

The role of microglia in the sympathetic control of blood pressure in normotension and hypertension

Komal Kapoor

BSc (Hons 1)

Supervisor: Professor Jacqueline K. Phillips and Professor Paul M. Pilowsky

Associate supervisor: Dr. Melissa M.J. Farnham

Department of Biomedical Sciences

The Faculty of Medicine and Health Sciences



Submitted: 9th June 2016

“This thesis is presented for the degree of Doctor of Philosophy”

Table of Contents

Abstract	ii
Declaration	iv
Acknowledgements	v
Publications and Communications	vii
List of Figures	xi
List of Tables	xiv
List of Plugins	xiv
List of Movies	xv
Abbreviations	xvi
Chapter 1 – Literature review	1
Chapter 2 – Methods	103
Chapter 3 – Microglial number is related to the number of tyrosine hydroxylase neurons in SHR and normotensive rats	133
Chapter 4 – Dynamic changes in the relationship of microglia to cardiovascular neurons in response to increases and decreases in blood pressure	157
Chapter 5 – Microglial response to changes in blood pressure in the rostral ventrolateral medulla is impaired in spontaneously hypertensive rats	199
Chapter 6 – Discussion and Conclusions	245
References	258
Appendix 1 – List of suppliers	297
Appendix 2 - Publications	302
Appendix 3 – Ethics	380

Abstract

Microglia are an essential component of the central nervous system (CNS), and are known to play a key role in the maintenance of neuronal/synaptic activity levels within their working physiological range. Microglia are present throughout the CNS and constantly survey their immediate environment for signs of over-, or under-, activity, or damage. Caudal and rostral ventrolateral medullary (CVLM and RVLM, respectively) regions of the brainstem are crucial in the cardiovascular arm of the sympathetic nervous system (SNS). Recently, dysfunction of normal microglial physiology in cardiovascular brain sites, involved in the sympathetic control of blood pressure (BP), is suggested to play a role in the pathology of neurogenic hypertension. The overall aim of this thesis was to determine if microglia in the ventrolateral medullary nuclei of the brainstem are involved in regulation of the cardiovascular system.

Data from Chapter 3 show that the microglial number, in a given catecholaminergic nucleus of the brainstem (such as A1, A2, C1, C3, A5 or A6), is closely related to the number of tyrosine hydroxylase immunoreactive (TH-ir) neurons in all 3 strains of rats examined (Sprague-Dawley (SD), Wistar-Kyoto (WKY) and spontaneously hypertensive rats (SHR)). The pattern of variation observed in the microglial number was similar to the pattern of variation observed in the TH-ir neuronal number, in catecholaminergic nuclei of the brainstem. This suggests that microglial distribution is strongly related to its local environment. Data from Chapter 4 show that microglia in the CVLM and the RVLM of SD rats are capable of sensing, and responding to, changes introduced in their local environment in response to altered baseline levels of BP. In this study, we demonstrate that alterations in BP do not induce any significant changes in microglial morphology, or require microglia to polarize to extreme activated phenotypes (M1/M2), in the CVLM and the RVLM. Instead, microglia, in the CVLM and the RVLM, alter their level of synaptic sampling (increased by $\approx 30\%$ following 6 h of phenylephrine induced hypertension and decreased by $>20\%$ following 6 h of hydralazine induced hypotension) accompanied by a subtle rearrangement of microglial spatial distribution. Data from Chapter 5 show that the microglial response to changes in BP is exaggerated in the RVLM of SHR (a model of neurogenic hypertension), when compared to that of the control strain (WKY). Following 2 h of phenylephrine induced hypertension, the % of colocalisation between microglia (Iba1) and synapses (synapsin) increased by $\approx 133\%$ in the RVLM of SHR, as compared to a decrease of $\approx 55\%$ seen in the RVLM of WKY. Similarly, following 2 h of hydralazine induced hypotension, the % of colocalisation between microglia (Iba1) and synapses (synapsin) increased by $\approx 72\%$ in the RVLM of SHR, but no changes were observed in the RVLM of WKY.

Collectively, data presented in this thesis highlight microglia as key elements of the CNS involved in the sympathetic control of BP homeostasis. We provide the first, and substantial, evidence that microglia in the ventrolateral medulla of the brainstem respond to changes in their local environment introduced by altered BP levels, and that this microglial response to altered BP in a strain with existing neurogenic hypertension (SHR) is impaired in the RVLM compared to its normotensive control.

Declaration

I certify that the work presented in this thesis, **“The role of microglia in the sympathetic control of blood pressure in normotension and hypertension”**, has not previously been submitted for, or as a part of, the requirements for a degree at any other university or institution other than the Macquarie University.

I also certify that this thesis is an original piece of research and the majority of the work included in this thesis was performed and written by me. I acknowledge and thank Mr. Amol M. Bhandare for his help with animal experiments described in Chapters 3, 4 and 5, and related data analysis (described in Chapters 4 and Chapter 5). Any further assistance that I have received in the completion of this work has been acknowledged appropriately.

Furthermore, I certify that all information sources and literature used are indicated in the thesis.

Part of the literature review is published in *Respiratory Physiology and Neurobiology* (Appendix 2) with the title “Alerted microglia and the sympathetic nervous system: A novel form of microglia in the development of hypertension”.

Chapter 3 (Appendix 2; (Kapoor et al., 2016a)) and Chapter 4 (Appendix 2; (Kapoor et al., 2016b)) are published with the following titles:

“Microglial number is related to the number of tyrosine hydroxylase neurons in SHR and normotensive rats” and

“Dynamic changes in the relationship of microglia to cardiovascular neurons in response to increases and decreases in blood pressure”.

Work described in Chapter 5 will be submitted shortly.

All the animal work conducted for this thesis was approved by the Sydney Local Health District Animal Welfare Committee, protocol no. 2013/081, and the Macquarie University Animal Care and Ethics Committee, Sydney, Australia.

Komal Kapoor

MQ student ID: 43115950

Acknowledgements

Past three and a half years have been filled with mixed emotions, happy at times and challenging at others, but most importantly this has been a journey full of emotional and intellectual development. None of this could have been possible without the support of many important people who deserve a special mention.

First, I wish to thank my supervisor Prof. Paul M. Pilowsky for giving me the opportunity to learn under his supervision, and being an amazing mentor I could ever have asked for. You have been a wonderful guide to me during the course of this PhD, not only as an advisor, but also as a fatherly figure. I would not have been able to complete this journey successfully without the ever-smiling face of yours. Thank you for showing tremendous amount of faith in me as a researcher and for helping me develop as an independent scientist. You have taught me many things including how to be a determined and a confident scientist, and how to learn ‘1 new word a day’.

I would also like to thank Prof. Jacqueline K. Phillips, my second supervisor, for making the journey of PhD, as an ‘Off site research student’, beautifully smooth. You have always just been a call away, despite of your busy schedule. I would also like to thank Jackie for her continuous motivation and support, and very constructive feedback on my work. Because of her, I was the lucky one who got the opportunity to enjoy the best of both worlds, Macquarie University and the Heart Research Institute.

Prior to acknowledging the tremendous support I received from everyone else; I would like to thank my lovely family who have always made sure that I receive the best of everything in life. My grandparents, parents, and my little brother, have really made my dream come true with their prayers, emotional and financial support. You have always been there for me, whether it’s a midnight international call or a skype conversation that continued for hours; assuring me in my difficult times that I am a good researcher and a strong individual. Thanks to my family for listening to my practice presentations and discussing my project, even though you had no idea of what ‘microglia’ are. Special thanks to my mum for being an amazing teacher throughout my life and for her very valuable support that helped me sail through the writing phase, very smoothly.

I would like to acknowledge and thank my associate supervisor Dr. Melissa M.J. Farnham for her continuous support, her amazing ‘attention to detail’ skills and very constructive feedback on almost every piece of work I wrote. Special thanks also goes to Dr. Suja Mohammed, who I

would like to think as an elder sister, for all her guidance during my candidature. I also thank Dr. Stephen Abbott for his valuable advice on ‘what to expect as a Post-Doctoral candidate’.

I would like to thank everyone in the High Blood Pressure team: Polina, Zohra, Sarah, Serene, Myfwany, Amol and Thara (apologies if I have missed anyone) for their very special (and supportive) company for tea and lunch breaks (especially for trips to pastry shops). All the ‘away from work’ breaks have really helped me get through this challenging journey. Saju, Asim and Nadia - you people are my family away from family; thanks for being there for me and for your support throughout this journey.

Lastly, none of this would have been possible without the financial support from the Macquarie University for funding my scholarship and all my conference presentations. Thanks to ‘Macquarie University postgraduate research fund’ for their very generous funding for my trip to the USA and presentation at the ‘Neuroscience’ conference. I would also like to thank the Heart Research Institute for funding my research that has taken the shape of this thesis.

I am surely going to miss this journey; all the late nights spent in the laboratory and all the weekends spent in dark microscopy room. Yet I look forward to the enormous amount of opportunities waiting for me.

Finally, I would like to dedicate this thesis to my grandfather (whose achievements have inspired me in my life) and in the loving memory of my grandmother. I could not have been able to succeed in life and my career, so far, without their love, motivation and faith in me.

“Education is not the learning of facts, but the training of mind to think”. Albert Einstein

Publications and Communications

Publications

1. **Kapoor, K.**, Bhandare, A.M., Mohammed, S., Farnham, M.M.J., Pilowsky, P.M., 2016. Microglial number is related to the number of tyrosine hydroxylase neurons in SHR and normotensive rats. *Autonomic Neuroscience*. 198, 10-8.
2. **Kapoor, K.**, Bhandare, A.M., Nedoboy, P.E., Mohammed, S., Farnham, M.M.J., Pilowsky, P.M., 2016. Dynamic changes in the relationship of microglia to cardiovascular neurons in response to increases and decreases in blood pressure. *Neuroscience*. 329, 12-29. **(Cover image of the issue - by Kapoor, K.)**
3. **Kapoor, K.**, Bhandare, A.M., Farnham, M.M.J., Pilowsky, P.M., 2015. Alerted microglia and the sympathetic nervous system: A novel form of microglia in the development of hypertension. *Respiratory Physiology and Neurobiology*. 226, 51-62. **(Cover image of the issue - by Kapoor, K.)**

Other publications arising from work conducted during the candidature

1. Nedoboy, P.E., Mohammed, S., **Kapoor, K.**, Bhandare, A.M., Farnham, M.M.J., Pilowsky, P.M., 2016. PSer40 tyrosine hydroxylase immunohistochemistry identifies the anatomical location of C1 neurons in rat RVLM that are activated by hypotension. *Neuroscience*. 317, 162-172.

Contribution by Kapoor, K. – brainstem tissue collected from animal experiments performed for Chapter 4 was shared with Nedoboy, P.E. for this study. K.K. also assisted with the conduct of immunohistochemistry experiments.

2. Bhandare, A.M., **Kapoor, K.**, Pilowsky, P.M., Farnham, M.M.J., 2016. Seizure-Induced sympathoexcitation is caused by activation of glutamatergic receptors in RVLM that also causes proarrhythmogenic changes mediated by PACAP and microglia in rats. *Journal of Neuroscience*. 36, 506-517. **(Cover image of the issue - by Kapoor, K.)**

Contribution by Kapoor, K. – assisted with tissue collection, and performed the molecular aspect of the study and related data analysis. K.K. provided images demonstrating the morphological relationship between cardiovascular neurons and microglia. Also provided the image for the cover art for this issue of the journal.

3. Bhandare, A.M., **Kapoor, K.**, Farnham, M.M.J., Pilowsky, P.M., 2015. Microglia PACAP and glutamate: Friends or foes in seizure-induced autonomic dysfunction and SUDEP? *Respiratory Physiology and Neurobiology*. 226, 39-50.

Contribution by Kapoor, K. – provided images demonstrating the morphological relationship between cardiovascular neurons and microglia. Contributed to final approval of the manuscript. Also provided the image for the cover art for this issue of the journal.

Publications “in preparation” or “under review”

1. **Kapoor, K.**, Bhandare, A.M., Farnham, M.M.J., Pilowsky, P.M., 2016. Microglial response to changes in blood pressure in the rostral ventrolateral medulla is impaired in spontaneously hypertensive rats. “In preparation”
2. Bhandare, A.M., **Kapoor, K.**, Powell, K.L., Briane, E., O’Brien, T.J., Farnham, M.M.J., Pilowsky, P.M., 2016. Microglial activation in the spinal cord mediates sympathoexcitatory and proarrhythmogenic changes in rats with chronic temporal lobe epilepsy. “In preparation”

Contribution by Kapoor, K. – assisted with tissue collection, the molecular aspect of the study and related data analysis. K.K. provided images demonstrating the morphological relationship between cardiovascular neurons and microglia.

Awards

1. **Heart Research Institute “Young Achievers award” – 2015** – was awarded “HRI excellence Young Achievers award” in recognition of performance during PhD candidature and conference presentations. This award is also associated with AUD\$5000 of funding to facilitate a presentation at an international conference in 2016.
2. **Travel award for Sydney Glia meeting – 2015** - \$300 was awarded to partially cover the costs associated with attendance at the Sydney Glia meeting 2015, Manly, Sydney.

Communications

1. **Kapoor, K.**, Bhandare, A.M., Mohammed, S., Farnham, M.M.J., Pilowsky, P.M. 2015. “Microglia and Hypertension: in cardiovascular nuclei in rat brainstem.” Oral presentation at the University of Rochester, New York, USA.

2. **Kapoor, K.**, Bhandare, A.M., Mohammed, S., Farnham, M.M.J., Pilowsky, P.M. 2015. "Microglia and Hypertension: in cardiovascular nuclei in rat brainstem." Oral presentation at the Mayo Clinic, Minnesota, USA.
3. **Kapoor, K.**, Bhandare, A.M., Mohammed, S., Farnham, M.M.J., Pilowsky, P.M. 2015. "Microglial alertness in rostral- and caudal- ventrolateral medullary nuclei is triggered by variations in neuronal activity in rat brainstem." Poster presentation at the Neuroscience (SfN) 2015, Chicago, USA.
4. **Kapoor, K.**, Bhandare, A.M., Mohammed, S., Farnham, M.M.J., Pilowsky, P.M. 2015. "Acute hypertension results in increased microglial contact with neuronal synapses in cardiovascular nuclei in rat brainstem." Oral presentation at the Sydney Glia meeting, Sydney, Australia.
5. **Kapoor, K.**, Bhandare, A.M., Mohammed, S., Farnham, M.M.J., Pilowsky, P.M. 2014. "Association of microglia with RVLM neurons during hypo- and hyper- tension." Poster presentation at the Oxford breathing meeting, Sydney, Australia.
6. **Kapoor, K.**, Bhandare, A.M., Mohammed, S., Farnham, M.M.J., Pilowsky, P.M. 2014. "Role of microglia in cardiovascular neurons: a morphological analysis." Poster presentation at the Central Cardiovascular Control: Future Directions, Melbourne, Australia.

Other communications arising from the work conducted during the candidature

1. Bhandare, A.M., **Kapoor, K.**, Pilowsky, P.M., Farnham, M.M.J. 2015. Cardiovascular autonomic dysfunction in seizure is caused by glutamatergic receptor activation in the rostral ventrolateral medulla; but not by pituitary adenylate cyclase activating polypeptide or microglia in rat. Poster presentation at the Neuroscience (SfN) 2015, Chicago, USA.
2. Bansal A., Nedoboy PE., Kim YJ., **Kapoor K.**, Pilowsky PM. 2015. Tyrosine hydroxylase neurons in hypothalamic neurons of WKY and hypertensive rats. Poster presentation at the Central Cardiorespiratory Control: Future Directions 2015, Sydney, Australia
3. Nedoboy PE., Mohammed S., Bhandare AM., **Kapoor K.**, Kim SJ., Farnham MMJ., Pilowsky PM. 2015. A novel set of mouse monoclonal antibodies to catecholaminergic antigens: tyrosine hydroxylase, Ser40-phosphorylated tyrosine hydroxylase and

norepinephrine transporter. Poster presentation at the Central Cardiorespiratory Control: Future Directions 2015, Sydney, Australia

4. Nedoboy PE., Mohammed S., Bhandare AM., **Kapoor K.**, Kim SJ., Farnham MMJ., Pilowsky PM. 2015. pSer40 tyrosine hydroxylase immunohistochemistry identifies the anatomical location of C1 neurons in rat RVLM that are activated by hypotension. Poster presentation at the Central Cardiorespiratory Control: Future Directions 2015, Sydney, Australia
5. Kim YJ., Bhandare AM., Nedoboy PE., **Kapoor K.**, Kim SJ., Farnham MMJ., Pilowsky PM. 2015. The effect of minocycline on sympathetic activity in the spontaneously hypertensive rat model of essential hypertension. Poster presentation at the Central Cardiorespiratory Control: Future Directions 2015, Sydney, Australia
6. Bhandare, A.M., **Kapoor, K.**, Mohammed, S, Pilowsky, P.M., Farnham, M.M.J. 2015. Antagonism of PACAP or microglia function worsens the cardiovascular consequences of kainic acid induced seizures in rat. Poster presentation at the ISN-APSN 2015, Cairns, Australia.
7. Bhandare, A.M., **Kapoor, K.**, Pilowsky, P.M., Farnham, M.M.J. Kainic acid-induced seizure causes dose dependent cardiorespiratory changes. Poster presentation at the Oxford breathing meeting, Sydney, Australia.
8. Bhandare, A.M., **Kapoor, K.**, Pilowsky, P.M., Farnham, M.M.J. Central autonomic and cardiovascular dysfunction in seizure and sudden unexpected death in epilepsy. Poster presentation at the Central Cardiovascular Control: Future Directions, Melbourne, Australia.

List of Figures

Chapter 1 – Literature review

Figure 1.1: Divisions of the Autonomic Nervous System (ANS)	5
Figure 1.2: Key sites in the brainstem involved in cardiovascular regulation.....	10
Figure 1.3: Efferent projections from the RVLM.....	20
Figure 1.4: C1 cells as “emergency medical technicians”	32
Figure 1.5: Segmental distribution of sympathetic preganglionic neurons (SPGNs).....	41
Figure 1.6: Location of various catecholaminergic nuclei, A1/A2/C1/C3/A5/A6, in the brainstem.....	43
Figure 1.7: Schematic representation of flow of the information between brainstem and peripheral organs involved in cardiovascular control of the SNS	48
Figure 1.8: The sympathetic baroreflex pathway	54
Figure 1.9: Sympathetic chemoreflex pathways.....	60
Figure 1.10: The Somatosympathetic reflex (SSR) pathway	65
Figure 1.11: Relationship between neurons and members of the ‘Glial family’ in the CNS ...	69
Figure 1.12: Schematic of P2R signalling and its contribution to central chemosensitivity in the retrotrapezoid nucleus (RTN).	71
Figure 1.13: Microglia in cardiovascular sites of the brainstem involved in the sympathetic control of BP.....	77
Figure 1.14: Activation stages of microglia in a healthy CNS, when subjected to a signal disturbing the homeostasis of the CNS.....	78
Figure 1.15: Microglia and the sympathetic control of blood pressure	92
Figure 1.16: Proposed model for immune/CNS interactions during hypertension.....	99
Figure 1.17: Schematic representation of aims of this thesis	102

Chapter 2 – Methods

Figure 2.1: Animal protocol.....	110
Figure 2.2: Pictorial representation of the Y shape of an IgG antibody	115
Figure 2.3: Expression of CD16 positive M1, amoeboid shaped, microglia.....	118
Figure 2.4: TH antibody characterisation	123

Chapter 3 – Microglial number is related to the number of tyrosine hydroxylase neurons in SHR and normotensive rats

Figure 3.1: Location of various catecholaminergic nuclei in the brainstem of a rat (SD, WKY or SHR).....	143
Figure 3.2: Microglia in the brainstem catecholaminergic nuclei of a SD	146
Figure 3.3: Microglia in the brainstem catecholaminergic nuclei of a WKY rat	147
Figure 3.4: Microglia in the brainstem catecholaminergic nuclei of an SHR	148
Figure 3.5: Intra- and inter- strain comparisons concerning the number of TH-ir neurons and microglia	149
Figure 3.6: Microglial morphology in the brainstem catecholaminergic nuclei.....	151
 Supplementary Figure 3.1: Intra-strain biological variability in the number of TH-ir neurons and microglia	 153

Chapter 4 – Dynamic changes in the relationship of microglia to cardiovascular neurons in response to increases and decreases in blood pressure

Figure 4.1: Effect of intravenous infusion of phenylephrine, saline and hydralazine on blood pressure	174
Figure 4.2: Effect of three different treatments (intravenous infusion of phenylephrine, saline or hydralazine) on the number of Fos-ir neurons in the RVLM region.....	175
Figure 4.3: Evidence of a close yet dynamic relationship between neurons (TH ⁺ neurons) and microglia	178
Figure 4.4: Effect of intravenous infusion of phenylephrine, saline or hydralazine on the number of microglia in the ventrolateral medullary region of SD rat	179
Figure 4.5: Effect of intravenous infusion of phenylephrine, saline or hydralazine on the spatial distribution pattern of microglia in the ventrolateral medullary region of SD rat.....	180
Figure 4.6: Effect of intravenous infusion of phenylephrine, saline or hydralazine on the number of synapses in contact with the microglial end point processes in the ventrolateral medullary region of SD rat.....	184
Figure 4.7: Effect of intravenous infusion of phenylephrine, saline or hydralazine on the morphological characteristics of microglia in the ventrolateral medullary region of SD rat	185

Figure 4.8: Microglial response to the intravenous infusion of phenylephrine, saline or hydralazine in the nucleus ambiguus (sub compact; NAsc) at 6 and 10 h time point.....	187
Figure 4.9: Effect of intravenous infusion of phenylephrine, saline or hydralazine on the expression levels of M1 and M2 phenotype in the brainstem region of SD rat	189
Figure 4.10: Microglial alertness induced in response to changes in levels of blood pressure	197

Chapter 5 – Microglial response to changes in blood pressure in the rostral ventrolateral medulla is impaired in spontaneously hypertensive rats

Figure 5.1: Tail-cuff phenotyping of WKY and SHR	212
Figure 5.2: Effect of intravenous infusion of phenylephrine, saline or hydralazine on AP, in WKY and SHR	214
Figure 5.3: Effects of intravenous infusion of phenylephrine, saline or hydralazine on MAP, of WKY and SHR, for 2 time points, 2 and 6 h	215
Figure 5.4: Fos-ir levels in response to intravenous infusion of phenylephrine, saline or hydralazine in the RVLM of WKY and SHR.....	217
Figure 5.5: Quantification of Fos-ir levels in the RVLM, of WKY and SHR, when subjected to intravenous infusion of phenylephrine, saline or hydralazine, for 2 and 6 h.....	219
Figure 5.6: Morphological relationship between microglia and cardiovascular neurons in the CVLM and the RVLM of WKY and SHR	221
Figure 5.7: Effects of intravenous infusion of phenylephrine, saline or hydralazine on the overall number of microglia	225
Figure 5.8: Effects of intravenous infusion of phenylephrine, saline or hydralazine on the IMD of microglia.....	226
Figure 5.9: Relationship between microglia (Iba1) and synapses (Synapsin) in the CVLM and the RVLM of WKY and SHR.....	230
Figure 5.10: Effects of intravenous infusion of phenylephrine, saline or hydralazine on the % of colocalisation between microglia (Iba1) and synapses (synapsin).....	231
Figure 5.11: Effects of intravenous infusion of phenylephrine, saline or hydralazine on microglial morphology	234
Figure 5.12: CD16 expression in response to intravenous infusion of phenylephrine, saline or hydralazine in WKY and SHR.....	236
Figure 5.13: CD206 expression in the ventrolateral medulla (VLM) of WKY and SHR	237

Figure 5.14: Expression levels of M2 microglia in response to intravenous infusion of phenylephrine, saline or hydralazine in WKY and SHR.	238
---	-----

Chapter 6 – Discussion and Conclusions

Figure 6.1: Microglia in the VLM region of the brainstem (controlling cardiovascular arm of the SNS) respond to altered BP	256
--	-----

List of Tables

Chapter 1 – Literature review

Table 1.1: Neurotransmitter-ir and their corresponding receptors on SPGNs.....	38
Table 1.2: Neurotransmitter receptors and their corresponding functions in the sympathetic control of BP and microglia (based on data from <i>in-vitro</i> studies)	84

Chapter 2 – Methods

Table 2.1: Considerations for choosing parametric vs non-parametric test	129
Table 2.2: List of parameters acquired in this study and appropriate statistical tests.....	130

List of Plugins

Chapter 2 – Methods

Plugin 1: To quantify the number of microglia, in a ROI, at 20X magnification.....	126
Plugin 2: Microglial skeleton analysis at 40X magnification.....	127
Plugin 3: Microglial skeleton analysis at 63X magnification.....	128
Plugin 4: To calculate the % of area occupied by microglia at 40X magnification	128

List of Movies

Chapter 4 – Dynamic changes in the relationship of microglia to cardiovascular neurons in response to increases and decreases in blood pressure

Movie 4.1: 3D reconstruction of Figure 4.3D197

Movie 4.2: 3D reconstruction of Figure 4.3E197

Chapter 5 – Microglial response to changes in blood pressure in the rostral ventrolateral medulla is impaired in spontaneously hypertensive rats

Movie 5.1: 3D reconstruction of Figure 5.6H238

Abbreviations

3v	3 rd ventricle
4v	4 th ventricle
5-HT	serotonin
7N	7 th nucleus
12N	12 th nucleus
AA	amino acids
ADN	aortic depressor nerve
ANOVA	analysis of variance
ANS	autonomic nervous system
AP	arterial blood pressure
ATP	adenosine triphosphate
AUC	area under curve
BDNF	brain derived neurotrophic factor
Böt	Bötzing
BP	blood pressure
CD	cluster of differentiation
ChAT	choline acetyltransferase
CNS	central nervous system
CPA	caudal pressor area
CPG	central pattern generator
CRN	central respiratory network
CVD	cardiovascular disorders
CVLM	caudal ventrolateral medulla
DBH	dopamine β hydroxylase
DH	dorsal horn
DMH	dorsomedial hypothalamus
EAA	excitatory amino acids
ELISA	enzyme-linked immunosorbent assay
EPSP	excitatory post synaptic potential
ERP	early reflex potential
GABA	γ -aminobutyric acid
GFAP	glial fibrillary acid protein
GFP	green fluorescent protein

H	Hours
HR	heart rate
IGF-1	insulin growth factor-1
IHC	immunohistochemistry
IL	interleukin
IML	intermediolateral cell column of the spinal cord
IMD	Inter-microglial distance
IO	inferior olives
Ir	Immunoreactivity
ISH	in situ hybridisation
JAM-1	junctional adhesion molecule-1
KCN	potassium cyanide
LC	locus coeruleus
LPS	lipopolysaccharide
LRP	late reflex potential
MAP	mean arterial pressure
MBP	mean blood pressure
MCPA	medullo-cervical pressor area
M-CSF	macrophage colony stimulating factor
MIP	maximum intensity projection
NAsc	nucleus ambiguus (sub compact)
NIH	National Institute of Health
NK-1	neurokinin-1
NMDA	N-methyl-D-aspartate
NMIIB	non-muscle myosin II B
NTS	nucleus of the solitary tract
PACAP	pituitary adenylate cyclase-activating polypeptide
PAG	periaqueductal gray
PBS	phosphate buffered saline
PBT	phosphate buffered saline with triton X-100
PFA	paraformaldehyde
PNMT	phenylethanolamine N-methyltransferase
Pre-Böt	Pre-Bötzinger
PSNS	parasympathetic nervous system

PVN	paraventricular nucleus of the hypothalamus
PVT	paraventricular nucleus of the thalamus
Pyr	pyramidal tract
RAS	renin angiotensin system
ROb	raphe obscurus
ROI	region of interest
ROS	reactive oxygen species
RPa	raphe pallidus
RTN	retrotrapezoid nucleus
RVLM	rostral ventrolateral medulla
RVMM	rostral ventromedial medulla
SBP	systolic blood pressure
SD	Sprague-Dawley
SHR	spontaneously hypertensive rats
SNA	sympathetic nerve activity
SND	sympathetic nerve discharge
SNP	sodium nitroprusside
SNS	sympathetic nervous system
Sp5	spinal trigeminal tract
SPGN	sympathetic preganglionic neurons
SSR	somatosympathetic reflex
SST	somatostatin
TGF β	transforming growth factor β
TH	tyrosine hydroxylase
TNF α	tumour necrosis factor- α
TPA	12-O-tetradecanoylphorbol-13-acetate
TPBS	phosphate buffered saline with tris
VII	facial nucleus
VMH	ventromedial nucleus of the hypothalamus
VLM	ventrolateral medulla
WKY	Wistar-Kyoto

Chapter 1

Literature review

Contents

1.1	Autonomic nervous system (ANS)	4
1.1.1	Parasympathetic nervous system (PSNS)	4
1.1.2	Sympathetic nervous system (SNS)	4
1.2	Sympathetic control of blood pressure (BP)	7
1.2.1	Key areas of the brain involved in the sympathetic control of BP	7
1.2.1.1	<i>Paraventricular nucleus of the hypothalamus (PVN)</i>	7
1.2.1.2	<i>A5</i>	12
1.2.1.3	<i>Caudal Raphe</i>	13
1.2.1.4	<i>Rostral ventromedial medullary (RVMM) neurons</i>	14
1.2.1.5	<i>Rostral ventrolateral medulla (RVLM)</i>	15
1.2.1.6	<i>Caudal ventrolateral medulla (CVLM)</i>	33
1.2.1.7	<i>Nucleus of the solitary tract (NTS)</i>	35
1.2.1.8	<i>Medullo-cervical pressor area (MCPA)</i>	36
1.2.1.9	<i>Sympathetic preganglionic neurons (SPGNs)</i>	37
1.2.2	Other catecholaminergic areas of the ANS	42
1.2.2.1	<i>A1</i>	44
1.2.2.2	<i>A2</i>	45
1.2.2.3	<i>C3</i>	45
1.2.2.4	<i>Locus coeruleus (LC) or A6 noradrenergic nucleus</i>	46
1.3	Autonomic reflex mechanisms	47
1.3.1	Baroreflex	49
1.3.2	Chemoreflex	55
1.3.2.1	<i>Peripheral chemoreflex</i>	55
1.3.2.2	<i>Central chemoreflex</i>	56
1.3.3	Somatosympathetic reflex (SSR)	62
1.4	Glia in CNS	67
1.4.1	Astroglia/astrocytes	67
1.4.2	Oligodendrocytes	73
1.4.3	Microglia	74
1.5	Microglia	74
1.5.1	Origin of microglia	74
1.5.2	History of microglia	74
1.5.3	Conventional activation paradigm	75
1.5.3.1	<i>Diverse microglial phenotypes</i>	75
1.5.3.2	<i>Activation pathway</i>	76

1.5.4	Activation signals – “on” or “off”	80
1.5.5	Microglial reaction to activation signal.....	80
1.6	Microglia and communication.....	80
1.6.1	Inter-microglial communication.....	80
1.6.2	Microglia and astrocytes	81
1.6.3	Microglia and neurons.....	81
1.6.3.1	<i>Glutamate receptors</i>	83
1.6.3.2	<i>GABA receptors</i>	83
1.6.3.3	<i>Purinergic receptors</i>	83
1.6.3.4	<i>Other neurotransmitter receptors</i>	84
1.7	Microglia and the CNS	87
1.7.1	Microglia in healthy CNS.....	88
1.7.2	Microglia during CNS injury	89
1.8	Microglia and sympathetic nervous system (SNS).....	90
1.9	Hypertension	94
1.9.1	Sympathetic nervous system and neurogenic hypertension	94
1.9.2	Possible involvement of microglia in hypertension	96
1.10	Aims.....	100

1.1 Autonomic nervous system (ANS)

The autonomic nervous system (ANS), a division of the vertebrate nervous system, is a complex network of neurons and ganglia; this network connects the brain and the spinal cord (central nervous system; CNS) to peripheral organs and glands (Figure 1.1). The ANS controls involuntary body systems, such as cardiorespiratory functions, temperature, osmolarity and digestion. The ANS consists of 2 parallel and separate arms, the sympathetic nervous system (SNS) and the parasympathetic nervous system (PSNS). Both systems, the SNS and the PSNS, comprise of 3 structural elements: preganglionic neurons (located in the CNS), ganglia and post-ganglionic neurons (located outside the CNS) (Figure 1.1) (McCorry, 2007). Sympathetic innervation of adrenal glands is an exception, where pre-ganglionic neurons from thoracic segments of the spinal cord innervate adrenal glands directly. Even though the SNS and the PSNS have opposite effects on peripheral organs, preganglionic elements of both of these systems are cholinergic in nature (Figure 1.1).

1.1.1 Parasympathetic nervous system (PSNS)

The PSNS is mainly responsible for functions associated with energy conservation and therefore, is activated during periods of “rest and digest” (Figure 1.1). Preganglionic neurons of the PSNS are located in the dorsal motor nucleus of the vagus (Olshansky et al., 2008), the nucleus ambiguus (Grkovic et al., 2005; Salo et al., 2006), the Edinger-Westphal nucleus in the brainstem (Reiner et al., 2009) and sacral columns (S2-S4) of the spinal cord (de Groat and Ryall, 1969) (Figure 1.1). The PSNS performs functions such as slowing down the heart rate (HR), constricting airways, and stimulating salivation and digestion. Approximately (\approx) 75% of the PSNS innervates the heart, and originates from the dorsal motor nucleus of the vagus (regulating contractile force) and the nucleus ambiguus (regulating HR) (Izzo et al., 1993; Rentero et al., 2002; Sampaio et al., 2014).

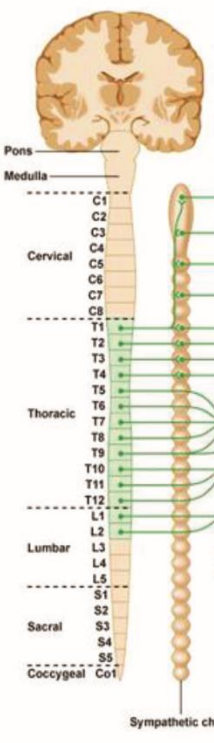

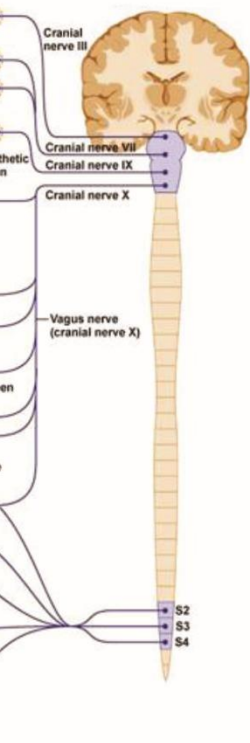
1.1.2 Sympathetic nervous system (SNS)

Contrary to the “rest and digest” arm of the ANS, the SNS is known as the “fight or flight” component and is generally associated with activities involved in expenditure of energy (Figure 1.1). Stimulation of the SNS elicits responses such as increase in vascular tone, stimulation of adrenal glands, generation of glucose, and inhibition of digestion. Unlike the PSNS, efferent arm of the SNS exits the CNS from thoracic and lumbar segments of the spinal cord to innervate adrenal glands and ganglia located in periphery and thereby, affects activity of peripheral organs

(Figure 1.1). Sympathetic preganglionic neurons (SPGNs) located in the intermediolateral (IML) cell column of the spinal cord are controlled by premotor neurons located in supra-spinal nuclei of the brainstem, such as the paraventricular nucleus of the hypothalamus (PVN), the rostral ventrolateral medulla (RVLM) and caudal raphe (Guyenet, 2006; Pilowsky et al., 2009).

Figure 1.1: Divisions of the Autonomic Nervous System (ANS)

There are 2 divisions of the ANS, the sympathetic nervous system (SNS) and the parasympathetic nervous system (PSNS). Preganglionic neurons of the SNS are located in the thoracic and lumbar segments of the spinal cord, and preganglionic nerves are comparatively shorter than postganglionic nerves. On the other hand, preganglionic neurons of the PSNS are located in the brainstem and sacral segments of the spinal cord; preganglionic nerves of the PSNS are comparatively longer than postganglionic nerves. The SNS and the PSNS exert opposing effects on target organs in periphery. For example, the SNS inhibits digestion, whereas the PSNS stimulates digestion. (Adapted from Chapter 11 from “droualb.faculty.mjc.edu”)

	Sympathetic Nervous System (SNS)	Target organs	Parasympathetic Nervous system (PSNS)
<p>Divisions of the autonomic nervous system (ANS)</p>			
<p>Preganglionic neuron</p>	<p>Soma of the neuron is usually in the thoracic and lumbar segments of the spinal cord</p>	<p>Soma of the neuron is usually in the brainstem or sacral segments of the spinal cord</p>	
	<p>Cholinergic</p>	<p>Cholinergic</p>	
<p>Postganglionic neurons</p>	<p>Soma of the neuron is in a sympathetic ganglion located closer to the spinal cord, except for innervations to adrenal glands</p>	<p>Soma of the neuron is in the ganglion located nearer to the target organ</p>	
	<p>Adrenergic or cholinergic</p>	<p>Cholinergic</p>	
<p>Response</p>	<p>Fight or flight</p>		<p>Rest and digest</p>

1.2 Sympathetic control of blood pressure (BP)

Blood pressure (BP) is defined as the pressure exerted by circulating blood on walls of peripheral vessels. According to recent guidelines from the American Heart Association, arterial BP (AP) is considered normal within the range of $\approx 100/60 - 120/80$ mmHg; this BP is sufficient for adequate tissue perfusion, oxygenation and waste removal.

BP, in general, is highly variable over a 24 hours (h) period, but is tightly regulated to avoid reaching extremes. Two factors determining AP levels are cardiac output and total peripheral resistance. In turn, cardiac output depends on end diastolic volume, myocardial contractility and HR. End diastolic volume is primarily governed by the SNS, however both the SNS and the PSNS play an important role in the regulation of myocardial contractility and HR ((Guyenet, 2006) and section 1.1.1). Despite the importance of the PSNS in control of AP, and various genetic factors influencing BP (Takami et al., 1999; Wong et al., 1999), this study is only focused upon the sympathetic control of BP.

1.2.1 Key areas of the brain involved in the sympathetic control of BP

1.2.1.1 Paraventricular nucleus of the hypothalamus (PVN)

The PVN is a major site involved in the autonomic and neuroendocrine control of the cardiovascular system (the hypothalamo-pituitary-adrenal axis, the thyroid axis, the reproductive axis, growth and development, and regulation of body fluid balance) (Badoer, 2010; Erdos et al., 2015), and is located on either side of the third ventricle of the hypothalamus (Figure 1.2) (Paxinos and Watson, 2007). Broadly, the PVN comprises of 2 cell populations, larger magnocellular neurons and smaller parvocellular neurons. Magnocellular neurons are associated with the neuroendocrine side of the PVN and are key in the secretion of vasopressin and oxytocin. The parvocellular PVN neuronal group is involved in the autonomic regulation of the cardiovascular system and is of interest here.

Afferent projections: The PVN receives afferent inputs from many sites ranging from other hypothalamic centers (such as the subfornical organ, the median preoptic nucleus and the suprachiasmatic nucleus) (Kawano and Masuko, 2010; Llewellyn et al., 2012; Silverman et al., 1981; Wang et al., 2003), to the pons (such as the locus coeruleus (LC)) (Hwang et al., 1998) and medullary regions (such as the nucleus of the solitary tract (NTS) (Affleck et al., 2012), the A1 nucleus (Day et al., 1984; McDonald et al., 2000) and the RVLM (Card et al., 2006; Xu et al., 2012)).

Efferent projections: Based on efferent projections from the PVN the neuronal population in this region can be divided into 2 main groups, the neuronal population (magnocellular neurons) that projects to the posterior pituitary (Swanson and Kuypers, 1980), and the population (parvocellular neurons) that projects to the median eminence (Swanson and Kuypers, 1980; Swanson et al., 1980) and dorsal vagal complex (Sawchenko and Swanson, 1982; Swanson and Kuypers, 1980; Swanson et al., 1980). Parvocellular neurons of the PVN are involved in the autonomic circuitry, and project directly to the RVLM region (Badoer, 1998; Badoer and Merolli, 1998; Kantzides and Badoer, 2005; Shi et al., 2009; Xu et al., 2012) and to SPGNs in the IML region of the spinal cord (Figure 1.2) (Badoer, 2010; Nunn et al., 2011; Sawchenko and Swanson, 1982; Strack et al., 1989). In addition to direct projections to the RVLM, ~30% of spinally projecting PVN neurons also send collateral projections to the RVLM (Badoer and Merolli, 1998). The PVN also sends direct bilateral glutamatergic projections to the medial sub-nucleus of the NTS, and these glutamatergic projections are tonically active (Kawabe et al., 2008). Thus, the PVN has the ability to exert its effects on peripheral cardiovascular organs via either direct or indirect projections to SPGNs.

Controversial evidence is reported concerning the role of the PVN in the sympathetic control of BP. Low intensity electrical stimulation of the PVN, in anesthetized rats, inhibited renal sympathetic nerve activity (SNA) (Kannan et al., 1988). On the other hand, high intensity electrical stimulation of the PVN, in anesthetized rats, evoked a transient excitatory effect followed by an inhibitory effect on renal SNA (Kannan et al., 1988). Chemical stimulation of the PVN in anesthetized rats, with glutamate, exerted a depressor response (Kannan et al., 1988). However, Coote et al., showed that chemical stimulation of PVN neurons (with D, L-homocysteic acid) in anesthetized rats exerted a pressor response, by exciting RVLM neurons (Coote et al., 1998). Horiuchi and colleagues (2011) showed that microinjection of bicuculline (GABA receptor antagonist) into the PVN of anaesthetised rats evoked increases in renal SNA; this effect could be greatly reduced in response to intravenous administration of 5-HT_{1A} receptor agonist (Horiuchi et al., 2011). Chemical inhibition of PVN neurons in conscious rabbits, with muscimol (GABA agonist, 10 nmol), elicited an increase in renal SNA and a reduction in HR, without any changes in mean arterial pressure (MAP) (Badoer et al., 2002).

Induction of either central hyper-, or hypo-, volemia evoked increases in the activity of PVN neurons (shown by Fos-ir)(Potts et al., 1999). Interestingly, the pattern of Fos-ir induced in the PVN of conscious rabbits in response to modulations in levels of blood volume did not

significantly differ between barointact and barodenervated rabbits, indicating that this response is primarily governed by inputs from cardiac receptors (Potts et al., 1999).

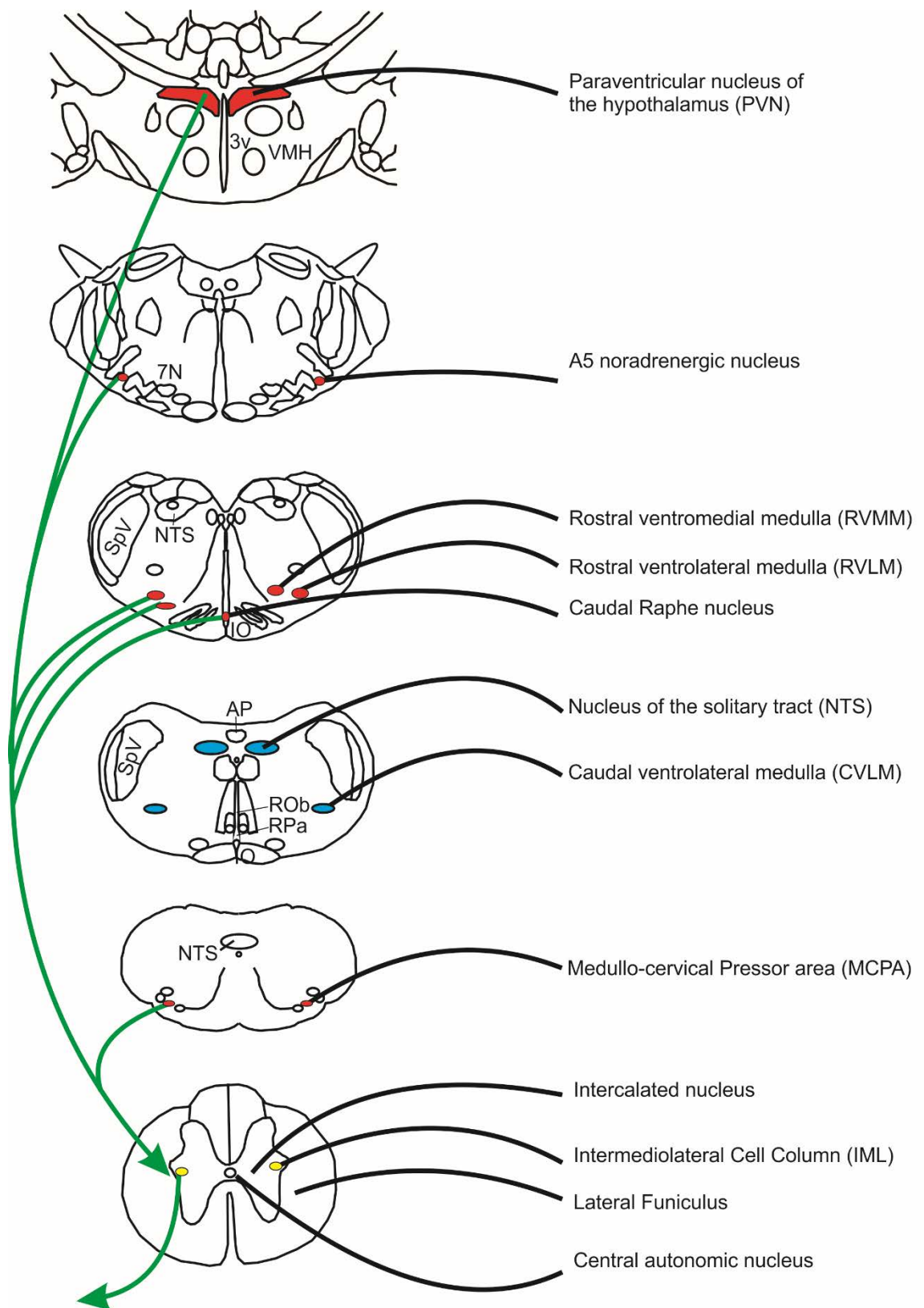
A recent study showed that intracerebroventricular administration of leptin and resistin caused an increase in neuronal activity levels in the PVN of rats (determined by Fos-ir) accompanied by an increase in renal SNA (Habeebullah et al., 2016); indirectly, this study has provided a link between activation of PVN neurons and increased renal SNA. All of the above-mentioned literature highlight the PVN as an integral component of the autonomic circuitry involved in cardiovascular regulation; however, the exact role of the PVN in regulation of the cardiovascular system is yet to be established.

Dysfunction in normal activity of the PVN is linked to the pathophysiology of various cardiovascular disorders (CVDs), such as hypertension (Ciriello et al., 1984; Erdos et al., 2015; Herzig et al., 1991; Li and Pan, 2007; Takeda et al., 1991) and heart failure (Badoer, 2010; Xu et al., 2012). The PVN mediated activation of the RVLM is exaggerated in animal models of heart failure, leading to higher levels of SNA (Coote, 2005). A study by Allen (2002) showed that basal sympathetic vasomotor tone under influence of the PVN is exaggerated in spontaneously hypertensive rats (SHR, an animal model for essential hypertension), and inhibition of the PVN region by GABA agonist significantly reduced this elevated sympathetic vasomotor tone in SHR (Allen, 2002).

Furthermore, PVN neurons are also thermosensitive, and modulate SNA in response to homeothermic challenges to thermoregulatory organs (such as brown adipose tissue, kidney, gut and the vasculature of rat tail) via its efferent projections to SPGNs and the RVLM (Badoer, 2010; Cham, 2006; Cham and Badoer, 2008a; Cham and Badoer, 2008b; Chen et al., 2008).

Figure 1.2: Key sites in the brainstem involved in cardiovascular regulation

There are 6 premotor nuclei (red), which project directly to the IML cell column (yellow) of the spinal cord, and play a key role in the sympathetic control of BP. In addition to these 6 premotor nuclei, the NTS (blue) and the CVLM (blue) also play an important role in the cardiovascular system. Majority of sympathetic preganglionic neurons (SPGNs) are located in the IML cell column and lateral funiculus of the spinal cord. Only a few SPGNs are located in the central autonomic and intercalated nucleus of the spinal cord. (Adapted from (Strack et al., 1988; Strack et al., 1989)). VMH, ventromedial nucleus of the hypothalamus; 3v, 3rd ventricle; 7N, facial nucleus; Sp5, spinal trigeminal tract; AP, area postrema; ROb, raphe obscurus nucleus; RPa, raphe pallidus nucleus; IO, inferior olives.



1.2.1.2 A5

The A5 noradrenergic nucleus of the brainstem is immunoreactive (ir) for tyrosine-hydroxylase (TH - an enzyme that is involved in the synthesis of catecholamines) and dopamine β hydroxylase (DBH). The A5 nucleus of the brainstem is located near the pontomesencephalic junction, mostly between the facial nerve fibers exiting the brainstem and the superior olive, at ≈ 10.56 mm caudal to bregma (Figure 1.2 and 1.6) (Badoer et al., 1987; Paxinos and Watson, 2007). A5 neurons of the brainstem are an important component of the ANS.

Afferent projections: The A5 group of neurons receive afferent projections from many nuclei including, but not limited to, the cuneiform nucleus, the PVN, the periaqueductal gray, the locus coeruleus (LC), parabrachial area, vestibular complex, the RVLM, intermediate and caudal NTS and the caudal ventral medullary reticular formation (Abbott et al., 2012; Bajic and Proudfit, 2013; Byrum and Guyenet, 1987; Li et al., 1992b; Stornetta et al., 2015).

Efferent projections: The A5 region projects to various nuclei involved in the autonomic control of BP, such as the NTS, the ipsilateral lateral funiculus of the spinal cord and the IML cell column of the spinal cord (Figure 1.2) (Bruinstroop et al., 2012; Byrum and Guyenet, 1987; Kanbar et al., 2011; Loewy et al., 1979b; Strack et al., 1989).

The exact role of A5 neurons in the ANS has been an area of debate for more than a decade. Loading of baroreceptors, in response to elevated levels of MAP, inhibited the firing of A5 neurons in urethane-anesthetized rats (Guyenet, 1984). In line with these findings, hypotension, induced by intravenous infusion of sodium nitroprusside (SNP), caused an elevation in levels of Fos-ir neurons in the A5 nucleus of conscious rabbits (Li and Dampney, 1994; Polson et al., 2002). Direct electrical stimulation, with 5 μ A currents, of A5 neurons, in anesthetized rats and conscious rabbits, resulted in an increased BP and pulse pressure, with no changes in HR (Loewy et al., 1979a; Maiorov et al., 1999). Whereas, chemical stimulation of the A5 region of anesthetized rats, with microinjections of L-glutamate, elicited reductions in MAP, HR, cardiac output and calculated stroke volume (Neil and Loewy, 1982; Stanek et al., 1984), or caused increases in the renal SNA, with no changes in AP (Maiorov et al., 1999). Reductions in MAP, following chemical stimulation of A5 neurons, is suggested to be mediated via projections from the A5 region to the spinal cord, and the neurotransmitter involved in this pathway is suggested to be GABA (Hara et al., 1997). However, the evidence supporting the presence of direct GABAergic projections from A5 neurons to the spinal cord is yet missing (Deuchars et al., 2005; Hara et al., 1997).

Microinjection of muscimol (agonist for GABA_A receptors) in the A5 region of conscious rabbits did not affect resting levels of MAP, HR and renal SNA (Maiorov et al., 2000). However, pretreatment of A5 neurons in conscious rabbits with muscimol increased renal sympathetic responses to baroreceptor unloading (with intravenous SNP), under normoxic conditions (Maiorov et al., 2000). This study highlighted that even though A5 neurons are not involved in the regulation of basal sympathetic tone, these neurons serve to limit the excitation of renal SPGNs caused by baroreceptor unloading.

A recent technique - optogenetic stimulation of channelrhodopsin-2 (a non-mammalian gene that codes for a light sensitive ion channel) expressed in neurons of interest – has proven to be quite promising. A study by Kanbar et al., (2011), utilizing the optogenetic technique in anesthetized rats, has shown that stimulation of channelrhodopsin-2 expressing neurons of the A5 region ($\approx 66\%$ of TH-ir A5 neurons) produced five-fold greater activation of renal than lumbar sympathetic chain (Kanbar et al., 2011).

In addition to the role of A5 nucleus in cardiovascular regulation, its role in respiratory modulation has also been reported (Guyenet et al., 1993; Kanbar et al., 2011; Li et al., 2008a). Furthermore, tachycardia and pressor responses evoked in response to electrical stimulation of the hypothalamic defence area are mediated through the A5 nucleus (Lopez-Gonzalez et al., 2013). This is supported by studies showing that blockade of A5 neurons, with muscimol, reduced the pressor response seen following stimulation of the hypothalamic defence area (Lopez-Gonzalez et al., 2013).

1.2.1.3 Caudal Raphe

Raphe nuclei of the brainstem are divided into 3 subtypes based on their neuro-anatomical location: raphe pallidus (RPa, Figure 1.2), raphe obscurus (ROb, Figure 1.2) and raphe magnus. All of these 3 sub-nuclei of the raphe nucleus can be immunohistochemically labelled with serotonin, 5-HT (Jansen et al., 1995). Neurons located in caudal sites of the raphe nucleus (Figure 1.2) are the ones that project to SPGNs (Strack et al., 1989). Some of these bulbospinal caudal raphe neurons, in addition to being 5-HT-ir, are also immunoreactive for substance P and thyrotropin releasing hormone (Charlton and Helke, 1987; Jansen et al., 1995).

Afferent projections: Afferent projections to caudal raphe neurons arise from a wide range of nuclei such as the medial preoptic nucleus, the hypothalamus, the central nucleus of amygdala and the RVLM (Berthoud et al., 2005; Card et al., 2006; Dampney, 1994; Hosoya, 1985; Stornetta et al., 2015; Verner et al., 2008).

Efferent projections: Efferent projections from caudal raphe neurons mediating its cardiovascular effects extend to both, the RVLM and the IML cell column of the spinal cord (Figure 1.2) (Bacon et al., 1990; Bago et al., 2002; Heslop et al., 2004; Strack et al., 1989).

The role of caudal raphe neurons in cardiovascular regulation can either be sympatho-excitatory or sympatho-inhibitory, depending on the neuronal subset stimulated (Morrison and Gebber, 1984). Both (sympatho-excitatory and sympatho-inhibitory) subsets of caudal raphe neurons are affected by activity of baroreceptors (Morrison and Gebber, 1984). However, only the sympatho-inhibitory neurons project to the IML cell column of the spinal cord (Morrison and Gebber, 1984).

Microinjection of GABA receptor antagonist (bicuculline) into RPa of conscious rats caused an increase in HR (Zaretsky et al., 2003). Chemical inhibition of RPa of conscious rats, with muscimol, did not affect HR, yet abolishes the air stress-induced tachycardia (Zaretsky et al., 2003). Microinjection of glutamate in the caudal raphe of anaesthetized rabbits induced a depressor response with decreases in MAP, renal SNA and HR (Coleman and Dampney, 1995). These observed depressor responses were similar in magnitude to the ones observed following chemical stimulation of the caudal ventrolateral medullary nucleus (CVLM) (Coleman and Dampney, 1995); this study highlighted caudal raphe nucleus as one of the key sites involved in cardiovascular regulation. Despite their role in cardiovascular regulation, caudal raphe neurons are not tonically active (Coleman and Dampney, 1995), but are inhibited by activation of baroreflex pathway (Pilowsky et al., 1995).

Moreover, caudal raphe neurons are also involved in other aspects of the ANS control, apart from their role in the cardiovascular regulation, such as chemoreception (Bernard et al., 1996), hemorrhage evoked response (Heslop et al., 2002; Kung et al., 2010) and thermoregulation (Berthoud et al., 2005; Nakamura and Morrison, 2007).

1.2.1.4 Rostral ventromedial medullary (RVMM) neurons

The RVMM pressor region (Figure 1.2) is located in the ventral medulla oblongata, ≈ 0.5 -1.5 mm lateral to the midline, and extends caudally from the rostral half of the facial nucleus to the rostral pole of the inferior olivary nucleus (Cox and Brody, 1989). The RVMM is sympatho-excitatory and receives projections from periaqueductal gray neurons (Morgan et al., 2008).

Efferent projections: Efferent projections from the RVMM extend to the spinal cord (Babic and Ciriello, 2004; Marinelli et al., 2002; Strack et al., 1989) (Figure 1.2), the nucleus ambiguus

(Babic et al., 2008), phrenic motoneurons (Dobbins and Feldman, 1994) and the NTS (Babic et al., 2008).

The role of RVMM neurons in modulation of nociceptive stimuli, at the level of the dorsal horn in the spinal cord, is well established (Fei et al., 2016; Heinricher et al., 2009; Marinelli et al., 2002). Neurons in the RVMM that are responsive to a nociceptive stimulus can be divided into 3 subclasses, based on their action potential response to a nociceptive stimulus: ON (increases action potential), OFF (decreases action potential) and NEUTRAL (no change in activity) (Fields et al., 1988).

In addition to the role of RVMM neurons in nociception, their role in cardiovascular regulation is also important. Neurons in the pressor region of the RVMM are immunoreactive for many neuro-transmitters/ neuro-peptides such as serotonin, adrenaline, thyrotropin releasing hormone, substance P, somatostatin (SST) and enkephalin (Jansen et al., 1995).

Bilateral microinjection of lidocaine in the RVMM of urethane-anaesthetized rats caused a reduction in MAP and renal, mesenteric and hindquarter vascular resistance (Cox and Brody, 1989). A study by Varner et al. (1989), also showed that the RVMM and the RVLN contribute equally to neurogenic maintenance of AP, and blockade of the RVMM reduced sympathetic outflow from renal, lumbar and splanchnic nerves (Varner et al., 1989). Electrical stimulation of the RVMM in anesthetized rats increased MAP and regional vascular resistance (Cox and Brody, 1989). In line with these findings, chemical stimulation of the RVMM in anesthetized rats, with glutamate or EAA (excitatory amino acids) analogues (NMDA), also exerted pressor effects; prior treatment with 5,7-dihydroxytryptamine abolished this pressor response (Minson et al., 1987; Varner et al., 1992). A role of the RVMM, under influence of the hypothalamus, in cardiovascular regulation has recently been revealed. Microinjection of corticotrophin releasing factor into the hypothalamus of rats caused an increase in the RVMM neuronal activity (Gao et al., 2016).

Further to the role of serotonergic RVMM neurons in nociception and cardiovascular regulation, neurons in this region of the brainstem are also involved in thermoregulation (Korsak and Gilbey, 2004; Morrison et al., 2008), respiration (Verner et al., 2004) and chemoreception (Bradley et al., 2002; Miura et al., 1996a; Richerson et al., 2001).

1.2.1.5 Rostral ventrolateral medulla (RVLN)

The RVLN (Figure 1.2 and Figure 1.4) neurons play an important role in the tonic and phasic regulation of BP and SNA (Guyenet, 2006). Different researchers define boundaries of the

RVLM differently (Farnham et al., 2008; Stornetta et al., 2001). For the purpose of this thesis, the RVLM is defined as the area located medial to the spinal trigeminal tract, lateral to the pyramids, ventral to the nucleus ambiguus and spans rostro-caudally from ≈ 12.00 mm to ≈ 12.8 mm caudal to bregma (Paxinos and Watson, 2007) (Figure 1.2). The C1 (catecholaminergic/adrenergic) group of RVLM neurons are immunoreactive for TH and PNMT (phenylethanolamine N-methyl transferase) (section 1.2.2). No known pan marker can label all RVLM neurons, C1 neurons and non-C1 neurons (non-catecholaminergic RVLM neurons). Preproenkephalin mRNA labels most of the non-C1 barosensitive bulbospinal neurons of the RVLM (Stornetta et al., 2001).

Bilateral destruction or inhibition of neurons in the RVLM of anesthetized cats caused profound falls in BP, similar to that observed following transection of the spinal cord (Feldberg and Guertzenstein, 1976; Guertzenstein and Silver, 1974). Even unilateral cytotoxic lesioning of the RVLM in conscious dogs (with microinjection of kainic acid) caused significant reductions in AP and total peripheral resistance, whereas no changes were observed in cardiac output and HR (Stith and Dormer, 1994). The depressor response to unilateral lesioning of the RVLM occurred in parallel to reductions in plasma levels of catecholamines (adrenaline and noradrenaline) and cortisol; these findings suggested a neuroendocrine relationship between the RVLM and AP (Stith and Dormer, 1994).

Electrical stimulation of the RVLM, in either conscious or anesthetized rats, elicited increases in MAP, HR, levels of plasma catecholamines (adrenaline, noradrenaline and dopamine) and vasopressin (Chen et al., 2013; Ross et al., 1984b). In line with these findings, chemical stimulation of the RVLM, by glutamate or NMDA microinjection in various species (such as conscious rabbits, anaesthetised rabbits, conscious rats and anesthetized rats), increased the AP, SNA to adrenal glands, renal SNA and lumbar SNA, and also enhanced resistance in the mesenteric, renal and hindquarter vascular beds (Blessing et al., 1981b; Chen et al., 2013; Chida et al., 1998; Dampney et al., 1982; Mueller et al., 2011; Reis et al., 1984; Ross et al., 1984b; Sakima et al., 2000; Willette et al., 1987). Conversely, microinjection of GABA, or tetrodotoxin (binds to voltage gated sodium channels exerting its neurotoxic effects), or muscimol (GABA_A mimetic), or baclofen, in the RVLM caused decreases in AP, renal SNA, HR and resistance in the mesenteric, renal and hindquarter vascular beds (Amano and Kubo, 1993; Reis et al., 1984; Ross et al., 1984b; Willette et al., 1987). Blockade of GABA receptors in the RVLM, with bicuculline or antagonists of GABA_A and GABA_B receptors, elevated baseline levels of AP (Amano and Kubo, 1993; Avanzino et al., 1994; Reis et al., 1984; Ross et al.,

1984b); this pressor response was possibly mediated due to the blockade of GABAergic input to the RVLM from the CVLM (section 1.3.1). Blockade of glycine receptors in the RVLM of anesthetized rats, with strychnine (glycine antagonist), had no significant effects on physiological parameters, such as MAP (Ross et al., 1984b). However, microinjection of glycine in the RVLM of anesthetized rats exerted a depressor response, accompanied with reduction in renal SNA (Amano and Kubo, 1993; Sakima et al., 2000). Therefore, it is suggested that RVLM neurons are sympatho-excitatory that exert an excitatory influence on sympathetic vasomotor neurons, adrenal medulla and the posterior pituitary; this area is under the tonic inhibitory control via GABAergic mechanisms (Guyenet, 2006; Pilowsky et al., 2009; Ross et al., 1984b).

In addition, the RVLM is a key site for the modulation of cardiovascular responses evoked by the activation of higher brain regions, such as the dorsomedial hypothalamus (DMH) (Fontes et al., 2001). The pressor and sympatho-excitatory responses evoked by microinjection of bicuculline (GABA antagonist) in the DMH of anaesthetised rats could be significantly interrupted by the bilateral microinjection of muscimol into the RVLM (Fontes et al., 2001).

- *Afferent inputs to the RVLM*

The RVLM is known to receive afferent inputs from many brain regions such as the NTS (Aicher et al., 1996; Dampney et al., 1982; Stornetta et al., 2015), the CVLM (Chan and Sawchenko, 1998; Schreihofer and Guyenet, 2002), caudal pressor area (Campos and McAllen, 1999; Campos et al., 2008; Sun and Panneton, 2005), the raphe (Nicholas and Hancock, 1990), the PAG (Farkas et al., 1998; Sartor and Verberne, 2003; Van Bockstaele et al., 1991), the PVN (Badoer, 1998; Badoer and Merolli, 1998; Coote et al., 1998), the DMH (Fontes et al., 2001) and orexinergic neurons of the dorsolateral hypothalamus (Guyenet et al., 2013; Puskas et al., 2010; Stornetta et al., 2015). Furthermore, retrograde labelling of afferent projections to the RVLM, with microinjections of wheat germ agglutinin conjugated with horseradish peroxidase in the RVLM, revealed afferent inputs from brain regions such as the ambiguous complex and the Kolliker-Fuse nucleus (Dampney et al., 1987).

Afferent projections to the RVLM arising from the NTS and the CVLM are of interest here. A study comparing afferent terminals to the RVLM from the NTS and the CVLM has shown that even though the morphology and vesicular content of these terminals were similar, CVLM efferent terminals were slightly larger than NTS efferent terminals (Aicher et al., 1996). NTS efferent terminals formed asymmetric synapses with RVLM neurons, which are sympatho-excitatory, and CVLM efferent terminals to the RVLM formed symmetric synapses that are

sympatho-inhibitory (Aicher et al., 1996). In addition, CVLM inhibitory inputs to the RVLM were speculated to be more influential than inputs from the NTS to the RVLM, because inputs from the CVLM are likely to contact the adrenergic RVLM neuronal somata (Aicher et al., 1996).

Sympatho-inhibitory effects exerted by CVLM inputs on to RVLM neurons are crucial in modulation of the sympathetic baroreflex pathway (section 1.3.1).

- *Efferent outputs from the RVLM*

RVLM neurons can be divided into 2 main categories based on their efferent outputs, bulbospinal RVLM neurons that project to SPGNs and non-bulbospinal RVLM neurons that project to other brain areas (Figure 1.3). Neurons in the caudal portion of the RVLM are non-bulbospinal neurons that project to areas such as the hypothalamic PVN (Coote, 2005; Haselton and Guyenet, 1990; Loewy et al., 1981), orexinergic neurons (Bochorishvili et al., 2014), raphe neurons (Card et al., 2006), PAG (Card et al., 2006; Herbert and Saper, 1992) or the locus coeruleus (LC) (Abbott et al., 2012; Chen et al., 2013; Pieribone et al., 1988; Pieribone and Aston-Jones, 1991).

Bulbospinal neurons are located in the rostral half of the RVLM, and send efferent projections mainly to the IML cell column of the spinal cord and to the central autonomic area (Figure 1.2 and 1.3) (Dampney et al., 1987; Guyenet et al., 2013; Stornetta et al., 2015; Strack et al., 1989). Many groups have demonstrated efferent projections from the RVLM to the IML cell column of the spinal cord (Figure 1.2 and Figure 1.3) (Card et al., 2006; Minson et al., 1990; Minson et al., 1991; Pyner and Coote, 1998; Ross et al., 1984a). These projections are highly specific in that there are no projections to thoracic dorsal and ventral horns (Ross et al., 1984a). Projections from the RVLM to SPGNs located in the IML cell column of the spinal cord are monosynaptic (Oshima et al., 2006; Oshima et al., 2008).

The sympathetic nerve discharge is differentially controlled by RVLM neurons (Barman et al., 1984). The firing pattern of RVLM neurons did not correlate to the same degree with different sympathetic outputs, suggesting that RVLM neurons exert their influence on various sympathetic outputs in a non-uniform fashion (Barman et al., 1984). Inhibition of RVLM neuronal discharge inhibited renal nerve discharge to a greater extent than splenic nerve discharge (Hayes and Weaver, 1990). Also, postganglionic responses to blockade of RVLM activity are greater than preganglionic responses (Hayes and Weaver, 1990). The findings mentioned here demonstrated that the nerve discharge of pre-, and post-, ganglionic

sympathetic fibers is dependent on the RVLM excitatory drive, and is differentially controlled by the same.

Chemical stimulation of the medial part of the RVLM, with glutamate, evoked activation of cutaneous fibres, whereas stimulation of more lateral region in the RVLM evoked activation of muscle vasoconstrictor fibres (Dampney and McAllen, 1988). Stimulation of RVLM neurons located ventro-medially and caudally to the pole of facial nucleus, with homocysteic acid, caused an increase in renal SNA, but do not change sympathetic activity of nerves projecting to skeletal muscle vasculature (Dean et al., 1992). Stimulation of caudal sites in the RVLM caused an increase in muscle SNA, and a simultaneous decrease in renal SNA (Dean et al., 1992). RVLM neurons that could evoke an excitatory response in the hindlimb muscle and mesenteric vascular beds were located caudally to the ones that evoked renal vasoconstriction (Lovick, 1987). In addition to this, RVLM neurons responsible for driving cardiac sympathetic nerves overlap with neurons that drive muscle vasoconstrictor activity (Campos and McAllen, 1997). This topographic organisation of RVLM neurons seems to be more related to the type of vascular bed/sympathetic nerves that they control, rather than the segmental level of SPGNs (McAllen and Dampney, 1990; Mueller et al., 2011). For example, RVLM premotor neurons driving the limb muscle vasculature were anatomically distinct from the ones driving renal nerve activity (McAllen and Dampney, 1990) whereas, RVLM neurons driving the forelimb and hindlimb muscle vasculature were anatomically inseparable (McAllen and Dampney, 1990). Microinjection of 100 mM of glutamate in the RVLM exerted a sympatho-excitatory response, with greater increases in SNA to adrenal glands as compared to the renal and lumbar SNA (Mueller et al., 2011).

Further to the above, a recent study by Nedoboy et al., (2016) showed that there is a topographical organisation of C1 neurons in the RVLM, which is responsible for responding differently to different physiological states (Nedoboy et al., 2016). Unloading of baroreceptors, with intravenous hydralazine, leading to a depressor response activated the central and medial group of C1 neurons (Nedoboy et al., 2016). On the other hand, baroreceptor loading, with intravenous phenylephrine, silenced the lateral group of C1 neurons, without affecting the baseline activation levels of the medial and central group of C1 neurons (Nedoboy et al., 2016).

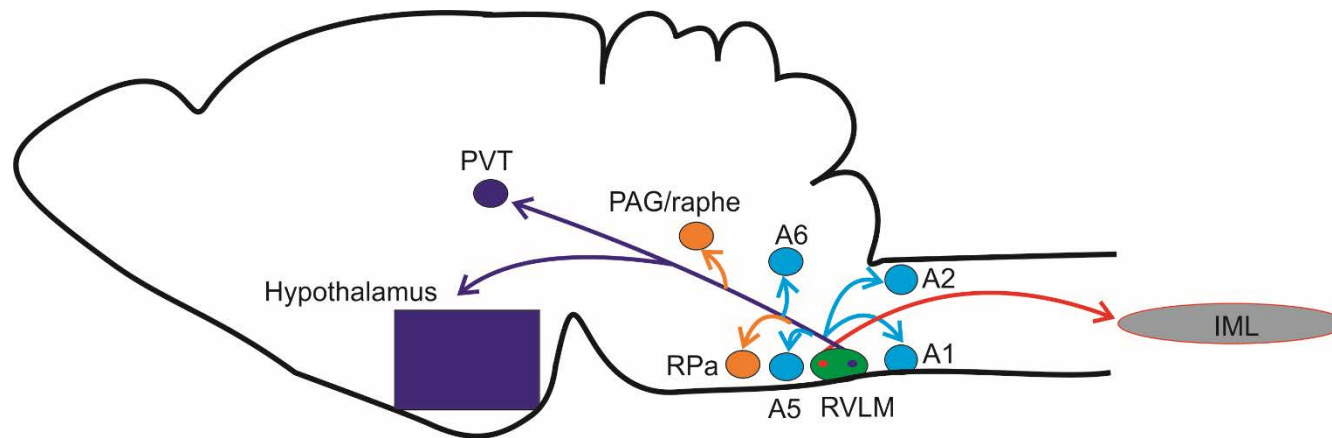


Figure 1.3: Efferent projections from the RVLM

Parasagittal view of the brain showing the location and main axonal projections from the RVLM. RVLM neurons (green) are located in the ventrolateral medulla (VLM). Non-bulbospinal RVLM neurons are located in the caudal portion of the RVLM (purple) and

project to nearby catecholaminergic nuclei (light blue), raphe nuclei (orange) and higher brain regions (purple). Higher brain regions include axonal projections to the PVT, and hypothalamic areas, such as the perifornical area, the dorsomedial nucleus, and the median and medial preoptic areas. Bulbospinal RVLM neurons are located in the rostral portion of the RVLM (red) and project to SPGNs in the spinal cord. PVT, paraventricular nucleus of the thalamus; RVLM, rostral ventrolateral medulla; IML, intermediolateral cell column of the spinal cord; RPa, raphe pallidus; PAG/raphe, periaqueductal grey matter/dorsal raphe. (Adapted from (Guyenet et al., 2013); used with permission)

- *RVLM neuronal characteristics*

Based on electrophysiological properties, RVLM neurons can be divided into 6 categories: type I that project to the spinal cord and are silenced by baroreceptor activation, type II that project to the hypothalamus and are silenced by baroreceptor activation, type III that project to the hypothalamus and are silenced by baroreceptor activation and nociceptive stimulation, type IV that project to the hypothalamus, are non-barosensitive and are activated by a somatic input, type V that project to the hypothalamus and are not sensitive to a baroreceptor or a somatic input, and type VI that project neither to the spinal cord or the hypothalamus, but respond to elevations in MAP (Verberne et al., 1999). Most of the type I, II and $\approx 50\%$ of type III cells are C1 neurons, and $\approx 91\%$ of C1 neurons receive inhibitory inputs from arterial and cardiopulmonary receptors (Verberne et al., 1999). As mentioned above, most of RVLM neurons that are barosensitive project to either the spinal cord or the hypothalamus (Abbott et al., 2009a; Oshima et al., 2006; Oshima et al., 2008; Stornetta et al., 2015; Verberne et al., 1999).

RVLM neurons express receptors for a variety of neurotransmitters/ neuropeptides such as GABA (Li and Guyenet, 1996), glutamate (Stornetta et al., 2002a; Stornetta et al., 2002b), SST2a (Burke et al., 2008), PACAP – pituitary adenylate cyclase-activating polypeptide (Farnham et al., 2012), orexin (Shahid et al., 2012), opioids (Aicher et al., 2001; Baraban et al., 1995; Punnen and Sapru, 1986), serotonin (5-HT) (Bergamaschi et al., 2014; Dean and Bago, 2002; Miyawaki et al., 2001), acetylcholine (Kumar et al., 2009; Padley et al., 2007) and angiotensin (Bergamaschi et al., 2014; de Kloet et al., 2016).

As discussed earlier, blockade of RVLM glutamate receptors did not alter baseline levels of BP; however, it blocked the excitatory input from peripheral receptors or other central nuclei in anesthetized rats (Guyenet et al., 1987; Sun and Guyenet, 1986; Urbanski and Sapru, 1988; Wang et al., 2009), and modulated the cardiovascular reflex responses (Gray et al., 2001). Therefore, it is not the glutamatergic input to the RVLM that drives the tonic activity of RVLM neurons. On the other hand, blockade of RVLM GABA receptors caused an increase in the RVLM neuronal discharge and exerted a pressor response (Amano and Kubo, 1993; Avanzino et al., 1994; Dampney et al., 1988; Kubo and Kihara, 1987a; Sun and Guyenet, 1985; Urbanski and Sapru, 1988). This GABAergic input to RVLM neurons can be either baroreceptor dependent or independent.

Cholinergic pathways in the RVLM

Immunoreactivity for choline acetyltransferase (ChAT-ir; an enzyme involved in the synthesis of acetylcholine)) was detected in cell bodies and processes in the RVLM area (Ruggiero et al., 1990). Interestingly, these ChAT-ir terminals found in the RVLM area overlapped with the bulbospinal group of RVLM neurons (Ruggiero et al., 1990). It was later shown that microiontophoretic application of acetylcholine onto the cell bodies of RVLM sympatho-excitatory neurons elicited an increase in the firing rate of RVLM neurons; an effect that was abolished by iontophoretic application of scopolamine (muscarinic receptor antagonist) onto the same neurons (Kubo et al., 1997). Microiontophoretic application of physostigmine (an acetylcholinesterase inhibitor) onto RVLM neurons increased the firing rate of these neurons (Kubo et al., 1997). Intravenous administration of physostigmine exerted a sympatho-excitatory effect on RVLM neurons (Giuliano et al., 1989; Kubo et al., 1997); this sympatho-excitatory effect onto RVLM neurons could be blocked by microinjection of scopolamine in the RVLM (an M2-selective muscarinic receptor antagonist) (Giuliano et al., 1989). It was suggested that the PVN is the main source of cholinergic inputs to RVLM neurons (Kubo et al., 2000).

Activation of the central muscarinic cholinergic receptors exerted a sympatho-excitatory response (increased AP, HR and SNA), which is primarily mediated by the bulbospinal non-C1 RVLM muscarinic cholinergic receptors (Padley et al., 2007).

Enkephalinergic pathways in the RVLM

Activation of the delta and mu opioid receptors (microinjections of agonist) in the RVLM inhibited lumbar SNA and attenuated responses to sympathetic reflexes, such as the sympathetic baroreflex and the somatosympathetic reflex (SSR) (Miyawaki et al., 2002b). One of the many sources of enkephalin terminals in the RVLM is the NTS (Morilak et al., 1989). Barosensitive bulbospinal RVLM neurons are a major source of enkephalinergic input to SPGNs (Stornetta et al., 2001). Approximately 54% of bulbospinal prepro-enkephalinergic neurons in the RVLM were Fos-ir in response to hydralazine induced hypotension (Stornetta et al., 2001). The barosensitive bulbospinal prepro-enkephalinergic RVLM neuronal group had faster axonal conduction velocity than those without prepro-enkephalinergic mRNA (Stornetta et al., 2001).

Angiotensin-related pathways in the RVLM

Microinjection of angiotensin II in the RVLM exerted a pressor effect (Allen et al., 1988) which could be reversed by systemic administration of hexamethonium bromide (ganglionic blocker) (Allen et al., 1988). Blockade of angiotensin II in the RVLM, with angiotensin II inhibitor, caused a significant decrease in baseline levels of BP, suggesting a role of angiotensin II in the tonic maintenance of BP (Andreatta et al., 1988). Intravenous administration of angiotensin II attenuated the barosensitivity of $\approx 50\%$ of barosensitive RVLM cardiovascular neurons (McMullan et al., 2007). A study by Arakawa and colleagues showed that microinjection of angiotensin (1-12) in the RVLM, a renin independent substrate for angiotensin II, caused an increase in MAP, HR and splanchnic SNA (Arakawa et al., 2013). Both, angiotensin converting enzyme and chymase, are required for the conversion of angiotensin (1-12) in the RVLM, and angiotensin (1-12) mediated sympatho-excitatory effects were due to its action on angiotensin 1 receptors (Arakawa et al., 2013). Angiotensin II can exert its effects on the SNS via 2 types of receptors, type I and type II receptors. Both of these receptors are present in the RVLM and counteract actions of each other (Gao et al., 2008a; Gao et al., 2008b; Kawabe et al., 2016). Unilateral blockade of angiotensin II type II receptors in the RVLM elicited a sympatho-excitatory effect (increases in MAP, HR and SNA); this sympatho-excitatory effect is attenuated in SHR, suggesting a role of angiotensin II type II receptors in the pathophysiology of hypertension (Kawabe et al., 2016).

Chen and colleagues (2010) showed that the pressor response to microinjection of angiotensin II in the RVLM were mediated through the angiotensin II type 1A receptors expressed on C1 neurons (Chen et al., 2010). However, despite the importance of angiotensin II type 1A receptors expressed on C1 neurons (Allen et al., 2009), it was recently shown that C1 neurons are not the only catecholaminergic neurons involved in the angiotensin II-induced hypertension (administered subcutaneously) (Jancovski et al., 2013; Jancovski et al., 2014). Selective deletion of angiotensin II type 1A receptors from the C1 neuronal group did not diminish the hypertensive response to subcutaneous administration of angiotensin-II in mice (Jancovski et al., 2014).

Other pathways in the RVLM

Microinjection of SST in the RVLM of anesthetized rats evoked a sympatho-inhibitory, hypotensive and bradycardiac response, which could be blocked by microinjection of an SST2a receptor antagonist (Burke et al., 2008). Supra-medullary brain regions, such as the

paratrigeminal nucleus, the lateral parabrachial nucleus, the Kölliker-Fuse nucleus, the ventrolateral periaqueductal grey area, the central nucleus of the amygdala and subnucleus of the extended amygdala, are putative sources of endogenous SST to the RVLM, and mediate its sympatho-inhibitory effects via SST2 receptors in the RVLM (Bou Farah et al., 2016).

Bilateral microinjection of mitogen-activated protein kinase inhibitor (PD98, 059), in the RVLM of WKY and SHR, caused significant reductions in AP, but did not attenuate the pressor response to glutamate microinjections in the RVLM (Seyedabadi et al., 2001). Bilateral microinjection of wortmannin (a phosphatidylinositol-4,5-bisphosphate 3-kinase inhibitor) into the RVLM exerted a depressor response in SHR, whereas no effect in the RVLM of WKY was observed (Seyedabadi et al., 2001). This study revealed that a PD98, 059-sensitive pathway in the RVLM of WKY and SHR is involved in tonic regulation of AP and a wortmannin-sensitive pathway is important in the maintenance of RVLM mediated hypertension in SHR (Seyedabadi et al., 2001).

Microinjection of 5-HT_{1A} (serotonin) receptor-selective agonist in the RVLM decreased AP and splanchnic SNA; this effect was blocked by pre-injection of 5-HT_{1A} receptor-selective antagonist (Miyawaki et al., 2001). Activation of 5-HT_{1A} receptors in the RVLM attenuated the SSR response, but did not affect the baroreflex or chemoreflex responses (Miyawaki et al., 2001). Microinjection of orexin-A into the RVLM elicited a pressor and sympatho-excitatory response, and modulated sympatho-excitation seen following activation of the chemoreflex (Shahid et al., 2012). Stimulation of orexin-A in the RVLM increased, or decreased, the sympatho-excitatory response observed following hypoxic, or hypercapnic, challenges, respectively (Shahid et al., 2012). Lower doses of neuromedin U in the RVLM of anesthetized rats caused an increase in AP, HR and SNA (splanchnic and lumbar) (Rahman et al., 2012). Whereas, higher doses of neuromedin U in the RVLM evoked a biphasic response, a brief hypertension and sympatho-excitation, followed by a prolonged hypotension and sympatho-inhibition (Rahman et al., 2012).

Microinjection of galanin into the RVLM of anesthetized rats reduced baseline levels of MAP, HR and splanchnic SNA (Abbott and Pilowsky, 2009). In addition to a depressor response, microinjection of galanin in the RVLM also attenuated the reflex response to activation of chemoreceptors, and increased the sympatho-inhibitory response to aortic depressor nerve (ADN) stimulation (Abbott and Pilowsky, 2009). Bilateral microinjection of SST in the RVLM

evoked a sympatho-inhibitory effect accompanied with bradycardia; it also attenuated the chemoreflex and the SSR responses (Burke et al., 2008).

In addition to expression of numerous receptors, RVLM neurons are also immunoreactive for a wide range of neurotransmitters/ neuropeptides, such as neuropeptide Y (Blessing et al., 1987; Stornetta et al., 1999; Tseng et al., 1993), cocaine and amphetamine regulated transcript (Burman et al., 2004; Dun et al., 2002), prepro-tachykinin (substance P) (Li et al., 2005; Urbanski et al., 1989), enkephalin (Stornetta et al., 2001), calbindin (Goodchild et al., 2000a) and PACAP (Farnham et al., 2008) (Stornetta, 2009). Immunoreactivity of neurotransmitters, and neuropeptides, in RVLM neurons is also indicative of their characteristics. For example, RVLM neurons expressing neuropeptide Y have a slower conduction velocity (may be unmyelinated) (Stornetta et al., 1999). Whereas, the enkephalinergic RVLM neurons have faster axonal conduction velocities (myelinated) (Stornetta et al., 2001). Another instance is that neuropeptide Y is more likely to be present in C1 neurons that project to the hypothalamus rather than the bulbospinal C1 neurons (Stornetta et al., 1999).

Even after localisation of a wide variety of neurotransmitters, glutamate is still considered the principal excitatory neurotransmitter mediating the effect of RVLM neurons on SPGNs. Most of bulbospinal neurons in the RVLM are also immunoreactive for phosphate activated glutaminase (a glutamate bio-synthetic enzyme) (Minson et al., 1991). Electrical excitation of RVLM neurons exerted an excitatory effect on SPGNs, which could be blocked by antagonism of glutamate receptors in the IML (Morrison, 2003). Also, anterogradely labelled terminals in the IML from the RVLM made asymmetric synapses (sympatho-excitatory) on local dendrites, and were immunoreactive for glutamate (Morrison, 2003). However, it is yet unclear which of the glutamate receptor subtype on SPGNs mediate the sympatho-excitatory effect of bulbospinal RVLM neurons.

- *Role of RVLM neurons in cardiovascular control*

Unilateral blockade/destruction of RVLM neurons is not sufficient enough to completely abolish the tonic maintenance of resting BP; this suggests that one side of the RVLM is capable of maintaining normal levels of BP (Guertzenstein and Silver, 1974). One possible explanation is that reductions in BP following unilateral blockade of the RVLM is detected by baroreceptors, which may provide a compensatory feedback to the contralateral side of RVLM neurons evoking an increase in their neuronal activity and thereby, maintaining the sympathetic tone (Horiuchi and Dampney, 1998). Another possibility is the presence of a non-linear

relationship between the degree of tonic excitatory output from RVLM neurons and activity of sympathetic vasomotor neurons (Horiuchi and Dampney, 1998). This non-linear relationship ensures that the activity of sympathetic vasomotor neurons is not significantly reduced unless there is a profound reduction in the excitatory output from RVLM neurons (Horiuchi and Dampney, 1998). Evidence in support of first explanation was provided in 1998, by Horiuchi and Dampney, when the unilateral blockade of RVLM neurons in anesthetized baroreceptor-denervated rabbits (with muscimol) caused profound decreases in MAP, HR and renal SNA (Horiuchi and Dampney, 1998).

As mentioned previously, the RVLM is critical for the maintenance of resting BP (Guyenet, 2006; Guyenet et al., 2013; Stornetta et al., 2015). Origin and maintenance of sympathetic tone by the RVLM has been an area of debate. Until now, there are 2 major theories explaining the possible mechanism behind origin of sympathetic tone by the RVLM:

- 1) Pacemaker theory - according to which RVLM neurons have an intrinsic property to generate action potentials (Dampney et al., 2000), and
- 2) Network theory - according to which the activity of RVLM neurons is determined by a balance between the tonic excitatory and inhibitory inputs to the RVLM from other brain regions (Dampney et al., 2000).

Furthermore, RVLM neurons also respond to changes in pO_2 or pCO_2 levels (Guyenet et al., 2013; Koganezawa and Paton, 2014; Reis et al., 1994; Seller et al., 1990).

The RVLM neuronal group also plays a critical role in modulation of sympathetic reflexes such as the sympathetic baroreflex (section 1.3.1), chemoreflexes (section 1.3.2) and SSR (section 1.3.3).

- *Origin of sympathetic tone – pacemaker theory*

Some RVLM neurons, even when deprived of all synaptic inputs (in slice preparation), exhibit tonic pacemaker like discharge activity (Sun et al., 1988c). Interestingly, none of these RVLM neurons exhibiting pacemaker like discharge were immunoreactive for PNMT (Sun et al., 1988c) or TH (Sun et al., 1988a), and $\approx 50\%$ of these neurons were bulbospinal (Sun et al., 1988c). However, the neuronal group immediately adjacent to RVLM neurons with pacemaker properties was silent, and $\approx 45\%$ of these silent neurons were TH-ir (Sun et al., 1988a). Furthermore, pacemaker-like discharge activity of RVLM neurons was insensitive to glutamate blockade by kynurenic acid (Sun et al., 1988b). Therefore, it was suggested that tonic discharge

of RVLM neurons was due to their intrinsic pacemaker-like activity, which could be modulated by a variety of synaptic inputs *in vivo* (Sun et al., 1988b). Contrary to this, few other studies have shown that C1 bulbospinal RVLM neurons exhibited intrinsic pacemaker-like properties (Li et al., 1995).

But, no intrinsic pacemaker-like properties of RVLM neurons were observed *in vivo* (Lipski et al., 1996). Therefore, it may be possible that in intact animals the discharge of RVLM neurons is derived by a fine balance between synaptic excitatory and inhibitory inputs (network theory) (Dampney et al., 2000; Lipski et al., 1996). However, under abnormal conditions, where the RVLM is deprived of its synaptic inputs, neuronal intrinsic pacemaker-like properties may become operational (Dampney et al., 2000; Koganezawa and Paton, 2014; Lipski et al., 1996).

- *Origin of sympathetic tone – network theory*

The network theory proposes that the final output activity from RVLM neurons is dependent on the tonic excitatory and inhibitory inputs to the RVLM.

The preganglionic and postganglionic sympathetic nerve discharge (SND) contains two major components based on frequency analyses, a prominent cardiac related 2-6 Hz rhythm and a strong additional 10 Hz component (Barman et al., 1992). Both of the components of SND were suggested to be generated by a network of brainstem regions, rather than intrinsic pacemaker-like properties (Zhong et al., 1993a; Zhong et al., 1993b). Activity of brainstem medullary neurons (RVLM, raphe or lateral tegmental field) contained a 2-6 Hz oscillation, and this 2-6 Hz activity was correlated with that in SND (Zhong et al., 1993a). Transection of the spinal cord abolished, or markedly reduced, SND but the 2-6 Hz oscillation in medullary activity was unchanged; this suggested that the 2-6 Hz oscillation component originates in the medulla (Zhong et al., 1993a). Activity of $\approx 25\%$ of RVLM and caudal raphe neurons was correlated to the 10 Hz rhythm in inferior cardiac postganglionic SND in cats (Barman and Gebber, 1992). Further to this, lesion of the RVLM eliminated the 2-6 Hz and 10 Hz component of the SND (Zhong et al., 1992). All of these studies are in support of the network theory, and highlight the RVLM as a central source of origin of sympathetic tone.

One of the major findings from Lipski et al., (1996) was that RVLM neurons are under the influence of tonic excitatory input (Lipski et al., 1996). Individual action potentials are usually preceded by identifiable fast EPSPs (excitatory post synaptic potentials) (Lipski et al., 1996). Blockade of glutamate receptors in the RVLM, in rabbits (Blessing and Nalivaiko, 2000), or in cats (Barman et al., 2000), caused decreases in MAP. Depressor response following blockade

of glutamatergic receptors (with kynurenic acid) in the RVLM seems to be mediated primarily via non-NMDA glutamate receptors (Abrahams et al., 1994). Contrary to this, a study by Ito and Sved (1997) failed to observe any significant changes in AP following the microinjection of kynurenic acid (antagonist of ionotropic glutamate receptors) in the RVLM of anesthetized rats (Ito and Sved, 1997). The discrepancy in findings between these studies could be merely due to a difference in species used for the experiments (rabbits or cats vs. rodents).

The RVLM is in receipt of excitatory inputs from many supra-medullary brain regions (Stornetta et al., 2015). RVLM neurons receive excitatory inputs from higher brain regions, such as the PVN in response to nociceptive stimuli (Tagawa and Dampney, 1999). Another source of glutamatergic input to the RVLM is neurons located in the pontine reticular formation (Krassioukov and Weaver, 1993). Blockade of pontine reticular formation neurons, with glycine, caused decreases in AP, HR and renal SNA; an effect that was interrupted by microinjection of kynurenate into the RVLM (Krassioukov and Weaver, 1993). However, the question as to what extent glutamatergic inputs contribute to the tonic activity of RVLM neurons remains unresolved.

An ideal example of the network theory was provided by Ito and Sved (1997) where removal of sympatho-inhibitory input to the RVLM, from the CVLM, elicited a pressor response (Ito and Sved, 1997). This pressor response could be blocked by microinjection of kynurenic acid into the RVLM (Ito and Sved, 1997). Therefore, in light of their findings, Ito and Sved proposed that microinjection of kynurenic acid in the RVLM blocks 2 types of inputs to RVLM presympathetic neurons, 1) direct excitatory glutamatergic input to RVLM neurons, and 2) excitatory input to local inhibitory neurons that are tonically active and synapse onto RVLM presympathetic neurons (Ito and Sved, 1997). Thus, the overall effect of kynurenic acid in the RVLM resulted in the removal of a direct excitatory and an indirect inhibitory input to these neurons and therefore, resulting in little change in their baseline activity (Ito and Sved, 1997).

It seems unlikely that inhibition provided to RVLM neurons by local inhibitory interneurons is the primary source of inhibitory input to the RVLM. Iontophoretic application of GABA receptor antagonist, bicuculline, increases the firing rate of RVLM neurons, suggesting the presence of a tonic inhibitory input to the RVLM (Sun and Guyenet, 1985), which in part is dependent on baroreceptor input. However, even after denervation of baroreceptors or lesions of the NTS in rabbits, microinjection of bicuculline in the RVLM caused large increases in BP (Dampney et al., 1988). Therefore, there may be other baroreceptor independent sources of

tonic GABAergic inhibitory input to the RVLM, such as the CVLM or caudal pressor area (Dampney et al., 2003a; Kvochina et al., 2007; Schreihofer and Guyenet, 2002).

Following blockade of both glutamate and GABA receptors in the RVLM very large increases in AP and renal SNA were observed (Tagawa et al., 1999). This study suggested that in absence of both inputs, glutamatergic and GABAergic, RVLM presympathetic neurons have a very high firing rate; this may reflect auto-activity of RVLM neurons, or may be indicative of a glutamate or GABA independent excitatory input. Angiotensin mediated excitatory inputs to RVLM neurons is independent of glutamate and GABA (Tagawa et al., 1999), and blockade of angiotensin receptors in the RVLM caused large decreases in AP, HR and renal SNA (Ito and Sved, 1996; Tagawa et al., 1999). Further to this, blockade of angiotensin II type I receptors attenuated the pressor effect of exogenously microinjected angiotensin II in the RVLM (Averill et al., 1994).

- *C1 adrenergic cell group*

C1 neurons of the RVLM (Figure 1.4 and Figure 1.6) contain $\approx 72\%$ of medullary PNMT-IR catecholaminergic neurons in rat brainstem (Minson et al., 1990). The other 2 PNMT-ir adrenergic neuronal groups in the medulla are, C2 group of neurons that contains $\approx 13\%$ and C3 group of neurons (section 1.2.2.3) that contains $\approx 15\%$ of medullary PNMT-ir neurons (Minson et al., 1990).

C1 neurons of the RVLM send direct monosynaptic efferent projections to SPGNs at all segmental levels of the thoracic spinal cord (Abbott et al., 2009a; Oshima et al., 2006; Oshima et al., 2008; Ross et al., 1984a; Stornetta et al., 2015). Approximately 71% of C1 neurons are bulbospinal with efferent projections to the thoracic level of the spinal cord (Haselton and Guyenet, 1989). C1 neurons were first described in 1974 as PNMT-ir neurons of the brainstem with a possible role in vasomotor and respiratory control (Bolme et al., 1974; Hökfelt et al., 1974). Most cells of the C1 neuronal group are bulbospinal, and are immunoreactive for TH, DBH and PNMT (Phillips et al., 2001). Catecholamine synthesizing C1 adrenergic neurons are also immunoreactive for neuro-peptides/ neuro-transmitters like neuropeptide-Y (Stornetta et al., 1999), enkephalin (Stornetta et al., 2001), PACAP (Farnham et al., 2008), cocaine- and amphetamine- regulated transcript (Burman et al., 2004; Dun et al., 2002) and many more (for a detailed review, see (Stornetta, 2009)).

Ultrastructural studies suggest that C1 neurons are good candidates for sensing O_2 levels as these neurons contain abundant mitochondria, and are in close proximity to blood vessels and

astrocytes (Milner et al., 1987). Presence of both, myelinated and unmyelinated, type of axons in C1 neurons imply that these neurons are capable of conducting with different velocities (Milner et al., 1987).

C1 neurons can form either symmetrical (inhibitory) or asymmetrical (excitatory) synapses with target neurons (such as SPGNs) depending on their site of termination, and the size of post-synaptic dendrite. (Milner et al., 1988). Pre-synaptic terminals from C1 neurons can also directly synapse onto the cell membrane of SPGNs, and these axosomatic synapses are exclusively symmetric (Milner et al., 1988).

Using a juxtacellular labelling technique in anaesthetized rats, Schreihöfer and Guyenet (1997) provided a comprehensive analysis of the proportion of C1 neurons that were bulbospinal and barosensitive. Each individual RVLM neuron was filled with biotinamide if the neuron was found to be spontaneously active, barosensitive and bulbospinal (Schreihöfer and Guyenet, 1997). Almost 70% of the bulbospinal RVLM neurons were found to be C1 cells, and with axonal conduction velocities of <1 m/s (Schreihöfer and Guyenet, 1997).

As discussed previously, RVLM neurons are sympatho-excitatory in nature. Even though, the role of C1 neurons in cardiovascular regulation is well established, C1 neurons also play a critical role in other physiological processes, such as endocrine responses to infection and inflammation, sleep-wake cycle, glucose homeostasis, reproduction and thermoregulation (Abbott et al., 2012; Guyenet et al., 2013). Due to their importance in physiology, C1 neurons have been termed as “emergency medical technicians” of the body (Figure 1.4) (Guyenet et al., 2013).

As C1 and non-C1 neurons of the RVLM are intermingled, studies blocking activity of RVLM neurons could not identify the individual level of involvement of these 2 cell groups in the sympathetic control of BP. Thus, development of an antibody that selectively lesions C1 neurons, anti-D β H-saporin, opened doors to the possibility of selectively targeting C1 neurons. Microinjection of anti-D β H-saporin in the RVLM selectively destroyed $\approx 90\%$ of C1 population, and did not alter the non-C1 population (Madden et al., 1999). Unilateral destruction of C1 neurons with anti-D β H-saporin reduced the pressor response to glutamate microinjection into the RVLM by nearly 40% (Madden et al., 1999). Following depletion of $>80\%$ of C1 neurons, with immunotoxin injection of anti-D β H-saporin in the RVLM, resting levels of AP were ≈ 10 mmHg lower as compared to control conscious rats (Madden and Sved, 2003b). Furthermore, sympatho-excitatory responses to cardiovascular reflexes, such as

baroreceptor unloading, chemoreceptor activation and electrical stimulation of the sciatic nerve (evoking a SSR), were attenuated following depletion of >80% of C1 neurons (Madden and Sved, 2003b). A study by Abbott et al., (2009) utilizing channelrhodopsin-2 selectively in catecholaminergic neurons, and photo-stimulating the transfected C1 neuronal population, has shown that selective activation of C1 neurons in the RVLM increased BP and splanchnic SNA (Abbott et al., 2009a). These studies have highlighted the role of C1 neurons in the maintenance of tonic vasomotor activity, and sympatho-excitatory responses to cardiovascular reflexes.

C1 neurons are essential for the hypotensive response evoked by microinjection of clonidine in the RVLM. Injection of clonidine into the RVLM of anaesthetised rats caused a decrease of ≈ 25 mmHg in AP; this depressor response was abolished following the depletion of C1 neurons (with the injection of anti-D β H-saporin in the RVLM) (Madden and Sved, 2003a). Contrary to this, another study failed to abolish the depressor response to clonidine following depletion of C1 neurons (Schreihöfer and Guyenet, 2000). However, in the study by Schreihöfer and Guyenet, depletion of C1 neurons was indirect i.e. anti-D β H-saporin was injected at the level of the thoracic spinal cord, and clonidine was administered intravenously (Schreihöfer and Guyenet, 2000).

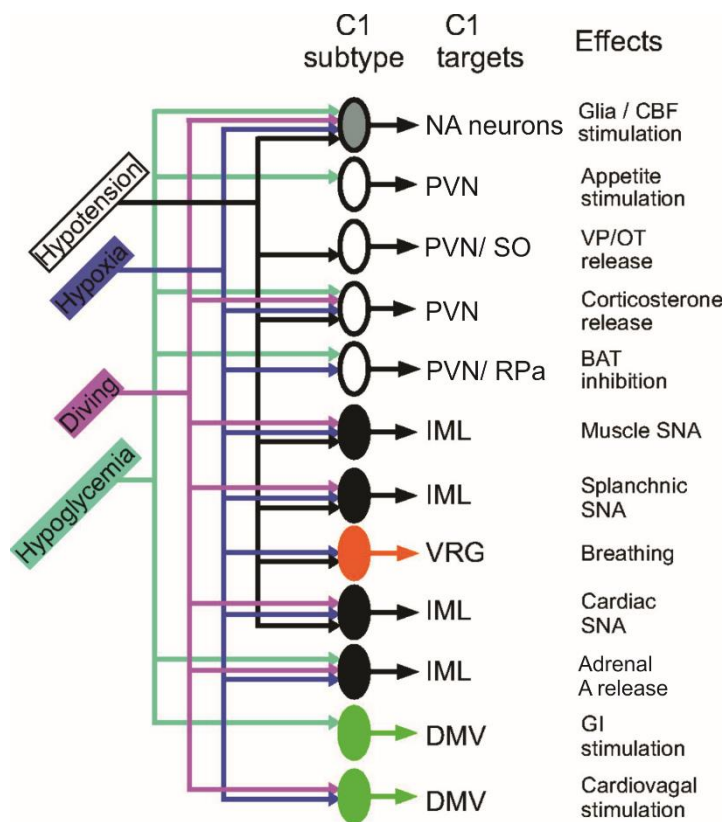


Figure 1.4: C1 cells as “emergency medical technicians”

Differential recruitment of subsets of C1 cells for different emergency responses. Hypothetical scheme that illustrates how the differential recruitment of 12 subsets of C1 cells by hypotension, hypoxia, diving, or hypoglycemia might produce a response pattern adapted to each situation. The anatomical target of each type of C1 cells, and the postulated physiological effect produced by their activation, are also indicated. Green: responses mediated

by C1 cells that innervate parasympathetic preganglionic neurons. Black: responses mediated by C1 cells that innervate sympathetic preganglionic neurons. White: responses mediated by C1 cells that innervate the PVN and other forebrain regions. Gray: responses mediated via activation of the CNS noradrenergic system (such as the locus coeruleus). Orange: response mediated by activation of the respiratory pattern generator. The number of C1 cell subsets could be smaller if some of the responses listed are produced by axonal collaterals. For example, the CNS noradrenergic neurons could be activated by collaterals of presympathetic neurons that regulate the circulation and by collaterals of glucose-sensitive cells (presympathetic or others). NA, noradrenaline-releasing cells; PVN, paraventricular nucleus of the hypothalamus; SO, supraoptic nucleus; RPa, raphe pallidus; IML, intermediolateral cell column of the spinal cord; VRG, ventral respiratory group; DMV, dorsal motor nucleus of the vagus; CBF, cerebral blood flow; VP, vasopressin; OT, oxytocin; BAT, brown adipose tissue; A, Adrenaline release; GI, gastrointestinal. (Figure and legend adapted from (Guyenet et al., 2013); used with permission)

1.2.1.6 Caudal ventrolateral medulla (CVLM)

The CVLM is defined as the area located medially to the spinal trigeminal tract, lateral to the pyramids, ventral to the nucleus ambiguus, and is intermingled with A1 noradrenergic neurons of the brainstem (Figure 1.2) (Paxinos and Watson, 2007).

Afferent projections: The CVLM receives afferent glutamatergic projections from the NTS and other regions, and is a major input of inhibitory monosynaptic GABAergic projections to the RVLM (Chalmers and Pilowsky, 1991; Mandel and Schreihofer, 2008; Pilowsky et al., 2009). In addition to excitatory inputs, CVLM neurons are also in receipt of inhibitory inputs, such as GABAergic (Blessing and Reis, 1983; Willette et al., 1984), glycinergic (Blessing and Reis, 1983) and opioids (Badoer and Chalmers, 1992; Drolet et al., 1991). Neurochemical phenotype of inhibitory CVLM neurons is quite diverse, as these neurons contain glycine and neuropeptide Y, in addition to GABA.

Small region of the CVLM is anatomically, and functionally, divided into 2 regions, 1) the rostral CVLM that contains neurons responsible for baroreflex-mediated inhibition, and 2) the caudal CVLM that contains neurons whose function is independent of baroreflex (Badoer et al., 1994; Cravo and Morrison, 1993). Selective lesioning of the rostral CVLM, with neurotoxic kainic acid, caused increases in AP and SNA, in baroreceptor intact and denervated rats (Cravo and Morrison, 1993). These findings suggested that the CVLM is an important source of tonic sympatho-inhibition (Cravo and Morrison, 1993; Sved et al., 2000).

Inhibition of CVLM neurons, by microinjection of muscimol, evoked a pressor response, accompanied by an increase in peripheral resistance and SNA (Horiuchi et al., 2004; Mandel and Schreihofer, 2008). This observed effect also highlights that CVLM neurons are tonically active, and provide tonic inhibition to RVLM neurons, which is critical in the regulation of resting BP levels. In line with these results, electrolytic lesion of the CVLM evoked a pressor response in conscious rabbits (Blessing et al., 1981b). Neurotoxicity induced in the CVLM, with kainic acid, also evoked a transient hypertensive effect accompanied with bradycardia (Blessing et al., 1981b; Cravo et al., 1991).

Microinjection of angiotensin II in the CVLM, in baroreceptor denervated rats, caused a dose dependent decrease in BP and renal SNA (Sasaki and Dampney, 1990). In addition, microinjection of angiotensin (1-12), a renin independent substrate for angiotensin II, in the CVLM evoked reductions in MAP, HR and splanchnic SNA; this effect was partly mediated by GABA receptors in the RVLM (Kawabe et al., 2014). Microinjection of angiotensin (1-12)

in the CVLM modulated the baroreflex response to intravenous injections of phenylephrine (loads baroreceptors) and SNP (unloads baroreceptors) (Kawabe et al., 2014). Microinjection of angiotensin-II specific antagonist in the CVLM caused an increase in BP and renal SNA (Sasaki and Dampney, 1990). These results suggest a tonic action facilitated by endogenous angiotensin II on the CVLM mediated sympatho-inhibitory effects.

Glutamate induced excitation of CVLM neurons exerted a depressor response, with reductions in HR, which may be attributed to a decrease in total peripheral resistance (Willette et al., 1987). Bilateral microinjection of either an NMDA or a selective AMPA receptor antagonist into the CVLM failed to attenuate the baroreflex response to the ADN stimulation (Miyawaki et al., 1997). However, microinjection of kynurenate, or a combination of NMDA and kainate receptor antagonist, abolished all components of the sympathetic baroreflex response to the ADN stimulation (Miyawaki et al., 1997).

The important component missing from previous work (described above) concerning the role of CVLM neurons in the sympathetic control of blood pressure is the failure to isolate actions exerted by CVLM neurons from other intermingled neurons, such as the A1 group of neurons. However, this earlier literature, concerning the role of CVLM neurons in the sympathetic control of BP, has provided an indication regarding the possible role of CVLM neurons in the sympathetic control of BP, and has set the stage for future non-trivial research.

Failure of tonic activity of CVLM neurons is linked to the pathology of hypertension (Smith and Barron, 1990). Inhibition of CVLM neurons, with microinjection of tetrodotoxin, in WKY (Wistar-Kyoto rats; normotensive control for SHR) and SHR, produced significantly larger increases in BP in WKY as compared to SHR (Smith and Barron, 1990). These findings suggest that a lower restrain of sympathetic output from CVLM neurons may be responsible for an exaggerated SNA in SHR (Smith and Barron, 1990).

In addition to tonic glutamatergic input from the NTS, studies have shown that CVLM neurons are also tonically excited by endogenous angiotensin II (see above) and NTS independent glutamatergic input. The NTS independent glutamatergic input to the CVLM was further strengthened by a study, which showed that the pressor response to sinoaortic denervation or lesioning of the NTS were worsened by the removal of CVLM (Dampney et al., 1988; Mandel and Schreihofer, 2008). In addition, a proportion of glutamatergic tonically active input to the CVLM, independent of the NTS-CVLM pathway, are sensitive to changes in central respiratory drive (Mandel and Schreihofer, 2008).

Another study by Chan and Sawchenko showed that induction of hypertension, with intravenous infusion of phenylephrine, evoked Fos-ir in CVLM neurons (projecting to the RVLM); the majority of these Fos-ir CVLM neurons were GABAergic, and only few were glycinergic (Chan and Sawchenko, 1998).

All of the above-mentioned literature highlights the CVLM as an area of the ventrolateral medulla (VLM) where excitatory and inhibitory inputs converge, and that it plays an important role in the maintenance of sympathetic vasomotor tone.

1.2.1.7 Nucleus of the solitary tract (NTS)

The NTS is a large nucleus of the brainstem, beginning at level of the cervical spinal cord and extends rostrally to the caudal part of the dorsal cochlear nucleus (Figure 1.2) (Paxinos and Watson, 2007).

Afferent projections: The NTS is a major site in the CNS that receives afferent inputs from many sensory peripheral receptors, such as those associated with the cardiovascular, visceral, respiratory and gustatory information, and is involved in the coordination of these inputs to the rest of CNS sites, such as the CVLM (section 1.3.1) and the RVLM (section 1.2.1.5) (Ciriello and Caverson, 2014; Dampney, 1994; Guyenet and Bayliss, 2015; Kumada et al., 1990; Lawrence and Jarrott, 1996; Pilowsky et al., 2009; van Giersbergen et al., 1992). Afferent projections to the NTS that affect the cardiovascular system are of interest here.

NTS neurons are the second order barosensitive neurons, receiving excitatory afferent inputs from baroreceptors located in the carotid sinus and the aortic arch. The role of NTS neurons in regulation of the cardiovascular system is well established. L-glutamate is suggested to be the most likely candidate released by baroreceptor afferent fibers at the level of the NTS (Kumada et al., 1990). On receipt of these afferent inputs (to dorsomedial, dorsolateral and commissural regions of the NTS), NTS neurons modulate their firing activity (either increase or decrease) to changes in BP (Zhang and Mifflin, 2000). Almost precise location of neurons receiving afferent inputs from peripheral baroreceptors varies from species to species (Kumada et al., 1990). Blockade of glutamate receptors in the NTS of anesthetized rats eliminated all responses to the baroreflex (Guyenet et al., 1987). Vice versa, chemical activation of the NTS mimicked the baroreflex response by decreasing BP and HR (Talman et al., 1984). To add to the complex neuro-functionality of the NTS, these neurons are immunoreactive for GABA_A receptors (Waldvogel et al., 2010), and blockade of GABA receptors in the medial area of the NTS of rats (with bicuculline) resulted in exaggeration of depressor and bradycardiac responses to the

ADN stimulation (Kubo and Kihara, 1988). Microinjection of GABA into the medial area of the NTS evoked a pressor response (Kubo and Kihara, 1987b). These studies have shown that NTS neurons are capable of modulating the baroreflex response via both, a glutamatergic and a GABAergic, neurotransmitter systems.

Induction of acute hypertension, with intravenous infusion of phenylephrine, caused significant increases in Fos-ir in caudal regions of the NTS (Chan and Sawchenko, 1994; Graham et al., 1995; Li and Dampney, 1994). Interestingly, even induction of hypotension, with hydralazine or SNP, increased Fos-ir in most regions of the NTS (Chan and Sawchenko, 1994; Graham et al., 1995). Induction of hypotensive hemorrhage also increased Fos-ir in the NTS of a rat (Chan and Sawchenko, 1994). The NTS consists of 2 distinct populations of neurons that can either be excited or inhibited by increased BP (Feldman and Felder, 1989). It may be that the group of NTS neurons that are inhibited in response to increased BP are the ones that are activated in response to reduced BP levels (Graham et al., 1995).

Even direct stimulation of the carotid sinus nerve, or induction of hypoxia, induced Fos like immunoreactivity in, and around, caudal and intermediate portions of the NTS (Miura et al., 1996b). Direct electrical stimulation of the ADN also induced Fos-ir in the NTS along with key sites involved in baroreflex modulation, such as the RVLM and the CVLM (McKittrick et al., 1992; Rutherford et al., 1992).

All of the above-mentioned literature highlights the importance of the NTS in autonomic control of the cardiovascular system.

1.2.1.8 Medullo-cervical pressor area (MCPA)

MCPA is an area located caudal to the CVLM region (≈ 14.6 mm caudal to bregma) and extends up to the caudal part of the third cervical segment of the spinal cord (Figure 1.2) (Seyedabadi et al., 2006). The MCPA sends direct efferent projections to the IML cell column of the spinal cord (Jansen and Loewy, 1997). Investigation of the neurochemical phenotype of MCPA neurons demonstrated the chemical heterogeneity of these neurons (Seyedabadi et al., 2006). Bulbospinal neurons located in the upper cervical spinal cord were distributed within 3 locations: the lateral cervical nucleus, the lateral spinal nucleus and the lateral funiculus (Jansen and Loewy, 1997).

Functionally, MCPA neurons are sympatho-excitatory in nature, and chemical stimulation of these neurons evoked a pressor response (Seyedabadi et al., 2006). Interestingly, the pressor response to glutamate microinjection in the MCPA was independent of the RVLM, and distinct

from axonal trajectory to the caudal pressor area (CPA) (Seyedabadi et al., 2006). Despite of the role played by MCPA neurons in the ANS, the MCPA does not contribute to sympathetic vasomotor tone. Intactness of the MCPA did not prevent falls observed in AP or SNA following blockade of the RVLM and transection below the CPA (Seyedabadi et al., 2006).

Exact role of the MCPA in the autonomic regulation of the cardiovascular system is yet to be established.

1.2.1.9 Sympathetic preganglionic neurons (SPGNs)

Autonomic regulation of the cardiovascular system involves a set of preganglionic nerves innervating sympathetic ganglionic chain (Juranek and Wojtkiewicz, 2015; Yau et al., 1991), which in turn are sites for autonomic postganglionic nerves (Figure 1.1). Sympathetic postganglionic nerves along with local auto regulatory mechanisms, and circulating hormones, control physiology of peripheral organs (Figure 1.1) (Dampney, 1994). Sympathetic preganglionic nerves arise from SPGNs that are located within the spinal cord, with the majority of SPGNs in the IML cell column and the lateral funiculus of the spinal cord; few of these SPGNs are located in the central autonomic and intercalated nucleus (Figure 1.2) (Dampney, 1994; Strack et al., 1988). SPGNs, due to their cholinergic phenotype, can be immunohistochemically identified with an antibody raised against choline acetyltransferase.

A detailed study by Strack et al., (1988), using retrograde transport of Fluoro-gold, showed that each sympathetic ganglion (such as the celiac, stellate or mesenteric ganglion) or adrenal medulla, received inputs from multiple spinal segments (Figure 1.5) (Strack et al., 1988). For example, stellate ganglion received inputs from the C8-T8 spinal segments (Figure 1.5) (Strack et al., 1988). SPGNs are immunoreactive for many neurotransmitters/neuro-peptides such as acetylcholine, SST, enkephalin, neurotensin, substance P and PACAP (also refer to Table 1.1) (Beaudet et al., 1998; Krukoff, 1987a; Krukoff, 1987b).

Based on electrophysiological properties, SPGNs can be divided into 3 categories: Type A, characterised by a high resting membrane potential and low input resistance; Type B, characterised by a lower resting membrane potential and high input resistance; Type C, similar to type B but their action potentials didn't show the 'after-depolarisation' effect (Dembowsky et al., 1986).

As discussed in previous sections, SPGNs receive direct inputs from many supra spinal sites, such as the PVN (section 1.2.1.1), A5 (section 1.2.1.2), caudal raphe (section 1.2.1.3), RVMM (section 1.2.1.4), RVLM (section 1.2.1.5) and the MCPA (section 1.2.1.8) (Seyedabadi et al.,

2006; Strack et al., 1989). Afferent projections from bulbospinal sites to SPGNs may exert their effects via neurotransmitters that include amino acids and neuropeptides (refer to Table 1.1). Moreover, terminals containing other compounds such as neurotensin (Chiba and Masuko, 1987; Krukoff et al., 1985), oxytocin (Chiba and Masuko, 1987) and vasoactive intestinal polypeptide (Chiba and Masuko, 1987) are also closely apposed to SPGNs; however, synaptic contacts have not yet been demonstrated. In addition to afferent projections from supra spinal sites, SPGNs are also innervated by spinal interneurons (Deuchars, 2007; Dun and Mo, 1989).

Table 1.1: Neurotransmitter-ir and their corresponding receptors on SPGNs

Neurotransmitter	Reference	Receptor	Reference
5-HT	(Bacon and Smith, 1988; Chiba, 1989; Jensen et al., 1995; Poulat et al., 1992; Vera et al., 1990)	5-HT 2	(Maeshima et al., 1998; Marlier et al., 1991)
		5-HT 1C/2	(Thor et al., 1993)
Angiotensin II	(Galabov, 1992)	Type 1 and type 2	(Ahmad et al., 2003; Chao et al., 2013)
Enkephalin	(Bowman and Goodchild, 2015; Stornetta et al., 2001; Vera et al., 1990)	Opioid receptors	(Bowman and Goodchild, 2015)
GABA	(Bacon and Smith, 1988; Bogan et al., 1989; Chiba and Semba, 1991)	GABA _A and GABA _B receptors	(Bowman and Goodchild, 2015; Brouillette and Couture, 2002)
Glutamate	(Llewellyn-Smith et al., 1992; Morrison et al., 1989a; Morrison et al., 1989b)	NMDA receptors	(Morrison, 2003; Poon et al., 2006; Young et al., 1999)
		Type I and II Metabotropic receptors	(Li et al., 1999)

Glycine	(Cabot et al., 1992; Chiba and Semba, 1991)	Glycine receptors	(Chiba and Semba, 1991)
PACAP	(Beaudet et al., 1998; Farnham et al., 2011; Inglott et al., 2011; Pettersson et al., 2004; Waschek, 2013)	PAC1 and VPAC receptors	(Inglott et al., 2012)
Substance P	(Bacon and Smith, 1988; Pilowsky et al., 1992; Poulat et al., 1992)	NK1 receptor	(Brouillette and Couture, 2002; Burman et al., 2001; Llewellyn-Smith et al., 1997)
Thyrotropin releasing hormone (TRH)	(Poulat et al., 1992)	TRH receptor	(Helke and Phillips, 1988; Suzuki et al., 1995)

Distribution of chemically distinct synaptic terminals is probably correlated with functional properties of SPGNs. For example, in adult cats even though most of the SPGNs are immunoreactive for catecholaminergic nerve terminals, the density varies between segmental levels (McLachlan and Oldfield, 1981). Catecholaminergic nerve terminals were found in most parts of the IML at the level of T1 to T8 and L2-L3 (McLachlan and Oldfield, 1981). However, between segmental levels of T9-L2, distribution of noradrenergic terminals in the IML was patchy; majority of these fibers projected to regions medial to the IML (McLachlan and Oldfield, 1981). Similar observations were made concerning the density of terminals to SPGNs that were immunoreactive for neurotransmitters such as glycine (Cabot et al., 1992), neuropeptide Y (Krukoff, 1987a), 5-HT, enkephalin, SST and substance P (Krukoff et al., 1985).

A plethora of neurotransmitters/ neuropeptides (Table 1.1) acting on SPGNs exert their effects in a combined fashion i.e. neuropeptides are co-released to evoke a response from SPGNs. For example, it is well established that adrenaline synthesizing RVLM neuronal projections on to SPGNs are sympatho-excitatory (section 1.3.1). However, iontophoretic application of adrenaline to SPGNs inhibited their activity (Coote, 1988). In this case, function of the co-released compound may be different from that of the isolated compound.

Glutamate and aspartate are considered the leading candidates evoking an EPSP in SPGNs, *in vitro* and *in vivo*. Sympatho-excitation produced by stimulation of the RVLM can be blocked by application of a glutamate antagonist in the spinal cord (Inokuchi et al., 1992). Further to this, in spinal cord slice from a cat, excitation of region dorsal to the IML evokes an EPSP; this EPSP could be depressed by EAA receptor antagonist, and could be enhanced by a glutamate uptake inhibitor (Inokuchi et al., 1992).

Stimulation of vasodepressor regions of the NTS, or stimulation of the ADN, evoked a membrane hyper-polarisation effect and induced reductions in cell input resistance of SPGNs (Lewis and Coote, 2008). This study ruled out the presence of a pacemaker like activity from SPGNs.

Intravenous injection of 2-deoxyglucose, leading to glucoprivation, increased the activity of SPGNs that regulated adrenaline secretion from chromaffin cells of adrenal medulla (Morrison and Cao, 2000). On the other hand, stimulation of the baroreflex inhibited the activity of SPGNs innervating noradrenergic chromaffin cells of the adrenal medulla; these SPGNs were sensitive to baroreceptor activation and not glucoprivation (Morrison and Cao, 2000).

Induction of acute hypotension, with infusion of SNP, caused increases in Fos-ir in SPGNs, of which $\approx 71\%$ had projections to sympatho-adrenal neurons; these neurons were most densely localised to the T8-T9 segments of the spinal cord (Minson et al., 1997a). SPGNs, projecting to the superior cervical ganglion, were not found to be barosensitive (Minson et al., 1997a). Anterograde tracing from the RVLM also showed that SPGNs responding to hypotension received projections from the RVLM (Minson et al., 1997a). A higher level of basal Fos-ir in SPGNs was seen in SHR (compared to WKY) following infusion of SNP, which may be responsible for elevated levels of BP in SHR (Minson et al., 1996). A recent study has also shown that induction of hypotension, with hydralazine, increased Fos-ir in SPGNs projecting to adrenal glands and the celiac ganglion (Parker et al., 2015).

All together, these findings suggest that SPGNs are highly critical in the autonomic control of the cardiovascular system.

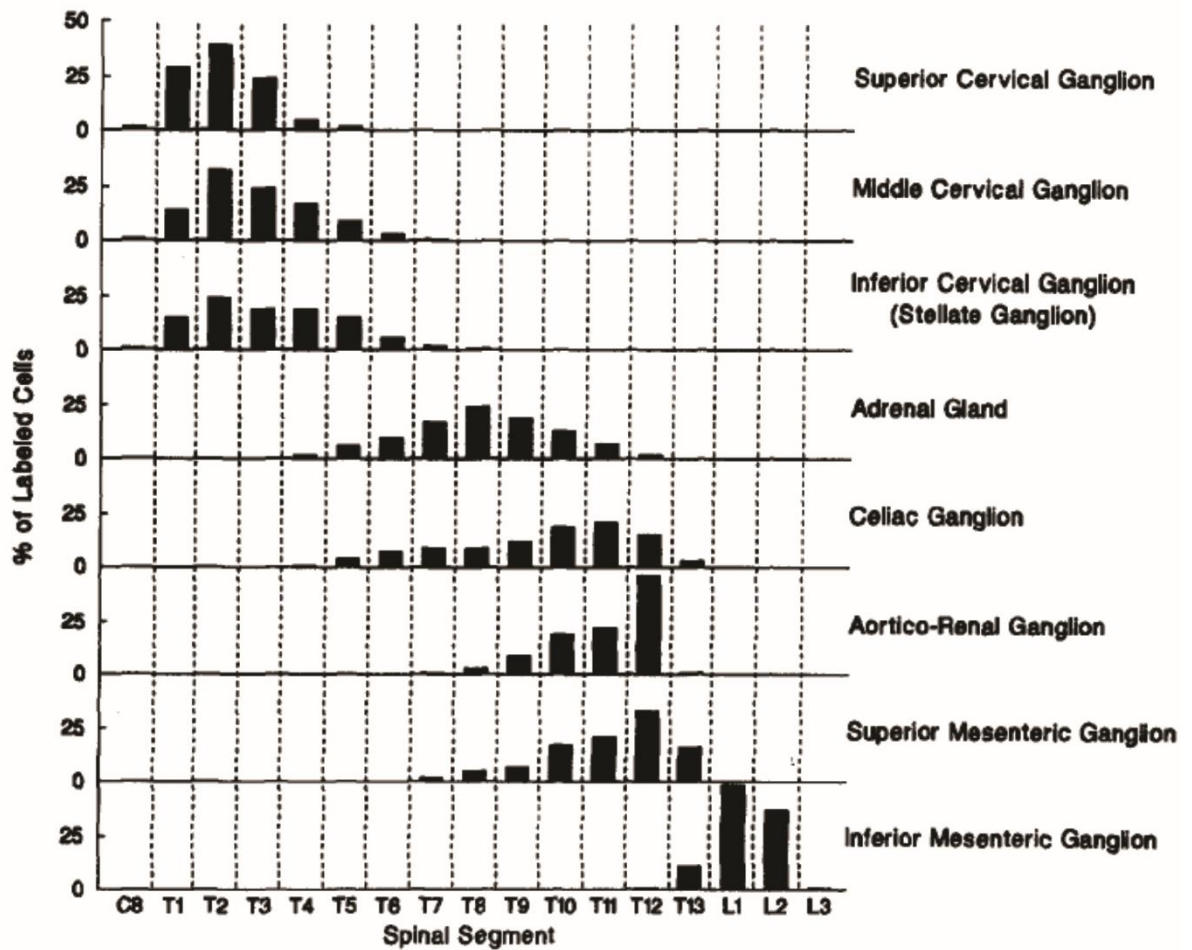


Figure 1.5: Segmental distribution of sympathetic preganglionic neurons (SPGNs)

Fluoro-gold injections into the major sympathetic ganglia, and adrenal glands, reveal that each sympathetic ganglion (or adrenal gland) receives projections from neurons located in multiple segments of the spinal cord. (Figure from (Strack et al., 1988); used with permission)

1.2.2 Other catecholaminergic areas of the ANS

Within the brainstem (extending rostrally from the CVLM to the rostral pons), there are many noradrenergic nuclei that are immunoreactive for TH and D β H; these include the A1 to A6 nuclei (Badoer et al., 1987; Burman et al., 2003; Dahlström and Fuxe, 1964; Li et al., 2008a). The presence of TH (rate limiting enzyme for dopamine synthesis) and D β H (enzyme that converts dopamine to noradrenaline) enables these neurons to synthesise noradrenaline (Armstrong et al., 1982). Adrenergic nuclei, such as C1-C3 cell groups, are immunoreactive for PNMT, in addition to TH and D β H (Armstrong et al., 1982; Minson et al., 1990; Seigny et al., 2012). PNMT catalyzes the synthesis of adrenaline from noradrenaline, and can be used to distinguish between adrenergic and noradrenergic catecholaminergic nuclei of the brainstem.

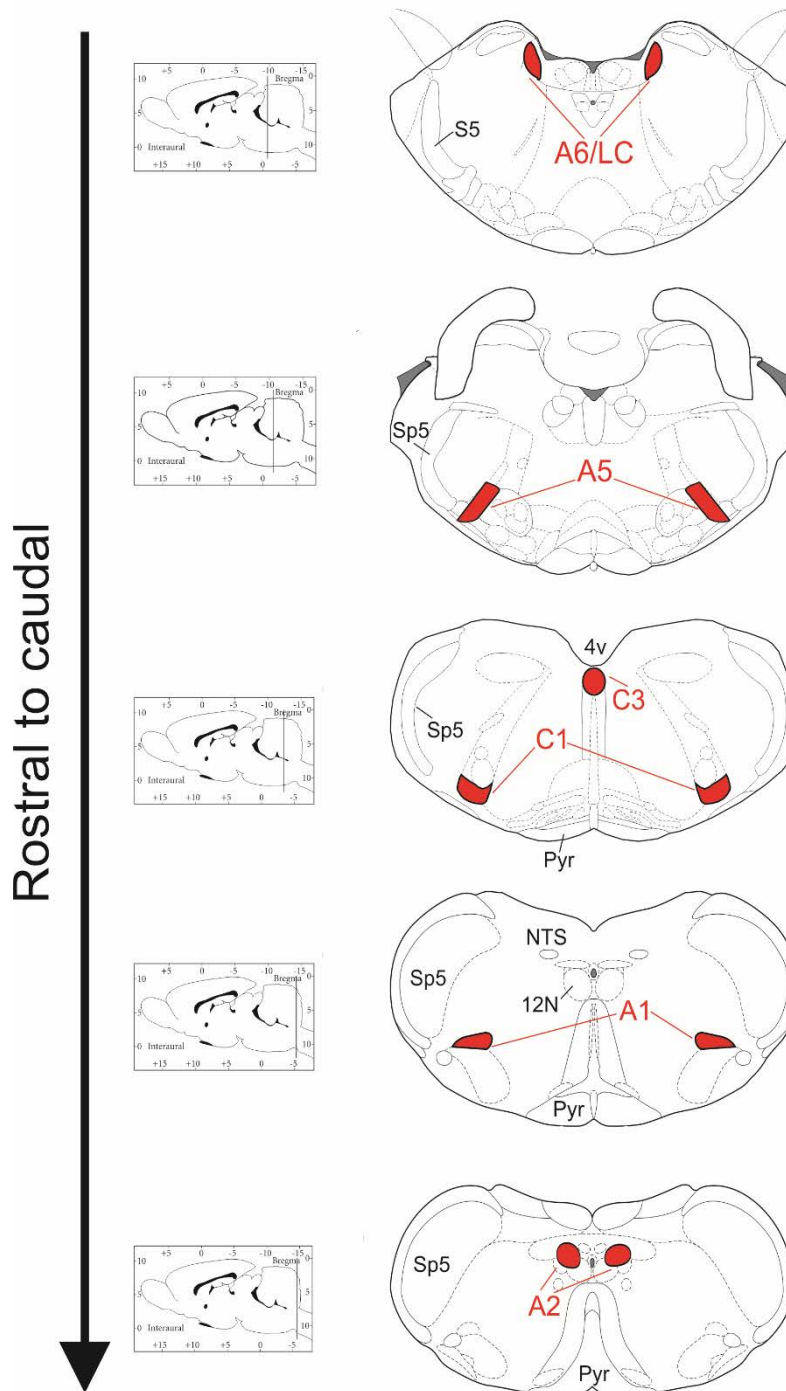


Figure 1.6: Location of various catecholaminergic nuclei, A1/A2/C1/C3/A5/A6, in the brainstem

Six catecholaminergic nuclei of interest

(A1/A2/C1/C3/A5/A6) are highlighted in red. S5, sensory root of the trigeminal nerve; Sp5, spinal trigeminal tract; 4v, 4th ventricle; Pyr, pyramidal tracts; NTS, nucleus of the solitary tract; 12N, 12th nucleus. (Adapted from (Kapoor et al., 2016a; Paxinos and Watson, 2007))

1.2.2.1 A1

A1 (Figure 1.6) noradrenergic neurons of the brainstem are immunoreactive for TH and D β H, and are intermingled with GABAergic neurons of the CVLM (Dahlström and Fuxe, 1964; Paxinos and Watson, 2007). A1 noradrenergic neurons are important in the hypothalamo-pituitary-adrenal axis, via their ascending efferent projections to neuroendocrine cells in the PVN (Blessing et al., 1982a; Cravo et al., 2009). A1 neurons are involved in the secretion of vasopressin (anti diuretic hormone) (Blessing et al., 1982b; Cravo et al., 2009; Day and Sibbald, 1990), and regulation of volume in extracellular compartments (Howe et al., 2004; Pedrino et al., 2008) (section 1.2.1.1). The absence of direct projections from A1 to SPGNs does not rule out the possibility that A1 neurons can modulate the activity of SPGNs. Few earlier studies have shown the presence of efferent projections from A1 neurons to the NTS (Blessing et al., 1981a), the PVN (Tanaka et al., 1997) and to the bulbospinal RVLM neurons (Dahlström and Fuxe, 1964). A1 neurons are in receipt of direct inputs from arterial baroreceptors (Day and Sibbald, 1990; Li et al., 1992a) and vagal cardiopulmonary volume receptors (Day et al., 1992).

Destruction of the area containing A1 neurons in rabbits, by either electrolytic lesioning or microinjection of kainic acid (neurotoxin), elevated plasma concentration levels of vasopressin, and induced acute hypertension accompanied by bradycardia (Blessing et al., 1982b; Elliott et al., 1985). Another study showed similar results where excitation of the region containing A1 cells in rabbits, with either a microinjection of L-glutamate or low frequency electrical stimulation, exerted a depressor response with reductions in HR (Blessing and Reis, 1982). Microinjection of GABA in the region containing A1 cells in rabbits exerted a pressor response (Blessing and Reis, 1982).

However, these results should be treated with caution as A1 neurons are intermingled with some of the key sites involved in cardiorespiratory regulation, such as the CVLM and the pre-Bötzinger nucleus; no attempt was made in these studies to functionally distinguish between the A1 group and other neuronal groups. A study by Head et al., (1987) highlighted that changes observed in MAP following electrical stimulation of the region containing A1 cells could be mediated through non-catecholaminergic neurons present in this region (Head et al., 1987)

Induction of hypotension, with intravenous administration of hydralazine or hypotensive hemorrhage, activated neurons in the A1 region (Benarroch, 1998; Smith et al., 1995). In line with this work, discharge from A1 neurons increased with reductions in AP, and vice versa (Li et al., 1992a). This role of A1 neurons in the cardiovascular regulation is suggested to be

mediated via its afferent pathway from baroreceptors, and efferent projections to the PVN (Buller et al., 1999; Kannan et al., 1986). Furthermore, A1 neurons also receive input from peripheral chemoreceptors, and modulate secretion of vasopressin accordingly (Li et al., 1992a).

1.2.2.2 A2

A2 neurons (Figure 1.6) of the brainstem are located within the dorsal vagal complex, and are centered within the intermediate and the caudal NTS (Badoer et al., 1987; Paxinos and Watson, 2007). Approximately 80% of A2 neurons are positive for vesicular glutamate transporter 2 (Stornetta et al., 2002a). Almost all of A2 neurons are positive for prolactin-releasing peptide (peptide hormone), suggesting a role of the A2 nucleus in regulation of the neuroendocrine system (Chen et al., 1999; Yamada et al., 2009). A2 neurons are also immunoreactive for neuropeptides such as PACAP (Das et al., 2007) and neuropeptide Y (Sawchenko et al., 1985).

A2 neurons receive direct afferent inputs from many sites such as area of the NTS innervated by visceral afferents (Appleyard et al., 2007), and projects to higher brain regions, such as the PVN (Yamada et al., 2009). Following induction of hyper-, and hypo-, tension in conscious rabbits (with phenylephrine and SNP, respectively), increased levels of Fos-ir (signifying neuronal activity) were observed in the A2 region (Li and Dampney, 1994). Destruction of A2 neurons in the brainstem of rats resulted in increased variability in AP without affecting MAP (Talman et al., 1980). However, A2 neurons do not receive a direct baroreceptor input as shown by single unit recordings (Moore and Guyenet, 1985).

In addition to a role of A2 neurons in the cardiovascular system, these neurons also play a critical role in systems associated with food intake, emotional and stress responses, affective behavior, and drug dependence (see review (Rinaman, 2011)).

1.2.2.3 C3

C3 TH-ir neurons are located in the medial longitudinal fasciculus in close proximity to the 4th ventricle, and at the level of the prepositus hypoglossal nucleus (Figure 1.6) (Paxinos and Watson, 2007; Ritter et al., 1998). C3 neurons express vesicular glutamate transporter 2 and hence, are glutamatergic in nature (Stornetta et al., 2002a). Efferent projections from C3 neurons extend to regions such as the IML cell column of the thoracic spinal cord, commissural and medial nuclei of the NTS and the PVN (Sevigny et al., 2012).

Increased expression of Fos in C3 neurons of the brainstem were observed following induction of glucoprivation by 2-deoxy-D-glucose (Ritter et al., 1998). C3 neuronal activity increased

(determined by Fos-ir) in response to induction of hypotension, with SNP (Murphy et al., 1994), but remained unaffected during hemorrhage (Dun et al., 1993). A recent study demonstrated that C3 neurons are sympatho-excitatory, and are critically involved in glucose homeostasis, but not hypotension (induced with hydralazine) (Menuet et al., 2014). The contradictory involvement of C3 neurons following hypotension shown between Murphy et al., (1994) and Menuet et al., (2014) could be attributed to the use of 2 different drugs to induce hypotension, SNP vs. hydralazine. Further work is required to establish the exact, and comprehensive, role of C3 neurons in the ANS.

1.2.2.4 Locus coeruleus (LC) or A6 noradrenergic nucleus

The LC/A6 nucleus (Figure 1.6) is located near the pontomesencephalic junction, and is the largest group of noradrenergic neurons in the CNS (Badoer et al., 1987; Dahlström and Fuxe, 1964; Paxinos and Watson, 2007). Multiple areas of the brain project to the LC, such as the PVN, the perifornical area, raphe nuclei, the periaqueductal grey matter, the RVLM and the spinal cord (Abbott et al., 2012; Luppi et al., 1995; Samuels and Szabadi, 2008). Projections from the RVLM to the LC are glutamatergic, and activation of RVLM neurons, via somatic or psychological stress, can activate LC neurons (Holloway et al., 2013).

LC is known for its well established role during the sleep-wake cycle (Aston-Jones and Bloom, 1981), cognitive performance (Usher et al., 1999) and emotional activation (Aston-Jones et al., 1996). Further to this, LC neurons project to many sites critical for the control of the cardiovascular system, such as the PVN, inhibitory projections to the RVLM, and caudal and dorsal raphe nuclei (see review (Samuels and Szabadi, 2008)). Glucose utilisation followed by induction of hemorrhage was increased in the area of the LC (Savaki et al., 1982).

Recent work from Bruinstroop and colleagues (2012) has shown that neurons of the A6/LC send efferent projections to all segments of the spinal cord (Bruinstroop et al., 2012). Interestingly, the density of axonal projections from the LC group of neurons to the spinal cord were similar in each spinal lamina at all levels of the spinal cord (Bruinstroop et al., 2012). The LC has the ability to modulate BP levels via direct projections (excitatory) to the IML cell column of the spinal cord (Jones and Yang, 1985), and indirect projections to premotor nuclei, such as the RVLM (inhibitory), and A5 noradrenergic neurons (excitatory) (Samuels and Szabadi, 2008; Stornetta et al., 2015). Blood volume load, or elevation of BP, reduced the firing rate of LC neurons; this effect persisted even after removal of afferents from arterial baroreceptors (Elam et al., 1984). In accordance with the previous study, significant increases

in Fos-ir in the LC were seen following induction of hypotension, via intravenous infusion of SNP (Li and Dampney, 1994).

Induction of hypercapnia, and hypoxia, resulted in an increased firing rate of neurons in the LC (Elam et al., 1981; Nattie, 2011). Effects of hypercapnia persisted even after the removal of afferents from peripheral chemoreceptors, suggesting that the observed effect was more central (Elam et al., 1981). However, the increased firing rate in response to hypoxia was abolished following removal of afferents from peripheral chemoreceptors (Elam et al., 1981). In accordance with these results, another study also showed increased Fos-ir in the LC in response to hypoxia or hypercapnia (Erickson and Millhorn, 1994; Teppema et al., 1997).

1.3 Autonomic reflex mechanisms

Autonomic reflexes are pathways that are governed by the ANS, and are involved in resumption of homeostasis when subjected to physiological disturbances. The most important (in context of the SNS), and extensively studied, autonomic reflexes are the sympathetic baroreflex, the chemoreflex and the SSR pathways.

The NTS (section 1.2.1.7), the CVLM (section 1.2.1.6) and the RVLM (section 1.2.1.5) are regions of the brainstem (Figure 1.7), which are crucial in regulation of tonic activity of the SNS, and integration of various autonomic reflex mechanisms. As discussed in previous sections, overall activity of sympatho-excitatory neurons in the RVLM is modulated by inputs from other key brain regions, such as the NTS (Koshiya and Guyenet, 1996) and the CVLM (Burke et al., 2008). Following integration of these inputs, RVLM neurons cause appropriate changes in physiology via bulbospinal sympatho-excitatory efferent pathways (Figure 1.7). SPGNs, found in the IML cell column of the spinal cord, receive monosynaptic inputs from RVLM neurons, and other supra-bulbar sites (Figure 1.7) (Guyenet, 2006; McAllen et al., 1994; Oshima et al., 2006; Oshima et al., 2008; Pilowsky et al., 1994; Pilowsky et al., 2009).

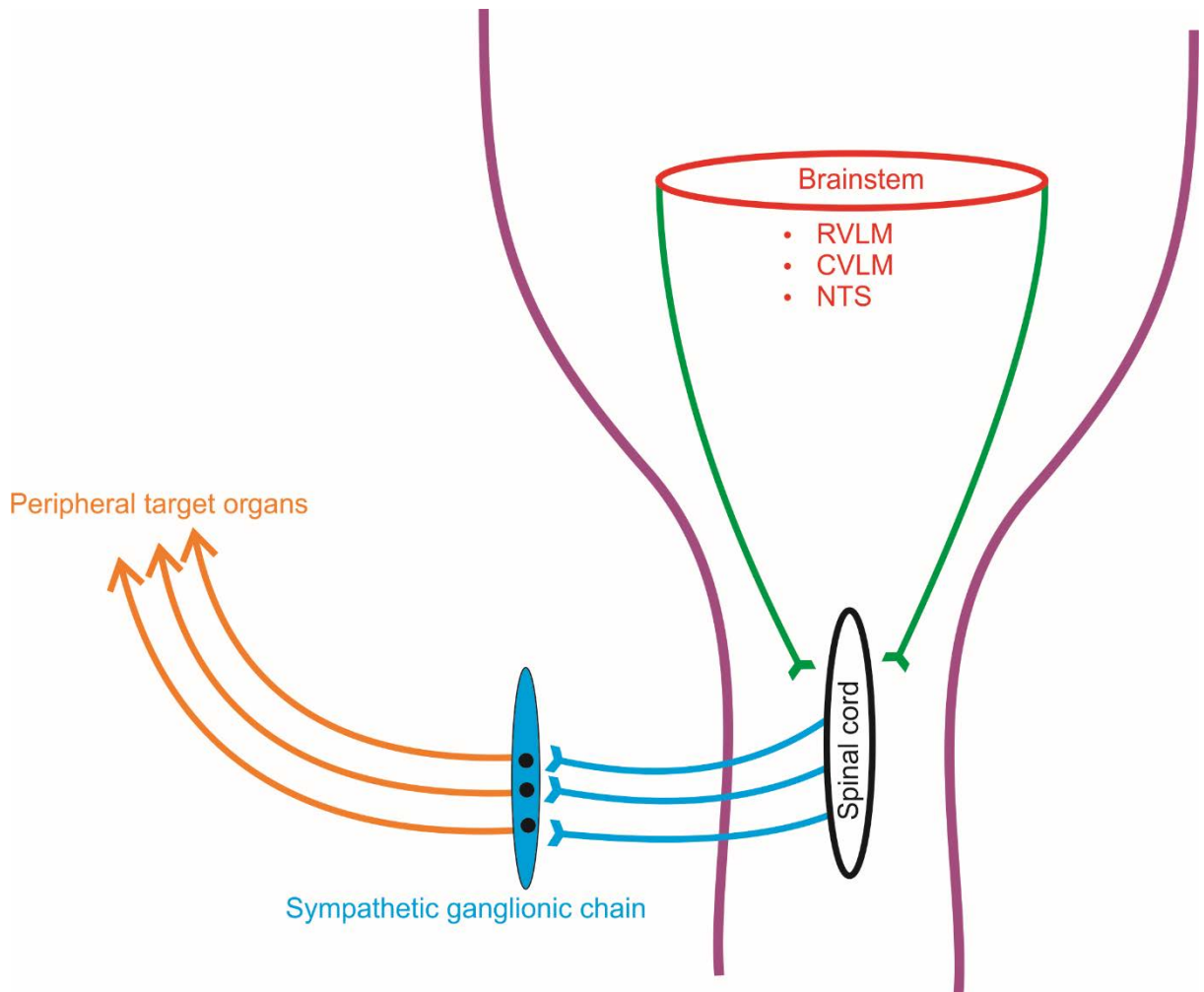


Figure 1.7: Schematic representation of flow of the information between brainstem and peripheral organs involved in cardiovascular control of the SNS

Brainstem premotor nuclei (red) send direct projections that innervate SPGNs located in the spinal cord (black). SPGNs control the activity of target organs via sympathetic ganglia (blue), which in turn gives rise to sympathetic postganglionic nerves (orange) innervating peripheral target organs. (Adapted from (Pilowsky and Goodchild, 2002))

1.3.1 **Baroreflex**

Baroreflexes are a series of negative feedback loops that are involved in the regulation of BP (Guyenet, 2006; Schreihofer and Guyenet, 2002; Sved et al., 2003). There are several types of baroreflexes including the vasopressin, HR and the sympathetic baroreflex (Figure 1.8).

The vasopressin baroreflex is, predominantly, a neuro-humoral reflex, which responds to unloading of arterial baroreceptors when subjected to decreases in blood volume. Under normal conditions, arterial baroreceptors provide inhibitory signals to areas of the CNS that are involved in release of vasopressin (potent vasoconstrictor), such as A1 noradrenergic neurons (section 1.2.2.1). When subjected to falls in blood volume, inhibitory signal to the CNS is reduced following unloading of baroreceptors, and subsequently increases the release of vasopressin. Increased plasma concentrations of vasopressin help to resume BP towards baseline levels. (Thrasher, 1994; Thrasher and Keil, 1998; Webb et al., 1986).

The HR baroreflex is governed by the PSNS and is primarily affected by loading state of aortic baroreceptors (section 1.1.1 and (Pickering et al., 2008)).

The focus of this thesis is the sympathetic baroreflex, which is critical in the short-term control of BP and is discussed in detail in the following sections. Role of the sympathetic baroreflex pathway in the long term regulation of BP remains a topic of considerable debate (Thrasher, 2005).

- *Baroreceptors*

Baroreceptors are primarily located in the aortic arch and the carotid sinus (where the common carotid artery bifurcates), and are specialised mechanoreceptors that are sensitive to stretch (Kougiass et al., 2010). Afferent fibres from carotid sinus baroreceptors join the glossopharyngeal (IX) nerve, and fibres from the aortic arch join the vagus (X) nerve; altogether these nerves provide an excitatory input to neurons in the NTS (Kougiass et al., 2010). Broadly speaking, increases in MAP loads baroreceptors evoking a depressor response in order to restore baseline levels of MAP. Conversely, decreases in MAP unloads baroreceptors, and elicits a pressor response via cardiovascular brainstem nuclei and the SNS. Arterial baroreceptors are in a loaded state during the systolic phase, and are in an unloaded state during the diastolic phase, of a single cardiac cycle.

There are 2 distinct subtypes of baroreceptor afferent fibres, myelinated A-type fibres and unmyelinated C-type fibres. A-type fibres generate high and regular discharge frequencies, whereas C-type fibres generate relatively low and irregular discharge frequencies. Electrical

activation of both, A- and C- type, baroreceptor afferents elicited a depressor response; the depressor response evoked by C-type fibres is powerful and longer lasting (Douglas et al., 1956). Blockade of large A-type fibre baroreceptors reduced the baroreflex sensitivity without any major changes in baseline levels of BP (Seagard et al., 1993). However, blockade of smaller A- and C- type fibres resulted in smaller decreases in baroreflex sensitivity but significantly elevated baseline levels of BP, indicating a loss of tonic control (Seagard et al., 1993).

- *Sympathetic baroreflex pathway (Figure 1.8)*

Baroreceptors increase their discharge rate in response to increased AP, and convey a message to the medulla oblongata via the glossopharyngeal and the vagus nerve; this ultimately modulates the vagal and sympathetic outflow to the heart and peripheral vasculature. The first site of termination for baroreceptor afferent nerves, in the medulla, is the caudal, medial and commissural regions of the NTS (Sun, 1995; Wallach and Loewy, 1980). NTS neurons process the excitatory input from baroreceptor afferents, and further excite neurons located in the CVLM via glutamatergic projections (Weston et al., 2003). CVLM neurons provide GABAergic inhibitory inputs to presympathetic neurons located in the RVLM, which in turn inhibit the activity of SPGNs, thereby lowering BP and SNA. (Guyenet, 2006; Pilowsky et al., 2009; Schreihofer and Guyenet, 2002; Sved et al., 2003)

- *Role of the NTS in the baroreflex pathway (Figure 1.8)*

Afferent fibres from baroreceptors, located in the carotid sinus and the aortic arch, have different sites of termination in the NTS. Dorsomedial and lateral sub-nuclei of the NTS are densely populated with afferent projections from the aortic nerve (Ciriello, 1983; Kougiass et al., 2010). Whereas, two distinct aggregations of afferents from the carotid sinus terminating in the NTS were observed, 1) rostral to the obex - within the lateral and dorsomedial sub-nuclei of the NTS; 2) caudal to the obex - within the commissural and ventrolateral sub-nuclei of the NTS (Housley et al., 1987). Further to this, ~85% of NTS neurons could only evoke a post-synaptic potential to electrical stimulation of only one of the 3 nerves investigated: the carotid sinus, aortic arch and vagal nerves (Donoghue et al., 1985). Approximately 76% of NTS neurons exhibited an EPSP in response to stimulation of baroreceptor afferent nerves, with a variable latency period ranging between 2-124 ms (Donoghue et al., 1985).

Glutamate is the most likely neurotransmitter conveying information from baroreceptor afferent fibres to NTS neurons. Blockade of glutamate receptors in the NTS, with kynurenic acid, significantly reduced responses to the sympathetic baroreflex (Guyenet et al., 1987). However,

the role of ionotropic glutamate receptors in translation of glutamate related depressor responses in the NTS was questioned when kynurenic acid was unable to block the depressor responses following exogenous glutamate (Talman, 1989). Therefore, it was suggested that the NTS contains a set of ionotropic and metabotropic glutamate receptors, of which activity of ionotropic glutamate receptors can be blocked by kynurenic acid (Pawloski-Dahm and Gordon, 1992). Activation of ionotropic glutamate receptors is required for modulation of baroreflex responses, and can be blocked by kynurenic acid (Pawloski-Dahm and Gordon, 1992). However, depressor responses seen following exogenous application of glutamate are mediated through metabotropic glutamate receptors, which are insensitive to kynurenic acid (Pawloski-Dahm and Gordon, 1992).

Please refer to section 1.2.1.7 for details on the role of the NTS in the baroreflex pathway, shown by changes in Fos-ir in response to activation of the baroreflex.

- *Role of the CVLM in the baroreflex pathway (Figure 1.8)*

It was initially thought that activation of NTS neurons in response to baroreflex provides direct inhibitory synaptic input to the RVLM nucleus, thereby reducing the activity of SPGNs (Chalmers, 1975). We have now known this for more than a decade that this is not the case. NTS neurons excited in response to baroreflex provide excitatory input to CVLM neurons (Aicher et al., 1995; Benarroch, 1998; Chalmers and Pilowsky, 1991; Guyenet, 2006; Miyawaki et al., 1997; Pilowsky and Goodchild, 2002; Pilowsky et al., 2009).

Anterogradely labelled neurons from the NTS are closely intermingled with the retrogradely labelled neurons from the RVLM (Yu and Gordon, 1996); this suggests that the pathway from the NTS to the CVLM to the RVLM mediates the baroreflex response. However, it was not confirmed whether NTS neurons providing efferent projections to the CVLM were the second order NTS neurons that received glutamatergic afferent projections from baroreceptor neurons. Therefore, the presence of interneurons in the NTS cannot be ruled out (Pilowsky and Goodchild, 2002).

Microinjection of EAA into the CVLM evoked a depressor response, analogous to baroreceptor reflexes (Gordon, 1987), providing an evidence that activation of the CVLM exerts a sympatho-inhibitory effect (section 1.2.1.6).

- *Role of the RVLM in the baroreflex pathway (Figure 1.8)*

As mentioned in the above section, and previous section 1.2.1.5, rostral CVLM neurons in the barosensory area provide monosynaptic sympatho-inhibitory output to cardiovascular

bulbospinal RVLM neurons (Cravo and Morrison, 1993; Guyenet, 2006; Jeske et al., 1995; Li and Dampney, 1994; Pilowsky and Goodchild, 2002; Pilowsky et al., 2009). Inhibition of the CVLM, with muscimol, increased BP and Fos-ir in the RVLM; $\approx 50\%$ of these Fos-ir neurons were bulbospinal RVLM neurons projecting to the upper thoracic spinal cord (Minson et al., 1994).

Depressor responses to baroreflex activation mediated by the CVLM act via GABA receptors, and not the glycinergic or α -adrenergic receptors, in the RVLM (Blessing, 1988). Induction of isovolemic hypotension with hydralazine or SNP, or hemorrhage-induced hypotension, increased Fos-ir in the RVLM (Badoer et al., 1993; Chan and Sawchenko, 1994; Graham et al., 1995; McAllen et al., 1992; Minson et al., 1997a).

Activation of μ -opioid receptors, but not Δ -opioid receptors, in the RVLM inhibited the sympathetic baroreceptor reflex, and inhibited lumbar and splanchnic SNA (Miyawaki et al., 2002b). Microinjection of galanin into the RVLM augmented the sympatho-inhibitory response following the ADN stimulation (Abbott and Pilowsky, 2009). Furthermore, microinjection of orexin-A, or catestatin, in the RVLM enhanced the reflex sympatho-inhibitory responses to intravenous administration of phenylephrine (Gaede and Pilowsky, 2010; Shahid et al., 2012).

- *Role of SPGNs in the baroreflex pathway (Figure 1.8)*

As discussed in section 1.2.1.9, the RVLM provides monosynaptic projections to SPGNs in the IML cell column of the spinal cord (Oshima et al., 2006; Oshima et al., 2008; Strack et al., 1988). SPGNs in the spinal cord are the last leg of the sympathetic baroreflex pathway, mediating sympatho-excitatory input received from supra-spinal brain areas to periphery, either via ganglia innervating the heart and vasculature or directly to adrenal chromaffin cells.

It was previously suggested that GABA acting at the spinal level was mediating the sympatho-inhibitory effects seen in response to baroreflex activation (Lewis and Coote, 1996). However, a later study revealed that intrathecal blockade of GABA, or glycine receptors, did not attenuate the sympatho-inhibitory response to the ADN stimulation (Goodchild et al., 2000b).

- *Baroreceptor resetting*

Baroreceptor resetting is a mechanism by which the BP threshold required to activate baroreceptors shifts in the direction of prevailing MAP. There appears to be 2 types of baroreflex resetting, acute and chronic. Acute baroreceptor resetting occurs due to rapid changes in BP, and is reversible in nature (Munch et al., 1983). However, changes in BP

threshold required to activate baroreceptors in chronic resetting affect the baroreceptor sensitivity and thus, are not reversible (Kougias et al., 2010).

Acute baroreflex resetting enables BP to rise over a wide range during appropriate day-to-day activities, such as exercise (DiCarlo and Bishop, 2001; Guyenet, 2006). In this case, GABA mediated input from peripheral receptors (such as nociceptors and muscle metabotropic receptors) and higher brain regions, such as the hypothalamus, provide inhibitory input to NTS neurons. Inhibition of NTS neurons reduces the excitatory input to the CVLM and therefore, reduces inhibition of the RVLM. This disinhibition of the RVLM leads to increased BP levels (Andresen et al., 2001; Guyenet, 2006; Potts et al., 2003).

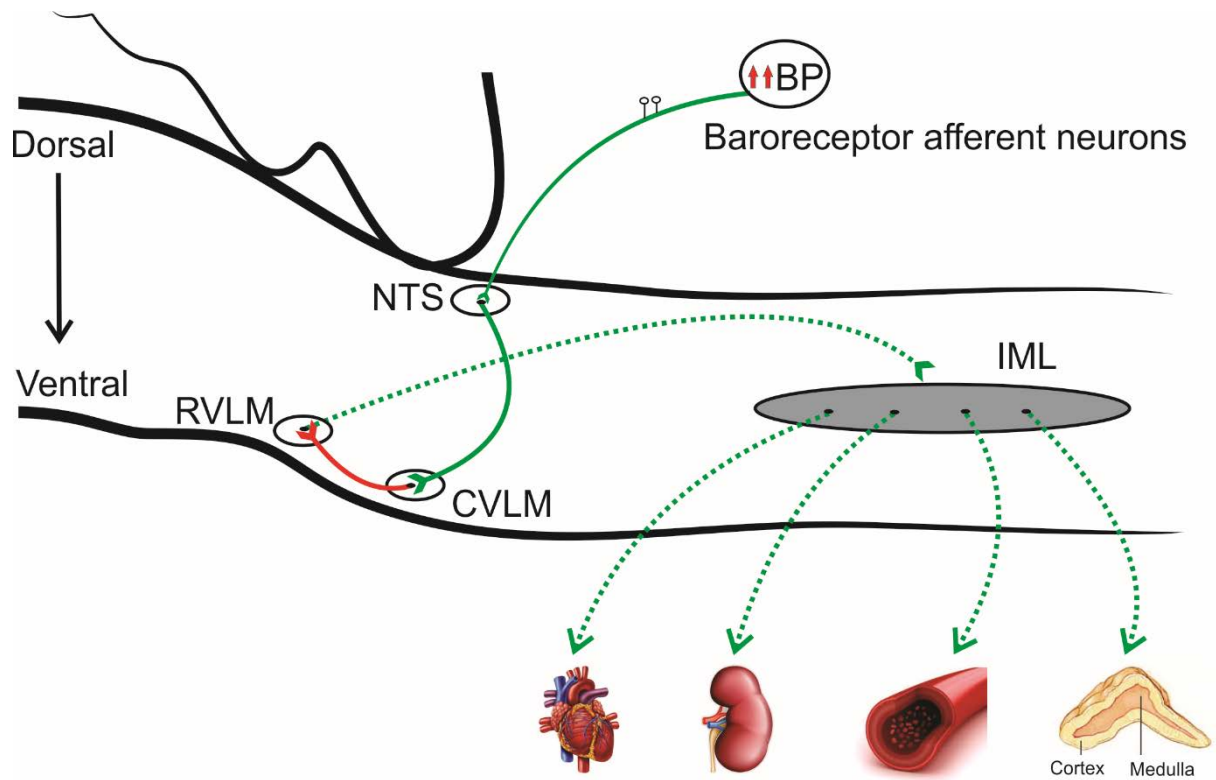


Figure 1.8: The sympathetic baroreflex pathway

Baroreceptor neurons located in the carotid sinus and the aortic arch send excitatory projections to the NTS located in the brainstem (green). Activated NTS neurons, in turn, send glutamatergic projections to the CVLM (green). Activated CVLM neurons send inhibitory projections to the RVLM (red) thereby, reducing the excitatory output (dotted green) to the IML cell column of the spinal cord. This reduced sympathetic output to the IML ultimately leads to reduced excitatory output to peripheral targets (dotted green), such as heart, kidneys, blood vessels and adrenal glands. BP, blood pressure; NTS, nucleus of the solitary tract; CVLM, caudal ventrolateral medulla; RVLM, rostral ventrolateral medulla; IML, intermediolateral cell column of the spinal cord. (Adapted from (Kapoor et al., 2015; Pilowsky et al., 2009))

1.3.2 Chemoreflex

Primary role of the chemoreflex system is to maintain $[H^+]$, PaO_2 and $PaCO_2$ within their homeostatic physiological levels. The chemoreflex arm of the ANS can be broadly divided into two subtypes, the peripheral and the central chemoreflex. Receptors that are sensitive to changing levels of O_2 are located peripherally in carotid bodies (Guyenet and Bayliss, 2015; Nattie, 1999). Receptors that detect, and respond to, disturbed levels of CO_2 concentration are located both, peripherally (carotid bodies) and centrally (brainstem) (Funk, 2013; Guyenet and Bayliss, 2015; Nattie, 1999). Up to a $PaCO_2$ value of 60-70 mmHg, contribution of carotid chemoreceptors is of the same magnitude as that of central chemoreceptors (Hanna et al., 1981); beyond this value of $PaCO_2$, contribution from carotid chemoreceptors declines, and that of the central chemoreceptors continues to increase (Hanna et al., 1981). Overall, activation of both, peripheral and central, chemoreceptors exert a sympatho-excitatory effect on the SNS accompanied with increases in AP.

1.3.2.1 *Peripheral chemoreflex*

Carotid bodies, located near the bifurcation of carotid arteries, are collections of chemosensitive cells that are activated in response to falls in the PaO_2 below 100 mmHg, and to increases in blood pH. Type I glomus cells of the carotid body are of neuronal phenotype, and are primary sites of sensory transduction (Kumar and Prabhakar, 2012; Prabhakar, 2000). Cryodestruction of glomus cells of the carotid body abolished the increased sensory discharge observed in response to hypoxia (Verna et al., 1975). Glomus cells, in isolation, are capable of responding to a hypoxic stimulus (Montoro et al., 1996). These glomus cells are a heterogeneous population of cells, with some cells depolarising (clustered) and others hyperpolarising (isolated) in response to a given hypoxic challenge (Pang and Eyzaguirre, 1992). These responses have been suggested to be either due to the presence, or absence, of sustentacular cells (glial cells), or could be due to the presence of sub-populations of functionally different glomus cells (Pang and Eyzaguirre, 1992). In addition to membrane potential, variations were also seen in intracellular pH (Pang and Eyzaguirre, 1993) and Ca^{2+} concentrations (Bright et al., 1996) in response to a hypoxic challenge (Kumar and Prabhakar, 2012; Prabhakar, 2000).

Glomus cells on sensing hypoxia (by either a heme and/or redox sensitive enzyme or K^+ channel) release an excitatory neurotransmitter, which acts on nearby afferent nerve endings, and leads to an increased sensory discharge (Kumar and Prabhakar, 2012; Prabhakar, 2000). Hypoxia also causes an increase in intracellular Ca^{2+} concentrations (from extracellular Ca^{2+}),

via voltage gated Ca^{2+} channels, which is critical for neurotransmitter release, such as dopamine (Overholt and Prabhakar, 1997; Shirahata and Fitzgerald, 1991).

Chemo stimulation of cells located in the carotid body provide glutamatergic input to the commissural and medial sub-nucleus of the NTS (Donoghue et al., 1984; Finley and Katz, 1992; Guyenet and Bayliss, 2015; Mifflin, 1992; Willette et al., 1987), ultimately leading to excitation of neurons in the RVLM (Figure 1.9A). RVLM neurons then excite cardiovascular SPGNs, thereby increasing sympathetic activity, plasma catecholamine levels and total peripheral resistance and thereby, leading to an increase in AP and a hyperventilatory response (Figure 1.9A) (Prabhakar et al., 2012).

1.3.2.2 Central chemoreflex

There is a dose-dependency in the way that central neurons respond to chemoreceptor inputs. In fact, almost every neuron in the brain will respond to changes in O_2 , CO_2 or acidity depending on the depth and duration of the stimulus. Central chemoreceptors are considered those neurons that respond vigorously within a physiological range. It was suggested by Putnam et al., (2004) that in order to be classified as a central chemosensitive neuron, a neuron has to fulfil 3 criteria (Putnam et al., 2004): 1) The neuron should be able to alter its firing rate according to changes in CO_2/H^+ concentration; 2) The neuron should intrinsically respond to changes in CO_2 , and not just respond to altered synaptic input; and 3) The neuron should be located in the region affected by acidification (Putnam et al., 2004).

Central chemoreceptors, unlike peripheral chemoreceptors, are thought to be distributed over a wide region of the brain including rostral sites, such as the hypothalamus (orexinergic neurons) (Nattie, 2011), to caudal sites, such as the retrotrapezoid nucleus (RTN) (Guyenet et al., 2016; Wang et al., 2013b) and serotonin positive rostral medullary raphe neurons (Guyenet and Bayliss, 2015; Nattie, 2011; Nattie and Li, 2012; Nattie and Li, 2001). Sunanaga and colleagues showed that induction of hypercapnia caused a marked increase in Fos-ir levels (signifying neuronal activity) in orexin-containing cells of the hypothalamus (Sunanaga et al., 2009). Central chemoreceptors located in the RTN are glutamatergic in nature (Holloway et al., 2015), are activated in response to changes in CO_2 levels (Figure 1.9B) (Guyenet et al., 2012; Kumar et al., 2015; Mulkey et al., 2004), and are silent above arterial pH 7.5 (Basting et al., 2015). Efferent neurons from the RTN innervate the central respiratory network (CRN)/CPG (central pattern generator) driving inspiration (Rosin et al., 2006), and the activity of RTN neurons is regulated by NTS neurons (Figure 1.9B) (Takakura et al., 2007). In addition to RTN neurons,

serotonergic neurons (in particular, the 5-HT_{2A} receptor positive neurons) located in the rostral brainstem are also chemosensitive and are capable of detecting changes in CO₂ levels (Buchanan et al., 2015). Furthermore, RVLM sympatho-excitatory neurons may be intrinsically sensitive to changes in pH, and/or be in receipt of excitatory synaptic input from RTN neurons (Figure 1.9B) (Moreira et al., 2006).

- *Role of the NTS in modulation of the chemoreflex (Figure 1.9)*

Glomus cells, in the carotid body, provide sympatho-excitatory input to NTS neurons (Donoghue et al., 1984; Finley and Katz, 1992; Mifflin, 1992) exerting a sympatho-excitatory pressor response (de Paula et al., 2007; Haibara et al., 1995; Zhang and Mifflin, 1993; Zhang and Mifflin, 1995). The pressor response observed following activation of carotid body afferents was abolished by microinjection of kynurenic acid into the NTS (Zhang and Mifflin, 1993); this finding suggests that the NTS mediated pressor response is due to EAA receptors in the NTS. NMDA receptors in the commissural NTS play an important role in the bradycardiac component following activation of the carotid body (Haibara et al., 1995). Blockade of NMDA receptors in the commissural NTS abolished the bradycardiac response to activation of carotid bodies, while leaving the pressor and hyperventilatory response intact (Haibara et al., 1995). In line with these results, another study showed that microinjection of kynurenic acid into the commissural NTS did not affect elevations in the thoracic SNA, and frequency of the phrenic nerve discharge, in response to chemoreflex activation (Braga and Machado, 2006).

Blockade of ionotropic, and not metabotropic, glutamate receptors in the lateral, and/or midline, commissural NTS partially reduced the pressor response to chemoreflex (Haibara et al., 1999). It has been suggested that the purinergic and the glutamatergic system in the commissural NTS work together, and constitute an integral component of the complex system responsible for the sympatho-excitatory component of chemoreflex activation (Braga et al., 2007).

Induction of acute hypoxia increased Fos-ir in the caudal NTS, and these Fos-ir NTS neurons project to the noncatecholaminergic group of RVLM neurons (Kline et al., 2010).

- *Role of the RVLM in modulation of the chemoreflex (Figure 1.9)*

Hypercapnia/hypoxia evoked a sympatho-excitatory response by increasing activity of RVLM neurons (Koganezawa and Paton, 2014; Moreira et al., 2006). Chemical inhibition of ionotropic glutamate receptors in the RVLM, with kynurenic acid, eliminated the phrenic nerve discharge in response to hypercapnia (Moreira et al., 2006). Neurons in the caudal NTS that are chemosensitive to a hypoxic stimulus project through the RVLM, and arborizes in this region

(Koshiya and Guyenet, 1996). As mentioned in section 1.2.1.5, a portion of NTS neurons provides monosynaptic projections to the C1 adrenergic group of neurons in the RVLM and thus, may be involved in modulation of sympatho-excitatory pathways, such as the chemoreceptor reflexes (Aicher et al., 1996).

Activity of RVLM bulbospinal neurons is affected by a hypoxic/hypercapnic stimulus in conditions where these neurons are deprived of their synaptic inputs (Boychuk et al., 2012; Koganezawa and Paton, 2014). As mentioned previously (section 1.2.1.5), abnormal conditions where RVLM neurons are devoid of their synaptic inputs may trigger RVLM neuronal intrinsic pacemaker-like properties. Two populations of bulbospinal RVLM neurons (deprived of their synaptic inputs) capable of responding to hypoxia/ hypercapnia were identified, 1) Low discharging RVLM neurons where the firing frequency was facilitated due to reduced inhibitory neurotransmission, and 2) High discharge RVLM neurons where the frequency was inhibited independent of a synaptic input (Boychuk et al., 2012). Therefore, it was concluded that the reduced inhibition of low discharging RVLM neurons is responsible for increased activity in response to hypoxia/ hypercapnia (Boychuk et al., 2012; Koganezawa and Paton, 2014).

It is proposed that the purinergic signalling system in the RVLM, P2Y1 in particular, is critical in modulation of responses to activation of the peripheral chemoreflex. Microinjection of a P2Y1-receptor specific agonist in the RVLM increased phrenic SNA and BP, mimicking responses seen following activation of the peripheral chemoreflex (Wenker et al., 2013). On the other hand, blockade of P2Y1-receptors in the RVLM decreased responses to the peripheral chemoreflex activation (Wenker et al., 2013). Neurons in the RVLM that are immunoreactive for P2Y1 are also positive for TH, confirming their identity as the C1 group of RVLM neurons, and lesion of C1 neurons *in vivo* abolished the response to a P2Y1-receptor agonist (Wenker et al., 2013).

Stimulation of carotid chemoreceptors, with brief N₂ inhalation, elicited increases in SND, MAP and the discharge rate of RVLM premotor neurons (Koshiya et al., 1993). Bilateral microinjection of kynurenic acid, blocking glutamate receptors, in the RVLM of anesthetized rats blocked sympatho-excitatory responses to activation of the chemoreflex (Koshiya et al., 1993).

- *Other areas of the brainstem involved in modulation of the chemoreflex*

Bilateral microinjection of kynurenic acid, or muscimol, into the CVLM did not affect sympatho-excitatory responses seen following activation of the chemoreflex with N₂ inhalation (Koshiya et al., 1993); this suggests that the CVLM does not play any role in modulation of the sympathetic chemoreflex. Thus, it is hypothesised that integration of information from the baroreflex and the chemoreflex before reaching SPGNs occurs post-synaptically at somata of the bulbospinal presympathetic RVLM neurons (Guyenet and Koshiya, 1995).

The A5 group of noradrenergic neurons, through their projections to either the spinal cord or medullary regions, also play an important role in the sympathetic chemoreflex (Guyenet and Koshiya, 1995). Chemical activation of GABA receptors, with muscimol, in the A5 region caused a reduction in the sympatho-excitatory response to the carotid chemoreflex activation by ≈65%, but did not affect the resting sympathetic tone (Koshiya and Guyenet, 1994).

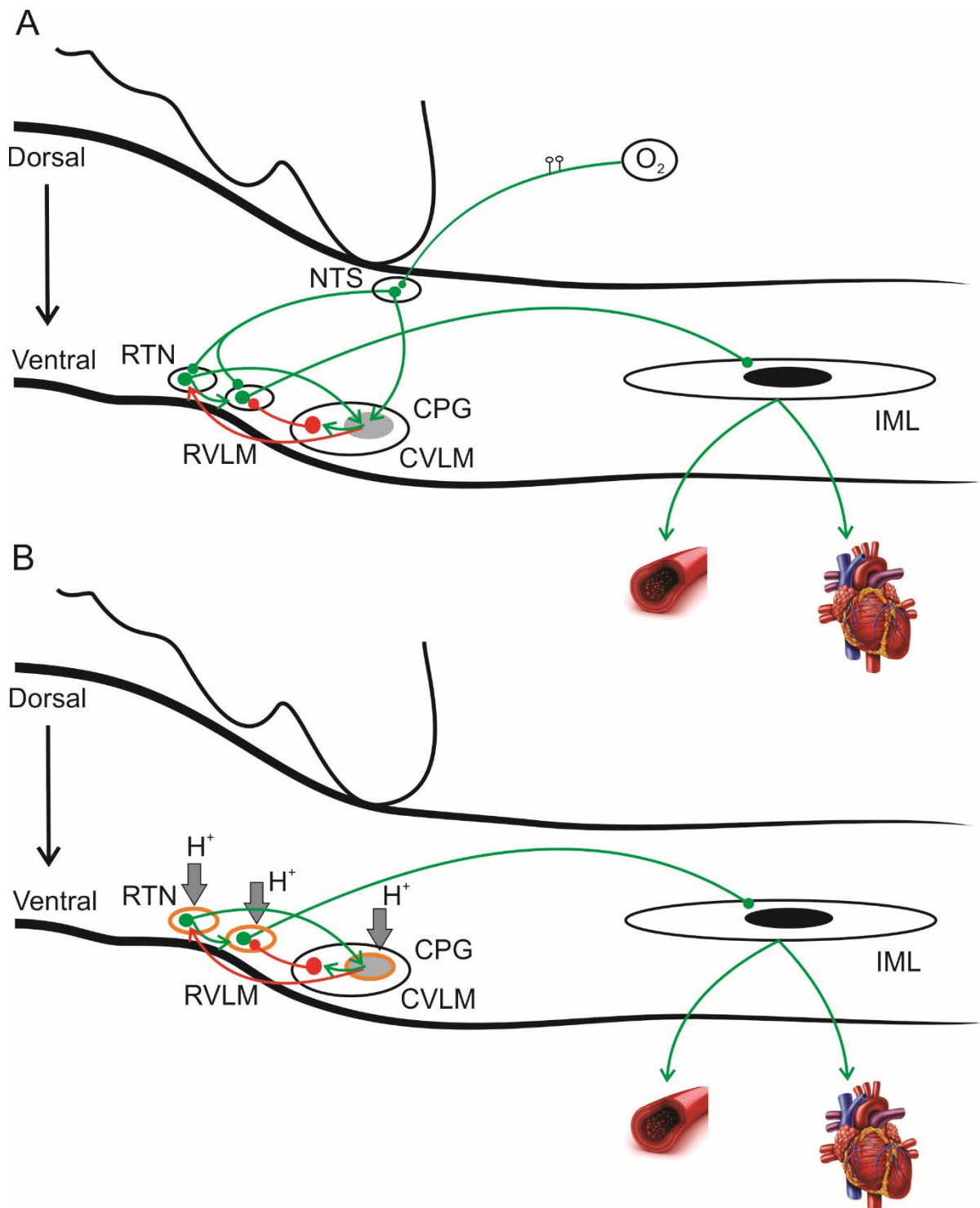
Intermittent activation of the chemoreflex, with injections of KCN (potassium cyanide), increased Fos-ir in the posterior parvocellular, the ventromedial parvocellular and the dorsal cap regions of the PVN (Cruz et al., 2008). Further to this, some of these Fos-ir PVN neurons were RVLM-projecting, but not NTS-projecting neurons (Cruz et al., 2008).

Figure 1.9: Sympathetic chemoreflex pathways

Increased SNA to peripheral organs is primarily due to increased nerve discharge of SPGNs located in the IML cell column of the spinal cord. This increased nerve discharge of SPGNs is driven by the excitatory output from bulbospinal sympatho-excitatory neurons of the RVLM.

A. Activation of **peripheral chemoreceptors**, by changing O_2 levels, causes activation of RVLM neurons via 2 pathways, a direct input from the NTS and a di-synaptic input relaying to the RTN. RTN neurons are intrinsically chemosensitive and thus, RTN→RVLM pathway is also affected by central chemoreceptors. Furthermore, activation of peripheral chemoreceptors also drives the CPG via NTS neurons. Respiratory-phasic activation of the CPG causes active inhibition of RVLM neurons via CVLM GABAergic neurons, and causes a disfacilitation of RVLM neurons via reduction in the discharge from RTN. In summary, these 2 processes attenuate the activation state of RVLM neurons during chemoreceptor stimulation and are responsible for respiratory modulation of SNA.

B. Activation of **central chemoreceptors** by changes in pH and CO_2 occurs in several brainstem sites, such as the RVLM, the RTN and the CPG, which are intrinsically chemosensitive (circled in orange). Increased SNA, in response to changes in pH and CO_2 , is driven via activation of the bulbospinal sympatho-excitatory neurons of the RVLM. Respiratory modulation of RVLM neurons and SNA has the same mechanism as in the case of the peripheral chemoreflex (CPG mediated inhibition of the RVLM via the CVLM and CPG mediated disfacilitation of the RVLM via the RTN). In addition to this, RVLM neurons are also chemosensitive. Chemosensitive RTN neurons are the principal source of CO_2 sensitive drive to the RVLM and the CPG. The scheme only applies to the effect of chemoreceptors on baro-regulated sympathetic efferents that control the heart and resistance vessels. The scheme is not applicable to other efferents such as skin and brown adipose fat. Excitatory neurons in green (large circles, cell bodies; small circles, ionotropic glutamatergic synapses; green arrows, neurochemically uncharacterised excitatory connections). In red, GABAergic CVLM neurons. Red arrow, neurochemically unidentified inhibitory input from the CPG to RTN neurons. Green lines show excitatory pathways and red lines show inhibitory pathways. CPG, central pattern generator; RTN, retrotrapezoid nucleus; RVLM; rostral ventrolateral medulla; CVLM, caudal ventrolateral medulla; NTS, nucleus of the solitary tract; O_2 , oxygen; IML, intermediolateral cell column of the spinal cord. (Adapted from (Kapoor et al., 2015; Moreira et al., 2006; Pilowsky et al., 2009)).



1.3.3 Somatosympathetic reflex (SSR)

The SSR pathway is involved in integration of signals from peripheral nociceptors located in the skin, muscle, joints and bone (sensitive to mechanical, chemical or temperature stimuli) with cardiovascular nuclei in the brain (Figure 1.10). For example, acute pain and exercise caused an increased HR, BP and muscle SNA (Burton et al., 2009; Kozelka et al., 1981). Increases in SNA in response to the SSR is mediated at both levels, spinal and supra-spinal levels (such as the RVLM). Two types of SSR pathways have been identified, 1) Spinal-SSR (dominant after spinal transection leading to loss of supra-spinal control) – peripheral information → spinal interneurons → SPGNs that affects SNA, 2) Spinal-bulbo-spinal-SSR (dominant in intact anatomy) – peripheral information → spinal interneurons → bulbospinal brainstem regions → SPGNs that affects SNA (Sato et al., 1967; Sato and Schmidt, 1971).

Spinal interneurons, located in the dorsal horn of the spinal cord (Figure 1.10) (Kozelka et al., 1981), receive afferent information from many peripheral receptors such as myelinated and unmyelinated nociceptors, visceral, cutaneous and muscle receptors (Pilowsky et al., 2009; Sato and Schmidt, 1973). These spinal interneurons then propagate the nociceptive stimulus to supra-spinal sites, such as the RVLM (Figure 1.10) (Burke et al., 2011; Makeham et al., 2005; Miyawaki et al., 2001; Stornetta et al., 1989). Activated RVLM neurons, in response to afferents from SSR sites, serve as sympathetic premotor nuclei, and enhance the activity of SPGNs in the IML of the spinal cord; thus increasing BP, HR and affecting SNA (Figure 1.10) (Stornetta et al., 1989).

Electrical stimulation of the sciatic nerve, in anaesthetized cats, produced two kinds of reflex potentials in the lumbar sympathetic trunk, 1) early reflex potential (ERP) characterized by a higher threshold and short latency, and 2) late reflex potential (LRP) characterized by a lower threshold and longer latency (Miyawaki et al., 2001; Sato et al., 1965). Spinal transection of C1 to T8 levels of the spinal cord diminished the LRP, whereas transection of medulla oblongata abolished the ERP (Sato et al., 1965). These findings indicated that the reflex center of LRP is located in medulla oblongata, and that of ERP is in the spinal cord (Sato et al., 1965). In addition to ERP and LRP, another phase “very late reflex potential” was observed when the lumbar white rami was recorded (Sato and Schmidt, 1971; Sato, 1972). This very late discharge was only seen in animals under light anaesthesia, and was reported to be mediated by supra-pontine brain structures (Sato and Schmidt, 1971; Sato, 1972; Sato and Schmidt, 1973). Further to this, another study reported that reflexes evoked by myelinated afferent fibers are mediated through spinal, supra-spinal and supra-medullary areas of the CNS; whereas, reflexes evoked by

unmyelinated afferent fibers are mediated through spinal and supra-spinal areas of the CNS (Janig et al., 1972).

Electrical stimulation of somatic nerves resulted in a pressor response characterised by an increase in BP and SNA (Sato and Schmidt, 1973). The sciatic nerve is a peripheral nerve that contains afferent nociceptors, and is, commonly, artificially stimulated to evoke a SSR response. Pressor response (increased BP and tachycardia) observed following electrical stimulation of the sciatic nerve was significantly reduced after chemical inhibition (with muscimol) of the RVLM (Kawabe et al., 2007). In addition to the RVLM, the NTS plays an important role in the SSR response. Bilateral chemical inhibition of the medial NTS in anesthetized rats, with muscimol, exaggerated the pressor response and tachycardia to the sciatic nerve stimulation (Kawabe et al., 2007). Microinjection of morphine into the intermediate and the caudal NTS of anesthetized rats caused a significant augmentation of the SSR response (Min Li et al., 1996). The SSR response augmentation induced by microinjection of morphine into the NTS was suggested to be either due to suppression of inhibitory baroreceptor information, or augmentation of excitatory chemoreceptor information (Min Li et al., 1996). Whereas, microinjection of morphine into the CVLM, or the LC, had no effect on the SSR response (Min Li et al., 1996).

Presence of crosstalk between the baroreflex and the SSR system was revealed by Kawabe and colleagues in 2007. Complete denervation of baroreceptor afferents or blockade of ionotropic glutamate receptors in the medial NTS of anesthetized rats caused an exaggeration of pressor response to the sciatic nerve stimulation (Kawabe et al., 2007). Vice versa, baroreflex stimulation, via electrical stimulation of the ADN, drastically reduced the pressor response seen after stimulation of the sciatic nerve (Kawabe et al., 2007). Further to this, activation of the chemoreflex, by hypercapnia, reduced the SSR response (Makeham et al., 2004), contrary to the suggestion made by Min et al., (1996), which states that activating the chemoreflex may enhance the SSR response (Min Li et al., 1996).

- *Role of the RVLM in modulation of the SSR (Figure 1.10)*

Pressor response to the SSR is suggested to be mediated via non-NMDA receptors in the RVLM. Blockade of non-NMDA receptors, prior to electrical stimulation of the sciatic nerve, markedly attenuated the pressor response (Kiely and Gordon, 1993).

Single nerve stimuli evoked an early and a late excitation of bulbospinal RVLM sympatho-excitatory neurons that paralleled, and preceded, biphasic increases in splanchnic SNA; this

demonstrated that the activation pathway of the SSR, mediated by the RVLM, involves both fast and slow conducting RVLM axons (Morrison and Reis, 1989) (Figure 1.10). Blockade of RVLM neurons, with muscimol, abolished the RVLM mediated peaks following electrical stimulation of the sciatic nerve (Burke et al., 2008). However, bilateral microinjection of SST in the RVLM eliminated first peak of the SSR response, indicating that SST inhibits a fast conducting sub-population of RVLM neurons that play an important role in the SSR (Burke et al., 2008; Burke et al., 2011) (Figure 1.10).

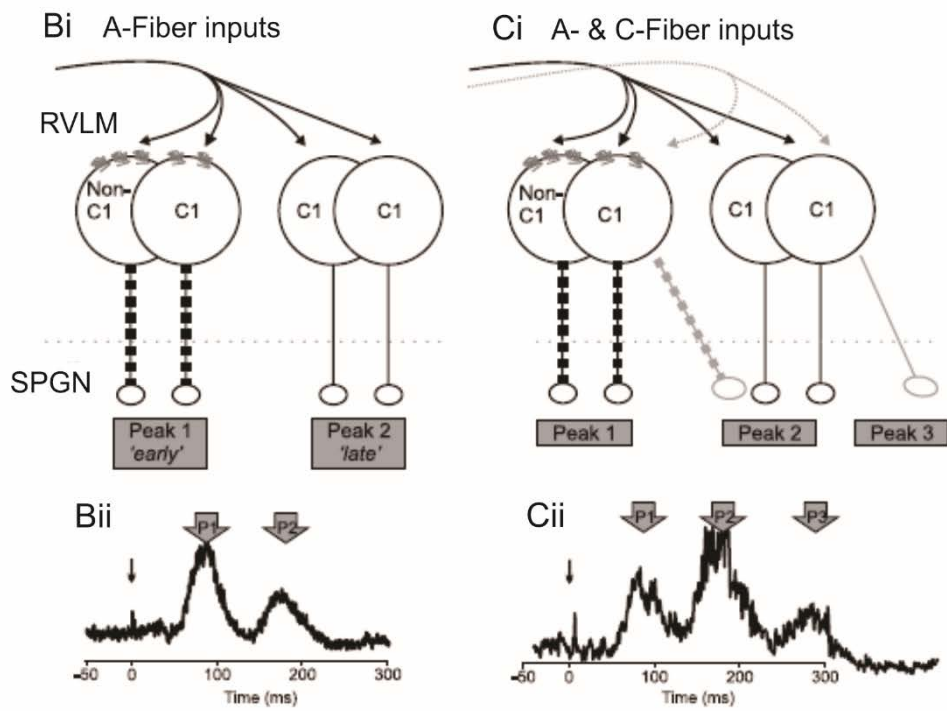
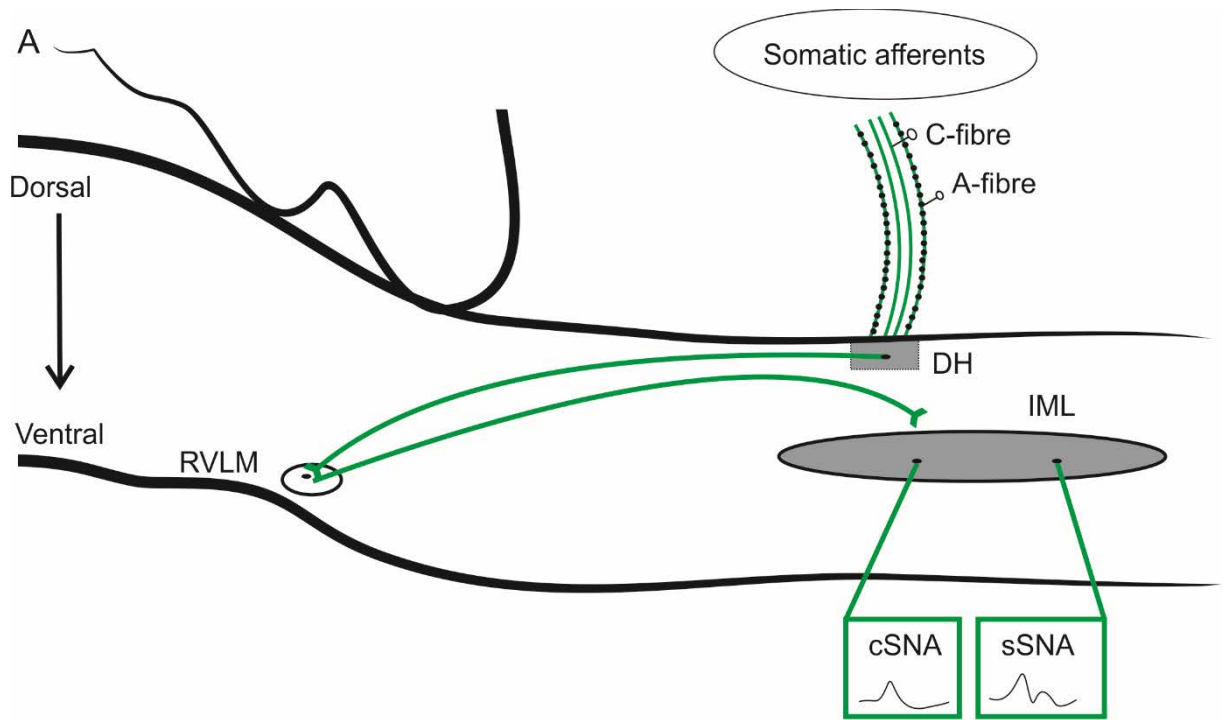
The sympathetic response to the SSR activation is highly dependent on target of the sympathetic output. For example, high intensity electrical stimulation of the sciatic nerve, activating A- and C- fibre afferents, evoked a biphasic response in the splanchnic SNA (Figure 1.10), whereas the same stimulation evoked a monophasic response in the cervical SNA (Figure 1.10) (McMullan et al., 2008). On the other hand, low intensity electrical stimulation of the sciatic nerve activating A-fibre afferents also evoked a biphasic response in SNA of renal, lumbar and splanchnic nerves, and evoked a monophasic response in the cervical SNA (Figure 1.10) (Burke et al., 2011). Stimulation of the ADN prior to stimulation of the sciatic nerve abolished the monophasic response in cervical SNA; whereas, it only abolished the first peak of splanchnic SNA leaving the second peak intact (McMullan et al., 2008). A potent inhibitory response to stimulation of the sciatic nerve exists in sympathetic nerves and most cardiovascular RVLM neurons (McMullan et al., 2008; Morrison and Reis, 1989; Wyszogrodski and Polosa, 1973).

Unmyelinated RVLM neurons are slow conducting neurons, which presumably belong to the C1 sub-population of RVLM neurons (Figure 1.10) (Schreihofer and Guyenet, 1997), and innervate splanchnic, lumbar and renal sympathetic nerves (Burke et al., 2011). Myelinated C1 and non-C1 neurons of the RVLM are fast conducting neurons, which innervate most of the sympathetic outflows: renal, lumbar, splanchnic and cervical (Figure 1.10) (Burke et al., 2011).

Activation of 5-HT_{1A} (Miyawaki et al., 2001), NK1 (Makeham et al., 2005), neuropeptide Y (Kashihara et al., 2008), or delta opioid receptors (Miyawaki et al., 2002b), in the RVLM significantly attenuated the SSR response. In addition to these, microinjection of morphine into the RVLM caused an augmentation of the SSR response, mediated by C-afferent fibres (Min Li et al., 1996).

Figure 1.10: The Somatosympathetic reflex (SSR) pathway

A. Afferent nociceptive pathways, myelinated (A-fiber) or unmyelinated (C-fiber), enter the spinal cord via the dorsal horn (DH). These afferent pathways activate local circuits, and activate neurons in the RVLM (green), in turn modulating the sympathetic output to periphery, via SPGNs in the IML cell column of the spinal cord (green). Activation of the SSR pathway generates a single peak in the cervical sympathetic nerve (cSNA), and two peaks in the splanchnic sympathetic nerve (sSNA). B and C. Schematic model illustrating the proposed mechanism by which stimulation of myelinated and unmyelinated somatic afferents generate patterns of sSNA. *Bi*: A-fiber inputs simultaneously activate fast (myelinated, thick hatched lines) and slow (unmyelinated, thin lines) conducting bulbospinal, sympatho-excitatory RVLM neurons and evoke a biphasic response in sSNA. *Bii*: sSNA biphasic response generated following low-intensity somatic afferent stimulation. *Ci*: C-fiber inputs (grey arrowed dotted lines) activate a subset of fast- and slow-conducting bulbospinal, sympatho-excitatory RVLM neurons ≈ 100 ms after the A-fiber activation (black arrowed lines). Hence, a second biphasic volley activates sSNA (grey inputs to *peaks 2 and 3*). The second sympathetic peak (P2, 190 ms) is a summation of both slow-conducting bulbospinal RVLM neurons activated by A-fiber afferents, as well as fast-conducting bulbospinal RVLM neurons activated by C-fiber afferents. The third sympathetic peak (290 ms) is generated by slow-conducting bulbospinal C1 neurons activated by C-fiber afferents. *Cii*: sSNA triphasic response generated following high-intensity somatic afferent stimulation. Small black arrows in *Bii* and *Cii* indicate time at which the stimulus is applied. DH, dorsal horn; RVLM, rostral ventrolateral medulla; IML, intermediolateral cell column of the spinal cord; C1, catecholaminergic neurons of the RVLM. (Adapted from (Burke et al., 2011; McMullan et al., 2008; Pilowsky et al., 2009).



1.4 Glia in CNS

Glia, derived from a Greek word meaning “glue”, are different from nerve cells; these cells do not directly participate in the synaptic transmission of signals between neurons. Glia were first described, by Virchow in 1846, as a connective tissue of the brain responsible for holding the brain together, and hence the name glia (Virchow, 1846). However, their ability to communicate with neurons, and impact neuronal physiology, affects synaptic transmission of signals (Funk et al., 2015). Glia are morphologically characterised by numerous processes extending from their cell bodies (Kettenmann et al., 2011). There are 3 types of glial cells in the CNS: astroglia, oligodendrocytes and microglia (Funk et al., 2015) (Figure 1.11).

1.4.1 Astroglia/astrocytes

Astrocytes form an integral component of the CNS while playing an important role in synaptic health (Figure 1.11B and 1.12), and originate from radial glial cells and oligodendrocyte precursor cells (Funk et al., 2015). Abnormal astrocytic physiology plays an important role in the pathogenesis of many neurodegenerative disorders, such as Huntington’s disease (Kim et al., 2015; Vis et al., 1998). Immunohistochemically, reactive astrocytes can be identified with antibodies raised against glial fibrillary acid protein (GFAP) (Funk et al., 2015; Kim et al., 2015). Broadly, astrocytes can be divided into 2 main categories, 1) Protoplasmic astrocytes that are found in grey matter and ensheath synapses and blood vessels with their processes, and 2) Fibrillary astrocytes that are found in white matter and are in contact with nodes of Ranvier and blood vessels (Funk et al., 2015; Sofroniew and Vinters, 2010). A single astrocyte can contact multiple synapses and fine blood vessels (Ventura and Harris, 1999).

A very important role of astrocytes in synaptogenesis was revealed in 1997, by Pfrieger and Barres, when *in vitro* retinal ganglion cells failed to show any significant synaptic activity (Pfrieger and Barres, 1997). In contrast, when purified retinal ganglion cells were co-cultured with astrocytes, or astrocytic conditioned media, the synaptic activity of retinal ganglion cells increased by ≈ 100 fold (Pfrieger and Barres, 1997). Another study showed that synapses formed in the absence of astrocytes are immature, and the presence of astrocytes was essential for the formation of mature, functional, synapses in the CNS (Ullian et al., 2001). The role of astrocytes in synaptogenesis can be attributed to their ability to release factors such as thrombospondin (Christopherson et al., 2005) and glia derived cholesterol (Mauch et al., 2001).

Inter-astrocytic communication, or astrocyte-neuron communication, is mediated by changes in their intracellular calcium concentrations (Charles et al., 1991). Enhanced astrocytic intracellular calcium concentrations can be triggered by changes in neuronal activity, and can augment the release of transmitters from astrocytes, such as glutamate, which affects neurons and other astrocytes (Sofroniew and Vinters, 2010; Volterra and Meldolesi, 2005).

Main role of astrocytes is in the maintenance of extracellular factors around synapses, such as fluid (Simard and Nedergaard, 2004), pH (Mulkey and Wenker, 2011; Obara et al., 2008), and ion balance (Simard and Nedergaard, 2004), thus ensuring a healthy synaptic transmission (Figure 1.11B) (Funk et al., 2015; Sofroniew and Vinters, 2010). Astrocytes also express high levels of transporters for neurotransmitters, such as glutamate (Sattler and Rothstein, 2006), hence preventing a glutamate mediated excitotoxicity (Figure 1.11B). Thus, astrocytes are treated as an integral physical component of synapses, giving rise to the concept of ‘tri-partite synapses’; consisting of pre-synaptic structure, astrocytic process and post synaptic structure (Figure 1.11A) (Perea et al., 2009). The term ‘tri-partite synapses’ refers to an important role of astrocyte in the synaptic physiology i.e. astrocytes are not only involved in a bi-directional communication with pre-, and post-, synaptic elements, but are also capable of influencing synaptic activity (Eroglu and Barres, 2010; Perea et al., 2009). Astrocytes can conduct many activities, such as glutamate uptake and release various transmitters (such as ATP), to maintain a healthy synaptic transmission (Figure 1.11B) (Sofroniew and Vinters, 2010).

Furthermore, recent work has accepted astrocytes as key chemosensory cells of the CNS (in addition to chemosensitive neurons; section 1.3.2.2) (Funk, 2010) (Figure 1.12). Astrocytes are an important source of ATP (Funk, 2010) and purinergic signalling pathways are key in the modulation of respiratory pathways (Alvares et al., 2014; Huxtable et al., 2009; Lorier et al., 2007; Miles et al., 2002; Zwicker et al., 2011). Therefore, astrocytes play a key role in the modulation of respiratory rhythm and the sympathetic chemoreflex pathways (Funk, 2013; Funk et al., 2015; Huxtable et al., 2010; Mulkey and Wenker, 2011; Rajani et al., 2015). Reductions in partial pressure of O₂ was sensed by astrocytes, and caused elevations in their intracellular calcium concentrations, mitochondrial depolarization and release of calcium from their intracellular stores (Angelova et al., 2015).

Figure 1.11: Relationship between neurons and members of the ‘Glial family’ in the CNS

In panel A., Astrocytes (green) are closely apposed to synaptic junctions between neurons, forming an integral component of the tri-partite synapse (pre-synapse, post-synapse and an astrocytic process). B. Green box represents the role of astrocytes in a healthy CNS. Astrocytes have processes in contact with synapses, blood vessels and Nodes of Ranvier. Astrocytes can also couple with neighboring astrocytes through gap junctions formed by connexins (inter-astrocytic communication). Astrocytes play an important role in synaptic health by maintaining levels of fluid, ion, pH and neurotransmitters (such as glutamate, GABA and glycine) in the synaptic interstitial fluid. Astrocytic contact with blood vessels enables astrocytes to titrate blood flow (by releasing factors such as NO) according to levels of synaptic activity, and to replenish the energy requirements (such as glucose) of neuronal environment. PGE, prostaglandins; NO, nitric oxide; AA; arachidonic acid. (Figure and legend adapted from (Sofroniew and Vinters, 2010); used with permission). In panel A., oligodendrocytes (blue) are supportive cells of the CNS, and their primary role is to myelinate neurons. C. Blue box represents the role of oligodendroglial exosomes in neuron-glia communication. (1) Electrically active axons release glutamate that provokes Ca^{2+} entry through oligodendroglial glutamate receptors. (2) Elevation of intracellular Ca^{2+} levels triggers exosome release from oligodendrocytes. (3) Neurons internalize exosomes and use their cargo. Ca^{2+} , calcium; NMDAR, NMDA receptor; AMPAR, AMPA receptor; MVB, multi-vesicular bodies. (Figure and legend from (Frühbeis et al., 2013); used with permission). In panel A., microglia (red), like astrocytes, are also closely apposed to synaptic junctions. D. Red box represents the role of microglia in phagocytosis of live cells (such as neuronal precursor cell, glioma cell and neutrophils) and neuronal structures (such as synapse) (Figure and legend adapted from (Brown and Neher, 2014); used with permission)

CHAPTER 1 – LITERATURE REVIEW

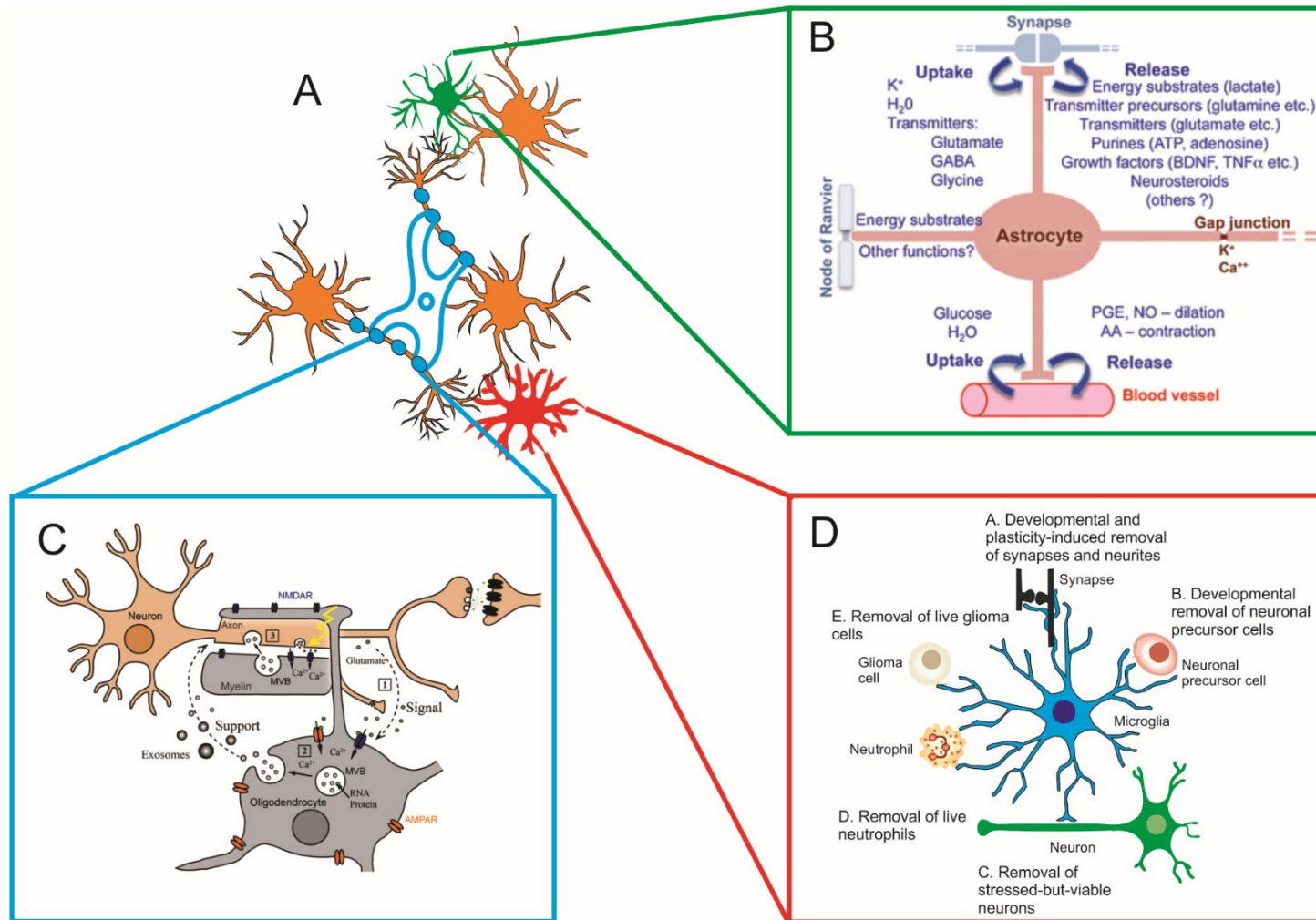
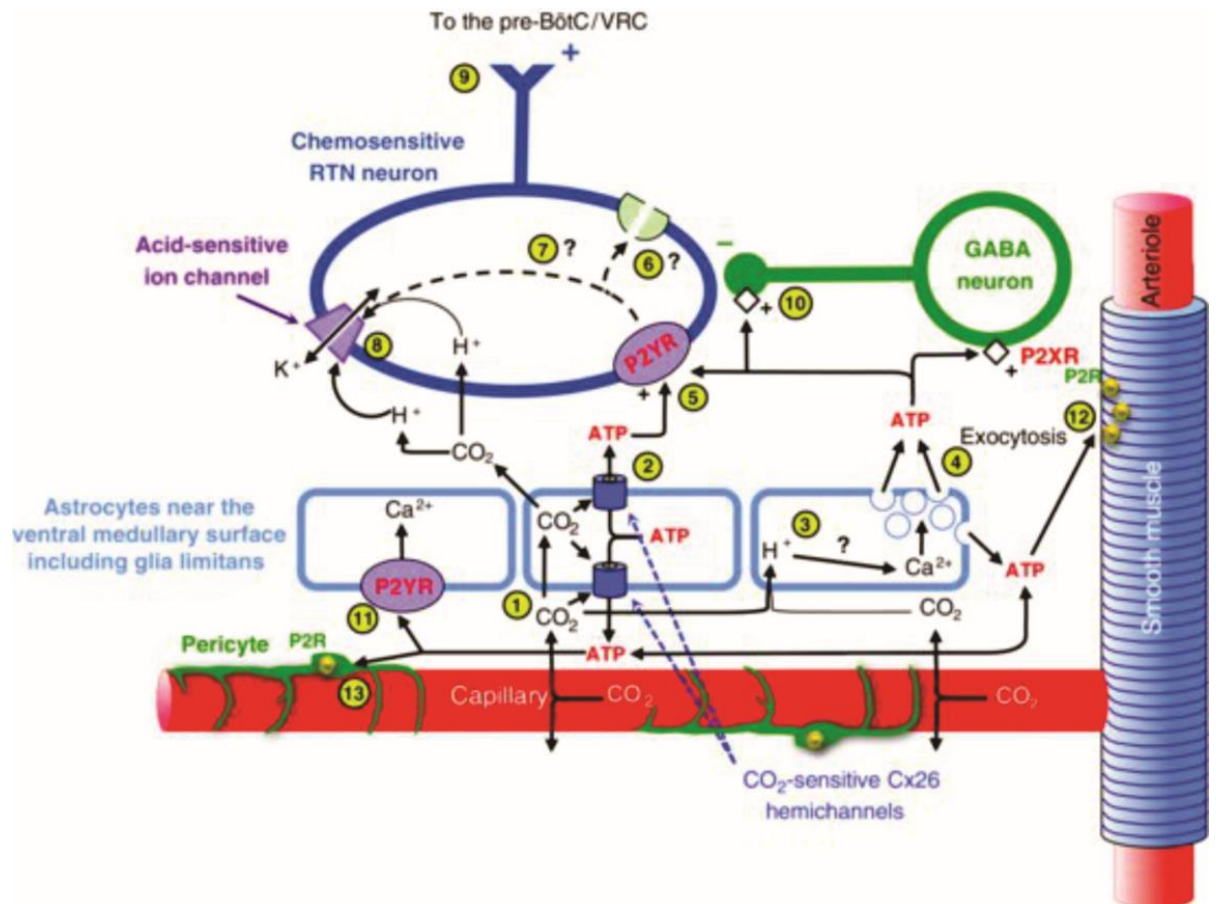


Figure 1.12: Schematic of P2R signalling and its contribution to central chemosensitivity in the retrotrapezoid nucleus (RTN).

Elevated CO₂ in the blood diffuses across the blood vessel/capillary wall, increasing CO₂ and H⁺ in the extracellular space surrounding neurons and astrocytes (1). Astrocytes near the ventral medullary surface including those in the glia limitans respond in two ways. Depicted in the middle astrocyte, elevated CO₂ (intracellular or extracellular) evokes release of ATP through CO₂-sensitive Cx26 hemichannels (i.e., Cx26 hemichannels act as the CO₂ sensor) (2). Depicted in the right astrocyte, CO₂ or H⁺ also cause the release of intracellular Ca²⁺ (3) and Ca²⁺-dependent, exocytotic release of ATP (4). ATP released via one or both of these mechanisms excites chemosensitive RTN neurons through a P2Y (5), G-protein coupled receptor-dependent mechanism that either modulates an unknown membrane conductance (6) or acid-sensitive ion channels directly (7). RTN neurons are also directly sensitive to intra- or extracellular acidification; the H⁺ sensor may be a K⁺ channel that is open at rest and closes in response to increased H⁺ (8). Note, however, that while closure of a K⁺ channel is strongly implicated in the depolarization of RTN neurons by acid, there is no direct evidence that the depolarization is produced by the direct action of acid or CO₂ on the K⁺ channel. Increased output from the RTN to the ventral respiratory column (VRC) including the pre-BötC (pre-Bötzinger) (9) causes ventilation to increase. The ATP-dependent excitatory processes mediate approximately 25% of the central chemosensory response. The remainder of the response reflects direct activation of RTN and other chemosensory neurons. Additional actions of extracellular ATP appear to include a P2XR-mediated, presynaptic excitation of inhibitory GABAergic inputs to RTN neurons (10) (the factors determining the balance to excitatory P2Y and indirect inhibitory P2XR mechanisms are not known) and an autocrine/paracrine P2YR-mediated excitation of astrocytes (11). ATP also has complex actions on the vasculature. Under conditions of normal oxygenation in other brain regions, ATP causes the contraction of vascular smooth muscle (12) as well pericytes (13). The resultant reduction in blood flow is hypothesized to increase the CO₂/pH stimulus and increase the response of local neurons/astrocytes. However, under conditions of reduced oxygen (hypoxia), there is growing evidence that the effects of ATP on both smooth muscle and pericytes reverses and facilitates restoration of blood flow to the hypoxic tissue. Whether the hypoxia-dependent effects of ATP on the vasculature influence CO₂/pH sensitivity of any respiratory chemosensory structure remains to be established. (Figure and legend from (Funk, 2013); used with permission)



1.4.2 Oligodendrocytes

Oligodendrocytes, initially called inter-fascicular glia, were first described by Rio Hortega in 1920s (Hortega, 1928), and arise from dedicated oligodendrocyte precursor cells (Funk et al., 2015). Oligodendrocytes' precursors originate from neuro-epithelial cells of ventricular zones during early stages of embryonic life (Bradl and Lassmann, 2010). Oligodendrocytes are capable of myelinating multiple axons; while its equivalent in periphery – the schwann cell – can only myelinate one segment of axon at a time (Figure 1.11C) (Bradl and Lassmann, 2010).

Gaps in myelin sheath along the axon are called nodes of Ranvier; at these nodes, axonal membrane is in direct contact with the extracellular space (Bradl and Lassmann, 2010; Bunge et al., 1962). Nodes of Ranvier allow fast saltatory conduction along axons, i.e. signal can jump from one node to another, rather than progressing slowly along axon (Bradl and Lassmann, 2010). Length of axons seem to participate in regulating the thickness of myelin, with thicker myelin sheaths found around longer axons (Waxman and Sims, 1984).

The main role of oligodendrocytes is in the formation of myelin sheath (rich in lipids and low water content) around axons with diameter above 0.2 μm (Figure 1.11C) (Bradl and Lassmann, 2010). Myelin sheath, due to its composition, leads to electrical insulation of axons, and supports fast conduction of electrical signals in nerve fibers over long distances. Direct close connections were demonstrated, by electron microscopy, between oligodendrocytes and myelin sheath (Bunge et al., 1962). Oligodendrocytes send out sail-like extensions of their cytoplasmic membrane, each of which forms a segment of myelin sheath around an axon.

A set of studies have shown that the onset and extent of myelination is dependent on electrical activity of neurons. Optic nerves of mice, reared in the dark, developed fewer myelinated axons (Gyllenstein and Malmfors, 1963), and myelination could be inhibited by blockade of sodium-dependent action potentials in developing optic nerves (Demerens et al., 1996). Vice versa, increased neuronal firing, with α -scorpion, enhanced myelination process (Demerens et al., 1996), and myelination could also be accelerated by artificial eye opening in optic nerves of rabbits (Tauber et al., 1980). The proposed mechanism is that the firing of neurons leads to release of adenosine (Kuperman et al., 1964; Maire et al., 1984), which inhibits proliferation of oligodendrocyte precursor cells, promoting their differentiation and also accelerates the formation of myelin (Stevens et al., 2002).

1.4.3 Microglia

Microglia are the tissue resident macrophages in the CNS (Figure 1.11D); these are equivalent to Kupffer cells in the liver, Langerhans cells in the skin and intestinal macrophages in the gastrointestinal tract. The main role of any tissue resident macrophage, regardless of their location, is to respond to a disturbed homeostatic situation in a protective manner, and to promote, post-injury, removal of debris. Abnormal microglial physiology plays an important role in the pathology of many neurodegenerative disorders (Shaikh et al., 2012) such as Parkinson's disease (Green and Nicholson, 2008; Shaikh and Nicholson, 2009), Alzheimer's disease (Ma and Nicholson, 2004) and Huntington's disease (Ma et al., 2003). Microglia, and their role in the CNS, are discussed, in detail, in further sections.

1.5 Microglia

Until recently, microglia were considered to play a role solely as immune cells of the CNS, where they were responsible for a wide range of functions during CNS damage (Kettenmann et al., 2011). Developments in the field, since 2005 (Nimmerjahn et al., 2005), suggest that microglia are more than just immune cells of the CNS. In fact, it seems that microglia are guardians of the CNS at all times; constantly working to maintain the dynamic neuronal physiology within its homeostatic levels (Hughes, 2012).

1.5.1 Origin of microglia

Microglia, like all macrophages, are cells of mesodermal origin that populate the CNS tissue during early stages of development. Erythroid/myeloid progenitor cells in the yolk sac, during early development, differentiate into tissue resident macrophage progenitor cells. These tissue resident macrophage progenitor cells, with amoeboid morphology, migrate into the brain and invade the brain tissue as microglial cells (Cronk and Kipnis, 2013). These microglial cells are self-renewing (Ajami et al., 2007), in case of depletion during inflammatory conditions. However, under special defined circumstances, when microglial cells in the CNS are depleted and are unable to replenish their pool, monocytes from bone marrow are capable of replenishing tissue resident macrophages of the CNS. (Cronk and Kipnis, 2013)

1.5.2 History of microglia

Microglia were also previously known as "Hortega cells", after Pio del Rio-Hortega first described these cells in the CNS, around 1932 (Kettenmann et al., 2011). According to studies

performed by del Rio-Hortega, using a modified silver staining technique, microglia are of mesodermal origin and are homogeneously distributed cells of the CNS (Figure 1.13), known for their inflammatory response towards any pathological event disturbing homeostasis of the CNS (Kettenmann et al., 2011). Subsequently, many studies were performed that aimed to describe these microglial/ “Hortega cells” and characterise their functions, but the advances made by Pio del Rio-Hortega still set the benchmark (Kettenmann et al., 2011).

1.5.3 Conventional activation paradigm

1.5.3.1 Diverse microglial phenotypes

Taking advantage of modern immunohistochemical methods, it is possible to identify all microglia in the brain using antibodies to different markers, in addition to the morphology of the cell. Microglial morphology is a useful indicator of its activation state and its potential role. Broadly speaking, microglial morphologies have been classed into 3 categories; M0, M1 or M2 (Butovsky et al., 2014; Hu et al., 2012). The M0 microglial phenotype (Figure 1.13 and 14), represents microglia in their resting/surveillance stage, characterised by a small cell body ($\approx 10 \mu\text{m}$ diameter) (Kozłowski and Weimer, 2012) and long thin processes/ramifications. On the other hand, M1/M2 phenotypes (Figure 1.13 and 14) share similar morphological characteristics; these are amoeboid in shape with shorter or no processes, but differ in their activities. Iba1 (ionised calcium-binding adaptor molecule 1) is a calcium binding protein that is also a pan microglial marker. M0, M1 and M2 microglia express Iba1. Expression of CD16 and CD32 is specific to M1 microglial phenotype, whereas expression of CD206 is specific for M2 microglial phenotype (David and Kroner, 2011; Hu et al., 2012).

The M0, surveillance microglial phenotype, monitors their local environment for the presence of pathogens, or for changes in the extracellular concentration of constitutively expressed neurochemicals (including neurotransmitters such as neuropeptides, glutamate or GABA) (Nimmerjahn et al., 2005; Tremblay et al., 2011) (Figure 1.14). Polarization of the M0 phenotype to an M1/M2 phenotype signifies a marked activation of microglia. The M1 phenotype, also known as the neurotoxic microglial phenotype, is associated with increased mRNA expression of molecules such as IL-6, TNF- α and IL-1 β (Chhor et al., 2013; Crain et al., 2013) (Figure 1.14) that are all associated with apoptosis of cells expressing receptors for these molecules. The M2 phenotype, which is a neuroprotective phenotype, releases molecules such as IL-10. The M2 phenotype is anti-apoptotic, and promotes tissue repair (Crain et al., 2013) (Figure 1.14).

1.5.3.2 Activation pathway

Most of our understanding related to the activation of microglia, is based on findings from experiments performed *in vitro*, in either cultured microglia or in freshly prepared brain tissue slices; this situation may differ *in vivo*.

The conventional microglial activation paradigm is divided into 3 distinct stages: a **withdrawal**, a **motility** and a **locomotory stage** (Stence et al., 2001). Ramified resting / surveilling microglia (M0) on sensing the presence of an activation signal enter a **withdrawal stage**, where these cells start to retract their existing processes. Whilst still withdrawing their existing branches, microglia initiate the process of developing new, short ramifications, which are highly dynamic in nature, enabling microglia to become highly motile. Replacement of long microglial fimbria, with short highly dynamic protrusions, permits microglia to enter a **motile stage**. Even though, long processes exhibited by microglia in their **resting/surveilling stage** are already dynamic (Davalos et al., 2005; Li et al., 2012; Nimmerjahn et al., 2005), the replacement of these long dynamic processes with short, highly dynamic, protrusions enables these microglia to migrate long distances (Stence et al., 2001). In their motile state, microglia develop a large cell body and very short processes, enabling them to migrate towards the site of injury and participate in inflammation (M1) or non-inflammation (M2) related activities (Figure 1.14). This last state is known as the **locomotory stage**. (Stence et al., 2001)

In addition to the M0 morphological polarization to either M1 or M2, microglia also undergo intracellular re-arrangements enabling them to translocate their cell body through the tissue. Recent studies indicate that the non-muscle myosin II B (NMIIB) is one of many intra-microglial molecules involved in microglial movement (Janssen et al., 2014). Microglial activation triggers rearrangement of the cellular distribution of NMIIB, enabling amoeboid microglia to become motile (Janssen et al., 2014). Increased expression levels of cell adhesion molecules, such as integrins (Hailer et al., 1996), may also permit amoeboid microglia to be locomotory. While changes observed in the morphology of activated microglia are obvious, subtle changes introduced in extracellular matrix proteins, such as laminin (Milner and Campbell, 2002), is another equally crucial process facilitating microglial movement through tissue.

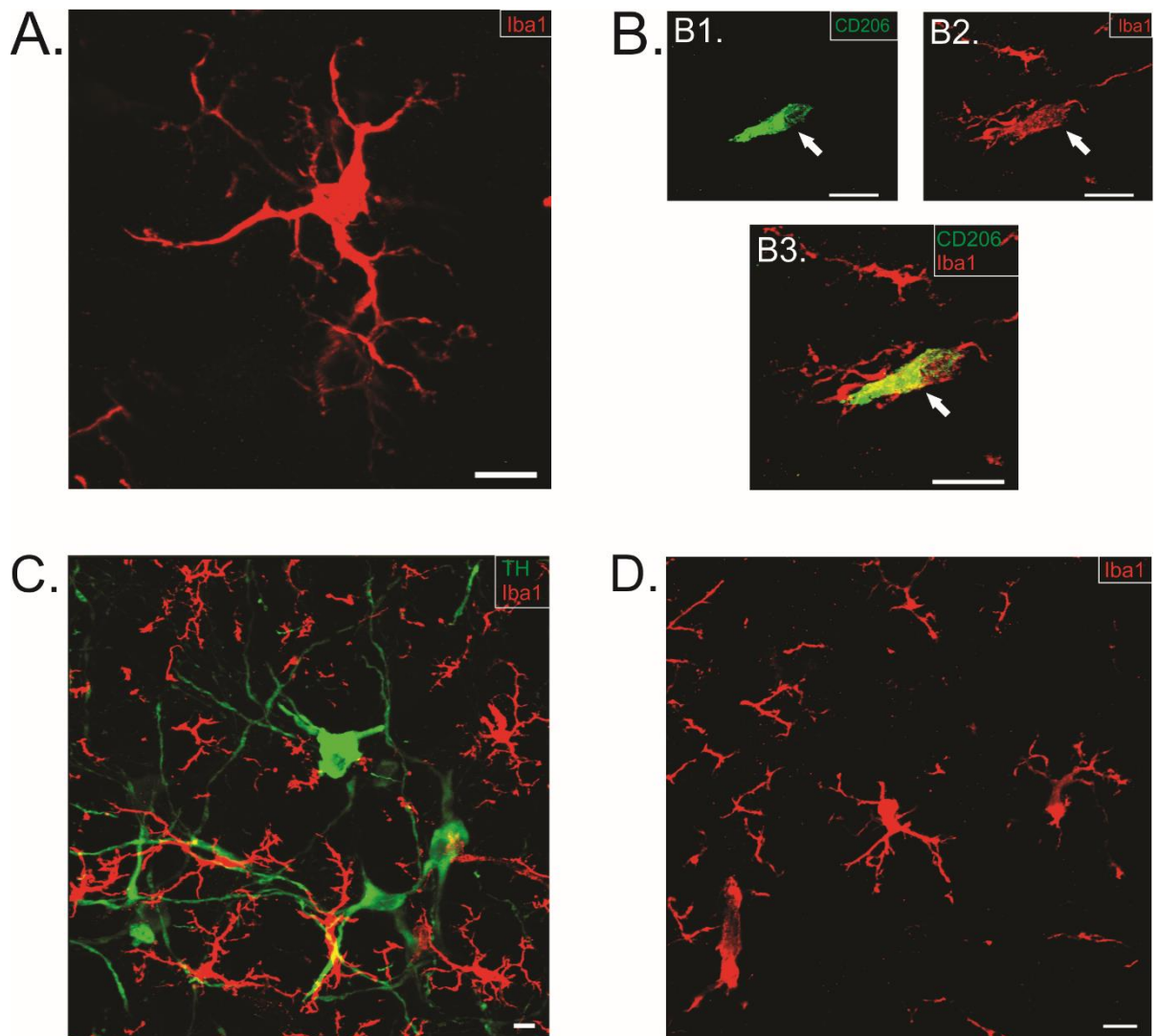


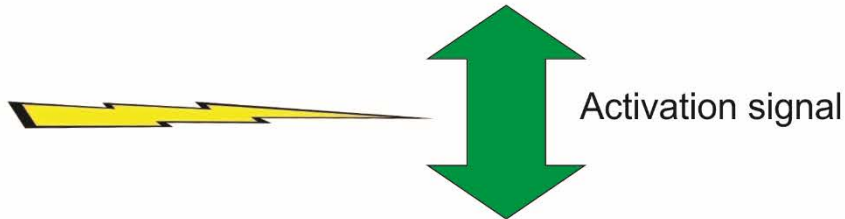
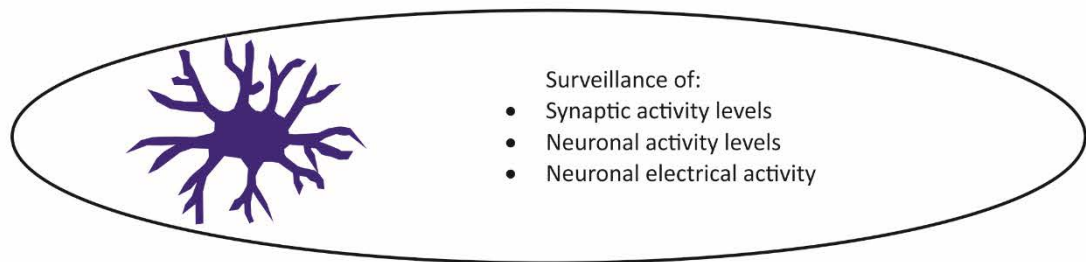
Figure 1.13: Microglia in cardiovascular sites of the brainstem involved in the sympathetic control of BP

A. Microglia in surveilling state in the brainstem of Sprague-Dawley (SD) rat. B. M2 positive microglia in the brainstem of a SD rat. B1. M2 microglial phenotype (CD206 positive, green). B2. Iba1 (red) positive microglia with an amoeboid morphology. B3. Merged image of B1 and B2 showing colocalisation of CD206 expression with Iba1 in M2 microglia. C. Microglia (Iba1, red) are intermingled with TH-ir (tyrosine hydroxylase-immunoreactive, green) neurons throughout the RVLM. D. Microglia (Iba1, red) in the CVLM region. Scale bar = 10 μm. (Z-stack images at 40X magnification were taken with the Zeiss Axio Imager Z2 epifluorescence microscope).

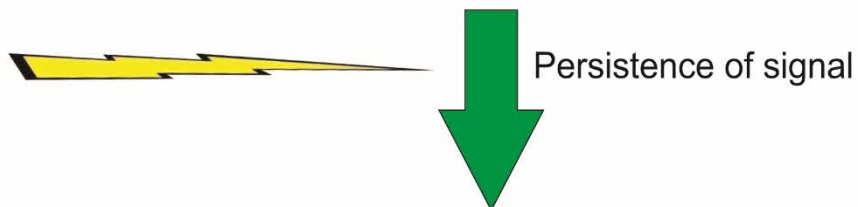
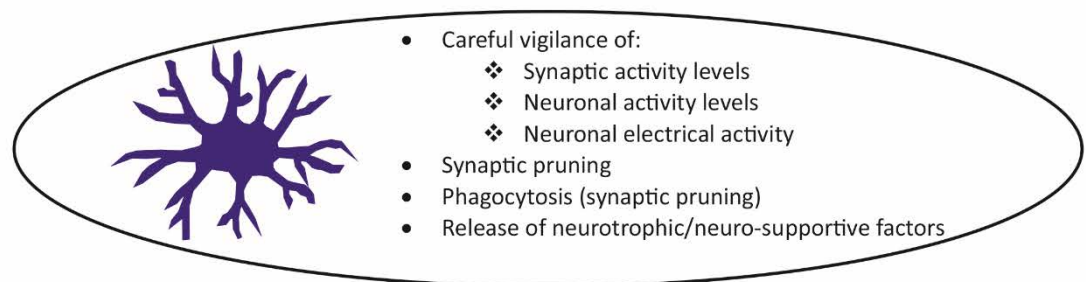
Figure 1.14: Activation stages of microglia in a healthy CNS, when subjected to a signal disturbing the homeostasis of the CNS

Surveilling/ resting microglia, in their highly ramified shape (M0), are distributed throughout the CNS. Sudden appearance or disappearance of any unexpected or expected molecule, respectively, triggers alertness in microglia. These “Alerted microglia” survey their local environment with extra vigilance, or conduct housekeeping activities to resume the CNS homeostatic levels. Due to persistence of the activation signal or when the CNS damage is permanent, M0 microglia polarize into either M1 (inflammatory) or M2 (anti-inflammatory) phenotype, depending on the situation. Although, M1 and M2 microglia perform different set of roles in the CNS, they do share a few functions and acquire similar morphology.

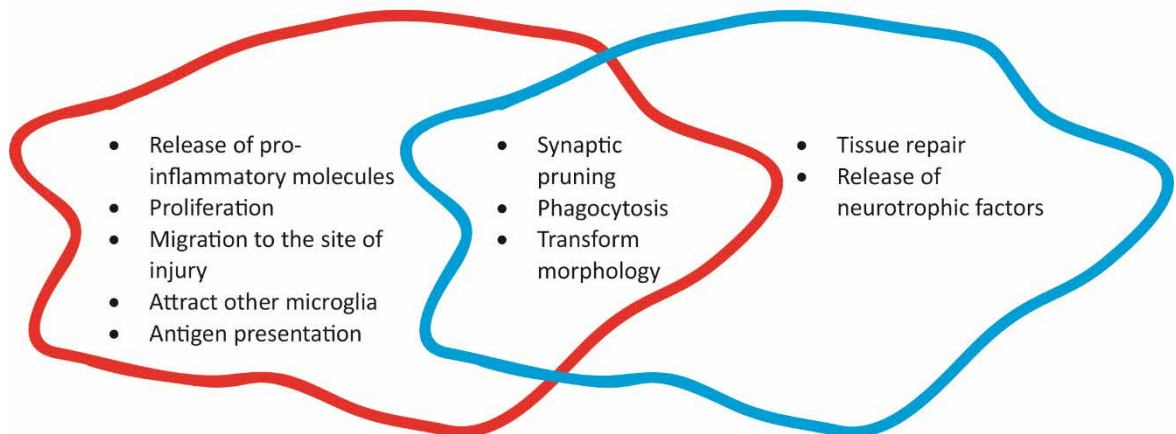
Surveilling/resting microglia (M0) - small cell body with long thin processes



Alerted microglia - morphology similar to M0 microglia



Activated microglia (M1/M2) - amoeboid morphology



1.5.4 Activation signals – “on” or “off”

Neurons are not simply passive recipients of microglial signalling. In fact, microglia and neurons are in constant, dynamic, communication thereby, affecting each other's physiological state. The ability of microglia and neurons to communicate, in response to changes in the extracellular environment, suggests a more subtle level of responsiveness by microglia, rather than being solely due to physical damage in the environment. Types of signals that alert microglia to changes in neuronal homeostasis are divided into 2 categories: “on” and “off” signals (Biber et al., 2007). “On” signals are defined as the appearance of unexpected molecules such as a pathogen or increases in the extracellular levels of intracellular constituents (released on cell death). Recently, the list of molecules leading to “on” signalling has been extended to include enhanced levels of neurotransmitters in the CNS. “Off” signalling, on the other hand, is triggered by the disappearance or disruption of constitutively expressed molecules, such as neurotransmitters or fractalkines (CX3CL1). (Biber et al., 2007; Hanisch and Kettenmann, 2007; van Rossum and Hanisch, 2004)

1.5.5 Microglial reaction to activation signal

Microglial perception of an activating signal and their response to the activating signal are 2 different processes. For example, addition of LPS (lipopolysaccharide) to cultured microglia can lead to the polarization of M0 to M1 (Butovsky et al., 2005); addition of IL-4 to cultured microglia results in the polarization of M0 to M2 (Butovsky et al., 2005). Appearance of both, LPS and IL-4, are examples of “on” signalling however, microglial reaction to these molecules are 2 different extremes of the spectrum. Our difficulty in understanding the role of microglia in normal physiological state, clearly identifies, a severe gap in our understanding concerning microglial function in the CNS.

1.6 Microglia and communication

1.6.1 Inter-microglial communication

Each microglial cell has its own surveilling territory (Figure 1.13), ranging from $\approx 15\ \mu\text{m}$ to $\approx 30\ \mu\text{m}$, and under normal conditions, microglia do not breach each other's territory (Figure 1.13C and D). However, exact molecular factors that determine the inter-microglial distance (IMD), and microglial pattern of distribution, are unknown. Microglia exhibit a heterogeneous distribution pattern, expression profile and morphology, which is highly region-specific (de

Haas et al., 2008; Lawson et al., 1990; Mittelbronn et al., 2001). Proteins expressed by microglia, which become evident during microglial responses to physiological and pathophysiological situations, are assumed to depend on the neuronal profile of their immediate environment (de Haas et al., 2008). A higher neuronal packing density may require more number of microglia, to maintain neurons in a healthy state. In addition, neuronal activity, and their release of signalling molecules, will further affect microglial expression profile. One can assume that the tessellated pattern of microglial distribution (Figure 1.13C and D) and precise inter-microglial distance is determined by a combination of neuronal packing density and neuronal activity levels, but this remains a matter of speculation.

Microglia release various factors such as cytokines, reactive oxygen species and neurotrophic factors, that not only affect neurons, but may also act on nearby microglia, and other cell types (such as astroglia, oligodendrocytes and blood vessels) in a paracrine signalling fashion (Kettenmann et al., 2011). Microglia also act as the antigen presenting cells in the CNS (Kettenmann et al., 2011) thereby, providing positive feedback to other microglia, and to infiltrating macrophages. Inter-microglial communication, over long distances, largely depends on the ability of microglia to translocate through the tissue, when in their amoeboid morphology.

1.6.2 Microglia and astrocytes

Even though the strands of communication between microglia and neurons are obvious, the importance of cross talk between microglia and astrocytes cannot be ignored. Astrocytes are an essential part of the CNS, mainly known for their supportive role towards neurons. Astrocytes play an important role in dampening the neurotoxic effects by microglia, such as release of iNOS (Pyo et al., 2003) and IL-12 (Aloisi et al., 1997). Microglia are also able to affect astrocytes. It was demonstrated that IL-1, released by activated microglia, promotes activation of astrocytes (Griffin, 2006). In addition, cultured astrocytes, treated with activated-microglial conditioned media, promote astrocytic gene expression of brain-derived neurotrophic factor (BDNF) (Savli et al., 2004) and astrocyte proliferation (Giulian and Baker, 1985).

1.6.3 Microglia and neurons

Since 2005, microglia are no longer considered to be passive or dormant cells in the CNS (Nimmerjahn et al., 2005). Rather, microglia are thought of as “busy bees” (Cronk and Kipnis, 2013) or the “constant gardeners” (Hughes, 2012) of the CNS. Microglia continuously monitor

their local environment, for the presence of any unexpected changes in the expression level of neurochemicals and other molecules. Microglia can also sense activity levels of synapses (Tremblay et al., 2010; Wake et al., 2009). In response to these changes, microglia constantly extend or retract their processes and survey the whole CNS over periods ranging from minutes to hours (Nimmerjahn et al., 2005). As the tip of the microglial process extends and contacts synapses, it enlarges, enabling the removal of excessive synaptic input, if necessary (Wake et al., 2009).

Microglia and neurons are in constant communication; this communication is possible because of the presence of receptors for nearly every neurotransmitter on the surface of microglia including: PACAP (pituitary adenylate cyclase- activating polypeptide), dopamine, substance P, glutamate and GABA (Pocock and Kettenmann, 2007) (Table 1.2). Microglia also express receptors for neurohormones/neuromodulators, such as neurotrophin (Kettenmann et al., 2011; Pocock and Kettenmann, 2007) (Table 1.2). Diverse range of receptors expressed by microglia allow them to perceive neuronal signals as an indicator of neuronal health and physiological levels. However, it is not yet clear whether or not neurons emit microglial-specific signals or the extent to which microglia detect neuron-neuron signalling.

Disruption to healthy neuron-neuron communication, leading to deviations in neuronal homeostasis, can lead to the development of neurological disorders such as Alzheimer's disease or hypertension, depending on the CNS area affected. Disturbances in an otherwise highly dynamic neuronal physiology are, more often than not, accompanied with changes in their neurochemistry, membrane potentials and concentration of molecules that diffuse across synapses in the extracellular matrix; these changes can be detected by microglia, as abnormal neuronal or synaptic activity (Biber et al., 2007; Hanisch and Kettenmann, 2007).

Recently, Glebov et al., (2015) showed that serotonergic neurons (derived from stem cells) stimulate the release of exosomes from microglia (Glebov et al., 2015). These exosomes may be one way by which microglia are provoked to release proteins, inflammatory molecules and cytokines, into the extracellular environment. Although this study (Glebov et al., 2015) was performed in a co-culture, *in vitro*, system, it does provide an example of direct microglia-neuron communication, driven by neurotransmitter release.

Some examples of microglial receptors corresponding to some commonly expressed neurotransmitters in the CNS include glutamate, GABA, purines, and peptides (see Table 1.2 for further examples).

1.6.3.1 Glutamate receptors

Glutamate is an excitatory neurotransmitter in the CNS. Glutamate receptors, broadly, can be divided into 2 subtypes: fast ionotropic (iGluRs) and slower metabotropic (mGluRs). Concerning iGluRs, evidence from transcription analysis has confirmed the presence of GluR1, GluR2, GluR3 and GluR4 on microglia (Kettenmann et al., 2011). Activation of glutamate receptors on microglia, via glutamate or kainate, can lead to the release of the pro-apoptotic peptide TNF- α (Hagino et al., 2004). iGluRs may also be involved in microglial chemotaxis; however, *in vivo* evidence in support of this idea is not yet available.

On the other hand, the evidence regarding the exact role of microglial mGluRs is controversial. Activation of group II mGluRs can enhance the neurotoxicity of microglia (Taylor et al., 2005). Whereas, activation of group III mGluRs tends to promote the neuroprotective effects of microglia (Taylor et al., 2003).

1.6.3.2 GABA receptors

Unlike glutamate receptors, the role of GABA receptors in microglial physiology is well established. GABA, acting on GABA receptors, is an inhibitory neurotransmitter and acts as a neuroprotective agent by acting on microglial GABA_A and GABA_B receptors (Lee, 2013; Pocock and Kettenmann, 2007). Both subunits of GABA_B receptors are expressed by microglia, with majority of them concentrated in the microglial lamellipodia (Kettenmann et al., 2011). Activation of GABA_B receptors in microglia, when subjected to LPS, can exert neuroprotective effects by reducing the release of inflammatory cytokines, such as IL-6 and IL-12 (Lee, 2013).

1.6.3.3 Purinergic receptors

Purinergic receptors, and their associated signalling systems, are found in almost all types of cells and tissues. The most abundant purinergic signalling molecule is adenosine triphosphate (ATP). ATP is a critical source of phosphate in kinase reactions that result in phosphorylation of intracellular proteins, and subsequent cellular activation. Purinergic receptors such as P2Y₆, P2Y₇, P2Y₈, P2Y₁₂ and P2X are abundantly expressed on the microglial surface (Funk, 2013; Pocock and Kettenmann, 2007). Broadly speaking, activation of purinergic signalling systems result in energy consuming processes, such as chemotaxis, movement of microglial fine ramifications, migration and cytokine release (Pocock and Kettenmann, 2007). Most ATP mediated functions are activated in response to physical injury. Activation of P2X₄ receptors on microglial surface may be a cause of chronic neuropathic pain (Inoue, 2006), and drugs that target these receptors are currently being actively investigated for clinical use.

Enhanced expression levels of P2X4 receptors, a type of P2X purinergic receptors, were observed in the spinal cord area in response to a nerve injury (Tsuda et al., 2003). Interestingly, this increased expression of P2X4 receptors was exclusive to microglia, and was not seen in either astrocytes or neurons (Tsuda et al., 2003). Furthermore, these P2X4 receptor positive microglia were found to be hyperactive (Tsuda et al., 2003), and pharmacological blockade of P2X4 receptors, *in vitro*, inhibited chemotaxis in microglia (Ohsawa et al., 2007). These, and many other studies (for review, see (Koizumi et al., 2013)), have provided a direct evidence of the role of purinergic receptors in the activation pathway of microglia.

1.6.3.4 Other neurotransmitter receptors

Microglia also express receptors for peptide neurotransmitters such as substance P and PACAP. Substance P activates neurokinin-1 (NK-1) receptors expressed by microglia, leading to activation of pro-inflammatory pathways, such as chemotaxis, and production of intracellular reactive oxygen species (Block et al., 2006; Rasley et al., 2002). Similarly, activation of bradykinin receptors expressed on microglial surface, can lead to enhancement of microglial motility features (Noda et al., 2003; Noda et al., 2006). Conversely, activation of PACAP receptors reduces chemokine production thereby, inhibiting the neurotoxic effects of microglia (Dejda et al., 2005).

Table 1.2: Neurotransmitter receptors and their corresponding functions in the sympathetic control of BP and microglia (based on data from *in-vitro* studies)

Neurotransmitter	SNS		Microglia	
	Effect	Reference	Effect	Reference
Angiotensin - II	Activates the AT ₁ receptor in circumventricular organs and exerts pressor effects via PVN and RVLM	(Cato and Toney, 2005; Li et al., 2003)	AT ₁ receptor expression is upregulated in response to LPS	(Miyoshi et al., 2008)
			Angiotensin-II activates microglia in PVN and causes an increased levels of pro-	(Shi et al., 2010)

			inflammatory cytokines	
			Angiotensin (1-7) exerts anti-inflammatory effects via Mas receptor expressed on microglia	(Liu et al., 2016)
Bradykinin	Microinjection of bradykinin in the RVLM elicits hypertensive effect	(Privitera et al., 1994)	Induces chemotaxis and enhances motility features	(Noda et al., 2003; Noda et al., 2006)
Dopamine	Microinjection of dopamine in the PVN results in decreased levels of renal SNA and BP in SD rats	(Zheng et al., 2014)	Stimulation of dopamine receptors enhances microglial migration abilities and suppresses nitric oxide production	(Farber et al., 2005)
GABA	Sympatho-inhibitory	(Guyenet, 2006)	Anti-inflammatory response in microglia	(Kuhn et al., 2004; Pocock and Kettenmann, 2007)
Galanin	Microinjection of galanin in the RVLM elicits a sympatho-inhibitory response by	(Abbott and Pilowsky, 2009)	Increases microglial motility	(Ifuku et al., 2011)

	decreasing BP and SNA			
	Microinjection of galanin in the respiratory sites of brainstem (BötC or PreBötC) causes a depression in the respiratory output	(Abbott et al., 2009)		
Glutamate	Sympatho-excitatory	(Guyenet, 2006)	Broadly, activation of glutamate receptors triggers pro-inflammatory responses (except mGluR group III)	(Pocock and Kettenmann, 2007)
Orexin	Microinjection of orexin A in RVLM causes a pressor and sympatho-excitatory response	(Shahid et al., 2012)	Microglial immunoreactivity for orexin 1 receptor increases with activation in response to traumatic brain injury	(Mihara et al., 2011)
			Orexin inhibits the ATP induced microglial motility	(Noda et al., 2011)
PACAP	Sympatho-excitatory	(Farnham et al., 2008;	Neuro-protective	(Dejda et al., 2005)

		Farnham et al., 2012; Inglott et al., 2011)		
Serotonin (5-HT)	Antagonism of 5-HT _{1A} receptor in RVLM blocks the hemorrhage induced sympatho-inhibition of SNS	(Dean and Bago, 2002)	Serotonin triggers the release of exosomes from microglia via 5-HT receptors	(Glebov et al., 2015)
SST	Microinjection of SST in RVLM causes a sympatho-inhibitory response and hypotension	(Burke et al., 2008)	Neuro-protective (inhibits microglial proliferation)	(Feindt et al., 1998)
Substance P	Microinjection of substance P analogue in the RVLM causes an increase in BP, HR and SNA	(Makeham et al., 2005)	Neurotoxic / pro-inflammatory	(Block et al., 2006; Rasley et al., 2002)

1.7 Microglia and the CNS

Microglia are ubiquitously distributed throughout the CNS, comprising for $\approx 10\text{-}20\%$ of the whole CNS cellular population (Kettenmann et al., 2011). Microglial cell bodies, labelled with Iba1 and visualized ultra-structurally, are closely apposed to neuronal cell bodies, implying the existence of close lines of communication between neurons and microglia (Shapiro et al., 2009).

Interestingly, microglial expression profiles throughout the CNS are not the same. For example, expression levels of CD11b, a pan-marker for microglia, are higher in the spinal cord as compared to the cerebral cortex (de Haas et al., 2008). These data highlight the fact that microglial profiles are significantly influenced by properties of their local microenvironment. The ability of microglia to be influenced by the neuronal diversity in their immediate environment, to be affected by neuronal physiology, and to play a critical role in healthy

neuron-neuron communication, further adds complexity to the already diverse microglial physiology.

1.7.1 Microglia in healthy CNS

As previously discussed, neurons are continuously being monitored by microglia (Nimmerjahn et al., 2005). Highly ramified processes on microglia that are closely apposed to sites of neuronal synaptic interaction enable microglia to monitor their local environment without having to translocate through the tissue. However, it is still possible that microglia are capable of migrating short distances while still in their surveilling stage (Karperien et al., 2013).

Microglia are not just the passive receivers of neuronal signals; microglia comprehend these neuronal signals and conduct activities that can influence neuronal function and physiology. Microglia are capable of performing activities, such as phagocytosis/synaptic pruning, without changing their morphology (Tremblay et al., 2011). During synaptic surveillance, microglia can sense whether synaptic spines are weak or over-worked. If spines are found to be in need of removal, microglia can strip them from the dendrite. Synaptic pruning process by microglia is normally a 3-step process: 1) microglia make, rather prolonged, contact with the pre-synaptic structure, 2) microglia attach firmly to, and strip the pre-synaptic structure and 3) phagocytose the stripped pre-synaptic structure (Kettenmann et al., 2013; Wake et al., 2009). It is not yet clear if microglia also phagocytose the post-synaptic structure.

Microglia are also capable of releasing neurotrophic factors, such as BDNF (Kettenmann et al., 2011), macrophage colony stimulating factor (M-CSF) (Murase and Hayashi, 1998), nerve growth factor (Elkabes et al., 1996) and insulin growth factor-1 (IGF-1) (Ueno et al., 2013). Controversial evidence is present regarding the exact role of microglia released neurotrophic factors. On the one hand, it is quite evident that BDNF released by microglia plays an important role in microglial activation (Zhang et al., 2014). On the other hand, it has also been proposed that BDNF released by microglia play a supportive role by promoting learning dependent synapse formation (Parkhurst et al.). It remains a question of whether the neurotrophic molecules released by microglia play a neuro-supportive or neuro-detrimental role and this, is another important, yet poorly understood, function of microglia that does not require polarization to either M1 or M2 phenotype.

Furthermore, there is direct evidence present that microglia can influence the excitability status of neurons. ATP-stimulated activated microglia, *in vitro*, caused an inversion in the polarity of

currents induced by GABA in spinal lamina I neurons in a nerve injury model (Coull et al., 2005). A recent study by Li and colleagues (2012) reported, using *in vivo* time lapse imaging in the optic tectum of larval zebrafish, that highly active neurons attract microglial processes to make contact (Li et al., 2012). The contact between microglia and highly active neurons reduced the spontaneous and visually evoked activities of the contacted neurons; an effect that persisted for several minutes after the removal of the microglial process (Li et al., 2012; Panatier and Robitaille, 2012).

1.7.2 Microglia during CNS injury

Most of the animal models, used to investigate microglial activation pathways, require either LPS-induced inflammation (Wu et al., 2012), or physical damage to the CNS (leading to neuronal stress and death) (Morrison and Filosa, 2013; Perego et al., 2011).

Previous work, focusing on the characterisation of correlation between neuronal activity and microglial activity, used stimuli such as binocular eye enucleation (Tremblay et al., 2010), tetrodotoxin injection into the retina (Wake et al., 2009), or ligation of left anterior descending coronary artery leading to ischemia (Dworak et al., 2014). These insults to the CNS affect the frequency with which microglia contact neuronal synapses. For example, reduced neuronal activity, in response to injection of tetrodotoxin in the retina or hypothermia, can reduce the frequency of microglial contact with synaptic structures by 40 to 50% (Wake et al., 2009). Furthermore, induction of transient cerebral ischemia, results in prolongation of contacts between surveilling microglial processes and synaptic boutons, in the region of somatosensory cortex, which lasts from about 5 minutes in the control state to around 80 minutes in the ischemic state (Wake et al., 2009). This extreme prolongation observed in microglial contact with synapses can be attributed to microglia carefully sensing synaptic health to either prune dead/weak synapses, or trying to restore their normal activity levels. No changes in microglial morphology, affected by transient cerebral ischemia, were reported. Another study showed that the microglial response to an activating signal runs parallel to developing cerebral brain injury, in response to ischemic stroke and reperfusion. The main finding, from this study, was the hyper- and de- ramification of microglia in relation to necrotic core, caused by the CNS injury (Morrison and Filosa, 2013).

Recent studies discussed above, identify a novel “alerted microglial” phenotype that is more active than ‘surveilling’, but not yet fully activated. This novel alerted state is characterized by a hyper-ramified or de-ramified morphology, or a morphology that is quite similar to surveilling

microglia. Alerted microglia (Hanisch and Kettenmann, 2007; Karperien et al., 2013; Kettenmann et al., 2011) may be the form adopted, prior to acquisition of an extreme activation phenotype, if this is necessary (Figure 1.14).

Under extreme circumstances, when ischemic conditions are left to develop for over 7 days, microglia exhibit carefully tailored biphasic behaviour that is neuroprotective before developing into a phagocytic phenotype (Perego et al., 2011). This biphasic response highlights another important trait of microglia: in the first instance, microglia tend to exhibit a neuroprotective/neuro-supportive behaviour in the CNS. However, when the CNS damage is very severe or irreversible, microglia initiate the process of eradicating dead/affected neurons in order to stop the spread of CNS injury and clear away debris. (Perego et al., 2011)

Although the microglial response to injury in higher brain regions is well established, studies have also identified these cells as an important mediator of spinal cord injury (Kigerl et al., 2009; Kroner et al., 2014; O'Carroll et al., 2013).

1.8 Microglia and sympathetic nervous system (SNS)

Microglia are present in all areas of the CNS. Within areas in the brain that are involved in the sympathetic control of BP, microglia (Figure 1.14 C and D) play a crucial role in surveillance of synaptic and neuronal activity levels. It is therefore somewhat surprising, considering the importance of the SNS in the regulation of the cardiorespiratory system, that the role of microglia in cardiorespiratory nuclei of the brain remains relatively unexplored. As discussed in previous sections, microglia express receptors for vast majority of neurotransmitters, as well as many other chemicals. Table 1.2 provides a brief overview of some of the neurotransmitters critical for cardiorespiratory function, and the presence of relevant receptors and their function that on local microglia.

Intracerebroventricular administration of IL-1 β (a pro-inflammatory cytokine) increases AP, HR and the renal SNA, within 20-25 min of administration (Kannan et al., 1996). A recent study from our laboratory found that inhibition of microglial activation, by minocycline, at the level of spinal cord, exaggerates the increase in SNA response seen in rats that develop seizures following an intraperitoneal dose of kainic acid (Bhandare et al., 2015). Our findings highlight the neuroprotective effect of microglia during seizure on SPGNs in the spinal cord. The protective effect of microglia towards seizure induced SNA might be mediated through their polarisation towards M2 phenotype, and an endogenous production of neurotrophic and anti-

apoptotic molecules, such as TGF- β and IL-10. Moreover, findings from this study also suggest that, as part of microglia-neuron communication, PACAP might be acting on microglial PAC1 and VPAC-1 receptors causing an increased expression of glutamate transporters on the surface of microglia and increasing glutamate uptake (Bhandare et al., 2015). These data highlight the possible neuroprotective behaviour of microglia when subjected to seizure.

Following myocardial infarction (a model for inflammation), in SD rats, there is an increased percentage of activated microglia in the PVN (Dworak et al., 2012; Rana et al., 2010), the RVLM (Dworak et al., 2014) and the NTS (Dworak et al., 2014). Furthermore, induction of diabetes (with streptozotocin) caused neuronal activation in brain regions (such as the PVN), accompanied by microglial activation in brain regions (such as the PVN and the NTS) (Rana et al., 2014). Interestingly, the delayed onset of microglial activation, following streptozotocin-induced diabetes, highlighted microglial activation as a consequence of over-excitation of neurons (Rana et al., 2014). Unfortunately, the lack of detailed analysis regarding the probable phenotype of these microglia with an activated morphology (in the PVN, RVLM and NTS in response to myocardial infarction or diabetes), makes it difficult to ascertain, whether or not, these activated microglia are playing a neuro-protective, a neuro-supportive, or a neurotoxic role.

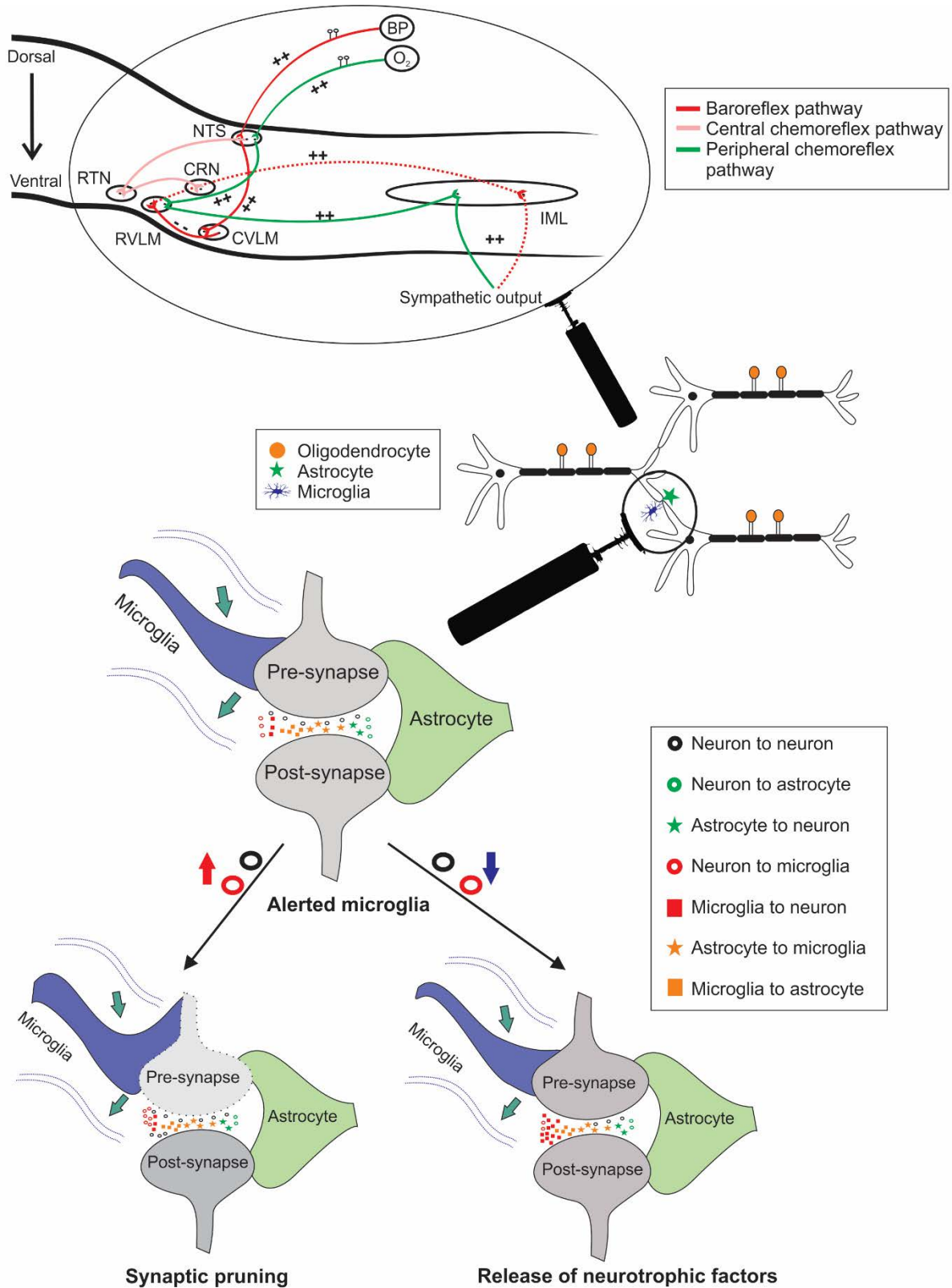
Furthermore, recent study has shown that respiratory depression in response to opioid administration (Hutchinson et al., 2008) is not mediated by microglia, at least in the pre-Bötzinger area (Zwicker et al., 2014).

The number of possible disorders that can occur, or be worsened by, increases in sympathetic activity is very large and include hypertension, diabetes, obesity, metabolic syndrome and heart failure. Given that microglia can regulate sympathetic activity (Bhandare et al., 2015), there is now a strong possibility that therapies affecting microglial function could play an important role in the treatment of sympathetic nerve related disorders, including cardiovascular disease. We hypothesize that, in addition to the important role that microglia play in the response to physical injury by adopting an M1 or M2 state, microglia can also detect changes in the level of neuronal/ synaptic activity in the VLM nuclei of the brainstem. Microglia may respond to normal adaptive reflexes by triggering a mild level of alertness in their normal behaviour (Figure 1.15). This alertness does not require polarisation to their extreme activation phenotypes: M1 or M2, instead, there is a more subtle change in microglial physiology. We propose that ‘alerted’ microglia have a morphology similar to that of surveilling microglia, but

are more attentive of synaptic activity levels (Figure 1.15) (Hanisch and Kettenmann, 2007; Kettenmann et al., 2011). Alerted microglia can perform activities such as synaptic pruning, in response to exaggerated levels of synaptic activity. In contrast to this, decreased synaptic activity levels can cause alerted microglia to release neuro-supportive substances, such as BDNF, nerve growth factor or IGF-1 (section 1.7.1), in order to restore normal homeostasis.

Figure 1.15: Microglia and the sympathetic control of blood pressure

Microglia play an important role in normal neuron-neuron communication and form an integral part of the tri-partite synaptic structure (pre-synapse, post synapse and astroglial process) in the SNS. The figure is divided into 3 stages. 1st stage refers to 3 important reflex pathways in the SNS: the sympathetic baroreflex (red), central chemoreflex (pink) and peripheral chemoreflex (green). Please refer to the text for details on these reflex pathways. 2nd stage of the figure shows the presence of different CNS elements, at the autonomic neuronal level. Oligodendrocytes are supportive cells for neurons, providing myelin sheath. Astrocytes and microglia are found in close apposition to the neuronal synaptic structure. Stage 3 of the figure shows the dynamics at the synaptic level. Unlike astrocytic process, microglial processes are not permanently associated with the synaptic structure. Rather, microglial processes are constantly moving, surveying neuronal activity levels. In case of enhanced levels of neuron-neuron/neuron-microglia communication, microglia perform functions such as synaptic pruning. During synaptic pruning, microglial process envelops the pre-synaptic structure, strip it from the spine and phagocytose the residue. On the contrary, decreased neuron-neuron/ neuron-microglial communication causes microglia to release neurotrophic factors (red squares), to support the weak synapse or increase the neuron-neuron communication. BP: blood pressure, O₂: oxygen, NTS: nucleus of the solitary tract, RVLM: rostral ventrolateral medulla, CVLM: caudal ventrolateral medulla, IML: intermediolateral cell column of spinal cord, RTN: retrotrapezoid nucleus and CRN: central respiratory network.



1.9 Hypertension

Hypertension is a pathological condition defined as a continuous elevation of AP beyond 130/85 mmHg; it is a risk factor for other CVDs, such as heart attack and stroke, and cerebrovascular disorders. Hypertension can be either primary (essential) or secondary, and can be due to either genetic or environmental influences. Diagnosis of hypertension can be difficult as symptoms are clinically silent, until it leads to end organ damage such as brain, kidney or heart.

Essential hypertension is responsible for $\approx 95\%$ of all cases of hypertension, and is generally neurogenic in origin (Guyenet, 2006). Almost all forms of neurogenic hypertension are associated with an exaggerated activity of the SNS (Schlaich et al., 2004).

1.9.1 Sympathetic nervous system and neurogenic hypertension

Elevated levels of noradrenaline in the plasma of patients suffering from hypertension suggested that the elevated SNA may well be the primary cause of neurogenic hypertension (Anderson et al., 1989; Fisher and Paton, 2012).

One of the common causes involved in the pathophysiology of neurogenic hypertension, leading to an exaggerated SNA, is the chronic over-activation of the SNS (de Kloet et al., 2013; Fisher and Paton, 2012; Grassi et al., 2010; Guyenet, 2006). This chronic over-activation of the SNS can lead to an increased sympathetic nerve firing rate (such as the muscle SNA), elevated levels of total systemic, cardiac and renal noradrenaline spillover, reduced neuronal noradrenaline reuptake and reduced facilitation of noradrenalin release by neuro-humoral factors (such as angiotensin II) (Schlaich et al., 2004).

Attenuated levels of the neuronal activity in cardiovascular nuclei of the brain, such as the NTS (Kawabe et al., 2015; Sato et al., 2002; Shan et al., 2013; Waki et al., 2006), the CVLM (Smith and Barron, 1990), the RVLM (Geraldes et al., 2014a; Li et al., 2013) and the PVN (Akine et al., 2003; Allen, 2002; Geraldes et al., 2014b), were seen in animal models of neurogenic hypertension (SHR). In addition to cardiovascular nuclei in the brain, brainstem respiratory sites, such as the pre-Bötzinger and Bötzingen nuclei, also showed increased neuronal activity in hypertensive models (Moraes et al., 2014).

The role of angiotensin-II in regulation of the cardiovascular arm of the SNS is well established (Arakawa et al., 2013; Chitravanshi and Sapru, 2011; Chitravanshi et al., 2012; Gao et al.,

2008b; Kawabe et al., 2014; McMullan et al., 2007; Sumners et al., 2015). Angiotensin II is a key neuropeptide involved in the long term regulation of BP, electrolyte and fluid homeostasis, via the renin-angiotensin system (RAS) (de Kloet et al., 2013). Angiotensin II is a vasoconstrictor, and exerts actions on proximal tubule to promote sodium reabsorption.

Angiotensin-II, along with the RAS, play an important role in the pathophysiology of neurogenic hypertension (Figure 1.16) (de Kloet et al., 2013; Fisher and Paton, 2012; Raizada et al., 1993). Data from SHR have shown that the central pathway involving angiotensin-II is attenuated in cardiovascular sites of the brain (Erdos et al., 2015; Kawabe et al., 2016). Furthermore, increased expression of angiotensin type II receptors (adenovirus associated vector) in the solitary-vagal complex (NTS, section 1.2.1.7) attenuated the development of renovascular hypertension and restored decreasing levels of angiotensin converting enzyme 2 to control levels (Blanch et al., 2014).

Central cholinergic system also plays an important role in the pathology of essential hypertension (Buccafusco and Spector, 1980; Giuliano and Brezenoff, 1987; Kumar et al., 2009). Intravenous administration of centrally acting cholinesterase inhibitor, physostigmine, evoked an enhanced pressor response in SHR, compared to WKY (Kubo and Tatsumi, 1979). Intracerebroventricular administration of cholinergic blocker exerted a depressor response only in SHR (Brezenoff and Caputi, 1980). Increased number of acetylcholine muscarinic receptors are present in the hypothalamus of SHR (Hershkowitz et al., 1982; Yamada et al., 1984). In addition, microinjection of physostigmine, a cholinesterase inhibitor, directly in the RVLM also exerted an enhanced pressor response in SHR as compared to WKY (Kubo et al., 1995). Whereas, bilateral microinjection of scopolamine in the RVLM (muscarinic cholinergic receptor antagonist) exerted a depressor response; this depressor response was greater in SHR than in WKY (Kubo et al., 1995). It was suggested that an alteration in the mRNA expression levels of muscarinic receptor subtypes in the RVLM of SHR compared to WKY (M2 receptors (elevated in SHR) and M4 receptors (reduced in SHR)) may contribute to a hypertensive phenotype of SHR (Kumar et al., 2009),

Interventions leading to reductions in the exaggerated SNA, such as the electrical activation of carotid sinuses, has shown promising results with respect to the treatment of hypertension in animal models (Lohmeier et al., 2004; McBryde et al., 2013), and human clinical trials (Illig et al., 2006; Papademetriou et al., 2011), without any adverse events.

1.9.2 Possible involvement of microglia in hypertension

Neurogenic hypertension is no longer viewed as, merely, a consequence of chronic activation of the SNS. Emerging evidence suggests that neurogenic hypertension is also an immune condition (Figure 1.16) (Cardinale et al., 2012; de Kloet et al., 2013; de Kloet et al., 2015; Zubcevic et al., 2011).

Induction of systemic inflammation (by peripheral LPS injection) can lead to the development of neurogenic hypertension, via activation of microglia and an increase in levels of oxidative stress in the RVLM (Wu et al., 2012). Genetically hypertensive rats develop larger cerebral infarctions following stroke (De Geyter et al., 2012); further highlighting a possible relationship between microglia and hypertension.

Recent work from Paton and colleagues has suggested a role of a pre-existing inflammatory condition in the NTS (section 1.2.1.7) of SHR in the pathophysiology of neurogenic hypertension (Waki et al., 2010). In the NTS of SHR, there is over-expression of pro-inflammatory molecules, such as JAM-1 (Waki et al., 2007; Waki et al., 2008a) and leukotriene B4 (Waki et al., 2013), and inflammatory markers, such as glycoprotein 39 precursor (Waki et al., 2008b). Over-expression of JAM-1 suggests that inflammation may play an important role in the genesis of neurogenic hypertension (Waki et al., 2007; Waki et al., 2008a; Waki et al., 2011). The possibility that JAM-1 plays a mechanistic role in the development of hypertension was addressed by demonstrating that over-expression of JAM-1 in the NTS of normotensive WKY caused hypertension (Waki et al., 2008a). This study highlighted an alternative explanation to the hypothesis: “microglia/neuro-inflammation may contribute to the pathophysiology of hypertension”. IL-6 is a cytokine that was found to be downregulated in the NTS of SHR (Waki et al., 2008b), and microinjection of IL-6 in the NTS of normotensive Wistar rats attenuated the baroreflex in response to increased AP (Takagishi et al., 2010). Altogether, these studies suggested that enhanced inflammation within the microvasculature of cardiovascular nuclei (such as the NTS) might be critical in the development of neurogenic hypertension.

Microinjection of fractalkine/CX3CL1 in either the PVN or the NTS of SD rats elicited a hypotensive response accompanied by an abnormal HR; this response was mediated via the activation of CX3CR1 receptors (Ruchaya et al., 2012; Ruchaya et al., 2014). CX3CR1 receptors are exclusively expressed by microglia in the CNS (Cardona et al., 2006), and activation of these receptors exerts ‘calming effects’ by suppressing microglial activation

(Pabon et al., 2011). Indirectly, the work from Ruchaya and colleagues have provided a link between the suppression of microglial activation and hypotension mediated via cardiovascular sympathetic nuclei of the brainstem (Ruchaya et al., 2012; Ruchaya et al., 2014).

A direct correlation between angiotensin-II induced hypertension and neuro-inflammation, in particular in the PVN, was investigated by Shi and colleagues (Shi et al., 2010a; Shi et al., 2010b; Shi et al., 2014). As mentioned in section 1.2.1.1, the PVN receives inputs from high brain regions and projects to both the RVLM and the IML, and therefore plays an important role in the co-ordination of efferent SNA (Guyenet, 2006). Angiotensin-II induced hypertension (McMullan et al., 2007) caused an activation of microglia in the PVN of SD rats (Shi et al., 2010a). This angiotensin-II mediated hypertension was abrogated, almost completely, by intracerebroventricular administration of minocycline (broad-spectrum tetracycline known to inhibit microglial activation via reductions in p38 MAPK phosphorylation (Garrido-Mesa et al., 2013)). On the other hand, overexpression of IL-10 (an anti-inflammatory cytokine) reduced the effect of angiotensin-II mediated hypertension (Jiang et al., 2013; Shi et al., 2010a). Taken together, these results suggest an important role for microglia in the development of neurogenic hypertension (Shi et al., 2010a). Furthermore, angiotensin (1-7), a protective component of the RAS system (Bennion et al., 2015a; Bennion et al., 2015b; Regenhardt et al., 2013; Sumners et al., 2013), exerted its anti-inflammatory effects (reduction of pro-inflammatory cytokines) in the hypothalamus via the Mas receptor expressed on microglia (Liu et al., 2016).

Macrophage migration inhibitory factor is a mysterious cytokine that can exert both, pro- and anti- inflammatory, effects on neighboring cellular elements (Cox et al., 2013; Nguyen et al., 2003). Restoration of expression levels of the macrophage migration inhibitory factor (counteracts the neuronal chronotropic actions of angiotensin II (Sun et al., 2004)) in the PVN of SHRs attenuated the time-dependent increases in BP, and restored stress-induced elevations in MAP (Erdos et al., 2015; Li et al., 2008b). However, restoration of expression levels of the macrophage migration inhibitory factor failed to reduce resting BP levels in SHR (Erdos et al., 2015). On the other hand, increased expression of macrophage migration inhibitory factor in the NTS of SHRs lowered MAP levels and restored baroreflex function (Freiria-Oliveira et al., 2013).

In clinical studies, reports suggested that there is $\approx 35\%$ increase in C-reactive protein levels (marker of systemic inflammation) in patients that are more vulnerable to develop peripheral arterial diseases and hypertension (Ridker et al., 1998). Even though, the detailed mechanism

behind these results is not clear, these findings do suggest novel directions in the investigation of microglia as critical players in neuro-inflammation, and hypertension.

The worldwide prevalence of neurogenic hypertension, involvement of the SNS in the pathophysiology of neurogenic hypertension and increasing literature suggesting close association between neuro-inflammatory elements of the CNS/microglia and neurogenic hypertension forms the foundation of the work conducted in this thesis.

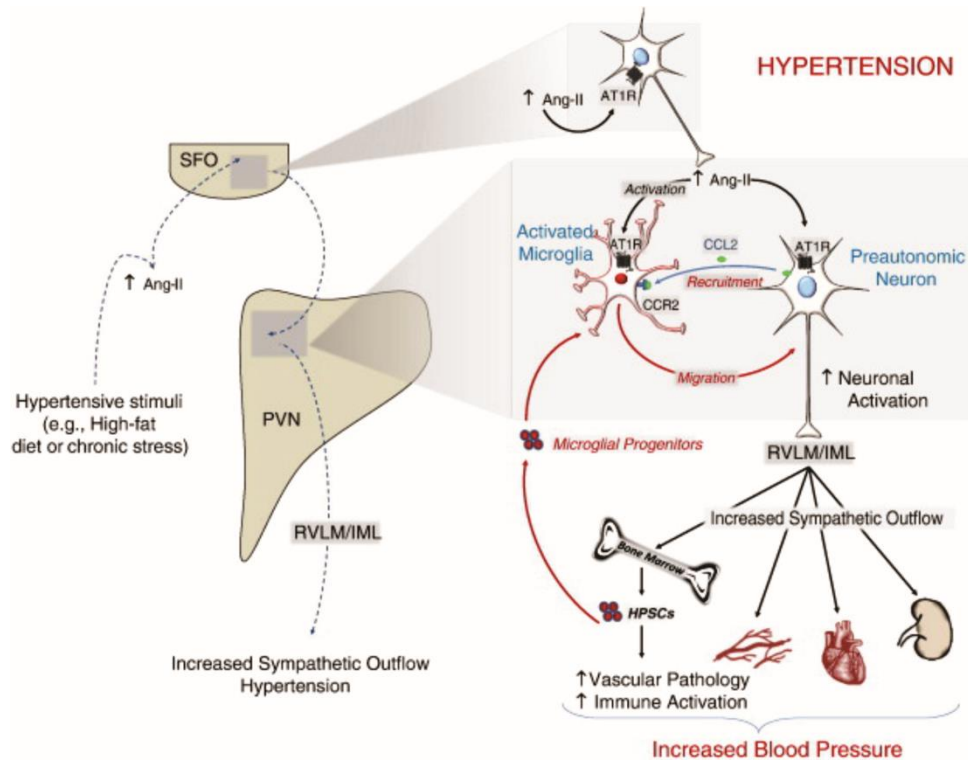


Figure 1.16: Proposed model for immune/CNS interactions during hypertension.

Hypertensive stimuli (such as obesity and chronic stress), cause increases in circulating factors (e.g., Ang-II) that are sensed by CVOs, such as the SFO. The SFO then transmits these signals to the pre-autonomic region of PVN, leading to stimulation of the IML and the RVLM projecting neurons and resulting in increased sympathetic outflow and BP. Furthermore, during neurogenic hypertension, the enhanced direct neuronal actions of Ang-II at AT1R (angiotensin type 1 receptor) in the PVN leads to an over-stimulation of pre-autonomic neurons. Direct effects of Ang-II at microglia lead to sustained induction of both the central and peripheral immune systems. It is proposed that initially, Ang-II directly activates microglia, and indirectly (via MCP-1/CCL-2 released from neurons) causes their migration towards pre-autonomic neurons. This pro-inflammatory microenvironment within the PVN then stimulates the brain to signal via the SNS to mobilize the peripheral immune system and to the bone marrow to mobilize microglial progenitors that are recruited to the PVN (likely via a CCL2/CCR2-dependent mechanism). This increase in microglial progenitors within the PVN then contributes to the population of innate immune cells within this nucleus, feeding-forward to activate pre-autonomic PVN neurons thereby, augmenting and sustaining the elevations in BP. Ang-II, angiotensin II; CVO, circumventricular organs; SFO, subfornical organ; HPSCs, haemopoietic pluripotent stem cells. (Figure and legend from (de Kloet et al., 2013); used with permission)

1.10 Aims

The overall aim of this thesis is to characterise the microglial distribution and morphology in healthy, uninjured, cardiovascular sites of the brainstem, and consequently, to identify if these microglia in the brainstem are vigilant of changes that occur around them in response to BP modulations. Alterations in BP are induced with the aid of continuous intravenous infusion of phenylephrine (to induce acute hypertension) and with intravenous administration of hydralazine (to induce acute hypotension). The 2 phases of hypertension explored in this study are acute (phenylephrine induced in SD) and chronic (SHR) hypertension.

Chapter 3 (Figure 1.17):

Before proceeding to characterise the microglial response to changes in BP, it is essential to identify the pattern of microglial distribution and morphology in cardiovascular sites of the brainstem. Thus, the aim of the experiments conducted in this Chapter is:

- To characterise the microglial distribution in various catecholaminergic nuclei ranging from the CVLM to the pons, in a healthy ANS, in normotensive and hypertensive rats (SD, WKY and SHR).
- To establish if the pattern of microglial distribution and morphology is related to the neuronal phenotype of different catecholaminergic nuclei.

Chapter 4: (Figure 1.17)

The overall aim of experiments conducted in this Chapter is to identify the microglial response, in the CVLM and the RVLM, to changes in BP (hyper- or hypo- tension) over a time spectrum ranging from 0.5 to 10 h. For the purpose of this aim, the microglial response was quantified according to the following microglial characteristics:

- Microglial spatial distribution
- Microglial morphology
- Microglial contact with synapses
- Microglial polarisation to either M1 or M2

Chapter 5: (Figure 1.17)

The overall aim of this Chapter is to identify if the microglial response, in the CVLM and the RVLM, to changes in BP (hyper- or hypo- tension) is impaired in SHR as compared to WKY, thereby contributing to the development of SHR hypertensive phenotype. For the purpose of

this aim, the microglial response was quantified according to the following microglial characteristics:

- Microglial spatial distribution
- Microglial morphology
- Microglial contact with synapses
- Microglial polarisation to either M1 or M2

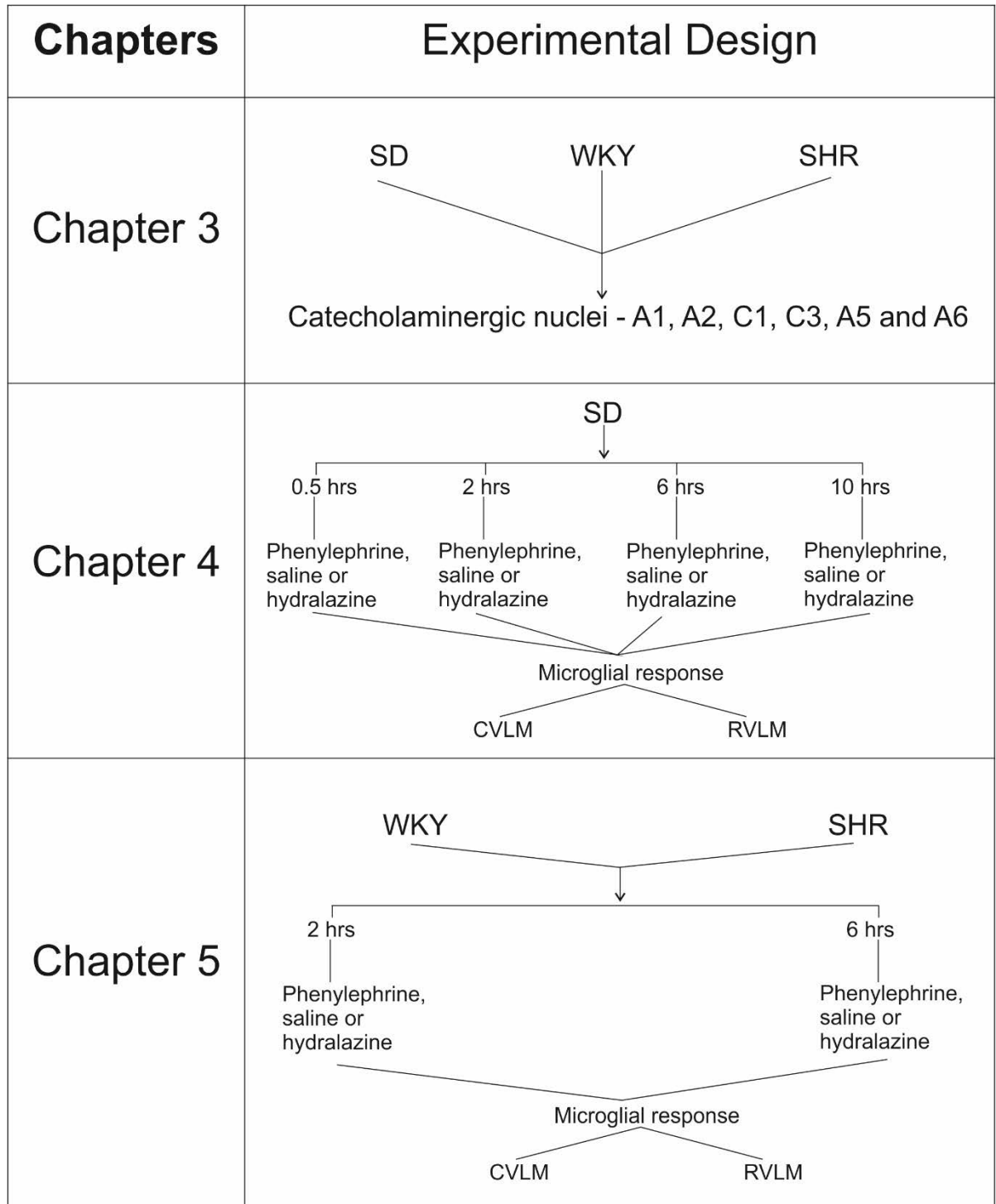


Figure 1.17: Schematic representation of aims of this thesis

Chapter 2

Methods

Contents

2.1	Animal experiments	105
2.1.1	Ethics.....	105
2.1.2	Strains.....	105
2.1.2.1	<i>Sprague-Dawley rats (SD)</i>	105
2.1.2.2	<i>Wistar-Kyoto rats (WKY)</i>	105
2.1.2.3	<i>Spontaneously hypertensive rats (SHR)</i>	106
2.1.3	Tail-cuff phenotyping of WKY and SHR	106
2.1.4	Anaesthesia.....	107
2.1.4.1	<i>Sodium pentobarbital</i>	107
2.1.4.2	<i>Urethane</i>	108
2.1.5	Cannulations.....	108
2.1.5.1	<i>Arterial and venous cannulations</i>	108
2.1.5.2	<i>Tracheal cannulation</i>	111
2.1.6	Alterations introduced in BP	111
2.1.6.1	<i>Phenylephrine induced hypertension</i>	111
2.1.6.2	<i>Hydralazine induced hypotension</i>	112
2.1.7	Transcardial perfusion.....	112
2.2	Immunohistochemistry (IHC)	113
2.2.1	Tissue harvesting and preparation.....	113
2.2.2	Immunohistochemistry (IHC)	113
2.2.2.1	<i>IHC protocol</i>	116
2.2.2.2	<i>Antibody characterisation</i>	116
2.2.3	Mounting	124
2.3	Data acquisition.....	124
2.3.1	Physiological data	124
2.3.1.1	<i>Tail-cuff BP data</i>	124
2.3.1.2	<i>BP data from animals under anaesthesia</i>	124
2.3.2	Microscopy.....	124
2.4	Analysis	125
2.4.1	Tail-cuff BP data	125
2.4.2	Physiological data	125
2.4.3	Histological data.....	126
2.5	Statistical analysis.....	129

2.1 Animal experiments

All experiments were conducted on adult male rats weighing between 300-420 g. Sprague-Dawley rats (SD), Wistar-Kyoto rats (WKY) and spontaneously hypertensive rats (SHR) were sourced from the Animal Resource Centre (Perth, WA). Upon arrival at the animal facility at the Heart Research Institute (Sydney, NSW), animals were housed in small groups (≤ 3 rats per cage), in environment enriched temperature controlled conditions (21 ± 2 °C), with fixed 12 h light/dark cycles. Animals were provided with access to standard chow pellets and water *ad libitum*.

2.1.1 Ethics

All procedures and protocols performed were approved by the Sydney Local Health District Animal Welfare Committee (protocol number 2013/081; Appendix 3) and the Macquarie University Animal Care and Ethics Committee, Sydney, Australia. All procedures were conducted in accordance with the standards and guidelines set by the Australian Code of Practice for the Care and Use of Animal for Scientific Purposes.

2.1.2 Strains

Three different strains of rats (*Rattus norvegicus*) were used for experiments described in this thesis: SD, WKY and SHR.

2.1.2.1 Sprague-Dawley rats (SD)

The SD strain of rat is a widely accepted healthy control model for studies in psychology, medicine and many other fields. In the context of the cardiovascular system, neuroanatomy and physiology of this strain is extensively investigated. SD rats sacrificed for experiments (Chapter 3 and Chapter 4) weighed between 300-420 g.

2.1.2.2 Wistar-Kyoto rats (WKY)

The first SHR was developed in 1963 by inbreeding a WKY with high blood pressure (Okamoto and Aoki, 1963) and therefore, WKY rats serve a normotensive control for SHR for studies on essential hypertension. Physiologically, WKY are not comparable to SD due to underlying behavioural and phenotypic differences. Data from Chapter 3 also highlight differences between SD and WKY. Therefore, the microglial response following BP modulations in SHR was compared with WKY, and not SD (Chapter 5). WKY rats sacrificed for experiments

(Chapter 3 and Chapter 5), weighed between 300-400 g and were age matched with SHR, i.e. >18 weeks of age.

2.1.2.3 Spontaneously hypertensive rats (SHR)

As mentioned above, SHR are WKY rats with high blood pressure (Okamoto and Aoki, 1963). SHR is a well-established animal model for essential/ neurogenic hypertension (Erdos et al., 2015; Li et al., 2008b; Waki et al., 2008a). Hypertension in SHR begins around 5-6 weeks of age. In addition to essential hypertension, SHR is also a good model for attention-deficit hyperactivity disorder. High blood pressure in SHR is linked to an exaggerated activity of the SNS, in particular the RVLM (Ito et al., 2000; Judy et al., 1976; Minson et al., 1996; Smith and Barron, 1990). SHRs sacrificed for experiments (Chapter 3 and Chapter 5) weighed between 300-400 g and were >18 weeks of age.

2.1.3 Tail-cuff phenotyping of WKY and SHR

Hypertensive and normotensive phenotype of SHR and WKY, respectively, was confirmed at the age of >18 weeks. Systolic and mean BP of SHR and WKY were recorded in conscious animals, non-invasively, using a customised sphygmomanometer cuffed around their tail (Chapter 3 and Chapter 5).

The IITC MRBP tail cuff BP system was used to measure BP in conscious rats. The system (including the automatic inflation pump, warming chamber and restrainer) was assembled and connected to the associated computer, switched on and allowed to warm up at least 15 min prior to transporting the animal in the chamber. The system was warmed up to 32 °C to avoid heat stress to the animal. Each rat was recovered from their cage, weighed and allowed to crawl freely into the warmed up restrainer. The restrainer was then placed into the warmed up chamber and an inflatable cuff was placed around the base of rats' tail. The inflatable cuff from the IITC MRBP system is connected to a transducer, which converts an analogue signal to a digital signal, and records the digitised signal on the computer screen in real time. The rat was then left untouched for a minimum of 5 min in the restrainer, allowing the rat to acclimatise to the chamber.

Two channels, at maximum, were in operation at the same time, allowing BP from 2 animals to be recorded simultaneously. The start pressure (high enough to occlude the artery) for SHR was selected as 220 mmHg and for WKY, it was selected as 160 mmHg. The termination pressure for both SHR and WKY was selected as 50 mmHg. Three inflation cycles recording

BP measurements were run consecutively with a delay of 10 seconds between each inflation cycle. The highest peak at which the tail-cuff pulse pressure could be detected was recorded as systolic blood pressure.

Hypertension was defined as a systolic pressure of >180 mmHg and normotension was defined as a systolic pressure of <150 mmHg (Chapter 3 and Chapter 5 (Farnham et al., 2012)).

2.1.4 Anaesthesia

Prior to commencement of any surgical procedure, animals were surgically anaesthetised. The type of anaesthetic used depended on the experiment. Animal stress during anaesthesia was kept to minimum by allowing the animal to, freely, enter a cone shaped fabric, and were only restrained for the anaesthetic injection. Both anaesthetics (urethane and sodium pentobarbital) used in the study were administered intraperitoneally mixed with atropine sulphate (muscarinic blocker to reduce bronchial secretions; 0.2 ml/kg) using a 26G needle. Temperature for all animals was maintained between 36.5 °C and 37.5 °C, using a rectal probe connected to a homeothermic heating blanket. Surgical procedures only commenced after the lack of a withdrawal response to a nociceptive stimulus, such as tail pinch.

2.1.4.1 *Sodium pentobarbital*

Sodium pentobarbital is a fast acting barbiturate, with short half-life. Animals sacrificed for shorter time point experiments (0.5, 2 and 6 hours (h)) were anaesthetised intraperitoneally with sodium pentobarbital (50 mg/kg). Room air flowing to the animal under anaesthesia was supplemented with 100% oxygen (rate 0.5–1.0 l/min) through a nose cone for the duration of the experiment (either 0.5, 2, 6 or 10 h depending on the experimental group). Exact concentration of oxygen in the air flowing to the animal was not a controlled parameter. This was only done to silence peripheral chemoreceptors by maintaining oxygen at supra-physiological levels. The depth of anaesthesia was monitored by observing reflex responses to nociceptive and tactile stimuli (periodic tail/paw pinches), pupillary responses to light stimuli and corneal touch reflex (involuntary blink). Additional anaesthetic – sodium pentobarbital (1.5-2.0 mg) – was administered to eliminate the response to nociceptive, or tactile stimuli, or corneal touch reflex.

2.1.4.2 Urethane

Urethane is a stable and longer acting anaesthetic with a half-life of ≈ 15 h. Urethane potentiates the function of neuronal nicotinic acetylcholine, GABA and glycine receptors, and it inhibits NMDA and α -amino-3-hydroxy-5-methyl-4-isoxazole propionic acid receptors in a concentration-dependent manner (Hara and Harris, 2002). SD rats sacrificed for the 10 h time point experiments (Chapter 4) were anaesthetised intraperitoneally with 10% urethane solution in 0.9% saline (1.0-1.5 g/kg). Animals were vagotomised (both vagus nerves were cut) and paralysed (neuromuscular blockade, pancuronium bromide; 0.4 mg was given as a 0.2 ml bolus injection followed by a continuous infusion of 10% pancuronium in 0.9% saline at a rate of 2 ml/h). Straight after vagotomy, animals were artificially ventilated and a CO₂ analyzer was connected to the expiratory line to monitor the expired CO₂. The depth of anaesthesia prior to vagotomy, and induction of paralysis, was monitored by observing reflex responses to nociceptive and tactile stimuli (periodic tail/paw pinches), pupillary responses to light stimuli and corneal touch reflex (involuntary blink). The depth of anaesthesia following vagotomy, and paralysis, was evaluated by continuously monitoring the BP trace for any excessive fluctuations, on its own or in response to a nociceptive stimulus. Any changes in BP exceeding 10% were regarded as signs of additional anaesthetic required. Additional anaesthetic – urethane (30-40 mg, 10% urethane i.v.) – was administered, when required.

2.1.5 Cannulations

2.1.5.1 Arterial and venous cannulations

In all experiments, the external jugular vein, the carotid artery and the femoral vein were cannulated for administration of additional anaesthetic (and neuromuscular blocker in 10 h experiments), recording of AP and administration of BP modulating drugs (phenylephrine/hydralazine), respectively (Figure 2.1).

The animal was placed in supine position and skin incisions were made to locate the jugular vein, the common carotid artery and the femoral vein (Figure 2.1). The external jugular vein is located beneath the subcutaneous tissue in the neck and can be exposed with an incision made in the midline of the neck area (Figure 2.1). The common carotid artery is located next to the trachea and is covered by a carotid sheath that contains the vagus nerve and the ADN (Figure 2.1). The femoral vein can be located in inner leg alongside the femoral artery (Figure 2.1). After identification of the required vessel, it was carefully isolated, cleared of connective tissue and was occluded at the distal end to the heart with silk sutures. A polyethylene tube (outer

diameter 0.96 mm and inner diameter 0.58 mm) was advanced into the lumen, towards the heart, and secured in place with silk sutures. The polyethylene tube/ cannula used for jugular/ femoral vein was filled with 0.9% saline and for the carotid artery (to prevent blood clotting), the cannula was filled with heparinised (≈ 10 IU heparin/ml) 0.9% saline, before advancing in the vessel.

The arterial cannula was connected to a BP transducer where the pulses from BP were converted into electrical signal. The analogue signal from the transducer was amplified and converted into digital signal (CED 1401, analogue to digital converter, Cambridge Electronic Design, UK), and was recorded using the Spike 2 acquisition and analysis software (version 8.01; Cambridge Electronic Design, UK).

Both wounds (in the neck and inner leg) were closed with silk sutures prior to the start of the protocol.

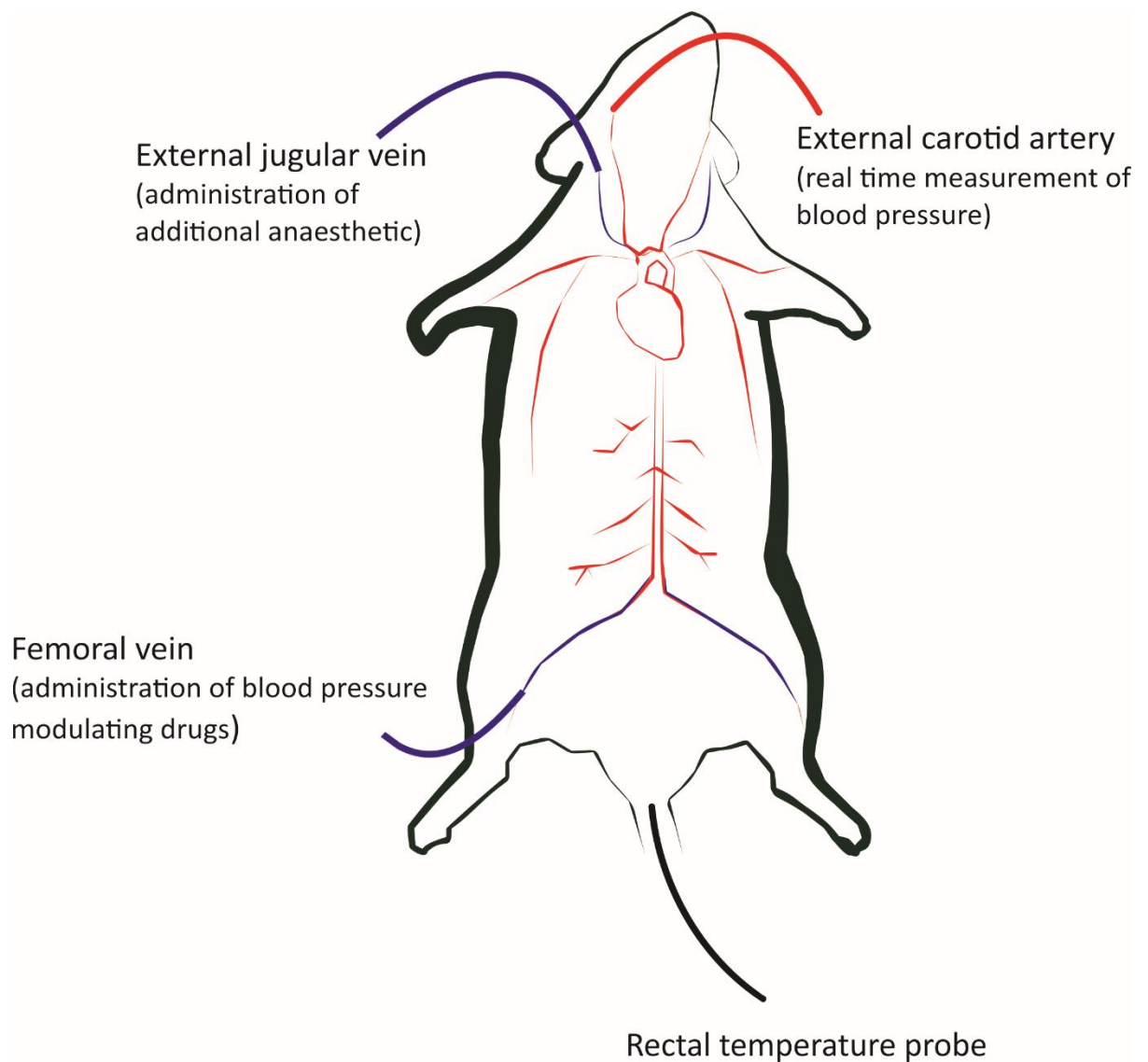


Figure 2.1: Animal protocol

The external jugular vein, carotid artery and femoral vein were cannulated in rats (SD, WKY and SHR) for the administration of additional anaesthetic, real time measurement of blood pressure and administration of blood pressure modulating drugs, respectively. A rectal temperature probe, connected to a homeothermic heating blanket, was used to maintain the temperature of the animal between 36.5 °C and 37.5 °C.

2.1.5.2 Tracheal cannulation

Tracheotomy was only performed for animals sacrificed for the 10 h time point experiments (Chapter 4) to facilitate artificial ventilation of the animal. The trachea was exposed by parting the strap muscles on the ventral surface of the neck. A 14G catheter was inserted through a small hole made in the trachea, below the larynx and was secured in place using silk sutures. The catheter was then connected to a rodent ventilator (UGO, Basile Biological Research Apparatus) and the expired CO₂ was recorded (Capstar 100 CO₂ analyser, CWE) as an indicator of animals' physiological condition.

The wound in the neck was closed with silk sutures, following the tracheal cannulation, prior to the start of the protocol.

2.1.6 Alterations introduced in BP

As mentioned in section 1.10, the main aim of our study was to characterise microglial response to acute and chronic changes in BP. For the purpose of this study, we infused phenylephrine, or hydralazine, (via femoral vein, Figure 2.1) to increase or decrease BP from baseline levels, respectively.

Induction of acute hyper-, or hypo-, tension to dissect the functional organisation of the CNS pathways has long been used (Curtis et al., 1999; Graham et al., 1995; Li and Dampney, 1994; Polson et al., 2002; Springell et al., 2005). One of the major advantages of these studies is that the internal physical milieu of the CNS is undisturbed.

2.1.6.1 Phenylephrine induced hypertension

Phenylephrine hydrochloride is a selective α_1 adrenergic receptor agonist and acts as a vasoconstrictor on blood vessels. Effects of intravenous phenylephrine are instantaneous, short acting, and the half-life of phenylephrine is ≈ 5 min. Thus, in order to maintain elevated levels of BP, a continuous infusion of phenylephrine is required. Prolonged infusions of phenylephrine causes desensitisation of α_1 adrenergic receptors (Minami et al., 1997) and therefore, is unable to maintain sustained elevated levels of BP for longer durations. Phenylephrine does not cross the blood brain barrier and thus, exerts its pressor effects on peripheral blood vessels (Olesen, 1972).

In our study, a continuous infusion of phenylephrine, at a dose of 10 $\mu\text{g/kg/min}$, was maintained to increase BP levels by at least 40 mmHg from baseline values (Graham et al., 1995). Rate of phenylephrine infusion was adjusted, when required, by at least 0.002 ml/min (at the dose of

60 µg/ml) to maintain elevated levels of BP throughout the protocol period (Graham et al., 1995). Please note that no exact dosage regime was followed to increase the rate of phenylephrine infusion as this entirely depended on the weight of animal, physiological desensitisation level of the animal towards phenylephrine and the duration of the protocol. However, special care was taken to maintain the elevated levels of BP by at least 40 mmHg (Graham et al., 1995), and not to induce hypervolemia.

2.1.6.2 Hydralazine induced hypotension

Hydralazine acts on arteries and arterioles, and relaxes smooth muscles, by influencing calcium dynamics in the walls of blood vessels, thereby acting as a vasodilator. SNP, another commonly used vasodilator, acts by generating nitric oxide that can influence a wide variety of tissues. Similar to phenylephrine, a continuous infusion of SNP is required to maintain lowered levels of BP. Whereas, a single bolus intravenous injection of hydralazine induces an instantaneous and stable hypotensive effect, which lasts for even long durations of the protocol, such as 10 h (Chapter 4). In addition, the nitric oxide generated by intravenous SNP can exert non-specific effects by acting on tissues other than blood vessels. Therefore, we used hydralazine, not SNP, in our study to maintain lowered levels of BP. A single bolus intravenous injection of hydralazine, at a dose of 10 mg/kg (Springell et al., 2005), was given to animals to lower BP by at least 40 mmHg.

2.1.7 Transcardial perfusion

Transcardial perfusion was conducted at the conclusion of animal experiments to harvest the brainstem tissue for further immunohistochemistry (IHC). Animals were deeply anaesthetised with an overdose of sodium pentobarbital (>72 mg/kg). Once the absence of any withdrawal reflex to a nociceptive stimulus was established, animals were immediately transferred to the nearby fume hood. A midline incision was made to expose the abdominal cavity and diaphragm. The heart was exposed after cutting the rib cage bilaterally, and an 18G needle connected to a peristaltic pump was inserted through the left ventricle and advanced into the ascending aorta. 1 ml of heparin (5000 IU/ml) was given to the animal to prevent coagulation and cause vasodilation. Following heparin, the right atrium was pierced and the animal was perfused with ≈400 ml of ice cold 0.1 M phosphate buffered saline (PBS), followed by ≈400 ml of ice cold 4% paraformaldehyde (PFA) in 0.1 M PBS at pH 7.4.

The brainstem tissue, caudal from the pons up to cervical segments of the spinal cord, was extracted and harvested for further IHC analysis.

2.2 Immunohistochemistry (IHC)

2.2.1 Tissue harvesting and preparation

Dura layer of the extracted tissue was removed with fine forceps and the tissue was fixed overnight in 4% PFA in 0.1 M PBS (pH 7.4) at 4 °C, while shaking. On the following day, the tissue was rinsed in 0.1 M PBS before sectioning. The brainstem was mounted on a sectioning platform with superglue and was embedded in 2% agar. Agar (2%), once set, provides a structural support to the tissue while sectioning. Brainstems were sectioned transversely using a vibrating microtome (Leica VT1200S) at a thickness of 40 µm. Sections were collected sequentially in 5 pots filled with cryoprotectant solution (30% RNase free sucrose, 30% ethylene glycol, 2% polyvinylpyrrolidone in 0.1 M PBS at pH 7.4). Brainstem sections were stored at -20 °C until further used for IHC.

2.2.2 Immunohistochemistry (IHC)

IHC is a well-established technique for labelling of antigens in tissue samples, and is an extension of immunocytochemistry (used to label antigens in cells). Use of immunocytochemistry was first reported in 1942 by Coones et al., (Coones et al., 1942). Since then, IHC is used in many neuroanatomical studies in the cardiovascular system (Graham et al., 1995; Li and Dampney, 1994; Nedoboy et al., 2016; Shahid et al., 2012). IHC is a way of **anatomical** labelling of the antigen based on its **immunological** and **biochemical** properties. Many other techniques are available for the qualitative and quantitative assessment of antigens/proteins, such as western blotting, ELISA (enzyme-linked immunosorbent assay) and spectrophotometric techniques. However, with the availability of advanced microscopy techniques, IHC enables one to identify the distribution and localisation of proteins.

Availability of multiple fluorophores with excitation ranging from ≈350 nm (AMCA, DAPI and Alexa Fluor 350) to fluorophores in the infrared range, excitation of ≈750 nm (Alexa Fluor 750 and Cy7), decreases the chance of bleed through between channels. This also allows multiple labelling of antigens in the same sample, and makes co-localisation studies feasible. However, in order to rule out the non-specific binding of antibody, rigorous methods to characterise and ensure the specificity of antigen-antibody binding, and appropriate blocking step before detection, are necessary. Further to this, appropriate controls are required to account for the bleed through of staining between channels. Bleed through between channels can also

be avoided by selection of fluorophores with distinct (not overlapping) excitation and emission wavelength spectra.

Primary antibodies used to detect the antigen, in question, are normally raised against a specific epitope sequence that matches the epitope sequence on the antigen surface, and is easily accessible on the antigen surface (Figure 2.2). The inaccessibility of epitope sequence on the antigen surface, due to reasons such as the 3D structure of protein, leads to lack of staining with the primary antibody. This is one of the most common reasons due to which primary antibodies designed for techniques such as western blotting (protein denaturation leads to easy accessibility of the epitope sequence) do not always work with techniques such as IHC (3D protein structure is intact and epitope sequence is hidden). Mammalian IgG antibodies are Y shaped proteins that comprises of 2 main structural components, Fab and Fc component (Figure 2.2). **Fab** component is the **fragment antigen-binding** component that binds to the antigen (Figure 2.2). **Fc** component, **fragment crystalizable**, is the stem of the Y shaped antibody, which interacts with the cell surface receptors called Fc receptors, and is specific to the animal where the antibody is raised (Figure 2.2). Thus, Fc fragment is part of the primary antibody where the secondary antibody binds. There are 5 types of antibody isotypes found in mammals: IgD, IgM, IgA, IgE and IgG. IgY is a special immunoglobulin that is only found in birds, reptiles and chickens.

Antibodies used in this study were either polyclonal or monoclonal in origin. Polyclonal antibodies are a mixture of antibody molecules that can recognise multiple epitopes on one antigen. Whereas, monoclonal antibodies consist of only one antibody subtype and recognise only one epitope on one antigen. In this study, we used an indirect detection step where a secondary antibody conjugated to fluorophore, specific to the Fc fragment of the antigen binding primary antibody, was used.

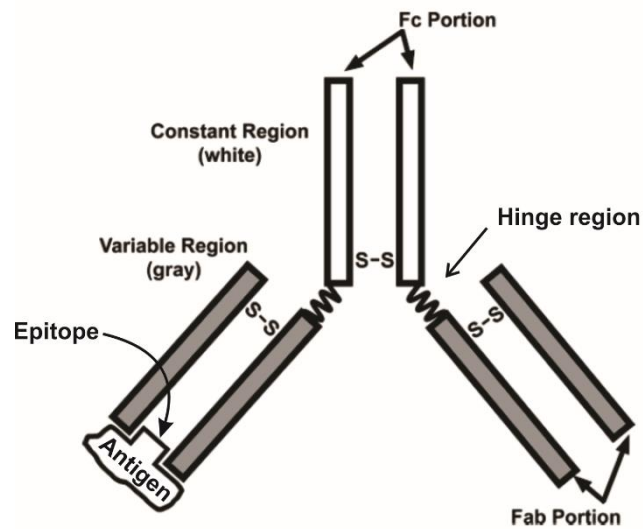


Figure 2.2: Pictorial representation of the Y shape of an IgG antibody

An antibody consists of a constant region (white) that contains the Fc portion (species specific) and a variable region (gray) that contains the epitope antigen-binding site, Fab portion. An IgG can be digested at the hinge region (flexible region) with a protease enzyme (papain/pepsin), and can be divided into an Fc end (constant end) and a Fab end (variable end). The antigen is the molecule used to immunize the animal, and the epitope is one of many portions of the antigen that can generate antibodies. S-S – disulphide bond. (Figure and legend adapted from (Burry, 2011); used with permission).

2.2.2.1 IHC protocol

Free-floating 40 µm brainstem sections, stored in cryoprotectant solution for less than 3 months, were washed in PBT (0.1 M PBS with 0.3% Triton X-100) for 3 times, 30 min each, at room temperature. 0.3% Triton X-100 was used to permeabilise tissue sections so that the primary antibody can access the antigen of interest. After washing, sections were incubated for >48 h in TTPBSm (10 mM Tris-HCl, 0.1 M PBS, 0.9% NaCl, 0.3% Triton X-100 and 0.1% merthiolate at pH 7.4). 0.1% merthiolate was used as a preservative for the incubation step. Normal donkey serum (10%) was added to sections as a blocking agent. Most of the secondary antibodies used in experiments, conducted as part of this thesis, were raised in donkey and thus, normal donkey serum was used to block reactive sites in the tissue where secondary antibody can bind non-specifically. Primary antibodies (depending on the experiment, refer to Appendix 1) were added to sections with solution containing TTPBSm and 10% normal donkey serum, and incubated for >48 h at 4 °C, while shaking. Sections were then washed 3 times, 30 min each, in TPBS (10 mM Tris-HCl, 0.1 M PBS and 0.9% NaCl at pH 7.4). Washed sections were then incubated overnight with secondary antibodies depending on the primary antibodies used (Appendix 1) in TPBSm (10 mM Tris-HCl, 0.1 M PBS, 0.9% NaCl and 0.1% merthiolate at pH 7.4) with 2% normal donkey serum at room temperature while shaking. Sections were then washed in TPBS 3 times, 30 min each, at room temperature while shaking.

2.2.2.2 Antibody characterisation

- *Cluster of differentiation-16 (CD16)*

The anti-CD16 monoclonal antibody was raised in mouse, IgG2a subtype specific (US biological, Life sciences, C2267-32), against whole white blood cells (clone ASH 1975). According to the manufacturer's specifications, this antibody is specific for CD16 antigen in humans, rat and mouse. In our hands, as expected, CD16 expression (M1) colocalised with Iba1 expression, and CD16 labelled microglia were amoeboid in shape. Further to this, brainstem sections (40 µm) from rats, where a physical injury was caused by a microinjection in the RVLM, were used to validate antibody staining (animal experiments were conducted by Dr. Farnham and Dr. Mohammed; Figure 2.3 A, B and C). Physical injury caused by a microinjection in the RVLM triggered the expression of M1 microglia that were positive for CD16 and CD68. CD68 represents a population of microglia that are phagocytosing, either M1 or M2. CD68 antibody, raised in rabbit (Abcam, ab125212), was used at a concentration of 1:2000 to label amoeboid microglia, which can be either M1 or M2 (Figure 2.3 A, B and C).

Skin samples (5 μ m) from 6-7 weeks old C57BL/6 mice from wound healing model (expected to be positive for M1 macrophages, animal experiments conducted by Dr. Anisyah Ridiandries; Figure 2.3D), were included as a positive control for CD16 staining (CD16 positive macrophages were observed, as expected).

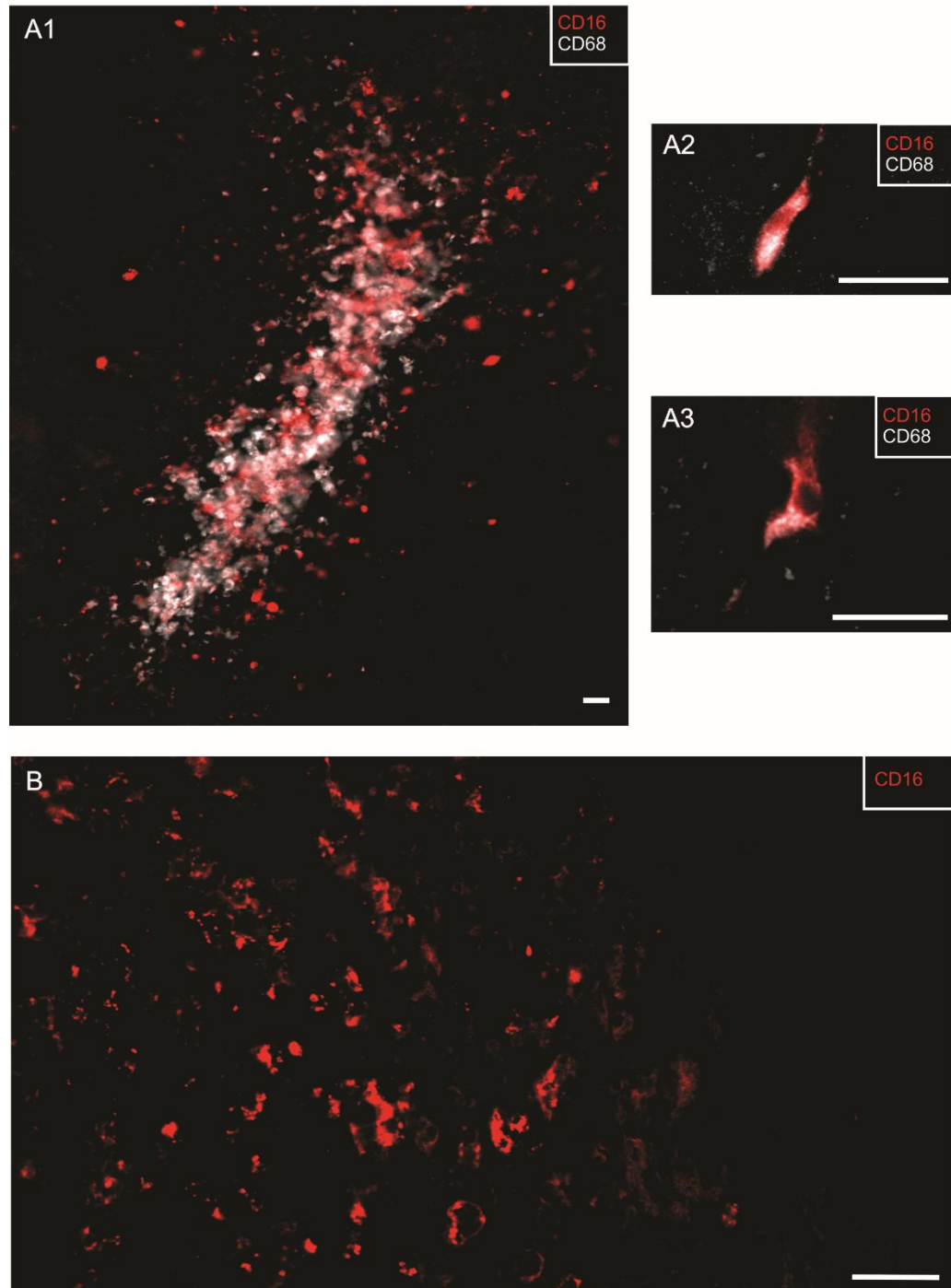


Figure 2.3: Expression of CD16 positive M1, amoeboid shaped, microglia

A. Images of the RVLM showing colocalisation of CD16 expression (red) and CD68 expression (white). A1 shows low magnification image of the RVLM (RVLM samples were collected from rats subjected to microinjection, causing physical injury). A2 and A3 are higher magnification images of M1 positive microglia shown in figure A1. B. Lower magnification image of M1 positive macrophages in skin samples collected from mice (from wound healing model). Scale bar = 20 μm .

- *Cluster of differentiation-206 (CD206)*

CD206/mannose receptor is known to, phenotypically, label microglia in an M2 state (David and Kroner, 2011; Perego et al., 2011). CD206 was used as an early marker to identify the presence of microglia exhibiting M2 phenotype in brainstem sections.

The anti-CD206 polyclonal antibody (Abcam, ab64693) was, raised in rabbit, against a synthetic peptide derived from within residues 1400 to the C-terminus of human Mannose receptor. Western blot analysis of rat liver lysate with this antibody resulted in only one band of size similar to that of the molecular weight of CD206 protein in rat (manufacturer's specifications). In Chapter 4 and Chapter 5, only CD206⁺ microglia that colocalised with Iba1 expression were counted as M2⁺ microglia.

- *Fos*

The proto-oncogene *c-Fos* belongs to a family of immediate early genes whose transcription is activated within minutes of application of a stimulus. Fos is a product of translation of the *c-fos* mRNA, which forms a heterodimer with Jun (protein product of another immediate early gene) (Rauscher et al., 1988), and this heterodimer controls the expression of late-genes in the cell/neuron (Dampney and Horiuchi, 2003; Simonson et al., 1992). In neurons, a stimulus causing neuronal depolarisation, such as synaptic excitation or hormones, induces the expression of c-Fos (Dampney and Horiuchi, 2003; Morgan and Curran, 1989). However, Fos labelling does not provide an indication of the degree of activation of neurons and whether the Fos⁺ neurons were activated in direct, or indirect, response to the provided stimulus (Appleyard, 2009). Another limitation of using Fos as a marker of activated neurons is that it fails to identify the group of neurons that were inhibited in response to a provided stimulus, and does not allow real-time measurement of neuronal activity (Kovacs, 2008). In addition, in some cases, it is possible that neuronal activation occurs without involving *c-Fos* gene (Appleyard, 2009; Kovacs, 2008). Furthermore, use of anaesthetic can greatly influence expression levels of Fos (Dampney et al., 1995; Dampney and Horiuchi, 2003; Dragunow and Faull, 1989). Despite these limitations, Fos is a useful, sensitive and readily available marker to label activated neurons. Furthermore, colocalised labelling can also be performed to identify the phenotype of Fos⁺ neurons.

The polyclonal Fos antibody (Synaptic Systems, 226 004) used in this study was, raised in Guinea pig, against synthetic peptide corresponding to the amino acid sequence 2-17 of rat Fos protein. Western blot analysis of lysate from nuclear extract of TPA stimulated HELA cells,

with this antibody, resulted in only one band of ≈ 60 kDa, corresponding to the molecular weight of Fos protein in rat (manufacturer's specifications). Further to this, absence of staining with this antibody in TPA untreated HELA cells was also confirmed using immunocytochemistry (manufacturer's specifications). In Chapter 4 and Chapter 5, the staining pattern obtained with this antibody was as expected to the provided stimulus (intravenous administration of phenylephrine, saline or hydralazine) (Graham et al., 1995).

As mentioned previously (sections 1.2.1.6, 1.2.1.7 and 1.3.1), modulations introduced in BP alter the level of neuronal activity (shown by changes in Fos-ir levels) in the NTS, the CVLM and the RVLM (Chan and Sawchenko, 1994; Graham et al., 1995; Li and Dampney, 1994; Minson et al., 1997b; Suzuki et al., 1994). The main aim of experiments performed in this thesis was to characterise the microglial response to alterations induced in BP levels. Therefore, as part of this thesis, changes in Fos-ir levels in response to the provided stimulus (phenylephrine induced hypertension or hydralazine induced hypotension) were only quantified in the RVLM, and not the CVLM, to validate the effect of the provided stimulus. Also, no attempt was made in this thesis to distinguish between the C1 Fos-ir group of RVLM neurons from the non-C1 Fos-ir group.

- *Ionized calcium-binding adaptor molecule-1 (Iba1)*

Iba1 is a pan marker for all microglial phenotypes: M0, M1 and M2. Iba1 is used, interchangeably with CD11b (clone OX-42), to phenotypically label and characterise microglia into different activation states based on their morphology (Dworak et al., 2012; Dworak et al., 2014; Morrison and Filosa, 2013; Shapiro et al., 2009; Smolny et al., 2014).

The polyclonal anti-Iba1 antibody (Wako, 019-19741, RRID AB_2314667) was raised in rabbit against the synthetic peptide "PTGPPAKKAISELP", corresponding to the C-terminus of Iba1. This antibody is specific for microglia and macrophages, and does not cross react with neurons and astrocytes (manufacturer's specifications). In our hands, no cross-reaction was observed between microglia stained with this antibody and TH neurons. This antibody recognised Iba1 antigen in swiss 3t3 cells transfected with Iba1 protein, whereas non-transfected cells were negative (manufacturer's technical information). This Iba1 antibody (Wako, 019-19741) is also listed in the *Journal of Comparative Neurology* antibody database, implying that the staining obtained with this antibody meets the stringent standards set to characterise antibody specificity.

The polyclonal anti-Iba1 antibody (Novus Biologicals, NB100-1028) was raised in goat against the synthetic peptide “TGPPAKKAISELP”, corresponding to the C-terminus of the Iba1 human protein, and is known to react with rat Iba1 protein. Western blot analysis of rat brain lysate labelled with this antibody resulted in only one band of ≈ 17 kDa corresponding to the molecular weight of Iba1 protein in rat (manufacturer’s specifications). Microglia stained with this antibody were similar in morphology and distribution pattern to the ones stained by polyclonal rabbit anti-Iba1 antibody (Wako, 019-19741).

- *Synapsin*

The synapsin antibody is a pre-synaptic marker, and is used in this study to label synaptic boutons. The polyclonal anti-synapsin 1/2 antibody (Synaptic Systems, 106 004) was raised in guinea pig against a synthetic peptide “NYLRRRLSDSNFMANLPNGYMTDLRQP”, corresponding to the N terminus of rat synapsin protein. This antibody detects proteins of expected size and the IHC signal was blocked by pre-adsorption with the immunogen (manufacturer’s technical information). In our hands, the staining observed with this antibody is enriched in the synaptic vesicle fraction, as expected, and matches the staining pattern observed by other synaptic markers such as Synaptophysin.

- *Tyrosine Hydroxylase*

As mentioned in section 1.2.2, TH is a marker of catecholaminergic nuclei in the brainstem, such as the A1 and the C1 nucleus. TH was used in this study to, anatomically, identify the location of A1, A2, C1, C3, A5 and A6 neurons in the brainstem.

The monoclonal anti-TH antibody from Sigma-Aldrich was raised in mouse (Sigma-Aldrich, St. Louis, MO; T1299, RRID AB_477560). According to the manufacturer’s specifications, indirect immunoblot analysis of proteins extracted from rat PC-12 pheochromocytoma cells resulted in a single band of ≈ 60 kDa corresponding to the molecular weight of TH protein from rat. All PNMT neurons identified with in-situ hybridization (ISH) in the brainstem were labelled with this TH antibody, as expected (Pilowsky et al., 2009). This TH antibody is also listed in the *Journal of Comparative Neurology* antibody database, implying that the staining obtained with this antibody meets the stringent standards set to characterise antibody specificity.

The monoclonal TH antibody, from Avanti antibodies, was raised in mouse (subtype specific for IgG1 κ), against synthetic peptide with sequence “CPRFIGRRQSLIEDARK” (Avanti antibodies; #AV1, RRID AB_2531895). This antibody is specific for TH in rat brainstem sections and is synthesised and characterised by the ‘High Blood Pressure group’ at the Heart

Research Institute, Sydney, NSW (Nedoboy et al., 2016). In the present study, TH neurons labelled with this antibody were similar in morphology, and staining pattern, to the ones labelled with the mouse monoclonal anti TH (T1299). In addition to this, the staining of this antibody was also characterised by colocalising the staining obtained with this antibody (Avanti antibodies, #AV1) with the expression of TH labelled with commercially available antibody from Abcam, Ab113 (Sheep polyclonal, 1:3000) (Figure 2.4).

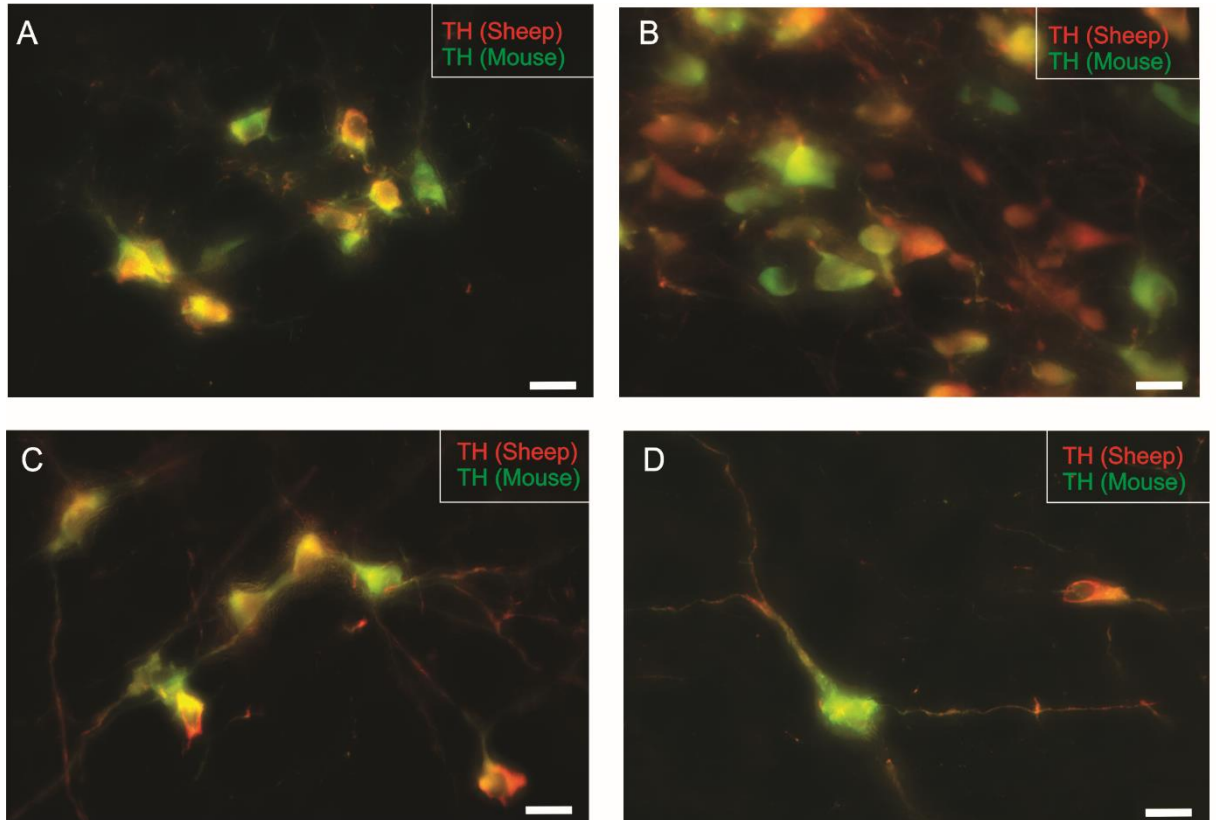


Figure 2.4: TH antibody characterisation

Colocalisation of staining was observed from TH antibody raised in mouse (Avanti antibodies, #AV1, green) and TH antibody raised in sheep (Abcam, Ab113, red) in the brainstem catecholaminergic nuclei, such as A1 (A), A2 (B), C1 (C) and A5 (D) regions. Scale bar = 20 μm .

2.2.3 Mounting

Sections processed for IHC were then mounted, caudal to rostral, on glass slides (Thermo Fisher Scientific) with a fine paint brush and air-dried. Caution was taken at this step not to over-dry sections, but semi-dry, so that sections will not move freely on the glass slide. Air-dried glass slides were cover-slipped with Vectashield (H-1000, Vector Laboratories) to prevent the fluorophores from photo-bleaching and these slides were then sealed with clear nail polish for imaging.

2.3 Data acquisition

2.3.1 Physiological data

2.3.1.1 *Tail-cuff BP data*

Systolic BP values, for conscious WKY and SHR, were acquired with the tail-cuff IITC MRBP system (section 2.1.3). Systolic BP values for each rat from each repeat (3 measurements/animal) were averaged using Microsoft Excel 2013.

2.3.1.2 *BP data from animals under anaesthesia*

Two physiological parameters were acquired with Spike 2 acquisition and analysis software (version 8.01, Cambridge Electronic Designs) during experimental protocols, BP and temperature. HR was derived from the BP data by logging each systolic peak, with an amplitude of >20 mmHg, and displaying the same as instant frequency in real time. HR and temperature traces were recorded to monitor the physiological health of the animal during the experiment and were not used in subsequent analysis.

2.3.2 Microscopy

Slides prepared following the IHC protocol were visualized, and images were acquired (20X, 40X or 63X magnification), with the Zeiss Axio Imager Z2 epifluorescence microscope (ZEISS, Germany) for Chapter 3 and Chapter 4. Data at lower magnifications, such as 20X and 40X, for Chapter 5 were acquired with a slide-scanning Axio Scan.Z1 microscope (ZEISS, Germany). For data concerning Iba1 and synapsin (Chapter 5), sections were visualised with an oil-immersion lens at 63X magnification, and data were acquired, with the Zeiss Axio Imager Z2 epifluorescence microscope (ZEISS, Germany). Images were adjusted for brightness and contrast to better visualize microglial morphology.

Each fluorophore was imaged individually with a filter cube (Semrock, USA) of appropriate excitation/emission wavelengths, with an Axiocam HRm digital camera (ZEISS, Germany). 4 non-overlapping fluorophores were used in this study: AMCA (350/445 -ex/em), Alexa Fluor 488 (496/519 – ex/em), Cy3 (550/570 – ex/em) and Cy5 (650/670 – ex/em). Images were captured as greyscale, and pseudo-coloring was applied to images for better visualization and colocalisation analysis.

Images obtained to demonstrate the morphological relationship between microglia and cardiovascular neurons were acquired with the Zeiss LSM 510 Spectral Meta confocal microscope (ZEISS, Germany) and Leica SPE-II confocal microscope (Leica, Germany). Both confocal microscopes, and Axio Scan.Z1 slide scanning microscope, are located at the ‘Advanced Microscope Facility’ at the Bosch Institute, University of Sydney. Four separate lasers were used for acquiring images using the Zeiss/Leica confocal microscope: 405 nm laser for AMCA, an argon laser (458, 477, 488 and 514 nm lines) for Alexa Fluor 488, 561 nm DPSS for Cy3 and 633 nm HeNe laser for Cy5.

2.4 Analysis

2.4.1 Tail-cuff BP data

Three consecutive values were acquired for systolic blood pressure (SBP) from each SHR and WKY. These repeat measurements were averaged in Excel 2013. The averaged value of SBP from each animal was then imported into GraphPad Prism 6.05 for further statistical analysis.

2.4.2 Physiological data

Area Under curve (AUC) values for MAP, at each time point for all strains (SD, WKY and SHR), were calculated with the Spike 2 software for area spanning between 2 cursors, one cursor placed at the start and the other cursor placed at the end of the protocol. The benefit of using AUC values, rather than MAP at a particular time point, is that AUC provides a more accurate representation of changes that have occurred during the whole treatment period. MAP values only account for the value of MAP at a particular time point. Whereas, AUC takes into account every change that has occurred during the protocol period and thus, provides an integrated value that is inclusive of the total change in blood pressure since the time the infusion started.

AUC values for MAP for SHR and WKY were highly variable, from animal to animal. Therefore, AUC values for the whole protocol period (either 2 or 6 h), for each animal, were normalized to AUC values obtained for area spanning 5 min before the start of the protocol (Chapter 5).

$$\text{Normalised AUC} = \frac{\text{AUC for the protocol period}}{\text{AUC for 5 min before the start of the protocol}} * 100$$

Normalised AUC values were exported to GraphPad Prism 6.05 for subsequent statistical analysis.

2.4.3 Histological data

- *Counts*

All the counting was performed in the Zen software (ZEISS, Germany) except for counting the number of microglia at 20X magnification. Microglia and Fos-ir/ TH-ir neurons present at the boundary of images were not included in the final count.

Number of microglia, Fos-ir and TH-ir neurons were counted manually at 40X magnification. A plugin was created using in-built features of Image J (NIH), with macros, to count the number of microglia at 20X magnification (Plugin 1). Below is a script of Plugin 1:

Plugin 1: To quantify the number of microglia, in a ROI, at 20X magnification

```
run("8-bit");
setOption("BlackBackground", true);
run("Make Binary");
run("Erode");
run("Particle Remover", "size=0-400 pixel summarize");
IJ.deleteRows(0, 0);
run("Make Binary");
run("Analyze Particles...", "size=0-Infinity summarize");
```

CD206⁺ microglia that colocalised with Iba1 labelled microglia (20X magnification) were the only ones counted for subsequent analysis.

- *Spatial distribution analysis*

Details of spatial distribution analysis are included in the “Experimental protocol” section 4.3.5.1 of Chapter 4. In brief, each image acquired at 40X magnification was divided into 6 equal parts with the grid feature of CorelDraw (version X7) and 1 microglia was chosen from each of these 6 parts. A series of 6 concentric circles were drawn around each microglia, first one centered at the soma with a radius of 8 μm , and consecutive circles increasing by radii of 5 μm . Number of microglial cell bodies intersecting with each of these circles were counted. This method is an adaptation of Sholl analysis (Morrison and Filosa, 2013; Sholl, 1953).

- *Morphological analysis*

Morphological analysis was performed as described by Morrison and Filosa (Morrison and Filosa, 2013). Plugins were created in Image J (NIH) to process images and analyse the microglial skeleton at 40X magnification (Plugin 2) and 63X magnification (Plugin 3). Another plugin was created in ImageJ (NIH) to calculate the % of area occupied by microglia at 40X magnification (Plugin 4). Below are scripts of Plugins 2, 3 and 4:

Plugin 2: Microglial skeleton analysis at 40X magnification

```
run("Set Scale...", "distance=310 known=50 pixel=1 unit=um");
run("8-bit");
run("Find Edges");
setOption("BlackBackground", true);
run("Make Binary");
run("Fill Holes");
run("Skeletonize (2D/3D)");
run("Analyze Skeleton (2D/3D)", "prune=none show");
```

Plugin 3: Microglial skeleton analysis at 63X magnification

```
run("Set Scale...", "distance=488.37 known=50 pixel=1 unit=um");
run("8-bit");
run("Find Edges");
setOption("BlackBackground", true);
run("Make Binary");
run("Fill Holes");
run("Skeletonize (2D/3D)");
run("Analyze Skeleton (2D/3D)", "prune=none show");
```

Plugin 4: To calculate the % of area occupied by microglia at 40X magnification

```
run("Set Scale...", "distance=310 known=50 pixel=1 unit=um");
run("8-bit");
run("Find Edges");
setOption("BlackBackground", true);
run("Make Binary");
run("Fill Holes");
run("Set Measurements...", "area shape area_fraction redirect=None decimal=3");
run("Measure");
```

Details are also included in Chapter 4 (section 4.3.5).

- *Synapsin co-localisation analysis*

Data obtained from SD animals (Chapter 4) for synapsin were analysed manually. 10 microglia from each image were chosen and the number of synaptic structures (labelled with synapsin) colocalising with microglial end-point processes were counted. However, this method is labor intensive and may include some user biasness.

In order to automate the colocalisation analysis for Chapter 5, a freely available ‘Colocalisation Finder’ plugin (<http://rsb.info.nih.gov/ij/plugins/colocalization-finder.html>) in Image J (NIH) was used. 10 microglia from each image, acquired at 63X magnification, were chosen. Individual images for each microglia (Iba1) and corresponding synapsin image were imported into Image J, in pairs, as black and white images, and then were converted to 8-bit images. All images were thresholded at the same intensity value to maintain consistency in the analysis.

‘Colocalisation Finder’ plugin was then used on these images to identify the % of area co-localising between each microglial (Iba1) and corresponding synapsin image; this refers to the % of Synapsin labelled synapses that had co-localised with Iba1 labelled microglia.

2.5 Statistical analysis

Statistical analysis on the acquired data, generally, is performed to estimate parameters for ‘whole population’ from data collected from a ‘subset of population’. There are 2 types of statistics, parametric and non-parametric. The main difference between these 2 types of statistics is that parametric statistics relies on 5 very important assumptions, which include that data is normally distributed, continuous in nature, samples are independent of each other, observations are sampled randomly and homogeneity of variances (Sokal and Rohlf, 2012). On the contrary, non-parametric statistics doesn’t rely on any assumption regarding distribution of the population from where the sample is drawn (also known as distribution-free methods) and the acquired data doesn’t need to be continuous (Sokal and Rohlf, 2012).

One drawback of non-parametric statistical tests is that these tests carry less power, which means there is a greater probability of missing the significance in the results. Non-parametric tests are more conservative. However, this can be taken as an advantage as this drawback decreases the likelihood of accounting for misinterpreted significant results, where there is no significance in reality (leading to Type I statistical errors i.e. falsely rejecting the null hypothesis).

Based on the characteristics listed in Table 2.1, each parameter acquired in this study was assigned to a category of statistics based on the type of data (parametric or non-parametric), and subsequently analysed with appropriate statistical tests (Sokal and Rohlf, 2012).

Table 2.1: Considerations for choosing parametric vs non-parametric test

Type of analysis	Parametric	Non-parametric
Assumed distribution	Normal distribution	Distribution free
Samples are independent	Yes	Not necessarily
Homogeneity of variance	Yes	No
Data type	Continuous	Discontinuous (counts)

Table 2.2: List of parameters acquired in this study and appropriate statistical tests

Type of parameter	Type of data	Parametric vs non-parametric	Statistical test	Purpose
% of area occupied by microglia	Continuous	Non-parametric	Kruskal-Wallis one-way analysis of variance	Compares three or more groups
% CD206 ⁺ to total microglia	Continuous	Non-parametric	Kruskal-Wallis one-way analysis of variance	Compares three or more groups
% of colocalisation between synapsin and microglia	Continuous	Non-parametric	Mann-Whitney U test	Compares 2 independent groups
Area under curve (AUC) for MAP	Continuous	Parametric	One-way ANOVA between treatment groups (phenylephrine, saline and hydralazine)	Compares three or more groups
Branch length (µm)/ microglia	Continuous	Non-parametric	Kruskal-Wallis one-way analysis of variance	Compares three or more groups
Distribution pattern of TH-ir neurons and/or microglia	Non-continuous	Non-parametric	Chi-square test of Independence	To identify if variables (distribution patterns) are independent or not

Number of end point processes/ microglia	Continuous	Non-parametric	Kruskal-Wallis one-way analysis of variance	Compares three or more groups
Number of microglia	Non- continuous	Non-parametric	Chi-square test for goodness-of- fit	If there is any difference between observed value and expected value of a variable
Number of neurons	Non- continuous	Non-parametric	Chi-square test for goodness-of- fit	If there is any difference between observed value and expected value of a variable
Number of synapses colocalising with microglial end point processes	Non- continuous	Non-parametric	Chi-square test for goodness-of- fit	If there is any difference between observed value and expected value of a variable
Systolic BP values (tail-cuff phenotyping of WKY and SHR)	Continuous	Parametric	Student's t-test (unpaired)	Compares 2 independent groups

All of the statistical tests mentioned in Table 2.2 were performed in GraphPad Prism version 6.05.

The Chi-square test is applicable for a variable whose values range from zero to positive infinity and therefore, unlike the normal distribution, the function approaches the X-axis only at the right-hand tail of the curve (Sokal and Rohlf, 2012). The Chi-square test for goodness-of-fit determines whether the observed value differs from the expected value to such a magnitude that it will cause the rejection of null hypothesis (Sokal and Rohlf, 2012). On the other hand, Chi-square test of independence provides an indication to whether one distribution (TH-ir neurons) is similar to another (Iba1-ir microglia) (Sokal and Rohlf, 2012). Data concerning the number of TH-ir/Fos-ir neurons, the number of microglia, the number of synapses colocalising with microglial end point processes and 'distribution patterns of TH-ir neurons and microglia' are categorical data, which are not continuous and do not follow a normal distribution. Therefore, these variables were analysed using the appropriate Chi-square tests (refer to Table 2.2).

The variables defining microglial morphological characteristics, or % of colocalisation between microglia and synapsin, did not follow a normal distribution, and thus, were analysed with distribution-free methods (non-parametric method) (Sokal and Rohlf, 2012). No attempt was made in this thesis to transform the acquire data to fit the assumptions of ANOVA. Data concerning microglial morphological characteristics (such as branch length (μm)/ microglia) were analysed using Kruskal-Wallis one-way analysis of variance. Data concerning the % of colocalisation between microglia and synapsin were analysed using Mann-Whitney U test. Kruskal-Wallis one-way analysis of variance is essentially a non-parametric equivalent of one-way ANOVA and Mann-Whitney U test is a non-parametric equivalent of Student's t-test.

Chapter 3

Microglial number is related
to the number of tyrosine
hydroxylase neurons in SHR
and normotensive rats

Contents

3.1	Abstract.....	137
3.2	Introduction.....	138
3.3	Experimental procedures	139
3.3.1	Animals	139
3.3.2	Experimental protocol	140
3.3.2.1	<i>Perfusion and tissue processing</i>	<i>140</i>
3.3.2.2	<i>Immunohistochemistry.....</i>	<i>140</i>
3.3.2.3	<i>Image acquisition</i>	<i>141</i>
3.3.3	Image analysis	141
3.3.4	Data analysis and statistics	142
3.4	Results	144
3.4.1	Intra-strain comparison demonstrating that microglial number is related to the number of TH-ir neurons in a catecholaminergic nucleus.....	144
3.4.2	Inter-strain comparison of TH neuronal and microglial number in various brainstem catecholaminergic nuclei.....	144
3.4.3	Microglial morphology doesn't vary considerably between catecholaminergic nuclei, regardless of the strain.....	145
3.5	Discussion	154

Abbreviations:

ANS – autonomic nervous system

CNS – central nervous system

DβH – dopamine β hydroxylase

PBS – phosphate buffered saline

SD – Sprague-Dawley

SHR – spontaneously hypertensive rats

TH – tyrosine hydroxylase

WKY – Wistar-Kyoto

Keywords: Microglia, Iba1, Tyrosine hydroxylase, SD, WKY, Hypertensive, Brainstem.

Highlights:

- Microglia are heterogeneously distributed in the sympathetic nervous system.
- Microglial distribution varies with the tyrosine hydroxylase neuronal number.
- Microglial morphology is similar across different catecholaminergic nuclei.

The work described in this chapter is published in “**Autonomic Neuroscience: Basic and Clinical**”.

Kapoor, K., Bhandare, A.M., Mohammed, S, Farnham, M.M.J., Pilowsky, P.M., 2016. Microglial number is related to the number of tyrosine hydroxylase neurons in SHR and normotensive rats. *Autonomic Neuroscience*. “In press”

The text of this chapter is an exact representation of the published material except for the figure numbers and the section numbers, which were modified to match the rest of this thesis.

Version of record published as: Kapoor, K., Bhandare, A. M., Mohammed, S., Farnham, M. M. J., Pilowsky, P. M. (2016) Microglial number is related to the number of tyrosine hydroxylase neurons in SHR and normotensive rats, *Autonomic Neuroscience*, Vol. 198, pp. 10-18, <https://doi.org/10.1016/j.autneu.2016.05.005>.

Declaration of contributions: Candidate contributed to the design of experiments, performed all experiments, analysed data, interpreted results and was the major contributor to the manuscript. Amol M. Bhandare (a PhD candidate) assisted with the animal experiments. Paul M. Pilowsky and Melissa M.J. Farnham contributed to conception and design of experiments, data analysis, interpretation of results, and editing and final approval of the manuscript. Suja Mohammed contributed to the design of IHC experiments.

3.1 Abstract

Microglia are ubiquitously distributed throughout the central nervous system (CNS) and play a critical role in the maintenance of neuronal homeostasis. Recent advances have shown that microglia, never resting cells of the CNS, continuously monitor and influence neuronal/synaptic activity levels, by communicating with neurons with the aid of their dynamic processes. The brainstem contains many catecholaminergic nuclei that are key to many aspects of brain function. This includes C1 neurons of the ventrolateral medulla that are thought to play a critical role in control of the circulation. Despite the role of catecholaminergic brainstem neurons in normal physiology, the presence of microglia that surrounds them is poorly understood. Here, we investigate the spatial distribution and morphology of microglia in catecholaminergic nuclei of the brainstem in 3 strains of rat: Sprague-Dawley (SD), Wistar-Kyoto (WKY) and spontaneously hypertensive rats (SHR). Our data reveal that microglia are heterogeneously distributed within and across different strains of rats. Interestingly, intra-strain comparison of tyrosine hydroxylase-immunoreactive (TH-ir) neuronal and microglial number reveals that microglial number varies with the TH-ir neuronal number in the brainstem. Even though microglial spatial distribution varies across brainstem nuclei, microglial morphology (% area covered, number of end point processes and branch length) does not differ significantly. This work provides the first evidence that even though microglia, in their surveilling state, do not vary appreciably in their morphology across brainstem areas, they do have a heterogeneous pattern of distribution that may be influenced by their local environment.

3.2 Introduction

Microglia are the tissue resident macrophages of the central nervous system (CNS). They are ubiquitously distributed, and comprise $\approx 10\text{--}15\%$ of cell population in the CNS (Xavier et al., 2014). Microglia are of mesodermal origin and populate the CNS during early stages of development, and are self-renewing in case of depletion (Ajami et al., 2007). Since 2005, microglia are no longer known solely for their critical role as immune cells of the CNS (Nimmerjahn et al., 2005). Recent work about the function of microglia concerns their role in maintaining normal brain homeostasis. The ability of microglia to communicate, detect changes, and influence the activity of neurons (Pocock and Kettenmann, 2007) and astrocytes (Aloisi et al., 1997; Pyo et al., 2003), highlights their role as an integral component of the “Glial Family”. Microglia, in their resting/ surveilling state, are capable of performing activities, such as release of neurotrophic factors (Karperien et al., 2013; Ueno et al., 2013) or synaptic pruning (Kettenmann et al., 2013; Miyamoto et al., 2013); during injury, microglia transform into a more macrophage-like ‘activated’ state removing debris, and enhancing tissue repair (David and Kroner, 2011; Kroner et al., 2014; Windelborn and Mitchell, 2012). The role of microglia in non-injurious situations is less clear.

Microglia are ubiquitously, yet heterogeneously, distributed in many areas of the CNS, including the hippocampus, olfactory telencephalon, cerebellum, cortex and spinal cord (de Haas et al., 2008; Lawson et al., 1990; Mittelbronn et al., 2001; Nikodemova et al., 2014). Heterogeneous microglial distribution, chemical expression profiles and morphology are hypothesised to be strongly influenced by their local environment (de Haas et al., 2008; Kapoor et al., 2015; Lawson et al., 1990; Mittelbronn et al., 2001; Nikodemova et al., 2014). However, exact factors responsible for the heterogeneity in microglial expression in a given environment are still unknown.

Catecholaminergic nuclei of the brainstem are involved in almost every aspect of cardiorespiratory control, ranging from the maintenance of tonic activity of the sympathetic nervous system (SNS) to somatosensory reflex responses (Pilowsky et al., 2009). Phenotypically, catecholaminergic nuclei are immunoreactive for tyrosine hydroxylase (TH), and extend from the caudal ventrolateral medullary region to the pons, including A1, A2, C1, C3, A5 and A6 (Dahlström and Fuxe, 1964). Studies using stimuli, such as hypotension, hypertension and glucoprivation, have shown that the neuronal activity of various catecholaminergic nuclei of the brainstem is affected by these homeostatic challenges

(Dampney and Horiuchi, 2003; Graham et al., 1995; Springell et al., 2005). For example, acute hypotension, induced by intravenous injection of hydralazine or infusion of sodium nitroprusside, causes activation of neurons located in the A1 (Benarroch, 1998), C1 (Minson et al., 1996; Miyawaki et al., 2002a), A5 (Dampney and Horiuchi, 2003) and A6 regions of the brainstem (Dampney and Horiuchi, 2003). On the other hand, induction of glucoprivation causes activation of A6 neurons (Ritter et al., 1998). The A2 catecholaminergic nucleus of brainstem not only responds to cardiorespiratory stimuli, but also responds to other diverse range of signals, such as hormonal, gastrointestinal and inflammatory (Rinaman, 2011). The function of C3 group of neurons of the brainstem is the least studied, but they may be sympathoexcitatory and respond to stimuli affecting glucose homeostasis (Menuet et al., 2014). In fact, it may be that C3 neurons are simply anatomically displaced C1 or C2 neurons that did not reach their final destination in the ventral or dorsal medulla oblongata.

Recent work has shown that close lines of communication exist between microglia and the SNS (Bhandare et al., 2015; Bhandare et al., 2016; Kapoor et al., 2016b; Shi et al., 2010a). As mentioned above, catecholaminergic nuclei in the brainstem are critical in the regulation of sympathetic nerve activity. The close link between microglia and the SNS, and previously proposed hypothesis that microglial distribution is influenced by their local environment (de Haas et al., 2008), formed the foundation of aims of the present study. Therefore, in this study, we aimed to identify if the microglial distribution is related to the neuronal heterogeneity in the SNS. For the purpose of this study, we used 3 different strains of rats: Sprague-Dawley (SD), the Wistar-Kyoto (WKY) and the spontaneously hypertensive rat (SHR).

3.3 Experimental procedures

3.3.1 Animals

Experiments were conducted in adult male rats from 3 different strains: SD, WKY (>18 weeks old) and SHR (>18 weeks old); n=3 per group (300-420 g; Animal Resource Centre; Perth, Australia) in accordance with the Australian code of practice for the care and use of animals for scientific purposes. All procedures and protocols performed were approved by the Sydney Local Health District Animal Welfare Committee and the Macquarie University Animal Care and Ethics Committee, Sydney, Australia.

The blood pressure phenotype of SHR and WKY was determined by tail-cuff sphygmomanometry at >18 weeks of age, prior to perfusion (Farnham et al., 2012). Hypertension was defined as a systolic pressure of >180 mmHg and normotension was defined as a systolic pressure of <150 mmHg.

3.3.2 Experimental protocol

3.3.2.1 *Perfusion and tissue processing*

Animals were deeply anaesthetized with sodium pentobarbital (>72 mg/kg i.p.; Cenvet Australia) and were transcardially perfused with ≈400 ml of ice cold 0.1 M phosphate buffered saline (PBS) followed by fixation with ≈400 ml of ice cold 4% paraformaldehyde in 0.1 M PBS (pH 7.4). Extracted brainstem tissue was fixed overnight in 4% paraformaldehyde in 0.1 M PBS (pH 7.4) at 4 °C, while shaking continuously. Brainstems were then sectioned transversely, using a vibrating microtome (VT1200S, Leica), at 40 µm and were collected sequentially into 5 pots. These sections were stored in cryoprotectant solution (30% sucrose, 30% ethylene glycol, 2% polyvinylpyrrolidone in 0.1 M PBS) at -20 °C until processed for immunohistochemistry.

3.3.2.2 *Immunohistochemistry*

Immunohistochemistry was conducted as described previously (Kapoor et al., 2016b; Nedoboy et al., 2016). Briefly, free floating 40 µm brainstem sections were washed in 0.1 M PBS with 0.3% Triton X-100, 3 times for 30 min each, at room temperature. After washing, sections were incubated for >48 h in TTPBSm (10 mM Tris-HCl, 0.1 M PBS, 0.9% NaCl, 0.3% Triton X-100 and 0.1% merthiolate at pH 7.4), 10% normal donkey serum with primary antibodies raised against TH (Mouse monoclonal (IgG1κ), Avanti antibodies, #AV1 (Nedoboy et al., 2016); 1:100) and Iba1 (Rabbit polyclonal, Wako Pure Chemical Industries Ltd., 019-19741; 1:2000) at 4 °C while shaking. Sections were then washed 3 times for 30 min each in TPBS (10 mM Tris-HCl, 0.1 M PBS and 0.9% NaCl at pH 7.4) and incubated overnight with secondary antibodies raised in donkey: donkey anti mouse Cy5 (Jacksons Immunoresearch 715-175-151; 1:500) and donkey anti rabbit Cy3 (Jacksons Immunoresearch 711-166-152; 1:500) in TPBSm (10 mM Tris-HCl, 0.1 M PBS, 0.9% NaCl and 0.1% merthiolate at pH 7.4) with 2% normal donkey serum at room temperature while shaking. Sections were then washed in TPBS 3 times for 30 min each at room temperature while shaking. These sections were then mounted, caudal to rostral, on glass slides (Thermo Fisher Scientific), cover-slipped with Vectashield (H-1000, Vector Laboratories) and sealed with clear nail polish for imaging.

3.3.2.3 Image acquisition

Brainstem sections were imaged using an Axio Imager Z2 (Zen software, Zeiss, Germany) for subsequent analysis. Each fluorochrome was imaged individually with appropriate filter cubes (TH-Cy5 with 650/670 nm (ex/em) and Iba1-Cy3 with 550/570 nm (ex/em)). Bilateral 'Z-stack' images of A1, A2, C1, A5 and A6 and medial 'Z-stack' images of C3 at 40X magnification were obtained, covering an area of 400 μ m X 400 μ m, 30 μ m in depth, at an interval of 0.62 μ m generating a stack of \approx 46 Z slices, for each repeat in each strain (3 strains; n=3 each; Figure 3.1).

A rat brain atlas (Paxinos and Watson, 2007) was used to define the anatomical location of the neuronal population analysed in this study. The A1 nucleus was defined as the area comprising of TH immunoreactive (TH-ir) neurons in the caudal ventrolateral medulla at the level of the area postrema and \approx 14.28 mm caudal to bregma (Figure 3.1). The A2 was defined as the area in and around the medial region of the nucleus of the solitary tract, at the level of \approx 14.64 mm caudal to bregma (Figure 3.1). The C1 was defined as a triangular area ventral to the nucleus ambiguus, medial to the spinal trigeminal tract and lateral to the pyramidal tracts at the level of \approx 12.36 mm caudal to bregma (Figure 3.1). The C3 was defined as the area populated with TH-ir neurons, in close proximity to 4th ventricle and at the level of \approx 12.36 mm caudal to bregma (Figure 3.1). The A5 was defined as the area nearer to the pontomesencephalic junction mostly between the descending facial nerve fibres and the superior olive, at the level of \approx 10.56 mm caudal to bregma (Figure 3.1). A6 neurons were located beside the fourth ventricle at the pontomesencephalic junction, rostral to the facial nucleus and at the level of \approx 9.72 mm caudal to bregma (Figure 3.1).

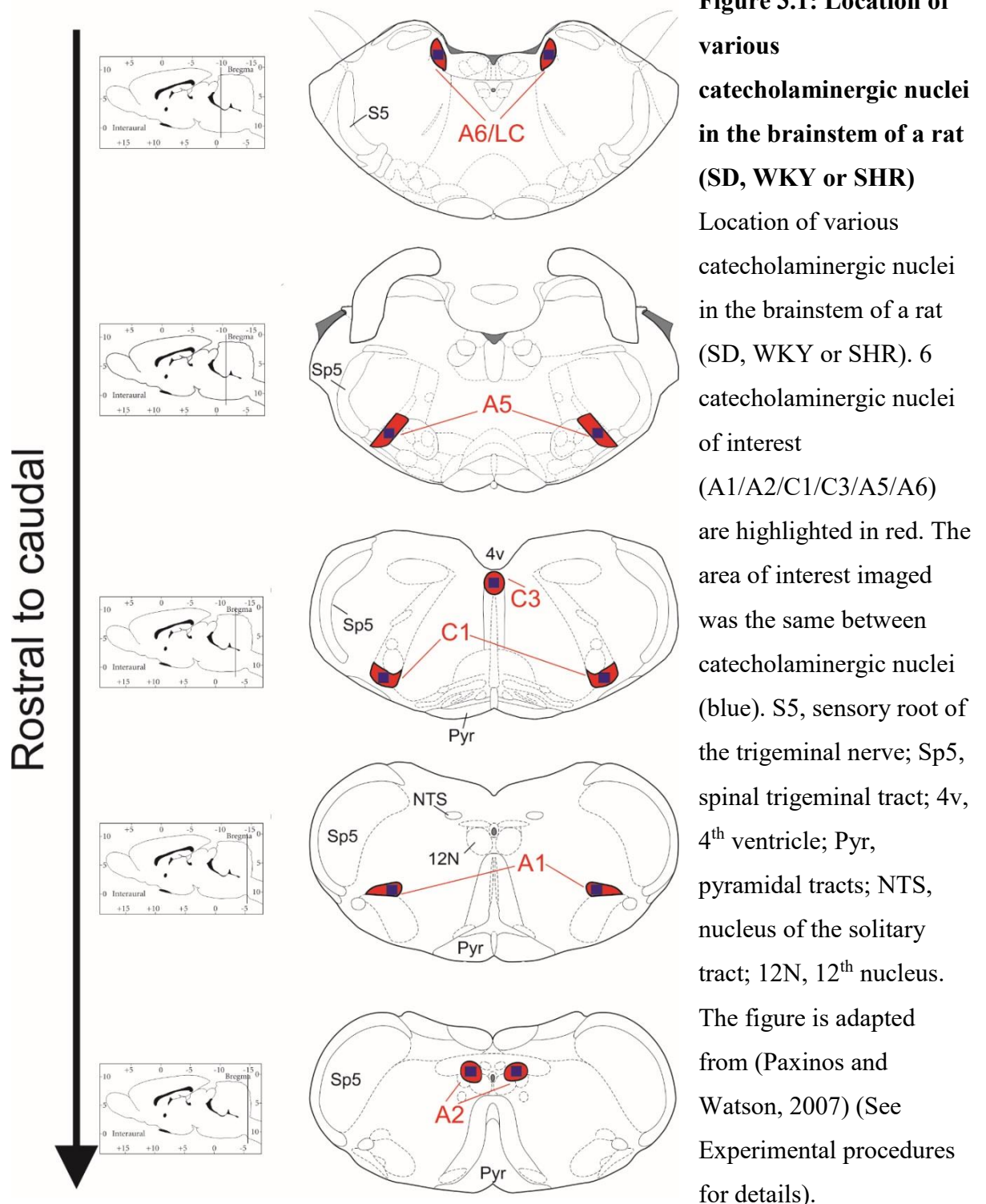
3.3.3 Image analysis

Maximum intensity projections of acquired 'Z-slices' were adjusted for brightness and contrast to highlight morphological features of microglia. Bilateral maximum intensity projection images acquired for A1, A2, C1, A5 and A6 regions, and medial images acquired for the C3 region, were used to quantify the overall number of TH-ir neurons, microglia and morphological characteristics of microglia. Number of TH-ir neurons and microglia were counted in images obtained for each region from each repeat; objects present at the boundary of images were excluded from the final counts. Microglial morphology was quantified as described by Morrison and Filosa (Morrison and Filosa, 2013). Briefly, the maximum intensity projection images were imported into Image J as 8-bit images and 'skeletonised' (Figure 3.6A).

The ‘skeletonised’ image was analysed using the “AnalyzeSkeleton” Image J plugin to acquire the number of end points and branch length (μm) which, when normalised to the number of microglia in that specific frame, provides an indication of the microglial morphology (Figure 3.6A). The percentage (%) of area occupied by microglia was quantified with the help of the “measure” feature in Image J software.

3.3.4 Data analysis and statistics

GraphPad Prism version 6.05 was used to perform all statistical analysis. Numbers of TH-ir neurons and microglia were treated as non-parametric non-continuous data, and were pooled from 3 repeats for each strain, for each brainstem nuclei (Kapoor et al., 2016b; Nedoboy et al., 2016; Sokal and Rohlf, 2012). Supplementary Figure 3.1 shows minor biological variability in the number of TH-ir neurons and microglia, within each strain. The relationship between the pattern of distribution of TH-ir neurons and microglia across different catecholaminergic nuclei, intra- and inter- strain, was analysed using the chi-square test of independence (Sokal and Rohlf, 2012). Parameters obtained highlighting the microglial morphology in catecholaminergic nuclei were treated as non-parametric continuous data, and were averaged across repeats ($n=3$), and analysed using a Kruskal-Wallis one-way analysis of variance.



3.4 Results

Microglia were distributed ubiquitously in catecholaminergic nuclei of the brainstem (A1, A2, C1, C3, A5 and A6) in the SD (Figure 3.2A-F), the WKY (Figure 3.3A-F) and the SHR (Figure 3.4A-F) strains of rats. However, TH neuronal and microglial number varied between regions and strains.

3.4.1 Intra-strain comparison demonstrating that microglial number is related to the number of TH-ir neurons in a catecholaminergic nucleus

Intra-strain (SD, WKY or SHR) comparisons of the number of TH-ir neurons in catecholaminergic nuclei of brainstem revealed that the TH-ir neuronal number varies between brainstem nuclei (Figure 3.5A-C). Microglial number also varied between catecholaminergic nuclei of brainstem in all 3 strains: SD, WKY and SHR. Interestingly, the pattern of variation observed in the microglial number was similar to the pattern of variation in the TH-ir neuronal number (Figure 3.5A-C). For example, TH-ir neuronal and microglial numbers were higher in A2 as compared to C1, C3 or A5, regardless of the strain (Figure 3.5A-C). Similarly, TH-neuronal and microglial number were lower in C3 as compared to A5 or A6, regardless of the strain (Figure 3.5A-C). However, some exceptions (24% - 11 comparisons out of 45) were observed, where the microglial number was not related to the TH-ir neuronal number, such as A1 vs A5 in SD and WKY (Figure 3.5A and B). But in majority ($\approx 76\%$) of intra-strain comparisons, the microglial number was related to the TH-ir neuronal number.

3.4.2 Inter-strain comparison of TH neuronal and microglial number in various brainstem catecholaminergic nuclei

A comparison of the distribution pattern of number of TH-ir neurons (Figure 3.5D) and microglia (Figure 3.5E) between strains revealed that the distribution varied in a similar pattern in catecholaminergic nuclei in all 3 strains of rat (SD, WKY and SHR; Figure 3.5D).

The highest number of TH-ir A6 neurons were observed in WKY when compared with SD (WKY was 28% higher than SD) and SHR (SHR was 19% lower than WKY) (Figure 3.5D). Microglial number in the brainstem catecholaminergic nuclei of WKY and SHR varied the most when compared with SD. Significant differences in the number of microglia were observed in A2, A5 and A6 brainstem regions, and the microglial number in these regions was the least in SD (Figure 3.5E).

3.4.3 Microglial morphology doesn't vary considerably between catecholaminergic nuclei, regardless of the strain

No significant differences were observed in the microglial morphological characteristics (% area, number of end point processes/microglia and branch length (μm)/microglia) within various catecholaminergic nuclei, in either intra-, or inter-, strain comparisons (Figure 3.6B-D).

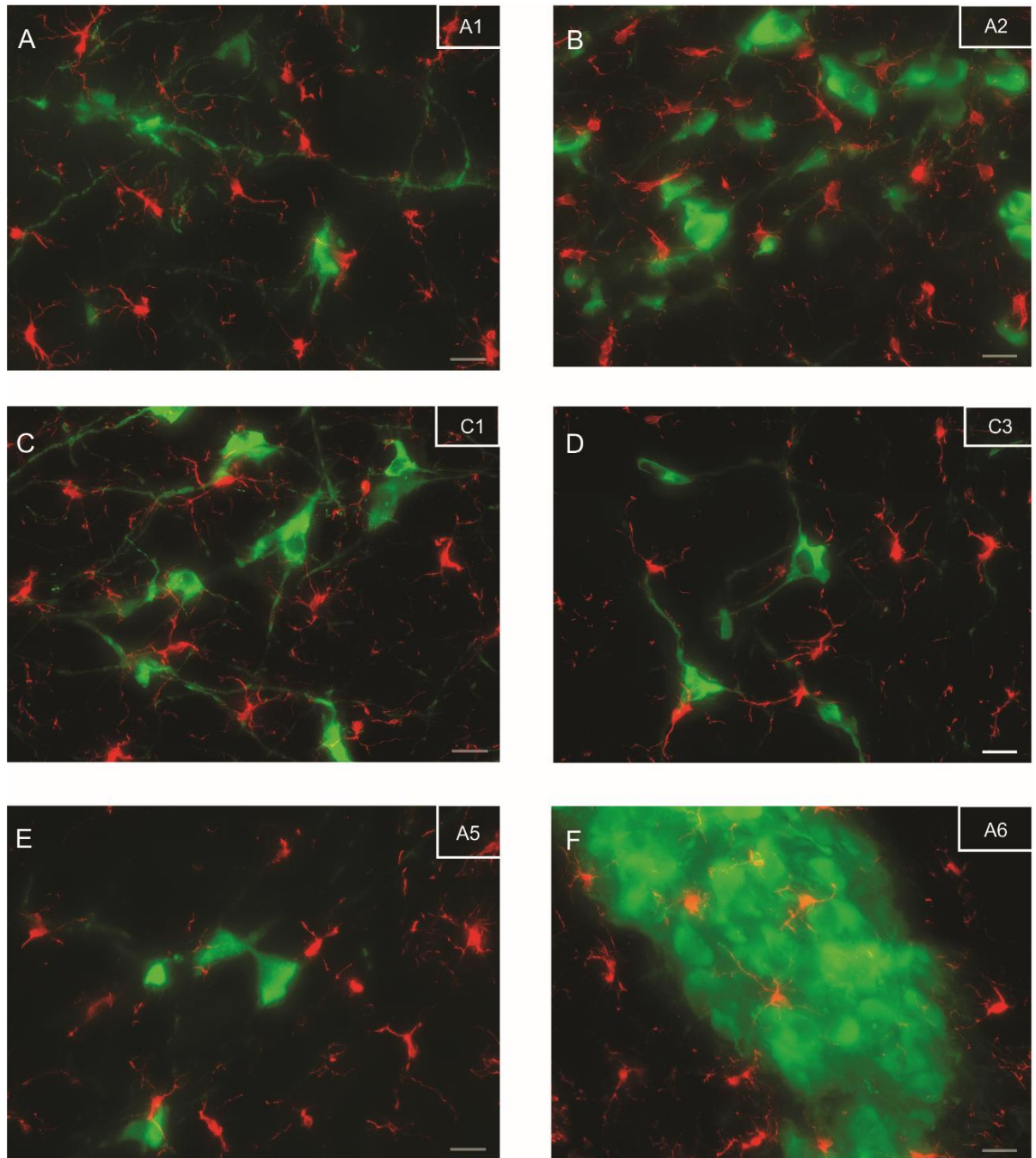


Figure 3.2: Microglia in the brainstem catecholaminergic nuclei of a SD

A. A1, B. A2, C. C1, D. C3, E. A5 and F. A6. Scale bar = 20 μ m. Microglia, Iba1 – red and TH – green. The region of interest was kept constant across all catecholaminergic nuclei.

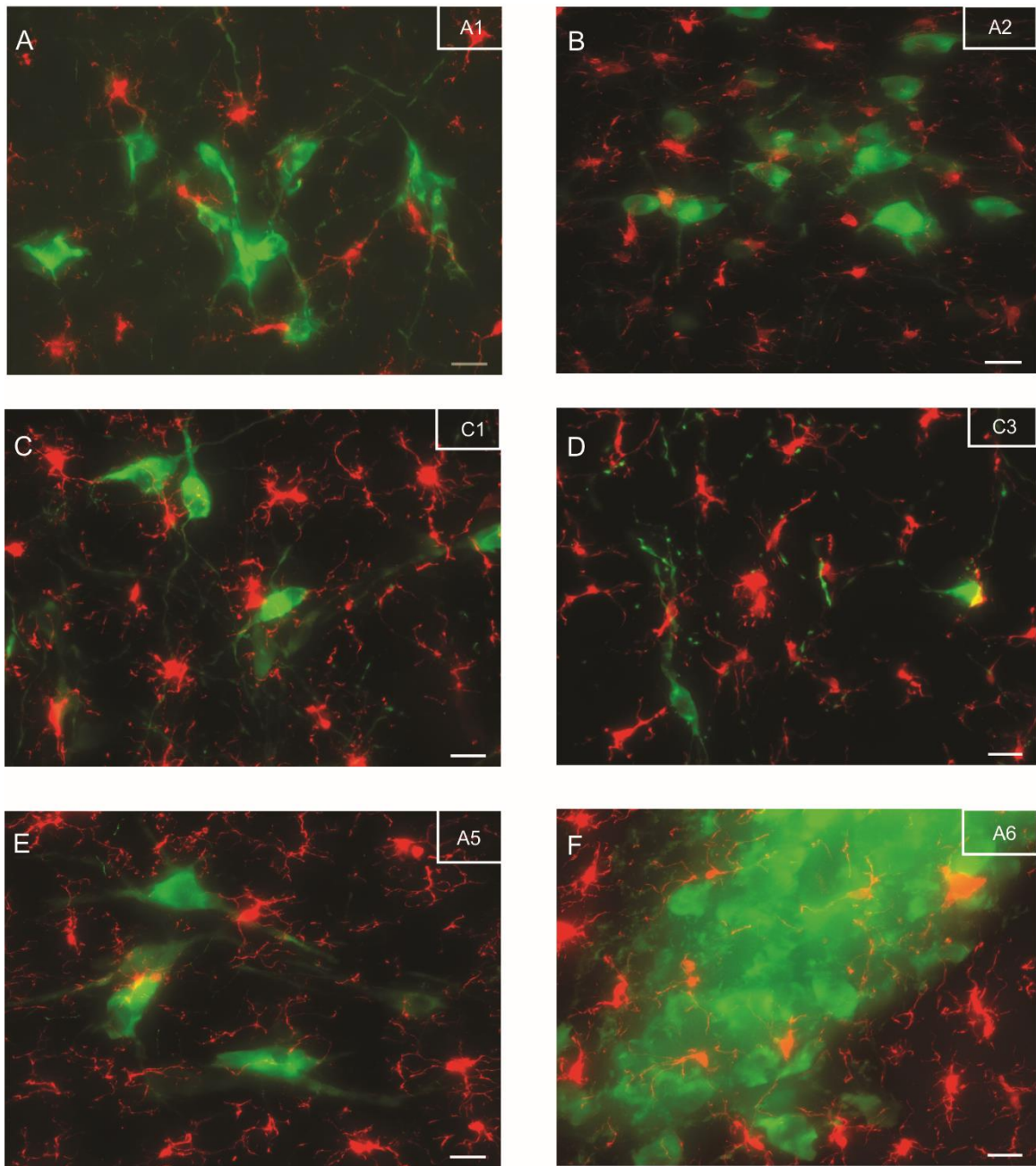


Figure 3.3: Microglia in the brainstem catecholaminergic nuclei of a WKY rat

A. A1, B. A2, C. C1, D. C3, E. A5 and F. A6. Scale bar = 20 μm. Microglia, Iba1 – red and TH – green. The region of interest was kept constant across all catecholaminergic nuclei.

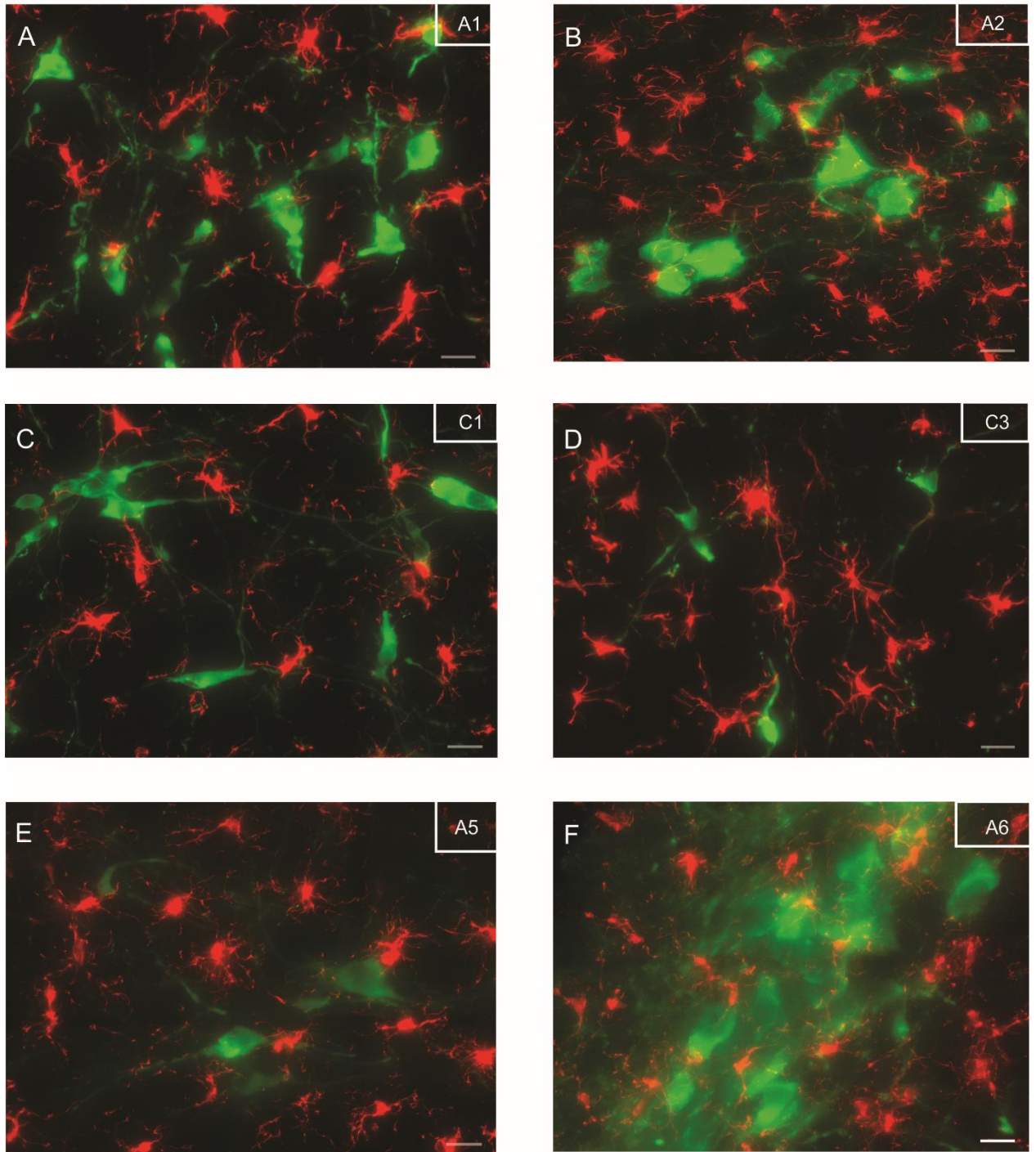


Figure 3.4: Microglia in the brainstem catecholaminergic nuclei of an SHR

A. A1, B. A2, C. C1, D. C3, E. A5 and F. A6. Scale bar = 20 μm . Microglia, Iba1 – red and TH – green. The region of interest was kept constant across all catecholaminergic nuclei.

Figure 3.5: Intra- and inter- strain comparisons concerning the number of TH-ir neurons and microglia

Intra-strain comparison of the pattern of distribution of TH-ir neuronal and microglial number in catecholaminergic nuclei of the brainstem of A. SD, B. WKY and C. SHR. Inter-strain (SD, WKY and SHR) comparison of the pattern of distribution of TH-ir neuronal (D) and microglial number (E) in catecholaminergic nuclei of the brainstem. Data are expressed as sum of counts from 3 animals for each strain. Statistical comparisons comparing the relationship between distribution patterns were made using the Chi-square test of independence. * $p \leq 0.05$, ** $p \leq 0.01$, *** $p \leq 0.001$ and **** $p \leq 0.0001$. (Refer to Supplementary Figure 3.1 for biological variability in the number of TH-ir neurons and microglia, in each strain)

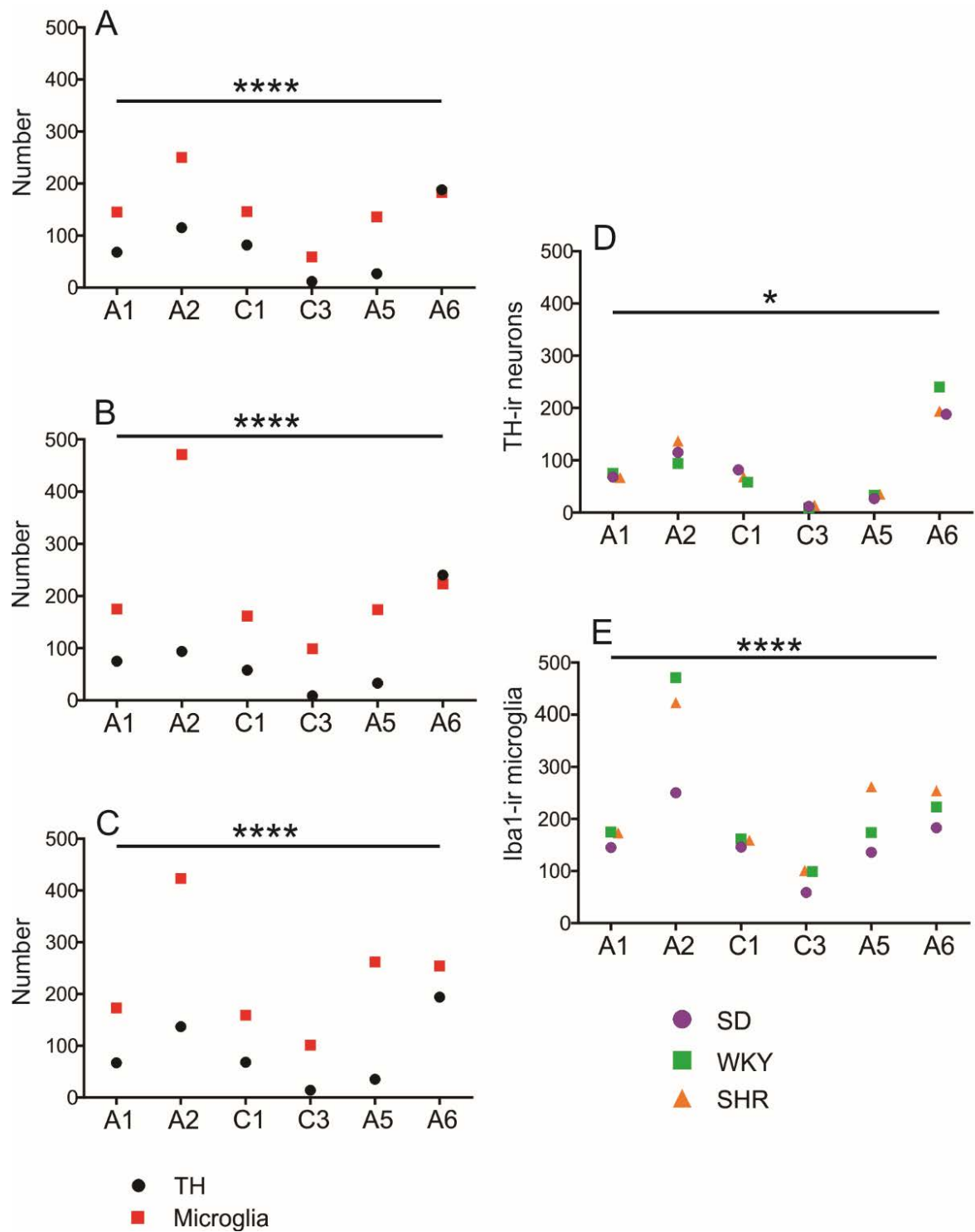
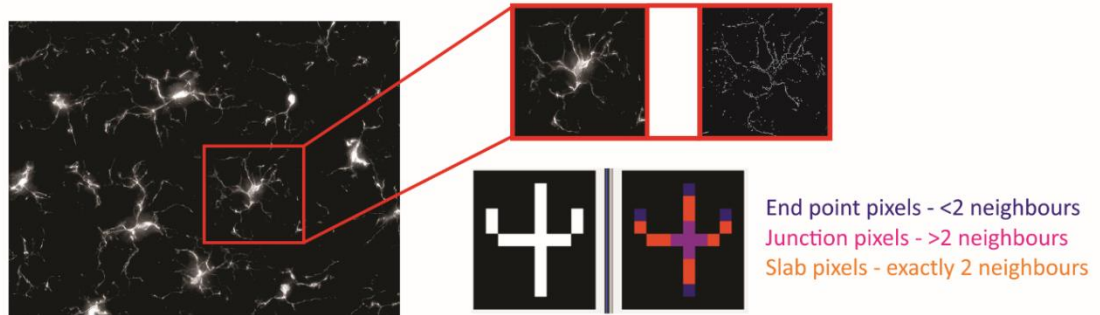


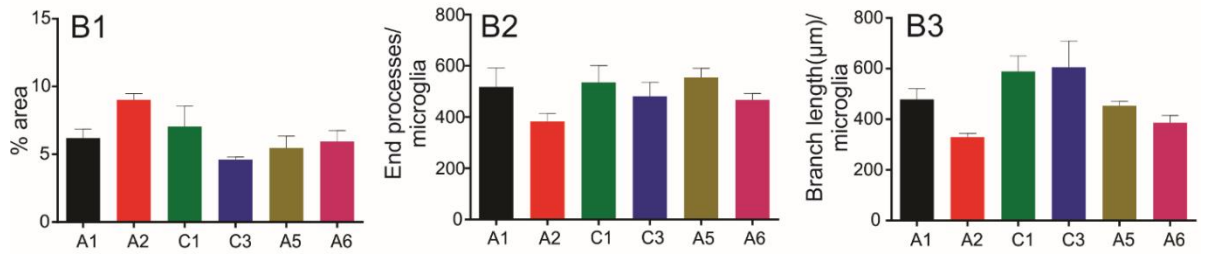
Figure 3.6: Microglial morphology in the brainstem catecholaminergic nuclei

A. Quantification of the number of end point processes/microglia and the branch length (μm)/microglia with Image J ‘AnalyzeSkeleton’ plugin (refer to Experimental procedures for details). 3 microglial morphological characteristics were quantified (% area, number of end processes/microglia and branch length (μm)/microglia) in the brainstem catecholaminergic nuclei of a B. SD rat, C. WKY rat and D. SHR. Data are expressed as mean \pm S.E.M. Statistical comparisons were made using a Kruskal-Wallis one-way analysis of variance. No significant differences were observed in the microglial morphology, intra-strain, across different catecholaminergic nuclei.

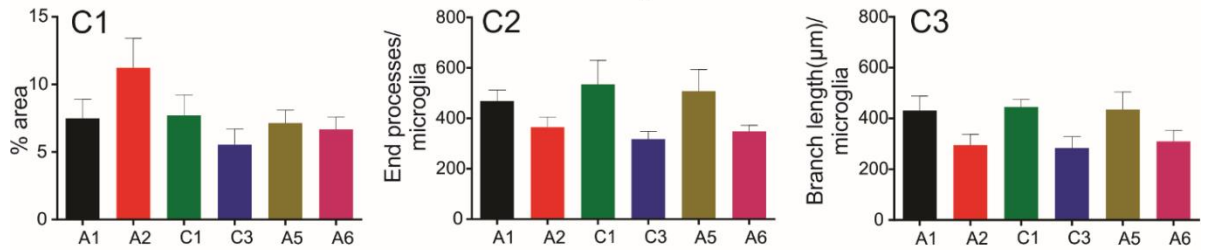
A. Morphological analysis



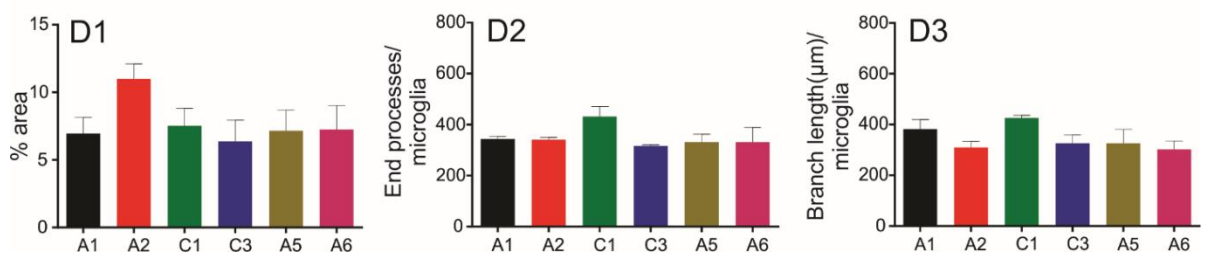
B. Sprague-Dawley rats

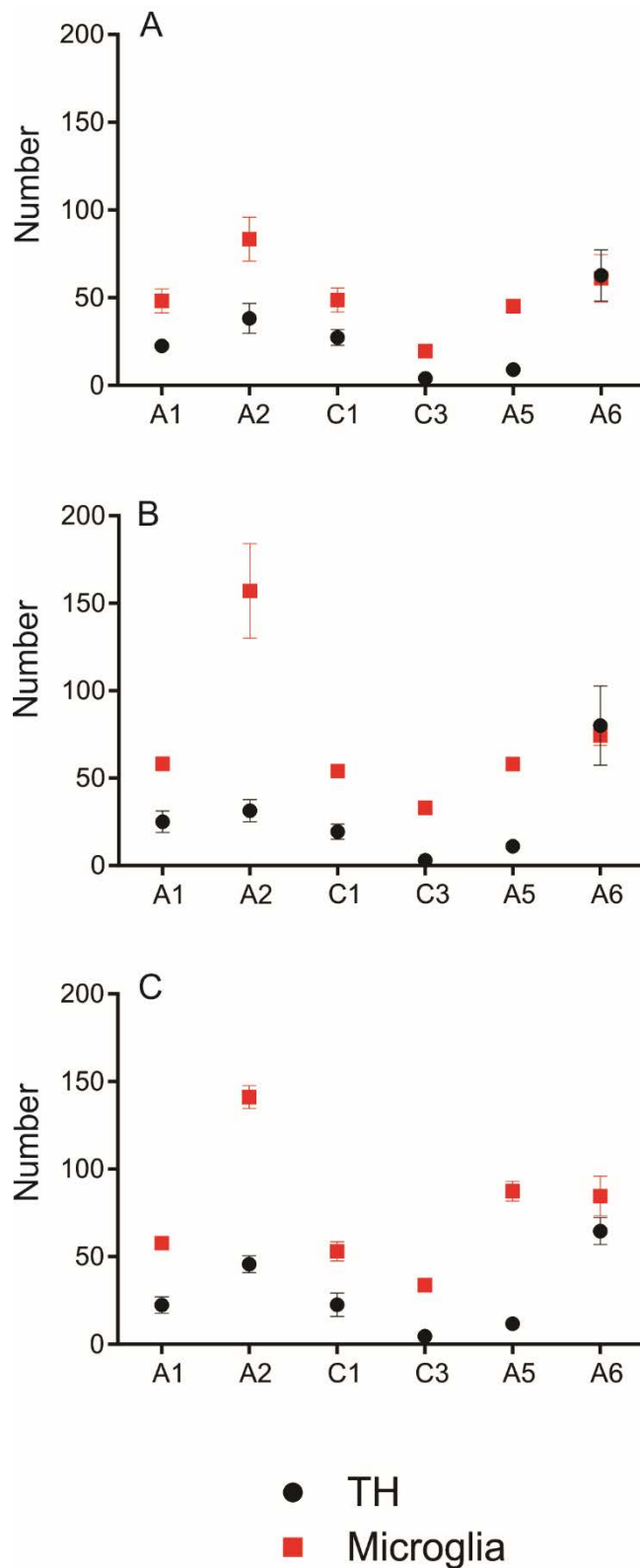


C. Wistar-Kyoto rats



D. Spontaneously hypertensive rats





Supplementary Figure 3.1: Intra-strain biological variability in the number of TH-ir neurons and microglia

Number of TH-ir neurons and microglia, in catecholaminergic nuclei of the brainstem, in A.SD, B. WKY and C. SHR from individual animals (n=3/ strain) highlighting minor biological variability between repeats. Data in Figure 3.5 are pooled from 3 repeats for each strain. Data are expressed as mean ± S.E.M.

3.5 Discussion

The main finding of our study is, first, that there is a ubiquitous and heterogeneous distribution of microglia in the brainstem catecholaminergic nuclei of the SNS of spontaneously hypertensive and normotensive rats. Secondly, the heterogeneous microglial distribution is related to the TH-ir neuronal distribution and thirdly, in all strains of rat, and in all catecholaminergic nuclei, microglia were found to be in a surveilling state with a ramified morphology.

We observed a highly heterogeneous microglial distribution in catecholaminergic nuclei of the SNS of spontaneously hypertensive and normotensive rats, which is related to the TH-ir neuronal number. Previous studies suggest that microglial distribution is region-specific and is thought to be influenced by the local microenvironment cues (Lawson et al., 1990; Mittelbronn et al., 2001; Nikodemova et al., 2014). For example, the grey matter of the CNS contains more microglia than the white matter, as detected by expression of the F4/80⁺ antigen, however the exact factor responsible for this is still unknown (Lawson et al., 1990). Also, microglial density was found to be 50% lower in lumbar segments of the spinal cord when compared with the cortex (Nikodemova et al., 2014). This heterogeneous distribution of microglia is not dependent on the proportion of monocytes recruited to the site of cell death during early development (Lawson et al., 1990). Microglial expression of immunoregulatory proteins is also quite region specific (de Haas et al., 2008; Nikodemova et al., 2014). These studies further highlight the diversity of microglia in the CNS, whose distribution, and chemical profile, is highly dependent on their local environment.

Our findings show that microglial number is related to the number of TH-ir neurons, which in turn relates to the type of catecholaminergic nucleus. It remains unclear if the presence of large numbers of catecholaminergic neurons cause changes in microglial number. As noted above, catecholaminergic neurons are an essential component of the CNS, in particular the SNS (Dampney and Horiuchi, 2003; Graham et al., 1995; Rinaman, 2011). As expected, the number of TH-ir neurons across various catecholaminergic nuclei in the brainstem was observed to be heterogeneous, in a given strain of rat. Interestingly, microglial number, in the same strain of rat, is equally heterogeneous, and is related to the TH-ir neuronal number. It is noteworthy that even though all of the nuclei observed in this study were catecholaminergic (A1/A2/C1/C3/A5/A6), the number of TH expressing neurons in these nuclei is variable. Moreover, the proportion and location of active TH neurons within these nuclei ultimately

affects the function of each nucleus in sympathetic regulation of the CNS (Badoer et al., 1987; Dampney and Horiuchi, 2003; Dampney et al., 2003b; Graham et al., 1995; Nedoboy et al., 2016). Therefore, the variability in TH-ir neuronal number between brainstem nuclei may well be responsible for differences in microglial number. Thus, in light of our own findings, and as hypothesised by other studies (de Haas et al., 2008; Kapoor et al., 2015; Lawson et al., 1990; Mittelbronn et al., 2001), we speculate that the local environment of a nucleus in the SNS, in particular the number of TH-ir neurons, influences the microglial distribution.

No major differences were observed in the microglial morphology, when compared intra-, or inter-, strain. Microglia continuously extend or retract their processes to contactsynapses to monitor, and regulate, their activity levels (Nimmerjahn et al., 2005; Wake et al., 2009). Microglial morphology in mice varies markedly between different CNS regions, particularly between the grey matter and the white matter (Lawson et al., 1990). In our study, only minor differences were observed in microglial morphology in their surveilling state. The difference in observations made between these 2 studies, may be due to different species (mice vs rat), or different antigens analysed. Our study looked at the expression of Iba1 (ionized calcium-binding adaptor molecule 1) as compared to F4/80⁺ antigen, and was performed at much lower magnification (40X vs 400X) albeit covering a region of interest (ROI) that was larger. There may be very subtle morphological differences that can only be observed at higher magnifications, but the biological relevance of such subtle morphological differences is unclear.

Even though, both SD and WKY are normotensive, WKY are not comparable to SD due to underlying behavioural defects. SHRs are inbred from WKY with high blood pressure (Okamoto and Aoki, 1963) and therefore, WKY, and not SD, is the most appropriate genetic and physiological control for SHR. Whether or not WKY is always the best control for SHR is still debated (H'Doubler et al., 1991). In our hands, we observed similarities in the pattern of distribution of TH-ir neurons and microglia in all 3 strains of rats (SD, WKY and SHR). The magnitude of microglial response to a CNS injury is more pronounced in SHR than WKY (De Geyter et al., 2012). Reduced striatal blood flow induces a larger infarction volume and more pronounced sensory deficits, and reduced microglial activation in SHR compared with WKY (De Geyter et al., 2012). According to our study, no major differences were observed in the overall microglial distribution pattern and morphology, between SHR and WKY. It is also hypothesised that neuro-inflammatory conditions in the CNS may play a detrimental role in the exaggeration of sympathetic nerve activity, and may contribute to the pathophysiology of cardiovascular disorders such as hypertension and heart failure (Liu et al.,

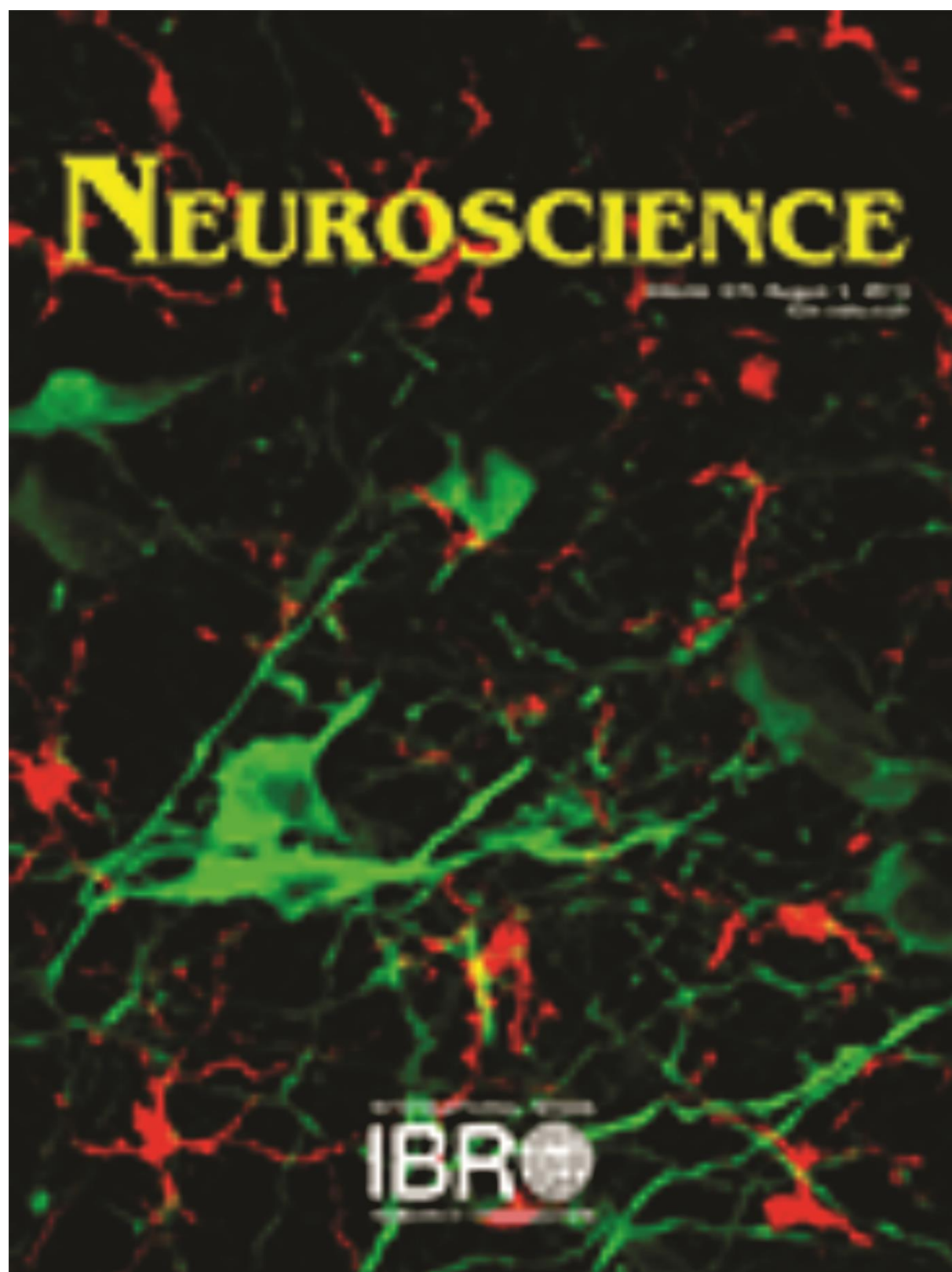
2016; Shi et al., 2010a; Wei et al., 2013; Wei et al., 2015). Thus, in light of our findings and previous studies, we speculate that the magnitude of the microglial response to an injury or disturbed homeostasis, rather than significant changes in basal microglial distribution, may be impaired in SHR than WKY.

Conclusion

Microglial distribution is markedly heterogeneous in the SNS of a rat (SD, WKY and SHR) and this heterogeneity seems to be related to the neuronal profile of their local environment. Hence, our study, in accordance with other studies, highlights that the microglial distribution profile is related to its local environment. Future studies focussed on the role of microglia, in addition to brain vascular macrophages (Waki et al., 2008a; Waki et al., 2011), in the sympathetic regulation of cardiovascular control will clarify if these brain immune cells play a protective or detrimental role in the pathology of hypertension.

Chapter 4

Dynamic changes in the relationship of microglia to cardiovascular neurons in response to increases and decreases in blood pressure



Contents

4.1	Abstract.....	163
4.2	Introduction.....	164
4.3	Experimental procedures.....	165
4.3.1	Animals	165
4.3.2	Experimental protocol	166
4.3.3	Perfusion and tissue processing.....	167
4.3.4	Immunohistochemistry	167
4.3.5	Image acquisition and analysis.....	168
4.3.5.1	<i>Microglial number and morphological analysis at 40X.....</i>	<i>168</i>
4.3.5.2	<i>M1 phenotype quantification</i>	<i>169</i>
4.3.5.3	<i>M2 phenotype quantification</i>	<i>169</i>
4.3.5.4	<i>Quantification of number of contacts made by microglial (Iba1) end point processes with synapses (Synapsin) and microglial morphology at 63X.....</i>	<i>170</i>
4.3.5.5	<i>Control experiments in the nucleus ambiguus (sub compact)</i>	<i>170</i>
4.3.6	Data analysis and statistics	171
4.4	Results	171
4.4.1	Effects of blood pressure modulations on the CVLM and the RVLM neuronal activity	171
4.4.1.1	<i>Variations induced in MAP</i>	<i>171</i>
4.4.1.2	<i>Fos-ir</i>	<i>172</i>
4.4.2	Microglial-neuronal relationship under homeostasis	176
4.4.3	Induction of acute hyper- and hypo- tension causes microglia to change their pattern of distribution in the ventrolateral medullary nuclei	176
4.4.3.1	<i>Overall number of microglia</i>	<i>176</i>
4.4.3.2	<i>Inter-microglial distance</i>	<i>176</i>
4.4.4	Microglial contact with synapses increases with the induction of acute hypertension in the ventrolateral medullary nuclei.....	181
4.4.5	Microglial contact with synapses decreases with the induction of acute hypotension in the ventrolateral medullary nuclei.....	181
4.4.6	Microglia do not change their morphology in response to induction of acute hyper- or hypo- tension (Figure 4.7B-E) in the ventrolateral medullary nuclei.....	182
4.4.7	Induction of acute hyper- or hypo- tension does not induce any microglial response in the nucleus ambiguus (sub compact, NAsc)	182
4.4.8	Expression levels of M1 or M2 phenotype do not change with the disturbances introduced in BP in the ventrolateral medullary nuclei.....	182

4.5	Discussion	191
------------	-------------------------	------------

Abbreviations:

AUC – area under curve

BP – blood pressure

CNS – central nervous system

CVLM – caudal ventrolateral medulla

Fos-ir – Fos immunoreactivity MAP – mean arterial pressure

NAsc – nucleus ambiguus (sub compact)

NTS – nucleus of the solitary tract

PBS – phosphate-buffered saline

RVLM – rostral ventrolateral medulla

SD – Sprague-Dawley SNS – sympathetic nervous system

TH – tyrosine hydroxylase

Keywords: CVLM, RVLM, microglia, blood pressure, sympathetic.

Highlights:

- Microglia alter spatial distribution in response to changes in blood pressure.
- Increased blood pressure causes microglia to contact more synapses.
- Decreased blood pressure reduces microglial contact with synapses.

The work in this chapter is published in “**Neuroscience**”.

Kapoor, K., Bhandare, A.M., Nedoboy, P.E., Mohammed, S, Farnham, M.M.J., Pilowsky, P.M., 2016. Dynamic changes in the relationship of microglia to cardiovascular neurons in response to increases and decreases in blood pressure. *Neuroscience*. 329, 12-29

(Cover image of the issue – by Kapoor, K.)

The text of this chapter is an exact representation of the published material except for the figure numbers and the section numbers, which were modified to match the rest of this thesis.

Declaration of contributions: Candidate contributed to the design of experiments, performed all experiments, analysed data, interpreted results and was the major contributor to the manuscript. Amol M. Bhandare (a PhD candidate) assisted with the animal experiments and data analysis related to physiological data (concerning BP). Paul M. Pilowsky and Melissa M.J. Farnham contributed to conception and design of experiments, data analysis, interpretation of results, and editing and final approval of the manuscript. Suja Mohammed contributed to the design of IHC experiments. Polina E. Nedoboy assisted with the TH antibody characterisation (Avanti antibodies, #AV1).

Version of record published as: Kapoor, K., Bhandare, A. M., Nedoboy, P. E., Mohammed, S., Farnham, M. M. J., Pilowsky, P. M. (2016) Dynamic changes in the relationship of microglia to cardiovascular neurons in response to increases and decreases in blood pressure, *Neuroscience*, Vol. 329, pp. 12-29, <https://doi.org/10.1016/j.neuroscience.2016.04.044>.

4.1 Abstract

Microglia are present throughout the central nervous system (CNS) and express receptors for every known neurotransmitter. During inflammation, microglia change into a state that either promotes removal of debris (M1), or into a state that promotes soothing (M2). Caudal- and rostral- ventrolateral medullary regions (CVLM and RVLM, respectively) of the brainstem are key nuclei involved in all aspects of the cardiovascular system. In this study, we investigate a novel role for microglia in cardiovascular control in the brainstem of adult male Sprague–Dawley (SD) rat. Here we show, that increases and decreases in blood pressure (BP) triggers alertness in the physiology of microglia in the brainstem region; inducing changes in microglial spatial distribution and the number of synapses in contact with microglial end processes. Following 6 h of acute hypertension, the number of synapses in contact with microglia increased by $\approx 30\%$ in both regions of the brainstem, CVLM and RVLM. Induction of acute hypotension for 6 h causes microglia to reduce the number of synaptic contacts by $>20\%$ in both, CVLM and RVLM, nuclei of the brainstem. Our analysis of the morphological characteristics of microglia, and expression levels of M1 and M2, reveals that the changes induced in microglial behavior do not require any obvious dramatic changes in their morphology. Taken together, our findings suggest that microglia play a novel, unexpected, physiological role in the uninjured autonomic nuclei of CNS; we therefore speculate that microglia act cooperatively with brainstem cardiovascular neurons to maintain them in a physiologically receptive state.

4.2 Introduction

Until recently, microglia were considered to be cells whose sole function was to detect and respond to inflammation, following any internal or external stimulus that threatens the integrity of the brain (Kettenmann et al., 2011; Kreutzberg, 1996; Perry et al., 1993). When subjected to strongly activating stimuli, microglia transform their phenotype from a highly ramified morphology with a small cell body to an amoeboid shape, allowing them to move easily, and phagocytose debris (Stence et al., 2001).

The idea that microglia are only important as inflammatory cells, now seems less certain. A growing body of evidence suggests that microglia are not only constantly alert and active; surveilling their immediate environment (Nimmerjahn et al., 2005; Tremblay et al., 2011), but may also play a physiological role in maintaining normal neuronal function. The idea that microglia constantly maintain neurons within their dynamic physiological working range, by regulating the number of excitatory synapses present on their post-synaptic membrane (Tremblay et al., 2010; Wake et al., 2009), is still poorly understood. Microglia are thought to perform this function by extending or retracting their processes, sensing the presence of any unexpected increase in extracellular chemical (“on- signalling”) or absence of any consistently expressed biological molecule (“off-signalling”) (Biber et al., 2007; Hanisch and Kettenmann, 2007; van Rossum and Hanisch, 2004). Microglia achieve this role by expressing receptors for all known neurotransmitters, and many other molecules (Pocock and Kettenmann, 2007), and by being in close proximity to neurons at all times (Shapiro et al., 2009). The close apposition of microglial processes to neuronal synapses in higher brain regions, such as the visual cortex, further strengthens the hypothesis of continuous neuron-microglia communication (Schafer et al., 2013; Tremblay et al., 2010; Wake et al., 2009). The possibility that this type of neuron-microglia relationship operates in a physiological state in the autonomic nervous system is unknown.

The caudal- and rostral- ventrolateral medullary (CVLM and RVLM, respectively) neurons of the brainstem are critical for the regulation of the sympathetic nervous system (SNS) and various reflex control mechanisms such as the chemoreflexes, baroreflex and somatosympathetic reflex (Pilowsky et al., 2009). Propriobulbar CVLM neurons provide an inhibitory GABAergic (γ -Aminobutyric acid) input to the excitatory bulbospinal glutamatergic presympathetic neurons located in the RVLM in response to elevated levels of blood pressure (BP); these inhibited RVLM neurons, in turn, reduces the activity of the sympathetic

preganglionic neurons (SPN) located in the spinal cord, thereby lowering BP and sympathetic activity (Guyenet, 2006; Pilowsky et al., 2009). Recently, we reported that inhibition of microglia led to an over-activation of sympathetic output, supporting the concept that microglia play an important physiological role in the SNS (Bhandare et al., 2015). However, the exact morphological relationship between microglia and cardiovascular neurons during the imposition of changes in BP remains unclear.

Here, we aimed to identify, first, the morphological relationship between surveilling microglia and cardiovascular neurons in the CVLM and the RVLM that control sympathetic output pathways, under homeostatic conditions. Secondly, we aimed to establish the extent to which the microglial-neuronal relationship, in the CVLM and RVLM regions of the brainstem, is affected by manipulations introduced in the basal levels of BP. Data concerning microglia were acquired following the induction of acute hyper- (phenylephrine) or hypo-(hydralazine) tension in adult male Sprague–Dawley (SD) rats at four different time points; 0.5, 2, 6 and 10 h (hrs). Our findings indicate that brainstem microglia behave as an essential element of the autonomic arm of the central nervous system (CNS), and that microglial responses to changes in levels of BP are carefully tailored according to the magnitude and duration of disturbances introduced in the homeostatic state. In particular, increased BP causes microglia to change their pattern of distribution, and make more contacts with synapses. On the contrary, decreased levels of BP, causes microglia to decrease the number of contacts with synapses and change their spatial distribution. This microglial behavior has all the characteristics of a physiological, as opposed to an inflammatory, destructive, response.

4.3 Experimental procedures

4.3.1 Animals

Experiments were conducted in 36 adult male SD rats (300–420 g; Animal resource center, Perth, Australia) in accordance with the Australian code of practice for the care and use of animals for scientific purposes. All procedures and protocols performed were approved by the Sydney Local Health District Animal Welfare Committee and the Macquarie University Animal care and Ethics Committee, Sydney, Australia.

4.3.2 Experimental protocol

The external jugular vein, carotid artery and femoral vein were cannulated, in anesthetized rats, for the administration of additional anesthetics, measurement of arterial BP and administration of BP altering drugs (phenylephrine, saline or hydralazine), respectively. Temperature for all animals was maintained between 36.5 °C and 37.5 °C, for the protocol period, using a rectal probe connected to a homeothermic heating blanket. Experiments were conducted at four time points: 0.5, 2, 6 and 10 h, with three treatment groups at each time point (n = 3 each treatment group at each time point): phenylephrine induced hypertension, saline served as control and hydralazine induced hypotension

0.5, 2 and 6 h: rats were anesthetized with sodium pentobarbital i.p. (50 mg/kg; Cenvet Australia) mixed with atropine sulfate (to reduce bronchial secretions; 0.2 ml/kg; Pfizer). Room air was supplemented with 100% oxygen (rate 0.5–1.0 l/min) through a nose cone. The depth of anaesthesia was monitored by observing reflex responses to nociceptive and tactile stimuli (withdrawal reflex to periodic tail/paw pinches), pupillary responses to light stimuli and the corneal touch reflex (involuntary blink). Additional anesthetic – sodium pentobarbital (1.5–2.0 mg) – was injected intravenously, when required, to eliminate nociceptive or corneal touch reflex responses.

10 h: rats were anesthetized with urethane i.p. (1.0–1.5 g/kg) mixed with atropine sulfate (to reduce bronchial secretions prior to vagotomy; 0.2 ml/kg), vagotomized (both, left and right cervical vagus nerves were cut), paralyzed with pancuronium bromide (neuromuscular blockade, 0.2-ml bolus i.v. injection containing 0.4 mg followed by 10% pancuronium in 0.9% saline at a rate of 2 ml/h; AstraZeneca) and artificially ventilated. Animals were vagotomized and paralyzed to prevent entrainment of breathing to the ventilator. The depth of anaesthesia, prior to induction of neuromuscular blockade, was monitored by observing reflex responses to nociceptive and tactile stimuli, pupillary responses to light stimuli and the corneal touch reflex (as explained above). Following neuromuscular blockade, the depth of anaesthesia was determined by continuously monitoring the resting levels of BP for excessive fluctuations, and any changes in BP in response to nociceptive stimuli. Additional anesthetic – urethane (30–40 mg, 10% urethane i.v.) – was injected intravenously, when nociceptive stimuli evoked changes in BP exceeding 10%.

Prior to the start of the protocol, arterial pressure was allowed to stabilize for at least 10 min. Baseline mean arterial pressure (MAP) was increased or decreased by at least 40 mmHg with

the aid of phenylephrine or hydralazine, respectively. A continuous infusion of phenylephrine, at the dose of 10 µg/kg/min (Graham et al., 1995), was maintained to induce acute hypertension. Rate of phenylephrine infusion was adjusted to maintain elevated levels of MAP. To induce acute hypotension, a bolus injection of hydralazine was given, at the dose of 10 mg/kg (Springell et al., 2005). To match the volume infused in the phenylephrine treatment group, hydralazine and saline treatment groups received a continuous infusion of saline at the rate of 10 µg/kg/min. Drug concentrations and infusion volumes were carefully determined in preliminary experiments and then adjusted to limit the maximum volume of infusion to 10 ml for the duration of protocol, to avoid hypervolemia.

4.3.3 Perfusion and tissue processing

All chemical reagents were purchased from Sigma–Aldrich, unless otherwise stated. At the end of the protocol, rats were deeply anesthetized with sodium pentobarbital (>72 mg/kg i.v.; Cenvet Australia) and were transcardially perfused with 400 ml of ice cold 0.1 M phosphate buffered saline (PBS) followed by fixation with ≈400 ml of ice cold 4% paraformaldehyde in 0.1 M PBS (pH 7.4). Brainstem was carefully extracted and post fixed overnight in the same fixative at 4 °C. Brainstems were sectioned transversely at 40 µm and were sequentially collected in five pots using vibrating microtome (VT1200S, Leica) and stored in cryoprotectant solution (30% sucrose, 30% ethylene glycol, 2% polyvinylpyrrolidone in 0.1 M PBS) at –20 °C, until processed for immunohistochemistry.

4.3.4 Immunohistochemistry

Methods were conducted as previously described (Bhandare et al., 2016; Nedoboy et al., 2016; Shahid et al., 2012). In brief, free floating 40-µm brainstem sections, previously stored in cryoprotectant solution, were washed 3 times, for 30 min each, in 0.1 M PBS containing 0.3% Triton X-100 at room temperature. Post washes, sections were incubated for >48 h in TTPBSm (10 mM Tris–HCl, 0.1 M PBS, 0.9% NaCl, 0.3% Triton X-100 and 0.1% merthiolate at pH 7.4), 10% normal donkey serum and primary antibodies (refer to Table 1) at 4 °C while shaking. Sections were then subsequently washed 3 times, 30 min each, in TPBS (10 mM Tris–HCl, 0.1 M PBS and 0.9% NaCl at pH 7.4). Depending on the primary antibodies, sections were incubated overnight with secondary antibodies (refer to Table 1) in TPBSm (10 mM Tris–HCl, 0.1 M PBS, 0.9% NaCl and 0.1% merthiolate at pH 7.4) with 2% normal donkey serum at room temperature while shaking. Sections were then washed in TPBS 3 times, 30 min each, at room

temperature followed by mounting sequentially on glass slides (Thermo Fisher Scientific, Victoria, Australia), cover-slipped with Vectashield (H-1000, Vector Laboratories, CA, USA) and sealed with clear nail polish.

4.3.5 Image acquisition and analysis

Brainstem sections, processed for immunohistochemistry, were imaged using an Axio Imager Z2 (ZEISS, Germany) at 20X, 40X or 63X magnification for subsequent analysis, depending on the target molecule. Images were adjusted for brightness and contrast to best represent the morphological characteristics of microglia. LSM 510 Meta spectral confocal microscope (ZEISS, Germany) was used for obtaining images to demonstrate the microglial-neuronal relationship.

A rat brain atlas was used to define the anatomical location of the neuronal population analysed in this study (Paxinos and Watson, 2007). The RVLM was defined as a triangular area, containing tyrosine hydroxylase positive (TH^+) neurons, ventral to the nucleus ambiguus (NA_{sc}), medial to the spinal trigeminal tract and lateral to the pyramidal tracts. Bilateral RVLM images were obtained from 4 serial sections, separated by 200 μ m between 12.00 and 12.8 mm caudal to the bregma (Graham et al., 1995; Guyenet et al., 2004). CVLM neurons were defined as the neurons located in close apposition with TH^+ neurons of the A1 region of brainstem (Graham et al., 1995; Paxinos and Watson, 2007). Bilateral CVLM images were taken between 12.8 and 13.6 mm caudal to the bregma, from four different sections bilaterally, 200 μ m apart (Graham et al., 1995; Guyenet et al., 2004).

4.3.5.1 Microglial number and morphological analysis at 40X

“Z-stack” images at 40X magnification were obtained covering an area of 400 μ m X 400 μ m, 30 μ m in depth, at an interval of 0.62 μ m generating a stack of \approx 46 Z slices. Maximum intensity projection images produced for CVLM and RVLM neurons at 40 X magnification were used to quantify the overall number of microglia, pattern of distribution and morphological characteristics of microglia. Number of Fos immunoreactive (Fos-ir) neurons and number of microglia were manually counted in the eight images obtained for each region from each repeat. Fos-ir neurons and microglia present at the boundary of images were excluded from the final counts. For spatial distribution analysis, each image was divided into six equal parts using the grid feature in CorelDRAW Graphics Suite X7 and one microglia from each of these six parts was chosen. A series of six concentric circles were drawn around each microglia with the first one centered at the soma of microglia starting at radius of 8 μ m and subsequent circles were

drawn with the increasing radii of 5 μm (Morrison and Filosa, 2013; Sholl, 1953). Microglial cell bodies intersecting with each of these concentric circles were counted to provide an estimate of inter-microglial distance variations with treatment (Figure 4.5A). This analysis is an adaptation of Sholl analysis, which is commonly used to quantify neuronal parameters (Sholl, 1953).

The method used to quantify the morphology acquired by microglia in response to different treatment paradigms was as described by Morrison and Filosa (2013) (Morrison and Filosa, 2013). In brief, brightness and contrast for each image was adjusted to highlight all the microglial end point processes. These images were then imported to Image J (NIH) as 8-bit images and ‘skeletonised’. The ‘skeletonised’ image obtained was analysed using the “AnalyzeSkeleton” Image J plugin to acquire the number of end points and branch length (μm), which when normalised to the number of microglia in that specific frame, provides an indication of the extent of ramified microglial morphology (Figure 4.7A). The percentage (%) of area occupied by microglia was also quantified with the help of in-built “measure” feature in Image J software.

4.3.5.2 M1 phenotype quantification

“Z-stack” images of the CVLM and the RVLM (Figure 4.9F) did not show any significant M1 expression and therefore, M1 expression levels were not quantified.

4.3.5.3 M2 phenotype quantification

“Z-stack” images at 20X magnification were obtained covering an area of 900 μm X 600 μm , 40 μm in depth, at an interval of 1.39 μm generating a stack of ≈ 29 Z slices. Maximum intensity projection images acquired for the CVLM and the RVLM region at 20X magnification were used to quantify the overall number of microglia (Figure 4.9A), with Image J, in the region of interest. The CD206 immunoreactive (CD206⁺) microglia (Figure 4.9B), co-localizing with the Iba1 positive (Iba1⁺) microglia (Figure 4.9C), were counted in the eight images obtained for each region at each time point in 3 treatment groups (n=3 each). Iba1⁺ and CD206⁺ microglia present at the boundary of images were excluded from the final counts. Expression levels of M2 microglia were expressed as a percentage of CD206⁺ microglia to the total number of microglia (Iba1⁺).

4.3.5.4 Quantification of number of contacts made by microglial (Iba1) end point processes with synapses (Synapsin) and microglial morphology at 63X

“Z-stack” images at 63X magnification were obtained covering an area of 400 μm X 300 μm , 30 μm in depth, at an interval of 0.5 μm generating a stack of ≈ 60 Z slices. For data concerning microglia and synapsin, the RVLM was defined as a triangular area, containing TH⁺ neurons, ventral to the NAsc, medial to the spinal trigeminal tract and lateral to the pyramidal tracts, 12.24 mm caudal to the bregma (Guyenet et al., 2004). CVLM neurons were defined as the neurons located in close apposition with TH⁺ neurons of the A1 region of brainstem, at 13.08 mm caudal to the bregma (Graham et al., 1995; Paxinos and Watson, 2007). Bilateral images for the CVLM and the RVLM for each animal repeat were obtained. Ten microglia from each image were chosen at random and the numbers of synaptic structures (Synapsin) co-localizing with microglial end point processes (Iba1) were manually counted. Thus, 60 microglia from each animal, from each treatment group (three treatments) at each time point (four time points), were analyzed.

4.3.5.5 Control experiments in the nucleus ambiguus (sub compact)

The nucleus ambiguus (sub compact; NAsc) was defined as the area, 12.24 mm caudal to bregma, dorsal to the TH⁺ neurons of the RVLM, medial to the spinal trigeminal tract and lateral to the raphe obscurus (Bieger and Hopkins, 1987; Paxinos and Watson, 2007). Images from the NAsc at the 6- and 10-h time point from all three treatment groups (phenylephrine, saline and hydralazine; $n = 3$ each group) served as a control for the images obtained from the CVLM and the RVLM, at each time point. Bilateral ‘Z-stack’ images at 40X magnification were obtained covering an area of 400 μm X 400 μm , 30 μm in depth, at an interval of 0.62 μm generating a stack of ≈ 46 Z slices. Maximum intensity projection images produced for the NAsc at 40X magnification were used to quantify the overall number of microglia, pattern of distribution and morphological characteristics of microglia: % area covered, number of end point processes/microglia and branch length (μm)/microglia (similar to the CVLM and RVLM). Bilateral “Z-stack” images at 63X magnification were obtained covering an area of 400 μm X 300 μm , 30 μm in depth, at an interval of 0.5 μm generating a stack of ≈ 60 Z slices. Ten microglia from each image were chosen at random and the number of synaptic structures (Synapsin) co-localizing with microglial end point processes (Iba1) were manually counted (similar to the CVLM and RVLM). Thus, 60 microglia from each animal, from each treatment group (three treatments) at the 6- and 10-h time points, were analyzed.

4.3.6 Data analysis and statistics

Area under curve (AUC) was calculated, using Spike two acquisition and analysis software (version 8.03; Cambridge Electronic Design, Cambridge, UK), for all treatment groups (phenylephrine, saline and hydralazine) at each time point (0.5, 2, 6 and 10 h), and was statistically analyzed using one-way ANOVA with Dunnett's multiple comparison tests. Non-parametric non-continuous data, such as the number of Fos-ir neurons, microglia and the number of microglial contacts made with synapses, from each repeat ($n = 3$), was summed and statistically analyzed using the Chi-square test for goodness of fit (Nedoboy et al., 2016; Sokal and Rohlf, 2012). Parameters obtained highlighting the microglial morphology variations between treatments (% of area occupied, number of end point processes per microglia and branch length (μm) per microglia) and percentage of CD206+ microglia to total microglia, were treated as non-parametric continuous data. Non-parametric continuous data were averaged across repeats ($n = 3$) and analyzed using Kruskal–Wallis one-way analysis of variance. All the statistical comparisons were made between treatment group (phenylephrine/hydralazine) and the saline group at the particular time point; no comparisons were made across time points in any of the groups. GraphPad Prism version 6.05 was used to perform all of the above mentioned statistical comparisons; one-way ANOVA, Chi-square test for goodness of fit and Kruskal–Wallis one-way analysis of variance.

4.4 Results

4.4.1 Effects of blood pressure modulations on the CVLM and the RVLM neuronal activity

4.4.1.1 Variations induced in MAP

Intravenous infusion of phenylephrine (an α_1 -adrenoreceptor agonist, which acts on blood vessels, and does not cross the blood-brain barrier) raised the baseline levels of MAP by 40 ± 10 mmHg, within 1 min following the start of infusion (Figure 4.1A1). However, the increase in MAP only lasted for 30 min, without changing the rate of infusion. The gradual reduction in arterial pressure following prolonged phenylephrine infusion is well known, and can be attributed to the desensitisation of α_1 -adrenoreceptors (Minami et al., 1997). Therefore, the rate of infusion was adjusted for subsequent time points to maintain the elevated levels of BP, where possible. Intravenous infusion of phenylephrine was maintained for 0.5, 2, 6 and 10 h, in four separate groups of rats ($n=3$ each). Each group of rats was sacrificed at each time point for

analysis. Slight variations in baseline levels of MAP were observed during intravenous infusion of saline in four separate group of rats: 0.5, 2, 6 and 10 h (n=3 each) (Figure 4.1A2) but overall BP levels were not affected.

Intravenous administration of hydralazine caused an instant, and sustained, hypotensive response of 40 ± 10 mmHg (Figure 4.1A3). The hypotensive stimulus was maintained for 0.5, 2, 6 and 10 h, respectively, in four separate groups of rats (n=3 each). Maintenance of the acute hyper-, and hypo-, tensive stimuli for the duration of the protocol, evoked significant differences in MAP, shown by AUC analysis (Figure 4.1B), indicating that alterations introduced in the MAP were maintained for the duration of the experimental period.

4.4.1.2 *Fos-ir*

It is well known that Fos-ir changes in response to altered MAP in the CVLM and the RVLM (Chan and Sawchenko, 1994; Graham et al., 1995; Li and Dampney, 1994; Minson et al., 1997b; Suzuki et al., 1994). Therefore, we did not perform a comprehensive quantification of Fos-ir in the CVLM, in response to provided stimuli; instead, Fos-ir was quantified in the RVLM region to indicate that the stimulus induced the expected changes in neuronal activity.

- *Neuronal activity in the RVLM increases in response to acute hypotension*

In agreement with previous studies, intravenous administration of hydralazine increased the number of Fos-ir neurons in the RVLM (Figure 4.2C), when compared to saline infusion (Figure 4.2B), at all of the four time points included in the study; 0.5, 2, 6 and 10 h (Graham et al., 1995). At 0.5 h, the number of Fos-ir neurons increased by 32% (88–116; $p \leq 0.05$) when compared with saline (Figure 4.2D). Consistent with the previous time point, 2 h of hydralazine administration increased the number of Fos-ir neurons by 255% (42–149; $p \leq 0.0001$ Figure 4.2D). The number of Fos-ir neurons in the RVLM continued to increase further by 149% at 6 h (from 148 to 368; $p \leq 0.0001$) and by 62% at 10 h (404–655; $p \leq 0.0001$) (Figure 4.2D).

Following 0.5 h of phenylephrine infusion, the number of Fos-ir neurons, observed in the RVLM, were not significantly different from that seen in saline treated rats (Figure 4.2D). However, increased levels of Fos-ir neurons were observed in the RVLM samples collected from rats subjected to acute hypertension, when compared with saline, for 2 h (increased by 110%; from 42 to 88; $p \leq 0.0001$), 6 h (increased by 44%; from 148 to 213; $p \leq 0.001$) and 10 h (increased by 53%; from 404 to 618; $p \leq 0.0001$) (Figure 4.2D). The increased levels of Fos-ir in the RVLM, in response to phenylephrine infusion when compared with saline infusion, may be attributed to the tendency of BP to return to baseline levels, following the initial 60 min of

phenylephrine infusion. However, the Fos-ir observed in the RVLM in response to intravenous phenylephrine (Figure 4.2A) was lower than the Fos-ir levels quantified in the same region in response to hydralazine administration (Figure 4.2C), at the 2 h (lower by 61; $p \leq 0.0001$) and 6 h time points (lower by 155; $p \leq 0.0001$) (Figure 4.2D).

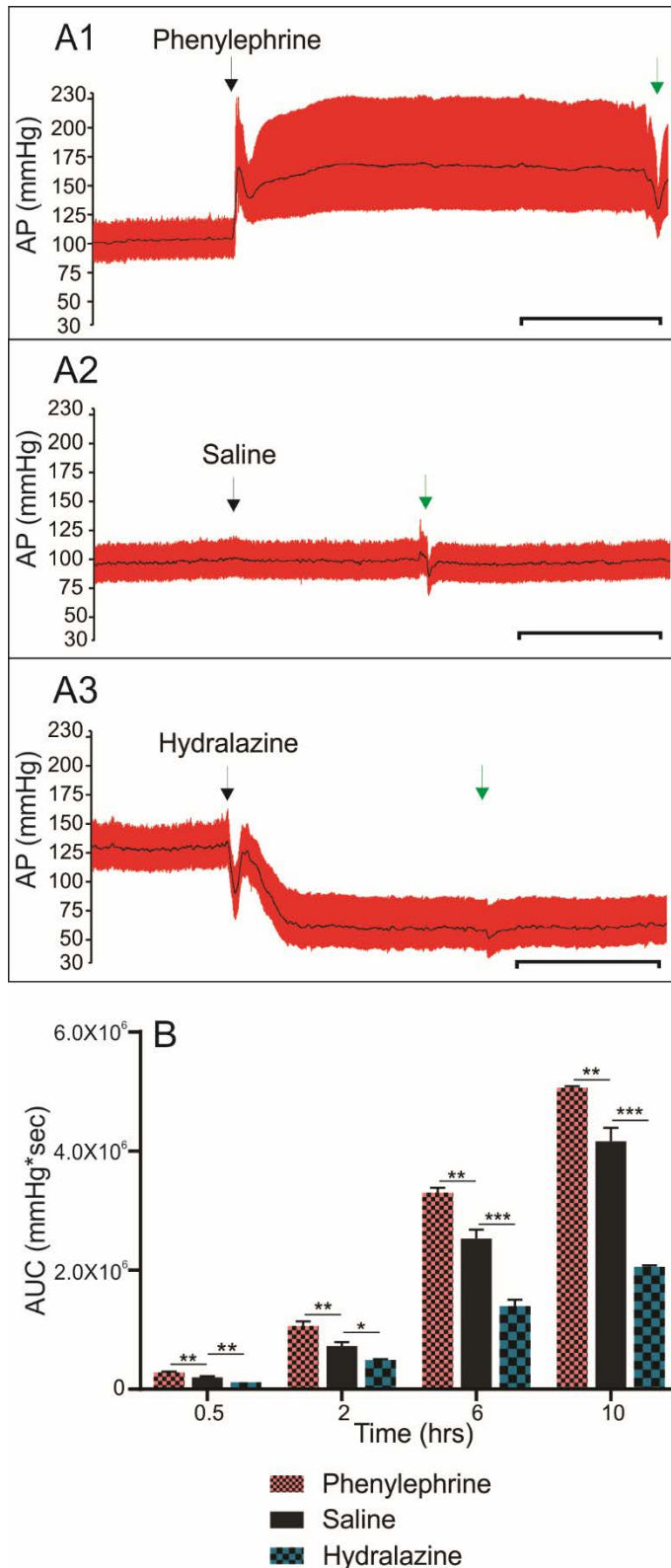


Figure 4.1: Effect of intravenous infusion of phenylephrine, saline and hydralazine on blood pressure

(A1) Effect of continuous intravenous infusion of phenylephrine at 10 $\mu\text{g/kg/min}$, (A2). Saline infusion and (A3). Effect of bolus injection of hydralazine at 10 mg/kg on arterial blood pressure (AP). Pinch reflex response and administration of additional anesthetic, when required (green arrow; please refer to methods for details). Scale bar = 5 min. (B) Effect of phenylephrine, saline and hydralazine on the area under curve (AUC) for mean arterial pressure (MAP) for the whole protocol period, where the stimulus was maintained continuously for 0.5, 2, 6 and 10 h in 4 separate group of rats ($n = 3$ each). Statistical comparisons were made with saline treatment group, at the particular time point, using one-way ANOVA with Dunnett's multiple comparison tests; $*p \leq 0.05$, $**p \leq 0.01$ and $***p \leq 0.001$. Data are expressed as mean \pm SEM, $n = 3$.

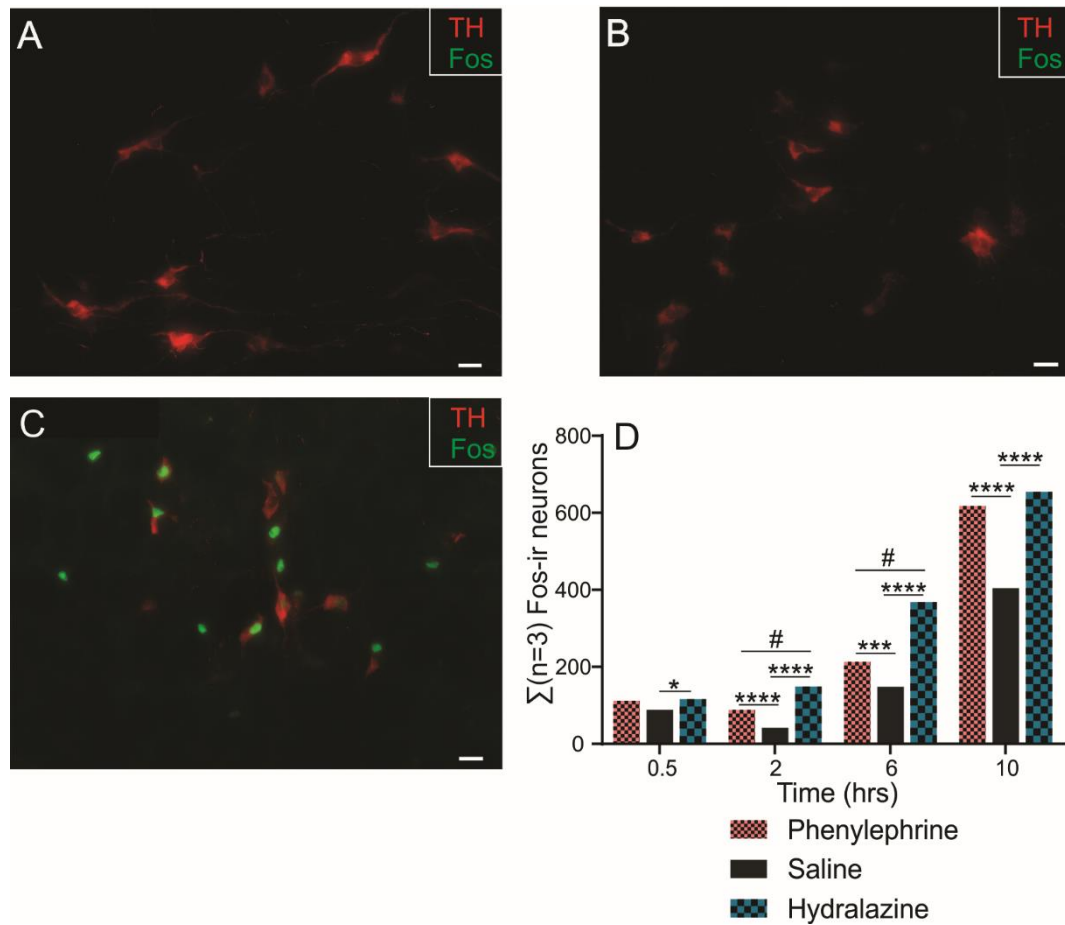


Figure 4.2: Effect of three different treatments (intravenous infusion of phenylephrine, saline or hydralazine) on the number of Fos-ir neurons in the RVLM region

(A) Fos-ir decreases in response to intravenous continuous infusion of phenylephrine. (B) Fos-ir stays minimal in response to intravenous continuous infusion of saline. (C) Fos-ir increases in response to intravenous administration of hydralazine. Scale bar = 20 μm. (D) Number of Fos-ir neurons in the RVLM region when stimuli were provided for 0.5, 2, 6 and 10 h in four separate group of rats (n = 3 each). *Statistical comparisons were made with the saline treatment group, at the particular time point, using the Chi-square test for goodness of fit; * $p \leq 0.05$, *** $p \leq 0.001$ and **** $p \leq 0.0001$. #Statistical comparisons were made between phenylephrine and hydralazine treatment groups, at the particular time point, using the Chi-square test for goodness of fit; # $p \leq 0.0001$. Data are summed for n = 3.

4.4.2 **Microglial-neuronal relationship under homeostasis**

Microglia (Iba1) are homogenously distributed in the cardiovascular nuclei of the brainstem, the CVLM (Figure 4.3A) and the RVLM (Figure 4.3B), and create a network with their processes covering the entire neuronal parenchyma. Microglial packing density varies depending on the neuronal packing density (Figure 4.3B). Microglial processes were observed to be in closer contact with the dendrites of TH⁺ RVLM neurons than the neuronal cell body (Figure 4.3B, C and E). Microglial processes were observed to wrap themselves around the TH⁺ neuronal cell body (Figure 4.3D and Movie 4.1) and dendrites (Figure 4.3E and Movie 4.2).

4.4.3 **Induction of acute hyper- and hypo- tension causes microglia to change their pattern of distribution in the ventrolateral medullary nuclei**

4.4.3.1 *Overall number of microglia*

- *CVLM*

Following intravenous administration of hydralazine, a change in the total number of microglia was only seen 6 h after the stimulus (Figure 4.4A), with a slight yet significant increment in the number of microglia (increased by $\approx 12\%$ from 661 to 742; $p \leq 0.05$). This increase returned to normal 10 h after hypotension (Figure 4.4A). Intravenous infusion of phenylephrine did not induce any changes in the overall number of microglia in the CVLM (Figure 4.4A).

- *RVLM*

Continuous intravenous infusion of phenylephrine for 0.5 h did not change the overall number of microglia (Figure 4.4B). However, following 2 h of phenylephrine infusion the number of microglia significantly increased by $\approx 14\%$ (from 596 to 683; $p \leq 0.05$) in the RVLM region when compared with saline (Figure 4.4B). These increased numbers of microglia returned to normal baseline levels at 6 h (Figure 4.4B) and remained unchanged 10 h following induction of hypertension (Figure 4.4B). No significant change in the number of microglia was observed in the hydralazine treatment group at any of the 4 time points analysed, when compared with saline treated group.

4.4.3.2 *Inter-microglial distance*

- *CVLM (Figure 4.5B-E)*

Induction of acute hypertension causes a rapid, but short term, change in the homogenous distribution of microglia. The number of microglia with an inter-microglial distance of $\approx 13 \mu\text{m}$ increased from 4 to 13 ($p \leq 0.05$) when compared with the saline group, following 0.5 h of

phenylephrine infusion (Figure 4.5B). This subtle change in the distribution of microglia returned to normal within 2 h of hypertension induction and stayed that way at subsequent time points (Figure 4.5C-E).

No rearrangement in the distribution of microglia was seen following hydralazine administration at 0.5 or 2 h (Figure 4.5B and 5C). However, at the 6-h time point, significant differences were seen in microglial distribution during acute hypotension. Increased numbers of microglia were observed with an inter-microglial distance of $\approx 23 \mu\text{m}$ (increased by 19; $p \leq 0.05$) and $33 \mu\text{m}$ (increased by 38; $p \leq 0.05$), when compared with saline (Figure 4.5D). These changes were not observed following 10 h of acute hypotension (Figure 4.5E).

- *RVLM (Figure 4.5F-I)*

A spatial distribution analysis revealed that the number of microglia with an inter-microglial distance of $\approx 13 \mu\text{m}$ increased from 0 to 7 ($p \leq 0.01$), when compared with saline, following 2 h of phenylephrine infusion (Figure 4.5G). Following 6 h of phenylephrine infusion, significant differences were observed in the number of microglia with an inter-microglial distance of $\approx 28 \mu\text{m}$, indicating the resumption of microglial homeostatic distribution. The number of microglia with an inter-microglial distance of $\approx 28 \mu\text{m}$ increased from 44 to 68 at 6 h ($p \leq 0.05$) (Figure 4.5H) and from 67 to 98 ($p \leq 0.05$) at 10 h (Figure 4.5I).

Data from induced hypotension showed a decrease in the inter-microglial distance starting at 2 h, continuing at 6 h and returning to normal at 10 h. The number of microglia at 2 h with an inter-microglial distance of $\approx 33 \mu\text{m}$ increased from 136 to 181 ($p \leq 0.05$) (Figure 4.5G). This distance between microglia continues to decrease to $\approx 23 \mu\text{m}$ (microglial number increased from 20 to 39; $p \leq 0.05$) and $28 \mu\text{m}$ (microglial number increased from 44 to 77; $p \leq 0.01$) at 6 h time point (Figure 4.5H). These changes in the spatial distribution of microglia returned to normal at 10 h (Figure 4.5I).

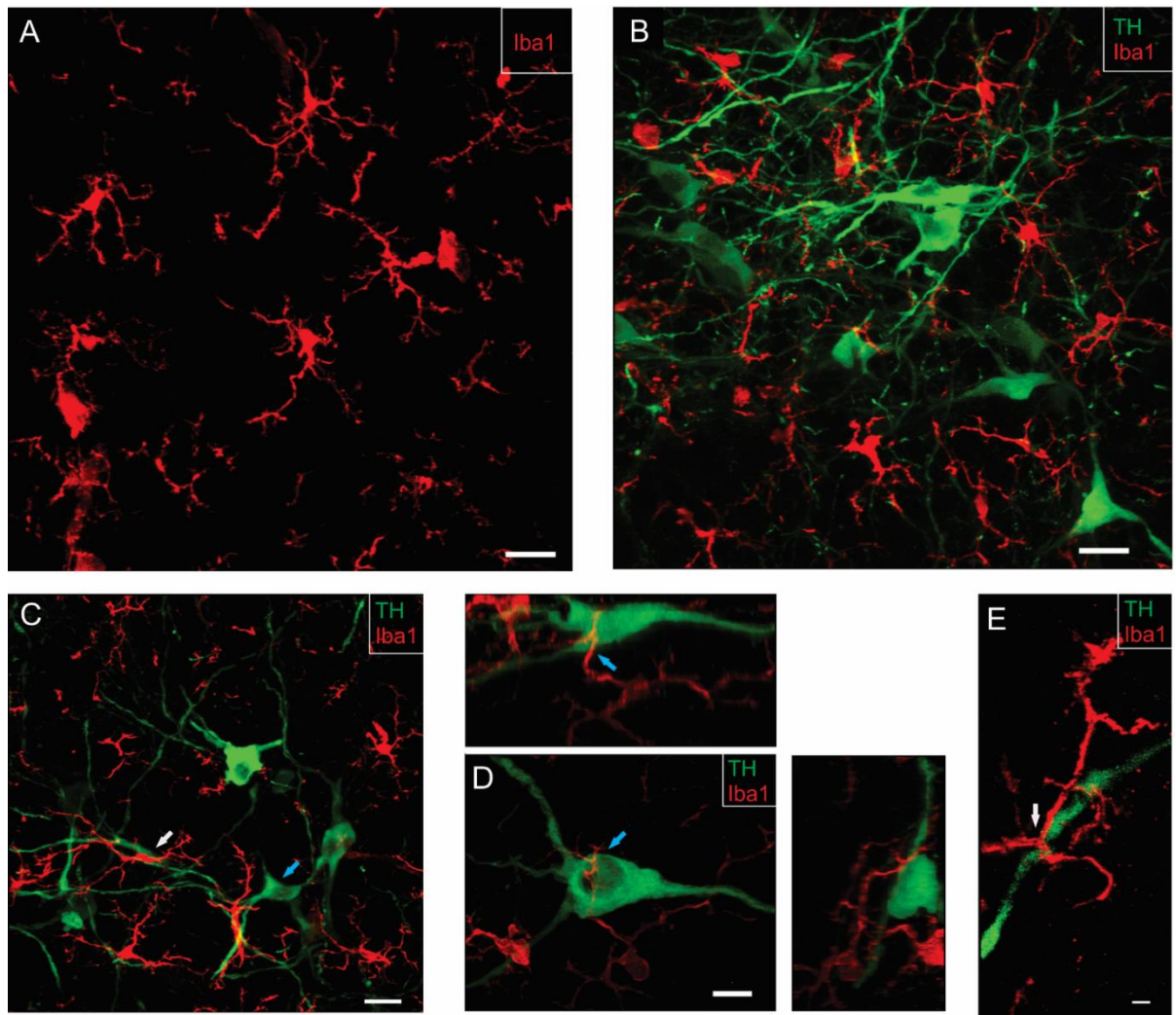


Figure 4.3: Evidence of a close yet dynamic relationship between neurons (TH⁺ neurons) and microglia

(A) Microglia are present in the CVLM region. Scale bar = 20 μ m. (B) Surveilling microglia cover the parenchyma of the RVLM region with their dynamic processes. Tyrosine hydroxylase (TH, green) is a marker for adrenergic RVLM neurons. Scale bar = 20 μ m. (C) Microglia are closely apposed to dendrites of TH⁺ RVLM neurons (white arrow) rather than the neuronal cell body (blue arrow). Scale bar = 20 μ m. (See ((Kapoor et al., 2015))); image used with permission) (D) Microglial processes appear to penetrate a neuronal cell body (blue arrow). Scale bar = 10 μ m. Also see Movie 4.1. (E) Microglial processes are wrapped around the dendrite of a TH⁺ neuron in the RVLM region (white arrow). Scale bar = 2 μ m. Also, see Movie 4.2.

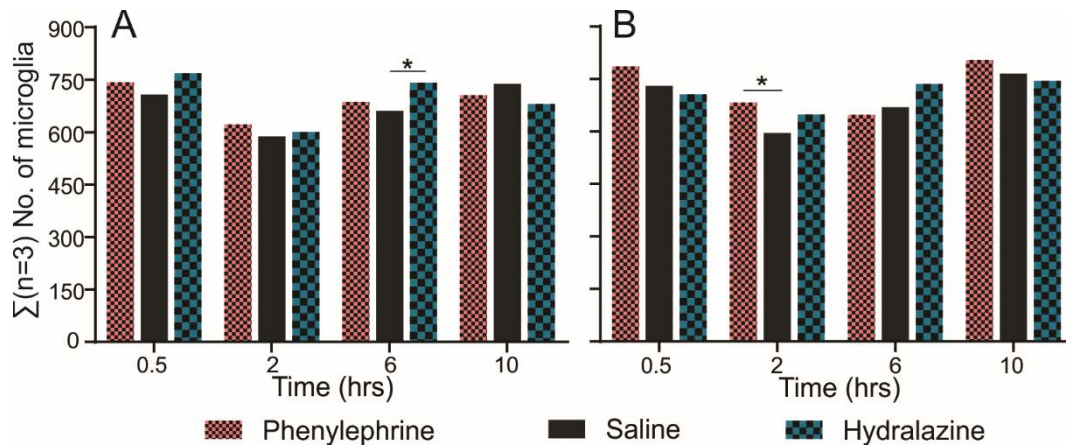


Figure 4.4: Effect of intravenous infusion of phenylephrine, saline or hydralazine on the number of microglia in the ventrolateral medullary region of SD rat

Number of microglia in the (A) CVLM and (B) RVLM, when stimuli were provided for 0.5, 2, 6 and 10 h. Statistical comparisons were made with the saline treatment group, at the particular time point, using the Chi-square test for goodness of fit; $*p \leq 0.05$. Data is summed from three animals.

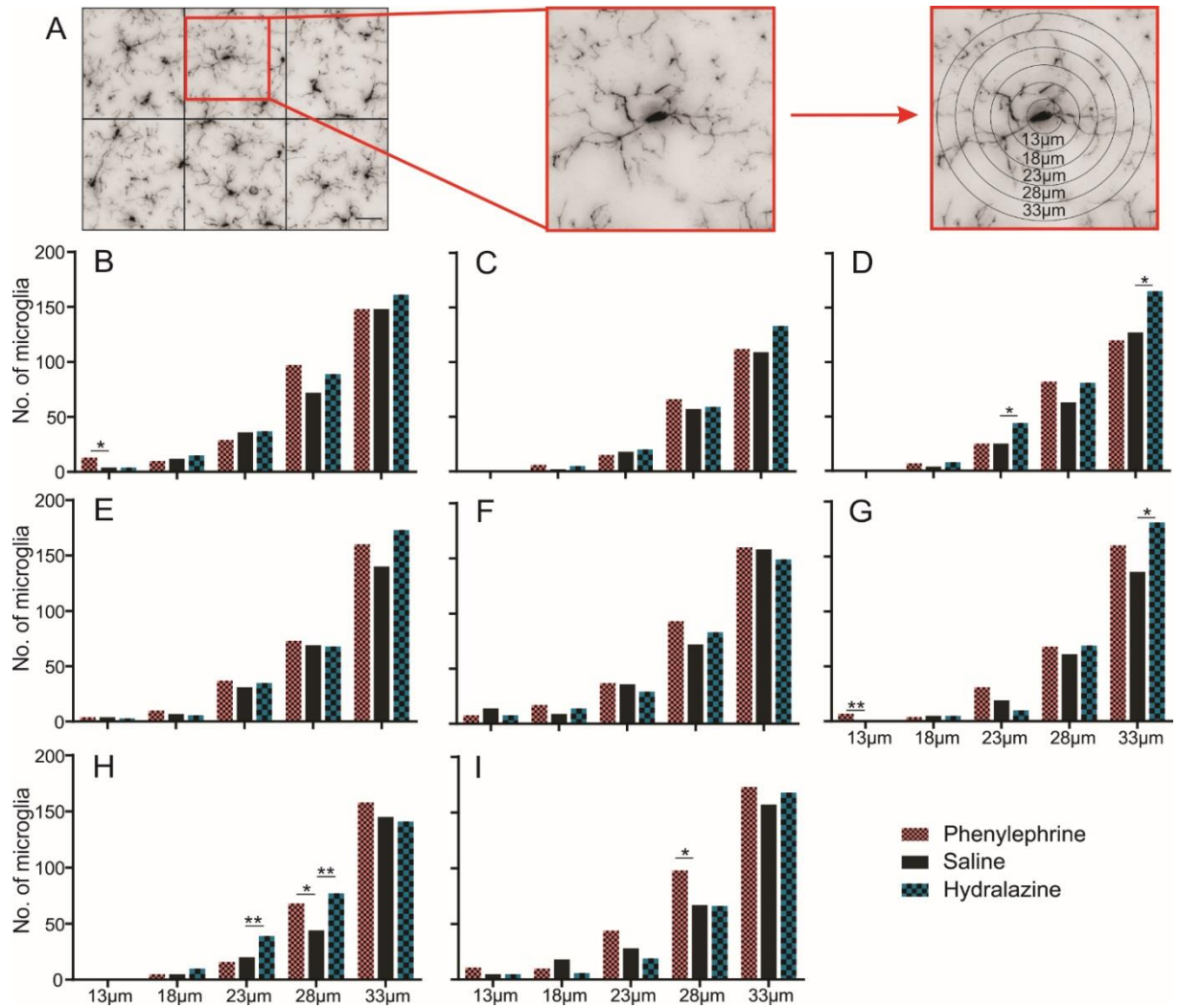


Figure 4.5: Effect of intravenous infusion of phenylephrine, saline or hydralazine on the spatial distribution pattern of microglia in the ventrolateral medullary region of SD rat

(A) Spatial distribution analysis: each image was divided into six equal parts using the grid feature in CorelDRAW X7. One microglia was chosen from each of these six regions and a series of six concentric circles were drawn centered around the soma of each of these microglia (modified Sholl analysis; see methods for details). Scale bar = 20 μm. Number of microglia plotted against the inter-microglial distance in the CVLM region when stimuli were provided for (B) 0.5 h, (C) 2 h, (D) 6 h and (E) 10 h and the RVLM region when stimuli were provided for (F) 0.5 h, (G) 2 h, (H) 6 h and (I) 10 h. Statistical comparisons were made with the saline treatment group, at the particular time point, using the Chi-square for goodness of fit; * $p \leq 0.05$ and ** $p \leq 0.01$. Data is summed from three animals.

4.4.4 Microglial contact with synapses increases with the induction of acute hypertension in the ventrolateral medullary nuclei

Microglial end point processes (Iba1) were seen to be in close contact with neuronal synapses (Synapsin), in the CVLM (Figure 4.6A) and the RVLM (Figure 4.6B) region of the brainstem.

- *CVLM*

Microglial contacts with neuronal synapses increased following 0.5 h of phenylephrine infusion and remained elevated until 10 h (Figure 4.6C). At 0.5 h, the number of synapses in close contact with microglial end point processes increased by 44% (from 252 to 362; $p \leq 0.0001$, Figure 4.6C). Following 2 h of phenylephrine infusion, the number of synapses in contact with microglia increased by 21% (from 312 to 378; $p \leq 0.05$ Figure 4.6C). Similar microglial responses were observed at 6 and 10 (Figure 4.6C). Number of microglial processes in contact with synapses increased by 31% (from 387 to 507; $p \leq 0.0001$) at 6 h and by 93% (from 289 to 558; $p \leq 0.0001$) at 10 h (Figure 4.6C).

- *RVLM*

In the RVLM, significant changes in the number of microglial processes contacting neuronal synapses started to appear following 6 h of phenylephrine infusion (Figure 4.6D). The number of synapses in contact with microglial end point processes increased by 32% (from 359 to 473; $p \leq 0.0001$) at 6 h and by 31% (from 404 to 529; $p \leq 0.0001$) at 10 h (Figure 4.6D).

4.4.5 Microglial contact with synapses decreases with the induction of acute hypotension in the ventrolateral medullary nuclei

- *CVLM*

Following 0.5 h of acute hypotension microglial contacts with neuronal synapses increased by 32% (from 252 to 332; $p \leq 0.001$; Figure 4.6C). Microglial contact with CVLM neuronal synapses decreases at 6 h (decreased by 35% from 387 to 252; $p \leq 0.0001$) and returned to normal at 10 h (Figure 4.6C).

- *RVLM*

Microglial contact with the RVLM neuronal synapses, in response to induction of acute hypotension, decreases with the increase in the duration of the stimulus (Figure 4.6D). At 2 h, the number of synapses contacted by microglia decreased by 17% (from 333 to 278; $p \leq 0.05$) and remained decreased at the following time points (Figure 4.6D). Number of synapses

contacted by microglial end point processes decreased by 21% (from 359 to 284; $p \leq 0.001$) at 6 h and by 25% (from 404 to 303; $p \leq 0.001$) at 10 h.

4.4.6 Microglia do not change their morphology in response to induction of acute hyper- or hypo- tension (Figure 4.7B-E) in the ventrolateral medullary nuclei

Analysis of the % of area covered by microglia, number of end point processes per microglia and branch length (μm) per microglia at 40X magnification did not show any significant differences between treatment groups. This observation was consistent during induction of acute hyper- or hypo- tension in either CVLM (Figure 4.7B) or RVLM (Figure 4.7C). Analysis of microglial morphology (number of end point processes/ microglia and branch length (μm)) at higher magnification (63X) also did not show any significant changes in microglial morphological characteristics in either CVLM (Figure 4.7D) or RVLM (Figure 4.7E).

4.4.7 Induction of acute hyper- or hypo- tension does not induce any microglial response in the nucleus ambiguus (sub compact, NAsc)

The microglial response to induction of hyper- or hypo- tension in the NAsc served as a control to the microglial response in the CVLM and the RVLM. No significant differences were observed in the overall number of microglia (Figure 4.8A1 and A2), microglial spatial distribution (Figure 4.8B1 and B2), number of synapses co-localising with microglial end point processes (Figure 4.8C1 and C2) and microglial morphology (Figure 4.8D1 and D2), at either 6 or 10 h time points, regardless of the provided treatment.

4.4.8 Expression levels of M1 or M2 phenotype do not change with the disturbances introduced in BP in the ventrolateral medullary nuclei

Iba1 (a pan marker for microglia) is known to label all microglia in the CNS regardless of their phenotype; M0, M1 or M2 (Figure 4.9A). The CD206/mannose receptor was used as a marker to identify activated microglia exhibiting a behavior similar to M2 type macrophages in the periphery (Figure 4.9B). The number of CD206⁺ microglia, co-localising with Iba1 expression (Figure 4.9C), was calculated and expressed as the percentage of CD206⁺ microglia to total microglia (% CD206⁺). The % CD206⁺ microglia, signifying the expression levels of M2 microglial phenotype, did not vary significantly between the three treatment groups at any of

the four time points; 0.5, 2, 6 and 10 h, in either of the regions analysed i.e. the CVLM (Figure 4.9D) or the RVLM (Figure 4.9E).

In addition to this, experiments were performed to quantify the expression levels of the M1 phenotype (labelled with CD16) in the CVLM and the RVLM region when animals were subjected to acute hyper- or hypo- tension at all of the four time points; 0.5, 2, 6 and 10 h. The results (Figure 4.9F) showed very slight, or no, expression of the M1 phenotype at any of the time points analysed, in any of the treatment groups, in either the CVLM or the RVLM region.

These results were in accordance with other studies, which showed basal M2 expression levels, and lack of M1 expression in the absence of physical CNS injury (Perego et al., 2011).

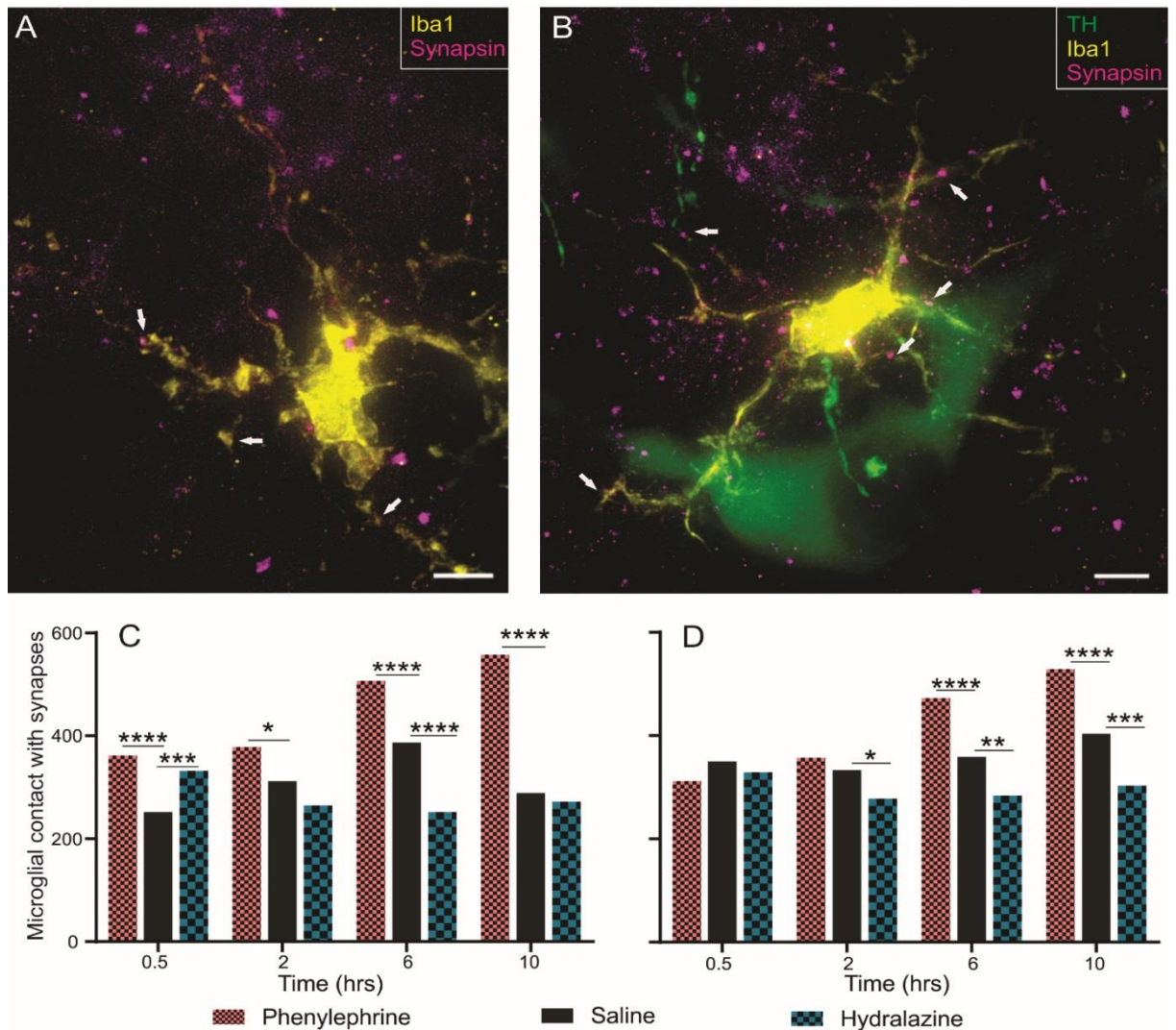


Figure 4.6: Effect of intravenous infusion of phenylephrine, saline or hydralazine on the number of synapses in contact with the microglial end point processes in the ventrolateral medullary region of SD rat

(A) Microglial end point processes in close contact with synapses (Synapsin) in the CVLM region (white arrows). Scale bar = 20 μ m. (B) Microglial end point processes in close contact with synapses (Synapsin) in the RVLM region (white arrows). Scale bar = 20 μ m. Yellow – Iba1, Green – TH and Violet – Synapsin. Number of microglia in contact with synapses in the (C) CVLM and the (D) RVLM when stimuli were provided for 0.5, 2, 6 and 10 h. Statistical comparisons were made with the saline treatment group, at the particular time point, using the Chi-square test for goodness of fit; * $p \leq 0.05$, ** $p \leq 0.01$, *** $p \leq 0.001$ and **** $p \leq 0.0001$. Data are summed from three animals.

Figure 4.7: Effect of intravenous infusion of phenylephrine, saline or hydralazine on the morphological characteristics of microglia in the ventrolateral medullary region of SD rat

(A) Quantification of morphological characteristics: binary images were ‘skeletonized’ with ImageJ and analyzed with the “AnalyzeSkeleton” plugin. Number of end point pixels (blue) and branch length (orange), obtained using AnalyzeSkeleton plugin of ImageJ, were normalized with the total number of microglia. Scale bar = 20 μm . The morphological characteristics examined at 40X magnification were: % of area covered by microglia calculated using ImageJ, Number of end point processes/microglia and branch length (μm)/microglia. Effect of intravenous infusion of blood pressure modulating drugs on the morphological characteristics of microglia (40X) in the (B) CVLM region and the (C) RVLM region where the stimulus was maintained for 0.5 h (B1 and C1), 2 h (B2 and C2), 6 h (B3 and C3) and 10 h (B4 and C4). The morphological characteristics examined at 63X magnification were: number of end point processes/microglia and branch length (μm)/microglia. Effect of intravenous infusion of blood pressure modulating drugs on the morphological characteristics of microglia (63X) in the (D) CVLM and the (E) RVLM region, where the stimulus was maintained for 0.5 h (D1 and E1), 2 h (D2 and E2), 6 h (D3 and E3) and 10 h (D4 and E4). Kruskal–Wallis one-way analysis of variance didn’t show any significant difference between treatments. Data are expressed as mean \pm SEM, $n = 3$.

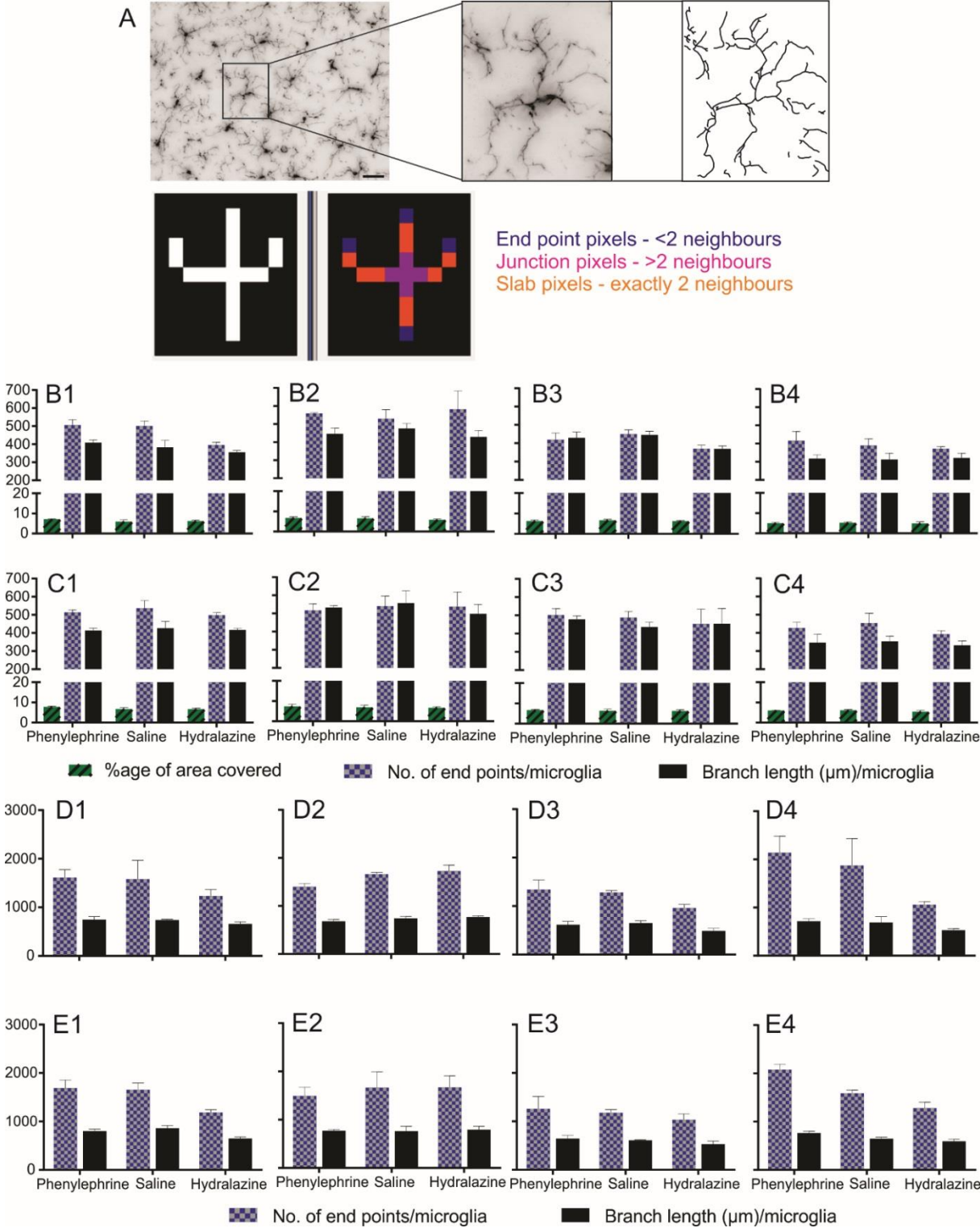


Figure 4.8: Microglial response to the intravenous infusion of phenylephrine, saline or hydralazine in the nucleus ambiguus (sub compact; NAsc) at 6 and 10 h time point

(A) Overall number of microglia at (A1) 6 h and (A2) 10 h. (B) Microglial spatial distribution at (B1) 6 h and (B2) 10 h. (C) No. of synapses in contact with microglial end point processes at (C1) 6 h and (C2) 10 h. (D) Microglial morphology: % of area covered, number of end point processes/microglia and branch length (μm)/microglia at (D1) 6 h and (D2) 10 h. The Chi-square test for goodness of fit didn't show any significant differences in the overall No. of microglia, microglial spatial distribution and number of synapses contacted by microglia. Statistical comparisons were made with the saline treatment group, at the particular time point; data is summed from three animals. Kruskal–Wallis one-way analysis of variance didn't show any significant difference between treatment groups. Data are expressed as mean \pm SEM, $n = 3$.

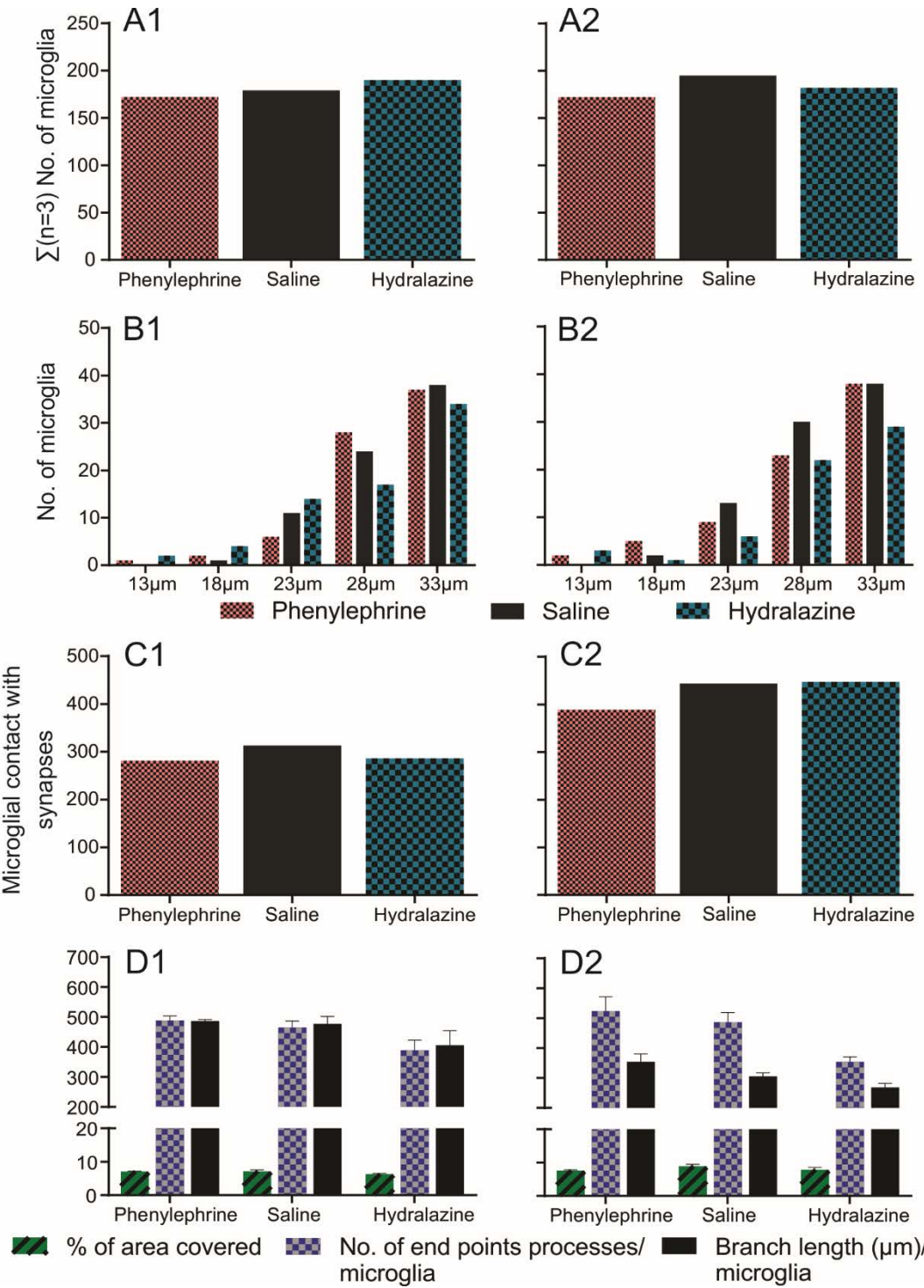
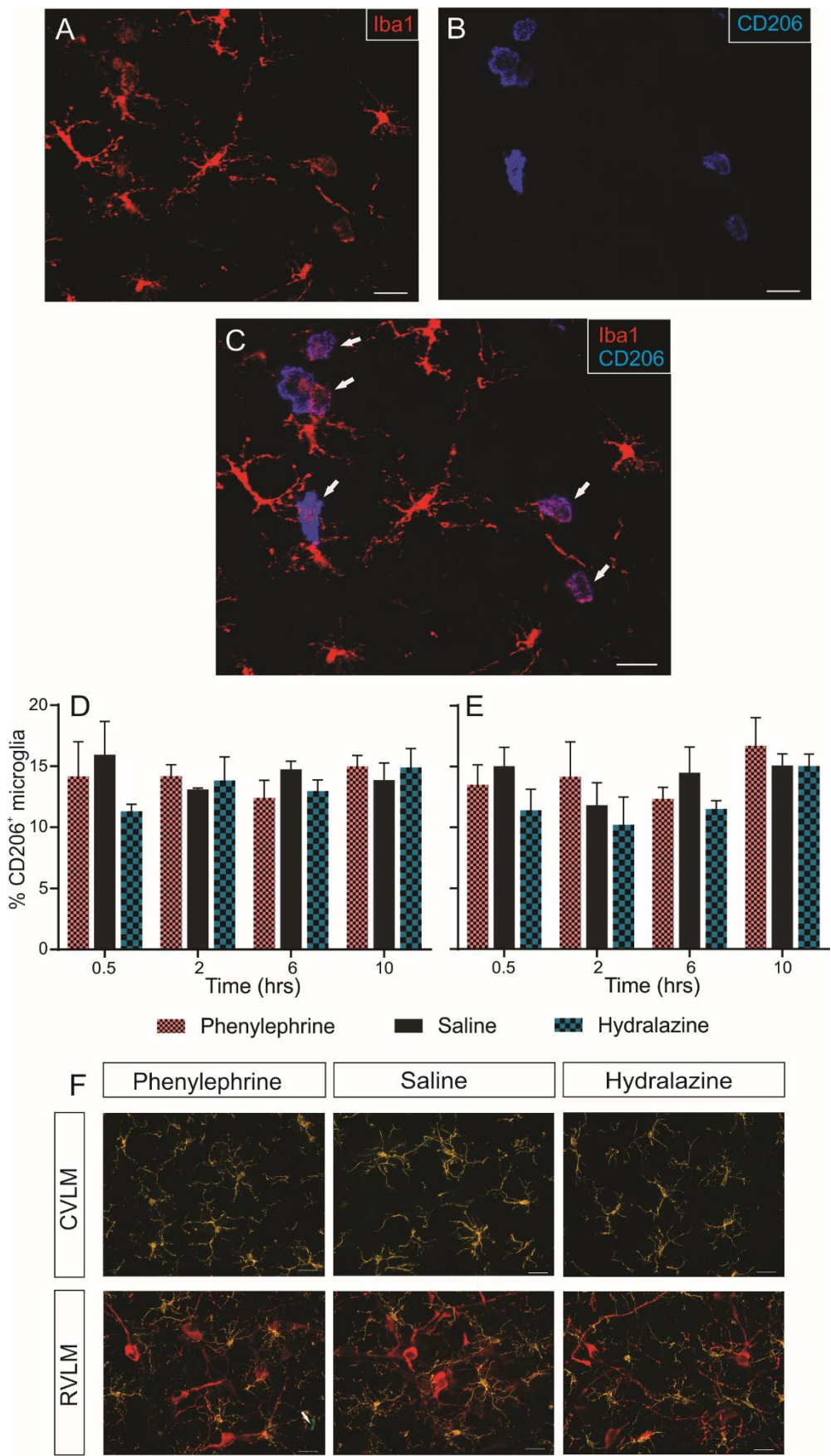


Figure 4.9: Effect of intravenous infusion of phenylephrine, saline or hydralazine on the expression levels of M1 and M2 phenotype in the brainstem region of SD rat

(A) Microglia (Iba1, red) in the RVLM region. (B) M2 microglia (CD206, blue) in the RVLM region. (C) Merged image of (A and B) showing the co-localization (white arrows) of M2 microglia and the Iba1 labeled microglia (pan marker for M0, M1 and M2). Scale bar = 20 μ m. % CD206⁺ microglia in response to blood pressure altering drugs in the (D) CVLM and the (E) RVLM when stimuli were provided for 0.5, 2, 6 and 10 h. Statistical comparisons were made using Kruskal–Wallis one-way analysis of variance. Data are expressed as mean \pm SEM, $n = 3$. (F) Representative images showing the expression levels of M1 phenotype (CD16, green, white arrow) and microglia (Iba1, yellow) in the CVLM and RVLM (TH, red) when stimuli were provided for 0.5, 2, 6 and 10 h. Scale bar = 20 μ m.



4.5 Discussion

The main finding of our study is that microglia do not play a passive role in the cardiovascular system but actively detect and respond to changes in the levels of BP; microglia dynamically change their distribution pattern and contacts made with synapses in response to changes in BP. Our first finding supports the hypothesis that microglia are well-placed to play a critical role within the CNS (Dworak et al., 2014; Hanisch and Kettenmann, 2007; Kettenmann et al., 2013; Wake et al., 2009) so as to ensure that cardiovascular autonomic neurons remain responsive to excitatory or inhibitory inputs. Secondly, our results reveal that microglia in the ventral medulla oblongata appear to monitor the local environment and respond to the magnitude and persistence of signals. Thirdly, increased or decreased levels of BP, ultimately affecting synaptic activity, changes microglial behavior. Interestingly, this microglial behavior is not manifested as polarization to activated microglial phenotypes, and does not require surveilling microglia to change their ramified morphology significantly. Instead, this modest change in microglial behavior may indicate an enhanced state of microglial alertness whereby they become more attentive to their local environment (Hanisch and Kettenmann, 2007; Kapoor et al., 2015; Karperien et al., 2013) . In response to increased BP, the spatial distribution of microglia is affected; as is the number of synapses contacted by surrounding microglia. On the other hand, decreased BP levels cause microglia to change their pattern of distribution, and reduce the number of synaptic structures contacted by microglial processes. This study is the first to describe the spatial distribution of microglia in the resting (saline) or ‘stressed’ states (hyper- or hypo- tension) within the ventral medulla of the brainstem that are critical for cardiorespiratory regulation.

Our first finding provides evidence for the existence of a mesh created by the fimbria of surveilling microglia covering the entire neuronal population in the CVLM and the RVLM region of brainstem. This microglial state is also defined as the M0 phenotype, which precedes the M1 (inflammatory activated microglia) and M2 (anti-inflammatory activated microglia) phenotypes (Butovsky et al., 2014; Hu et al., 2012).

Induction of acute hypertension increases the glutamatergic input to CVLM neurons of brainstem (Minson et al., 1997b; Oshima et al., 2012). This glutamate-mediated activation at synapses in the CVLM region induces a rapid microglial response (within 0.5 h), causing microglia to move closer to, and contact, synapses more frequently. The rearrangement in the pattern of distribution of microglia was a short-term response to increased BP levels and was

not seen at any subsequent time points. However, the increased microglial contact with neuronal synapses was a rapid and long-term effect and did not return to normal levels even following 10 h of phenylephrine infusion. Augmented inhibitory output (GABAergic transmission) from CVLM neurons, in response to increased BP levels, shuts down neurons in the RVLM region (Pilowsky et al., 1985; Pilowsky et al., 2009). In the RVLM, microglial numbers increased and changed their distribution pattern following 2 h of continuous hypertension. This change observed in the spatial distribution of microglia did not change the level of synapses sampled by microglia. The number of synapses contacted by microglia, in the RVLM region, starts to increase at 6 h and remained elevated at 10 h. A lack of microglial response, in the RVLM region, following 0.5 h of hypertensive stimulus, may be attributed to microglia sensing the decreased synaptic activity in the RVLM region as a temporary disturbance. However, the persistence of stimuli in the RVLM alerts microglia to under-excited neurons.

We performed the same study in another animal group where acute hypotension was induced, by intravenous administration of hydralazine. Lowering of BP reduces the excitatory (glutamatergic) inputs to the CVLM (Guyenet, 2006; Miyawaki et al., 1997; Pilowsky et al., 2009). This reduced synaptic activity of CVLM neurons, in response to reduced glutamatergic input from nucleus of the solitary tract (NTS), caused microglia to increase the number of contacts made with synapses at 0.5 h. Following 6 h of hypotension, microglia changed their pattern of distribution and reduced the number of synaptic contacts. The initial increase (0.5 h) in microglial contacts with synapses, in the CVLM, may be a means by which microglia analyze the nature of any homeostatic disturbance. The lack of a microglial response at 2 h may be attributed to the possibility that microglia assess the homeostatic imbalance as a harmless change. The subsequent persistence of the stimulus may then lead to a microglial reaction. A reduction of inhibitory inputs from CVLM neurons reduces the levels of GABA in the synapses of RVLM neurons and leads to their over-excitation (Miyawaki et al., 1997; Miyawaki et al., 2002a). This reduced synaptic activity of RVLM neurons induces a fairly rapid (following 2 h of treatment) change in microglial behavior causing inter-microglial distance to decrease until 6 h of hypotension. This change in the spatial distribution of microglia is accompanied by a reduction in the number of synapses contacted by microglia.

Our data strongly supports the hypothesis that microglia and neurons are constantly communicating with each other (Pocock and Kettenmann, 2007; van Rossum and Hanisch, 2004). Any changes in neuronal activity are, more often than not, accompanied with changes in their neurochemistry that possess the power to disrupt the constitutive release of

neurotransmitters, released by neurons in homeostatic circumstances, such as GABA and glutamate (Pilowsky, 2014). Augmented, or reduced, synaptic levels of constitutively expressed neurotransmitters, depending on the stimulus, are sensed by microglia that may cause them to shift to an ‘alerted’ state. In this ‘alerted/ intermediate’ state, microglia monitor the local environment with extra vigilance by changing the level of synaptic sampling and conducting the required action (Hanisch and Kettenmann, 2007; Kapoor et al., 2015; Karperien et al., 2013). This shift can be attributed to “on” (due to an increased synaptic activity) or “off” (due to a decreased synaptic activity) signalling mechanisms (Biber et al., 2007). In this study, the microglial behavior induced in response to increased BP levels/ synaptic activity, possibly via “on” signalling, causes rearrangement of their pattern of distribution and increases the number of synapses contacted by microglia. This microglial behavior might be necessary to conduct activities such as synaptic pruning (Miyamoto et al., 2013; Wake et al., 2009), to reduce the activity levels of affected synapses. Changes in microglial behavior observed in response to decreased BP levels/ synaptic activity, possibly via “off” signalling, can be attributed to their ability to release neurotrophic factors. Such factors may include insulin growth factor-1 (Ueno et al., 2013) and macrophage-colony stimulating factor (Murase and Hayashi, 1998) that may support, or increase, the activity of silent synapses. In the case of “off signalling”, we speculate that fewer microglia may spend longer with affected synapses. The rearrangement induced in the pattern of microglial distribution may or may not be accompanied by changes in the overall number of microglia. In our hands, the first signs of a microglial response, to the changes induced in the basal levels of BP, were observed in the CVLM region, in both hyper-, and hypo-, tension.

It is now believed that microglial responses to any stimuli can no longer be viewed as an “all or none” activity; rather, they elaborate a graded response (Kettenmann et al., 2011). At one extreme, microglia respond to damage caused by inflammation or other severe injury. At the other extreme, the findings presented here support the notion that microglia continuously interact with neuronal synapses in a homeostatic manner to maintain a physiologically balanced state (Miyamoto et al., 2013; Wake et al., 2009). CNS injuries can result in irreversible damage that requires dramatic morphological rearrangement of surveilling microglia, resulting in microglial polarization to either of the activated phenotypes; M1 or M2 (David and Kroner, 2011; Perego et al., 2011). In our case, our morphological analysis revealed that brainstem microglia in cardiovascular nuclei do not significantly change their morphology when subjected to either hyper-, or hypo-, tension. This is further supported by the lack of significant changes

observed in the expression levels of M1 or M2 phenotype. Our data also reveal that the brainstem microglial response to increased or decreased levels of BP does not require an obvious change to an “activated phenotype”. Therefore, we speculate, in accordance with other studies, that the microglial behavior observed here is may be exhibited as an intermediate state by “alerted microglia” that succeeds the surveilling phenotype (M0), but precedes the activated phenotypes (M1/M2), that are observed during even mild disturbances in the local environment, and act to restore homeostasis (Hanisch and Kettenmann, 2007; Kapoor et al., 2015; Karperien et al., 2013). Recent literature suggests that microglia, in their ramified state, are capable of a number of neuro-supportive functions, including synaptic pruning (Tremblay et al., 2011), and release of neurotrophic substances (Karperien et al., 2013); this earlier work further supports the hypothesis for the existence of an ‘alerted’ microglial phenotype in addition to the quiescent M0, and activated M1/M2 states (Hanisch and Kettenmann, 2007; Karperien et al., 2013; Kettenmann et al., 2011). Our findings therefore illustrate a novel dimension to sympathetic neurophysiology, and illustrate the way that ‘alerted’ microglia may play a critical role in interacting with neurons to maintain a healthy CNS in normal homeostasis.

Microglial migration to the site of injury enables them to execute their immune functions, and requires a highly dynamic morphology (Stence et al., 2001) that comes with the ability to cope with extreme cellular rearrangements in a short period of time (Janssen et al., 2014). There is a possibility that there may be subtle changes introduced in the morphology of surveilling microglia enabling them to change their pattern of distribution while they are in a normal but ‘alerted’ state. Other studies also suggest that microglia may be capable of migrating short distances to conduct their housekeeping activities without acquiring an amoeboid morphology (Amadio et al., 2013; Karperien et al., 2013).

Changes in the levels of BP, by loading or unloading of baroreceptors, affects the synaptic activity levels in the CVLM or the RVLM, fairly rapidly, within minutes of the provided stimulus (Miyawaki et al., 1997; Schreihöfer and Guyenet, 2003). These rapidly induced changes in the levels of synaptic activity may be sensed by microglia in the vicinity of the affected synapses, and microglia may contribute to mechanisms such as baroreflex resetting. Baroreflex resetting is a mechanism by which the operating point of baroreceptor sensitivity changes, over a wide range of BP, and allows elevation of BP during appropriate behaviors, such as exercise (DiCarlo and Bishop, 2001; Guyenet, 2006). The earliest time point employed in our study was 0.5 h and the latest time point was 10 h; at 0.5 h, no significant changes in the microglial spatial distribution, except in the CVLM following phenylephrine infusion, were

observed. Microglia increased the number of CVLM neuronal synapses contacted at 0.5 h, following phenylephrine and hydralazine administration, but no changes were observed in the RVLM. We speculate that the persistence of the stimulus, rather than the appearance, evokes a more settled microglial response. However, the possibility that the microglial response to altered levels of BP, in the ventrolateral medullary nuclei, may begin and peak earlier than 0.5 h cannot be ignored; further work at earlier time points would be needed to clarify such a possibility.

Technical consideration: vertebrates under anesthesia cannot breathe adequately for longer durations without the aid of artificial ventilation: in this study, 6 h was the maximum. Thus, in the 10 h experiments animals were vagotomized (both left and right cervical vagus nerves were cut, to prevent inputs from pulmonary afferent nerves) and paralyzed with pancuronium bromide (to prevent entrainment of breathing to the ventilator (Pilowsky et al., 1990; Sun et al., 2011)), and were artificially ventilated. In preliminary experiments combining the use of sodium pentobarbital, pancuronium bromide and phenylephrine, there was a severe deterioration in the condition of the animal. Thus, the anesthetic was changed to urethane, so that all 3 drugs (anesthetic, paralyzing agent and phenylephrine) could be administered in the same animal. The control experiments (saline), at the 10 h time-point were conducted, where the animals were treated in the same way as the test treatments (phenylephrine/ hydralazine), to rule out the effect of change in anesthetic and surgical procedures, and isolate the effect of altered BP, on the microglial response. The microglial response observed at the 10 h time point reached a ‘plateau phase’, where microglial response either returned to baseline or no new additional changes were observed at 10 h compared to 6 h. This is reflected in the data from the control experiments (10 h in the NAsc) where no changes were seen in the microglial number, spatial distribution, morphology or level of synaptic sampling, following 10 h of either hyper-, or hypo-, tension.

In summary, we speculate that while changes in BP do not require polarization of microglia to an activation state, but that a transition to an ‘alerted’ state is essential to maintain a normal homeostatic environment. Microglia constantly sense changes in synaptic activity and change their pattern of distribution or packing density along with the level of synaptic surveillance, but without requiring an obvious transformation in their phenotype. The alertness induced in microglial behavior in response to synaptic activity variations may be attributed to the ability of microglia to conduct neuro-protective/ neuro-supportive activities such as synaptic pruning

or release of neurotrophic factors, to resume homeostasis without causing inflammation or long-term neuronal damage (Figure 4.10).

Our study, therefore, provides the first evidence concerning the relationship of microglia to cardiovascular neurons in the ventral brainstem. Importantly, the microglial response that follows imposed variations in BP does not induce a conventional inflammatory activation of microglia; revealing yet another function of surveilling microglia in the uninjured CNS. With increasing literature suggesting that microglial activation contributes to the exaggerated activity of the SNS (Shi et al., 2010a), we propose a plausible neuro-supportive role of microglia in the SNS.

Figure 4.10: Microglial alertness induced in response to changes in levels of blood pressure

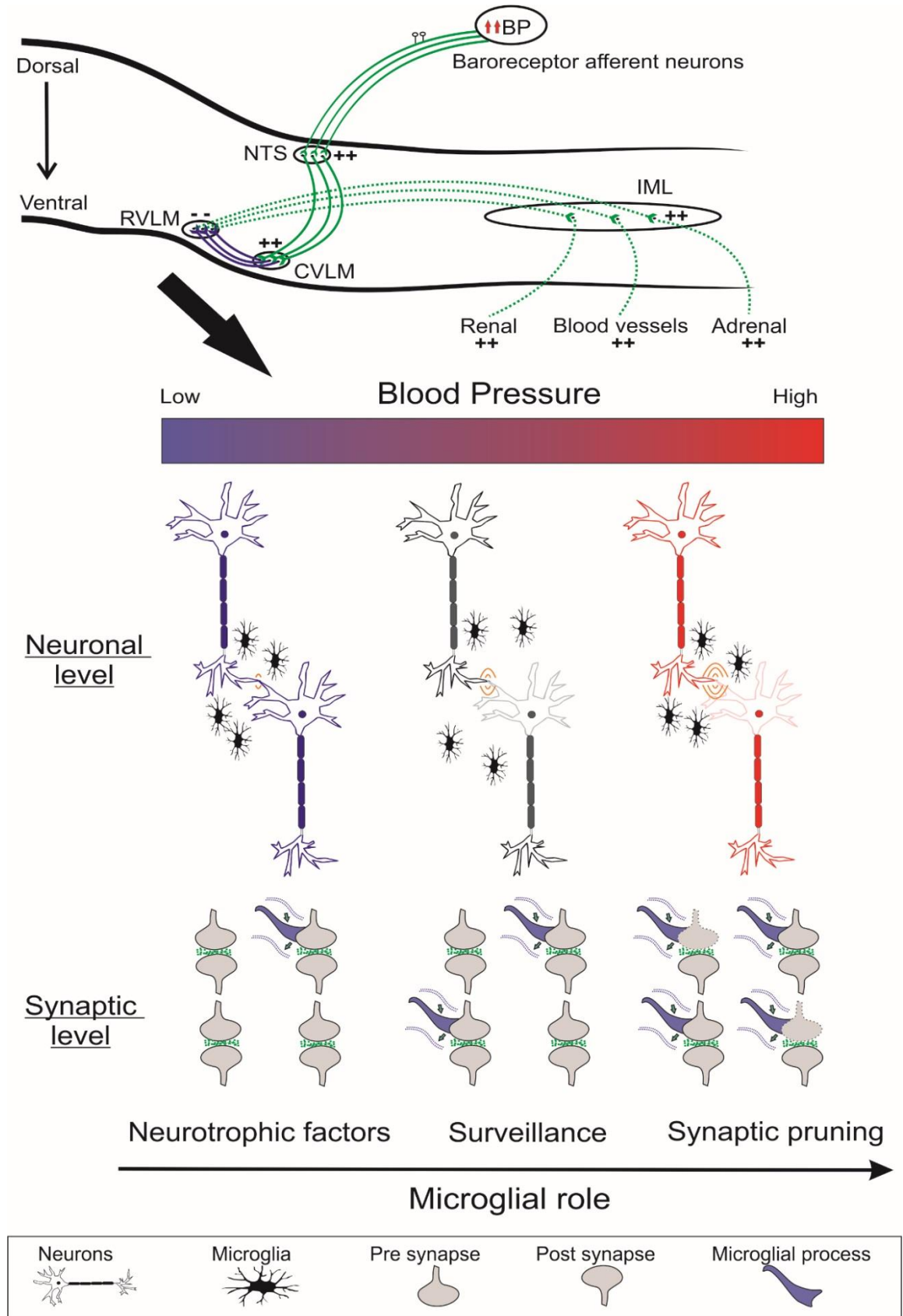
Baroreceptor afferent neurons located in the carotid sinus and aortic arch provide excitatory input (green) to the nucleus of the solitary tract (NTS) neurons in response to increased levels of blood pressure. Excited NTS neurons then activate (green) the caudal ventrolateral medullary (CVLM) neurons which in turn provide inhibitory input (blue) to rostral ventrolateral medullary (RVLM) neurons. This inhibition of RVLM neurons results in reduced sympatho-excitatory (dotted green) outflow to peripheral organs via neurons located in the intermediolateral (IML) cell column of the spinal cord. Modulations in arterial blood pressure levels further alter the levels of synaptic activity which in turn triggers “on” or “off” signaling alertness in microglial behavior. Low blood pressure levels (blue neurons) may cause “off” signaling microglial alertness resulting in microglia to move closer and reduce the number of synaptic contacts. Whereas, increased levels of blood pressure (red neurons) may trigger “on” signaling in microglial activity causing microglia to move closer to each other and increase the number of contacts made with synapses.

Movie 4.1: 3D reconstruction of Figure 4.3D

Demonstrating the proximity of microglial processes (Iba1, red) and cell body of a TH⁺ RVLM neuron (green). Microglial processes seem to penetrate a TH⁺ neuronal cell body in the RVLM. (Movies are included in .wmv format in the CD at the back of this thesis)

Movie 4.2: 3D reconstruction of Figure 4.3E

Demonstrating the morphological relationship between microglial processes (Iba1, red) and dendrite of a TH⁺ RVLM neuron (green). The microglial processes are wrapped around the neuronal dendrite. (Movies are included in .wmv format in the CD at the back of this thesis)



Chapter 5

Microglial response to changes in blood pressure in the rostral ventrolateral medulla is impaired in spontaneously hypertensive rats

Contents

5.1	Abstract.....	203
5.2	Introduction.....	204
5.3	Experimental procedures	206
5.3.1	Animals	206
5.3.2	Tail-cuff phenotyping.....	206
5.3.3	Experimental protocol	206
5.3.3.1	<i>Induction of acute hyper-, or hypo-, tension.....</i>	<i>206</i>
5.3.3.2	<i>Perfusion and tissue processing</i>	<i>207</i>
5.3.3.3	<i>Immunohistochemistry.....</i>	<i>207</i>
5.3.4	Image acquisition	208
5.3.5	Image analysis	209
5.3.5.1	<i>Fos-immunoreactivity (Fos-ir) and microglial spatial distribution</i>	<i>209</i>
5.3.5.2	<i>Microglial contact with synapses</i>	<i>209</i>
5.3.5.3	<i>Microglial morphology.....</i>	<i>209</i>
5.3.5.4	<i>M1 and M2 phenotype quantification.....</i>	<i>210</i>
5.3.6	Data analysis and statistics	210
5.4	Results	211
5.4.1	Tail-cuff phenotyping of WKY and SHR	211
5.4.2	Induction of acute hyper-, or hypo-, tension in WKY and SHR	213
5.4.3	Fos-ir increases in the RVLM in response to hypotension.....	216
5.4.4	Microglial-neuronal relationship	220
5.4.5	Microglia change their pattern of distribution in response to disturbances introduced in BP	223
5.4.5.1	<i>Number of microglia.....</i>	<i>223</i>
5.4.5.2	<i>Spatial distribution</i>	<i>223</i>
5.4.6	Microglia (Iba1) dynamically change the % of colocalisation with synapses (synapsin) in response to alterations in BP	228
5.4.7	Microglia do not change their morphology in response to disturbances introduced in BP levels	233
5.4.8	Microglia do not polarize to either M1 or M2 phenotype in response to disturbances introduced in BP levels.....	233
5.5	Discussion	239

Abbreviations:

BP – blood pressure

CNS – central nervous system

CVLM – caudal ventrolateral medulla

Fos-ir – Fos immunoreactivity

GABA – γ -aminobutyric acid

GFP – green fluorescent protein

H – hours

IMD – inter-microglial distance

JAM-1 – junctional adhesion molecule-1

MAP – mean arterial pressure

MBP – mean blood pressure

MIP – maximum intensity projection

NTS – nucleus of the solitary tract

PBS – phosphate buffered saline

RVLM – rostral ventrolateral medulla

SBP – systolic blood pressure

SHR – spontaneously hypertensive rats

SNS – sympathetic nervous system

STED – simulated emission depletion

TH – tyrosine hydroxylase

TREM2 – triggering receptor expressed on myeloid cells 2

VLM – ventrolateral medulla

WKY – Wistar-Kyoto rats

Keywords: CVLM, RVLM, microglia, blood pressure, SHR, WKY.

Highlights:

- Microglia change their spatial distribution to changes in blood pressure
- Microglial physiology is impaired in the RVLM of SHR
- Microglial response to altered blood pressure is impaired in the RVLM of SHR

The work in this chapter will be submitted shortly.

Kapoor, K., Bhandare, A.M., Farnham, M.M.J., Pilowsky, P.M., 2016. Microglial response to changes in blood pressure in the rostral ventrolateral medulla is impaired in spontaneously hypertensive rats. “In preparation”

Declaration of contributions: Candidate contributed to the design of experiments, performed all experiments, analysed data, interpreted results and was the major contributor to the manuscript. Amol M. Bhandare (a PhD candidate) assisted with the animal experiments and data analysis related to physiological data (concerning BP). Paul M. Pilowsky and Melissa M.J. Farnham contributed to conception and design of experiments, data analysis, interpretation of results, and editing and final approval of the manuscript.

5.1 Abstract

Microglia are the tissue resident macrophages of the central nervous system (CNS), and continuously survey their immediate environment for any homeostatic disturbances. Microglia are capable of detecting changes in neuronal activity levels by virtue of their close proximity to neurons and synapses. Microglia express receptors for almost every known neurotransmitter. Microglial processes constantly extend or retract in response to chemical gradients generated by changes in the activity of neurons. During over-activity of neurons/synapses, microglia remove synaptic structures leading to a more quiescent state. The caudal-, and rostral-, ventrolateral medullary (CVLM and RVLM, respectively) nuclei are critical in regulation of the cardiovascular system. Recently, an impairment in normal microglial physiology, leading to a failure to conduct housekeeping activities in the brain, was hypothesized to be involved in the pathology of hypertension. Here, we aimed to determine if the microglial response, in the ventrolateral medullary nuclei (VLM) of the brainstem, to induced alterations in blood pressure (BP) differs in normotensive and hypertensive rats. To achieve this study, we induced acute hyper-, (phenylephrine infusion) or hypo-, (hydralazine bolus injection) tension in Wistar-Kyoto rats (WKY) and spontaneously hypertensive rats (SHR). Microglia in the VLM dynamically change their spatial distribution and the extent of synaptic contact (% colocalisation between microglia and synapsin) in response to altered BP levels; this microglial behaviour does not induce significant changes in the microglial morphology. The key finding of this study is that the microglial response (pattern of distribution and % of colocalisation with synapses), to induced acute hyper-, (phenylephrine), or hypo- (hydralazine), tension, was impaired in the RVLM of SHR, when compared with WKY. The percentage of colocalisation between microglia (Iba1) and synapses (synapsin) increased by >70% in the RVLM of SHR, when subjected to either phenylephrine induced hypertension, or hydralazine induced hypotension. On the other hand, induction of phenylephrine induced hypertension caused a reduction (by $\approx 55\%$) in the percentage of colocalisation between microglia and synapsin in the RVLM of WKY; whereas, no changes were observed in the RVLM of WKY when subjected to hydralazine induced hypotension. Therefore, we speculate that the microglial physiology is impaired in the RVLM of SHR, which coincides with the hypertensive phenotype of SHR.

5.2 Introduction

Microglia are an essential component of the central nervous system (CNS) (Hanisch and Kettenmann, 2007; Kettenmann et al., 2011), and are continuously monitoring their local environment, with the help of their dynamic processes, to maintain homeostasis in a healthy CNS (Kapoor et al., 2015; Nimmerjahn et al., 2005; Tremblay et al., 2011). Microglia are capable of sensing changes in neuronal activity due to their close apposition to neurons/synaptic structures (Kapoor et al., 2016b; Schafer et al., 2013; Shapiro et al., 2009), and due to the expression of receptors for almost every known neurotransmitter and neuropeptide, including glutamate, GABA, ATP and angiotensin receptors (Farber et al., 2005; Kapoor et al., 2015; Kettenmann et al., 2011; Liu et al., 2016; Pocock and Kettenmann, 2007). When subjected to disturbances in normal neuronal/synaptic activity, microglia sense the change, and respond by altering the frequency of contacts made with neuronal synapses (Tremblay et al., 2010; Wake et al., 2009). Microglia can perform many activities that lead to a resumption of homeostasis, ranging from release of neurotrophic factors (Karperien et al., 2013; Ueno et al., 2013) to removal of unhealthy synapses (synaptic pruning) (Kettenmann et al., 2013; Miyamoto et al., 2013; Tremblay et al., 2010; Wake et al., 2009). Interestingly, microglia do not need to change their morphology, significantly, in order to conduct housekeeping activities, such as synaptic pruning (Kapoor et al., 2016b; Kettenmann et al., 2013; Miyamoto et al., 2013; Tremblay et al., 2010; Wake et al., 2009). Only in situations of extreme physical injury do microglia acquire an amoeboid morphology (Stence et al., 2001), and polarize into either a, macrophage-like, neurotoxic (M1) or a neuro-protective (M2) phenotype (David and Kroner, 2011; Hu et al., 2012; Wang et al., 2013a).

As discussed in sections 1.2.1.5 and 1.2.1.6, the caudal and rostral ventrolateral medullary (CVLM and RVLM, respectively) nuclei in the brainstem are involved in almost every aspect of cardiovascular control by the sympathetic nervous system (SNS) (Guyenet, 2006; Pilowsky and Goodchild, 2002; Pilowsky et al., 2009). Data in Chapter 4 show that microglia in the VLM area are capable of responding to changes in blood pressure (BP) levels, and respond to altered BP by changing their spatial distribution and number of contacts made with synapses (Kapoor et al., 2016b).

It is suggested that an impairment in normal microglial physiology (Liu et al., 2016; Rodríguez et al., 2016; Shi et al., 2010a; Shi et al., 2010b), or exaggerated vascular inflammation (Waki et al., 2010; Waki et al., 2011; Waki et al., 2013), in cardiovascular areas of the brain, may be

involved in the pathology of hypertension. Waki and colleagues reported that JAM-1 (junctional adhesion molecule -1, a pro-inflammatory molecule), and monocyte chemoattractant protein-1, are over expressed in the nucleus of the solitary tract (NTS, section 1.2.1.7) of spontaneously hypertensive rats (model for neurogenic hypertension; SHR) (Waki et al., 2007; Waki et al., 2008a; Waki et al., 2008b). Adenovirus mediated over-expression of JAM-1 in the NTS of Wistar-Kyoto rats (normotensive control for SHR; WKY) evoked a hypertensive response (Waki et al., 2007). Antagonism of microglial activation (with intracerebroventricular administration of minocycline) significantly attenuated the angiotensin-II induced hypertension (Shi et al., 2010a). Furthermore, over-expression of IL-10 (an anti-inflammatory cytokine; with adenovirus mediated gene transfer) in the PVN mimicked the anti-hypertensive effects of minocycline (blockade of microglial activation) (Shi et al., 2010a). In addition, a physical CNS injury, such as ischemic stroke, induced reduced microglial activation in SHR than WKY (De Geyter et al., 2012). Therefore, based on these studies, it was proposed that impairment of neuro-inflammation (vascular inflammation or microglia) related molecules might contribute to the pathophysiology of neurogenic hypertension.

Data in Chapter 3 show that microglia are ubiquitously distributed throughout the central autonomic regions of the brain that control the SNS in WKY and SHR, but their number varies with the tyrosine hydroxylase-immunoreactive (TH-ir) neuronal number (Kapoor et al., 2016a). Further to this, data in Chapter 3 also suggest that there are no basal differences in the number of microglia, or microglial morphology, between WKY and SHR (Kapoor et al., 2016a). It may be the microglial response to a homeostatic disturbance, which is different in SHR (compared to its normotensive phenotype) contributing to its hypertensive phenotype. Thus, the aim of this study was to identify if the microglial response to altered BP levels (homeostatic challenge) differs between SHR and WKY. This study was conducted at 2 different time points, based on the previous study (Chapter 4), 2 and 6 hours (h) (Kapoor et al., 2016b). Major findings from this study, in accordance with the previous work (Chapter 4 (Kapoor et al., 2016b)), are that, first, microglia in the ventrolateral medulla (VLM) of WKY and SHR are capable of sensing changes in their local environment evoked by alterations in BP. This microglial response, in the CVLM and the RVLM of WKY and SHR, is manifested as a change in their spatial distribution and the percentage of colocalisation with synapsin. Secondly, microglial response in the RVLM of SHR is different, regardless of the provided stimulus (acute hyper-, or hypo-, tension), when compared with the microglial response in the RVLM of WKY.

5.3 Experimental procedures

5.3.1 Animals

Experiments were conducted in 36 adult male rats from 2 different strains (WKY and SHR; n=18 each strain (300-400 g; Animal resource centre, Perth, Australia)) in accordance with the Australian code of practice for the care and use of animals for scientific purposes. All procedures and protocols performed were approved by the Sydney Local Health District Animal Welfare Committee and the Macquarie University Animal Care and Ethics Committee, Sydney, Australia.

5.3.2 Tail-cuff phenotyping

The hypertensive and normotensive phenotype of SHR and WKY, respectively, was determined by tail-cuff sphygmomanometry (non-invasive) at >18 weeks age, prior to using animals for further experiments. Detailed method for tail-cuff sphygmomanometry is included in section 2.1.3 (Farnham et al., 2012). Hypertension was defined as a systolic BP of >180 mmHg and normotension was defined as a systolic BP of <150 mmHg (Figure 5.1).

5.3.3 Experimental protocol

5.3.3.1 Induction of acute hyper-, or hypo-, tension

Experimental design included induction of acute hyper-, or hypo-, tension in WKY and SHR at 2 different time points, 2 and 6 h. 3 treatment groups (phenylephrine induced hypertension, saline served as control and hydralazine induced hypotension) were included in the study at each time point (2 and 6 h) and in each strain (WKY and SHR). 3 repeats for each time point, each treatment group in each strain, were conducted. 3 treatment groups (phenylephrine, saline and hydralazine) *2 time points (2 and 6 h) *3 repeats each = 18 animals per strain (2 strains, WKY and SHR).

Experimental protocol was followed as described previously (Kapoor et al., 2016b). In brief, animals were anaesthetised with sodium pentobarbital (50 mg/kg, i.p.; Cenvet Australia) mixed with atropine sulphate (to reduce bronchial secretions, 0.2 ml/ kg). The external jugular vein, the carotid artery and the femoral vein were cannulated to administer additional anaesthetic, measurement of AP and administration of BP modulating drugs, respectively. The depth of anaesthesia was monitored by observing reflex responses to nociceptive and tactile stimuli

(periodic tail/paw pinches), pupillary responses to light stimuli and corneal touch reflex (involuntary blink). Additional anaesthetic (i.v.) – sodium pentobarbital (1.5-2 mg) – was administered to eliminate the withdrawal response to nociceptive or tactile stimuli, or involuntary blink to corneal touch reflex. Temperature for all animals was maintained continuously, for the protocol period, between 36.5 °C and 37.5 °C using a rectal probe connected to a homeothermic heating blanket. The air flowing to animals was supplemented with 100% oxygen (at a rate of 0.5-1.0 l/min; please refer to section 2.1.4.1 for details).

A continuous infusion of phenylephrine, at a dose of 10 µg/kg/ml, was maintained intravenously to induce acute hypertension, i.e. to increase BP by at least 40 mmHg (Graham et al., 1995). The infusion rate of phenylephrine was adjusted, when required, by at least 0.002 ml/ min (at the dose of 60 µg/ml) to maintain elevated levels of BP (please refer to section 2.1.6.1 for details) (Graham et al., 1995). A bolus injection of hydralazine, at a dose of 10 mg/kg, was administered intravenously to lower BP by at least 40 mmHg and induce acute hypotension (Springell et al., 2005). Both animal groups, belonging to the saline control group and hydralazine induced hypotension group, received a continuous infusion of saline at a dose of 10 µg/kg/ml, to match the volume of saline infused in the phenylephrine treatment group. The concentration of drugs was adjusted to limit the maximum volume infused to 10 ml, over the whole protocol period, to avoid induction of hypervolemia.

5.3.3.2 Perfusion and tissue processing

At the conclusion of the infusion protocol, animals were deeply anaesthetized with sodium pentobarbital (>72 mg/kg i.v.; Cenvet Australia), and were perfused transcardially with ≈400 ml of ice cold 0.1 M phosphate buffered saline (PBS), followed by fixation with ≈400 ml of ice cold 4% paraformaldehyde in 0.1 M PBS (pH 7.4). Extracted brainstem tissue was fixed overnight in 4% paraformaldehyde in 0.1 M PBS (pH 7.4) at 4 °C, while shaking continuously. Brainstems were then sectioned transversely, using a vibrating microtome (VT1200S, Leica), at 40 µm and collected sequentially into 5 pots. These sections were stored in cryoprotectant solution (30% RNase free sucrose, 30% ethylene glycol, 2% polyvinylpyrrolidone in 0.1 M PBS) at -20 °C until processed for immunohistochemistry.

5.3.3.3 Immunohistochemistry

Immunohistochemistry was conducted as described previously in section 2.2.2 and 2.2.3 (Kapoor et al., 2016a; Kapoor et al., 2016b). Briefly, free floating 40 µm brainstem sections were washed in 0.1 M PBS with 0.3% Triton X-100, 3 times for 30 min each, at room

temperature. After washing, sections were incubated for >48 h in TTPBSm (10 mM Tris-HCl, 0.1 M PBS, 0.9% NaCl, 0.3% Triton X-100 and 0.1% merthiolate at pH 7.4), 10% normal donkey serum with primary antibodies (Appendix 1) at 4 °C while shaking. Sections were then washed 3 times for 30 min each in TPBS (10 mM Tris-HCl, 0.1 M PBS and 0.9% NaCl at pH 7.4) and incubated overnight with secondary antibodies (Appendix 1) in TPBSm (10 mM Tris-HCl, 0.1 M PBS, 0.9% NaCl and 0.1% merthiolate at pH 7.4) with 2% normal donkey serum at room temperature, while shaking. Sections were then washed in TPBS 3 times, for 30 min each, at room temperature while shaking. These sections were then mounted, caudal to rostral, on glass slides (Thermo Fisher Scientific), cover-slipped with Vectashield (H-1000, Vector Laboratories) and sealed with clear nail polish for imaging.

5.3.4 Image acquisition

Brainstem sections were imaged using a slide-scanning Axio Scan.Z1 microscope (ZEISS, Germany), at 20X or 40X magnification (depending on the target molecule), for subsequent analysis. Axio Imager Z2 (ZEISS, Germany) was used to acquire images, at 63X magnification with oil-immersion lens, concerning Iba1 labelled microglia and synapsin labelled synaptic structures. Each fluorophore was imaged individually with appropriate filter cubes (section 2.3.2).

LSM 510 Meta spectral confocal microscope (ZEISS, Germany) was used to acquire images to demonstrate a close morphological relationship between microglia and cardiovascular neurons.

A rat brain atlas (Paxinos and Watson, 2007) was used to define the anatomical location of the neuronal population (the CVLM and the RVLM) analysed in this study, and the sampling of brainstem sections was similar to that in Chapter 4 (Kapoor et al., 2016b). The CVLM was defined as the area located in close apposition with A1 noradrenergic neurons (TH-ir) of the brainstem, between ≈ 12.8 mm and ≈ 13.6 mm caudal to bregma (Guyenet et al., 2004). The RVLM was defined as the area located medially to the spinal trigeminal tract, lateral to the pyramids, ventral to the nucleus ambiguus, populated with TH-ir neurons and spans rostro-caudally from ≈ 12.00 mm to ≈ 12.8 mm caudal to bregma (Guyenet et al., 2004). 4 consecutive brainstem sections, separated by 200 μ m, were chosen for each nuclei (the CVLM and the RVLM) between the defined bregma levels and were imaged.

5.3.5 Image analysis

Microglial analysis was split into 4 categories: microglial spatial distribution (number of microglia and inter-microglial distance), microglial contact with synapses, morphology and polarisation into either M1 or M2.

5.3.5.1 *Fos-immunoreactivity (Fos-ir) and microglial spatial distribution*

Bilateral ‘Z-stack’ images from 4 consecutive sections for each VLM nuclei, the CVLM and the RVLM, at 40X magnification were obtained, covering an area of 400 μm X 400 μm , 30 μm in depth, at an interval of 0.62 μm , generating a stack of ≈ 46 Z slices, from each animal in each strain. Maximum intensity projections (MIP) of acquired ‘Z-slices’ were adjusted for brightness and contrast to highlight morphological characteristics of microglia. These MIP images, at 40X magnification, were used to quantify the overall number of Fos-ir neurons and microglia, and microglial spatial distribution (as previously described in section 2.4.3 and 4.3.5.1; Figure 5.8I) (Kapoor et al., 2016b). The number of Fos-ir neurons and microglia were counted in acquired images; objects present at the boundary were excluded from final counts.

5.3.5.2 *Microglial contact with synapses*

Bilateral ‘Z-stack’ images of the CVLM (at ≈ 13.08 mm caudal to bregma) and the RVLM (at ≈ 12.24 mm caudal to bregma) were obtained, at 63X magnification, covering an area of 400 μm X 300 μm , 30 μm in depth, at an interval of 0.5 μm , generating a stack of ≈ 60 Z slices, for each animal in each strain. 10 microglia from each side, for the CVLM and the RVLM, were chosen, and microglial (Iba1) and synapsin images were imported into Image J (NIH, USA), in pairs, as 8-bit images. All images were thresholded at the same intensity to maintain consistency in the analysis. The Image J plugin, ‘Colocalisation finder’, was then used to identify the % of area colocalising between each microglial (Iba1) and corresponding synapsin image (refer to section 2.4.3 for details).

5.3.5.3 *Microglial morphology*

MIP of bilateral ‘Z-stack’ images previously acquired at 40X magnification (for quantification of microglial spatial distribution) were processed for quantification of microglial morphological characteristics. Microglial morphology was quantified as described by Morrison and Filosa (Morrison and Filosa, 2013) (refer to section 4.3.5.1 and Figure 5.11A (Kapoor et al., 2016b)). Briefly, MIP images acquired at 40X magnification were imported into Image J as 8-bit images and ‘skeletonised’. The ‘skeletonised’ image was analysed using the ‘AnalyzeSkeleton’ Image J plugin (Plugin 2) to quantify the number of end points and branch length (μm), which when

normalised to the number of microglia in that specific frame, provides an indication of the microglial morphology. % of area occupied by microglia was quantified with the “measure” feature in Image J software (Plugin 4).

Microglial morphological characteristics (number of end point processes/microglia and branch length (μm)/microglia) were also quantified for MIP images obtained at 63X magnification (Plugin 3).

5.3.5.4 M1 and M2 phenotype quantification

As seen in Chapter 4 (Kapoor et al., 2016b), none or very few M1 positive microglia (colocalisation of CD16 expression with Iba1) were seen in the CVLM (Figure 5.12) and the RVLM (Figure 5.12), regardless of the treatment group or time point or strain. Thus, expressions levels of M1 phenotype was not quantified.

Bilateral ‘Z-stack’ images were obtained, at 20X magnification, covering an area of 900 μm X 600 μm , 40 μm in depth, at an interval of 1.39 μm , generating a stack of ≈ 29 slices. MIP images were adjusted for brightness to highlight the microglial morphology (labelled with Iba1). CD206 was used to label activated microglia with M2 phenotype. Total number of microglia (Iba1-ir) were quantified with Image J (Plugin 1). Only the CD206⁺ microglia where the CD206 expression colocalised with Iba1 expression were counted as M2 microglia (Figure 5.13). % of M2⁺ microglia was calculated from the number of CD206⁺ microglia and the total number of microglia (Iba1) in a region of interest.

5.3.6 Data analysis and statistics

GraphPad Prism version 6.05 was used to perform all the statistical tests. Numbers of Fos-ir neurons and microglia were treated as non-parametric non-continuous data, and data were pooled from 3 repeats for each strain for each treatment group at each time point, for each brainstem nuclei (Kapoor et al., 2016b). The number of Fos-ir neurons and microglia were analysed using the Chi-square test for goodness-of-fit (Kapoor et al., 2016a; Kapoor et al., 2016b; Sokal and Rohlf, 2012). Parameters obtained highlighting microglial morphology, % of CD206⁺ microglia and % of colocalisation between microglia (Iba1) and synapses (synapsin) were treated as non-parametric continuous data, and were averaged across repeats and analysed using a Kruskal-Wallis one-way analysis of variance. Area under curve (AUC) values for MAP were normalised to baseline values (section 2.4.2) and were analysed using one-way ANOVA

with Dunnett's multiple comparison tests. Systolic and mean BP values obtained from tail-cuff phenotyping of rats were analysed using Student's t-test (unpaired).

5.4 Results

5.4.1 Tail-cuff phenotyping of WKY and SHR

The systolic BP for, conscious and restrained, WKY (>18 weeks of age) was 140.3 ± 2.19 mmHg (Figure 5.1). On the other hand, higher values for systolic BP (198.1 ± 3.2 mmHg) for SHR (>18 weeks of age) were recorded (Figure 5.1). At this stage, the normotensive and hypertensive phenotype of WKY and SHR, respectively, was confirmed before proceeding to the experimental protocol.

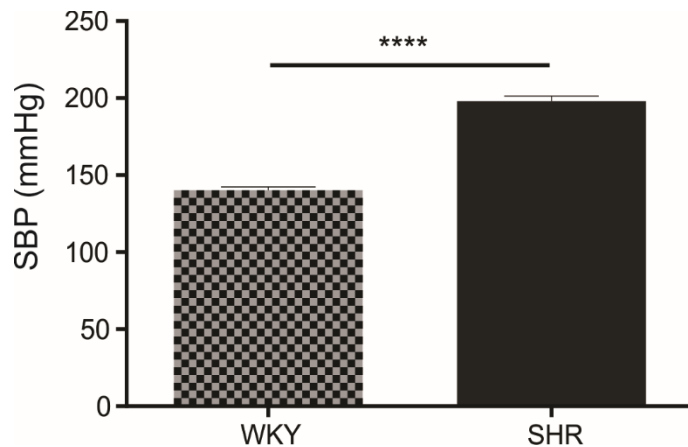


Figure 5.1: Tail-cuff phenotyping of WKY and SHR

Systolic blood pressure (SBP) values were recorded for WKY and SHR via tail-cuff sphygmomanometry. WKY had a SBP of 140.3±2.19 mmHg and SHR had a SBP of 198.1±3.2 mmHg.

Hypertension was defined as a SBP of >180 mmHg and normotension was defined as a SBP of <150 mmHg. Therefore, WKY and SHR used in this study were normotensive and hypertensive, respectively. Data are expressed as mean ±SEM. Statistical significance was determined by a Student's T-test. * $p \leq 0.05$, ** $p \leq 0.01$, *** $p \leq 0.001$ and **** $p \leq 0.0001$.

5.4.2 Induction of acute hyper-, or hypo-, tension in WKY and SHR

Mean arterial pressure (MAP) for WKY following continuous intravenous infusion of phenylephrine (10 $\mu\text{g/kg/min}$) rose rapidly by at least 40 mmHg (Figure 5.2A shows a representative BP trace). Continuous intravenous infusion of phenylephrine, at a dose of 10 $\mu\text{g/kg/min}$, maintained additional hypertension in SHR (Figure 5.2B shows a representative BP trace). However, over time, MAP raised by phenylephrine had a tendency to return to baseline values, regardless of the strain. As mentioned previously, and seen in Chapter 4, prolonged periods of phenylephrine infusion leads to desensitization of α_1 -adrenoreceptors in periphery (Kapoor et al., 2016b; Minami et al., 1997). MAP values for animals infused with saline, serving as control group, did not change significantly over time for either WKY or SHR (Figure 5.2C and D).

Within a min of hydralazine administration (10 mg/kg), MAP for WKY (Figure 5.2 E shows a representative BP trace) and for SHR (Figure 5.2 F shows a representative BP trace) fell by at least 40 mmHg, inducing acute hypotension in both strains of rat. The hypotensive effect of one bolus intravenous injection of hydralazine (10 mg/kg) was sustained until the end of the protocol in both WKY and SHR at both time points, 2 and 6 h.

Comparison of AUC values for MAP for WKY and SHR showed that significant differences were induced in baseline levels of BP, when treated with either phenylephrine or hydralazine, for the whole protocol period, 2 h (Figure 5.3A) and 6 h (Figure 5.3B).

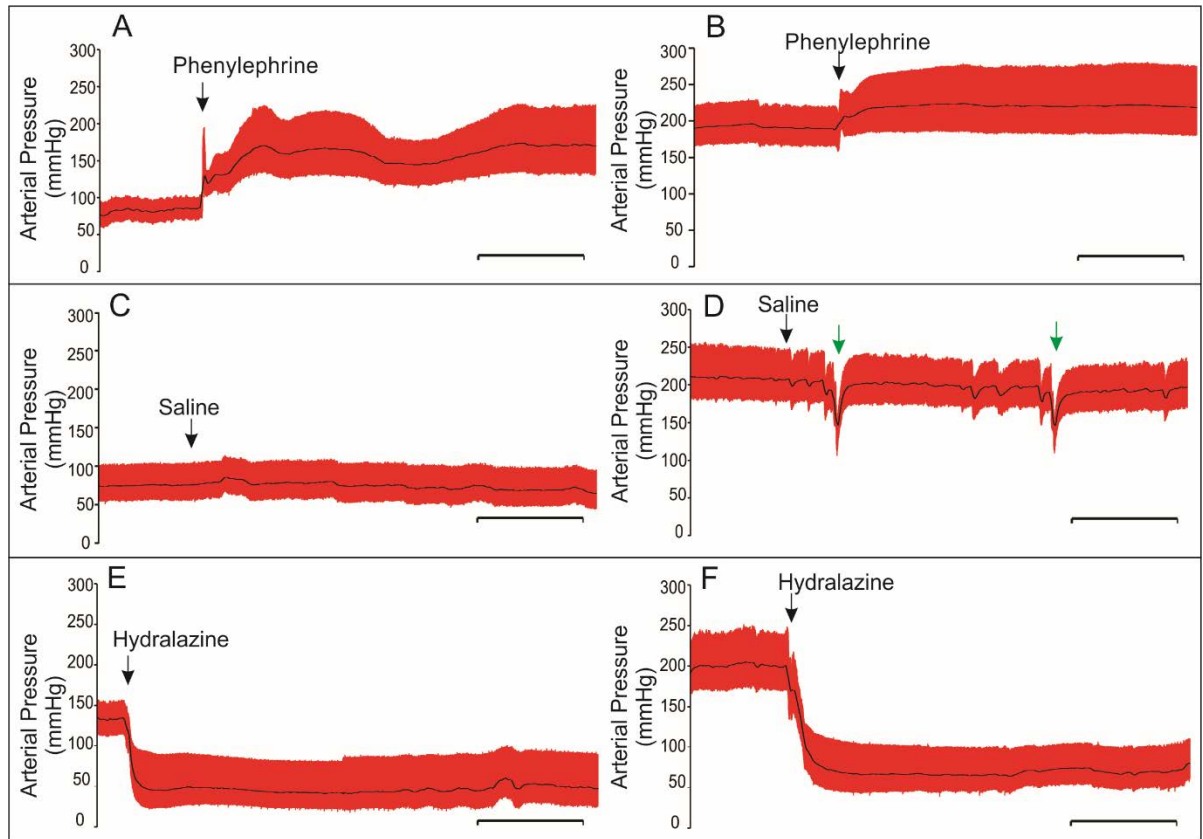


Figure 5.2: Effect of intravenous infusion of phenylephrine, saline or hydralazine on AP, in WKY and SHR

Continuous intravenous infusion of phenylephrine at a dose of 10 $\mu\text{g/kg/min}$, in A. WKY and B. SHR, induced acute hypertension. Continuous intravenous infusion of saline (at the rate of 10 $\mu\text{g/kg/min}$) served as a control group in WKY (C) and SHR (D). A bolus intravenous injection of hydralazine (10 mg/kg), followed by a continuous intravenous infusion of saline (at the rate of $\mu\text{g/kg/min}$), in E. WKY and F. SHR, induced acute hypotension. Black arrows show the start of treatment and green arrows show the reflex response to a nociceptive stimulus to check the depth of anaesthesia. Scale bar = 10 min.

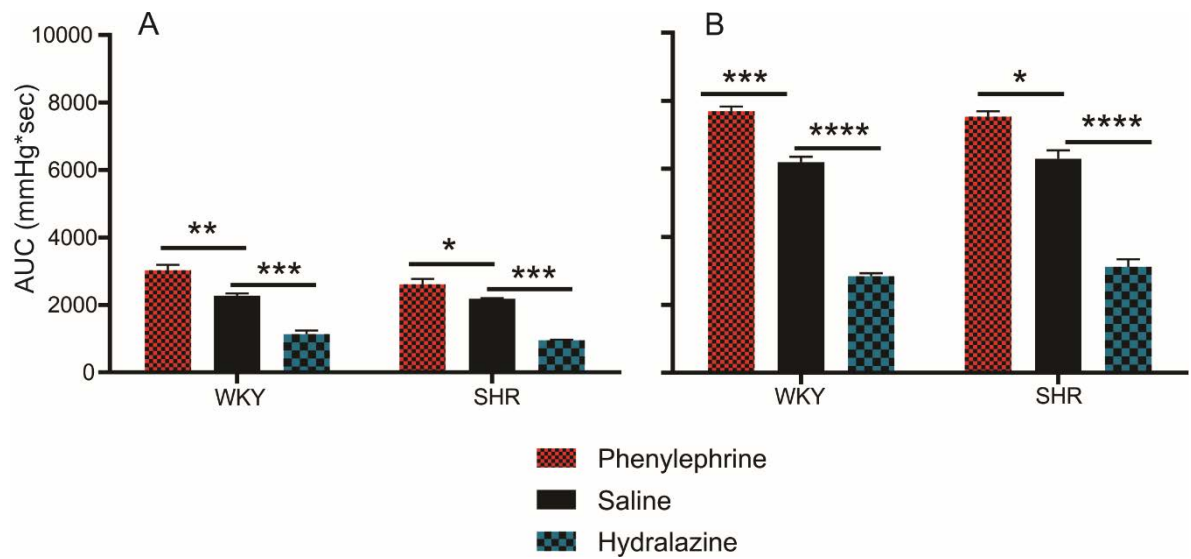


Figure 5.3: Effects of intravenous infusion of phenylephrine, saline or hydralazine on MAP, of WKY and SHR, for 2 time points, 2 and 6 h

Effect of intravenous administration of phenylephrine, saline or hydralazine on the area under curve (AUC) for mean arterial pressure (MAP) for the whole protocol period, where the stimulus was maintained continuously for either 2 h (A) or 6 h (B) in 2 separate group of rats (n=3 each treatment). Data are expressed as mean \pm SEM. Statistical significance was determined by one-way ANOVA with Dunnett's multiple comparison tests. * $p \leq 0.05$, ** $p \leq 0.01$, *** $p \leq 0.001$ and **** $p \leq 0.0001$.

5.4.3 Fos-ir increases in the RVLM in response to hypotension

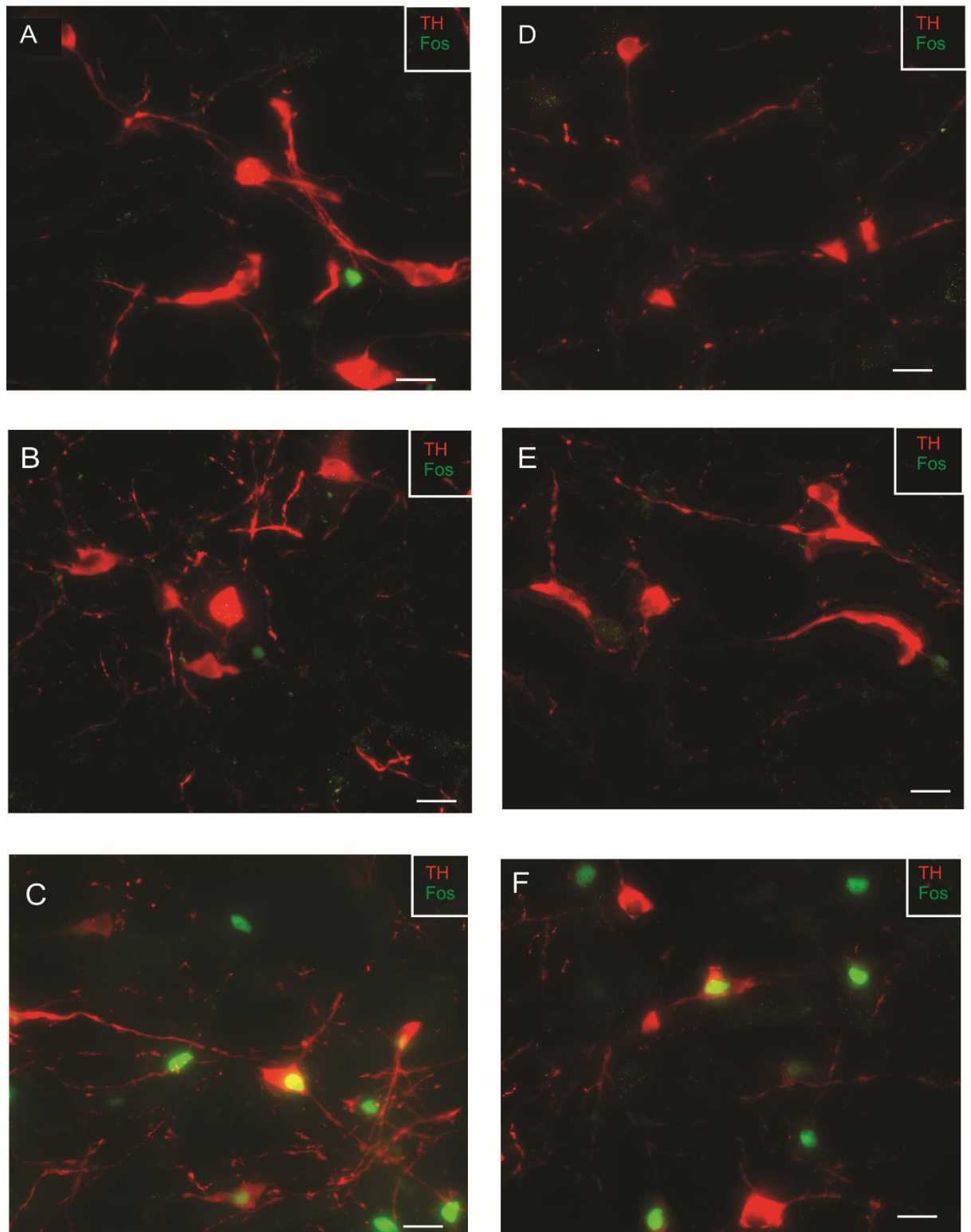
As previously done in Chapter 4, Fos-ir levels for WKY and SHR at both, 2 and 6 h, time points were only quantified in the RVLM to validate the effect of stimuli (phenylephrine induced hypertension or hydralazine induced hypotension) on neuronal activity. Overall, higher levels of Fos-ir were seen in the RVLM in response to hydralazine induced acute hypotension, in both strains of rats, WKY (Figure 5.4C) and SHR (Figure 5.4F).

At the 2 h time point, Fos-ir drastically increased in the RVLM of both, WKY (by 120%, increased from 93 to 205; $p \leq 0.0001$) and SHR (by 221%, increased from 75 to 241; $p \leq 0.0001$), when treated with hydralazine (inducing acute hypotension) (Figure 5.5A). No significant differences were observed in Fos-ir levels in the RVLM of WKY when subjected to phenylephrine induced hypertension for 2 h (Figure 5.5A). However, Fos-ir in the RVLM of SHR increased by 53% (increased from 75 to 115; $p \leq 0.01$), when treated with phenylephrine for 2 h (Figure 5.5A). Fos-ir in the RVLM of both, WKY (lower by 107; $p \leq 0.0001$) and SHR (lower by 126; $p \leq 0.0001$), was lower in the animal group treated with phenylephrine than the group treated with hydralazine, at the 2 h time point (Figure 5.5A).

Similar to the 2 h time point, maintenance of hypotension (induced by hydralazine) for 6 h induced enhanced levels of Fos-ir in the RVLM of both, WKY (by 308%, increased from 69 to 282; $p \leq 0.0001$) and SHR (by 194%, increased from 71 to 209; $p \leq 0.0001$) (Figure 5.5B). Despite the continuous infusion of phenylephrine for 6 h, Fos-ir in the RVLM of WKY increased by 191%, when compared with saline (increased from 69 to 201; $p \leq 0.0001$) (Figure 5.5B). However, Fos-ir levels were higher in the RVLM of WKY when treated with hydralazine than phenylephrine (higher by 81; $p \leq 0.001$) (Figure 5.5B). No significant differences were observed in Fos-ir levels in the RVLM of SHR, when subjected to phenylephrine induced hypertension for 6 h (Figure 5.5B)

Figure 5.4: Fos-ir levels in response to intravenous infusion of phenylephrine, saline or hydralazine in the RVLM of WKY and SHR

Induction of acute hypertension via continuous infusion of phenylephrine reduced Fos-ir expression levels in both WKY (A) and SHR (D). Minimal Fos-ir was observed following continuous infusion of saline in WKY (B) and SHR (E). On the other hand, a bolus injection of hydralazine significantly increased expression levels of Fos-ir in the RVLM of WKY (C) and SHR (F). TH expressing C1 neurons of the RVLM are in red and Fos-ir neurons are in green. Scale bar = 20 μ m. (Brightness and contrast of images was intentionally adjusted for better visualization of TH neuronal dendrites and Fos-ir nuclei)



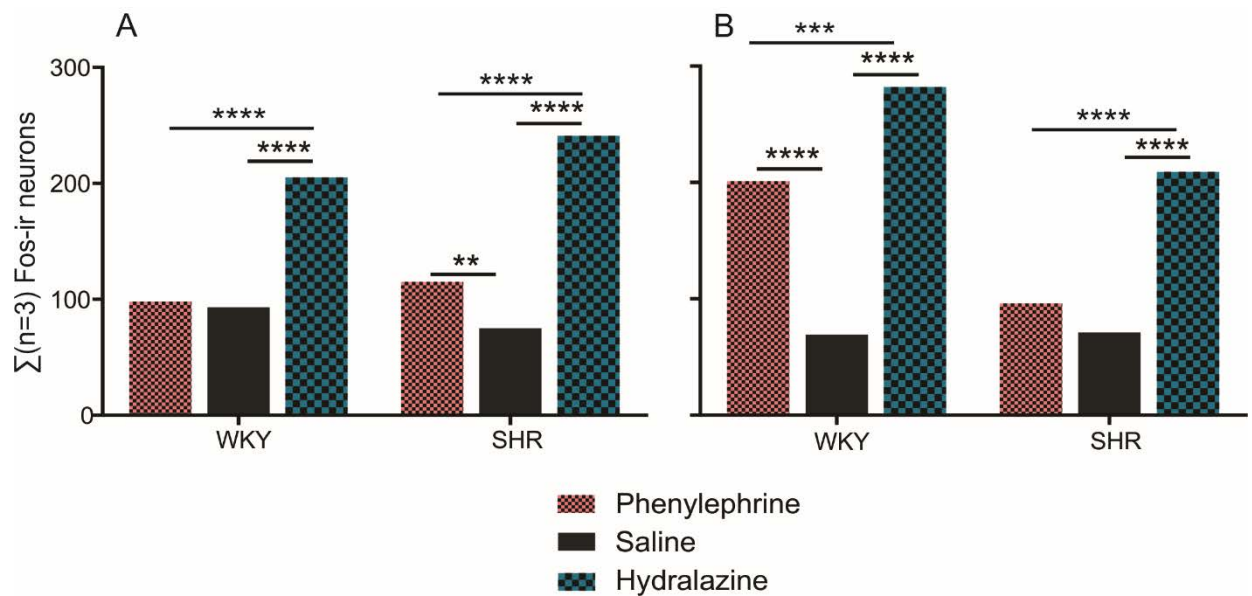


Figure 5.5: Quantification of Fos-ir levels in the RVLM, of WKY and SHR, when subjected to intravenous infusion of phenylephrine, saline or hydralazine, for 2 and 6 h

Fos-ir expression levels were significantly higher in the RVLM of both WKY and SHR, when subjected to hydralazine induced hypotension, for 2 h (A) and 6 h (B). See section 5.4.3 for details. All statistical comparisons were made between treatment groups (phenylephrine or hydralazine) and the saline group, at the particular time point; no comparisons were made across time points. Data are pooled from 3 animals, in each treatment group, at each time point, for each strain. Statistical significance was determined by the Chi-square test for goodness of fit. * $p \leq 0.05$, ** $p \leq 0.01$, *** $p \leq 0.001$ and **** $p \leq 0.0001$

5.4.4 Microglial-neuronal relationship

Microglia (Iba1) are ubiquitously distributed in the CVLM (Figure 5.6A and B) and the RVLM (Figure 5.6C and D) of both strains of rats, WKY and SHR. In some cases, microglial processes were closely apposed to TH neuronal dendrites in the RVLM of both WKY (Figure 5.6E) and SHR (Figure 5.6F). In line with the observations of Chapter 4 (Kapoor et al., 2016b), a microglial process seemed to penetrate through a TH neuronal cell body (Figure 5.6G). Multiple microglial cell bodies were seen to be in close proximity to each other (Figure 5.6H and Movie 5.1); this suggests that within a brain nucleus, microglial distribution is not homogenous, and the inter-microglial distance (IMD) is highly dynamic.

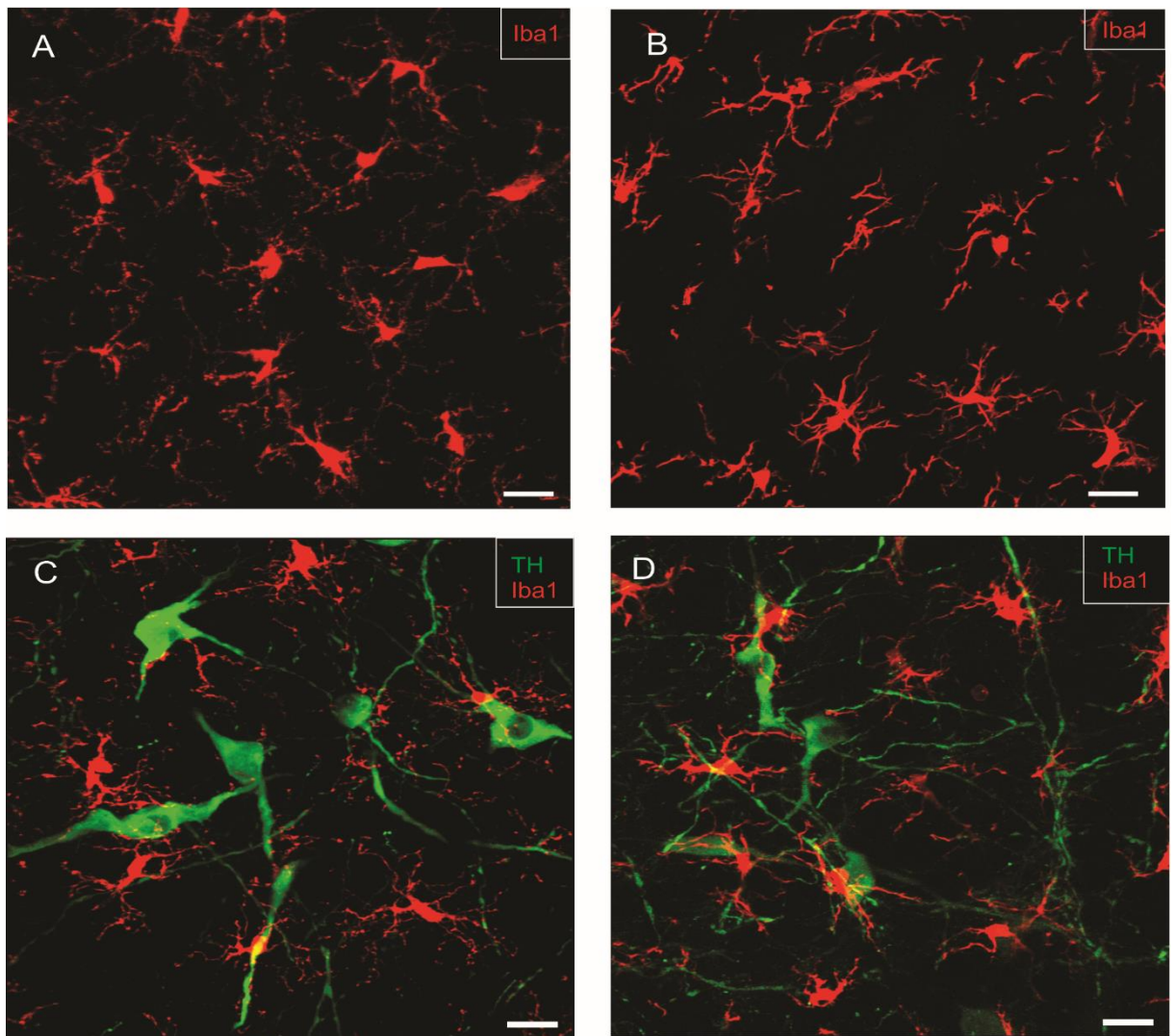


Figure 5.6: Morphological relationship between microglia and cardiovascular neurons in the CVLM and the RVLM of WKY and SHR

Microglia (Iba1, red) are ubiquitously distributed throughout the CVLM of WKY (A) and SHR (B), and the RVLM of WKY (C) and SHR (D). TH expressing C1 neurons of the RVLM are in green. Scale bar = 20 μ m. (P.T.O. for rest of the Figure 5.6)

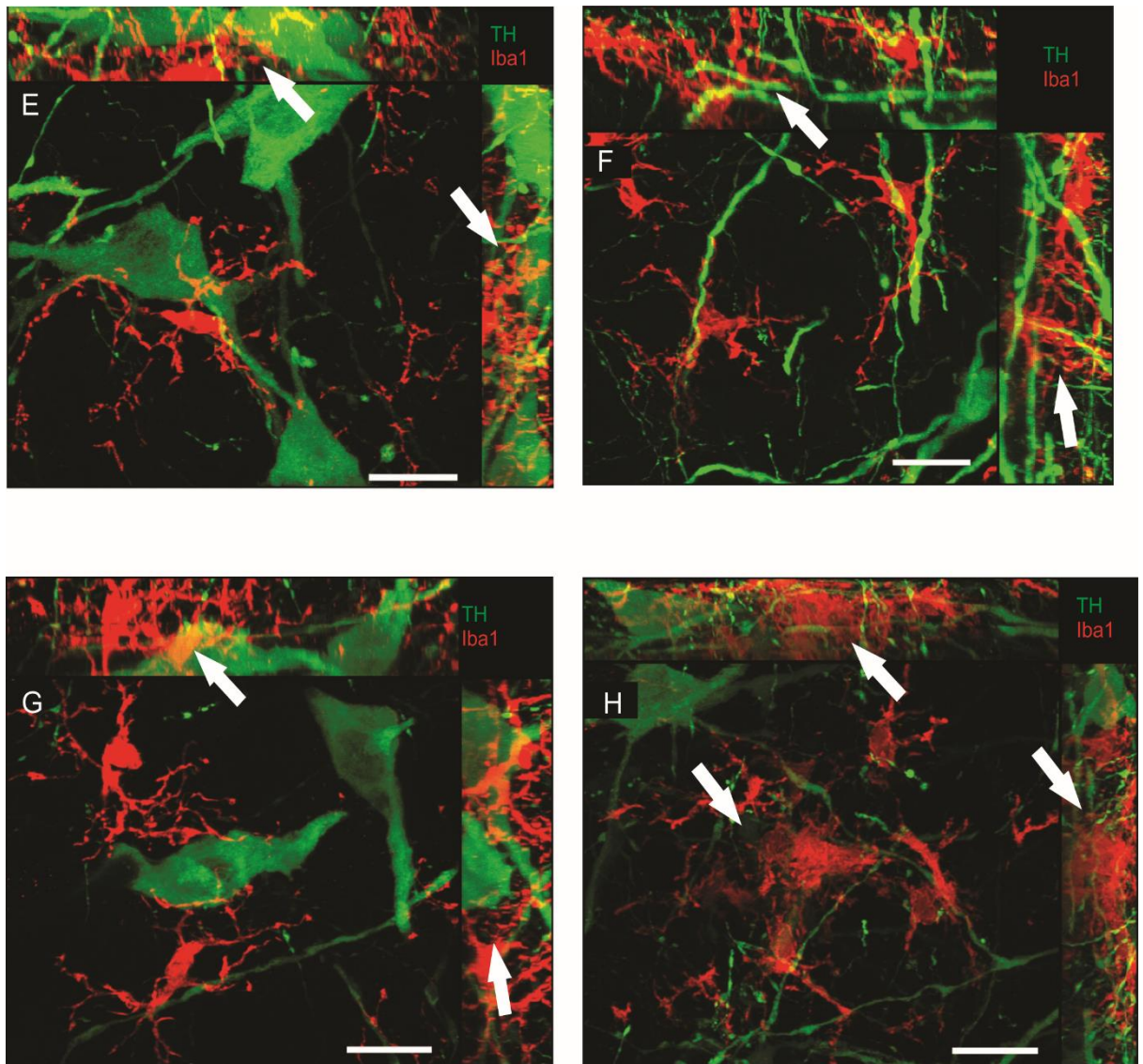


Figure 5.6: Morphological relationship between microglia and cardiovascular neurons in the CVLM and the RVLM of WKY and SHR

Microglial processes (Iba1, red) are in close contact with TH neuronal dendrites in the RVLM (white arrows in orthogonal projections) of WKY (E) and SHR (F). G. A microglial process in the RVLM of WKY seem to penetrate through a TH neuronal cell body (white arrows in orthogonal projections). H. Multiple microglial cell bodies in the RVLM of SHR are in close proximity to each other showing that IMD is variable within a brain nucleus (white arrows in the image and in orthogonal projections). Also, see Movie 5.1. TH expressing C1 neurons of the RVLM are in green. Scale bar = 20 μm .

5.4.5 Microglia change their pattern of distribution in response to disturbances introduced in BP

5.4.5.1 Number of microglia

No significant changes in the overall number of microglia were observed at any one of the two time points (2 and 6 h), regardless of the brainstem area (CVLM/RVLM), in WKY rats when treated with either phenylephrine or hydralazine (Figure 5.7).

- *CVLM*

Significant changes in the number of microglia were only observed following the induction of hypotension (hydralazine) in the CVLM of SHR. The number of microglia increased by $\approx 10\%$ (from 728 to 807; $p \leq 0.05$) in the CVLM of SHR when subjected to hypotension for 2 h (Figure 5.7A). Following 6 h of hydralazine induced hypotension, the number of microglia in the CVLM of SHR decreased by $\approx 13\%$ (from 850 to 739; $p \leq 0.05$) (Figure 5.7B).

- *RVLM*

No significant changes in the number of microglia were observed in the RVLM of SHR following 2 h of hypotension (Figure 5.7C). However, following 6 h of hypotension, the number of microglia in the RVLM of SHR decreased by 11% (from 935 to 829; $p \leq 0.05$) (Figure 5.7D).

5.4.5.2 Spatial distribution

- *CVLM*

- WKY

No changes in the microglial pattern of distribution were observed in the CVLM of WKY in response to intravenous infusion of phenylephrine, at either 2 h (Figure 5.8A) or 6 h (Figure 5.8C). Following hydralazine induced hypotension, the number of microglia with an IMD of $\approx 33 \mu\text{m}$ increased from 134 to 182 ($p \leq 0.01$, Figure 5.8A). These changes were not seen at the 6 h time point (Figure 5.8C).

- SHR

With regards to SHR, following the infusion of phenylephrine for 2 h, the number of microglia with an IMD of $\approx 33 \mu\text{m}$ increased from 148 to 195 ($p \leq 0.05$, Figure 5.8B) and with an IMD of $\approx 23 \mu\text{m}$ increased by 56% (from 53 to 83; $p \leq 0.05$, Figure 5.8B); an effect that persisted at the 6 h time point (microglia with an IMD of $\approx 23 \mu\text{m}$ increased from 53 to 80; $p \leq 0.05$, Figure 5.8D). Induction of hypotension (hydralazine) for 2 h caused the number of microglia with an

IMD of $\approx 33 \mu\text{m}$ to increase from 148 to 189 ($p \leq 0.05$, Figure 5.8B); this effect was not seen at the 6 h time point.

- *RVLM*
 - WKY

Consistent with the microglial response seen in the CVLM following phenylephrine infusion in WKY, no changes in the microglial pattern of distribution were observed in the RVLM of WKY (Figure 5.8E and G). On the other hand, hydralazine administration in WKY introduced changes in the microglial spatial distribution, in the RVLM, at the 2 and 6 h time point. The number of microglia with an IMD of $\approx 28 \mu\text{m}$ increased from 73 to 112 ($p \leq 0.01$, Figure 5.8E) following 2 h of hypotension (hydralazine). Following 6 h of hydralazine induced hypotension in WKY, the number of microglia in the RVLM continued to move closer; the number of microglia with an IMD of $\approx 23 \mu\text{m}$ increased from 20 to 39 ($p \leq 0.05$, Figure 5.8G).

- SHR

Induction of acute hypertension (phenylephrine) caused the IMD in the RVLM of SHR to decrease; the number of microglia with an IMD of $\approx 18 \mu\text{m}$ increased from 14 to 39 ($p \leq 0.001$, Figure 5.8F), and the number with an IMD of $\approx 23 \mu\text{m}$ increased from 39 to 68 ($p \leq 0.01$, Figure 5.8F). Following infusion of phenylephrine for 6 h in SHR, changes seen in the microglial spatial distribution at the previous time point (2 h) in the RVLM started to return to normal; the number of microglia with an IMD of $\approx 28 \mu\text{m}$ increased from 133 to 179 ($p \leq 0.01$, Figure 5.8H).

At the 2 h time point, following hydralazine treatment in the SHR, the number of microglia with an IMD of $\approx 23 \mu\text{m}$ increased from 39 to 61 ($p \leq 0.05$, Figure 5.8F). Following 6 h of hypotension in SHR, the number of microglia with an IMD of $\approx 18 \mu\text{m}$, $\approx 23 \mu\text{m}$ and $\approx 28 \mu\text{m}$ decreased in the RVLM (Figure 5.8H). The number of microglia with an IMD of $\approx 18 \mu\text{m}$ decreased from 25 to 7 ($p \leq 0.01$), with an IMD of $\approx 23 \mu\text{m}$ decreased from 57 to 37 ($p \leq 0.05$), and with an IMD of $\approx 28 \mu\text{m}$ decreased from 133 to 99 ($p \leq 0.05$, Figure 5.8H).

Changes introduced in the microglial spatial distribution, in WKY and SHR, in response to provided stimuli (phenylephrine induced hypertension and hydralazine induced hypotension) are summarized in a tabular form in Figure 5.8J.

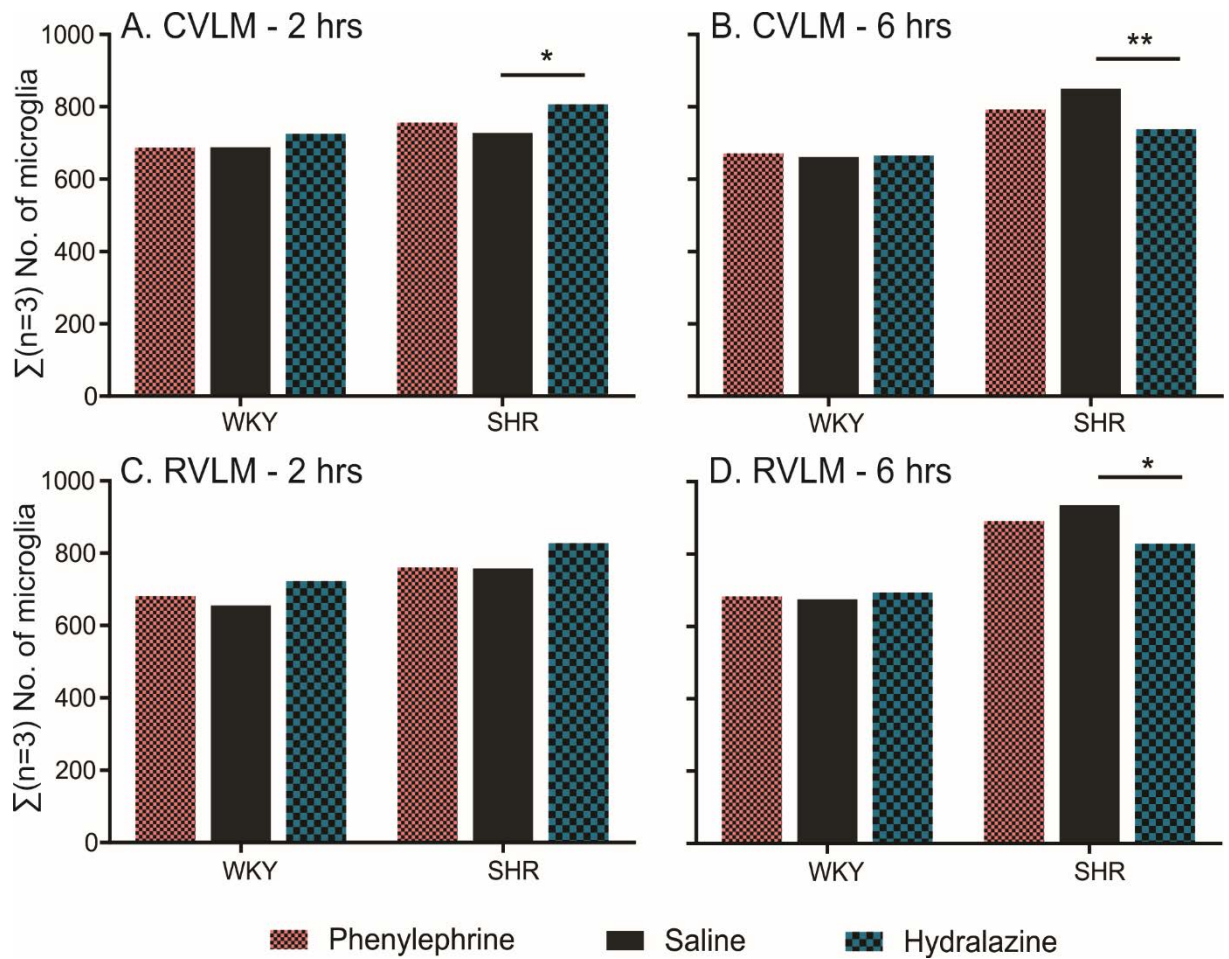
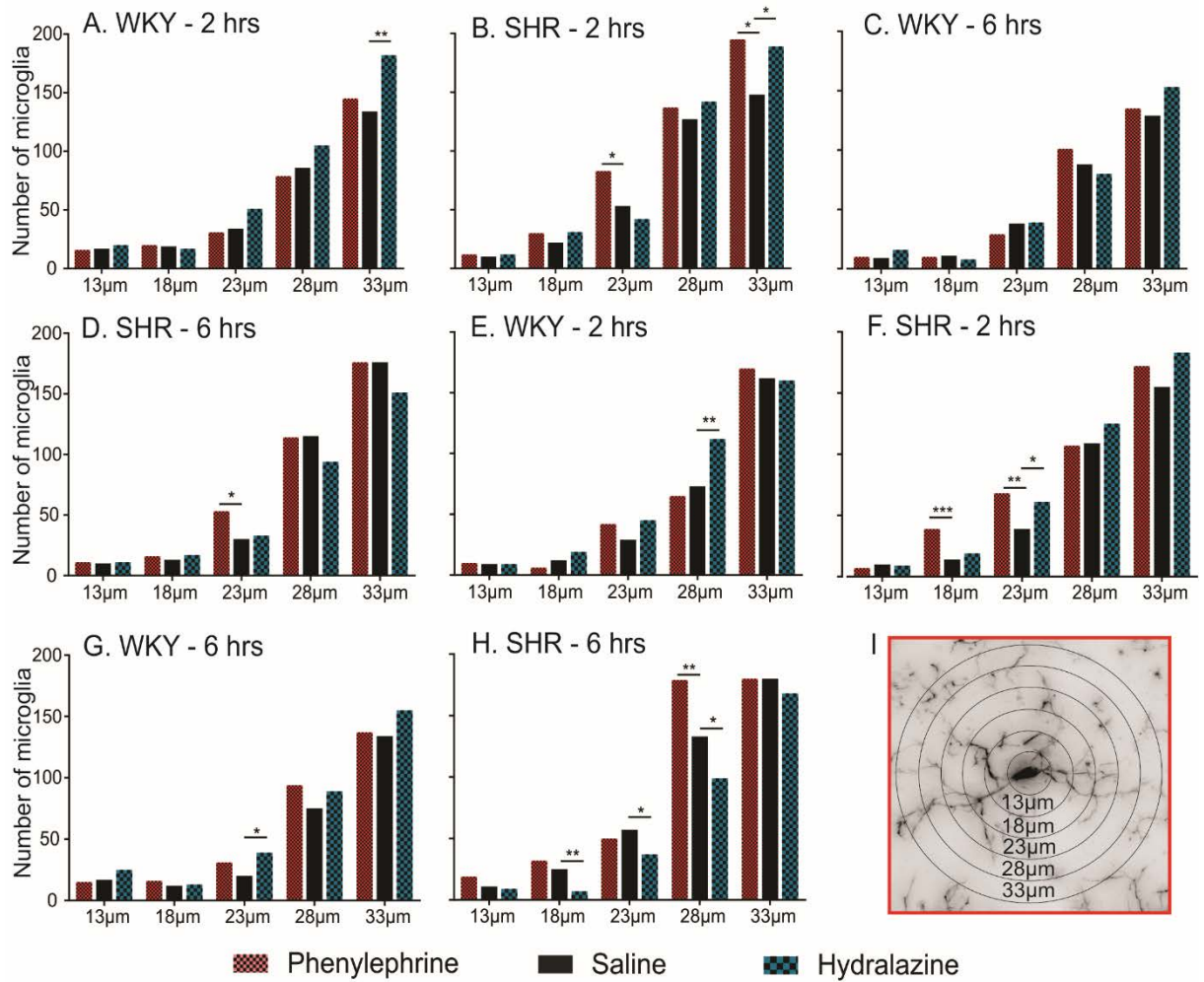


Figure 5.7: Effects of intravenous infusion of phenylephrine, saline or hydralazine on the overall number of microglia

Changes in the overall number of microglia in the CVLM (A and B) and the RVLM (C and D) of WKY and SHR, when subjected to phenylephrine induced acute hypertension, saline served as control or hydralazine induced acute hypotension, for 2 and 6 h. See section 5.4.5.1 for details. All statistical comparisons were made between treatment groups (phenylephrine or hydralazine) and the saline group, at the particular time point; no comparisons were made across time points. Data are pooled from 3 animals, in each treatment group, at each time point, for each strain. Statistical significance was determined by the Chi-square test for goodness of fit. * $p \leq 0.05$, ** $p \leq 0.01$, *** $p \leq 0.001$ and **** $p \leq 0.0001$.

Figure 5.8: Effects of intravenous infusion of phenylephrine, saline or hydralazine on the IMD of microglia

Changes in the spatial distribution of microglia in the CVLM (A-D) and the RVLM (E-H) of WKY and SHR, when subjected to phenylephrine induced hypertension, saline served as control or hydralazine induced hypotension, for 2 and 6 h. I. An example of a microglial image with 6 concentric circles drawn around the cell body to quantify the IMD. J. Summary of data represented in graphs A–H in a tabular form. All statistical comparisons were made between treatment groups (phenylephrine or hydralazine) and the saline group, at the particular time point; no comparisons were made across time points. Data are pooled from 3 animals, in each treatment group, at each time point, for each strain. * $p \leq 0.05$, ** $p \leq 0.01$, *** $p \leq 0.001$ and **** $p \leq 0.0001$.



J		Treatment	Phenylephrine		Hydralazine	
Blood pressure			↑		↓	
Brainstem region			CVLM	RVLM	CVLM	RVLM
Strain	Time point	Changes in inter-microglial distance in response to altered blood pressure				
WKY	2 hrs	—	—	—	Move closer; ≈33μm	Move closer; ≈28μm
	6 hrs	—	—	—	—	Move closer; ≈23μm
SHR	2 hrs	Move closer; ≈23μm and ≈33μm	Move closer; ≈18μm	—	Move closer; ≈33μm	Move closer; ≈23μm
	6 hrs	Move closer; ≈23μm	Starts to return to normal	—	—	Move further apart; ≈28μm

5.4.6 Microglia (Iba1) dynamically change the % of colocalisation with synapses (synapsin) in response to alterations in BP

Microglial cell bodies and end point processes (Iba1) colocalise with synaptic structures (synapsin) in the CVLM and the RVLM of both WKY and SHR (Figure 5.9)

- *CVLM*
 - WKY

Following the induction of hypertension (phenylephrine) in WKY for 2 h, % colocalisation between microglia and synapsin increases by $\approx 66\%$ (from 3 ± 0.3 to 5 ± 0.5 , $p \leq 0.05$; Figure 5.10A). On the contrary, persistence of hypertension in WKY for 6 h causes % of colocalisation between microglia and synapsin to decrease by $\approx 28\%$ (from 4.2 ± 0.37 to 2.9 ± 0.3 , $p \leq 0.05$; Figure 5.10B). Similar to hypertension, induction of hypotension for 2 h in WKY induces an increment of $\approx 42\%$ in the % of co-localisation between microglia and synapsin (from 3.0 ± 0.33 to 4.3 ± 0.39 , $p \leq 0.05$; Figure 5.10A); an effect that returned to normal at the subsequent time point, 6 h (Figure 5.10B).

- SHR

No changes were observed in the % of co-localisation between microglia and synapsin in the CVLM of SHR, when subjected to either hyper-, or hypo-, tension, regardless of the time point (Figure 5.10A and B).

- *RVLM*
 - WKY

Following the induction of hypertension for 2 h, the % of co-localisation decreased by $\approx 55\%$ between microglia and synapsin in the RVLM of WKY (from 3.1 ± 0.3 to 1.45 ± 0.23 , $p \leq 0.0001$; Figure 5.10C); this effect returned to normal at the 6 h time point (Figure 5.10D). No significant changes were observed in the % of colocalisation between microglia and synapsin in the RVLM of WKY, when subjected to hydralazine induced hypotension, at either time point (2 or 6 h; Figure 5.10C and D).

- SHR

Following induction of both, hyper-, and hypo-, tension, in SHR for 2 h, % of colocalisation between microglia and synapsin increased in the RVLM. % of colocalisation between microglia and synapsin in the RVLM of SHR following phenylephrine induced hypertension for 2 h increased by $\approx 133\%$ (from 3.3 ± 0.5 to 7.7 ± 0.7 , $p \leq 0.0001$). Similarly, % of colocalisation

between microglia and synapsin in the RVLM of SHR following hydralazine induced hypotension for 2 h increased by $\approx 72\%$ (from 3.3 ± 0.5 to 5.7 ± 0.54 , $p \leq 0.0001$; Figure 5.10C). However, persistence of the stimulus (either hypertension or hypotension) for 6 h evoked no significant changes in the % of colocalisation between microglia and synapsin (Figure 5.10D).

Data presented in graphs, Figure 5.10A, B, C or D, are summarized in a tabular form in Figure 5.10E.

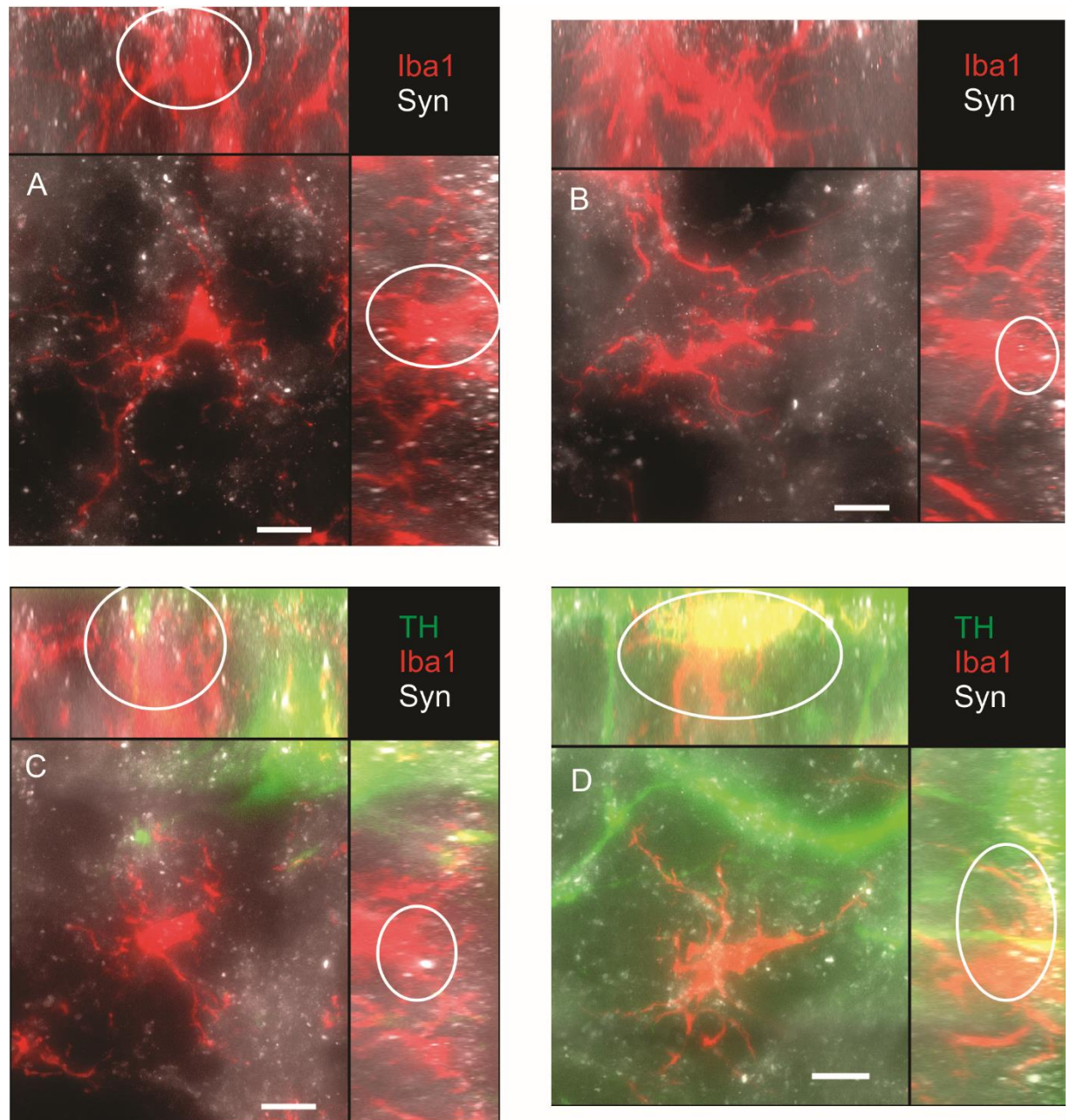
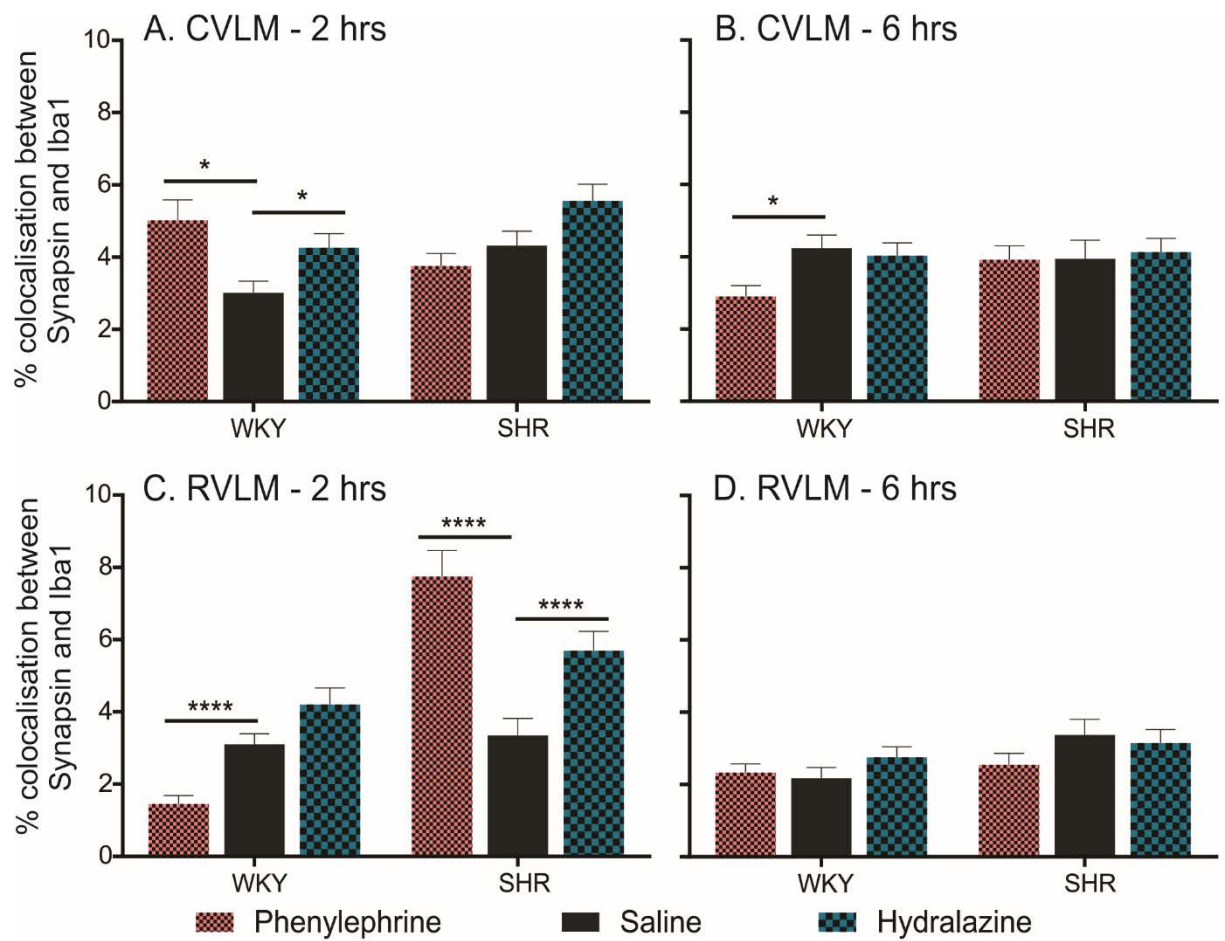


Figure 5.9: Relationship between microglia (Iba1) and synapses (Synapsin) in the CVLM and the RVLM of WKY and SHR

Microglia labelled with Iba1 (red) colocalised with synaptic structures labelled with synapsin (Syn, white). Colocalised pixels are shown in white circles in orthogonal projections. A. CVLM of WKY, B. CVLM of SHR, C. RVLM of WKY and D. RVLM of SHR. TH-ir RVLM neurons are in green. Scale bar = 20 μm .

Figure 5.10: Effects of intravenous infusion of phenylephrine, saline or hydralazine on the % of colocalisation between microglia (Iba1) and synapses (synapsin)

Changes in the % of colocalisation between microglia and synapses in the CVLM (A and B) and the RVLM (C and D) of WKY and SHR, as quantified with ImageJ (see method for details), when subjected to phenylephrine induced hypertension, saline served as control or hydralazine induced hypotension, for 2 and 6 h. E. Summary of data represented in graphs A–D in a tabular form. All statistical comparisons were made between treatment groups (phenylephrine or hydralazine) and the saline group, at the particular time point; no comparisons were made across time points. Data are expressed as mean \pm SEM. Statistical significance was determined by a Kruskal-Wallis one-way analysis of variance. * $p \leq 0.05$, ** $p \leq 0.01$, *** $p \leq 0.001$ and **** $p \leq 0.0001$.



Treatment		Phenylephrine		Hydralazine	
Blood pressure		↑		↓	
Brainstem region		CVLM	RVLM	CVLM	RVLM
Strain	Time point	% colocalisation between microglia (Iba1) and synapses (Synapsin)			
WKY	2 hrs	Increases	Decreases	Increases	—
	6 hrs	Decreases	—	—	—
SHR	2 hrs	—	Increases	—	Increases
	6 hrs	—	—	—	—

5.4.7 Microglia do not change their morphology in response to disturbances introduced in BP levels

Microglial morphological characteristics were analysed at 2 different magnifications, 40X and 63X. 3 different microglial morphological characteristics were analysed at 40X magnification: % of area covered by microglia in a region of interest, number of end point processes/ microglia and branch length (μm)/ microglia. At 40X magnification, regardless of the treatment (phenylephrine/hydralazine) or the strain (WKY/SHR) or the time point (2 or 6 h), no significant changes in microglial morphology were observed in either the CVLM (Figure 5.11B-E) or the RVLM (Figure 5.11 F-I).

Similar results were seen at 63X magnification. 2 different microglial morphological characteristics analysed at 63X magnification were the number of end point processes/ microglia and branch length (μm)/ microglia. No significant changes in the microglial morphology were observed in either of the rat strain (WKY or SHR), regardless of the provided treatment (phenylephrine/hydralazine) or the time point (2 or 6 h), in either the CVLM (Figure 5.11 J-M) or the RVLM (Figure 5.11N-Q).

5.4.8 Microglia do not polarize to either M1 or M2 phenotype in response to disturbances introduced in BP levels

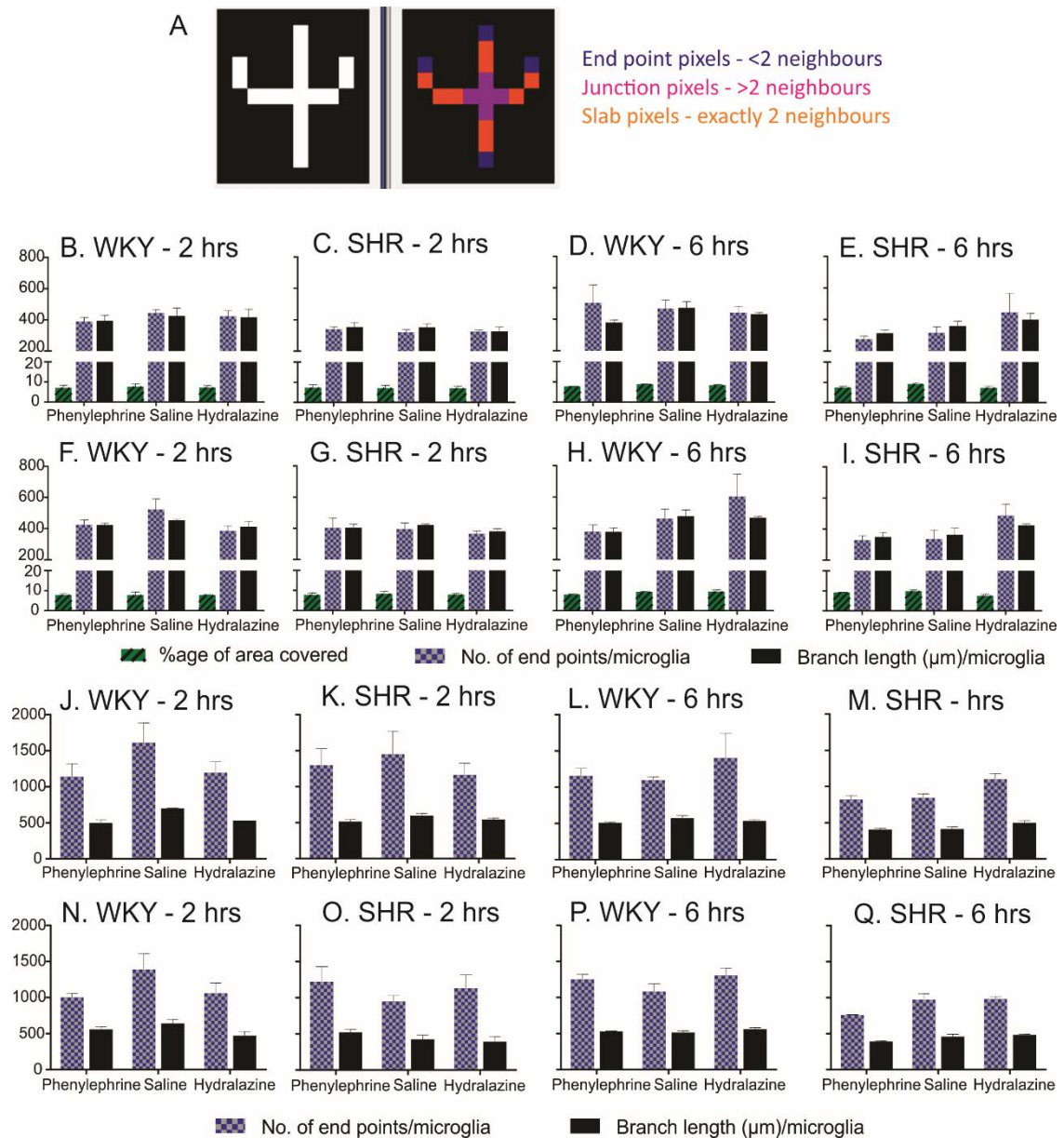
Consistent with findings from Chapter 4 (Kapoor et al., 2016b), disturbances introduced in BP levels did not induce microglial polarization to extreme activated phenotypes, either M1 or M2.

Very little, or almost no, M1 expression was seen following induction of either phenylephrine induced hypertension or hydralazine induced hypotension in WKY and SHR, in either the CVLM (Figure 5.12) or the RVLM (Figure 5.12), regardless of the time point, 2 or 6 h.

With regards to the expression of M2 microglial phenotype, baseline expression levels were observed in both rat strains, WKY (Figure 5.13A2) and SHR (Figure 5.13B2). Only the CD206⁺ microglia (Figure 5.12A2 and B2) that were also positive for Iba1 (Figure 5.13A1 and B1) were counted as M2⁺ microglia (Figure 5.13A3 and B3). However, no significant changes in expression levels of M2 microglia were observed following alterations introduced in BP (phenylephrine or hydralazine) regardless of the strain (WKY or SHR) at any time point (2 or 6 h), in either the CVLM (Figure 5.14A and B) or the RVLM (Figure 5.14C and D).

Figure 5.11: Effects of intravenous infusion of phenylephrine, saline or hydralazine on microglial morphology

A. ImageJ quantification of microglial morphological characteristics (number of end point processes/microglia and branch length (μm)/ microglia) with 'AnalyzeSkeleton' plugin (see methods for details). Changes in microglial morphology were quantified under 2 different magnifications, 40X and 63X. Three characteristics of microglial morphology quantified under 40X magnification were, % of area covered by microglia, number of end point processes/microglia and branch length (μm)/microglia. Two microglial morphological characteristics quantified at 63X magnification were, number of end point processes/ microglia and branch length (μm)/ microglia. No changes were observed in microglial morphology at 40X in the CVLM (B-E) or the RVLM (F-I). No changes were observed in microglial morphology at 63X in the CVLM (J-M) and the RVLM (N-Q), of WKY and SHR, when subjected to phenylephrine induced hypertension, saline served as control or hydralazine induced hypotension, for 2 and 6 h. All statistical comparisons were made between treatment groups (phenylephrine or hydralazine) and the saline group, at the particular time point; no comparisons were made across time points. Data are expressed as mean \pm SEM. Statistical significance was determined by a Kruskal-Wallis one-way analysis of variance. * $p \leq 0.05$, ** $p \leq 0.01$, *** $p \leq 0.001$ and **** $p \leq 0.0001$.



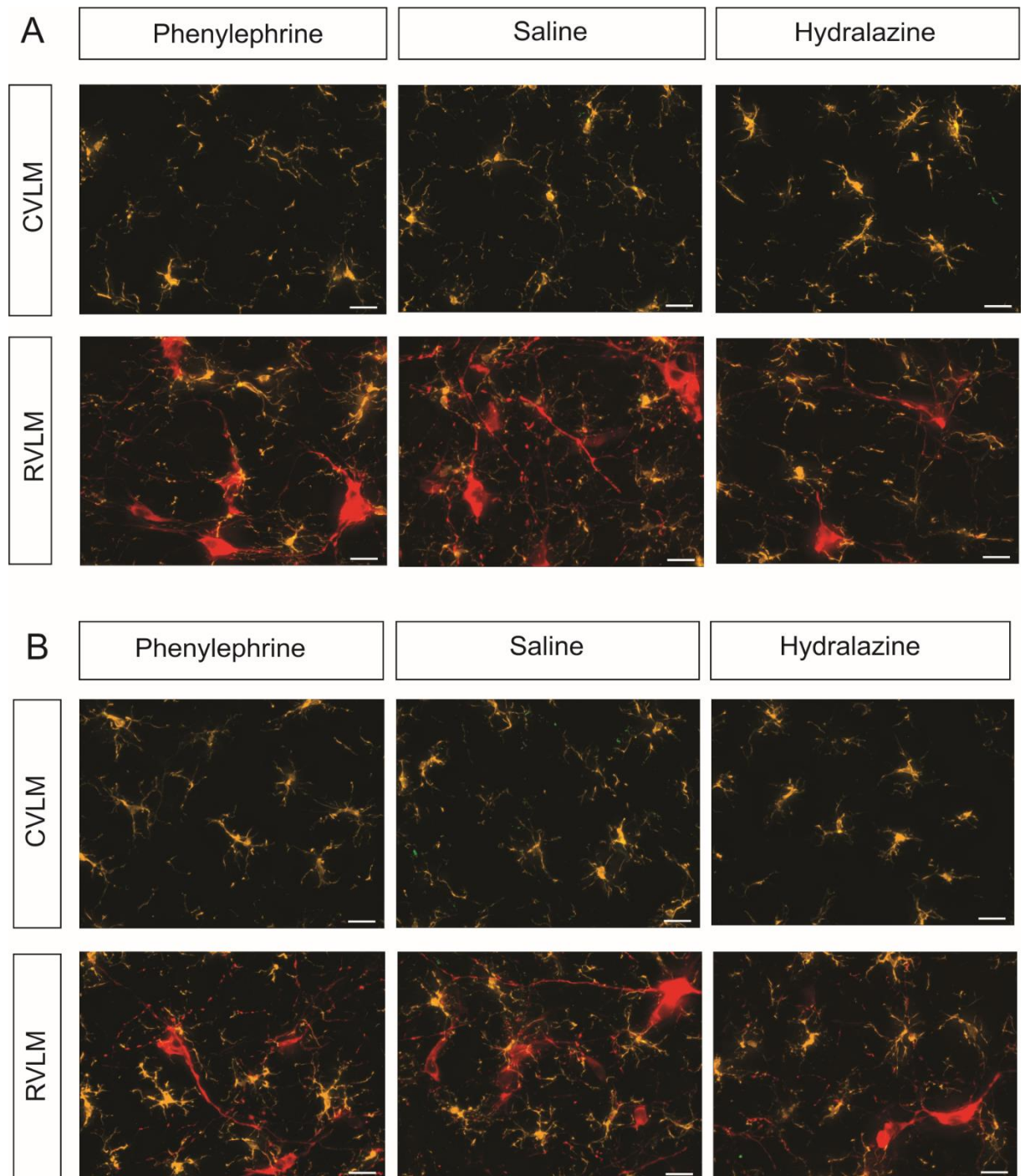


Figure 5.12: CD16 expression in response to intravenous infusion of phenylephrine, saline or hydralazine in WKY and SHR

Induction of hypertension (phenylephrine), normotension (saline) or hypotension (hydralazine) did not induce CD16 expression in either the CVLM or the RVLM, of either WKY (A) or SHR (B). Iba1 labelled microglia are in yellow and TH expressing C1 neurons of the RVLM are in red. Scale bar = 20 μ m.

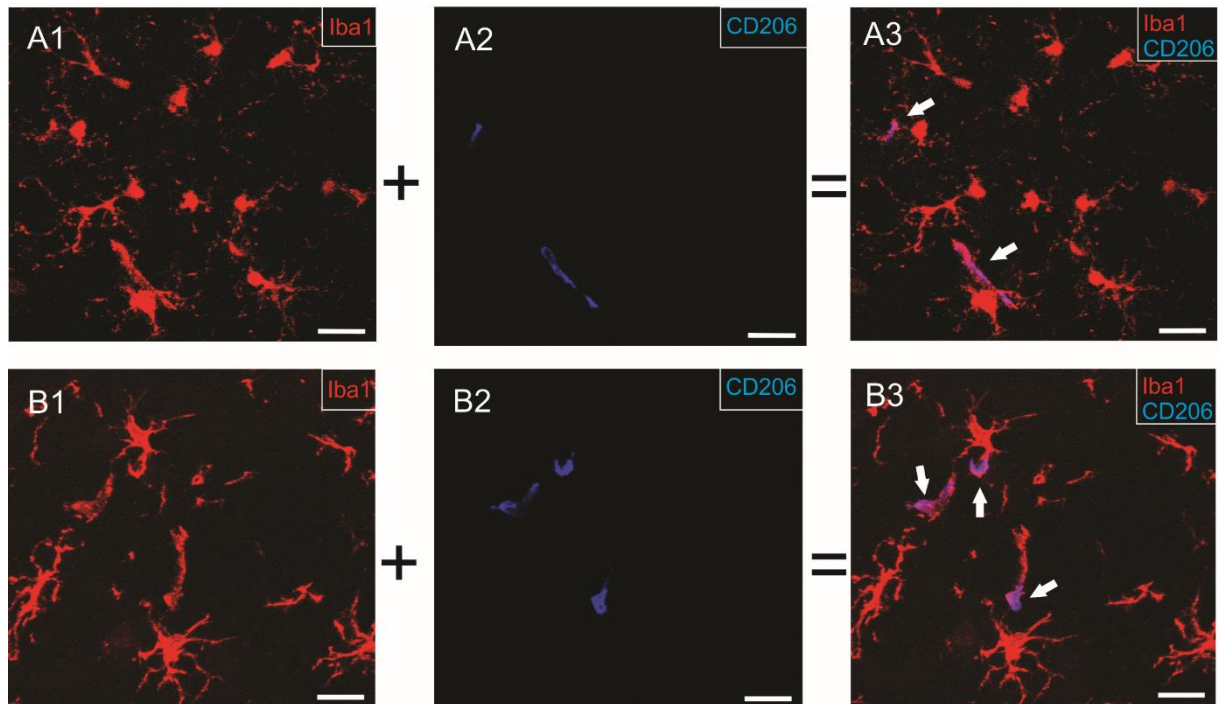


Figure 5.13: CD206 expression in the ventrolateral medulla (VLM) of WKY and SHR

A1 and B1 show the Iba1 labelled microglia (red) in the VLM of WKY and SHR, respectively. A2 and B2 show amoeboid shaped CD206⁺ M2 microglia (blue) in the VLM of WKY and SHR, respectively. A3 and B3 are merged images of Iba1 labelled and CD206⁺ microglia showing the colocalisation of Iba1 and CD206 in M2 microglia (white arrows). Scale bar = 20 μm.

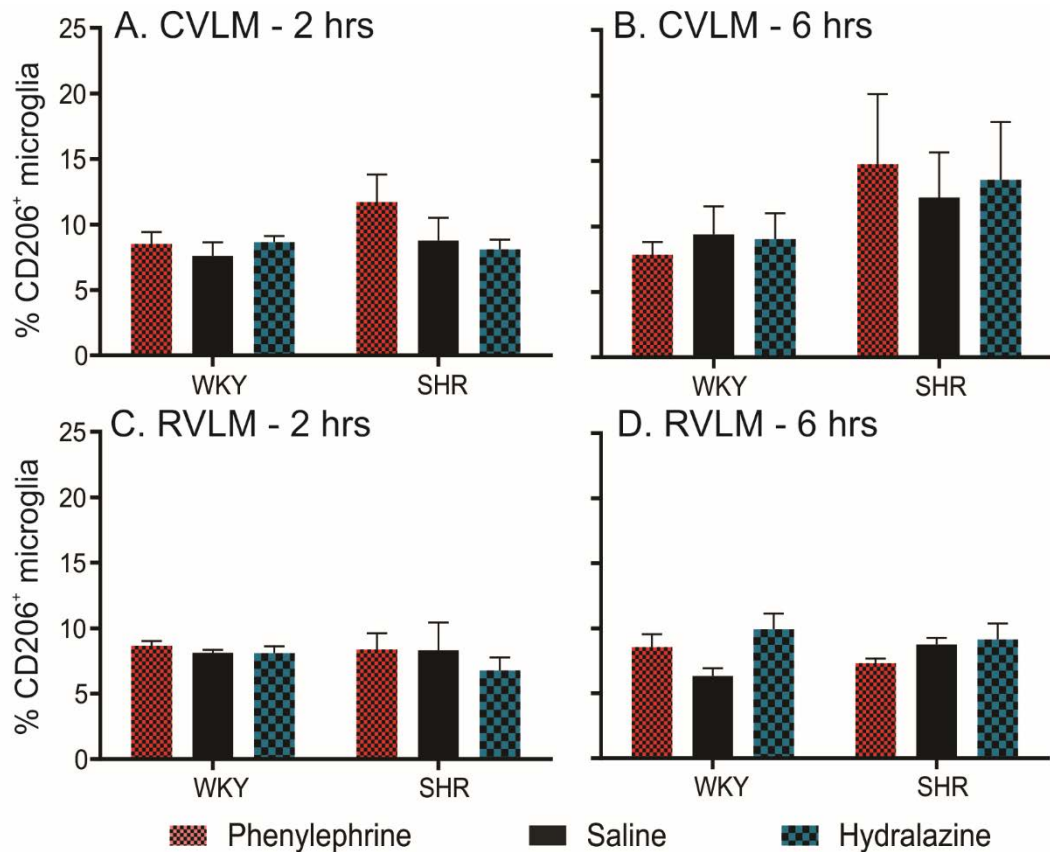


Figure 5.14: Expression levels of M2 microglia in response to intravenous infusion of phenylephrine, saline or hydralazine in WKY and SHR.

Induction of hypertension (phenylephrine), normotension (saline) or hypotension (hydralazine), for 2 and 6 h, did not induce any changes in the baseline expression levels of CD206 in the CVLM (A and B) or the RVLM (C and D), of either WKY or SHR. All statistical comparisons were made between treatment groups (phenylephrine or hydralazine) and the saline group, at the particular time point; no comparisons were made across time points. Data are expressed as mean \pm SEM. Statistical significance was determined by a Kruskal-Wallis one-way analysis of variance.

Movie 5.1: 3D reconstruction of Figure 5.6H

Demonstrating the proximity of multiple microglial cell bodies in the RVLM of SHR. The inter-microglial distance (IMD) is highly variable and microglia can breach each other's surveilling territory. Exact factors determining an IMD are yet unknown. According to findings from Chapter 3 (Kapoor et al., 2016a), and as speculated by other studies (de Haas et al., 2008; Lawson et al., 1990; Nikodemova et al., 2014), microglial distribution is closely related to, and is influenced by, their local neuronal environment. (Movies are included in .wmv format in the CD at the back of this thesis)

5.5 Discussion

Our first finding is in accordance with findings from Chapter 3 (Kapoor et al., 2016a), which show that microglia are ubiquitously distributed in the VLM area of the brainstem in both strains of rat, WKY and SHR. Secondly, microglia dynamically change their pattern of distribution, and the % of colocalisation with synapses, in response to altered BP. In accordance with Chapter 4 (Kapoor et al., 2016b), microglial response to induced alterations in BP is neither manifested as a significant change in microglial morphology, nor does it induce microglial polarization to extreme activation phenotypes (either M1 or M2). Most importantly, as speculated in Chapter 3 (Kapoor et al., 2016a), the findings described here suggest that it is the ‘microglial response’ to altered BP in the VLM area that is different in SHR when compared to WKY, and this impaired microglial response in the VLM of SHR coincides with the hypertensive phenotype of SHR.

First, as seen in Chapter 3, microglia exhibit a ubiquitous, and heterogeneous, distribution in the VLM area of WKY and SHR (Kapoor et al., 2016a). In accordance with previous work (Kapoor et al., 2016a; Kapoor et al., 2016b; Schafer et al., 2013; Shapiro et al., 2009), our findings show that microglial processes are closely apposed to neuronal dendrites in both WKY and SHR; this makes it easier for microglia to sense, and respond to, changes in neuronal/synaptic activity levels.

- *Changes in microglial spatial distribution to altered BP*

Induction of acute hypertension, with intravenous administration of phenylephrine, increases neuronal activity in the CVLM (section 1.3.1 and (Chan and Sawchenko, 1998)). In WKY, phenylephrine induced hypertension did not induce any changes in microglial spatial distribution in the CVLM, at any time point (2 or 6 h). However, following infusion of phenylephrine, microglia in the CVLM of SHR moved closer relative to each other, at both time points (2 and 6 h). Enhanced CVLM neuronal activity in response to increased BP (phenylephrine) provides an inhibitory GABAergic input to RVLM neurons, reducing overall RVLM neuronal activity (section 1.3.1 and (Cravo and Morrison, 1993; Jeske et al., 1995; Minson et al., 1994)). Phenylephrine induced hypertension in WKY, at either 2 or 6 h time point, did not induce any changes in the pattern of distribution of microglia in the RVLM area. On the other hand, in the RVLM of SHR, following the infusion of phenylephrine for 2 h, microglia moved closer relative to each other (up to 18 μ m); however, microglia started to return to a normal IMD at the subsequent time point, 6 h.

Intravenous injection of hydralazine evokes a hypotensive response, which causes unloading of baroreceptors (Graham et al., 1995; Springell et al., 2005; Stornetta et al., 2001). Unloading of baroreceptors, in turn, reduces the glutamatergic input to the NTS, further reducing excitation of CVLM neurons (section 1.3.1 and (Pilowsky and Goodchild, 2002; Pilowsky et al., 2009)). Changes in the CVLM neuronal activity, following the induction of hypotension (hydralazine) for 2 h, are detected by microglia in the vicinity causing the IMD to decrease in both WKY and SHR. Persistence of hypotensive stimulus for 6 h caused the IMD in the CVLM to return to normal levels in both WKY and SHR. Even though, no significant changes were seen in the IMD in the CVLM of SHR at the 6 h time point, following induction of hypotension (hydralazine), yet reductions were seen in the overall number of microglia. Reduced CVLM neuronal activity, in response to unloading of baroreceptors, evokes an enhanced neuronal activity in the RVLM (Chan and Sawchenko, 1994; Dun et al., 1993; Graham et al., 1995). This enhanced RVLM neuronal activity induced reductions in the IMD, at the 2 h time point, in both WKY and SHR; microglia in the SHR moved closer by $\approx 23 \mu\text{m}$ whereas in WKY, microglia moved closer up to $28 \mu\text{m}$. On the one hand, persistence of hypotension for 6 h caused the IMD to continue to decrease in the RVLM of WKY; on the other hand, the IMD started to increase in the RVLM of SHR, which was accompanied by a reduction in their overall number.

To summarize, microglia in both the CVLM and the RVLM of SHR moved closer relative to each other when subjected to either phenylephrine induced hypertension or hydralazine induced hypotension. No changes in the microglial spatial distribution were seen in either the CVLM or the RVLM in response to phenylephrine induced hypertension in SHR's normotensive phenotype, WKY. At this stage, it is difficult to comprehend the reason behind a lack of any microglial response in the VLM area of brainstem of WKY, to phenylephrine-induced hypertension. One possible explanation is that the microglial response, for some reason, is disrupted in WKY rats. However, our main aim is to identify the difference between microglial response to altered BP levels observed in the VLM of WKY and SHR. So keeping the focus of experiments in mind, it is quite evident that induction of acute hypertension in SHR induces an exaggerated microglial response, compared to WKY, in the VLM (CVLM and RVLM) nucleus of the brainstem; this was seen in the form of rearrangement in microglial spatial distribution. In case of hypotension, the pattern of changes introduced in the microglial spatial distribution in the CVLM are similar in both WKY and SHR. However, an impaired microglial response was seen, with respect to their spatial distribution, in the RVLM of SHR as compared to WKY, following maintenance of hydralazine induced hypotension for 6 h; the IMD increased in SHR

rather than decreasing (as observed in WKY). Changes observed in the IMD, as seen in Chapter 4 (Kapoor et al., 2016b), may or may not be accompanied by changes in the overall number of microglia. Subtle changes in the IMD may not result in significant variations in the overall microglial number in a given brainstem nucleus.

- *Changes in the % of colocalisation between microglia (Iba1) and synapses (synapsin)*

The presence of PSD95 immunoreactive-puncta, a marker of excitatory post-synaptic density, inside GFP labelled microglia revealed intra-microglial localization of synaptic proteins (Paolicelli et al., 2011). Therefore, Paolicelli et al., (2011) referred to the extent of colocalisation between microglia and synaptic markers (PSD95), confirmed by confocal, STED (stimulated emission depletion) and electron microscopy, as the degree of synaptic pruning performed by microglia (Paolicelli et al., 2011). Microglia are known to prune pre-synaptic structures, whereas the fate of post-synaptic structure and dendrite is still a question (Kettenmann et al., 2013; Wake et al., 2009). As we did not employ microscopy techniques such as STED or electronic microscopy, the percentage of colocalisation between microglia and synapses in this study was referred to as the extent of contact between these 2 structures. Therefore, any changes in the percentage of colocalisation between microglia and synapses highlight the level of synaptic sampling conducted by microglia.

Following phenylephrine induced hypertension in WKY, an increased extent of contact (% of colocalisation) between microglia (Iba1) and synapses (synapsin) was observed. However, with the persistence of phenylephrine induced hypertension for 6 h in WKY, % of microglial colocalisation with synapsin in the CVLM reduced. At this stage it is unclear, if the reduced microglial colocalisation with synapses in the CVLM following 6 h of hypertension (phenylephrine) is a cause, or a result, of the tendency of BP to return to baseline levels following prolonged infusions of phenylephrine (Kapoor et al., 2016b). No changes in the % of colocalisation between microglia and synapsin were seen in the CVLM of SHR, following induction of hypertension (phenylephrine), which indicates an impairment of microglial normal behaviour in the CVLM of SHR (compared to microglial response in WKY).

Following hydralazine induced hypotension, % of colocalisation between microglia (Iba1) and synapsin increased in the CVLM of WKY at the 2 h time point, and no response was seen in SHR; indicative of an impairment of microglial physiology in SHR. A previous study has shown that SHRs have a lower level of tonic activity in the CVLM that may be responsible for an exaggerated sympathetic nerve activity (SNA), as compared to WKY (Smith and Barron,

1990). Reduced tonic activity of the CVLM of SHR may cause subtle changes in neuronal activity levels in response to altered BP and therefore, may be one explanation for a lack of microglial response observed in the CVLM of SHR. However, these results should be treated with caution. As explained in the literature review, CVLM neurons are intermingled with A1 neurons (section 1.2.1.6 and (Aicher et al., 1995; Paxinos and Watson, 2007)). Reduced BP levels exert an opposite effect on the A1 and the CVLM neuronal activity. GABAergic neurons of the CVLM are regulated by baroreceptor afferent neurons; reductions in BP causes reductions in the CVLM neuronal activity (section 1.3.1 and (Chan and Sawchenko, 1998; Pilowsky and Goodchild, 2002; Pilowsky et al., 2009)). However, reduced BP evokes an enhanced A1 neuronal activity (section 1.2.2.1 (Kannan et al., 1986; Li et al., 1992a)). No attempt in this study was made to distinguish between synapses of GABAergic CVLM neurons (GAD67⁺) and synapses of A1 neurons (TH⁺). Thus, it is difficult, within the scope of this study, to interpret the level of microglial-synaptic contact with CVLM neuronal synapses only, following induction of either hypertension (phenylephrine) or hypotension (hydralazine). In spite of that, a deviation in the expected microglial response in the CVLM of SHR when compared with WKY (in response to either phenylephrine induced hypertension or hydralazine induced hypotension), shows an impairment of microglial physiology in SHR.

Induction of hypertension for 2 h in the RVLM of WKY caused a reduction in the % of microglial colocalisation with synapsin, whereas the same stimulus caused an increased % of microglial colocalisation with synapsin in the RVLM of SHR. A decreased % of colocalisation between microglia and synapsin in the RVLM of WKY suggests that microglia are spending longer in contact with synapses, indicative of a neuro-supportive microglial role (reduced synaptic pruning or increased release of neurotrophic factors) (Kapoor et al., 2016b). However, an impairment/exaggeration of the expected microglial response was observed in the RVLM of SHR (decreased % of colocalisation in the RVLM of WKY vs. increased % of colocalisation in the RVLM of SHR).

Hydralazine administration induces reductions in BP levels, followed by reductions in GABAergic input from the CVLM (section 1.2.1.5), and an enhanced RVLM neuronal activity (shown by For-ir; Figure 5.5) (Graham et al., 1995). Regardless of disturbances introduced in synaptic/ neuronal activity levels, reduced BP levels were detected by microglia as a non-harmful disturbance in homeostasis, inducing no change in the % of colocalisation between microglia and synapsin in the RVLM of WKY. On the other hand, an exaggerated microglial response in the RVLM of SHR to decreased BP levels was seen. The % of colocalisation

between microglia and synapsin increased in the RVLM of SHR following hydralazine administration. This again highlights an impaired/ exaggerated microglial response in the RVLM of SHR when compared with the RVLM of WKY.

The impaired/ exaggerated microglial response seen in the RVLM of SHR, when compared with the RVLM of WKY, could be due to a compromised microglial physiology in the RVLM of SHR (Kapoor et al., 2016a); microglia in the RVLM of SHR may exhibit a hypervigilant M0 state that responds to homeostatic disturbances in an exaggerated manner. An alternative interpretation to the impaired microglial response seen in the RVLM of SHR is the level of RVLM neuronal activity. As discussed earlier (section 1.2.1.5), the RVLM is also in receipt of glutamatergic inputs from brain areas, such as the NTS (Aicher et al., 1996) and the PVN (Yang et al., 2001), in addition to GABAergic input from the CVLM. It was previously suggested that tonically active glutamatergic input to the RVLM is increased in hypertensive rats (Ito et al., 2000; Ito et al., 2001; Zha et al., 2013). Perhaps the ‘off’ balance between excitatory and inhibitory input to SHR RVLM neuronal synapses (Ito and Sved, 1997), following either phenylephrine or hydralazine administration, is manifested as an increased microglial-synaptic contact.

In summary, an exaggerated level of microglial-synaptic contact (% of colocalisation between microglia and synapsin) was observed in the RVLM of SHR as compared to WKY, regardless of the treatment provided (phenylephrine or hydralazine). Microglial response to either hyper-, or hypo-, tension, in the RVLM of SHR, was to initially increase the level of synaptic sampling (microglial-synaptic contact). Future studies differentiating between A1 and CVLM neurons, and quantifying the extent of microglial contact with CVLM neuronal synapses only (GABAergic synapses) will elaborate on the microglial response to altered BP levels in the CVLM of SHR.

- *General discussion*

Interestingly, as reported in Chapter 4 (Kapoor et al., 2016b), alterations in BP levels, regardless of the rat strain, do not induce significant changes in microglial morphology. This further supports the hypothesis that the microglial response to a physical injury, or disturbed homeostasis, is a gradual transformation in their phenotype (Kettenmann et al., 2011). An ‘alerted’ microglial state does exist, where microglia are not entirely surveilling, and are alerted to homeostatic disturbances, yet have not acquired an activated amoeboid phenotype (Hanisch and Kettenmann, 2007; Kapoor et al., 2015; Kapoor et al., 2016b; Karperien et al., 2013;

Kettenmann et al., 2011). Acquisition of an extreme activated microglial phenotype indicates a point-of-no-return in microglial physiology (Kettenmann et al., 2011), which is not necessary in response to homeostatic deviations where microglial activities (such as synaptic pruning/release of neurotrophic factors) can control the situation and help resume homeostasis. Microglia are capable of performing neuro-supportive activities, such as synaptic pruning (Kettenmann et al., 2013; Tremblay et al., 2011) or release of neurotrophic factors (Elkabes et al., 1996; Kettenmann et al., 2011; Ueno et al., 2013) in normal brain.

Changes seen in microglial spatial distribution, as observed in Chapter 4, further supports the hypothesis that microglia can displace their cell body over short distances to perform housekeeping activities (Kapoor et al., 2016b; Karperien et al., 2013). IMD is dynamic and fluctuates in response to persistence of a stimulus inducing variations in synaptic/neuronal physiology.

In conclusion, regardless of the provided stimulus, microglia in the RVLM of SHR exhibit an impaired response to a homeostatic disturbance, which can be seen in the form of changes introduced in microglial spatial distribution and altered levels of microglial contact with synapses. We speculate, based on increased % of colocalisation between Iba1 and synapsin in the RVLM of SHR, that the initial response of microglia is to prune affected synapses, which shows an impairment of microglial physiology in SHR. This impairment of microglial physiology in the RVLM of SHR was not reflected in their morphology. However, one key question that remains to be resolved is whether the impaired microglial response observed in the RVLM of SHR is due to a compromised neuronal activity levels, or whether the failure of microglia to respond appropriately to altered BP is a reason of an exaggerated SNA in SHR, leading to their hypertensive phenotype. Future studies aimed at the characterisation of microglial response to modulations introduced in BP levels performed in young pre-hypertensive SHRs (>18 weeks old), and age-matched WKY, would resolve the ‘what happened first: impairment in microglial physiology or hypertensive phenotype’ paradigm (pers. comm. with Prof. Ruth Stornetta).

Chapter 6

Discussion & Conclusions

Discussion

Microglia, ‘never resting cells of the CNS’, play a crucial role in the maintenance of physiological homeostasis. Microglia, in their non-activated/surveilling/‘M0’ state, continuously scan their local environment with the aid of their dynamic processes for sudden, or gradual, appearance or disappearance of any unexpected or expected molecules, respectively (Biber et al., 2007; Kapoor et al., 2015; Nimmerjahn et al., 2005). When subjected to a physical injury threatening the integrity of the CNS, microglia sense the situation and polarize into extreme activation phenotypes (M1 or M2 depending on the insult), characterized by an amoeboid shape (David and Kroner, 2011; Stebbing et al., 2015; Stence et al., 2001). These activated microglial phenotypes are capable of conducting activities such as release of pro-inflammatory cytokines and reactive oxygen species (M1) or release of anti-inflammatory cytokines (M2) (Crain et al., 2013; David and Kroner, 2011; Kettenmann et al., 2011).

The SNS plays a critical role in the cardiovascular arm of the ANS. Brainstem areas, such as the NTS (section 1.2.1.7), the CVLM (section 1.2.1.6) and the RVLM (section 1.2.1.5), are involved in almost every aspect of the cardiovascular system including the modulation of adaptive reflexes, such the sympathetic baroreflex, the chemoreflexes or the SSR (section 1.3 (Guyenet, 2006; Moreira et al., 2006; Pilowsky et al., 2009)). Despite the importance of brainstem regions, such as the CVLM and the RVLM, in homeostasis of physiological parameters such as BP, distribution and role of microglia in these regions is still unknown.

The overall aim of this thesis was to characterise the microglial distribution and the microglial response to homeostatic disturbances induced by modulation of BP levels in cardiovascular sites of the brainstem that control the SNS, in 3 different strains of rat: SD (normotensive), WKY (normotensive control for SHR) and SHR (model of neurogenic hypertension). Main findings of this thesis are as following:

Microglial distribution in catecholaminergic nuclei of the brainstem in spontaneously hypertensive and normotensive rats (Chapter 3 (Kapoor et al., 2016a))

- Microglia are ubiquitously, and heterogeneously, distributed in catecholaminergic nuclei of the brainstem in all 3 strains of rats: SD, WKY and SHR.
- Microglial morphology does not vary considerably within, and between, different strains of rats.
- Number of microglia are closely related to the number of TH-ir neurons in catecholaminergic nuclei of the brainstem.

Microglial density and expression profile is highly influenced by their local neuronal environment (de Haas et al., 2008; Lawson et al., 1990; Mittelbronn et al., 2001; Nikodemova et al., 2014). Findings from Chapter 3 show that microglia are ubiquitously distributed throughout various catecholaminergic nuclei of the brainstem. TH-ir neurons are either adrenaline or noradrenaline synthesizing neurons of the brainstem that play an important role in the CNS. Interestingly, results from Chapter 3 show that the number of TH-ir neurons are not only involved in control of peripheral target organ activity (section 1.2.1 and 1.2.2), but are also strongly related to the number of microglia in a brainstem nucleus.

However, at this stage, it is yet to be established if the microglial number is influenced by the TH-ir neuronal number or *vice versa*. This study highlights the extent to which microglial distribution is related to their local environment in the brainstem, catecholaminergic nuclei in particular.

Microglial response to alterations in BP in the VLM of a SD rat (Chapter 4 (Kapoor et al., 2016b))

- Microglia are in close proximity to neuronal dendrites and synaptic structures (synapsin) in the ventrolateral medulla (VLM) of the brainstem.
- Microglia detect alterations in homeostatic levels of BP and respond to the same by changing their pattern of distribution (by moving closer relative to each other).
- Microglia contact more synapses (synapsin) when subjected to acute hypertension.
- Microglial contact with synapses (synapsin) decreases with reductions in BP.
- Microglia do not change their morphology significantly or acquire extreme activation phenotypes, such as an M1 or M2 state, in response to disturbance in BP homeostasis.

Findings from Chapter 4 show that microglia in the CVLM and the RVLM of the brainstem can detect changes in BP. Microglia can translocate their cell body in an amoeboid shape (Stence et al., 2001), over long distances, to reach an area of injury and conduct activities such as phagocytosis of debris and tissue repair (Hu et al., 2012; Kroner et al., 2014). However, data here show that microglia are capable of introducing subtle changes in their pattern of distribution in response to homeostatic challenges that do not threaten the physical integrity of the CNS.

Furthermore, our study shows, as shown in other areas of the brain, that microglia dynamically change the number of synapses contacted in response to homeostatic disturbances introduced their local neuronal environment (Li et al., 2012; Tremblay et al., 2010; Wake et al., 2009).

A review of the available literature shows that CD206 is a commonly used marker for M2 microglia. Many studies have used CD206, Ym1 and Arginase-1 as phenotypic markers for identification of M2 microglia (David and Kroner, 2011; Perego et al., 2011). Markers such as TGF- β are cytokines released by microglia (Kroner et al., 2014) and therefore, cannot phenotypically label microglia. Ym1 is a molecule that is associated with tissue recovery from an injury and its expression was reported 24 h following permanent middle cerebral artery occlusion; whereas expression of CD206 was observed 6 h post injury (Perego et al., 2011). Arginase-1 is a marker expressed by M2 microglia, which are contributing to wound healing and matrix deposition. A 2 fold increase in expression levels of both, CD206 and arginase-1, was observed 7 days following tissue injury and the expression was associated with the tissue recovery phase (Kroner et al., 2014). Another previous study shows similar results where expression of CD206 and arginase-1 were induced at approximately similar time post injury (Kigerl et al., 2009). Even in human studies, CD206 has proven to be a successful marker for identification of microglia in M2 state (Aron-Wisnewsky et al., 2009).

In our study, due to a lack of physical injury to the CNS, and 10 h being the maximum time point analysed, CD206 was used as an early marker for detection of M2. Arginase-1 and Ym1 expression levels are associated with wound healing and tissue recovery, and therefore were not explored in our study.

Many studies have only used changes in microglial morphology as a marker of microglial activation (Dworak et al., 2012; Dworak et al., 2014; Morrison and Filosa, 2013; Rana et al., 2010; Rana et al., 2014; Shi et al., 2010a). In these studies, microglial polarization to an amoeboid phenotype even after induction of extreme insults to the CNS was not observed, such as myocardial infarction (Dworak et al., 2012; Dworak et al., 2014; Rana et al., 2010) or temporary middle cerebral artery occlusion (Morrison and Filosa, 2013). In addition, researchers in the “microglia” field are moving away from the concept of presence of activated microglial phenotypes (M1/M2) in a healthy, non-injured, CNS (pers. comm. with Dr. Anja Majewska and Dr. Dorothy Schafer).

Thus, we speculate that microglial reaction (manifested as altered microglial spatial distribution and altered level of synaptic sampling) observed in response to cardiovascular challenges, such

as modulation of BP, induces a microglial physiological state – ‘alerted microglia’. Microglia in their ‘alerted’ state are not entirely surveilling or dormant, but they are more vigilantly aware of their surroundings (compared to M0). ‘Alerted’ microglial state is neither accompanied by an obvious change in microglial morphology, nor does it require microglial polarisation to extreme activated phenotypes (M1/M2).

Microglia in the CVLM and the RVLM of WKY respond to alterations in BP levels; a response that is compromised in SHR (Chapter 5)

- Similar to SD, microglia are in close proximity to neuronal dendrites and synaptic structures (synapsin) in the VLM of the brainstem of WKY and SHR.
- Microglial spatial distribution is dynamic and heterogeneous within a brainstem nucleus.
- Microglia in the VLM of SHR respond to induction of acute hypertension (intravenous phenylephrine) by changing their pattern of distribution, whereas no response was seen in the VLM of WKY following the infusion of phenylephrine.
- % of colocalisation between microglia (Iba1) and synapses (synapsin), reflecting the degree of synaptic sampling/pruning, increased in the RVLM of SHR regardless of the stimulus provided (phenylephrine induced hypertension or hydralazine induced hypotension). This shows an exaggerated microglial response in the RVLM of SHR to alterations in BP, as compared to WKY.
- In accordance with results from Chapter 4, microglial morphology, or expression levels of activated microglial states (M1/M2), do not change significantly in response to altered levels of BP.

A recent study showed that microglia in the PVN of stroke-prone SHR were comparatively smaller in size than the ones in WKY (Takesue et al., 2016). Inhibition of microglial activation (with oral minocycline) in stroke-prone SHR increased microglial size in the PVN, further supporting that microglial activation is a gradual, and reversible, process (Takesue et al., 2016). However, our morphological analysis (Chapter 3 and Chapter 5) shows that microglial morphology in the VLM of SHR and WKY is not significantly different. The discrepancy between these 2 studies could be due to different strains of rats used (stroke-prone SHR vs SHR) or due to difference in the area of the brain investigated (PVN vs VLM). As mentioned previously, SHR is a well-established model for neurogenic hypertension (section 2.1.2.3), whereas stroke-prone SHR is a model of hypertension-induced hemorrhagic stroke (Regenhardt

et al., 2014). Another possible explanation to the discrepancy in results between these 2 studies is the type of statistical tests used to analyse the data. Takesue et al., (2016) analysed microglial cell sizes using two-way ANOVA, whereas in our study, we used Kruskal-Wallis one-way analysis of variance to analyse the microglial morphological characteristics ((Takesue et al., 2016) and Chapter 5).

Similar to WKY, a lack of expression levels of M1 microglial phenotype was observed in saline treated SHR rats, in either the CVLM or the RVLM area. Taken together findings from Chapter 3 and Chapter 5 suggest that no changes in microglial number, morphology or activation state exist at baseline in the VLM of SHR, when compared with WKY. Clearly, microglia in the VLM of SHR respond to altered BP levels in an impaired manner, as compared to WKY. However, it is unclear at this stage if the impaired microglial behaviour in SHR is a causative factor of their hypertensive phenotype, or is a result of enhanced SNA and affected neuronal activity levels in SHR.

General Discussion

Findings from Chapter 4 and Chapter 5 suggest that the initial response of microglia to administration of BP modulating drugs is to change their pattern of distribution, and move closer relative to each other. This microglial response was independent of the direction of induced BP alterations. Even though, phenylephrine and hydralazine exert opposing effects on the VLM neuronal activity (section 1.3.1 and (Guyenet, 2006; Pilowsky et al., 2009), microglia move closer relative to each other in both cases (please refer to section 4.4.3 and 5.4.5 for details); the exact reason behind this is yet to be established. However, we speculate that microglia in the VLM area change their spatial distribution in response to the magnitude and persistence of the stimulus rather than the direction of BP. Furthermore, many researchers have also suggested previously that microglia respond to both, appearance and disappearance, of a constitutively expressed stimulus (Biber et al., 2007; Hanisch and Kettenmann, 2007); the evidence supporting this phenomenon is yet missing.

In Chapter 4, microglial contact with synapses increased in response to phenylephrine induced hypertension, and decreased in response to hydralazine induced hypotension (section 4.4). Again, this microglial response was independent of the changes induced in neuronal activity levels (Guyenet, 2006; Pilowsky et al., 2009), but varied with the direction of induced BP modulations. Whereas, in Chapter 5, inconsistent microglial response was seen with regards to the level of microglial-synaptic contact (please refer to section 5.5 for a detailed discussion).

One reason behind the inconsistency seen in findings between Chapter 4 and Chapter 5 could be the difference in method of analysis (please refer to section 2.4.3 for detailed methods). Synaptic contact with microglial end point processes was quantified in Chapter 4, whereas in Chapter 5, % of colocalisation between microglia (including cell body) and synapsin was quantified. As suggested by Paolicelli and colleagues, this may refer to the degree of synaptic pruning performed by microglia (Paolicelli et al., 2011). The alternative reason behind the discrepancy between findings from Chapter 4 and Chapter 5 could be due to the different strains of rats used, SD vs. WKY and SHR (section 2.1 and Chapter 3).

Interestingly, as seen in Chapter 4 and Chapter 5, changes observed in the extent of microglial contact with synapses and changes in the microglial spatial distribution do not always occur simultaneously. This could be due to heterogeneity in the microglial population within a brain nucleus. Microglial density and expression of immune-regulatory proteins is highly dependent on their neuronal environment and thus, is region-specific (Chapter 3 and (de Haas et al., 2008; Lawson et al., 1990; Mittelbronn et al., 2001; Nikodemova et al., 2014)). Even within a regional microglial population, sub-populations of specialized microglia exist with specific expression profiles of immune-regulatory proteins, such as neurotrophins and TREM-2 (Elkabes et al., 1996; Hanisch, 2013; Kettenmann et al., 2011; Schmid et al., 2002; Schmid et al., 2009). This cell-to-cell variability in microglia, within a brain nucleus, may explain the lack of synchronization between microglial response observed in context of their spatial distribution and degree of colocalisation with synapsin. Microglial population inducing a change in their pattern of distribution and microglial population varying the level of synaptic sampling may be from 2 different microglial sub-populations, within a brain nucleus.

Technical considerations

Several technical considerations have limited the scope of this work. First, the task of gaining a better understanding of the role of microglia in a healthy CNS requires use of state-of-the-art microscopy, and non-invasive, techniques. Employment of, easily available, extensively invasive techniques currently utilized in neuroscience (such as direct brain access, opening of skull or decapitation) may contribute to activation of microglia (Stence et al., 2001; Xu et al., 2007). Experiments performed while characterising the antibody raised against CD16 (labels M1 microglia, Figure 2.3), showed that microinjection of drugs locally into specific areas of the brainstem lead to activation of microglia. For the purpose of this thesis, care was taken not to disturb the internal milieu of brainstem sites that are involved in the sympathetic control of

BP, to avoid microglial activation in response to surgical procedures. Thus, drugs widely used to alter BP levels with their peripheral actions, such as phenylephrine or hydralazine, were used to modulate BP levels.

Secondly, the CVLM is an area, which is intermingled with neurons that are critical for cardiorespiratory functions, such as pre-bötzinger neurons (respiratory) and A1 neurons. A1 neurons play an important role in the hypothalamo-pituitary-adrenal axis (section 1.2.2.1) and pre-bötzinger neurons are crucial for the generation of respiratory rhythm (Figure 1.9) (Moreira et al., 2006). A1 neurons are TH-ir (Chapter 3), and both, CVLM (Chan and Sawchenko, 1998) and pre-bötzinger neurons (Kuwana et al., 2006), are GABAergic and glycinergic. Thus, separation of the CVLM group of neurons from the pre-bötzinger group of neurons, with markers such as GAD67 (glutamic acid decarboxylase 67) without intracellular recordings, is a difficult task. No attempt was made in the present study to distinguish between CVLM, A1 and pre-bötzinger neurons for the purpose of quantification of Fos-ir or microglial response. Our main aim was to identify if microglia in, and around, the CVLM area respond to changes in BP. Hence, future studies need to be conducted that aim at the identification of changes in microglial relationship with CVLM neurons in response to alterations induced in BP levels.

Thirdly, without the use of electron microscopy, it is difficult to estimate the extent of physical proximity between microglial processes and neuronal structures, such as cell body, dendrites or synapses. Previously, it was shown that Iba1 labelled microglial cell bodies are adjacent to neurons and capillaries (Shapiro et al., 2009). Furthermore, close association and contact between microglia and synaptic structures has also been shown (Tremblay et al., 2010; Wake et al., 2009). Yet, the question whether microglial processes can penetrate the neuronal cell body, as raised in Chapter 4 and Chapter 5, remains unanswered. Future studies at ultra-structural level will increase our understanding of the exact morphological relationship between microglia and neurons.

BP is a physiological parameter, which is tightly regulated by various brain nuclei (section 1.2). The topographical organization of BP controlling neurons provides a wide ROI to be explored, in response to phenylephrine induced hypertension or hydralazine induced hypotension. Studies using advanced microscopy techniques, such as *in vivo* two photon imaging (Wake et al., 2009), targeting an individual microglia, and covering a smaller ROI, may have missed subtle changes introduced in the distribution pattern or microglial packing density in the ROI. Therefore, future studies employing advanced microscopy techniques, covering a wide ROI and at an ultra-

structural level, to reveal mechanisms involved behind microglial behaviour (observed in Chapter 4 and Chapter 5), will surely enhance our understanding concerning microglial physiology and activation paradigm.

In summary, further work is required to not only understand the role of microglia in hypertension, but to also identify techniques with minimal physiological manipulations. This will enable us to evaluate the nature and mechanism of changes introduced in microglial physiology or the extracellular matrix, when subjected to a homeostatic disturbance.

Future directions

The work conducted in this thesis has highlighted microglia as dynamic elements of the ANS, capable of sensing, and responding to, changes in their local environment, triggered by disruptions in BP homeostasis. To our knowledge, the work presented in this thesis is a first attempt at connecting microglia and the VLM region of the brainstem, in context of essential hypertension, in the absence of any injury or inflammation. Previous work focusing on the role of microglia in the VLM is either in response to systemic inflammation (Wu et al., 2012) or in response to myocardial infarction (Dworak et al., 2014).

Much of the work connecting ‘brainstem sites involved in the sympathetic control of blood pressure’, ‘microglia’ and ‘essential hypertension’ is focused on brain regions other than the VLM, such as the supra-optic nucleus (Ayoub and Salm, 2003) or the PVN (Dworak et al., 2012; Dworak et al., 2014; Liu et al., 2016; Rana et al., 2010; Rana et al., 2014; Shi et al., 2010a; Takesue et al., 2016).

Findings of this thesis have answered questions regarding the extent to which microglia are influenced by their neuronal environment in the VLM region, and the close relationship between microglia and cardiovascular neurons. However, it also raises a plethora of questions concerning our current understanding of microglia. With the current available understanding of microglia, it is quite difficult to identify the exact mechanism behind the observed microglial behaviour, and we can only speculate at this stage regarding the existence of ‘alerted microglial’ state.

Alternative methods such as stimulation of the ADN (Abbott et al., 2009b; Kubo and Kihara, 1988; Willette et al., 1987) will isolate the microglial response to changes in neuronal activity from side-effect of BP modulating drugs, such as the effect of hydralazine (lowering of BP) on respiratory neurons and the effect of continuous infusion of drugs (or saline) on tissue perfusion.

Clonidine is a sympatholytic drug that can cross blood brain barrier (Andre et al., 2009) and is known to exert its hypotensive effects via sites such as the RVLM (Punnen et al., 1987; Yamazato et al., 2001). Use of drugs such as clonidine will elaborate on current findings, to understand the extent to which microglia in the RVLM are affected in response to sympatho-inhibition. Another factor that should be considered is the effect of anaesthesia on the microglial response to changes in BP. Studies have suggested that the use of an anaesthetic influences the response to a provided stimulus, and triggers a response pattern that is different from the one that could be seen in conscious animals (de Abreu et al., 2009; Lacerda et al., 2003). Thus, the use of an anaesthetic, such as sodium pentobarbital or urethane, may have evoked different microglial responses to alterations in BP as opposed to a situation where BP alterations would be induced in a conscious animal. Future experiments focusing on the microglial response to alterations induced in BP (either phenylephrine induced hypertension or hydralazine induced hypotension) in conscious animals will provide insights on the effects of anaesthesia on microglia.

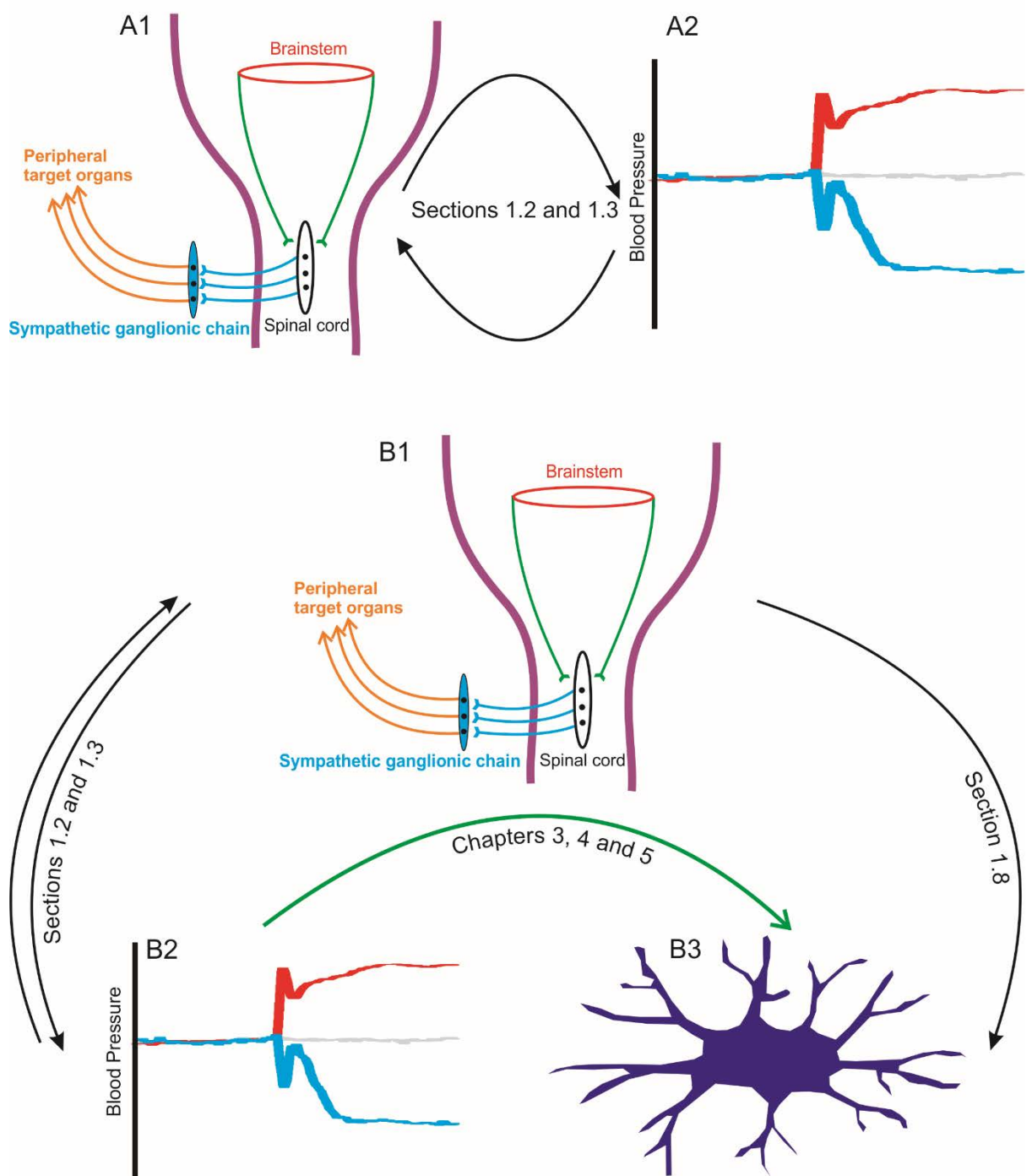
So far, attempting to predict the fate or role (neuro-protective or neurotoxic) of microglia in cardiovascular sites in the brain that control the SNS, following a conventional flow chart, is proving to be a formidable task. Inhibition of microglial function *in vivo* is a difficult task. Minocycline is a broad spectrum tetracycline that even though is known to inhibit microglial activation (Shi et al., 2010a) is not specific for microglia (Cai et al., 2010; Gonzalez et al., 2007; Stirling et al., 2004). Recent developments have suggested that even though the expression, and internalization, of anti-CD11b antibody (OX42) is specific for microglia, the internalization of this antibody also elicits a strong immune response (Smolny et al., 2014). The absence of substantial EGFP expression (conjugated to anti-CD11b antibody), *in vitro* and *in vivo*, and presence of non-specific fluorescent labelling, showed limitations of manipulating microglial gene expression (Smolny et al., 2014). Even though this study highlights CD11b as a potential and microglia specific target for future studies, it also provides further evidence that manipulations in ‘Microglial internal environment’ are a relatively challenging task (Smolny et al., 2014). Therefore, future research focusing on exogenous priming of microglia (Perry and Holmes, 2014) towards protective effects of M2 phenotype, rather than inhibition of microglial activity, may prove to be fruitful in 2 ways, 1) it will advance our understanding of the role of naïve (non-primed) microglia in a healthy CNS, and 2) will reveal therapeutic effects of M2 microglial phenotype.

Conclusions (Figure 6.1)

Studies described in this thesis provide novel data supporting the hypothesis that microglia play an important role in the function of a healthy, uninjured, VLM that controls the cardiovascular arm of the SNS (Figure 6.1). Here, we provide an evidence, for the first time, that microglia in the VLM area of the brainstem are highly dynamic, and respond to changes in their local neuronal environment triggered by alterations in BP. Microglia in the VLM area not only respond to disturbance in BP homeostasis, but also carefully tailor their response to the magnitude, and persistence, of changes introduced in BP homeostasis. Results described in this thesis show that microglia are heterogeneously distributed in brainstem catecholaminergic nuclei of the CNS. Very little, or no, expression of M1 microglia was observed in the CVLM and the RVLM, in absence of any physical injury. Basal expression levels of M2 microglia are present even in the absence of a physical injury, where CD206 expression colocalises with Iba1 expression. Microglia in the VLM of the brainstem detect changes in BP, and respond to them by varying the IMD and the level of synaptic contact. Emerging evidence suggests that activation of microglia can no longer be viewed as an “all or none” process. Rather, it is a gradual, morphological and physiological, transformation of microglia, which is reversible up to the point where an extreme activation phenotype (M1 or M2) is acquired. Thus, in light of our findings, we speculate that the microglial response to changes in BP is due to an intermediate microglial ‘alerted’ physiological state, which precedes activation states (M1/M2) and succeeds surveilling/M0 state. Our data also reveal that microglial function in the VLM area of the brainstem is impaired in SHR as compared to WKY. However, this impairment of microglial function is more related to the difference in microglial physiology and microglial response to homeostatic disturbance, and is not manifested as significant basal differences in microglial number or morphology between SHR and WKY.

Figure 6.1: Microglia in the VLM region of the brainstem (controlling cardiovascular arm of the SNS) respond to altered BP

A. Central autonomic regions in the brainstem (A1) are responsible for the maintenance of baseline levels of BP (A2). Any alterations in BP homeostasis cause changes in SNA, which in turn helps in the resumption of BP homeostasis; this pathway is known as the sympathetic baroreflex pathway. B. Work described in this thesis has added a 3rd dimension to BP homeostasis, i.e. microglia. As mentioned in panel A, the sympathetic baroreflex is a negative feedback loop system where baseline levels of BP and SNA are maintained in coordination with each other. The work described in this thesis shows that any changes in BP homeostasis (B2) affects microglial activity (B3) in the VLM area of the brainstem that is involved in the sympathetic control of BP (B1). Microglial response to altered BP levels is manifested as changes in the microglial spatial distribution and the level of synaptic sampling (conducted by microglia).



References

- Abbott, S.B., Pilowsky, P.M., 2009. Galanin microinjection into rostral ventrolateral medulla of the rat is hypotensive and attenuates sympathetic chemoreflex. *Am J Physiol Regul Integr Comp Physiol.* 296, R1019-26.
- Abbott, S.B., Stornetta, R.L., Socolovsky, C.S., West, G.H., Guyenet, P.G., 2009a. Photostimulation of channelrhodopsin-2 expressing ventrolateral medullary neurons increases sympathetic nerve activity and blood pressure in rats. *J Physiol.* 587, 5613-31.
- Abbott, S.B., Kanbar, R., Bochorishvili, G., Coates, M.B., Stornetta, R.L., Guyenet, P.G., 2012. C1 neurons excite locus coeruleus and A5 noradrenergic neurons along with sympathetic outflow in rats. *J Physiol.* 590, 2897-915.
- Abbott, S.B.G., Burke, P.G.R., Pilowsky, P.M., 2009b. Galanin microinjection into the PreBötzinger or the Bötzing Complex terminates central inspiratory activity and reduces responses to hypoxia and hypercapnia in rat. *Respir Physiol Neurobiol.* 167, 299-306.
- Abrahams, T.P., Hornby, P.J., Chen, K., Dasilva, A.M.T., Gillis, R.A., 1994. The non-NMDA subtype of excitatory amino acid receptor plays the major role in control of cardiovascular function by the subretrofacial nucleus in cats. *J Pharmacol Exp Ther.* 270, 424-432.
- Affleck, V.S., Coote, J.H., Pyner, S., 2012. The projection and synaptic organisation of NTS afferent connections with presympathetic neurons, GABA and nNOS neurons in the paraventricular nucleus of the hypothalamus. *Neuroscience.* 219, 48-61.
- Ahmad, Z., Milligan, C.J., Paton, J.F., Deuchars, J., 2003. Angiotensin type 1 receptor immunoreactivity in the thoracic spinal cord. *Brain Res.* 985, 21-31.
- Aicher, S.A., Kurucz, O.S., Reis, D.J., Milner, T.A., 1995. Nucleus tractus solitarius efferent terminals synapse on neurons in the caudal ventrolateral medulla that project to the rostral ventrolateral medulla. *Brain Res.* 693, 51-63.
- Aicher, S.A., Saravay, R.H., Cravo, S., Jeske, I., Morrison, S.F., Reis, D.J., Milner, T.A., 1996. Monosynaptic projections from the nucleus tractus solitarii to C1 adrenergic neurons in the rostral ventrolateral medulla: comparison with input from the caudal ventrolateral medulla. *J Comp Neurol.* 373, 62-75.
- Aicher, S.A., Schreihöfer, A.M., Kraus, J.A., Sharma, S., Milner, T.A., Guyenet, P.G., 2001. Mu-opioid receptors are present in functionally identified sympathoexcitatory neurons in the rat rostral ventrolateral medulla. *J Comp Neurol.* 433, 34-47.
- Ajami, B., Bennett, J.L., Krieger, C., Tetzlaff, W., Rossi, F.M., 2007. Local self-renewal can sustain CNS microglia maintenance and function throughout adult life. *Nat Neurosci.* 10, 1538-43.
- Akine, A., Montanaro, M., Allen, A.M., 2003. Hypothalamic paraventricular nucleus inhibition decreases renal sympathetic nerve activity in hypertensive and normotensive rats. *Auton Neurosci.* 108, 17-21.
- Allen, A.M., Dampney, R.A., Mendelsohn, F.A., 1988. Angiotensin receptor binding and pressor effects in cat subretrofacial nucleus. *Am J Physiol.* 255, H1011-7.
- Allen, A.M., 2002. Inhibition of the Hypothalamic Paraventricular Nucleus in Spontaneously Hypertensive Rats Dramatically Reduces Sympathetic Vasomotor Tone. *Hypertension.* 39, 275-280.
- Allen, A.M., O'Callaghan, E.L., Chen, D., Bassi, J.K., 2009. Central neural regulation of cardiovascular function by angiotensin: a focus on the rostral ventrolateral medulla. *Neuroendocrinology.* 89, 361-9.
- Aloisi, F., Penna, G., Cerase, J., Menendez Iglesias, B., Adorini, L., 1997. IL-12 production by central nervous system microglia is inhibited by astrocytes. *J Immunol.* 159, 1604-12.

- Alvares, T.S., Revill, A.L., Huxtable, A.G., Lorenz, C.D., Funk, G.D., 2014. P2Y1 receptor-mediated potentiation of inspiratory motor output in neonatal rat in vitro. *J Physiol.* 592, 3089-111.
- Amadio, S., De Ninno, A., Montilli, C., Businaro, L., Gerardino, A., Volonte, C., 2013. Plasticity of primary microglia on micropatterned geometries and spontaneous long-distance migration in microfluidic channels. *BMC Neurosci.* 14, 121.
- Amano, M., Kubo, T., 1993. Involvement of both GABAA and GABAB receptors in tonic inhibitory control of blood pressure at the rostral ventrolateral medulla of the rat. *Naunyn Schmiedeberg's Arch Pharmacol.* 348, 146-53.
- Anderson, E.A., Sinkey, C.A., Lawton, W.J., Mark, A.L., 1989. Elevated sympathetic nerve activity in borderline hypertensive humans. Evidence from direct intraneural recordings. *Hypertension.* 14, 177-83.
- Andre, P., Debray, M., Scherrmann, J.M., Cisternino, S., 2009. Clonidine transport at the mouse blood-brain barrier by a new H⁺ antiporter that interacts with addictive drugs. *J Cereb Blood Flow Metab.* 29, 1293-304.
- Andreatta, S.H., Averill, D.B., Santos, R.A., Ferrario, C.M., 1988. The ventrolateral medulla. A new site of action of the renin-angiotensin system. *Hypertension.* 11, 1163-6.
- Andresen, M.C., Doyle, M.W., Jin, Y.H., Bailey, T.W., 2001. Cellular mechanisms of baroreceptor integration at the nucleus tractus solitarius. *Ann N Y Acad Sci.* 940, 132-41.
- Angelova, P.R., Kasymov, V., Christie, I., Sheikhabaie, S., Turovsky, E., Marina, N., Korsak, A., Zwicker, J., Teschemacher, A.G., Ackland, G.L., Funk, G.D., Kasparov, S., Abramov, A.Y., Gourine, A.V., 2015. Functional Oxygen Sensitivity of Astrocytes. *J Neurosci.* 35, 10460-73.
- Appleyard, S.M., Marks, D., Kobayashi, K., Okano, H., Low, M.J., Andresen, M.C., 2007. Visceral afferents directly activate catecholamine neurons in the solitary tract nucleus. *J Neurosci.* 27, 13292-302.
- Appleyard, S.M., 2009. Lighting Up Neuronal Pathways: The Development of a Novel Transgenic Rat that Identifies Fos-Activated Neurons Using a Red Fluorescent Protein. *Endocrinology.* 150, 5199-5201.
- Arakawa, H., Kawabe, K., Sapru, H.N., 2013. Angiotensin-(1-12) in the rostral ventrolateral medullary pressor area of the rat elicits sympathoexcitatory responses. *Exp Physiol.* 98, 94-108.
- Armstrong, D.M., Ross, C.A., Pickel, V.M., Joh, T.H., Reis, D.J., 1982. Distribution of dopamine-, noradrenaline-, and adrenaline-containing cell bodies in the rat medulla oblongata: demonstrated by the immunocytochemical localization of catecholamine biosynthetic enzymes. *J Comp Neurol.* 212, 173-87.
- Aron-Wisnewsky, J., Tordjman, J., Poitou, C., Darakhshan, F., Hugol, D., Basdevant, A., Aissat, A., Guerre-Millo, M., Clement, K., 2009. Human adipose tissue macrophages: m1 and m2 cell surface markers in subcutaneous and omental depots and after weight loss. *J Clin Endocrinol Metab.* 94, 4619-23.
- Aston-Jones, G., Bloom, F.E., 1981. Activity of norepinephrine-containing locus coeruleus neurons in behaving rats anticipates fluctuations in the sleep-waking cycle. *J Neurosci.* 1, 876-86.
- Aston-Jones, G., Rajkowski, J., Kubiak, P., Valentino, R.J., Shipley, M.T., 1996. Role of the locus coeruleus in emotional activation. *Prog Brain Res.* 107, 379-402.
- Avanzino, G.L., Ruggeri, P., Bianchi, D., Cogo, C.E., Ermirio, R., Weaver, L.C., 1994. GABAB receptor-mediated mechanisms in the RVLM studied by microinjections of two GABAB receptor antagonists. *Am J Physiol.* 266, H1722-8.
- Averill, D.B., Tsuchihashi, T., Khosla, M.C., Ferrario, C.M., 1994. Losartan, nonpeptide angiotensin II-type 1 (AT1) receptor antagonist, attenuates pressor and

- sympathoexcitatory responses evoked by angiotensin II and L-glutamate in rostral ventrolateral medulla. *Brain Res.* 665, 245-52.
- Ayoub, A.E., Salm, A.K., 2003. Increased morphological diversity of microglia in the activated hypothalamic supraoptic nucleus. *J Neurosci.* 23, 7759-66.
- Babic, T., Ciriello, J., 2004. Medullary and spinal cord projections from cardiovascular responsive sites in the rostral ventromedial medulla. *J Comp Neurol.* 469, 391-412.
- Babic, T., de Oliveira, C.V., Ciriello, J., 2008. Collateral axonal projections from rostral ventromedial medullary nitric oxide synthase containing neurons to brainstem autonomic sites. *Brain Res.* 1211, 44-56.
- Bacon, S.J., Smith, A.D., 1988. Preganglionic sympathetic neurones innervating the rat adrenal medulla: immunocytochemical evidence of synaptic input from nerve terminals containing substance P, GABA or 5-hydroxytryptamine. *J Auton Nerv Syst.* 24, 97-122.
- Bacon, S.J., Zagon, A., Smith, A.D., 1990. Electron microscopic evidence of a monosynaptic pathway between cells in the caudal raphe nuclei and sympathetic preganglionic neurons in the rat spinal cord. *Exp Brain Res.* 79, 589-602.
- Badoer, E., Head, G.A., Aberdeen, J.A., Korner, P.I., 1987. Localization of the main noradrenergic neuron groups in the pons and medulla of the rabbit and the importance of cathodal lesions for prolonged survival. *J Neurosci Methods.* 19, 11-27.
- Badoer, E., Chalmers, J., 1992. Interactions of endogenous opioid and excitatory amino acid inputs to the caudal ventrolateral medulla of the rat. *Neuropharmacology.* 31, 857-62.
- Badoer, E., McKinley, M.J., Oldfield, B.J., McAllen, R.M., 1993. A comparison of hypotensive and non-hypotensive hemorrhage on Fos expression in spinally projecting neurons of the paraventricular nucleus and rostral ventrolateral medulla. *Brain Res.* 610, 216-23.
- Badoer, E., McKinley, M.J., Oldfield, B.J., McAllen, R.M., 1994. Localization of barosensitive neurons in the caudal ventrolateral medulla which project to the rostral ventrolateral medulla. *Brain Res.* 657, 258-268.
- Badoer, E., 1998. Neurons in the hypothalamic paraventricular nucleus that project to the rostral ventrolateral medulla are not activated by hypotension. *Brain Res.* 801, 224-227.
- Badoer, E., Merolli, J., 1998. Neurons in the hypothalamic paraventricular nucleus that project to the rostral ventrolateral medulla are activated by haemorrhage. *Brain Res.* 791, 317-320.
- Badoer, E., Ng, C.W., De Matteo, R., 2002. Tonic sympathoinhibition arising from the hypothalamic PVN in the conscious rabbit. *Brain Res.* 947, 17-24.
- Badoer, E., 2010. Role of the hypothalamic PVN in the regulation of renal sympathetic nerve activity and blood flow during hyperthermia and in heart failure. *Am J Physiol Renal Physiol.* 298, F839-46.
- Bago, M., Marson, L., Dean, C., 2002. Serotonergic projections to the rostroventrolateral medulla from midbrain and raphe nuclei. *Brain Res.* 945, 249-58.
- Bajic, D., Proudfit, H.K., 2013. Projections from the rat cuneiform nucleus to the A7, A6 (locus coeruleus), and A5 pontine noradrenergic cell groups. *J Chem Neuroanat.* 50-51, 11-20.
- Baraban, S.C., Stornetta, R.L., Guyenet, P.G., 1995. Effects of morphine and morphine withdrawal on adrenergic neurons of the rat rostral ventrolateral medulla. *Brain Res.* 676, 245-57.
- Barman, S.M., Gebber, G.L., Calaresu, F.R., 1984. Differential control of sympathetic nerve discharge by the brain stem. *Am J Physiol.* 247, R513-9.
- Barman, S.M., Gebber, G.L., 1992. Rostral ventrolateral medullary and caudal medullary raphe neurons with activity correlated to the 10-Hz rhythm in sympathetic nerve discharge. *J Neurophysiol.* 68, 1535-47.
- Barman, S.M., Gebber, G.L., Zhong, S., 1992. The 10-Hz rhythm in sympathetic nerve discharge. *Am J Physiol.* 262, R1006-R1014.
- Barman, S.M., Gebber, G.L., Orer, H.S., 2000. Medullary lateral tegmental field: an important source of basal sympathetic nerve discharge in the cat. *Am J Physiol.* 278, R995-R1004.

- Basting, T.M., Burke, P.G., Kanbar, R., Viar, K.E., Stornetta, D.S., Stornetta, R.L., Guyenet, P.G., 2015. Hypoxia silences retrotrapezoid nucleus respiratory chemoreceptors via alkalosis. *J Neurosci.* 35, 527-43.
- Beaudet, M.M., Braas, K.M., May, V., 1998. Pituitary adenylate cyclase activating polypeptide (PACAP) expression in sympathetic preganglionic projection neurons to the superior cervical ganglion. *J Neurobiol.* 36, 325-36.
- Benarroch, E., 1998. *The Lower Brainstem and Bodily Homeostasis.* By William Blessing, Oxford, UK. *Ann Neurol.* 43, 839-839.
- Bennion, D.M., Haltigan, E., Regenhardt, R.W., Steckelings, U.M., Sumners, C., 2015a. Neuroprotective mechanisms of the ACE2-angiotensin-(1-7)-Mas axis in stroke. *Curr Hypertens Rep.* 17, 3.
- Bennion, D.M., Haltigan, E.A., Irwin, A.J., Donnangelo, L.L., Regenhardt, R.W., Pioquinto, D.J., Purich, D.L., Sumners, C., 2015b. Activation of the neuroprotective angiotensin-converting enzyme 2 in rat ischemic stroke. *Hypertension.* 66, 141-148.
- Bergamaschi, C.T., Silva, N.F., Pires, J.G., Campos, R.R., Neto, H.A., 2014. Participation of 5-HT and AT1 Receptors within the Rostral Ventrolateral Medulla in the Maintenance of Hypertension in the Goldblatt 1 Kidney-1 Clip Model. *Int J Hypertens.* 2014, 723939.
- Bernard, D.G., Li, A., Nattie, E.E., 1996. Evidence for central chemoreception in the midline raphe. *J Appl Physiol* (1985). 80, 108-15.
- Berthoud, H.R., Patterson, L.M., Sutton, G.M., Morrison, C., Zheng, H., 2005. Orexin inputs to caudal raphe neurons involved in thermal, cardiovascular, and gastrointestinal regulation. *Histochem Cell Biol.* 123, 147-56.
- Bhandare, A.M., Mohammed, S., Pilowsky, P.M., Farnham, M.M., 2015. Antagonism of PACAP or microglia function worsens the cardiovascular consequences of kainic-acid-induced seizures in rats. *J Neurosci.* 35, 2191-9.
- Bhandare, A.M., Kapoor, K., Pilowsky, P.M., Farnham, M.M., 2016. Seizure-Induced Sympathoexcitation Is Caused by Activation of Glutamatergic Receptors in RVLm That Also Causes Proarrhythmogenic Changes Mediated by PACAP and Microglia in Rats. *J Neurosci.* 36, 506-17.
- Biber, K., Neumann, H., Inoue, K., Boddeke, H.W., 2007. Neuronal 'On' and 'Off' signals control microglia. *Trends Neurosci.* 30, 596-602.
- Bieger, D., Hopkins, D.A., 1987. Viscerotopic representation of the upper alimentary tract in the medulla oblongata in the rat: the nucleus ambiguus. *J Comp Neurol.* 262, 546-62.
- Blanch, G.T., Freiria-Oliveira, A.H., Speretta, G.F., Carrera, E.J., Li, H., Speth, R.C., Colombari, E., Sumners, C., Colombari, D.S., 2014. Increased expression of angiotensin II type 2 receptors in the solitary-vagal complex blunts renovascular hypertension. *Hypertension.* 64, 777-83.
- Blessing, W., Costa, M., Furness, J., West, M., Chalmers, J., 1981a. Projection from A1 neurons towards the nucleus tractus solitarius in rabbit. *Cell Tiss Res.* 220, 27-40.
- Blessing, W.W., West, M.J., Chalmers, J., 1981b. Hypertension, bradycardia, and pulmonary edema in the conscious rabbit after brainstem lesions coinciding with the A1 group of catecholamine neurons. *Circ Res.* 49, 949-58.
- Blessing, W.W., Jaeger, C.B., Ruggiero, D.A., Reis, D.J., 1982a. Hypothalamic projections of medullary catecholamine neurons in the rabbit: a combined catecholamine fluorescence and HRP transport study. *Brain Res Bull.* 9, 279-86.
- Blessing, W.W., Reis, D.J., 1982. Inhibitory cardiovascular function of neurons in the caudal ventrolateral medulla of the rabbit: relationship to the area containing A1 noradrenergic cells. *Brain Res.* 253, 161-71.
- Blessing, W.W., Sved, A.F., Reis, D.J., 1982b. Destruction of noradrenergic neurons in rabbit brainstem elevates plasma vasopressin, causing hypertension. *Science.* 217, 661-3.

- Blessing, W.W., Reis, D.J., 1983. Evidence that GABA and glycine-like inputs inhibit vasodepressor neurons in the caudal ventrolateral medulla of the rabbit. *Neurosci Lett.* 37, 57-62.
- Blessing, W.W., Oliver, J.R., Hodgson, A.H., Joh, T.H., Willoughby, J.O., 1987. Neuropeptide Y-like immunoreactive C1 neurons in the rostral ventrolateral medulla of the rabbit project to sympathetic preganglionic neurons in the spinal cord. *J Auton Nerv Syst.* 18, 121-9.
- Blessing, W.W., 1988. Depressor neurons in rabbit caudal medulla act via GABA receptors in rostral medulla. *Am J Physiol.* 254, H686-92.
- Blessing, W.W., Nalivaiko, E., 2000. Regional blood flow and nociceptive stimuli in rabbits: Patterning by medullary raphe, not ventrolateral medulla. *J Physiol.* 524, 279-292.
- Block, M.L., Li, G., Qin, L., Wu, X., Pei, Z., Wang, T., Wilson, B., Yang, J., Hong, J.S., 2006. Potent regulation of microglia-derived oxidative stress and dopaminergic neuron survival: substance P vs. dynorphin. *FASEB J.* 20, 251-8.
- Bochorishvili, G., Nguyen, T., Coates, M.B., Viar, K.E., Stornetta, R.L., Guyenet, P.G., 2014. The orexinergic neurons receive synaptic input from C1 cells in rats. *J Comp Neurol.* 522, 3834-46.
- Bogan, N., Mennone, A., Cabot, J.B., 1989. Light microscopic and ultrastructural localization of GABA-like immunoreactive input to retrogradely labeled sympathetic preganglionic neurons. *Brain Res.* 505, 257-70.
- Bolme, P., Corrodi, H., Fuxe, K., Hokfelt, T., Lidbrink, P., Goldstein, M., 1974. Possible involvement of central adrenaline neurons in vasomotor and respiratory control. Studies with clonidine and its interactions with piperoxane and yohimbine. *Eur J Pharmacol.* 28, 89-94.
- Bou Farah, L., Bowman, B.R., Bokinić, P., Karim, S., Le, S., Goodchild, A.K., McMullan, S., 2016. Somatostatin in the rat rostral ventrolateral medulla: Origins and mechanism of action. *J Comp Neurol.* 524, 323-42.
- Bowman, B.R., Goodchild, A.K., 2015. GABA and enkephalin tonically alter sympathetic outflows in the rat spinal cord. *Auton Neurosci.* 193, 84-91.
- Boychuk, C.R., Woerman, A.L., Mendelowitz, D., 2012. Modulation of bulbospinal rostral ventral lateral medulla neurons by hypoxia/hypercapnia but not medullary respiratory activity. *Hypertension.* 60, 1491-7.
- Bradl, M., Lassmann, H., 2010. Oligodendrocytes: biology and pathology. *Acta Neuropathol.* 119, 37-53.
- Bradley, S.R., Pieribone, V.A., Wang, W., Severson, C.A., Jacobs, R.A., Richerson, G.B., 2002. Chemosensitive serotonergic neurons are closely associated with large medullary arteries. *Nat Neurosci.* 5, 401-2.
- Braga, V.A., Machado, B.H., 2006. Chemoreflex sympathoexcitation was not altered by the antagonism of glutamate receptors in the commissural nucleus tractus solitarii in the working heart-brainstem preparation of rats. *Exp Physiol.* 91, 551-9.
- Braga, V.A., Soriano, R.N., Bracciulli, A.L., de Paula, P.M., Bonagamba, L.G., Paton, J.F., Machado, B.H., 2007. Involvement of L-glutamate and ATP in the neurotransmission of the sympathoexcitatory component of the chemoreflex in the commissural nucleus tractus solitarii of awake rats and in the working heart-brainstem preparation. *J Physiol.* 581, 1129-45.
- Brezenoff, H.E., Caputi, A.P., 1980. Intracerebroventricular injection of hemicholinium-3 lowers blood pressure in conscious spontaneously hypertensive rats but not in normotensive rats. *Life Sci.* 26, 1037-1045.
- Bright, G.R., Agani, F.H., Haque, U., Overholt, J.L., Prabhakar, N.R., 1996. Heterogeneity in cytosolic calcium responses to hypoxia in carotid body cells. *Brain Res.* 706, 297-302.

- Brouillette, J., Couture, R., 2002. Evidence for a GABA(B) receptor component in the spinal action of Substance P (SP) on arterial blood pressure in the awake rat. *Br J Pharmacol.* 136, 1169-77.
- Brown, G.C., Neher, J.J., 2014. Microglial phagocytosis of live neurons. *Nat Rev Neurosci.* 15, 209-16.
- Bruinstroop, E., Cano, G., Vanderhorst, V.G., Cavalcante, J.C., Wirth, J., Sena-Esteves, M., Saper, C.B., 2012. Spinal projections of the A5, A6 (locus coeruleus), and A7 noradrenergic cell groups in rats. *J Comp Neurol.* 520, 1985-2001.
- Buccafusco, J.J., Spector, S., 1980. Role of central cholinergic neurons in experimental hypertension. *J Cardiovasc Pharmacol.* 2, 347-55.
- Buchanan, G.F., Smith, H.R., MacAskill, A., Richerson, G.B., 2015. 5-HT_{2A} receptor activation is necessary for CO₂-induced arousal. *J Neurophysiol.* 114, 233-43.
- Buller, K.M., Smith, D.W., Day, T.A., 1999. Differential recruitment of hypothalamic neuroendocrine and ventrolateral medulla catecholamine cells by non-hypotensive and hypotensive hemorrhages. *Brain Res.* 834, 42-54.
- Bunge, M.B., Bunge, R.P., Pappas, G.D., 1962. Electron microscopic demonstration of connections between glia and myelin sheaths in the developing mammalian central nervous system. *J Cell Biol.* 12, 448-453.
- Burke, P.G., Li, Q., Costin, M.L., McMullan, S., Pilowsky, P.M., Goodchild, A.K., 2008. Somatostatin 2A receptor-expressing presympathetic neurons in the rostral ventrolateral medulla maintain blood pressure. *Hypertension.* 52, 1127-33.
- Burke, P.G., Neale, J., Korim, W.S., McMullan, S., Goodchild, A.K., 2011. Patterning of somatosympathetic reflexes reveals nonuniform organization of presympathetic drive from C1 and non-C1 RVLM neurons. *Am J Physiol.* 301, R1112-22.
- Burman, K.J., McKittrick, D.J., Minson, J.B., West, A., Arnolda, L.F., Llewellyn-Smith, I.J., 2001. Neurokinin-1 receptor immunoreactivity in hypotension sensitive sympathetic preganglionic neurons. *Brain Res.* 915, 238-43.
- Burman, K.J., Ige, A.O., White, J.H., Marshall, F.H., Pangalos, M.N., Emson, P.C., Minson, J.B., Llewellyn-Smith, I.J., 2003. GABAB receptor subunits, R1 and R2, in brainstem catecholamine and serotonin neurons. *Brain Res.* 970, 35-46.
- Burman, K.J., Sartor, D.M., Verberne, A.J., Llewellyn-Smith, I.J., 2004. Cocaine- and amphetamine-regulated transcript in catecholamine and noncatecholamine presympathetic vasomotor neurons of rat rostral ventrolateral medulla. *J Comp Neurol.* 476, 19-31.
- Burry, R.W., 2011. Controls for immunocytochemistry: an update. *J Histochem Cytochem.* 59, 6-12.
- Burton, A.R., Birznies, I., Bolton, P.S., Henderson, L.A., Macefield, V.G., 2009. Effects of deep and superficial experimentally induced acute pain on muscle sympathetic nerve activity in human subjects. *J Physiol.* 587, 183-93.
- Butovsky, O., Talpalar, A.E., Ben-Yaakov, K., Schwartz, M., 2005. Activation of microglia by aggregated beta-amyloid or lipopolysaccharide impairs MHC-II expression and renders them cytotoxic whereas IFN-gamma and IL-4 render them protective. *Mol Cell Neurosci.* 29, 381-93.
- Butovsky, O., Jedrychowski, M.P., Moore, C.S., Cialic, R., Lanser, A.J., Gabriely, G., Koeglperger, T., Dake, B., Wu, P.M., Doykan, C.E., Fanek, Z., Liu, L., Chen, Z., Rothstein, J.D., Ransohoff, R.M., Gygi, S.P., Antel, J.P., Weiner, H.L., 2014. Identification of a unique TGF-beta-dependent molecular and functional signature in microglia. *Nat Neurosci.* 17, 131-43.
- Byrum, C.E., Guyenet, P.G., 1987. Afferent and efferent connections of the A5 noradrenergic cell group in the rat. *J Comp Neurol.* 261, 529-42.
- Cabot, J.B., Alessi, V., Bushnell, A., 1992. Glycine-like immunoreactive input to sympathetic preganglionic neurons. *Brain Res.* 571, 1-18.

- Cai, Z.Y., Yan, Y., Chen, R., 2010. Minocycline reduces astrocytic reactivation and neuroinflammation in the hippocampus of a vascular cognitive impairment rat model. *Neurosci Bull.* 26, 28-36.
- Campos, R.R., McAllen, R.M., 1997. Cardiac sympathetic premotor neurons. *Am J Physiol.* 272, R615-20.
- Campos, R.R., McAllen, R.M., 1999. Tonic drive to sympathetic premotor neurons of rostral ventrolateral medulla from caudal pressor area neurons. *Am J Physiol.* 276, R1209-13.
- Campos, R.R., Carillo, B.A., Oliveira-Sales, E.B., Silva, A.M., Silva, N.F., Futuro Neto, H.A., Bergamaschi, C.T., 2008. Role of the caudal pressor area in the regulation of sympathetic vasomotor tone. *Braz J Med Biol Res.* 41, 557-62.
- Card, J.P., Sved, J.C., Craig, B., Raizada, M., Vazquez, J., Sved, A.F., 2006. Efferent projections of rat rostroventrolateral medulla C1 catecholamine neurons: Implications for the central control of cardiovascular regulation. *J Comp Neurol.* 499, 840-59.
- Cardinale, J.P., Sriramula, S., Mariappan, N., Agarwal, D., Francis, J., 2012. Angiotensin II-induced hypertension is modulated by nuclear factor-kappaB in the paraventricular nucleus. *Hypertension.* 59, 113-21.
- Cardona, A.E., Pioro, E.P., Sasse, M.E., Kostenko, V., Cardona, S.M., Dijkstra, I.M., Huang, D., Kidd, G., Dombrowski, S., Dutta, R., Lee, J.C., Cook, D.N., Jung, S., Lira, S.A., Littman, D.R., Ransohoff, R.M., 2006. Control of microglial neurotoxicity by the fractalkine receptor. *Nat Neurosci.* 9, 917-24.
- Chalmers, J., Pilowsky, P., 1991. Brainstem and bulbospinal neurotransmitter systems in the control of blood pressure. *J Hypertens.* 9, 675-94.
- Chalmers, J.P., 1975. Brain amines and models of experimental hypertension. *Circ Res.* 36, 469-80.
- Cham, J.L., 2006. Activation of spinally projecting and nitrergic neurons in the PVN following heat exposure. *Am J Physiol.* 291, R91-R101.
- Cham, J.L., Badoer, E., 2008a. Exposure to a hot environment can activate rostral ventrolateral medulla-projecting neurones in the hypothalamic paraventricular nucleus in conscious rats. *Exp Physiol.* 93, 64-74.
- Cham, J.L., Badoer, E., 2008b. Hypothalamic paraventricular nucleus is critical for renal vasoconstriction elicited by elevations in body temperature. *Am J Physiol Renal Physiol.* 294, F309-15.
- Chan, R.K., Sawchenko, P.E., 1994. Spatially and temporally differentiated patterns of c-fos expression in brainstem catecholaminergic cell groups induced by cardiovascular challenges in the rat. *J Comp Neurol.* 348, 433-60.
- Chan, R.K., Sawchenko, P.E., 1998. Organization and transmitter specificity of medullary neurons activated by sustained hypertension: implications for understanding baroreceptor reflex circuitry. *J Neurosci.* 18, 371-87.
- Chao, J., Gao, J., Parbhu, K.J., Gao, L., 2013. Angiotensin type 2 receptors in the intermediolateral cell column of the spinal cord: negative regulation of sympathetic nerve activity and blood pressure. *Int J Cardiol.* 168, 4046-55.
- Charles, A.C., Merrill, J.E., Dirksen, E.R., Sanderson, M.J., 1991. Intercellular signaling in glial cells: calcium waves and oscillations in response to mechanical stimulation and glutamate. *Neuron.* 6, 983-92.
- Charlton, C.G., Helke, C.J., 1987. Substance P-containing medullary projections to the intermediolateral cell column: identification with retrogradely transported rhodamine-labeled latex microspheres and immunohistochemistry. *Brain Res.* 418, 245-254.
- Chen, C., Dun, S.L., Dun, N.J., Chang, J.K., 1999. Prolactin-releasing peptide-immunoreactivity in A1 and A2 noradrenergic neurons of the rat medulla. *Brain Res.* 822, 276-9.
- Chen, C.Y., Kuo, T.B., Hsieh, I.T., Yang, C.C., 2013. Electrical stimulation of the rostral ventrolateral medulla promotes wakefulness in rats. *Sleep Med.* 14, 1076-84.

- Chen, D., Bassi, J.K., Walther, T., Thomas, W.G., Allen, A.M., 2010. Expression of angiotensin type 1A receptors in C1 neurons restores the sympathoexcitation to angiotensin in the rostral ventrolateral medulla of angiotensin type 1A knockout mice. *Hypertension*. 56, 143-150.
- Chen, F., Dworak, M., Wang, Y., Joo, L.C., Badoer, E., 2008. Role of the hypothalamic PVN in the reflex reduction in mesenteric blood flow elicited by hyperthermia. *Am J Physiol-Regul Integr Comp Physiol*. 295, R1874-R1881.
- Chhor, V., Le Charpentier, T., Lebon, S., Ore, M.V., Celador, I.L., Josserand, J., Degos, V., Jacotot, E., Hagberg, H., Savman, K., Mallard, C., Gressens, P., Fleiss, B., 2013. Characterization of phenotype markers and neuronotoxic potential of polarised primary microglia in vitro. *Brain Behav Immun*. 32, 70-85.
- Chiba, T., Masuko, S., 1987. Synaptic structure of the monoamine and peptide nerve terminals in the intermediolateral nucleus of the guinea pig thoracic spinal cord. *J Comp Neurol*. 262, 242-55.
- Chiba, T., 1989. Direct synaptic contacts of 5-hydroxytryptamine-, neuropeptide Y-, and somatostatin-immunoreactive nerve terminals on the preganglionic sympathetic neurons of the guinea pig. *Neurosci Lett*. 105, 281-6.
- Chiba, T., Semba, R., 1991. Immuno-electronmicroscopic studies on the gamma-aminobutyric acid and glycine receptor in the intermediolateral nucleus of the thoracic spinal cord of rats and guinea pigs. *J Auton Nerv Syst*. 36, 173-181.
- Chida, K., Miyagawa, M., Kawamura, H., Takasu, T., 1998. Effects of chemical stimulation of the rostral ventrolateral medulla on cerebral and renal microcirculation in spontaneously hypertensive rats. *J Auton Nerv Syst*. 70, 51-5.
- Chitravanshi, V.C., Sapru, H.N., 2011. Cardiovascular responses elicited by a new endogenous angiotensin in the nucleus tractus solitarius of the rat. *Am J Physiol- Heart Circ Physiol*. 300, H230-H240.
- Chitravanshi, V.C., Proddutur, A., Sapru, H.N., 2012. Cardiovascular actions of angiotensin-(1-12) in the hypothalamic paraventricular nucleus of the rat are mediated via angiotensin II. *Exp Physiol*. 97, 1001-1017.
- Christopherson, K.S., Ullian, E.M., Stokes, C.C.A., Mallowney, C.E., Hell, J.W., Agah, A., Lawler, J., Mosher, D.F., Bornstein, P., Barres, B.A., 2005. Thrombospondins are astrocyte-secreted proteins that promote CNS synaptogenesis. *Cell*. 120, 421-433.
- Ciriello, J., 1983. Brainstem projections of aortic baroreceptor afferent fibers in the rat. *Neurosci Lett*. 36, 37-42.
- Ciriello, J., Kline, R.L., Zhang, T.X., Caverson, M.M., 1984. Lesions of the paraventricular nucleus alter the development of spontaneous hypertension in the rat. *Brain Res*. 310, 355-9.
- Ciriello, J., Caverson, M.M., 2014. Carotid chemoreceptor afferent projections to leptin receptor containing neurons in nucleus of the solitary tract. *Peptides*. 58, 30-5.
- Coleman, M.J., Dampney, R.A., 1995. Powerful depressor and sympathoinhibitory effects evoked from neurons in the caudal raphe pallidus and obscurus. *Am J Physiol*. 268, R1295-302.
- Coones, A.H., Creech, H.J., Jones, R.N., Berliner, E., 1942. The Demonstration of Pneumococcal Antigen in Tissues by the Use of Fluorescent Antibody. *J Immunol*. 45, 159-170.
- Coote, J.H., 1988. The organisation of cardiovascular neurons in the spinal cord. *Rev Physiol Bioch P*. 110, 147-285.
- Coote, J.H., Yang, Z., Pyner, S., Deering, J., 1998. Control of sympathetic outflows by the hypothalamic paraventricular nucleus. *Clin Exp Pharmacol Physiol*. 25, 461-3.
- Coote, J.H., 2005. A role for the paraventricular nucleus of the hypothalamus in the autonomic control of heart and kidney. *Exp Physiol*. 90, 169-73.

- Coull, J.A., Beggs, S., Boudreau, D., Boivin, D., Tsuda, M., Inoue, K., Gravel, C., Salter, M.W., De Koninck, Y., 2005. BDNF from microglia causes the shift in neuronal anion gradient underlying neuropathic pain. *Nature*. 438, 1017-21.
- Cox, B.F., Brody, M.J., 1989. Subregions of rostral ventral medulla control arterial pressure and regional hemodynamics. *Am J Physiol*. 257, R635-R640.
- Cox, G.M., Kithcart, A.P., Pitt, D., Guan, Z., Alexander, J., Williams, J.L., Shawler, T., Dagia, N.M., Popovich, P.G., Satoskar, A.R., Whitacre, C.C., 2013. Macrophage migration inhibitory factor potentiates autoimmune-mediated neuroinflammation. *J Immunol*. 191, 1043-54.
- Crain, J.M., Nikodemova, M., Watters, J.J., 2013. Microglia express distinct M1 and M2 phenotypic markers in the postnatal and adult central nervous system in male and female mice. *J Neurosci Res*. 91, 1143-51.
- Cravo, S.L., Morrison, S.F., Reis, D.J., 1991. Differentiation of two cardiovascular regions within caudal ventrolateral medulla. *Am J Physiol*. 261, R985-94.
- Cravo, S.L., Morrison, S.F., 1993. The caudal ventrolateral medulla is a source of tonic sympathoinhibition. *Brain Res*. 621, 133-6.
- Cravo, S.L., Campos, R.R., Colombari, E., Sato, M.A., Bergamaschi, C.M., Pedrino, G.R., Ferreira-Neto, M.L., Lopes, O.U., 2009. Role of the medulla oblongata in normal and high arterial blood pressure regulation: the contribution of Escola Paulista de Medicina - UNIFESP. *An Acad Bras Cienc*. 81, 589-603.
- Cronk, J.C., Kipnis, J., 2013. Microglia - the brain's busy bees. *F1000Prime Rep*. 5, 53.
- Cruz, J.C., Bonagamba, L.G., Machado, B.H., Biancardi, V.C., Stern, J.E., 2008. Intermittent activation of peripheral chemoreceptors in awake rats induces Fos expression in rostral ventrolateral medulla-projecting neurons in the paraventricular nucleus of the hypothalamus. *Neuroscience*. 157, 463-72.
- Curtis, K.S., Cunningham, J.T., Heesch, C.M., 1999. Fos expression in brain stem nuclei of pregnant rats after hydralazine-induced hypotension. *Am J Physiol*. 277, R532-40.
- Dahlström, A., Fuxe, K., 1964. Evidence for the existence of monoamine-containing neurons in the central nervous system. I. Demonstration of monoamines in the cell bodies of brain stem neurons. *Acta Physiol Scand*. 62, 1-55.
- Dampney, R.A., Goodchild, A.K., Robertson, L.G., Montgomery, W., 1982. Role of ventrolateral medulla in vasomotor regulation: a correlative anatomical and physiological study. *Brain Res*. 249, 223-35.
- Dampney, R.A., Blessing, W.W., Tan, E., 1988. Origin of tonic GABAergic inputs to vasopressor neurons in the subretrofacial nucleus of the rabbit. *J Auton Nerv Syst*. 24, 227-39.
- Dampney, R.A., McAllen, R.M., 1988. Differential control of sympathetic fibres supplying hindlimb skin and muscle by subretrofacial neurones in the cat. *J Physiol*. 395, 41-56.
- Dampney, R.A., Li, Y.W., Hirooka, Y., Potts, P., Polson, J.W., 1995. Use of c-fos functional mapping to identify the central baroreceptor reflex pathway: advantages and limitations. *Clin Exp Hypertens*. 17, 197-208.
- Dampney, R.A., Horiuchi, J., Tagawa, T., Fontes, M.A., Potts, P.D., Polson, J.W., 2003a. Medullary and supramedullary mechanisms regulating sympathetic vasomotor tone. *Acta Physiol Scand*. 177, 209-18.
- Dampney, R.A.L., Czachurski, J., Dembowski, K., Goodchild, A.K., Seller, H., 1987. Afferent connections and spinal projections of the pressor region in the rostral ventrolateral medulla of the cat. *J Auton Nerv Syst*. 20, 73-86.
- Dampney, R.A.L., 1994. Functional organization of central pathways regulating the cardiovascular system. *Physiol Rev*. 74, 323-364.
- Dampney, R.A.L., Tagawa, T., Horiuchi, J., Fontes, M., Polson, J.W., 2000. What Drives The Tonic Activity Of Presympathetic Neurons In The Rostral Ventrolateral Medulla? *Clin Exper Pharm Physiol*. 27, 1049-1053.

- Dampney, R.A.L., Horiuchi, J., 2003. Functional organisation of central cardiovascular pathways: Studies using c-fos gene expression. *Prog Neurobiol.* 71, 359-384.
- Dampney, R.A.L., Polson, J.W., Potts, P.D., Hirooka, Y., Horiuchi, J., 2003b. Functional organization of brain pathways subserving the baroreceptor reflex: Studies in conscious animals using immediate early gene expression. *Cell Mol Neurobiol.* 23, 597-616.
- Das, M., Vihlen, C.S., Legradi, G., 2007. Hypothalamic and brainstem sources of pituitary adenylate cyclase-activating polypeptide nerve fibers innervating the hypothalamic paraventricular nucleus in the rat. *J Comp Neurol.* 500, 761-76.
- Davalos, D., Grutzendler, J., Yang, G., Kim, J.V., Zuo, Y., Jung, S., Littman, D.R., Dustin, M.L., Gan, W.B., 2005. ATP mediates rapid microglial response to local brain injury in vivo. *Nat Neurosci.* 8, 752-8.
- David, S., Kroner, A., 2011. Repertoire of microglial and macrophage responses after spinal cord injury. *Nat Rev Neurosci.* 12, 388-399.
- Day, T.A., Ferguson, A.V., Renaud, L.P., 1984. Facilitatory influence of noradrenergic afferents on the excitability of rat paraventricular nucleus neurosecretory cells. *J Physiol.* 355, 237-49.
- Day, T.A., Sibbald, J.R., 1990. Involvement of the A1 cell group in baroreceptor inhibition of neurosecretory vasopressin cells. *Neurosci Lett.* 113, 156-62.
- Day, T.A., Sibbald, J.R., Smith, D.W., 1992. A1 neurons and excitatory amino acid receptors in rat caudal medulla mediate vagal excitation of supraoptic vasopressin cells. *Brain Res.* 594, 244-52.
- de Abreu, S.B., Lenhard, A., Mehanna, A., de Souza, H.C., Correa, F.M., Hasser, E.M., Martins-Pinge, M.C., 2009. Role of paraventricular nucleus in exercise training-induced autonomic modulation in conscious rats. *Auton Neurosci.* 148, 28-35.
- De Geyter, D., Stoop, W., Zgavc, T., Sarre, S., Michotte, Y., De Keyser, J., Kooijman, R., 2012. Spontaneously hypertensive rats display reduced microglial activation in response to ischemic stroke and lipopolysaccharide. *J Neuroinflamm.* 9, 114.
- de Groat, W.C., Ryall, R.W., 1969. Reflexes to sacral parasympathetic neurones concerned with micturition in the cat. *J Physiol.* 200, 87-108.
- de Haas, A.H., Boddeke, H.W., Biber, K., 2008. Region-specific expression of immunoregulatory proteins on microglia in the healthy CNS. *Glia.* 56, 888-94.
- de Kloet, A.D., Krause, E.G., Shi, P.D., Zubcevic, J., Raizada, M.K., Sumners, C., 2013. Neuroimmune communication in hypertension and obesity: a new therapeutic angle? *Pharmacol Ther.* 138, 428-40.
- de Kloet, A.D., Liu, M., Rodriguez, V., Krause, E.G., Sumners, C., 2015. Role of neurons and glia in the CNS actions of the renin-angiotensin system in cardiovascular control. *Am J Physiol Regul Integr Comp Physiol.* 309, R444-58.
- de Kloet, A.D., Wang, L., Ludin, J.A., Smith, J.A., Pioquinto, D.J., Hiller, H., Steckelings, U.M., Scheuer, D.A., Sumners, C., Krause, E.G., 2016. Reporter mouse strain provides a novel look at angiotensin type-2 receptor distribution in the central nervous system. *Brain Struct Funct.* 221, 891-912.
- de Paula, P.M., Tolstykh, G., Mifflin, S., 2007. Chronic intermittent hypoxia alters NMDA and AMPA-evoked currents in NTS neurons receiving carotid body chemoreceptor inputs. *Am J Physiol.* 292, R2259-65.
- Dean, C., Seagard, J.L., Hopp, F.A., Kampine, J.P., 1992. Differential control of sympathetic activity to kidney and skeletal muscle by ventral medullary neurons. *J Auton Nerv Syst.* 37, 1-10.
- Dean, C., Bago, M., 2002. Renal sympathoinhibition mediated by 5-HT(1A) receptors in the RVLM during severe hemorrhage in rats. *Am J Physiol Regul Integr Comp Physiol.* 282, R122-30.
- Dejda, A., Sokolowska, P., Nowak, J.Z., 2005. Neuroprotective potential of three neuropeptides PACAP, VIP and PHI. *Pharmacol Rep.* 57, 307-20.

- Dembowsky, K., Czachurski, J., Seller, H., 1986. Three types of sympathetic preganglionic neurones with different electrophysiological properties are identified by intracellular recordings in the cat. *Pflugers Arch.* 406, 112-20.
- Demerens, C., Stankoff, B., Logak, M., Anglade, P., Allinquant, B., Couraud, F., Zalc, B., Lubetzki, C., 1996. Induction of myelination in the central nervous system by electrical activity. *Proc Natl Acad Sci U S A.* 93, 9887-92.
- Deuchars, S.A., Milligan, C.J., Stornetta, R.L., Deuchars, J., 2005. GABAergic neurons in the central region of the spinal cord: a novel substrate for sympathetic inhibition. *J Neurosci.* 25, 1063-70.
- Deuchars, S.A., 2007. Multi-tasking in the spinal cord--do 'sympathetic' interneurons work harder than we give them credit for? *J Physiol.* 580, 723-9.
- DiCarlo, S.E., Bishop, V.S., 2001. Central baroreflex resetting as a means of increasing and decreasing sympathetic outflow and arterial pressure. *Ann N Y Acad Sci.* 940, 324-37.
- Dobbins, E.G., Feldman, J.L., 1994. Brainstem network controlling descending drive to phrenic motoneurons in rat. *J Comp Neurol.* 347, 64-86.
- Donoghue, S., Felder, R.B., Jordan, D., Spyer, K.M., 1984. The central projections of carotid baroreceptors and chemoreceptors in the cat: a neurophysiological study. *J Physiol.* 347, 397-409.
- Donoghue, S., Felder, R.B., Gilbey, M.P., Jordan, D., Spyer, K.M., 1985. Post-synaptic activity evoked in the nucleus tractus solitarius by carotid sinus and aortic nerve afferents in the cat. *J Physiol.* 360, 261-273.
- Douglas, W.W., Ritchie, J.M., Schaumann, W., 1956. Depressor reflexes from medullated and non-medullated fibres in the rabbit's aortic nerve. *J Physiol.* 132, 187-198.
- Dragunow, M., Faull, R., 1989. The use of c-fos as a metabolic marker in neuronal pathway tracing. *J Neurosci Methods.* 29, 261-265.
- Drolet, G., Morilak, D.A., Chalmers, J., 1991. Endogenous opioids tonically inhibit the depressor neurones in the caudal ventrolateral medulla of rabbits: mediation through delta- and kappa-receptors. *Neuropharmacology.* 30, 383-90.
- Dun, N.J., Mo, N., 1989. Inhibitory postsynaptic potentials in neonatal rat sympathetic preganglionic neurones in vitro. *J Physiol.* 410, 267-81.
- Dun, N.J., Dun, S.L., Chiaia, N.L., 1993. Hemorrhage induces Fos immunoreactivity in rat medullary catecholaminergic neurons. *Brain Res.* 608, 223-232.
- Dun, S.L., Ng, Y.K., Brailoiu, G.C., Ling, E.A., Dun, N.J., 2002. Cocaine- and amphetamine-regulated transcript peptide-immunoreactivity in adrenergic C1 neurons projecting to the intermediolateral cell column of the rat. *J Chem Neuroanat.* 23, 123-32.
- Dworak, M., Stebbing, M., Kompa, A.R., Rana, I., Krum, H., Badoer, E., 2012. Sustained activation of microglia in the hypothalamic PVN following myocardial infarction. *Auton Neurosci.* 169, 70-76.
- Dworak, M., Stebbing, M., Kompa, A.R., Rana, I., Krum, H., Badoer, E., 2014. Attenuation of microglial and neuronal activation in the brain by ICV minocycline following myocardial infarction. *Auton Neurosci.* 185, 43-50.
- Elam, M., Yao, T., Thoren, P., Svensson, T.H., 1981. Hypercapnia and hypoxia: chemoreceptor-mediated control of locus coeruleus neurons and splanchnic, sympathetic nerves. *Brain Res.* 222, 373-81.
- Elam, M., Yoa, T., Svensson, T.H., Thoren, P., 1984. Regulation of locus coeruleus neurons and splanchnic, sympathetic nerves by cardiovascular afferents. *Brain Res.* 290, 281-287.
- Elkabes, S., DiCicco-Bloom, E.M., Black, I.B., 1996. Brain microglia/macrophages express neurotrophins that selectively regulate microglial proliferation and function. *J Neurosci.* 16, 2508-21.
- Elliott, J.M., Kapoor, V., Cain, M., West, M.J., Chalmers, J.P., 1985. The mechanism of hypertension and bradycardia following lesions of the caudal ventrolateral medulla in

- the rabbit: the role of sympathetic nerves, circulating adrenaline, vasopressin and renin. *Clin Exp Hypertens A*. 7, 1059-82.
- Erdos, B., Clifton, R.R., Liu, M., Li, H., McCowan, M.L., Sumners, C., Scheuer, D.A., 2015. Novel mechanism within the paraventricular nucleus reduces both blood pressure and hypothalamic pituitary-adrenal axis responses to acute stress. *Am J Physiol Heart Circ Physiol*. 309, H634-45.
- Erickson, J.T., Millhorn, D.E., 1994. Hypoxia and electrical stimulation of the carotid sinus nerve induce Fos-like immunoreactivity within catecholaminergic and serotonergic neurons of the rat brainstem. *J Comp Neurol*. 348, 161-82.
- Eroglu, C., Barres, B.A., 2010. Regulation of synaptic connectivity by glia. *Nature*. 468, 223-31.
- Farber, K., Pannasch, U., Kettenmann, H., 2005. Dopamine and noradrenaline control distinct functions in rodent microglial cells. *Mol Cell Neurosci*. 29, 128-38.
- Farkas, E., Jansen, A.S., Loewy, A.D., 1998. Periaqueductal gray matter input to cardiac-related sympathetic premotor neurons. *Brain Res*. 792, 179-92.
- Farnham, M.M., Li, Q., Goodchild, A.K., Pilowsky, P.M., 2008. PACAP is expressed in sympathoexcitatory bulbospinal C1 neurons of the brain stem and increases sympathetic nerve activity in vivo. *Am J Physiol Regul Integr Comp Physiol*. 294, R1304-11.
- Farnham, M.M., Inglott, M.A., Pilowsky, P.M., 2011. Intrathecal PACAP-38 causes increases in sympathetic nerve activity and heart rate but not blood pressure in the spontaneously hypertensive rat. *Am J Physiol Heart Circ Physiol*. 300, H214-22.
- Farnham, M.M., Lung, M.S., Tallapragada, V.J., Pilowsky, P.M., 2012. PACAP causes PAC1/VPAC2 receptor mediated hypertension and sympathoexcitation in normal and hypertensive rats. *Am J Physiol Heart Circ Physiol*. 303, H910-7.
- Fei, Y., Wang, X., Chen, S., Zhou, Q., Zhang, C., Li, Y., Sun, L., Zhang, L., 2016. Role of the RVM in Descending Pain Regulation Originating from the Cerebrospinal Fluid-Contacting Nucleus. *Neurochem Res*. 41, 1651-61.
- Feldberg, W., Guertzenstein, P.G., 1976. Vasodepressor effects obtained by drugs acting on the ventral surface of the brain stem. *J Physiol*. 258, 337-55.
- Feldman, P.D., Felder, R.B., 1989. α 2-Adrenergic modulation of synaptic excitability in the rat nucleus tractus solitarius. *Brain Res*. 480, 190-197.
- Fields, H.L., Barbaro, N.M., Heinricher, M.M., 1988. Brain stem neuronal circuitry underlying the antinociceptive action of opiates. *Prog Brain Res*. 77, 245-57.
- Finley, J.C., Katz, D.M., 1992. The central organization of carotid body afferent projections to the brainstem of the rat. *Brain Res*. 572, 108-16.
- Fisher, J.P., Paton, J.F.R., 2012. The sympathetic nervous system and blood pressure in humans: Implications for hypertension. *J Hum Hypertens*. 26, 463-475.
- Fontes, M.A., Tagawa, T., Polson, J.W., Cavanagh, S.J., Dampney, R.A., 2001. Descending pathways mediating cardiovascular response from dorsomedial hypothalamic nucleus. *Am J Physiol Heart Circ Physiol*. 280, H2891-901.
- Freiria-Oliveira, A.H., Blanch, G.T., Li, H., Colombari, E., Colombari, D.S., Sumners, C., 2013. Macrophage migration inhibitory factor in the nucleus of solitary tract decreases blood pressure in SHR. *Cardiovasc Res*. 97, 153-60.
- Frühbeis, C., Fröhlich, D., Kuo, W.P., Krämer-Albers, E.-M., 2013. Extracellular vesicles as mediators of neuron-glia communication. *Front Cell Neurosci*. 7.
- Funk, G.D., 2010. The 'connexin' between astrocytes, ATP and central respiratory chemoreception. *J Physiol*. 588, 4335-7.
- Funk, G.D., 2013. Neuromodulation: purinergic signaling in respiratory control. *Compr Physiol*. 3, 331-63.
- Funk, G.D., Rajani, V., Alvares, T.S., Revill, A.L., Zhang, Y., Chu, N.Y., Biancardi, V., Linhares-Taxini, C., Katzell, A., Reklow, R., 2015. Neuroglia and their roles in central

- respiratory control; an overview. *Comp Biochem Physiol A Mol Integr Physiol.* 186, 83-95.
- Gaede, A.H., Pilowsky, P.M., 2010. Catestatin in rat RVLM is sympathoexcitatory, increases barosensitivity, and attenuates chemosensitivity and the somatosympathetic reflex. *Am J Physiol Regul Integr Comp Physiol.* 299, R1538-45.
- Galabov, P.G., 1992. Ultrastructural localization of angiotensin II-like immunoreactivity (A II-LI) in the vegetative networks of the spinal cord of the guinea pig. *J Auton Nerv Syst.* 40, 215-22.
- Gao, H.R., Zhuang, Q.X., Li, B., Li, H.Z., Chen, Z.P., Wang, J.J., Zhu, J.N., 2016. Corticotropin releasing factor excites neurons of posterior hypothalamic nucleus to produce tachycardia in rats. *Sci Rep.* 6, 20206.
- Gao, L., Wang, W.-Z., Wang, W., Zucker, I.H., 2008a. Imbalance of Angiotensin Type 1 Receptor and Angiotensin II Type 2 Receptor in the Rostral Ventrolateral Medulla: Potential Mechanism for Sympathetic Overactivity in Heart Failure. *Hypertension.* 52, 708-714.
- Gao, L., Wang, W., Wang, W., Li, H., Sumners, C., Zucker, I.H., 2008b. Effects of angiotensin type 2 receptor overexpression in the rostral ventrolateral medulla on blood pressure and urine excretion in normal rats. *Hypertension.* 51, 521-7.
- Garrido-Mesa, N., Zarzuelo, A., Galvez, J., 2013. Minocycline: far beyond an antibiotic. *Br J Pharmacol.* 169, 337-52.
- Geraldes, V., Goncalves-Rosa, N., Liu, B., Paton, J.F., Rocha, I., 2014a. Essential role of RVL medullary neuronal activity in the long term maintenance of hypertension in conscious SHR. *Auton Neurosci.* 186, 22-31.
- Geraldes, V., Goncalves-Rosa, N., Liu, B., Paton, J.F., Rocha, I., 2014b. Chronic depression of hypothalamic paraventricular neuronal activity produces sustained hypotension in hypertensive rats. *Exp Physiol.* 99, 89-100.
- Giulian, D., Baker, T.J., 1985. Peptides released by ameboid microglia regulate astroglial proliferation. *J Cell Biol.* 101, 2411-5.
- Giuliano, R., Brezenoff, H.E., 1987. Increased central cholinergic activity in rat models of hypertension. *J Cardiovasc Pharmacol.* 10, 113-22.
- Giuliano, R., Ruggiero, D.A., Morrison, S., Ernsberger, P., Reis, D.J., 1989. Cholinergic regulation of arterial pressure by the C1 area of the rostral ventrolateral medulla. *J Neurosci.* 9, 923-42.
- Glebov, K., Löchner, M., Jabs, R., Lau, T., Merkel, O., Schloss, P., Steinhäuser, C., Walter, J., 2015. Serotonin stimulates secretion of exosomes from microglia cells. *Glia.* 63, 626-634.
- Gonzalez, J.C., Egea, J., Del Carmen Godino, M., Fernandez-Gomez, F.J., Sanchez-Prieto, J., Gandia, L., Garcia, A.G., Jordan, J., Hernandez-Guijo, J.M., 2007. Neuroprotectant minocycline depresses glutamatergic neurotransmission and Ca(2+) signalling in hippocampal neurons. *Eur J Neurosci.* 26, 2481-95.
- Goodchild, A.K., Llewellyn-Smith, I.J., Sun, Q.J., Chalmers, J., Cunningham, A.M., Pilowsky, P.M., 2000a. Calbindin-immunoreactive neurons in the reticular formation of the rat brainstem: catecholamine content and spinal projections. *J Comp Neurol.* 424, 547-62.
- Goodchild, A.K., Van Deurzen, B.T., Sun, Q.J., Chalmers, J., Pilowsky, P.M., 2000b. Spinal GABA(A) receptors do not mediate the sympathetic baroreceptor reflex in the rat. *Am J Physiol.* 279, R320-31.
- Gordon, F.J., 1987. Aortic baroreceptor reflexes are mediated by NMDA receptors in caudal ventrolateral medulla. *Am J Physiol.* 252, R628-33.
- Graham, J.C., Hoffman, G.E., Sved, A.F., 1995. c-Fos expression in brain in response to hypotension and hypertension in conscious rats. *J Auton Nerv Syst.* 55, 92-104.
- Grassi, G., Seravalle, G., Quarti-Trevano, F., 2010. The 'neuroadrenergic hypothesis' in hypertension: current evidence. *Exp Physiol.* 95, 581-6.

- Gray, T.K., Lewis, E., 3rd, Maher, T.J., Ally, A., 2001. AMPA-receptor blockade within the RVLM modulates cardiovascular responses via glutamate during peripheral stimuli. *Pharmacol Res.* 43, 47-54.
- Green, C.R., Nicholson, L.F., 2008. Interrupting the inflammatory cycle in chronic diseases--do gap junctions provide the answer? *Cell Biol Int.* 32, 1578-83.
- Griffin, W.S., 2006. Inflammation and neurodegenerative diseases. *Am J Clin Nutr.* 83, 470S-474S.
- Grkovic, I., Fernandez, K., McAllen, R.M., Anderson, C.R., 2005. Misidentification of cardiac vagal pre-ganglionic neurons after injections of retrograde tracer into the pericardial space in the rat. *Cell Tissue Res.* 321, 335-40.
- Guertzenstein, P.G., Silver, A., 1974. Fall in blood pressure produced from discrete regions of the ventral surface of the medulla by glycine and lesions. *J Physiol.* 242, 489-503.
- Guyenet, P.G., 1984. Baroreceptor-mediated inhibition of A5 noradrenergic neurons. *Brain Res.* 303, 31-40.
- Guyenet, P.G., Filtz, T.M., Donaldson, S.R., 1987. Role of excitatory amino acids in rat vagal and sympathetic baroreflexes. *Brain Res.* 407, 272-84.
- Guyenet, P.G., Koshiya, N., Huangfu, D., Verberne, A.J., Riley, T.A., 1993. Central respiratory control of A5 and A6 pontine noradrenergic neurons. *Am J Physiol.* 264, R1035-44.
- Guyenet, P.G., Koshiya, N., 1995. Working model of the sympathetic chemoreflex in rats. *Clin Exp Hypertens.* 17, 167-79.
- Guyenet, P.G., Stornetta, R.L., Weston, M.C., McQuiston, T., Simmons, J.R., 2004. Detection of amino acid and peptide transmitters in physiologically identified brainstem cardiorespiratory neurons. *Auton Neurosci.* 114, 1-10.
- Guyenet, P.G., 2006. The sympathetic control of blood pressure. *Nat Rev Neurosci.* 7, 335-46.
- Guyenet, P.G., Stornetta, R.L., Abbott, S.B., Depuy, S.D., Kanbar, R., 2012. The retrotrapezoid nucleus and breathing. *Adv Exp Med Biol.* 758, 115-22.
- Guyenet, P.G., Stornetta, R.L., Bochorishvili, G., Depuy, S.D., Burke, P.G., Abbott, S.B., 2013. C1 neurons: the body's EMTs. *Am J Physiol Regul Integr Comp Physiol.* 305, R187-204.
- Guyenet, P.G., Bayliss, D.A., 2015. Neural Control of Breathing and CO₂ Homeostasis. *Neuron.* 87, 946-61.
- Guyenet, P.G., Bayliss, D.A., Stornetta, R.L., Ludwig, M.G., Kumar, N.N., Shi, Y., Burke, P.G., Kanbar, R., Basting, T.M., Holloway, B.B., Wenker, I.C., 2016. Proton detection and breathing regulation by the retrotrapezoid nucleus. *J Physiol.* 594, 1529-51.
- Gyllenstein, L., Malmfors, T., 1963. Myelination of the optic nerve and its dependence on visual function--a quantitative investigation in mice. *J Embryol Exp Morphol.* 11, 255-66.
- H'Doubler, P.B., Jr., Peterson, M., Shek, W., Auchincloss, H., Abbott, W.M., Orkin, R.W., 1991. Spontaneously hypertensive and Wistar Kyoto rats are genetically disparate. *Lab Anim Sci.* 41, 471-3.
- Habeebullah, H., Alsuhaymi, N., Stebbing, M.J., Jenkins, T.A., Badoer, E., 2016. Central leptin and resistin combined elicits enhanced central effects on renal sympathetic nerve activity. *Exp Physiol.* 101, 791-800.
- Hagino, Y., Kariura, Y., Manago, Y., Amano, T., Wang, B., Sekiguchi, M., Nishikawa, K., Aoki, S., Wada, K., Noda, M., 2004. Heterogeneity and potentiation of AMPA type of glutamate receptors in rat cultured microglia. *Glia.* 47, 68-77.
- Haibara, A.S., Colombari, E., Chianca, D.A., Jr., Bonagamba, L.G., Machado, B.H., 1995. NMDA receptors in NTS are involved in bradycardic but not in pressor response of chemoreflex. *Am J Physiol.* 269, H1421-7.
- Haibara, A.S., Bonagamba, L.G., Machado, B.H., 1999. Sympathoexcitatory neurotransmission of the chemoreflex in the NTS of awake rats. *Am J Physiol.* 276, R69-80.

- Hailer, N.P., Järhult, J.D., Nitsch, R., 1996. Resting microglial cells in vitro: Analysis of morphology and adhesion molecule expression in organotypic hippocampal slice cultures. *Glia*. 18, 319-331.
- Hanisch, U.K., Kettenmann, H., 2007. Microglia: active sensor and versatile effector cells in the normal and pathologic brain. *Nat Neurosci*. 10, 1387-94.
- Hanisch, U.K., 2013. Functional diversity of microglia - how heterogeneous are they to begin with? *Front Cell Neurosci*. 7, 65.
- Hanna, B.D., Lioy, F., Polosa, C., 1981. Role of carotid and central chemoreceptors in the CO₂ response of sympathetic preganglionic neurons. *J Auton Nerv Syst*. 3, 421-35.
- Hara, K., Miyawaki, T., Minson, J., Arnolda, L., Llewellyn-Smith, I., Chalmers, J., Pilowsky, P., 1997. Role of spinal GABA receptors in depressor responses to chemical stimulation of the A5 area in normal and hypertensive rats. *J Auton Nerv Syst*. 66, 53-61.
- Hara, K., Harris, R.A., 2002. The anesthetic mechanism of urethane: the effects on neurotransmitter-gated ion channels. *Anesth Analg*. 94, 313-8.
- Haselton, J.R., Guyenet, P.G., 1989. Electrophysiological characterization of putative C1 adrenergic neurons in the rat. *Neuroscience*. 30, 199-214.
- Haselton, J.R., Guyenet, P.G., 1990. Ascending collaterals of medullary barosensitive neurons and C1 cells in rats. *Am J Physiol*. 258, R1051-63.
- Hayes, K., Weaver, L.C., 1990. Selective control of sympathetic pathways to the kidney, spleen and intestine by the ventrolateral medulla in rats. *J Physiol*. 428, 371-385.
- Head, G.A., Badoer, E., Korner, P.I., 1987. Cardiovascular role of A1 catecholaminergic neurons in the rabbit. Effect of chronic lesions on responses to methyl dopa, clonidine and 6-OHDA induced transmitter release. *Brain Res*. 412, 18-28.
- Heinricher, M.M., Tavares, I., Leith, J.L., Lumb, B.M., 2009. Descending control of nociception: Specificity, recruitment and plasticity. *Brain Res Rev*. 60, 214-25.
- Helke, C.J., Phillips, E.T., 1988. Thyrotropin-releasing hormone receptor activation in the spinal cord increases blood pressure and sympathetic tone to the vasculature and the adrenals. *J Pharmacol Exp Ther*. 245, 41-6.
- Herbert, H., Saper, C.B., 1992. Organization of medullary adrenergic and noradrenergic projections to the periaqueductal gray matter in the rat. *J Comp Neurol*. 315, 34-52.
- Hershkowitz, M., Eliash, S., Cohen, S., 1982. The muscarinic cholinergic receptors in the posterior hypothalamus of hypertensive and normotensive rats. *Eur J Pharmacol*. 86, 229-36.
- Herzig, T.C., Buchholz, R.A., Haywood, J.R., 1991. Effects of paraventricular nucleus lesions on chronic renal hypertension. *Am J Physiol*. 261, H860-7.
- Heslop, D.J., Keay, K.A., Bandler, R., 2002. Haemorrhage-evoked compensation and decompensation are mediated by distinct caudal midline medullary regions in the urethane-anaesthetised rat. *Neuroscience*. 113, 555-567.
- Heslop, D.J., Bandler, R., Keay, K.A., 2004. Haemorrhage-evoked decompensation and recompensation mediated by distinct projections from rostral and caudal midline medulla in the rat. *Eur J Neurosci*. 20, 2096-110.
- Ho"kfelt, T., Fuxe, K., Goldstein, M., Johansson, O., 1974. Immunohistochemical evidence for the existence of adrenaline neurons in the rat brain. *Brain Res*. 66, 235-251.
- Holloway, B.B., Stornetta, R.L., Bochorishvili, G., Erisir, A., Viar, K.E., Guyenet, P.G., 2013. Monosynaptic glutamatergic activation of locus coeruleus and other lower brainstem noradrenergic neurons by the C1 cells in mice. *J Neurosci*. 33, 18792-805.
- Holloway, B.B., Viar, K.E., Stornetta, R.L., Guyenet, P.G., 2015. The retrotrapezoid nucleus stimulates breathing by releasing glutamate in adult conscious mice. *Eur J Neurosci*. 42, 2271-82.
- Horiuchi, J., Dampney, R.A., 1998. Dependence of sympathetic vasomotor tone on bilateral inputs from the rostral ventrolateral medulla in the rabbit: role of baroreceptor reflexes. *Neurosci Lett*. 248, 113-6.

- Horiuchi, J., Killinger, S., Dampney, R.A., 2004. Contribution to sympathetic vasomotor tone of tonic glutamatergic inputs to neurons in the RVLM. *Am J Physiol* 287, R1335-43.
- Horiuchi, J., Atik, A., Iigaya, K., McDowall, L.M., Killinger, S., Dampney, R.A., 2011. Activation of 5-hydroxytryptamine-1A receptors suppresses cardiovascular responses evoked from the paraventricular nucleus. *Am J Physiol Regul Integr Comp Physiol* 301, R1088-97.
- Hortega, D.R., 1928. Tercera aportacion al conocimiento morfologico e interpretacion funcional de la oligodendroglia. *Memor Real Soc Esp Hist Nat.* 14, 5-122.
- Hosoya, Y., 1985. Hypothalamic projections to the ventral medulla oblongata in the rat, with special reference to the nucleus raphe pallidus: a study using autoradiographic and HRP techniques. *Brain Res.* 344, 338-50.
- Housley, G.D., Martin-Body, R.L., Dawson, N.J., Sinclair, J.D., 1987. Brain stem projections of the glossopharyngeal nerve and its carotid sinus branch in the rat. *Neuroscience.* 22, 237-50.
- Howe, B.M., Bruno, S.B., Higgs, K.A., Stigers, R.L., Cunningham, J.T., 2004. FosB expression in the central nervous system following isotonic volume expansion in unanesthetized rats. *Exp Neurol.* 187, 190-8.
- Hu, X., Li, P., Guo, Y., Wang, H., Leak, R.K., Chen, S., Gao, Y., Chen, J., 2012. Microglia/macrophage polarization dynamics reveal novel mechanism of injury expansion after focal cerebral ischemia. *Stroke.* 43, 3063-3070.
- Hughes, V., 2012. Microglia: The constant gardeners. *Nature.* 485, 570-2.
- Hutchinson, M.R., Northcutt, A.L., Chao, L.W., Kearney, J.J., Zhang, Y., Berkelhammer, D.L., Loram, L.C., Rozeske, R.R., Bland, S.T., Maier, S.F., Gleeson, T.T., Watkins, L.R., 2008. Minocycline suppresses morphine-induced respiratory depression, suppresses morphine-induced reward, and enhances systemic morphine-induced analgesia. *Brain Behav Immun.* 22, 1248-56.
- Huxtable, A.G., Zwicker, J.D., Poon, B.Y., Pagliardini, S., Vrouwe, S.Q., Greer, J.J., Funk, G.D., 2009. Tripartite purinergic modulation of central respiratory networks during perinatal development: the influence of ATP, ectonucleotidases, and ATP metabolites. *J Neurosci.* 29, 14713-25.
- Huxtable, A.G., Zwicker, J.D., Alvares, T.S., Ruangkittisakul, A., Fang, X., Hahn, L.B., Posse de Chaves, E., Baker, G.B., Ballanyi, K., Funk, G.D., 2010. Glia contribute to the purinergic modulation of inspiratory rhythm-generating networks. *J Neurosci.* 30, 3947-58.
- Hwang, K.R., Chan, S.H., Chan, J.Y., 1998. Noradrenergic neurotransmission at PVN in locus ceruleus-induced baroreflex suppression in rats. *Am J Physiol.* 274, H1284-92.
- Illig, K.A., Levy, M., Sanchez, L., Trachiotis, G.D., Shanley, C., Irwin, E., Pertile, T., Kieval, R., Cody, R., 2006. An implantable carotid sinus stimulator for drug-resistant hypertension: surgical technique and short-term outcome from the multicenter phase II Rheos feasibility trial. *J Vasc Surg.* 44, 1213-1218.
- Inglott, M.A., Farnham, M.M., Pilowsky, P.M., 2011. Intrathecal PACAP-38 causes prolonged widespread sympathoexcitation via a spinally mediated mechanism and increases in basal metabolic rate in anesthetized rat. *Am J Physiol Heart Circ Physiol.* 300, H2300-7.
- Inglott, M.A., Lerner, E.A., Pilowsky, P.M., Farnham, M.M., 2012. Activation of PAC(1) and VPAC receptor subtypes elicits differential physiological responses from sympathetic preganglionic neurons in the anaesthetized rat. *Br J Pharmacol.* 167, 1089-98.
- Inokuchi, H., Yoshimura, M., Yamada, S., Polosa, C., Nishi, S., 1992. Fast excitatory postsynaptic potentials and the responses to excitant amino acids of sympathetic preganglionic neurons in the slice of the cat spinal cord. *Neuroscience.* 46, 657-667.
- Inoue, K., 2006. The function of microglia through purinergic receptors: neuropathic pain and cytokine release. *Pharmacol Ther.* 109, 210-26.

- Ito, S., Sved, A.F., 1996. Blockade of angiotensin receptors in rat rostral ventrolateral medulla removes excitatory vasomotor tone. *Am J Physiol.* 270, R1317-23.
- Ito, S., Sved, A.F., 1997. Tonic glutamate-mediated control of rostral ventrolateral medulla and sympathetic vasomotor tone. *Am J Physiol.* 273, R487-94.
- Ito, S., Komatsu, K., Tsukamoto, K., Sved, A.F., 2000. Excitatory amino acids in the rostral ventrolateral medulla support blood pressure in spontaneously hypertensive rats. *Hypertension.* 35, 413-7.
- Ito, S., Komatsu, K., Tsukamoto, K., Sved, A.F., 2001. Tonic Excitatory Input to the Rostral Ventrolateral Medulla in Dahl Salt-Sensitive Rats. *Hypertension.* 37, 687-691.
- Izzo, P.N., Deuchars, J., Spyer, K.M., 1993. Localization of cardiac vagal preganglionic motoneurons in the rat: immunocytochemical evidence of synaptic inputs containing 5-hydroxytryptamine. *J Comp Neurol.* 327, 572-83.
- Jancovski, N., Bassi, J.K., Carter, D.A., Choong, Y.T., Connelly, A., Nguyen, T.P., Chen, D., Lukoshkova, E.V., Menuet, C., Head, G.A., Allen, A.M., 2013. Stimulation of angiotensin type 1A receptors on catecholaminergic cells contributes to angiotensin-dependent hypertension. *Hypertension.* 62, 866-71.
- Jancovski, N., Carter, D.A., Connelly, A.A., Stevens, E., Bassi, J.K., Menuet, C., Allen, A.M., 2014. Angiotensin type 1A receptor expression in C1 neurons of the rostral ventrolateral medulla contributes to the development of angiotensin-dependent hypertension. *Exp Physiol.* 99, 1597-610.
- Janig, W., Sato, A., Schmidt, R.F., 1972. Reflexes in postganglionic cutaneous fibres by stimulation of group I to group IV somatic afferents. *Pflugers Arch.* 331, 244-56.
- Jansen, A.S., Loewy, A.D., 1997. Neurons lying in the white matter of the upper cervical spinal cord project to the intermediolateral cell column. *Neuroscience.* 77, 889-98.
- Jansen, A.S.P., Wessendorf, M.W., Loewy, A.D., 1995. Transneuronal labeling of CNS neuropeptide and monoamine neurons after pseudorabies virus injections into the stellate ganglion. *Brain Res.* 683, 1-24.
- Janssen, S., Gudi, V., Prajeeth, C.K., Singh, V., Stahl, K., Heckers, S., Skripuletz, T., Pul, R., Trebst, C., Tsiavaliaris, G., Stangel, M., 2014. A pivotal role of nonmuscle myosin II during microglial activation. *Exp Neurol.* 261, 666-76.
- Jensen, I., Llewellyn-Smith, I.J., Pilowsky, P., Minson, J.B., Chalmers, J., 1995. Serotonin inputs to rabbit sympathetic preganglionic neurons projecting to the superior cervical ganglion or adrenal medulla. *J Comp Neurol.* 353, 427-38.
- Jeske, I., Reis, D.J., Milner, T.A., 1995. Neurons in the barosensory area of the caudal ventrolateral medulla project monosynaptically on to sympathoexcitatory bulbospinal neurons in the rostral ventrolateral medulla. *Neuroscience.* 65, 343-353.
- Jiang, N., Shi, P., Desland, F., Kitchen-Pareja, M.C., Sumners, C., 2013. Interleukin-10 inhibits angiotensin II-induced decrease in neuronal potassium current. *Am J Physiol Cell Physiol.* 304, C801-7.
- Jones, B.E., Yang, T.Z., 1985. The efferent projections from the reticular formation and the locus coeruleus studied by anterograde and retrograde axonal transport in the rat. *J Comp Neurol.* 242, 56-92.
- Judy, W.V., Watanabe, A.M., Henry, D.P., Besch, H.R., Jr., Murphy, W.R., Hockel, G.M., 1976. Sympathetic nerve activity: role in regulation of blood pressure in the spontaneously hypertensive rat. *Circ Res.* 38, 21-9.
- Juranek, J.K., Wojtkiewicz, J.A., 2015. Origins and neurochemical complexity of preganglionic neurons supplying the superior cervical ganglion in the domestic pig. *J Mol Neurosci.* 55, 297-304.
- Kanbar, R., Depuy, S.D., West, G.H., Stornetta, R.L., Guyenet, P.G., 2011. Regulation of visceral sympathetic tone by A5 noradrenergic neurons in rodents. *J Physiol.* 589, 903-17.

- Kannan, H., Osaka, T., Kasai, M., Okuya, S., Yamashita, H., 1986. Electrophysiological properties of neurons in the caudal ventrolateral medulla projecting to the paraventricular nucleus of the hypothalamus in rats. *Brain Res.* 376, 342-50.
- Kannan, H., Nijima, A., Yamashita, H., 1988. Effects of stimulation of the hypothalamic paraventricular nucleus on blood pressure and renal sympathetic nerve activity. *Brain Res Bull.* 20, 779-83.
- Kannan, H., Tanaka, Y., Kunitake, T., Ueta, Y., Hayashida, Y., Yamashita, H., 1996. Activation of sympathetic outflow by recombinant human interleukin-1 beta in conscious rats. *Am J Physiol.* 270, R479-85.
- Kantzides, A., Badoer, E., 2005. nNOS-containing neurons in the hypothalamus and medulla project to the RVLM. *Brain Res.* 1037, 25-34.
- Kapoor, K., Bhandare, A.M., Farnham, M.M., Pilowsky, P.M., 2015. Alerted microglia and the sympathetic nervous system: A novel form of microglia in the development of hypertension. *Respir Physiol Neurobiol.* 226, 51-62.
- Kapoor, K., Bhandare, A.M., Mohammed, S., Farnham, M.M., Pilowsky, P.M., 2016a. Microglial number is related to the number of tyrosine hydroxylase neurons in SHR and normotensive rats. *Auton Neurosci.* 198, 10-8.
- Kapoor, K., Bhandare, A.M., Nedoboy, P.E., Mohammed, S., Farnham, M.M., Pilowsky, P.M., 2016b. Dynamic changes in the relationship of microglia to cardiovascular neurons in response to increases and decreases in blood pressure. *Neuroscience.* 329, 12-29.
- Karperien, A., Ahammer, H., Jelinek, H.F., 2013. Quantitating the subtleties of microglial morphology with fractal analysis. *Front Cell Neurosci.* 7, 3.
- Kashihara, K., McMullan, S., Lonergan, T., Goodchild, A.K., Pilowsky, P.M., 2008. Neuropeptide Y in the rostral ventrolateral medulla blocks somatosympathetic reflexes in anesthetized rats. *Auton Neurosci.* 142, 64-70.
- Kawabe, T., Kawabe, K., Sapru, H.N., 2007. Cardiovascular responses to somatosensory stimulation and their modulation by baroreflex mechanisms. *Clin Exp Hypertens.* 29, 403-18.
- Kawabe, T., Chitravanshi, V.C., Kawabe, K., Sapru, H.N., 2008. Cardiovascular function of a glutamatergic projection from the hypothalamic paraventricular nucleus to the nucleus tractus solitarius in the rat. *Neuroscience.* 153, 605-617.
- Kawabe, T., Kawabe, K., Sapru, H.N., 2014. Cardiovascular effect of angiotensin-(1-12) in the caudal ventrolateral medullary depressor area of the rat. *Am J Physiol Heart Circ Physiol.* 306, H438-49.
- Kawabe, T., Ueyama, T., Hano, T., Sapru, H.N., 2015. Cardiovascular responses to microinjections of endomorphin-2 into the nucleus of the solitary tract are attenuated in the spontaneously hypertensive rat. *Clin Exp Hypertens.* 37, 197-206.
- Kawabe, T., Iwasa, M., Kawabe, K., Sapru, H.N., 2016. Attenuation of angiotensin type 2 receptor function in the rostral ventrolateral medullary pressor area of the spontaneously hypertensive rat. *Clin Exp Hypertens.* 38, 209-17.
- Kawano, H., Masuko, S., 2010. Region-specific projections from the subfornical organ to the paraventricular hypothalamic nucleus in the rat. *Neuroscience.* 169, 1227-34.
- Kettenmann, H., Hanisch, U.K., Noda, M., Verkhratsky, A., 2011. Physiology of microglia. *Physiol Rev.* 91, 461-553.
- Kettenmann, H., Kirchhoff, F., Verkhratsky, A., 2013. Microglia: new roles for the synaptic stripper. *Neuron.* 77, 10-8.
- Kiely, J.M., Gordon, F.J., 1993. Non-NMDA receptors in the rostral ventrolateral medulla mediate somatosympathetic pressor responses. *J Auton Nerv Syst.* 43, 231-9.
- Kigerl, K.A., Gensel, J.C., Ankeny, D.P., Alexander, J.K., Donnelly, D.J., Popovich, P.G., 2009. Identification of two distinct macrophage subsets with divergent effects causing either neurotoxicity or regeneration in the injured mouse spinal cord. *J Neurosci.* 29, 13435-44.

- Kim, J., Waldvogel, H.J., Faull, R.L., Curtis, M.A., Nicholson, L.F., 2015. The RAGE receptor and its ligands are highly expressed in astrocytes in a grade-dependant manner in the striatum and subependymal layer in Huntington's disease. *J Neurochem.* 134, 927-42.
- Kline, D.D., King, T.L., Austgen, J.R., Heesch, C.M., Hasser, E.M., 2010. Sensory afferent and hypoxia-mediated activation of nucleus tractus solitarius neurons that project to the rostral ventrolateral medulla. *Neuroscience.* 167, 510-527.
- Koganezawa, T., Paton, J.F., 2014. Intrinsic chemosensitivity of rostral ventrolateral medullary sympathetic premotor neurons in the in situ arterially perfused preparation of rats. *Exp Physiol.* 99, 1453-66.
- Koizumi, S., Ohsawa, K., Inoue, K., Kohsaka, S., 2013. Purinergic receptors in microglia: functional modal shifts of microglia mediated by P2 and P1 receptors. *Glia.* 61, 47-54.
- Korsak, A., Gilbey, M.P., 2004. Rostral ventromedial medulla and the control of cutaneous vasoconstrictor activity following i.c.v. prostaglandin E(1). *Neuroscience.* 124, 709-17.
- Koshiya, N., Huangfu, D., Guyenet, P.G., 1993. Ventrolateral medulla and sympathetic chemoreflex in the rat. *Brain Res Rev.* 609, 174-184.
- Koshiya, N., Guyenet, P.G., 1994. A5 noradrenergic neurons and the carotid sympathetic chemoreflex. *Am J Physiol.* 267, R519-26.
- Koshiya, N., Guyenet, P.G., 1996. NTS neurons with carotid chemoreceptor inputs arborize in the rostral ventrolateral medulla. *Am J Physiol.* 270, R1273-8.
- Kougias, P., Weakley, S.M., Yao, Q., Lin, P.H., Chen, C., 2010. Arterial baroreceptors in the management of systemic hypertension. *Med Sci Monit.* 16, RA1-8.
- Kovacs, K.J., 2008. Measurement of immediate-early gene activation- c-fos and beyond. *J Neuroendocrinol.* 20, 665-72.
- Kozelka, J.W., Chung, J.M., Wurster, R.D., 1981. Ascending spinal pathways mediating somato-cardiovascular reflexes. *J Auton Nerv Syst.* 3, 171-5.
- Kozlowski, C., Weimer, R.M., 2012. An automated method to quantify microglia morphology and application to monitor activation state longitudinally in vivo. *PLoS ONE.* 7.
- Krassioukov, A.V., Weaver, L.C., 1993. Connections between the pontine reticular formation and rostral ventrolateral medulla. *Am J Physiol.* 265, H1386-H1392.
- Kreutzberg, G.W., 1996. Microglia: a sensor for pathological events in the CNS. *Trends Neurosci.* 19, 312-318.
- Kroner, A., Greenhalgh, A.D., Zaruk, J.G., PassosdosSantos, R., Gaestel, M., David, S., 2014. TNF and Increased Intracellular Iron Alter Macrophage Polarization to a Detrimental M1 Phenotype in the Injured Spinal Cord. *Neuron.* 83, 1098-1116.
- Krukoff, T.L., Ciriello, J., Calaresu, F.R., 1985. Segmental distribution of peptide- and 5HT-like immunoreactivity in nerve terminals and fibers of the thoracolumbar sympathetic nuclei of the cat. *J Comp Neurol.* 240, 103-16.
- Krukoff, T.L., 1987a. Neuropeptide Y-like immunoreactivity in cat spinal cord with special reference to autonomic areas. *Brain Res.* 415, 300-8.
- Krukoff, T.L., 1987b. Coexistence of neuropeptides in sympathetic preganglionic neurons of the cat. *Peptides.* 8, 109-12.
- Kubo, T., Tatsumi, M., 1979. Increased pressor responses to physostigmine in spontaneously hypertensive rats. *Naunyn Schmiedebergs Arch Pharmacol.* 306, 81-3.
- Kubo, T., Kihara, M., 1987a. Studies on GABAergic mechanisms responsible for cardiovascular regulation in the rostral ventrolateral medulla of the rat. *Arch Int Pharmacodyn Ther.* 285, 277-87.
- Kubo, T., Kihara, M., 1987b. Evidence for the presence of GABAergic and glycine-like systems responsible for cardiovascular control in the nucleus tractus solitarii of the rat. *Neurosci Lett.* 74, 331-336.
- Kubo, T., Kihara, M., 1988. Evidence for gamma-aminobutyric acid receptor-mediated modulation of the aortic baroreceptor reflex in the nucleus tractus solitarii of the rat. *Neurosci Lett.* 89, 156-60.

- Kubo, T., Ishizuka, T., Asari, T., Fukumori, R., 1995. Acetylcholine release in the rostral ventrolateral medulla of spontaneously hypertensive rats. *Clin Exp Pharmacol Physiol Suppl.* 22, S40-2.
- Kubo, T., Taguchi, K., Sawai, N., Ozaki, S., Hagiwara, Y., 1997. Cholinergic mechanisms responsible for blood pressure regulation on sympathoexcitatory neurons in the rostral ventrolateral medulla of the rat. *Brain Res Bull.* 42, 199-204.
- Kubo, T., Hagiwara, Y., Sekiya, D., Chiba, S., Fukumori, R., 2000. Cholinergic inputs to rostral ventrolateral medulla pressor neurons from hypothalamus. *Brain Res Bull.* 53, 275-82.
- Kumada, M., Terui, N., Kuwaki, T., 1990. Arterial baroreceptor reflex: its central and peripheral neural mechanisms. *Prog Neurobiol.* 35, 331-61.
- Kumar, N.N., Ferguson, J., Padley, J.R., Pilowsky, P.M., Goodchild, A.K., 2009. Differential muscarinic receptor gene expression levels in the ventral medulla of spontaneously hypertensive and Wistar-Kyoto rats: role in sympathetic baroreflex function. *J Hypertens.* 27, 1001-8.
- Kumar, N.N., Velic, A., Soliz, J., Shi, Y., Li, K., Wang, S., Weaver, J.L., Sen, J., Abbott, S.B., Lazarenko, R.M., Ludwig, M.G., Perez-Reyes, E., Mohebbi, N., Bettoni, C., Gassmann, M., Suply, T., Seuwen, K., Guyenet, P.G., Wagner, C.A., Bayliss, D.A., 2015. Regulation of breathing by CO(2) requires the proton-activated receptor GPR4 in retrotrapezoid nucleus neurons. *Science.* 348, 1255-60.
- Kumar, P., Prabhakar, N.R., 2012. Peripheral chemoreceptors: function and plasticity of the carotid body. *Compr Physiol.* 2, 141-219.
- Kung, L.-H., Glasgow, J., Ruszaj, A., Gray, T., Scrogin, K.E., 2010. Serotonin neurons of the caudal raphe nuclei contribute to sympathetic recovery following hypotensive hemorrhage. *Am J Physiol.* 298, R939-R953.
- Kuperman, A.S., Volpert, W.A., Okamoto, M., 1964. Release of Adenine Nucleotide from Nerve Axons. *Nature.* 204, 1000-1.
- Kuwana, S., Tsunekawa, N., Yanagawa, Y., Okada, Y., Kuribayashi, J., Obata, K., 2006. Electrophysiological and morphological characteristics of GABAergic respiratory neurons in the mouse pre-Botzinger complex. *Eur J Neurosci.* 23, 667-74.
- Kvochina, L., Hasser, E.M., Heesch, C.M., 2007. Pregnancy increases baroreflex-independent GABAergic inhibition of the RVLM in rats. *Am J Physiol Regul Integr Comp Physiol.* 293, R2295-305.
- Lacerda, J.E.C., Campos, R.R., Araujo, G.C., Andreatta-Van Leyen, S., Lopes, O.U., Guertzenstein, P.G., 2003. Cardiovascular responses to microinjections of GABA or anesthetics into the rostral ventrolateral medulla of conscious and anesthetized rats. *Braz J Med Biol Res.* 36, 1269-1277.
- Lawrence, A.J., Jarrott, B., 1996. Neurochemical modulation of cardiovascular control in the nucleus tractus solitarius. *Prog Neurobiol.* 48, 21-53.
- Lawson, L.J., Perry, V.H., Dri, P., Gordon, S., 1990. Heterogeneity in the distribution and morphology of microglia in the normal adult mouse brain. *Neuroscience.* 39, 151-170.
- Lee, M., 2013. Neurotransmitters and microglial-mediated neuroinflammation. *Curr Protein Pept Sci.* 14, 21-32.
- Lewis, D.I., Coote, J.H., 1996. Baroreceptor-induced inhibition of sympathetic neurons by GABA acting at a spinal site. *Am J Physiol.* 270, H1885-92.
- Lewis, D.I., Coote, J.H., 2008. Electrophysiological characteristics of vasomotor preganglionic neurons and related neurons in the thoracic spinal cord of the rat: An intracellular study in vivo. *Neuroscience.* 152, 534-546.
- Li, A., Emond, L., Nattie, E., 2008a. Brainstem catecholaminergic neurons modulate both respiratory and cardiovascular function. *Adv Exp Med Biol.* 605, 371-6.
- Li, A., Hindmarch, C.C., Nattie, E.E., Paton, J.F., 2013. Antagonism of orexin receptors significantly lowers blood pressure in spontaneously hypertensive rats. *J Physiol.* 591, 4237-48.

- Li, D.-P., Pan, H.-L., 2007. Glutamatergic Inputs in the Hypothalamic Paraventricular Nucleus Maintain Sympathetic Vasomotor Tone in Hypertension. *Hypertension*. 49, 916-925.
- Li, H., Gao, Y., Qi, Y., Katovich, M.J., Jiang, N., Braseth, L.N., Scheuer, D.A., Shi, P., Sumners, C., 2008b. Macrophage migration inhibitory factor in hypothalamic paraventricular nucleus neurons decreases blood pressure in spontaneously hypertensive rats. *FASEB J*. 22, 3175-85.
- Li, Q., Goodchild, A.K., Seyedabadi, M., Pilowsky, P.M., 2005. Pre-protachykinin A mRNA is colocalized with tyrosine hydroxylase-immunoreactivity in bulbospinal neurons. *Neuroscience*. 136, 205-16.
- Li, X.C., Beart, P.M., Monn, J.A., Jones, N.M., Widdop, R.E., 1999. Type I and II metabotropic glutamate receptor agonists and antagonists evoke cardiovascular effects after intrathecal administration in conscious rats. *Br J Pharmacol*. 128, 823-9.
- Li, Y., Du, X.F., Liu, C.S., Wen, Z.L., Du, J.L., 2012. Reciprocal regulation between resting microglial dynamics and neuronal activity in vivo. *Dev Cell*. 23, 1189-202.
- Li, Y.W., Gieroba, Z.J., Blessing, W.W., 1992a. Chemoreceptor and baroreceptor responses of A1 area neurons projecting to supraoptic nucleus. *Am J Physiol*. 263, R310-7.
- Li, Y.W., Wesselingh, S.L., Blessing, W.W., 1992b. Projections from rabbit caudal medulla to C1 and A5 sympathetic premotor neurons, demonstrated with phaseolus leucoagglutinin and herpes simplex virus. *J Comp Neurol*. 317, 379-95.
- Li, Y.W., Dampney, R.A., 1994. Expression of Fos-like protein in brain following sustained hypertension and hypotension in conscious rabbits. *Neuroscience*. 61, 613-34.
- Li, Y.W., Bayliss, D.A., Guyenet, P.G., 1995. C1 neurons of neonatal rats: intrinsic beating properties and alpha 2-adrenergic receptors. *Am J Physiol*. 269, R1356-69.
- Li, Y.W., Guyenet, P.G., 1996. Activation of GABA(B) receptors increases a potassium conductance in rat bulbospinal neurons of the C1 area. *Am J Physiol*. 271, R1304-R1310.
- Lipski, J., Kanjhan, R., Kruszkowska, B., Rong, W., 1996. Properties of presympathetic neurones in the rostral ventrolateral medulla in the rat: An intracellular study 'in vivo'. *J Physiol*. 490, 729-744.
- Liu, M., Shi, P., Sumners, C., 2016. Direct anti-inflammatory effects of angiotensin-(1-7) on microglia. *J Neurochem*. 136, 163-71.
- Llewellyn-Smith, I.J., Phend, K.D., Minson, J.B., Pilowsky, P.M., Chalmers, J.P., 1992. Glutamate-immunoreactive synapses on retrogradely-labelled sympathetic preganglionic neurons in rat thoracic spinal cord. *Brain Res*. 581, 67-80.
- Llewellyn-Smith, I.J., Martin, C.L., Minson, J.B., Pilowsky, P.M., Arnolda, L.F., Basbaum, A.I., Chalmers, J.P., 1997. Neurokinin-1 receptor-immunoreactive sympathetic preganglionic neurons: target specificity and ultrastructure. *Neuroscience*. 77, 1137-49.
- Llewellyn, T., Zheng, H., Liu, X., Xu, B., Patel, K.P., 2012. Median preoptic nucleus and subfornical organ drive renal sympathetic nerve activity via a glutamatergic mechanism within the paraventricular nucleus. *Am J Physiol Regul Integr Comp Physiol*. 302, R424-32.
- Loewy, A.D., Gregorie, E.M., McKellar, S., Baker, R.P., 1979a. Electrophysiological evidence that the A5 catecholamine cell group is a vasomotor center. *Brain Res*. 178, 196-200.
- Loewy, A.D., McKellar, S., Saper, C.B., 1979b. Direct projections from the A5 catecholamine cell group to the intermediolateral cell column. *Brain Res*. 174, 309-14.
- Loewy, A.D., Wallach, J.H., McKellar, S., 1981. Efferent connections of the ventral medulla oblongata in the rat. *Brain Res*. 228, 63-80.
- Lohmeier, T.E., Irwin, E.D., Rossing, M.A., Serdar, D.J., Kieval, R.S., 2004. Prolonged activation of the baroreflex produces sustained hypotension. *Hypertension*. 43, 306-11.
- Lopez-Gonzalez, M.V., Diaz-Casares, A., Peinado-Aragones, C.A., Lara, J.P., Barbancho, M.A., Dawid-Milner, M.S., 2013. Neurons of the A5 region are required for the tachycardia evoked by electrical stimulation of the hypothalamic defence area in anaesthetized rats. *Exp Physiol*. 98, 1279-94.

- Lorier, A.R., Huxtable, A.G., Robinson, D.M., Lipski, J., Housley, G.D., Funk, G.D., 2007. P2Y1 receptor modulation of the pre-Botzinger complex inspiratory rhythm generating network in vitro. *J Neurosci.* 27, 993-1005.
- Lovick, T.A., 1987. Differential control of cardiac and vasomotor activity by neurones in nucleus paragigantocellularis lateralis in the cat. *J Physiol.* 389, 23-35.
- Luppi, P.H., Aston-Jones, G., Akaoka, H., Chouvet, G., Jouvet, M., 1995. Afferent projections to the rat locus coeruleus demonstrated by retrograde and anterograde tracing with cholera-toxin B subunit and Phaseolus vulgaris leucoagglutinin. *Neuroscience.* 65, 119-160.
- Ma, L., Morton, A.J., Nicholson, L.F., 2003. Microglia density decreases with age in a mouse model of Huntington's disease. *Glia.* 43, 274-80.
- Ma, L., Nicholson, L.F., 2004. Expression of the receptor for advanced glycation end products in Huntington's disease caudate nucleus. *Brain Res.* 1018, 10-7.
- Madden, C.J., Satoru, I., Rinaman, L., Wiley, R.G., Sved, A.F., 1999. Lesions of the C1 catecholaminergic neurons of the ventrolateral medulla in rats using anti-D β H-saporin. *Am J Physiol.* 277, R1063-R1075.
- Madden, C.J., Sved, A.F., 2003a. Rostral ventrolateral medulla C1 neurons and cardiovascular regulation. *Cell Mol Neurobiol.* 23, 739-49.
- Madden, C.J., Sved, A.F., 2003b. Cardiovascular regulation after destruction of the C1 cell group of the rostral ventrolateral medulla in rats. *Am J Physiol.* 285, H2734-48.
- Maeshima, T., Ito, R., Hamada, S., Senzaki, K., Hamaguchi-Hamada, K., Shutoh, F., Okado, N., 1998. The cellular localization of 5-HT_{2A} receptors in the spinal cord and spinal ganglia of the adult rat. *Brain Res.* 797, 118-24.
- Maierov, D.N., Wilton, E.R., Badoer, E., Petrie, D., Head, G.A., Malpas, S.C., 1999. Sympathetic response to stimulation of the pontine A5 region in conscious rabbits. *Brain Res.* 815, 227-36.
- Maierov, D.N., Malpas, S.C., Head, G.A., 2000. Influence of pontine A5 region on renal sympathetic nerve activity in conscious rabbits. *Am J Physiol Regul Integr Comp Physiol.* 278, R311-9.
- Maire, J.C., Medilanski, J., Straub, R.W., 1984. Release of adenosine, inosine and hypoxanthine from rabbit non-myelinated nerve fibres at rest and during activity. *J Physiol.* 357, 67-77.
- Makeham, J.M., Goodchild, A.K., Costin, N.S., Pilowsky, P.M., 2004. Hypercapnia selectively attenuates the somato-sympathetic reflex. *Respir Physiol Neurobiol.* 140, 133-43.
- Makeham, J.M., Goodchild, A.K., Pilowsky, P.M., 2005. NK1 receptor activation in rat rostral ventrolateral medulla selectively attenuates somato-sympathetic reflex while antagonism attenuates sympathetic chemoreflex. *Am J Physiol Regul Integr Comp Physiol.* 288, R1707-15.
- Mandel, D.A., Schreihöfer, A.M., 2008. Glutamatergic inputs to the CVLM independent of the NTS promote tonic inhibition of sympathetic vasomotor tone in rats. *Am J Physiol Heart Circ Physiol.* 295, H1772-9.
- Marinelli, S., Vaughan, C.W., Schnell, S.A., Wessendorf, M.W., Christie, M.J., 2002. Rostral ventromedial medulla neurons that project to the spinal cord express multiple opioid receptor phenotypes. *J Neurosci.* 22, 10847-55.
- Marlier, L., Teilhac, J.R., Cerruti, C., Privat, A., 1991. Autoradiographic mapping of 5-HT₁, 5-HT_{1A}, 5-HT_{1B} and 5-HT₂ receptors in the rat spinal cord. *Brain Res.* 550, 15-23.
- Mauch, D.H., Nägler, K., Schumacher, S., Göritz, C., Müller, E.C., Otto, A., Pfrieger, F.W., 2001. CNS synaptogenesis promoted by glia-derived cholesterol. *Science.* 294, 1354-1357.
- McAllen, R.M., Dampney, R.A.L., 1990. Vasomotor neurons in the rostral ventrolateral medulla are organized topographically with respect to type of vascular bed but not body region. *Neurosci Lett.* 110, 91-96.

- McAllen, R.M., Badoer, E., Shafton, A.D., Oldfield, B.J., McKinley, M.J., 1992. Hemorrhage induces c-fos immunoreactivity in spinally projecting neurons of cat subretrofacial nucleus. *Brain Res.* 575, 329-32.
- McAllen, R.M., Habler, H.J., Michaelis, M., Peters, O., Janig, W., 1994. Monosynaptic excitation of preganglionic vasomotor neurons by subretrofacial neurons of the rostral ventrolateral medulla. *Brain Res.* 634, 227-34.
- McBryde, F.D., Abdala, A.P., Hendy, E.B., Pijacka, W., Marvar, P., Moraes, D.J., Sobotka, P.A., Paton, J.F., 2013. The carotid body as a putative therapeutic target for the treatment of neurogenic hypertension. *Nat Commun.* 4, 2395.
- McCorry, L.K., 2007. Physiology of the autonomic nervous system. *Am J Pharm Educ.* 71, 78.
- McDonald, T.J., Le, W.W., Hoffman, G.E., 2000. Brainstem catecholaminergic neurons activated by hypoxemia express GR and are coordinately activated with fetal sheep hypothalamic paraventricular CRH neurons. *Brain Res.* 885, 70-8.
- McKittrick, D.J., Krukoff, T.L., Calaresu, F.R., 1992. Expression of c-fos protein in rat brain after electrical stimulation of the aortic depressor nerve. *Brain Res.* 599, 215-22.
- McLachlan, E.M., Oldfield, B.J., 1981. Some observations on the catecholaminergic innervation of the intermediate zone of the thoracolumbar spinal cord of the cat. *J Comp Neurol.* 200, 529-44.
- McMullan, S., Goodchild, A.K., Pilowsky, P.M., 2007. Circulating angiotensin II attenuates the sympathetic baroreflex by reducing the barosensitivity of medullary cardiovascular neurones in the rat. *J Physiol.* 582, 711-22.
- McMullan, S., Pathmanandavel, K., Pilowsky, P.M., Goodchild, A.K., 2008. Somatic nerve stimulation evokes qualitatively different somatosympathetic responses in the cervical and splanchnic sympathetic nerves in the rat. *Brain Res.* 1217, 139-47.
- Menuet, C., Sevigny, C.P., Connelly, A.A., Bassi, J.K., Jancovski, N., Williams, D.A., Anderson, C.R., Llewellyn-Smith, I.J., Fong, A.Y., Allen, A.M., 2014. Catecholaminergic C3 neurons are sympathoexcitatory and involved in glucose homeostasis. *J Neurosci.* 34, 15110-22.
- Mifflin, S.W., 1992. Arterial chemoreceptor input to nucleus tractus solitarius. *Am J Physiol.* 263, R368-75.
- Miles, G.B., Parkis, M.A., Lipski, J., Funk, G.D., 2002. Modulation of phrenic motoneuron excitability by ATP: consequences for respiratory-related output in vitro. *J Appl Physiol* (1985). 92, 1899-910.
- Milner, R., Campbell, I.L., 2002. Cytokines regulate microglial adhesion to laminin and astrocyte extracellular matrix via protein kinase C-dependent activation of the $\alpha 6 \beta 1$ integrin. *J Neurosci.* 22, 1562-72.
- Milner, T.A., Pickel, V.M., Park, D.H., Joh, T.H., Reis, D.J., 1987. Phenylethanolamine N-methyltransferase-containing neurons in the rostral ventrolateral medulla of the rat. I. Normal ultrastructure. *Brain Res.* 411, 28-45.
- Milner, T.A., Morrison, S.F., Abate, C., Reis, D.J., 1988. Phenylethanolamine N-methyltransferase-containing terminals synapse directly on sympathetic preganglionic neurons in the rat. *Brain Res.* 448, 205-22.
- Min Li, W., Sato, A., Sato, Y., Schmidt, R.F., 1996. Morphine microinjected into the nucleus tractus solitarius and rostral ventrolateral medullary nucleus enhances somatosympathetic A- and C-reflexes in anesthetized rats. *Neurosci Lett.* 221, 53-56.
- Minami, N., Imai, Y., Nishiyama, H., Abe, K., 1997. Role of nitric oxide in the development of vascular $\alpha 1$ -adrenoreceptor desensitization and pressure diuresis in conscious rats. *Hypertension.* 29, 969-75.
- Minson, J., Llewellyn-Smith, I., Neville, A., Somogyi, P., Chalmers, J., 1990. Quantitative analysis of spinally projecting adrenaline-synthesising neurons of C1, C2 and C3 groups in rat medulla oblongata. *J Auton Nerv Syst.* 30, 209-20.

- Minson, J., Pilowsky, P., Llewellyn-Smith, I., Kaneko, T., Kapoor, V., Chalmers, J., 1991. Glutamate in spinally projecting neurons of the rostral ventral medulla. *Brain Res.* 555, 326-331.
- Minson, J., Arnolda, L., Llewellyn-Smith, I., Pilowsky, P., Chalmers, J., 1996. Altered c-fos in rostral medulla and spinal cord of spontaneously hypertensive rats. *Hypertension.* 27, 433-41.
- Minson, J.B., Chalmers, J.P., Caon, A.C., Renaud, B., 1987. Separate areas of rat medulla oblongata with populations of serotonin- and adrenaline-containing neurons alter blood pressure after L-glutamate stimulation. *J Auton Nerv Syst.* 19, 39-50.
- Minson, J.B., Llewellyn-Smith, I.J., Arnolda, L.F., Pilowsky, P.M., Oliver, J.R., Chalmers, J.P., 1994. Disinhibition of the rostral ventral medulla increases blood pressure and Fos expression in bulbospinal neurons. *Brain Res.* 646, 44-52.
- Minson, J.B., Llewellyn-Smith, I.J., Arnolda, L.F., Pilowsky, P.M., Chalmers, J.P., 1997a. C-fos expression in central neurons mediating the arterial baroreceptor reflex. *Clin Exp Hypertens.* 19, 631-43.
- Minson, J.B., Llewellyn-Smith, I.J., Chalmers, J.P., Pilowsky, P.M., Arnolda, L.F., 1997b. c-fos identifies GABA-synthesizing barosensitive neurons in caudal ventrolateral medulla. *Neuroreport.* 8, 3015-21.
- Mittelbronn, M., Dietz, K., Schluesener, H.J., Meyermann, R., 2001. Local distribution of microglia in the normal adult human central nervous system differs by up to one order of magnitude. *Acta Neuropathol.* 101, 249-255.
- Miura, M., Okada, J., Takayama, K., 1996a. Parapyramidal rostroventromedial medulla as a respiratory rhythm modulator. *Neurosci Lett.* 203, 41-4.
- Miura, M., Okada, J., Takayama, K., Jingu, H., 1996b. Barosensitive and chemosensitive neurons in the rat medulla: a double labeling study with c-Fos/glutamate, GAD, PNMT and calbindin. *J Auton Nerv Syst.* 61, 17-25.
- Miyamoto, A., Wake, H., Moorhouse, A.J., Nabekura, J., 2013. Microglia and synapse interactions: fine tuning neural circuits and candidate molecules. *Front Cell Neurosci.* 7, 70.
- Miyawaki, T., Suzuki, S., Minson, J., Arnolda, L., Chalmers, J., Llewellyn-Smith, I., Pilowsky, P., 1997. Role of AMPA/kainate receptors in transmission of the sympathetic baroreflex in rat CVLM. *Am J Physiol.* 272, R800-12.
- Miyawaki, T., Goodchild, A.K., Pilowsky, P.M., 2001. Rostral ventral medulla 5-HT1A receptors selectively inhibit the somatosympathetic reflex. *Am J Physiol Regul Integr Comp Physiol.* 280, R1261-8.
- Miyawaki, T., Goodchild, A.K., Pilowsky, P.M., 2002a. Evidence for a tonic GABA-ergic inhibition of excitatory respiratory-related afferents to presympathetic neurons in the rostral ventrolateral medulla. *Brain Res.* 924, 56-62.
- Miyawaki, T., Goodchild, A.K., Pilowsky, P.M., 2002b. Activation of mu-opioid receptors in rat ventrolateral medulla selectively blocks baroreceptor reflexes while activation of delta opioid receptors blocks somato-sympathetic reflexes. *Neuroscience.* 109, 133-44.
- Montoro, R.J., Urena, J., Fernandez-Chacon, R., Alvarez de Toledo, G., Lopez-Barneo, J., 1996. Oxygen sensing by ion channels and chemotransduction in single glomus cells. *J Gen Physiol.* 107, 133-143.
- Moore, S.D., Guyenet, P.G., 1985. Effect of blood pressure on A2 noradrenergic neurons. *Brain Res.* 338, 169-72.
- Moraes, D.J.A., Machado, B.H., Paton, J.F.R., 2014. Specific respiratory neuron types have increased excitability that drive presympathetic neurones in neurogenic hypertension. *Hypertension.* 63, 1309-1318.
- Moreira, T.S., Takakura, A.C., Colombari, E., Guyenet, P.G., 2006. Central chemoreceptors and sympathetic vasomotor outflow. *J Physiol.* 577, 369-86.

- Morgan, J.I., Curran, T., 1989. Stimulus-transcription coupling in neurons: role of cellular immediate-early genes. *Trends Neurosci.* 12, 459-62.
- Morgan, M.M., Whittier, K.L., Hegarty, D.M., Aicher, S.A., 2008. Periaqueductal Gray neurons project to spinally projecting GABAergic neurons in the rostral ventromedial medulla. *Pain.* 140, 376-386.
- Morilak, D.A., Somogyi, P., McIlhinney, R.A., Chalmers, J., 1989. An enkephalin-containing pathway from nucleus tractus solitarius to the pressor area of the rostral ventrolateral medulla of the rabbit. *Neuroscience.* 31, 187-94.
- Morrison, H.W., Filosa, J.A., 2013. A quantitative spatiotemporal analysis of microglia morphology during ischemic stroke and reperfusion. *J Neuroinflamm.* 10, 4.
- Morrison, S.F., Gebber, G.L., 1984. Raphe neurons with sympathetic-related activity: baroreceptor responses and spinal connections. *Am J Physiol.* 246, R338-48.
- Morrison, S.F., Callaway, J., Milner, T.A., Reis, D.J., 1989a. Glutamate in the spinal sympathetic intermediolateral nucleus: localization by light and electron microscopy. *Brain Res.* 503, 5-15.
- Morrison, S.F., Ernsberger, P., Milner, T.A., Callaway, J., Gong, A., Reis, D.J., 1989b. A glutamate mechanism in the intermediolateral nucleus mediates sympathoexcitatory responses to stimulation of the rostral ventrolateral medulla. *Prog Brain Res.* 81, 159-69.
- Morrison, S.F., Reis, D.J., 1989. Reticulospinal vasomotor neurons in the RVL mediate the somatosympathetic reflex. *Am J Physiol.* 256, R1084-97.
- Morrison, S.F., Cao, W.H., 2000. Different adrenal sympathetic preganglionic neurons regulate epinephrine and norepinephrine secretion. *Am J Physiol Regul Integr Comp Physiol.* 279, R1763-75.
- Morrison, S.F., 2003. Glutamate transmission in the rostral ventrolateral medullary sympathetic premotor pathway. *Cell Mol Neurobiol.* 23, 761-72.
- Morrison, S.F., Nakamura, K., Madden, C.J., 2008. Central control of thermogenesis in mammals. *Exp Physiol.* 93, 773-97.
- Mueller, P.J., Mischel, N.A., Scislo, T.J., 2011. Differential activation of adrenal, renal, and lumbar sympathetic nerves following stimulation of the rostral ventrolateral medulla of the rat. *Am J Physiol Regul Integr Comp Physiol.* 300, R1230-40.
- Mulkey, D.K., Stornetta, R.L., Weston, M.C., Simmons, J.R., Parker, A., Bayliss, D.A., Guyenet, P.G., 2004. Respiratory control by ventral surface chemoreceptor neurons in rats. *Nat Neurosci.* 7, 1360-9.
- Mulkey, D.K., Wenker, I.C., 2011. Astrocyte chemoreceptors: mechanisms of H⁺ sensing by astrocytes in the retrotrapezoid nucleus and their possible contribution to respiratory drive. *Exp Physiol.* 96, 400-6.
- Munch, P.A., Andresen, M.C., Brown, A.M., 1983. Rapid resetting of aortic baroreceptors in vitro. *Am J Physiol.* 244, H672-80.
- Murase, S., Hayashi, Y., 1998. Expression pattern and neurotrophic role of the c-fms proto-oncogene M-CSF receptor in rodent Purkinje cells. *J Neurosci.* 18, 10481-92.
- Murphy, A.Z., Ennis, M., Shipley, M.T., Behbehani, M.M., 1994. Directionally specific changes in arterial pressure induce differential patterns of fos expression in discrete areas of the rat brainstem: a double-labeling study for Fos and catecholamines. *J Comp Neurol.* 349, 36-50.
- Nakamura, K., Morrison, S.F., 2007. Central efferent pathways mediating skin cooling-evoked sympathetic thermogenesis in brown adipose tissue. *Am J Physiol Regul Integr Comp Physiol.* 292, R127-36.
- Nattie, E., 1999. CO₂, brainstem chemoreceptors and breathing. *Prog Neurobiol.* 59, 299-331.
- Nattie, E., 2011. Julius H. Comroe, Jr., distinguished lecture: central chemoreception: then ... and now. *J Appl Physiol (1985).* 110, 1-8.

- Nattie, E., Li, A., 2012. Central chemoreceptors: locations and functions. *Compr Physiol.* 2, 221-54.
- Nattie, E.E., Li, A., 2001. CO₂ dialysis in the medullary raphe of the rat increases ventilation in sleep. *J Appl Physiol* (1985). 90, 1247-57.
- Nedoboy, P.E., Mohammed, S., Kapoor, K., Bhandare, A.M., Farnham, M.M., Pilowsky, P.M., 2016. pSer40 tyrosine hydroxylase immunohistochemistry identifies the anatomical location of C1 neurons in rat RVLM that are activated by hypotension. *Neuroscience.* 317, 162-72.
- Neil, J.J., Loewy, A.D., 1982. Decreases in blood pressure in response to L-glutamate microinjections into the A5 catecholamine cell group. *Brain Res.* 241, 271-8.
- Nguyen, M.T., Lue, H., Kleemann, R., Thiele, M., Tolle, G., Finkelmeier, D., Wagner, E., Braun, A., Bernhagen, J., 2003. The cytokine macrophage migration inhibitory factor reduces pro-oxidative stress-induced apoptosis. *J Immunol.* 170, 3337-47.
- Nicholas, A.P., Hancock, M.B., 1990. Evidence for projections from the rostral medullary raphe onto medullary catecholamine neurons in the rat. *Neurosci Lett.* 108, 22-8.
- Nikodemova, M., Small, A.L., Smith, S.M., Mitchell, G.S., Watters, J.J., 2014. Spinal but not cortical microglia acquire an atypical phenotype with high VEGF, galectin-3 and osteopontin, and blunted inflammatory responses in ALS rats. *Neurobiol Dis.* 69, 43-53.
- Nimmerjahn, A., Kirchhoff, F., Helmchen, F., 2005. Neuroscience: Resting microglial cells are highly dynamic surveillants of brain parenchyma in vivo. *Science.* 308, 1314-1318.
- Noda, M., Kariura, Y., Amano, T., Manago, Y., Nishikawa, K., Aoki, S., Wada, K., 2003. Expression and function of bradykinin receptors in microglia. *Life Sci.* 72, 1573-81.
- Noda, M., Kettenmann, H., Wada, K., 2006. Anti-inflammatory effects of kinins via microglia in the central nervous system. *Biol Chem.* 387, 167-71.
- Nunn, N., Womack, M., Dart, C., Barrett-Jolley, R., 2011. Function and pharmacology of spinally-projecting sympathetic pre-autonomic neurones in the paraventricular nucleus of the hypothalamus. *Curr Neuropharmacol.* 9, 262-77.
- O'Carroll, S.J., Gorrie, C.A., Velamoor, S., Green, C.R., Nicholson, L.F., 2013. Connexin43 mimetic peptide is neuroprotective and improves function following spinal cord injury. *Neurosci Res.* 75, 256-67.
- Obara, M., Szeliga, M., Albrecht, J., 2008. Regulation of pH in the mammalian central nervous system under normal and pathological conditions: facts and hypotheses. *Neurochem Int.* 52, 905-19.
- Ohsawa, K., Irino, Y., Nakamura, Y., Akazawa, C., Inoue, K., Kohsaka, S., 2007. Involvement of P2X₄ and P2Y₁₂ receptors in ATP-induced microglial chemotaxis. *GLIA.* 55, 604-616.
- Okamoto, K., Aoki, K., 1963. Development of a strain of spontaneously hypertensive rats. *Jpn Circ J.* 27, 282-93.
- Olesen, J., 1972. The effect of intracarotid epinephrine, norepinephrine, and angiotensin on the regional cerebral blood flow in man. *Neurology.* 22, 978-87.
- Olshansky, B., Sabbah, H.N., Hauptman, P.J., Colucci, W.S., 2008. Parasympathetic Nervous System and Heart Failure: Pathophysiology and Potential Implications for Therapy. *Circulation.* 118, 863-871.
- Oshima, N., McMullan, S., Goodchild, A.K., Pilowsky, P.M., 2006. A monosynaptic connection between baroinhibited neurons in the RVLM and IML in Sprague-Dawley rats. *Brain Res.* 1089, 153-61.
- Oshima, N., Kumagai, H., Onimaru, H., Kawai, A., Pilowsky, P.M., Iigaya, K., Takimoto, C., Hayashi, K., Saruta, T., Itoh, H., 2008. Monosynaptic excitatory connection from the rostral ventrolateral medulla to sympathetic preganglionic neurons revealed by simultaneous recordings. *Hypertens Res.* 31, 1445-54.

- Oshima, N., Kumagai, H., Igaya, K., Onimaru, H., Kawai, A., Nishida, Y., Saruta, T., Itoh, H., 2012. Baro-excited neurons in the caudal ventrolateral medulla (CVLM) recorded using the whole-cell patch-clamp technique. *Hypertens Res.* 35, 500-6.
- Overholt, J.L., Prabhakar, N.R., 1997. Ca²⁺ Current in Rabbit Carotid Body Glomus Cells Is Conducted by Multiple Types of High-Voltage-Activated Ca²⁺ Channels. *J Neurophysiol.* 78, 2467-2474.
- Pabon, M.M., Bachstetter, A.D., Hudson, C.E., Gemma, C., Bickford, P.C., 2011. CX3CL1 reduces neurotoxicity and microglial activation in a rat model of Parkinson's disease. *J Neuroinflamm.* 8, 9.
- Padley, J.R., Kumar, N.N., Li, Q., Nguyen, T.B., Pilowsky, P.M., Goodchild, A.K., 2007. Central command regulation of circulatory function mediated by descending pontine cholinergic inputs to sympathoexcitatory rostral ventrolateral medulla neurons. *Circ Res.* 100, 284-91.
- Panatier, A., Robitaille, R., 2012. The soothing touch: microglial contact influences neuronal excitability. *Dev Cell.* 23, 1125-6.
- Pang, L., Eyzaguirre, C., 1992. Different effects of hypoxia on the membrane potential and input resistance of isolated and clustered carotid body glomus cells. *Brain Res.* 575, 167-73.
- Pang, L., Eyzaguirre, C., 1993. Hypoxia affects differently the intracellular pH of clustered and isolated glomus cells of the rat carotid body. *Brain Res.* 623, 349-55.
- Paolicelli, R.C., Bolasco, G., Pagani, F., Maggi, L., Scianni, M., Panzanelli, P., Giustetto, M., Ferreira, T.A., Guiducci, E., Dumas, L., Ragozzino, D., Gross, C.T., 2011. Synaptic pruning by microglia is necessary for normal brain development. *Science.* 333, 1456-8.
- Papademetriou, V., Doumas, M., Faselis, C., Tsioufis, C., Douma, S., Gkaliagkousi, E., Zamboulis, C., 2011. Carotid baroreceptor stimulation for the treatment of resistant hypertension. *Int J Hypertens.* 2011, 964394.
- Parker, L.M., Damanhuri, H.A., Fletcher, S.P., Goodchild, A.K., 2015. Hydralazine administration activates sympathetic preganglionic neurons whose activity mobilizes glucose and increases cardiovascular function. *Brain Res.* 1604, 25-34.
- Parkhurst, C.N., Yang, G., Ninan, I., Savas, J.N., Yates, J.R., 3rd, Lafaille, J.J., Hempstead, B.L., Littman, D.R., Gan, W.B., 2013. Microglia promote learning-dependent synapse formation through brain-derived neurotrophic factor. *Cell.* 155, 1596-609.
- Pawloski-Dahm, C., Gordon, F.J., 1992. Evidence for a kynurenate-insensitive glutamate receptor in nucleus tractus solitarii. *Am J Physiol.* 262, H1611-5.
- Paxinos, G., Watson, C., 2007. The rat brain in stereotaxic coordinates. Vol. Sixth, Elsevier Academic Press.
- Pedrinio, G.R., Rosa, D.A., Korim, W.S., Cravo, S.L., 2008. Renal sympathoinhibition induced by hypernatremia: involvement of A1 noradrenergic neurons. *Auton Neurosci.* 142, 55-63.
- Perea, G., Navarrete, M., Araque, A., 2009. Tripartite synapses: astrocytes process and control synaptic information. *Trends Neurosci.* 32, 421-31.
- Perego, C., Fumagalli, S., De Simoni, M.G., 2011. Temporal pattern of expression and colocalization of microglia/macrophage phenotype markers following brain ischemic injury in mice. *J Neuroinflamm.* 8, 174.
- Perry, V.H., Andersson, P.-B., Gordon, S., 1993. Macrophages and inflammation in the central nervous system. *Trends Neurosci.* 16, 268-273.
- Perry, V.H., Holmes, C., 2014. Microglial priming in neurodegenerative disease. *Nat Rev Neurol.* 10, 217-224.
- Pettersson, L.M., Heine, T., Verge, V.M., Sundler, F., Danielsen, N., 2004. PACAP mRNA is expressed in rat spinal cord neurons. *J Comp Neurol.* 471, 85-96.
- Pfriege, F.W., Barres, B.A., 1997. Synaptic efficacy enhanced by glial cells in vitro. *Science.* 277, 1684-1687.

- Phillips, J.K., Goodchild, A.K., Dubey, R., Sesiasvili, E., Takeda, M., Chalmers, J., Pilowsky, P.M., Lipski, J., 2001. Differential expression of catecholamine biosynthetic enzymes in the rat ventrolateral medulla. *J Comp Neurol.* 432, 20-34.
- Pickering, A.E., Simms, A.E., Paton, J.F., 2008. Dominant role of aortic baroreceptors in the cardiac baroreflex of the rat in situ. *Auton Neurosci.* 142, 32-9.
- Pieribone, V.A., Aston-Jones, G., Bohn, M.C., 1988. Adrenergic and non-adrenergic neurons in the C1 and C3 areas project to locus coeruleus: a fluorescent double labeling study. *Neurosci Lett.* 85, 297-303.
- Pieribone, V.A., Aston-Jones, G., 1991. Adrenergic innervation of the rat nucleus locus coeruleus arises predominantly from the C1 adrenergic cell group in the rostral medulla. *Neuroscience.* 41, 525-42.
- Pilowsky, P., West, M., Chalmers, J., 1985. Renal sympathetic nerve responses to stimulation, inhibition and destruction of the ventrolateral medulla in the rabbit. *Neurosci Lett.* 60, 51-5.
- Pilowsky, P., Llewellyn-Smith, I.J., Lipski, J., Chalmers, J., 1992. Substance P immunoreactive boutons form synapses with feline sympathetic preganglionic neurons. *J Comp Neurol.* 320, 121-35.
- Pilowsky, P., Llewellyn-Smith, I.J., Arnolda, L., Minson, J., Chalmers, J., 1994. Intracellular recording from sympathetic preganglionic neurons in cat lumbar spinal cord. *Brain Res.* 656, 319-28.
- Pilowsky, P.M., Jiang, C., Lipski, J., 1990. An intracellular study of respiratory neurons in the rostral ventrolateral medulla of the rat and their relationship to catecholamine-containing neurons. *J Comp Neurol.* 301, 604-17.
- Pilowsky, P.M., Miyawaki, T., Minson, J.B., Sun, Q.J., Arnolda, L.F., Llewellyn-Smith, I.J., Chalmers, J.P., 1995. Bulbospinal sympatho-excitatory neurons in the rat caudal raphe. *J Hypertens.* 13, 1618-23.
- Pilowsky, P.M., Goodchild, A.K., 2002. Baroreceptor reflex pathways and neurotransmitters: 10 years on. *J Hypertens.* 20, 1675-88.
- Pilowsky, P.M., Lung, M.S., Spirovski, D., McMullan, S., 2009. Differential regulation of the central neural cardiorespiratory system by metabotropic neurotransmitters. *Philos Trans R Soc Lond B Biol Sci.* 364, 2537-52.
- Pilowsky, P.M., 2014. Peptides, serotonin, and breathing: the role of the raphe in the control of respiration. *Prog Brain Res.* 209, 169-89.
- Pocock, J.M., Kettenmann, H., 2007. Neurotransmitter receptors on microglia. *Trends Neurosci.* 30, 527-35.
- Polson, J.W., Mrljak, S., Potts, P.D., Dampney, R.A., 2002. Fos expression in spinally projecting neurons after hypotension in the conscious rabbit. *Auton Neurosci.* 100, 10-20.
- Poon, Y.Y., Chang, A.Y., Chan, S.H., 2006. Differential contribution of N-methyl-D-aspartate and non-N-methyl-D-aspartate receptors in the intermediolateral cell column of the thoracic spinal cord to sympathetic vasomotor tone during experimental endotoxemia in the rat. *Shock.* 26, 372-8.
- Potts, J.T., Paton, J.F., Mitchell, J.H., Garry, M.G., Kline, G., Anguelov, P.T., Lee, S.M., 2003. Contraction-sensitive skeletal muscle afferents inhibit arterial baroreceptor signalling in the nucleus of the solitary tract: role of intrinsic GABA interneurons. *Neuroscience.* 119, 201-14.
- Potts, P.D., Ludbrook, J., Gillman-Gaspari, T.A., Horiuchi, J., Dampney, R.A.L., 1999. Activation of brain neurons following central hypervolaemia and hypovolaemia: contribution of baroreceptor and non-baroreceptor inputs. *Neuroscience.* 95, 499-511.
- Poulat, P., Marlier, L., Rajaofetra, N., Privat, A., 1992. 5-Hydroxytryptamine, substance P and thyrotropin-releasing hormone synapses in the intermediolateral cell column of the rat thoracic spinal cord. *Neurosci Lett.* 136, 19-22.

- Prabhakar, N.R., 2000. Oxygen sensing by the carotid body chemoreceptors. *J Appl Physiol* (1985). 88, 2287-95.
- Punnen, S., Sapru, H.N., 1986. Cardiovascular responses to medullary microinjections of opiate agonists in urethane-anesthetized rats. *J Cardiovasc Pharmacol.* 8, 950-6.
- Punnen, S., Urbanski, R., Krieger, A.J., Sapru, H.N., 1987. Ventrolateral medullary pressor area: site of hypotensive action of clonidine. *Brain Res.* 422, 336-46.
- Puskas, N., Papp, R.S., Gallatz, K., Palkovits, M., 2010. Interactions between orexin-immunoreactive fibers and adrenaline or noradrenaline-expressing neurons of the lower brainstem in rats and mice. *Peptides.* 31, 1589-97.
- Putnam, R.W., Filosa, J.A., Ritucci, N.A., 2004. Cellular mechanisms involved in CO(2) and acid signaling in chemosensitive neurons. *Am J Physiol-Cell Physiol.* 287, C1493-526.
- Pyner, S., Coote, J.H., 1998. Rostroventrolateral medulla neurons preferentially project to target-specified sympathetic preganglionic neurons. *Neuroscience.* 83, 617-31.
- Pyo, H., Yang, M.S., Jou, I., Joe, E.H., 2003. Wortmannin enhances lipopolysaccharide-induced inducible nitric oxide synthase expression in microglia in the presence of astrocytes in rats. *Neurosci Lett.* 346, 141-4.
- Rahman, A.A., Shahid, I.Z., Pilowsky, P.M., 2012. Differential cardiorespiratory and sympathetic reflex responses to microinjection of neuromedin U in rat rostral ventrolateral medulla. *J Pharmacol Exp Ther.* 341, 213-24.
- Raizada, M.K., Summers, C., Lu, D., 1993. Angiotensin II type 1 receptor mRNA levels in the brains of normotensive and spontaneously hypertensive rats. *J Neurochem.* 60, 1949-52.
- Rajani, V., Zhang, Y., Revill, A.L., Funk, G.D., 2015. The role of P2Y receptor signaling in central respiratory control. *Respir Physiol Neurobiol.* 226, 3-10.
- Rana, I., Stebbing, M., Kompa, A., Kelly, D.J., Krum, H., Badoer, E., 2010. Microglia activation in the hypothalamic PVN following myocardial infarction. *Brain Res.* 1326, 96-104.
- Rana, I., Badoer, E., Alahmadi, E., Leo, C.H., Woodman, O.L., Stebbing, M.J., 2014. Microglia are selectively activated in endocrine and cardiovascular control centres in streptozotocin-induced diabetic rats. *J Neuroendocrinol.* 26, 413-25.
- Rasley, A., Bost, K.L., Olson, J.K., Miller, S.D., Marriott, I., 2002. Expression of functional NK-1 receptors in murine microglia. *Glia.* 37, 258-67.
- Rauscher, F.J., 3rd, Voulalas, P.J., Franza, B.R., Jr., Curran, T., 1988. Fos and Jun bind cooperatively to the AP-1 site: reconstitution in vitro. *Genes Dev.* 2, 1687-99.
- Regenhardt, R.W., Desland, F., Mecca, A.P., Pioquinto, D.J., Afzal, A., Mocco, J., Summers, C., 2013. Anti-inflammatory effects of angiotensin-(1-7) in ischemic stroke. *Neuropharmacology.* 71, 154-63.
- Regenhardt, R.W., Mecca, A.P., Desland, F., Ritucci-Chinni, P.F., Ludin, J.A., Greenstein, D., Banuelos, C., Bizon, J.L., Reinhard, M.K., Summers, C., 2014. Centrally administered angiotensin-(1-7) increases the survival of stroke-prone spontaneously hypertensive rats. *Exp Physiol.* 99, 442-53.
- Reiner, A., Erichsen, J.T., Cabot, J.B., Evinger, C., Fitzgerald, M.E.C., Karten, H.J., 2009. Neurotransmitter organization of the nucleus of Edinger–Westphal and its projection to the avian ciliary ganglion. *Visual Neurosci.* 6, 451.
- Reis, D.J., Ross, C.A., Ruggiero, D.A., Granata, A.R., Joh, T.H., 1984. Role of adrenaline neurons of ventrolateral medulla (the C1 group) in the tonic and phasic control of arterial pressure. *Clin Exp Hypertens A.* 6, 221-41.
- Reis, D.J., Golanov, E.V., Ruggiero, D.A., Sun, M.K., 1994. Sympatho-excitatory neurons of the rostral ventrolateral medulla are oxygen sensors and essential elements in the tonic and reflex control of the systemic and cerebral circulations. *J Hypertens.* 12, S159-S180.

- Rentero, N., Cividjian, A., Trevaks, D., Pequignot, J.M., Quintin, L., McAllen, R.M., 2002. Activity patterns of cardiac vagal motoneurons in rat nucleus ambiguus. *Am J Physiol Regul Integr Comp Physiol.* 283, R1327-34.
- Richerson, G.B., Wang, W., Tiwari, J., Bradley, S.R., 2001. Chemosensitivity of serotonergic neurons in the rostral ventral medulla. *Respir Physiol.* 129, 175-89.
- Ridker, P.M., Cushman, M., Stampfer, M.J., Tracy, R.P., Hennekens, C.H., 1998. Plasma concentration of C-reactive protein and risk of developing peripheral vascular disease. *Circulation.* 97, 425-8.
- Rinaman, L., 2011. Hindbrain noradrenergic A2 neurons: diverse roles in autonomic, endocrine, cognitive, and behavioral functions. *Am J Physiol Regul Integr Comp Physiol.* 300, R222-35.
- Ritter, S., Llewellyn-Smith, I., Dinh, T.T., 1998. Subgroups of hindbrain catecholamine neurons are selectively activated by 2-deoxy-d-glucose induced metabolic challenge. *Brain Res.* 805, 41-54.
- Rodríguez, V., De Kloet, A.D., Sumners, C., 2016. Hypertension and brain inflammation: Role of RAS-induced glial activation. In *Hypertension and the Brain as an End-Organ Target.* pp. 181-194.
- Rosin, D.L., Chang, D.A., Guyenet, P.G., 2006. Afferent and efferent connections of the rat retrotrapezoid nucleus. *J Comp Neurol.* 499, 64-89.
- Ross, C.A., Ruggiero, D.A., Joh, T.H., Park, D.H., Reis, D.J., 1984a. Rostral ventrolateral medulla: selective projections to the thoracic autonomic cell column from the region containing C1 adrenaline neurons. *J Comp Neurol.* 228, 168-85.
- Ross, C.A., Ruggiero, D.A., Park, D.H., Joh, T.H., Sved, A.F., Fernandez-Pardal, J., Saavedra, J.M., Reis, D.J., 1984b. Tonic vasomotor control by the rostral ventrolateral medulla: effect of electrical or chemical stimulation of the area containing C1 adrenaline neurons on arterial pressure, heart rate, and plasma catecholamines and vasopressin. *J Neurosci.* 4, 474-94.
- Ruchaya, P.J., Paton, J.F.R., Murphy, D., Yao, S.T., 2012. A cardiovascular role for fractalkine and its cognate receptor, CX3CR1, in the rat nucleus of the solitary tract. *Neuroscience.* 209, 119-127.
- Ruchaya, P.J., Antunes, V.R., Paton, J.F., Murphy, D., Yao, S.T., 2014. The cardiovascular actions of fractalkine/CX3CL1 in the hypothalamic paraventricular nucleus are attenuated in rats with heart failure. *Exp Physiol.* 99, 111-22.
- Ruggiero, D.A., Giuliano, R., Anwar, M., Stornetta, R., Reis, D.J., 1990. Anatomical substrates of cholinergic-autonomic regulation in the rat. *J Comp Neurol.* 292, 1-53.
- Rutherford, S.D., Widdop, R.E., Sannajust, F., Louis, W.J., Gundlach, A.L., 1992. Expression of c-fos and NGFI-A messenger RNA in the medulla oblongata of the anaesthetized rat following stimulation of vagal and cardiovascular afferents. *Brain Res Mol Brain Res.* 13, 301-12.
- Sakima, A., Yamazato, M., Sesoko, S., Muratani, H., Fukiyama, K., 2000. Cardiovascular and sympathetic Effects of L-glutamate and glycine injected into the rostral ventrolateral medulla of conscious rats. *Hypertension Res.* 23, 633-641.
- Salo, L.M., Campos, R.R., McAllen, R.M., 2006. Differential control of cardiac functions by the brain. *Clin Exp Pharmacol Physiol.* 33, 1255-8.
- Sampaio, K.N., Mauad, H., Michael Spyer, K., Ford, T.W., 2014. Chronotropic and dromotropic responses to localized glutamate microinjections in the rat nucleus ambiguus. *Brain Res.* 1542, 93-103.
- Samuels, E.R., Szabadi, E., 2008. Functional neuroanatomy of the noradrenergic locus coeruleus: its roles in the regulation of arousal and autonomic function part I: principles of functional organisation. *Curr Neuropharmacol.* 6, 235-53.

- Sartor, D.M., Verberne, A.J., 2003. Phenotypic identification of rat rostroventrolateral medullary presympathetic vasomotor neurons inhibited by exogenous cholecystokinin. *J Comp Neurol.* 465, 467-79.
- Sasaki, S., Dampney, R.A., 1990. Tonic cardiovascular effects of angiotensin II in the ventrolateral medulla. *Hypertension.* 15, 274-83.
- Sato, A., Tsushima, N., Fujimori, B., 1965. Reflex Potentials of Lumbar Sympathetic Trunk. With Sciatic Nerve Stimulation in Cats. *Jpn J Physiol.* 15, 532-539.
- Sato, A., Sato, N., Ozawa, T., Fujimori, B., 1967. Further observation of reflex potentials in the lumbar sympathetic trunk in cats. *Jpn J Physiol.* 17, 294-307.
- Sato, A., Schmidt, R.F., 1971. Spinal and supraspinal components of the reflex discharges into lumbar and thoracic white rami. *J Physiol.* 212, 839-50.
- Sato, A., 1972. Somato-sympathetic reflex discharges evoked through supramedullary pathways. *Pflugers Arch.* 332, 117-26.
- Sato, A., Schmidt, R.F., 1973. Somatosympathetic reflexes: afferent fibers, central pathways, discharge characteristics. *Physiol Rev.* 53, 916-47.
- Sato, M.A., Colombari, E., Morrison, S.F., 2002. Inhibition of neurons in commissural nucleus of solitary tract reduces sympathetic nerve activity in SHR. *Am J Physiol Heart Circ Physiol.* 282, H1679-84.
- Sattler, R., Rothstein, J.D., 2006. Regulation and dysregulation of glutamate transporters. *Handb Exp Pharmacol.* 277-303.
- Savaki, H.E., Macpherson, H., McCulloch, J., 1982. Alterations in local cerebral glucose utilization during hemorrhagic hypotension in the rat. *Circ Res.* 50, 633-44.
- Savli, H., Gulkac, M.D., Esen, N., 2004. The effect of stimulated microglia conditioned media on BDNF gene expression of striatal astrocytes: quantification by real-time PCR. *Int J Neurosci.* 114, 1601-12.
- Sawchenko, P.E., Swanson, L.W., 1982. Immunohistochemical identification of neurons in the paraventricular nucleus of the hypothalamus that project to the medulla or to the spinal cord in the rat. *J Comp Neurol.* 205, 260-72.
- Sawchenko, P.E., Swanson, L.W., Grzanna, R., Howe, P.R., Bloom, S.R., Polak, J.M., 1985. Colocalization of neuropeptide Y immunoreactivity in brainstem catecholaminergic neurons that project to the paraventricular nucleus of the hypothalamus. *J Comp Neurol.* 241, 138-53.
- Schafer, D.P., Lehrman, E.K., Stevens, B., 2013. The "quad-partite" synapse: microglia-synapse interactions in the developing and mature CNS. *Glia.* 61, 24-36.
- Schlaich, M.P., Lambert, E., Kaye, D.M., Krozowski, Z., Campbell, D.J., Lambert, G., Hastings, J., Aggarwal, A., Esler, M.D., 2004. Sympathetic augmentation in hypertension: role of nerve firing, norepinephrine reuptake, and Angiotensin neuromodulation. *Hypertension.* 43, 169-75.
- Schmid, C.D., Sautkulis, L.N., Danielson, P.E., Cooper, J., Hasel, K.W., Hilbush, B.S., Sutcliffe, J.G., Carson, M.J., 2002. Heterogeneous expression of the triggering receptor expressed on myeloid cells-2 on adult murine microglia. *J Neurochem.* 83, 1309-20.
- Schmid, C.D., Melchior, B., Masek, K., Puntambekar, S.S., Danielson, P.E., Lo, D.D., Sutcliffe, J.G., Carson, M.J., 2009. Differential gene expression in LPS/IFN γ activated microglia and macrophages: in vitro versus in vivo. *J Neurochem.* 109 Suppl 1, 117-25.
- Schreihöfer, A.M., Guyenet, P.G., 1997. Identification of C1 presympathetic neurons in rat rostral ventrolateral medulla by juxtacellular labeling in vivo. *J Comp Neurol.* 387, 524-36.
- Schreihöfer, A.M., Guyenet, P.G., 2000. Role of presympathetic C1 neurons in the sympatholytic and hypotensive effects of clonidine in rats. *Am J Physiol Regul Integr Comp Physiol.* 279, R1753-62.

- Schreihofer, A.M., Guyenet, P.G., 2002. The baroreflex and beyond: control of sympathetic vasomotor tone by GABAergic neurons in the ventrolateral medulla. *Clin Exp Pharmacol Physiol.* 29, 514-21.
- Schreihofer, A.M., Guyenet, P.G., 2003. Baro-activated neurons with pulse-modulated activity in the rat caudal ventrolateral medulla express GAD67 mRNA. *J Neurophysiol.* 89, 1265-77.
- Seagard, J.L., Hopp, F.A., Drummond, H.A., Van Wynsberghe, D.M., 1993. Selective contribution of two types of carotid sinus baroreceptors to the control of blood pressure. *Circ Res.* 72, 1011-22.
- Seller, H., Konig, S., Czachurski, J., 1990. Chemosensitivity of sympathoexcitatory neurones in the rostroventrolateral medulla of the cat. *Pflugers Arch.* 416, 735-41.
- Sevigny, C.P., Bassi, J., Williams, D.A., Anderson, C.R., Thomas, W.G., Allen, A.M., 2012. Efferent projections of C3 adrenergic neurons in the rat central nervous system. *J Comp Neurol.* 520, 2352-68.
- Seyedabadi, M., Goodchild, A.K., Pilowsky, P.M., 2001. Differential role of kinases in brain stem of hypertensive and normotensive rats. *Hypertension.* 38, 1087-1092.
- Seyedabadi, M., Li, Q., Padley, J.R., Pilowsky, P.M., Goodchild, A.K., 2006. A novel pressor area at the medullo-cervical junction that is not dependent on the RVLM: efferent pathways and chemical mediators. *J Neurosci.* 26, 5420-7.
- Shahid, I.Z., Rahman, A.A., Pilowsky, P.M., 2012. Orexin A in rat rostral ventrolateral medulla is pressor, sympatho-excitatory, increases barosensitivity and attenuates the somato-sympathetic reflex. *Br J Pharmacol.* 165, 2292-303.
- Shaikh, S.B., Nicholson, L.F., 2009. Effects of chronic low dose rotenone treatment on human microglial cells. *Mol Neurodegener.* 4, 55.
- Shaikh, S.B., Uy, B., Perera, A., Nicholson, L.F., 2012. AGEs-RAGE mediated up-regulation of connexin43 in activated human microglial CHME-5 cells. *Neurochem Int.* 60, 640-51.
- Shan, Z., Zubcevic, J., Shi, P., Jun, J.Y., Dong, Y., Murca, T.M., Lamont, G.J., Cuadra, A., Yuan, W., Qi, Y., Li, Q., Paton, J.F., Katovich, M.J., Sumners, C., Raizada, M.K., 2013. Chronic knockdown of the nucleus of the solitary tract AT1 receptors increases blood inflammatory-endothelial progenitor cell ratio and exacerbates hypertension in the spontaneously hypertensive rat. *Hypertension.* 61, 1328-33.
- Shapiro, L.A., Perez, Z.D., Foresti, M.L., Arisi, G.M., Ribak, C.E., 2009. Morphological and ultrastructural features of Iba1-immunolabeled microglial cells in the hippocampal dentate gyrus. *Brain Res.* 1266, 29-36.
- Shi, P., Jiang, N., Li, H., Mecca, A.P., Raizada, M.K., Sumners, C., 2009. Paraventricular nucleus (PVN) neurons projecting to the rostral ventrolateral medulla (RVLM) contain both oxytocin and glutamate. *FASEB J.* 23, 967.6.
- Shi, P., Diez-Freire, C., Jun, J.Y., Qi, Y., Katovich, M.J., Li, Q., Sriramula, S., Francis, J., Sumners, C., Raizada, M.K., 2010a. Brain microglial cytokines in neurogenic hypertension. *Hypertension.* 56, 297-303.
- Shi, P., Raizada, M.K., Sumners, C., 2010b. Brain cytokines as neuromodulators in cardiovascular control. *Clin Exp Pharmacol Physiol.* 37, e52-7.
- Shi, P., Grobe, J.L., Desland, F.A., Zhou, G., Shen, X.Z., Shan, Z., Liu, M., Raizada, M.K., Sumners, C., 2014. Direct pro-inflammatory effects of prorenin on microglia. *PLoS One.* 9, e92937.
- Shirahata, M., Fitzgerald, R.S., 1991. Dependency of hypoxic chemotransduction in cat carotid body on voltage-gated calcium channels. *J Appl Physiol* (1985). 71, 1062-9.
- Sholl, D.A., 1953. Dendritic organization in the neurons of the visual and motor cortices of the cat. *J Anat.* 87, 387-406.
- Silverman, A.J., Hoffman, D.L., Zimmerman, E.A., 1981. The descending afferent connections of the paraventricular nucleus of the hypothalamus (PVN). *Brain Res Bull.* 6, 47-61.

- Simard, M., Nedergaard, M., 2004. The neurobiology of glia in the context of water and ion homeostasis. *Neuroscience*. 129, 877-96.
- Simonson, M.S., Jones, J.M., Dunn, M.J., 1992. Differential regulation of fos and jun gene expression and AP-1 cis-element activity by endothelin isopeptides. Possible implications for mitogenic signaling by endothelin. *J Biol Chem*. 267, 8643-9.
- Smith, D.W., Sibbald, J.R., Khanna, S., Day, T.A., 1995. Rat vasopressin cell responses to simulated hemorrhage: stimulus-dependent role for A1 noradrenergic neurons. *Am J Physiol*. 268, R1336-42.
- Smith, J.K., Barron, K.W., 1990. Cardiovascular effects of L-glutamate and tetrodotoxin microinjected into the rostral and caudal ventrolateral medulla in normotensive and spontaneously hypertensive rats. *Brain Res*. 506, 1-8.
- Smolny, M., Rogers, M.L., Shafton, A., Rush, R.A., Stebbing, M.J., 2014. Development of non-viral vehicles for targeted gene transfer into microglia via the integrin receptor CD11b. *Front Mol Neurosci*. 7, 79.
- Sofroniew, M.V., Vinters, H.V., 2010. Astrocytes: biology and pathology. *Acta Neuropathol*. 119, 7-35.
- Sokal, R.R., Rohlf, F.J., 2012. *Biometry*. Vol. Fourth, W.H. Freeman and Company, New York.
- Springell, D.A., Costin, N.S., Pilowsky, P.M., Goodchild, A.K., 2005. Hypotension and short-term anaesthesia induce ERK1/2 phosphorylation in autonomic nuclei of the brainstem. *Eur J Neurosci*. 22, 2257-70.
- Stanek, K.A., Neil, J.J., Sawyer, W.B., Loewy, A.D., 1984. Changes in regional blood flow and cardiac output after L-glutamate stimulation of A5 cell group. *Am J Physiol*. 246, H44-51.
- Stebbing, M.J., Cottee, J.M., Rana, I., 2015. The Role of Ion Channels in Microglial Activation and Proliferation - A Complex Interplay between Ligand-Gated Ion Channels, K(+) Channels, and Intracellular Ca(2.). *Front Immunol*. 6, 497.
- Stence, N., Waite, M., Dailey, M.E., 2001. Dynamics of microglial activation: a confocal time-lapse analysis in hippocampal slices. *Glia*. 33, 256-66.
- Stevens, B., Porta, S., Haak, L.L., Gallo, V., Fields, R.D., 2002. Adenosine: a neuron-glial transmitter promoting myelination in the CNS in response to action potentials. *Neuron*. 36, 855-68.
- Stirling, D.P., Khodarahmi, K., Liu, J., McPhail, L.T., McBride, C.B., Steeves, J.D., Ramer, M.S., Tetzlaff, W., 2004. Minocycline treatment reduces delayed oligodendrocyte death, attenuates axonal dieback, and improves functional outcome after spinal cord injury. *J Neurosci*. 24, 2182-90.
- Stith, R.D., Dormer, K.J., 1994. Pressor and endocrine responses to lesions of canine rostral ventrolateral medulla. *Am J Physiol*. 266, H2520-6.
- Stornetta, R.L., Morrison, S.F., Ruggiero, D.A., Reis, D.J., 1989. Neurons of rostral ventrolateral medulla mediate somatic pressor reflex. *Am J Physiol*. 256, R448-62.
- Stornetta, R.L., Akey, P.J., Guyenet, P.G., 1999. Location and electrophysiological characterization of rostral medullary adrenergic neurons that contain neuropeptide Y mRNA in rat medulla. *J Comp Neurol*. 415, 482-500.
- Stornetta, R.L., Schreihofer, A.M., Pelaez, N.M., Sevigny, C.P., Guyenet, P.G., 2001. Preproenkephalin mRNA is expressed by C1 and non-C1 barosensitive bulbospinal neurons in the rostral ventrolateral medulla of the rat. *J Comp Neurol*. 435, 111-26.
- Stornetta, R.L., Sevigny, C.P., Guyenet, P.G., 2002a. Vesicular glutamate transporter DNPI/VGLUT2 mRNA is present in C1 and several other groups of brainstem catecholaminergic neurons. *J Comp Neurol*. 444, 191-206.
- Stornetta, R.L., Sevigny, C.P., Schreihofer, A.M., Rosin, D.L., Guyenet, P.G., 2002b. Vesicular glutamate transporter DNPI/VGLUT2 is expressed by both C1 adrenergic and nonaminergic presympathetic vasomotor neurons of the rat medulla. *J Comp Neurol*. 444, 207-20.

- Stornetta, R.L., 2009. Neurochemistry of bulbospinal presympathetic neurons of the medulla oblongata. *J Chem Neuroanat.* 38, 222-30.
- Stornetta, R.L., Inglis, M.A., Viar, K.E., Guyenet, P.G., 2015. Afferent and efferent connections of C1 cells with spinal cord or hypothalamic projections in mice. *Brain Struct Funct.* 1-18.
- Strack, A.M., Sawyer, W.B., Marubio, L.M., Loewy, A.D., 1988. Spinal origin of sympathetic preganglionic neurons in the rat. *Brain Res.* 455, 187-91.
- Strack, A.M., Sawyer, W.B., Hughes, J.H., Platt, K.B., Loewy, A.D., 1989. A general pattern of CNS innervation of the sympathetic outflow demonstrated by transneuronal pseudorabies viral infections. *Brain Res.* 491, 156-62.
- Sumners, C., Horiuchi, M., Widdop, R.E., McCarthy, C., Unger, T., Steckelings, U.M., 2013. Protective arms of the renin-angiotensin-system in neurological disease. *Clin Exp Pharmacol Physiol.* 40, 580-8.
- Sumners, C., de Kloet, A.D., Krause, E.G., Unger, T., Steckelings, U.M., 2015. Angiotensin type 2 receptors: blood pressure regulation and end organ damage. *Curr Opin Pharmacol.* 21, 115-21.
- Sun, C., Li, H., Leng, L., Raizada, M.K., Bucala, R., Sumners, C., 2004. Macrophage migration inhibitory factor: an intracellular inhibitor of angiotensin II-induced increases in neuronal activity. *J Neurosci.* 24, 9944-52.
- Sun, M.-K., Young, B.S., Hackett, J.T., Guyenet, P.G., 1988a. Rostral ventrolateral medullary neurons with intrinsic pacemaker properties are not catecholaminergic. *Brain Res.* 451, 345-349.
- Sun, M.K., Guyenet, P.G., 1985. GABA-mediated baroreceptor inhibition of reticulospinal neurons. *Am J Physiol.* 249, R672-80.
- Sun, M.K., Guyenet, P.G., 1986. Hypothalamic glutamatergic input to medullary sympathoexcitatory neurons in rats. *Am J Physiol.* 251, R798-810.
- Sun, M.K., Hackett, J.T., Guyenet, P.G., 1988b. Sympathoexcitatory neurons of rostral ventrolateral medulla exhibit pacemaker properties in the presence of a glutamate-receptor antagonist. *Brain Res.* 438, 23-40.
- Sun, M.K., Young, B.S., Hackett, J.T., Guyenet, P.G., 1988c. Reticulospinal pacemaker neurons of the rat rostral ventrolateral medulla with putative sympathoexcitatory function: an intracellular study in vitro. *Brain Res.* 442, 229-39.
- Sun, M.K., 1995. Central neural organization and control of sympathetic nervous system in mammals. *Prog Neurobiol.* 47, 157-233.
- Sun, Q.J., Bautista, T.G., Berkowitz, R.G., Zhao, W.J., Pilowsky, P.M., 2011. The temporal relationship between non-respiratory burst activity of expiratory laryngeal motoneurons and phrenic apnoea during stimulation of the superior laryngeal nerve in rat. *J Physiol.* 589, 1819-30.
- Sun, W., Panneton, W.M., 2005. Defining projections from the caudal pressor area of the caudal ventrolateral medulla. *J Comp Neurol.* 482, 273-93.
- Sunanaga, J., Deng, B.S., Zhang, W., Kanmura, Y., Kuwaki, T., 2009. CO₂ activates orexin-containing neurons in mice. *Respir Physiol Neurobiol.* 166, 184-6.
- Suzuki, S., Pilowsky, P., Minson, J., Arnold, L., Llewellyn-Smith, I.J., Chalmers, J., 1994. c-fos antisense in rostral ventral medulla reduces arterial blood pressure. *Am J Physiol.* 266, R1418-22.
- Suzuki, S., Pilowsky, P., Minson, J., Arnold, L., Llewellyn-Smith, I., Chalmers, J., 1995. Antisense to thyrotropin releasing hormone receptor reduces arterial blood pressure in spontaneously hypertensive rats. *Circ Res.* 77, 679-83.
- Sved, A.F., Ito, S., Madden, C.J., 2000. Baroreflex dependent and independent roles of the caudal ventrolateral medulla in cardiovascular regulation. *Brain Res Bull.* 51, 129-33.
- Sved, A.F., Ito, S., Sved, J.C., 2003. Brainstem mechanisms of hypertension: role of the rostral ventrolateral medulla. *Curr Hypertens Rep.* 5, 262-8.

- Swanson, L.W., Kuypers, H.G., 1980. The paraventricular nucleus of the hypothalamus: cytoarchitectonic subdivisions and organization of projections to the pituitary, dorsal vagal complex, and spinal cord as demonstrated by retrograde fluorescence double-labeling methods. *J Comp Neurol.* 194, 555-70.
- Swanson, L.W., Sawchenko, P.E., Wiegand, S.J., Price, J.L., 1980. Separate neurons in the paraventricular nucleus project to the median eminence and to the medulla or spinal cord. *Brain Res.* 198, 190-5.
- Tagawa, T., Dampney, R.A.L., 1999. AT1 receptors mediate excitatory inputs to rostral ventrolateral medulla pressor neurons from hypothalamus. *Hypertension.* 34, 1301-1307.
- Tagawa, T., Horiuchi, J., Potts, P.D., Dampney, R.A.L., 1999. Sympathoinhibition after angiotensin receptor blockade in the rostral ventrolateral medulla is independent of glutamate and γ -aminobutyric acid receptors. *J Auton Nerv Syst.* 77, 21-30.
- Takagishi, M., Waki, H., Bhuiyan, M.E., Gouraud, S.S., Kohsaka, A., Cui, H., Yamazaki, T., Paton, J.F., Maeda, M., 2010. IL-6 microinjected in the nucleus tractus solitarii attenuates cardiac baroreceptor reflex function in rats. *Am J Physiol Regul Integr Comp Physiol.* 298, R183-90.
- Takakura, A.C., Moreira, T.S., West, G.H., Gwilt, J.M., Colombari, E., Stornetta, R.L., Guyenet, P.G., 2007. GABAergic pump cells of solitary tract nucleus innervate retrotrapezoid nucleus chemoreceptors. *J Neurophysiol.* 98, 374-81.
- Takami, S., Wong, Z.Y.H., Stebbing, M., Harrap, S.B., 1999. Linkage analysis of glucocorticoid and β 2-adrenergic receptor genes with blood pressure and body mass index. *Am J Physiol.* 276, H1379-H1384.
- Takeda, K., Nakata, T., Takesako, T., Itoh, H., Hirata, M., Kawasaki, S., Hayashi, J., Oguro, M., Sasaki, S., Nakagawa, M., 1991. Sympathetic inhibition and attenuation of spontaneous hypertension by PVN lesions in rats. *Brain Res.* 543, 296-300.
- Takesue, K., Kishi, T., Hirooka, Y., Sunagawa, K., 2016. Activation of microglia within paraventricular nucleus of hypothalamus is NOT involved in maintenance of established hypertension. *J Cardiol.*
- Talman, W.T., Snyder, D., Reis, D.J., 1980. Chronic lability of arterial pressure produced by destruction of A2 catecholaminergic neurons in rat brainstem. *Circ Res.* 46, 842-53.
- Talman, W.T., Granata, A.R., Reis, D.J., 1984. Glutamatergic mechanisms in the nucleus tractus solitarius in blood pressure control. *Fed Proc.* 43, 39-44.
- Talman, W.T., 1989. Kynurenic acid microinjected into the nucleus tractus solitarius of rat blocks the arterial baroreflex but not responses to glutamate. *Neurosci Lett.* 102, 247-52.
- Tanaka, J., Hayashi, Y., Watai, T., Fukami, Y., Johkoh, R., Shimamune, S., 1997. A1 noradrenergic modulation of AV3V inputs to PVN neurosecretory cells. *Neuroreport.* 8, 3147-50.
- Tauber, H., Waehneltd, T.V., Neuhoff, V., 1980. Myelination in rabbit optic nerves is accelerated by artificial eye opening. *Neurosci Lett.* 16, 235-8.
- Taylor, D.L., Diemel, L.T., Pocock, J.M., 2003. Activation of microglial group III metabotropic glutamate receptors protects neurons against microglial neurotoxicity. *J Neurosci.* 23, 2150-60.
- Taylor, D.L., Jones, F., Kubota, E.S., Pocock, J.M., 2005. Stimulation of microglial metabotropic glutamate receptor mGlu2 triggers tumor necrosis factor alpha-induced neurotoxicity in concert with microglial-derived Fas ligand. *J Neurosci.* 25, 2952-64.
- Teppema, L.J., Veening, J.G., Kranenburg, A., Dahan, A., Berkenbosch, A., Olivier, C., 1997. Expression of c-fos in the rat brainstem after exposure to hypoxia and to normoxic and hyperoxic hypercapnia. *J Comp Neurol.* 388, 169-90.

- Thor, K.B., Nickolaus, S., Helke, C.J., 1993. Autoradiographic localization of 5-hydroxytryptamine_{1A}, 5-hydroxytryptamine_{1B} and 5-hydroxytryptamine_{1C/2} binding sites in the rat spinal cord. *Neuroscience*. 55, 235-52.
- Thrasher, T.N., 1994. Baroreceptor regulation of vasopressin and renin secretion: low-pressure versus high-pressure receptors. *Front Neuroendocrinol*. 15, 157-96.
- Thrasher, T.N., Keil, L.C., 1998. Arterial baroreceptors control blood pressure and vasopressin responses to hemorrhage in conscious dogs. *Am J Physiol*. 275, R1843-57.
- Thrasher, T.N., 2005. Baroreceptors, baroreceptor unloading, and the long-term control of blood pressure. *Am J Physiol Regul Integr Comp Physiol*. 288, R819-27.
- Tremblay, M.E., Lowery, R.L., Majewska, A.K., 2010. Microglial interactions with synapses are modulated by visual experience. *PLoS Biol*. 8.
- Tremblay, M.E., Stevens, B., Sierra, A., Wake, H., Bessis, A., Nimmerjahn, A., 2011. The role of microglia in the healthy brain. *J Neurosci*. 31, 16064-9.
- Tseng, C.J., Lin, H.C., Wang, S.D., Tung, C.S., 1993. Immunohistochemical study of catecholamine enzymes and neuropeptide Y (NPY) in the rostral ventrolateral medulla and bulbospinal projection. *J Comp Neurol*. 334, 294-303.
- Tsuda, M., Shigemoto-Mogami, Y., Koizumi, S., Mizokoshi, A., Kohsaka, S., Salter, M.W., Inoue, K., 2003. P2X₄ receptors induced in spinal microglia gate tactile allodynia after nerve injury. *Nature*. 424, 778-783.
- Ueno, M., Fujita, Y., Tanaka, T., Nakamura, Y., Kikuta, J., Ishii, M., Yamashita, T., 2013. Layer V cortical neurons require microglial support for survival during postnatal development. *Nat Neurosci*. 16, 543-51.
- Ullian, E.M., Sapperstein, S.K., Christopherson, K.S., Barres, B.A., 2001. Control of synapse number by glia. *Science*. 291, 657-661.
- Urbanski, R.W., Sapru, H.N., 1988. Putative neurotransmitters involved in medullary cardiovascular regulation. *J Auton Nerv Syst*. 25, 181-93.
- Urbanski, R.W., Murugaian, J., Krieger, A.J., Sapru, H.N., 1989. Cardiovascular effects of substance P receptor stimulation in the ventrolateral medullary pressor and depressor areas. *Brain Res*. 491, 383-9.
- Usher, M., Cohen, J.D., Servan-Schreiber, D., Rajkowski, J., Aston-Jones, G., 1999. The role of locus coeruleus in the regulation of cognitive performance. *Science*. 283, 549-554.
- Van Bockstaele, E.J., Aston-Jones, G., Pieribone, V.A., Ennis, M., Shipley, M.T., 1991. Subregions of the periaqueductal gray topographically innervate the rostral ventral medulla in the rat. *J Comp Neurol*. 309, 305-27.
- van Giersbergen, P.L., Palkovits, M., De Jong, W., 1992. Involvement of neurotransmitters in the nucleus tractus solitarii in cardiovascular regulation. *Physiol Rev*. 72, 789-824.
- van Rossum, D., Hanisch, U.K., 2004. Microglia. *Metab Brain Dis*. 19, 393-411.
- Varner, K.J., Grosskreutz, C.L., Cox, B.F., Brody, M.J., 1989. Differential regulation of sympathetic nerve activity by lateral and medial subregions of the rostral ventral medulla. *Prog Brain Res*. 81, 99-103.
- Varner, K.J., Rutherford, D.S., Vasquez, E.C., Brody, M.J., 1992. Identification of cardiovascular neurons in the rostral ventromedial medulla in anesthetized rats. *Hypertension*. 19, 1193-7.
- Ventura, R., Harris, K.M., 1999. Three-dimensional relationships between hippocampal synapses and astrocytes. *J Neurosci*. 19, 6897-6906.
- Vera, P.L., Holets, V.R., Miller, K.E., 1990. Ultrastructural evidence of synaptic contacts between substance P-, enkephalin-, and serotonin-immunoreactive terminals and retrogradely labeled sympathetic preganglionic neurons in the rat: a study using a double-peroxidase procedure. *Synapse*. 6, 221-9.
- Verberne, A.J., Stornetta, R.L., Guyenet, P.G., 1999. Properties of C1 and other ventrolateral medullary neurones with hypothalamic projections in the rat. *J Physiol*. 517 (Pt 2), 477-94.

- Verna, A., Roumy, M., Leitner, L.M., 1975. Loss of chemoreceptive properties of the rabbit carotid body after destruction of the glomus cells. *Brain Res.* 100, 13-23.
- Verner, T.A., Goodchild, A.K., Pilowsky, P.M., 2004. A mapping study of cardiorespiratory responses to chemical stimulation of the midline medulla oblongata in ventilated and freely breathing rats. *Am J Physiol Regul Integr Comp Physiol.* 287, R411-21.
- Verner, T.A., Pilowsky, P.M., Goodchild, A.K., 2008. Retrograde projections to a discrete apneic site in the midline medulla oblongata of the rat. *Brain Res.* 1208, 128-36.
- Virchow, R., 1846. Ueber das granulirte Aussehen der Wandungen der Gehirnvventrikel. *Allg Z Psychiat.* 3, 242-2502.
- Vis, J.C., Nicholson, L.F., Faull, R.L., Evans, W.H., Severs, N.J., Green, C.R., 1998. Connexin expression in Huntington's diseased human brain. *Cell Biol Int.* 22, 837-47.
- Volterra, A., Meldolesi, J., 2005. Astrocytes, from brain glue to communication elements: the revolution continues. *Nat Rev Neurosci.* 6, 626-40.
- Wake, H., Moorhouse, A.J., Jinno, S., Kohsaka, S., Nabekura, J., 2009. Resting microglia directly monitor the functional state of synapses in vivo and determine the fate of ischemic terminals. *J Neurosci.* 29, 3974-80.
- Waki, H., Murphy, D., Yao, S.T., Kasparov, S., Paton, J.F.R., 2006. Endothelial NO synthase activity in nucleus tractus solitarii contributes to hypertension in spontaneously hypertensive rats. *Hypertension.* 48, 644-650.
- Waki, H., Liu, B., Miyake, M., Katahira, K., Murphy, D., Kasparov, S., Paton, J.F.R., 2007. Junctional adhesion molecule-1 is upregulated in spontaneously hypertensive rats: Evidence for a prohypertensive role within the brain stem. *Hypertension.* 49, 1321-1327.
- Waki, H., Gouraud, S.S., Maeda, M., Paton, J.F., 2008a. Specific inflammatory condition in nucleus tractus solitarii of the SHR: novel insight for neurogenic hypertension? *Auton Neurosci.* 142, 25-31.
- Waki, H., Gouraud, S.S., Maeda, M., Paton, J.F., 2008b. Gene expression profiles of major cytokines in the nucleus tractus solitarii of the spontaneously hypertensive rat. *Auton Neurosci.* 142, 40-4.
- Waki, H., Gouraud, S.S., Maeda, M., Paton, J.F., 2010. Evidence of specific inflammatory condition in nucleus tractus solitarii of spontaneously hypertensive rats. *Exp Physiol.* 95, 595-600.
- Waki, H., Gouraud, S.S., Maeda, M., Raizada, M.K., Paton, J.F., 2011. Contributions of vascular inflammation in the brainstem for neurogenic hypertension. *Respir Physiol Neurobiol.* 178, 422-8.
- Waki, H., Hendy, E.B., Hindmarch, C.C.T., Gouraud, S., Toward, M., Kasparov, S., Murphy, D., Paton, J.F.R., 2013. Excessive leukotriene B4 in nucleus tractus solitarii is prohypertensive in spontaneously hypertensive rats. *Hypertension.* 61, 194-201.
- Waldvogel, H.J., Baer, K., Eady, E., Allen, K.L., Gilbert, R.T., Mohler, H., Rees, M.I., Nicholson, L.F., Faull, R.L., 2010. Differential localization of gamma-aminobutyric acid type A and glycine receptor subunits and gephyrin in the human pons, medulla oblongata and uppermost cervical segment of the spinal cord: an immunohistochemical study. *J Comp Neurol.* 518, 305-28.
- Wallach, J.H., Loewy, A.D., 1980. Projections of the aortic nerve to the nucleus tractus solitarius in the rabbit. *Brain Res.* 188, 247-51.
- Wang, D., Cui, L.N., Renaud, L.P., 2003. Pre- and postsynaptic GABA(B) receptors modulate rapid neurotransmission from suprachiasmatic nucleus to parvocellular hypothalamic paraventricular nucleus neurons. *Neuroscience.* 118, 49-58.
- Wang, G., Zhang, J., Hu, X., Zhang, L., Mao, L., Jiang, X., Liou, A.K., Leak, R.K., Gao, Y., Chen, J., 2013a. Microglia/macrophage polarization dynamics in white matter after traumatic brain injury. *J Cereb Blood Flow Metab.* 33, 1864-74.

- Wang, S., Shi, Y., Shu, S., Guyenet, P.G., Bayliss, D.A., 2013b. Phox2b-expressing retrotrapezoid neurons are intrinsically responsive to H⁺ and CO₂. *J Neurosci.* 33, 7756-61.
- Wang, W.-Z., Gao, L., Wang, H.-J., Zucker, I.H., Wang, W., 2009. Tonic Glutamatergic Input in The Rostral Ventrolateral Medulla is Increased in Rats With Chronic Heart Failure. *Hypertension.* 53, 370-374.
- Waschek, J.A., 2013. VIP and PACAP: neuropeptide modulators of CNS inflammation, injury, and repair. *Br J Pharmacol.* 169, 512-23.
- Waxman, S.G., Sims, T.J., 1984. Specificity in central myelination: evidence for local regulation of myelin thickness. *Brain Res.* 292, 179-85.
- Webb, R.L., Osborn Jr, J.W., Cowley Jr, A.W., 1986. Cardiovascular actions of vasopressin: Baroreflex modulation in the conscious rats. *Am J Physiol.* 251.
- Wei, S.G., Zhang, Z.H., Beltz, T.G., Yu, Y., Johnson, A.K., Felder, R.B., 2013. Subfornical organ mediates sympathetic and hemodynamic responses to blood-borne proinflammatory cytokines. *Hypertension.* 62, 118-125.
- Wei, S.G., Yu, Y., Zhang, Z.H., Felder, R.B., 2015. Proinflammatory cytokines upregulate sympathoexcitatory mechanisms in the subfornical organ of the rat. *Hypertension.* 65, 1126-1133.
- Wenker, I.C., Sobrinho, C.R., Takakura, A.C., Mulkey, D.K., Moreira, T.S., 2013. P2Y₁-receptors expressed by C1 neurons determine peripheral chemoreceptor modulation of breathing, sympathetic activity and blood pressure. *Hypertension.* 62, 263-273.
- Weston, M., Wang, H., Stornetta, R.L., Sevigny, C.P., Guyenet, P.G., 2003. Fos expression by glutamatergic neurons of the solitary tract nucleus after phenylephrine-induced hypertension in rats. *J Comp Neurol.* 460, 525-41.
- Willette, R.N., Barcas, P.P., Krieger, A.J., Sapru, H.N., 1984. Endogenous GABAergic mechanisms in the medulla and the regulation of blood pressure. *J Pharmacol Exp Ther.* 230, 34-9.
- Willette, R.N., Punnen-Grandy, S., Krieger, A.J., Sapru, H.N., 1987. Differential regulation of regional vascular resistance by the rostral and caudal ventrolateral medulla in the rat. *J Auton Nerv Syst.* 18, 143-51.
- Windelborn, J.A., Mitchell, G.S., 2012. Glial activation in the spinal ventral horn caudal to cervical injury. *Respir Physiol Neurobiol.* 180, 61-8.
- Wong, Z.Y., Stebbing, M., Ellis, J.A., Lamantia, A., Harrap, S.B., 1999. Genetic linkage of beta and gamma subunits of epithelial sodium channel to systolic blood pressure. *Lancet.* 353, 1222-5.
- Wu, K.L., Chan, S.H., Chan, J.Y., 2012. Neuroinflammation and oxidative stress in rostral ventrolateral medulla contribute to neurogenic hypertension induced by systemic inflammation. *J Neuroinflamm.* 9, 212.
- Wyszogrodski, I., Polosa, C., 1973. The inhibition of sympathetic preganglionic neurons by somatic afferents. *Can J Physiol Pharmacol.* 51, 29-38.
- Xavier, A.L., Menezes, J.R., Goldman, S.A., Nedergaard, M., 2014. Fine-tuning the central nervous system: microglial modelling of cells and synapses. *Philos Trans R Soc Lond B Biol Sci.* 369, 20130593.
- Xu, B., Zheng, H., Patel, K.P., 2012. Enhanced activation of RVLM-projecting PVN neurons in rats with chronic heart failure. *Am J Physiol Heart Circ Physiol.* 302, H1700-11.
- Xu, H.T., Pan, F., Yang, G., Gan, W.B., 2007. Choice of cranial window type for in vivo imaging affects dendritic spine turnover in the cortex. *Nat Neurosci.* 10, 549-51.
- Yamada, S., Ishima, T., Hayashi, M., Tomita, T., Hayashi, E., 1984. Muscarinic cholinergic receptors and choline acetyltransferase activity in the hypothalamus of spontaneously hypertensive rats. *Life Sci.* 34, 2151-8.

- Yamada, T., Mochiduki, A., Sugimoto, Y., Suzuki, Y., Itoi, K., Inoue, K., 2009. Prolactin-releasing peptide regulates the cardiovascular system via corticotrophin-releasing hormone. *J Neuroendocrinol.* 21, 586-93.
- Yamazato, M., Sakima, A., Nakazato, J., Sesoko, S., Muratani, H., Fukiyama, K., 2001. Hypotensive and sedative effects of clonidine injected into the rostral ventrolateral medulla of conscious rats. *Am J Physiol* 281, R1868-76.
- Yang, Z., Bertram, D., Coote, J.H., 2001. The role of glutamate and vasopressin in the excitation of RVL neurones by paraventricular neurones. *Brain Res.* 908, 99-103.
- Yau, J.I., Wu, J.J., Liu, J.C., 1991. Origins of the afferent fibers to the cat superior cervical ganglion. *Proc Natl Sci Counc Repub China B.* 15, 1-7.
- Young, M.M., Smith, M.E., Coote, J.H., 1999. Effect of sympathectomy on the expression of NMDA receptors in the spinal cord. *J Neurol Sci.* 169, 156-60.
- Yu, D., Gordon, F.J., 1996. Anatomical evidence for a bi-neuronal pathway connecting the nucleus tractus solitarius to caudal ventrolateral medulla to rostral ventrolateral medulla in the rat. *Neurosci Lett.* 205, 21-4.
- Zaretsky, D.V., Zaretskaia, M.V., Samuels, B.C., Cluxton, L.K., DiMicco, J.A., 2003. Microinjection of muscimol into raphe pallidus suppresses tachycardia associated with air stress in conscious rats. *J Physiol.* 546, 243-50.
- Zha, Y.P., Wang, Y.K., Deng, Y., Zhang, R.W., Tan, X., Yuan, W.J., Deng, X.M., Wang, W.Z., 2013. Exercise training lowers the enhanced tonically active glutamatergic input to the rostral ventrolateral medulla in hypertensive rats. *CNS Neurosci Ther.* 19, 244-51.
- Zhang, J., Mifflin, S.W., 2000. Responses of aortic depressor nerve-evoked neurones in rat nucleus of the solitary tract to changes in blood pressure. *J Physiol.* 529, 431-443.
- Zhang, W., Mifflin, S.W., 1993. Excitatory amino acid receptors within NTS mediate arterial chemoreceptor reflexes in rats. *Am J Physiol.* 265, H770-H773.
- Zhang, W., Mifflin, S.W., 1995. Excitatory amino-acid receptors contribute to carotid sinus and vagus nerve evoked excitation of neurons in the nucleus of the tractus solitarius. *J Auton Nerv Syst.* 55, 50-6.
- Zhang, X., Zeng, L., Yu, T., Xu, Y., Pu, S., Du, D., Jiang, W., 2014. Positive feedback loop of autocrine BDNF from microglia causes prolonged microglia activation. *Cell Physiol Biochem.* 34, 715-23.
- Zhong, S., Barman, S.M., Gebber, G.L., 1992. Effects of brain stem lesions on 10-Hz and 2- to 6-Hz rhythms in sympathetic nerve discharge. *Am J Physiol.* 262, R1015-24.
- Zhong, S., Huang, Z.S., Gebber, G.L., Barman, S.M., 1993a. Role of the brain stem in generating the 2- to 6-Hz oscillation in sympathetic nerve discharge. *Am J Physiol.* 265, R1026-35.
- Zhong, S., Huang, Z.S., Gebber, G.L., Barman, S.M., 1993b. The 10-Hz sympathetic rhythm is dependent on raphe and rostral ventrolateral medullary neurons. *Am J Physiol.* 264, R857-R866.
- Zubcevic, J., Waki, H., Raizada, M.K., Paton, J.F.R., 2011. Autonomic-Immune-Vascular Interaction: An Emerging Concept for Neurogenic Hypertension. *Hypertension.* 57, 1026-1033.
- Zwicker, J.D., Rajani, V., Hahn, L.B., Funk, G.D., 2011. Purinergic modulation of preBotzinger complex inspiratory rhythm in rodents: the interaction between ATP and adenosine. *J Physiol.* 589, 4583-600.
- Zwicker, J.D., Zhang, Y., Ren, J., Hutchinson, M.R., Rice, K.C., Watkins, L.R., Greer, J.J., Funk, G.D., 2014. Glial TLR4 signaling does not contribute to opioid-induced depression of respiration. *J Appl Physiol* (1985). 117, 857-68.

Appendix 1

List of suppliers and product codes of all items used during the candidature

Name	Product code	Company	Country
Agar	A1296-500G	Sigma-Aldrich	Australia
Atropine sulphate	1957699	Pfizer	USA
Diethylpyrocarbonate (DEPC)	D5758-25ML	Sigma-Aldrich	Australia
Ethylene glycol	324558-1L	Sigma-Aldrich	Australia
Hydrochloric acid	H9892-100ML	Sigma-Aldrich	Australia
Heparin	H1290	Cenvet	Australia
Hydralazine	H1753-10G	Sigma-Aldrich	Australia
Sodium hydroxide	S2770-100ML	Sigma-Aldrich	Australia
Pancuronium bromide	1256060	Pfizer	USA
Paraformaldehyde	158127-3KG	Sigma-Aldrich	Australia
Phenylephrine hydrochloride	P1626-10G	Sigma-Aldrich	Australia
PBS tablets	P4417-100TAB	Sigma-Aldrich	Australia
Polyvinylpyrrolidone (PVP-40)	PVP40-500G	Sigma-Aldrich	Australia
Potassium chloride	PA054-500G	Chem-supply	Australia
RNAse free sucrose	84097-1KG	Sigma-Aldrich	Australia
Sodium chloride	SA046-3KG	Chem-supply	Australia
Sodium Pentobarbital	N1660	Cenvet	Australia
Sodium phosphate dibasic (Na ₂ HPO ₄)	S3264-1KG	Sigma-Aldrich	Australia
Sodium phosphate monobasic (NaH ₂ PO ₄)	S3139-1KG	Sigma-Aldrich	Australia
Thimerosal (merthiolate)	T5125-100G	Sigma-Aldrich	Australia
Tris buffer	T1503-1KG	Sigma-Aldrich	Australia
Triton X-100	T8787-250ML	Sigma-Aldrich	Australia
Urethane	U2500-100G	Sigma-Aldrich	Australia
Vectashield	H-1000	Abacus ALS	Australia

Equipment	Model	Company	Country
Axio scan slide scanning microscope	Axio scan. Z1 slide scanner	Carl Zeiss	Germany
Axiocam digital camera	HRm	Carl Zeiss	Germany
Blood gas analyzer	Vetstat Electrolyte and Blood gas analyzer	IDEXX	Australia
BP amplifier	BMA-931	CWE	USA
BP transducer		Argon Critical care systems	Singapore
Cambridge Electronic Design ADC system	CED 1401	Cambridge Electronic Design	UK
Cautery		RB medical engineering Ltd.	
CO ₂ analyzer	Capstar 100	CWE	USA
Epifluorescence microscope	Axio Imager Z2	Carl Zeiss	Germany
Filter cubes: AMCA, FITC, Cy3 and Cy5		Semrock	USA
Homeothermic heating blanket	TC-1000	CWE	
IITC MRBP system	For rodents	IITC Life Sciences	USA
Infusion pump	702208	Harvard Apparatus	USA
Leica confocal microscope	SPE-II	Leica	Germany
Medical Oxygen flowmeter	G8801	Gascon	Australia
Oxygen Cylinder	202150	Coregas	Australia
Oxygen regulator (Series-O)	518800	Addtech+	Australia
Polyethylene tubing	PE9050	Microtube Extrusions	Australia
Silk sutures		Pearsalls	UK
Ventilator	Rodent ventilator	UGO Basile Biological Research Apparatus	Italy
Vibratome	VT1200S	Leica	Germany
ZEISS confocal microscope	LSM 510 Meta Spectral	Carl Zeiss	Germany

Name	Version	Company	Country
Corel Draw	X7	Corel cooperation	Australia
End Note	X7	Thomson Reuters	USA
GraphPad Prism	6.05	GraphPad Prism	USA
Spike 2	8.01	Cambridge Electronic Design	UK
Microsoft Office	2013	Microsoft	Australia
Image J	1.50b	National Institutes of Health (NIH)	USA
Zen	2012	Carl Zeiss	Germany

Primary and corresponding secondary antibodies used for immunohistochemistry experiments

Name	Immunogen	Host/ clonality	Company/ catalogue number	Concen tration used*	Secondary antibody**
CD16	Whole white blood cells (clone ASH 1975)	Mouse monoclonal (IgG2a)	US biological, Life Sciences/C2 267-32	1:400	AlexaFluor488 Goat anti Mouse – 115-545-206
CD206	Synthetic peptide derived from within residues 1400 to the C-terminus of Human Mannose receptor	Rabbit polyclonal	Abcam/ab6 4693	1:2000	AlexaFluor 488 Donkey anti Rabbit - 711-546-152
CD68	Synthetic peptide corresponding to mouse CD68 (internal sequence)	Rabbit polyclonal	Abcam/ ab125212	1:2000	Cy3 Donkey anti Rabbit - 711-166-152

c-Fos	Synthetic peptide amino acid 2-17 in rat	Guinea Pig polyclonal	Synaptic Systems/22 6 004	1:2000	AlexaFluor 488 Donkey anti Guinea Pig - 706-546- 148
Iba1	Synthetic peptide to C-terminus of Iba1	Rabbit polyclonal	Wako Pure Chemical Industries, Ltd./019- 19741	1:2000	Cy3 Donkey anti Rabbit - 711-166-152
Iba1	Synthetic peptide: TGPPAKKAISELP	Goat polyclonal	Novus Biologicals/ NB100- 1028	1:1000	Cy3 Donkey anti Goat - 705-546-147
Synapsin	Synthetic peptide “NYLRRRLSDSNFM ANLPNGYMTDLRQ P” corresponding to N terminus of rat synapsin protein	Guinea Pig Polyclonal	Synaptic Systems/ 106004	1:1000	AMCA Donkey anti Guinea Pig 706-156-148
TH	Rat PC-12 pheochromocytoma cell tyrosine hydroxylase (clone TH-2)	Mouse monoclon al (IgG1)	Sigma- Aldrich/T12 99	1:500	Cy5 Donkey anti Mouse – 715-175-151
TH	Synthetic peptide: CPRFIGRRQSLIEDA RK	Mouse monoclon al (IgG1κ)	Avanti antibodies/# AV1	1:100	Cy5 Donkey anti Mouse – 715-175-151 Cy5 Goat anti- mouse – 115- 175-205

TH	Full length native protein (purified) corresponding to rat TH protein	Sheep polyclonal	Abcam/ Ab113	1:3000	Cy3 Donkey anti Sheep - 713-166-147
----	---	------------------	--------------	--------	-------------------------------------

*optimum concentration for all primary antibodies was determined by titration on the basis of manufacturer's recommendations using fixed brainstem tissue collected from SD rats perfused with 0.1 M PBS followed by fixation with 4% paraformaldehyde.

**all the secondary antibodies were purchased from Jacksons Immunoresearch and used at 1:500 concentration unless, otherwise stated

Appendix 2

Publications



Microglial number is related to the number of tyrosine hydroxylase neurons in SHR and normotensive rats



Komal Kapoor^{a,b}, Amol M. Bhandare^{a,b}, Suja Mohammed^{b,c}, Melissa M.J. Farnham^{b,c}, Paul M. Pilowsky^{b,c,*}

^a Faculty of Medicine and Health Sciences, Macquarie University, Sydney, New South Wales 2109, Australia

^b The Heart Research Institute, Sydney, New South Wales 2042, Australia

^c Department of Physiology, University of Sydney, Sydney, New South Wales 2006, Australia

ARTICLE INFO

Article history:

Received 7 February 2016

Received in revised form 19 May 2016

Accepted 20 May 2016

Keywords:

Microglia

Iba1

Tyrosine hydroxylase

SD

WKY

Hypertensive

Brainstem

ABSTRACT

Microglia are ubiquitously distributed throughout the central nervous system (CNS) and play a critical role in the maintenance of neuronal homeostasis. Recent advances have shown that microglia, never resting cells of the CNS, continuously monitor and influence neuronal/synaptic activity levels, by communicating with neurons with the aid of their dynamic processes. The brainstem contains many catecholaminergic nuclei that are key to many aspects of brain function. This includes C1 neurons of the ventrolateral medulla that are thought to play a critical role in control of the circulation. Despite the role of catecholaminergic brainstem neurons in normal physiology, the presence of microglia that surrounds them is poorly understood. Here, we investigate the spatial distribution and morphology of microglia in catecholaminergic nuclei of the brainstem in 3 strains of rat: Sprague-Dawley (SD), Wistar-Kyoto (WKY) and spontaneously hypertensive rats (SHR). Our data reveal that microglia are heterogeneously distributed within and across different strains of rats. Interestingly, intra-strain comparison of tyrosine hydroxylase-immunoreactive (TH-ir) neuronal and microglial number reveals that microglial number varies with the TH-ir neuronal number in the brainstem. Even though microglial spatial distribution varies across brainstem nuclei, microglial morphology (% area covered, number of end point processes and branch length) does not differ significantly. This work provides the first evidence that even though microglia, in their surveilling state, do not vary appreciably in their morphology across brainstem areas, they do have a heterogeneous pattern of distribution that may be influenced by their local environment.

Crown Copyright © 2016 Published by Elsevier B.V. All rights reserved.

1. Introduction

Microglia are the tissue resident macrophages of the central nervous system (CNS). They are ubiquitously distributed, and comprise ≈10–15% of cell population in the CNS (Xavier et al., 2014). Microglia are of mesodermal origin and populate the CNS during early stages of development, and are self-renewing in case of depletion (Ajami et al., 2007). Since 2005, microglia are no longer known solely for their critical role as immune cells of the CNS (Nimmerjahn et al., 2005). Recent work about the function of microglia concerns their role in maintaining normal brain homeostasis. The ability of microglia to communicate, detect changes, and influence the activity of neurons (Pocock and Kettenmann, 2007) and astrocytes (Aloisi et al., 1997; Pyo et al., 2003), highlights their role as an integral component of the “Glial Family”. Microglia, in their resting/surveilling state, are capable of performing activities, such as release of neurotrophic factors (Karperien et al., 2013; Ueno et al., 2013) or synaptic

pruning (Kettenmann et al., 2013; Miyamoto et al., 2013); during injury, microglia transform into a more macrophage-like ‘activated’ state removing debris, and enhancing tissue repair (David and Kroner, 2011; Kroner et al., 2014; Windelborn and Mitchell, 2012). The role of microglia in non-injurious situations is less clear.

Microglia are ubiquitously, yet heterogeneously, distributed in many areas of the CNS, including the hippocampus, olfactory telencephalon, cerebellum, cortex and spinal cord (de Haas et al., 2008; Lawson et al., 1990; Mittelbronn et al., 2001; Nikodemova et al., 2014). Heterogeneous microglial distribution, chemical expression profiles and morphology are hypothesised to be strongly influenced by their local environment (de Haas et al., 2008; Kapoor et al., in press; Lawson et al., 1990; Mittelbronn et al., 2001; Nikodemova et al., 2014). However, exact factors responsible for the heterogeneity in microglial expression, in a given environment, are still unknown.

Catecholaminergic nuclei of the brainstem are involved in almost every aspect of cardiorespiratory control, ranging from the maintenance of tonic activity of the sympathetic nervous system (SNS) to somatosensory reflex responses (Pilowsky et al., 2009). Phenotypically, catecholaminergic nuclei are immunoreactive for tyrosine hydroxylase (TH), and extend from the caudal ventrolateral medullary region to the pons, including A1, A2, C1, C3, A5 and A6

Abbreviations: ANS, autonomic nervous system; CNS, central nervous system; DBH, dopamine β-hydroxylase; PBS, phosphate buffered saline; SD, Sprague-Dawley; SHR, spontaneously hypertensive rats; TH, tyrosine hydroxylase; WKY, Wistar-Kyoto.

* Corresponding author at: University of Sydney & Heart Research Institute, 7 Eliza St. Newtown 2042, Australia.

E-mail address: paul.pilowsky@hri.org.au (P.M. Pilowsky).

<http://dx.doi.org/10.1016/j.autneu.2016.05.005>

1566-0702/Crown Copyright © 2016 Published by Elsevier B.V. All rights reserved.

(Dahlström and Fuxe, 1964). Studies using stimuli, such as hypotension, hypertension and glucoprivation, have shown that the neuronal activity of various catecholaminergic nuclei of the brainstem is affected by these homeostatic challenges (Dampney and Horiuchi, 2003; Graham et al., 1995; Springell et al., 2005). For example, acute hypotension, induced by intravenous injection of hydralazine or infusion of sodium nitroprusside, causes activation of neurons located in the A1 (Benarroch, 1998), C1 (Minson et al., 1996; Miyawaki et al., 2002), A5 (Dampney and Horiuchi, 2003) and A6 regions of the brainstem (Dampney and Horiuchi, 2003). On the other hand, induction of glucoprivation causes activation of A6 neurons (Ritter et al., 1998). The A2 catecholaminergic nucleus of brainstem not only responds to cardiorespiratory stimuli, but also responds to other diverse range of signals such as hormonal, gastrointestinal and inflammatory (Rinaman, 2011). The function of C3 group of neurons of the brainstem is the least studied, but they may be sympathoexcitatory and respond to stimuli affecting glucose homeostasis (Menuet et al., 2014). In fact, it may be that C3 neurons are simply anatomically displaced C1 or C2 neurons that did not reach their final destination in the ventral or dorsal medulla oblongata.

Recent work has shown that close lines of communication exist between microglia and the SNS (Bhandare et al., 2016; Bhandare et al., 2015; Kapoor et al., in press; Shi et al., 2010). As mentioned above, catecholaminergic nuclei in the brainstem are critical in the regulation of sympathetic nerve activity. The close link between microglia and the SNS, and previously proposed hypothesis that microglial distribution is influenced by their local environment (de Haas et al., 2008), formed the foundation of aims of the present study. Therefore, in this study, we aimed to identify if the microglial distribution is related to the neuronal heterogeneity in the SNS. For the purpose of this study, we used 3 different strains of rats: Sprague-Dawley (SD), the Wistar-Kyoto (WKY) and the spontaneously hypertensive rat (SHR).

2. Experimental procedures

2.1. Animals

Experiments were conducted in adult male rats from 3 different strains: SD, WKY (>18 weeks old) and SHR (>18 weeks old); $n = 3$ per group (300–420 g; Animal Resource Centre; Perth, Australia) in accordance with the Australian code of practice for the care and use of animals for scientific purposes. All procedures and protocols performed were approved by the Sydney Local Health District Animal Welfare Committee and the Macquarie University Animal Care and Ethics Committee, Sydney, Australia.

The blood pressure phenotype of SHR and WKY was determined by tail-cuff sphygmomanometry at >18 weeks of age, prior to perfusion (Farnham et al., 2012). Hypertension was defined as a systolic pressure of >180 mm Hg and normotension was defined as a systolic pressure of <150 mm Hg.

2.2. Experimental protocol

2.2.1. Perfusion and tissue processing

Animals were deeply anaesthetized with sodium pentobarbital (>72 mg/kg i.p.; Cenvet Australia) and were transcardially perfused with ≈ 400 ml of ice cold 0.1 M phosphate buffered saline (PBS) followed by fixation with ≈ 400 ml of ice cold 4% paraformaldehyde in 0.1 M PBS (pH 7.4). Extracted brainstem tissue was fixed overnight in 4% paraformaldehyde in 0.1 M PBS (pH 7.4) at 4 °C, while shaking continuously. Brainstems were then sectioned transversely, using a vibrating microtome (VT1200S, Leica), at 40 μ m and were collected sequentially into 5 pots. These sections were stored in cryoprotectant solution (30% sucrose, 30% ethylene glycol, 2% polyvinylpyrrolidone in 0.1 M PBS) at -20 °C until processed for immunohistochemistry.

2.2.2. Immunohistochemistry

Immunohistochemistry was conducted as described previously (Kapoor et al., in press; Nedoboy et al., 2016). Briefly, free floating 40 μ m brainstem sections were washed in 0.1 M PBS with 0.3% Triton X-100, 3 times for 30 min each, at room temperature. After washing, sections were incubated for >48 h in TPBSm (10 mM Tris-HCl, 0.1 M PBS, 0.9% NaCl, 0.3% Triton X-100 and 0.1% merthiolate at pH 7.4), 10% normal donkey serum with primary antibodies raised against TH (mouse monoclonal (IgG1 κ), Avanti antibodies, #AV1 (Nedoboy et al., 2016); 1:100) and Iba1 (rabbit polyclonal, Wako Pure Chemical Industries Ltd., 019-19741; 1:2000) at 4 °C while shaking. Sections were then washed 3 times for 30 min each in TPBS (10 mM Tris-HCl, 0.1 M PBS and 0.9% NaCl at pH 7.4) and incubated overnight with secondary antibodies raised in donkey: donkey anti mouse Cy5 (Jacksons Immunoresearch 715-175-151; 1:500) and donkey anti rabbit Cy3 (Jacksons Immunoresearch 711-166-152; 1:500) in TPBSm (10 mM Tris-HCl,

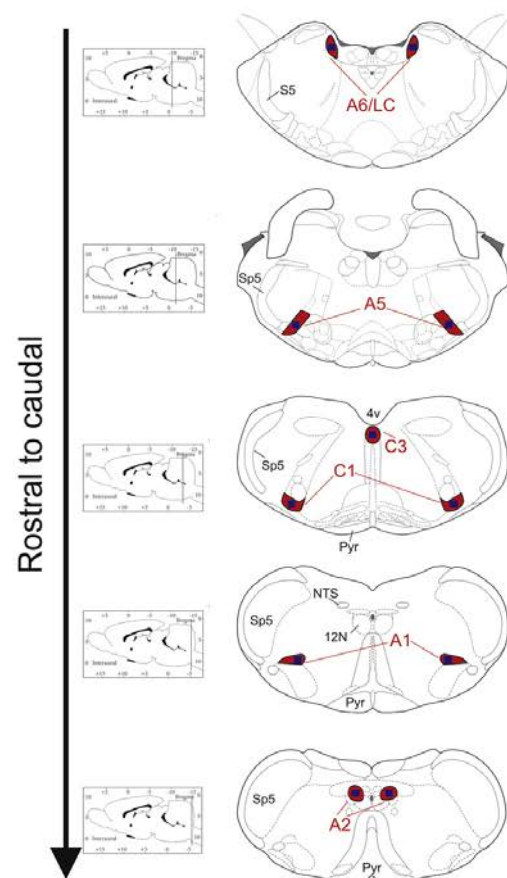


Fig. 1. Location of various catecholaminergic nuclei in the brainstem of a rat (SD, WKY or SHR). 6 catecholaminergic nuclei of interest (A1/A2/C1/C3/A5/A6) are highlighted in red. The area of interest imaged was the same between catecholaminergic nuclei (blue). S5, sensory root of the trigeminal nerve; Sp5, spinal trigeminal tract; 4v, 4th ventricle; Pyr, pyramidal tracts; NTS, nucleus of the solitary tract; 12N, 12th nucleus. The figure is adapted from Paxinos and Watson (2007) (see Experimental procedures for details).

0.1 M PBS, 0.9% NaCl and 0.1% merthiolate at pH 7.4) with 2% normal donkey serum at room temperature while shaking. Sections were then washed in TPBS 3 times for 30 min each at room temperature while shaking. These sections were then mounted, caudal to rostral, on glass slides (Thermo Fisher Scientific), cover-slipped with Vectashield (H-1000, Vector Laboratories) and sealed with clear nail polish for imaging.

2.2.3. Image acquisition

Brainstem sections were imaged using an Axio Imager Z2 (Zen software, Zeiss, Germany) for subsequent analysis. Each fluorochrome was imaged individually with appropriate filter cubes (TH-Cy5 with 650/670 nm (ex/em) and Iba1-Cy3 with 550/570 nm (ex/em)). Bilateral 'Z-stack' images of A1, A2, C1, A5 and A6 and medial 'Z-stack' images of C3 at 40 \times magnification were obtained, covering an area of 400 μ m \times 400 μ m, 30 μ m in depth, at an interval of 0.62 μ m generating a stack of \approx 46 Z slices, for each repeat in each strain (3 strains; n = 3 each; Fig. 1).

A rat brain atlas (Paxinos and Watson, 2007) was used to define the anatomical location of the neuronal population analysed in this study. The A1 nucleus was defined as the area comprising of TH immunoreactive (TH-ir) neurons in the caudal ventrolateral medulla at the level of the area postrema and \approx 14.28 mm caudal to bregma (Fig. 1). The A2 was defined as the area in and around the medial region of the nucleus of the solitary tract, at the level of \approx 14.64 mm caudal to bregma (Fig. 1). The C1 was defined as a triangular area ventral to the nucleus ambiguus, medial to the spinal trigeminal tract and lateral to the pyramidal tracts at the level of \approx 12.36 mm caudal to bregma (Fig. 1). The C3 was defined as the area populated with TH-ir neurons, in close proximity to 4th ventricle and at the level of \approx 12.36 mm caudal to bregma (Fig. 1). The A5 was defined as the area nearer to the pontomesencephalic junction mostly between the descending facial nerve fibres and the superior olive, at the level of \approx 10.56 mm caudal to bregma (Fig. 1). A6 neurons were located beside the fourth ventricle at the pontomesencephalic junction, rostral to the facial nucleus and at the level of \approx 9.72 mm caudal to bregma (Fig. 1).

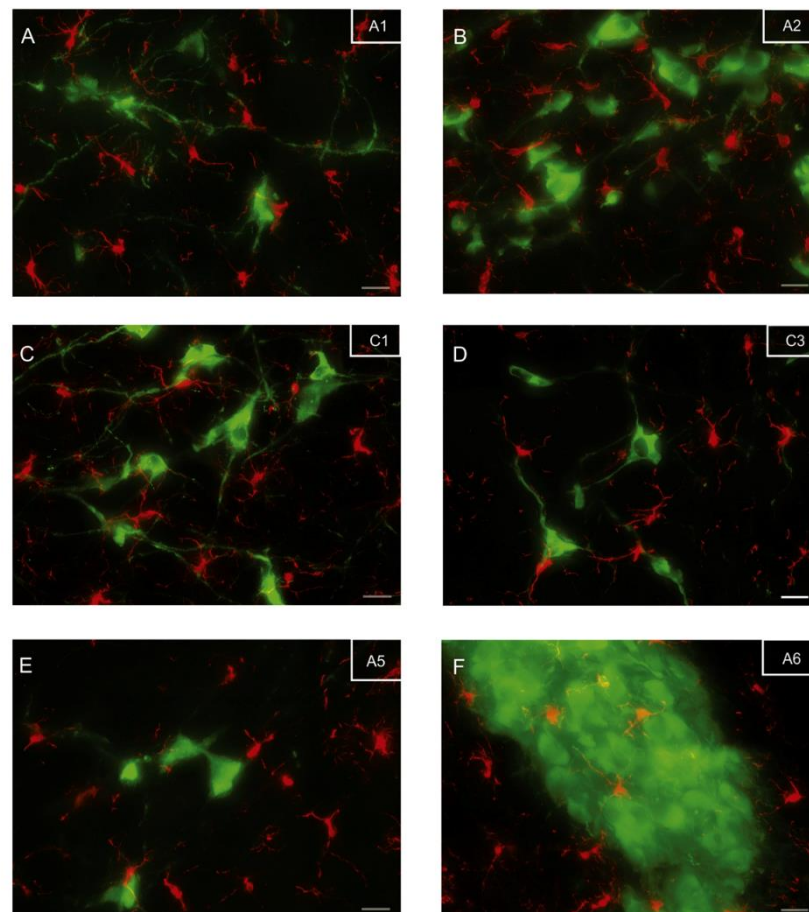


Fig. 2. Microglia in brainstem catecholaminergic nuclei of a SD. A. A1, B. A2, C. C1, D. C3, E. A5 and F. A6. Scale bar = 20 μ m. Microglia, Iba1 – red and TH – green. The region of interest was kept constant across all catecholaminergic nuclei.

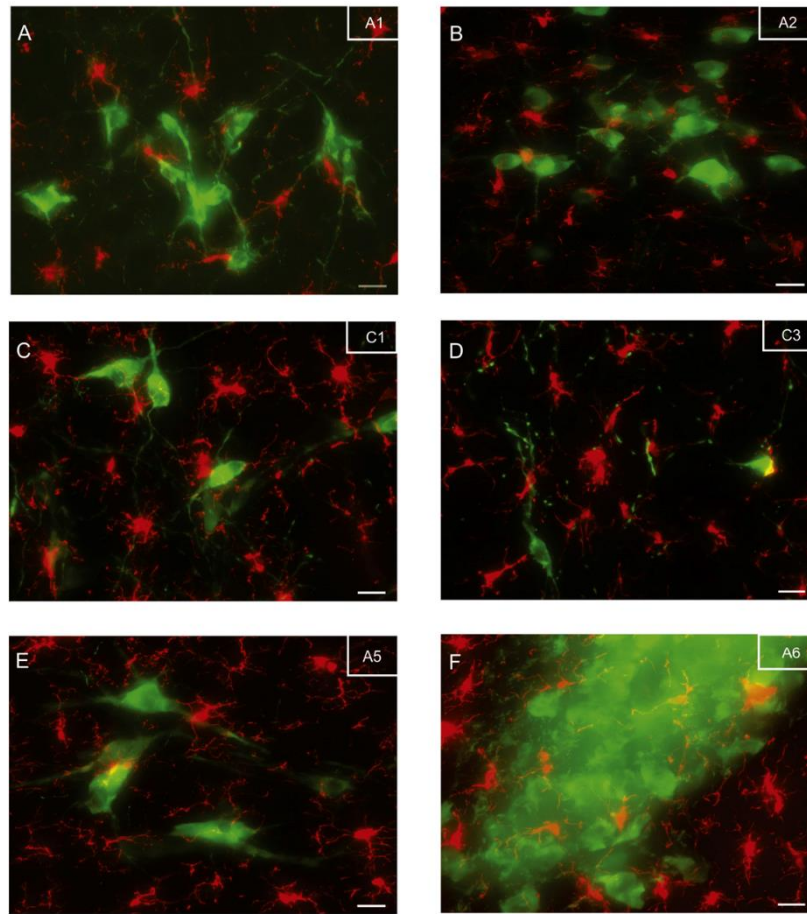


Fig. 3. Microglia in brainstem catecholaminergic nuclei of a WKY rat. A. A1, B. A2, C. C1, D. C3, E. A5 and F. A6. Scale bar = 20 μ m. Microglia, Iba1 – red and TH – green. The region of interest was kept constant across all catecholaminergic nuclei.

2.2.4. Image analysis

Maximum intensity projections of acquired ‘Z-slices’ were adjusted for brightness and contrast to highlight morphological features of microglia. Bilateral maximum intensity projection images acquired for A1, A2, C1, A5 and A6 regions, and medial images acquired for the C3 region, were used to quantify the overall number of TH-ir neurons, microglia and morphological characteristics of microglia. Number of TH-ir neurons and microglia were counted in images obtained for each region from each repeat; objects present at the boundary of images were excluded from the final counts. Microglial morphology was quantified as described by Morrison and Filosa (2013). Briefly, the maximum intensity projection images were imported into Image J as 8 bit images and ‘skeletonised’ (Fig. 6A). The ‘skeletonised’ image was analysed using the ‘AnalyzeSkeleton’ Image J plugin to acquire the number of end points and branch length (μ m) which, when normalised to the number of microglia in that specific frame, provides an indication of microglial morphology (Fig. 6A). The percentage (%) of area occupied by microglia was quantified with the help of the ‘measure’ feature in Image J software.

2.2.5. Data analysis and statistics

GraphPad Prism version 6.05 was used to perform all statistical analysis. Numbers of TH-ir neurons and microglia were treated as non-parametric non-continuous data, and were pooled from 3 repeats for each strain, for each brainstem nuclei (Kapoor et al., in press; Nedoboy et al., 2016; Sokal and Rohlf, 2012). Supplementary Fig. 1 shows minor biological variability in the number of TH-ir neurons and microglia, within each strain. The relationship between the pattern of distribution of TH-ir neurons and microglia across different catecholaminergic nuclei, intra- and inter- strain, was analysed using the Chi-square test of independence (Sokal and Rohlf, 2012). Parameters obtained highlighting the microglial morphology in catecholaminergic nuclei were treated as non-parametric continuous data, and were averaged across repeats ($n = 3$), and analysed using a Kruskal-Wallis one-way analysis of variance.

3. Results

Microglia were distributed ubiquitously in catecholaminergic nuclei of brainstem (A1, A2, C1, C3, A5 and A6) in the SD (Fig. 2A–F), the WKY

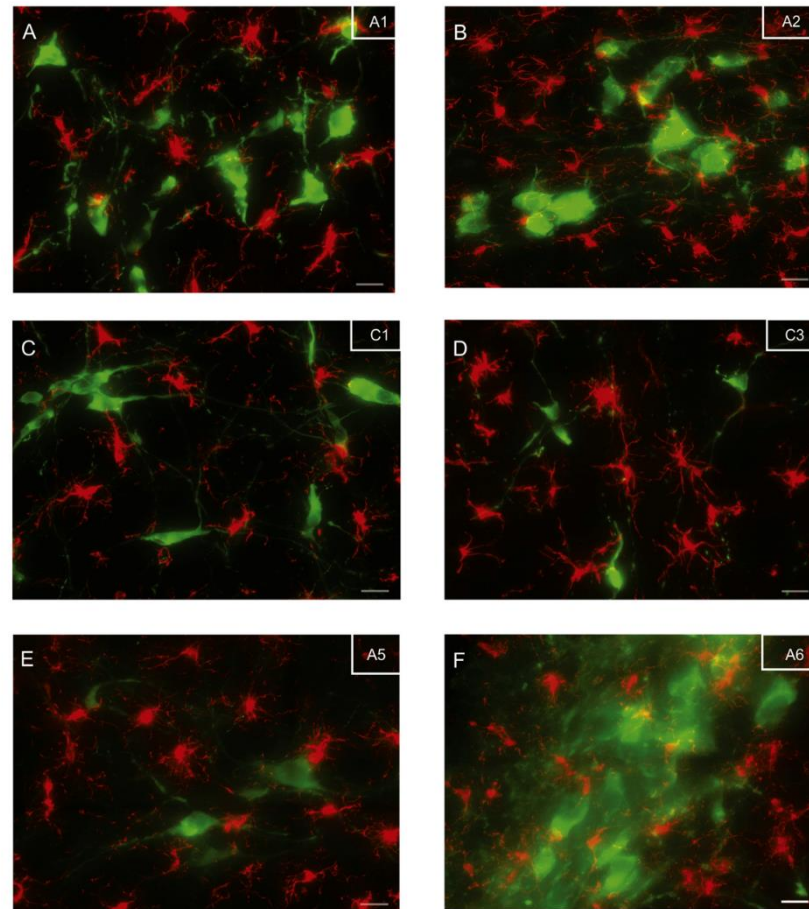


Fig. 4. Microglia in brainstem catecholaminergic nuclei of an SHR. A. A1, B. A2, C. C1, D. C3, E. A5 and F. A6. Scale bar = 20 μ m. Microglia, Iba1 – red and TH – green. The region of interest was kept constant across all catecholaminergic nuclei.

(Fig. 3A–F) and the SHR (Fig. 4A–F) strains of rats. However, TH neuronal and microglial number varied between regions and strains.

3.1. Intra-strain comparison demonstrating that microglial number is related to the number of TH-ir neurons in a catecholaminergic nucleus

Intra-strain (SD, WKY or SHR) comparisons of the number of TH-ir neurons in catecholaminergic nuclei of brainstem revealed that the TH-ir neuronal number varies between brainstem nuclei (Fig. 5A–C). Microglial number also varied between catecholaminergic nuclei of brainstem in all 3 strains: SD, WKY and SHR. Interestingly, the pattern of variation observed in the microglial number was similar to the pattern of variation in the TH-ir neuronal number (Fig. 5A–C). For example, TH-ir neuronal and microglial numbers were higher in A2 as compared to C1, C3 or A5, regardless of the strain (Fig. 5A–C). Similarly, TH-neuronal and microglial number were lower in C3 as compared to A5 or A6, regardless of the strain (Fig. 5A–C). However, some exceptions (24% – 11 comparisons out of 45) were observed, where the microglial number was not related to the TH-ir neuronal number, such as A1 vs A5 in SD and WKY (Fig.

5A and B). But in majority ($\approx 76\%$) of intra-strain comparisons, the microglial number was related to the TH-ir neuronal number.

3.2. Inter-strain comparison of TH neuronal and microglial number in various brainstem catecholaminergic nuclei

A comparison of the distribution pattern of number of TH-ir neurons (Fig. 5D) and microglia (Fig. 5E) between strains revealed that the distribution varied in a similar pattern in catecholaminergic nuclei in all 3 strains of rat (SD, WKY and SHR; Fig. 5D).

The highest number of TH-ir A6 neurons were observed in WKY when compared with SD (WKY was 28% higher than SD) and SHR (SHR was 19% lower than WKY) (Fig. 5D). Microglial number in the brainstem catecholaminergic nuclei of WKY and SHR varied the most when compared with SD. Significant differences in the number of microglia were observed in A2, A5 and A6 brainstem regions, and the microglial number in these regions was the least in SD (Fig. 5E).

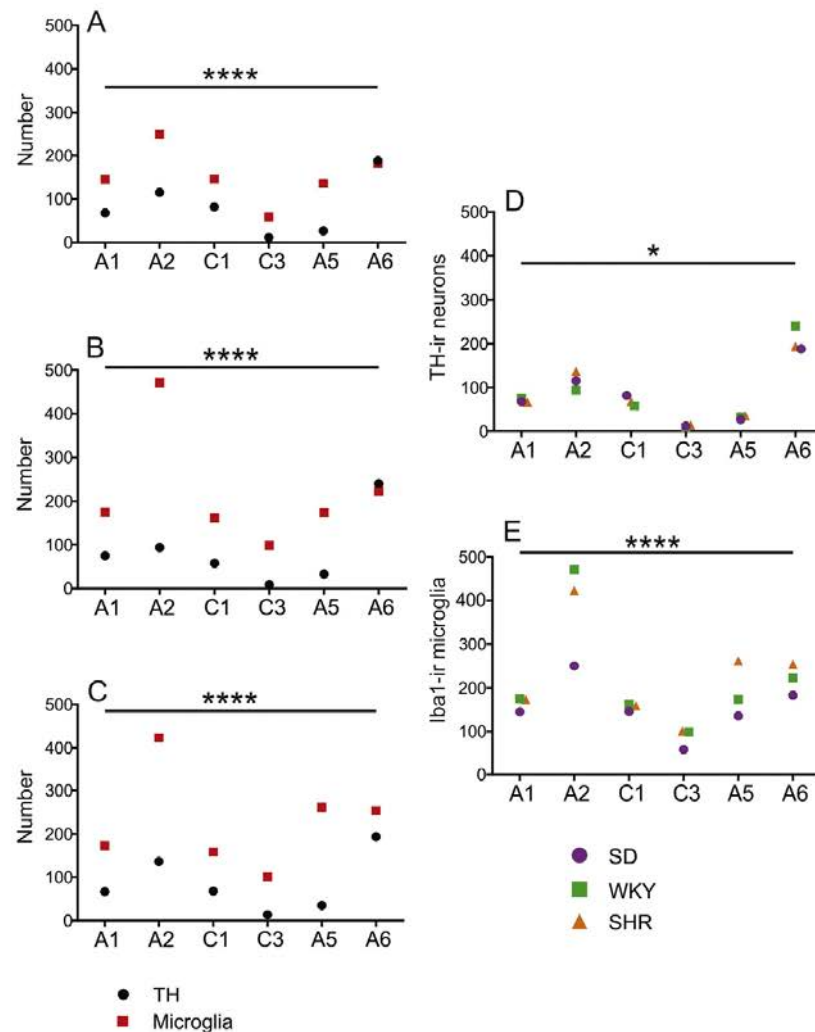


Fig. 5. Intra- and inter- strain comparisons concerning the number of TH-ir neurons and microglia. Intra-strain comparison of the pattern of distribution of TH-ir neuronal and microglial number in catecholaminergic nuclei of the brainstem of A. SD, B. WKY and C. SHR. Inter-strain (SD, WKY and SHR) comparison of the pattern of distribution of TH-ir neuronal (D) and microglial number (E) in catecholaminergic nuclei of the brainstem. Data are expressed as sum of counts from 3 animals for each strain. Statistical comparisons comparing the relationship between distribution patterns were made using the Chi-square test of independence. * $p \leq 0.05$, ** $p \leq 0.01$, *** $p \leq 0.001$ and **** $p \leq 0.0001$. (Refer to Supplementary Fig. 1 for biological variability in the number of TH-ir neurons and microglia, in each strain).

3.3. Microglial morphology doesn't vary considerably between catecholaminergic nuclei, regardless of the strain (Fig. 6)

No significant differences were observed in the microglial morphological characteristics (% area, number of end point processes/microglia and branch length (μm)/microglia) within various catecholaminergic nuclei, in either intra-, or inter-, strain comparisons (Fig. 6B–D).

4. Discussion

The main finding of our study is, first, that there is a ubiquitous and heterogeneous distribution of microglia in the brainstem catecholaminergic

nuclei of the SNS of spontaneously hypertensive and normotensive rats. Secondly, the heterogeneous microglial distribution is related to the TH-ir neuronal distribution and thirdly, in all strains of rat, and in all catecholaminergic nuclei, microglia were found to be in a surveilling state with a ramified morphology.

We observed a highly heterogeneous microglial distribution in catecholaminergic nuclei of the SNS of spontaneously hypertensive and normotensive rats, which is related to the TH-ir neuronal number. Previous studies suggest that microglial distribution is region-specific and is thought to be influenced by the local microenvironment cues (Lawson et al., 1990; Mittelbronn et al., 2001; Nikodemova et al., 2014). For example, the grey matter of the CNS

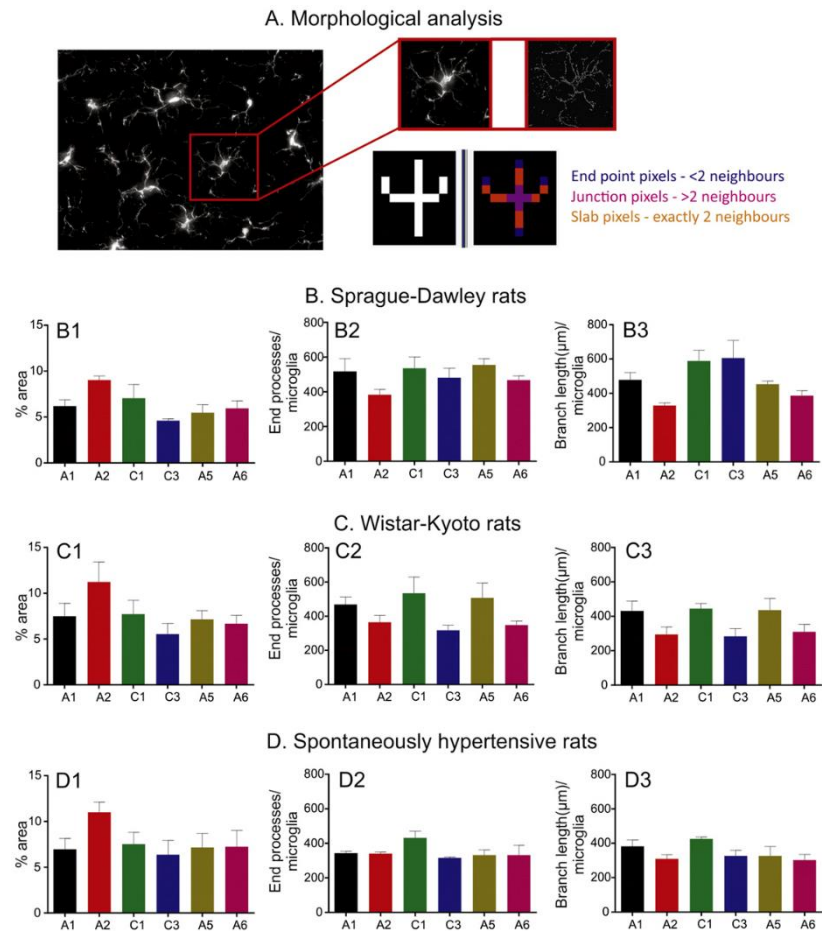


Fig. 6. Microglial morphology in the brainstem catecholaminergic nuclei. A. Quantification of the number of end point processes/microglia and the branch length (μm)/microglia with Image J 'AnalyzeSkeleton' plugin (refer to Experimental procedures for details). 3 microglial morphological characteristics were quantified (% area, number of end processes/microglia and branch length (μm)/microglia) in the brainstem catecholaminergic nuclei of a B. SD rat, C. WKY rat and D. SHR. Data are expressed as mean ± S.E.M. Statistical comparisons were made using a Kruskal-Wallis one-way analysis of variance. No significant differences were observed in the microglial morphology, intra-strain, across different catecholaminergic nuclei.

contains more microglia than the white matter, as detected by expression of the F4/80⁺ antigen, however the exact factor responsible for this is still unknown (Lawson et al., 1990). Also, microglial density was found to be 50% lower in lumbar segments of the spinal cord when compared with the cortex (Nikodemova et al., 2014). This heterogeneous distribution of microglia is not dependent on the proportion of monocytes recruited to the site of cell death during early development (Lawson et al., 1990). Microglial expression of immunoregulatory proteins is also quite region specific (de Haas et al., 2008; Nikodemova et al., 2014). These studies further highlight the diversity of microglia in the CNS, whose distribution, and chemical profile, is highly dependent on their local environment.

Our findings show that microglial number is related to the number of TH-ir neurons, which in turn relates to the type of catecholaminergic nucleus. It remains unclear if the presence of large numbers of catecholaminergic neurons cause changes in microglial number. As noted above, catecholaminergic neurons are an essential component of the CNS, in

particular the SNS (Dampney and Horiuchi, 2003; Graham et al., 1995; Rinaman, 2011). As expected, the number of TH-ir neurons across various catecholaminergic nuclei in the brainstem was observed to be heterogeneous, in a given strain of rat. Interestingly, microglial number, in the same strain of rat, is equally heterogeneous, and is related to the TH-ir neuronal number. It is noteworthy that even though all of the nuclei observed in this study were catecholaminergic (A1/A2/C1/C3/A5/A6), the number of TH expressing neurons in these nuclei is variable. Moreover, the proportion and location of active TH neurons within these nuclei ultimately affects the function of each nucleus in sympathetic regulation of the CNS (Badoer et al., 1987; Dampney and Horiuchi, 2003; Dampney et al., 2003; Graham et al., 1995; Nedoboy et al., 2016). Therefore, the variability in TH-ir neuronal number between brainstem nuclei may well be responsible for differences in microglial number. Thus, in light of our own findings, and as hypothesised by other studies (de Haas et al., 2008; Kapoor et al., 2015; Lawson et al., 1990; Mittelbronn et al., 2001), we speculate that

the local environment of a nucleus in the SNS, in particular the number of TH-ir neurons, influences the microglial distribution.

No major differences were observed in the microglial morphology, when compared intra-, or inter-, strain. Microglia continuously extend or retract their processes to contact synapses to monitor, and regulate, their activity levels (Nimmerjahn et al., 2005; Wake et al., 2009). Microglial morphology in mice varies markedly between different CNS regions, particularly between the grey matter and the white matter (Lawson et al., 1990). In our study, only minor differences were observed in microglial morphology in their surveilling state. The difference in observations made between these 2 studies, may be due to different species (mice vs rat), or different antigens analysed. Our study looked at the expression of Iba1 (ionized calcium-binding adaptor molecule 1) as compared to F4/80⁺ antigen, and was performed at much lower magnification (40× vs 400×) albeit covering a region of interest (ROI) that was larger. There may be very subtle morphological differences that can only be observed at higher magnifications, but the biological relevance of such subtle morphological differences is unclear.

Even though, both SD and WKY are normotensive, WKY are not comparable to SD due to underlying behavioural defects. SHR are inbred from WKY with high blood pressure (Okamoto and Aoki, 1963) and therefore, WKY, and not SD, is the most appropriate genetic and physiological control for SHR. Whether or not WKY is always the best control for SHR is still debated (H'Doubler et al., 1991). In our hands, we observed similarities in the pattern of distribution of TH-ir neurons and microglia in all 3 strains of rats (SD, WKY and SHR).

The magnitude of microglial response to a CNS injury is more pronounced in SHR than WKY (De Geyter et al., 2012). Reduced striatal blood flow induces a larger infarction volume and more pronounced sensory deficits, and reduced microglial activation, in SHR compared with WKY (De Geyter et al., 2012). According to our study, no major differences were observed in the overall microglial distribution pattern and morphology, between SHR and WKY. It is also hypothesised that neuro-inflammatory conditions in the CNS may play a detrimental role in the exaggeration of sympathetic nerve activity, and may contribute to the pathophysiology of cardiovascular disorders such as hypertension and heart failure (Liu et al., 2016; Shi et al., 2010; Wei et al., 2015; Wei et al., 2013). Thus, in light of our findings and previous studies, we speculate that the magnitude of the microglial response to an injury or disturbed homeostasis, rather than significant changes in basal microglial distribution, may be impaired in SHR than WKY.

5. Conclusion

Microglial distribution is markedly heterogeneous in the SNS of a rat (SD, WKY and SHR) and this heterogeneity seems to be related to the neuronal profile of their local environment. Hence, our study, in accordance with other studies, highlights that the microglial distribution profile is related to its local environment. Future studies focussed on the role of microglia, in addition to brain vascular macrophages (Waki et al., 2008; Waki et al., 2011), in the sympathetic regulation of cardiovascular control will clarify if these brain immune cells play a protective or detrimental role in the pathology of hypertension.

Supplementary data to this article can be found online at <http://dx.doi.org/10.1016/j.autneu.2016.05.005>.

Acknowledgements

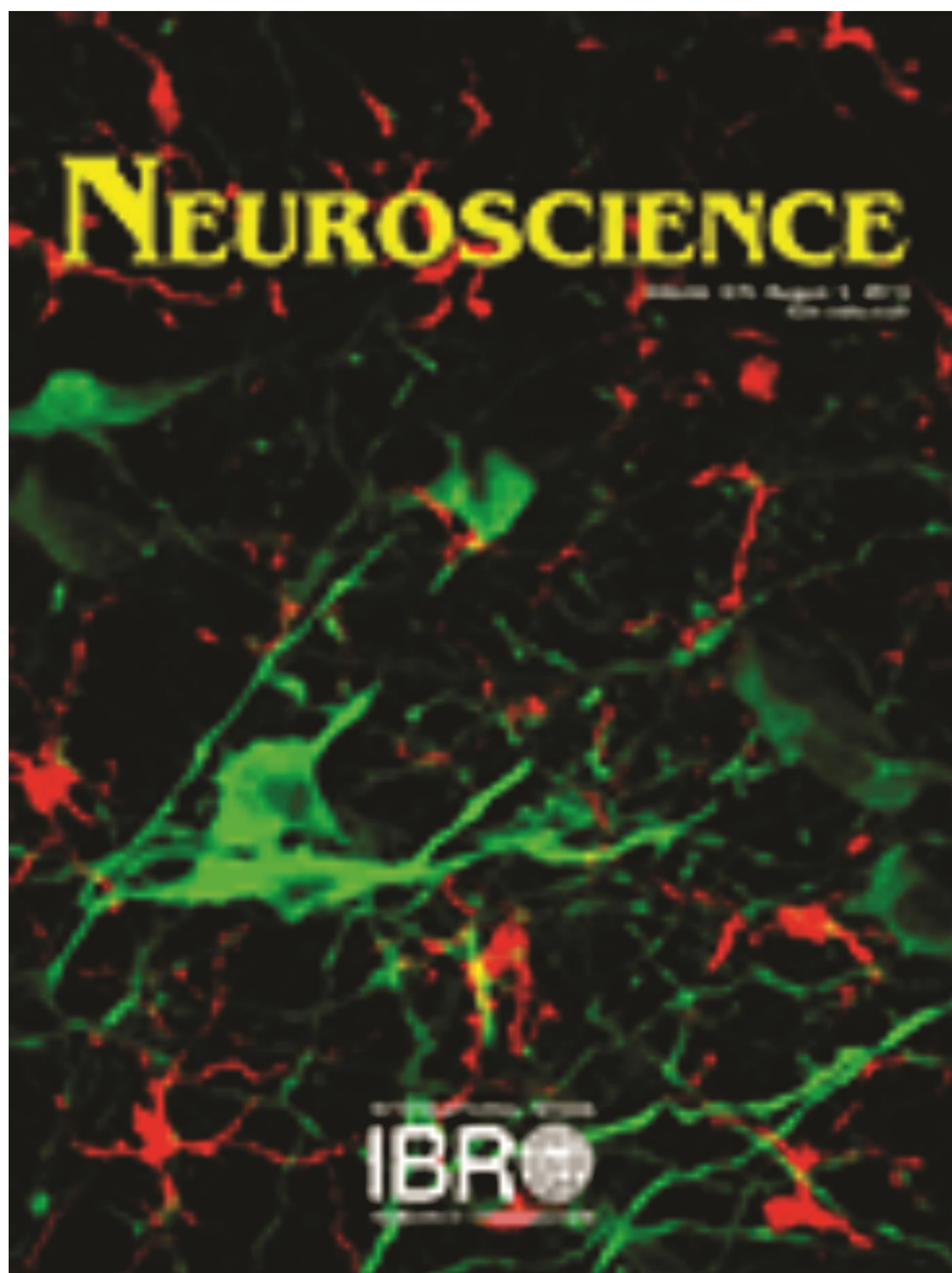
Work in the authors' laboratory is supported by funding from the Australian Research Council (DE120100992), the National Health and Medical Research Council of Australia (1082215, 1065485 and 1024489), The Heart Research Institute, the University of Sydney and the Macquarie University (2012112 and 2012219).

The authors declare no competing financial interests.

References

- Ajami, B., Bennett, J.L., Krieger, C., Tetzlaff, W., Rossi, F.M., 2007. Local self-renewal can sustain CNS microglia maintenance and function throughout adult life. *Nat. Neurosci.* 10, 1538–1543.
- Aloisi, F., Penna, G., Cerase, J., Menendez Iglesias, B., Adorini, L., 1997. IL-12 production by central nervous system microglia is inhibited by astrocytes. *J. Immunol.* 159, 1604–1612.
- Badoer, E., Head, G.A., Aberdeen, J.A., Korner, P.L., 1987. Localization of the main noradrenergic neuron groups in the pons and medulla of the rabbit and the importance of cathodal lesions for prolonged survival. *J. Neurosci. Methods* 19, 11–27.
- Benarroch, E., 1998. The lower brainstem and bodily homeostasis. By William Blessing. Oxford, UK. *Ann. Neurol.* 43, 839.
- Bhandare, A.M., Mohammed, S., Pilowsky, P.M., Farnham, M.M., 2015. Antagonism of PACAP or microglia function worsens the cardiovascular consequences of kainic acid-induced seizures in rats. *J. Neurosci.* 35, 2191–2199.
- Bhandare, A.M., Kapoor, K., Pilowsky, P.M., Farnham, M.M., 2016. Seizure-induced sympathoexcitation is caused by activation of glutamatergic receptors in RVLM that also causes proarrhythmic changes mediated by PACAP and microglia in rats. *J. Neurosci.* 36, 506–517.
- Dahlström, A., Fuxe, K., 1964. Evidence for the existence of monoamine-containing neurons in the central nervous system. I. Demonstration of monoamines in the cell bodies of brain stem neurons. *Acta Physiol. Scand.* 62, 1–55.
- Dampney, R.A.L., Horiuchi, J., 2003. Functional organisation of central cardiovascular pathways: studies using c-fos gene expression. *Prog. Neurobiol.* 71, 359–384.
- Dampney, R.A.L., Polson, J.W., Potts, P.D., Hirooka, Y., Horiuchi, J., 2003b. Functional organization of brain pathways subserving the baroreceptor reflex: studies in conscious animals using immediate early gene expression. *Cell Mol. Neurobiol.* 23, 597–616.
- David, S., Kroner, A., 2011. Repertoire of microglial and macrophage responses after spinal cord injury. *Nat. Rev. Neurosci.* 12, 388–399.
- De Geyter, D., Stoop, W., Zgavc, T., Sarre, S., Michotte, Y., De Keyser, J., Koijman, R., 2012. Spontaneously hypertensive rats display reduced microglial activation in response to ischemic stroke and lipopolysaccharide. *J. Neuroinflamm.* 9, 114.
- de Haas, A.H., Boddeke, H.W., Biber, K., 2008. Region-specific expression of immunoregulatory proteins on microglia in the healthy CNS. *Glia* 56, 888–894.
- Farnham, M.M., Lung, M.S., Tallapragada, V.J., Pilowsky, P.M., 2012. PACAP causes PAC1/VPAC2 receptor mediated hypertension and sympathoexcitation in normal and hypertensive rats. *Am. J. Phys.* 303, H910–H917.
- Graham, J.C., Hoffman, G.E., Sved, A.F., 1995. c-Fos expression in brain in response to hypotension and hypertension in conscious rats. *J. Auton. Nerv. Syst.* 55, 92–104.
- H'Doubler Jr., P.B., Peterson, M., Shek, W., Auchincloss, H., Abbott, W.M., Orkin, R.W., 1991. Spontaneously hypertensive and Wistar Kyoto rats are genetically disparate. *Lab. Anim. Sci.* 41, 471–473.
- Kapoor, K., Bhandare, A.M., Farnham, M.M., Pilowsky, P.M., 2015. Alerted microglia and the sympathetic nervous system: a novel form of microglia in the development of hypertension. *Respir. Physiol. Neurobiol.*
- Kapoor, K., Bhandare, A.M., Nedoboy, P.E., Mohammed, S., Farnham, M.M.J., Pilowsky, P.M., 2016. Dynamic changes in the relationship of microglia to cardiovascular neurons in response to increases and decreases in blood pressure. *Neuroscience* (in press).
- Karperien, A., Ahammer, H., Jelinek, H.F., 2013. Quantitating the subtleties of microglial morphology with fractal analysis. *Front. Cell. Neurosci.* 7, 3.
- Kettenmann, H., Kirchhoff, F., Verkhratsky, A., 2013. Microglia: new roles for the synaptic stripper. *Neuron* 77, 10–18.
- Kroner, A., Greenhalgh, A.D., Zaruk, J.G., PassosdosSantos, R., Gaestel, M., David, S., 2014. TNF and increased intracellular iron alter macrophage polarization to a detrimental M1 phenotype in the injured spinal cord. *Neuron* 83, 1098–1116.
- Lawson, L.J., Perry, V.H., Dri, P., Gordon, S., 1990. Heterogeneity in the distribution and morphology of microglia in the normal adult mouse brain. *Neuroscience* 39, 151–170.
- Liu, M., Shi, P., Summers, C., 2016. Direct anti-inflammatory effects of angiotensin-(1–7) on microglia. *J. Neurochem.* 136, 163–171.
- Menuet, C., Sevigny, C.P., Connelly, A.A., Bassi, J.K., Janovski, N., Williams, D.A., Anderson, C.R., Uweylyn-Smith, I.J., Fong, A.Y., Allen, A.M., 2014. Catecholaminergic C3 neurons are sympathoexcitatory and involved in glucose homeostasis. *J. Neurosci.* 34, 15110–15122.
- Minson, J., Arnold, L., Uweylyn-Smith, I., Pilowsky, P., Chalmers, J., 1996. Altered c-fos in rostral medulla and spinal cord of spontaneously hypertensive rats. *Hypertension* 27, 433–441.
- Mittelbronn, M., Dietz, K., Schluesener, H.J., Meyerermann, R., 2001. Local distribution of microglia in the normal adult human central nervous system differs by up to one order of magnitude. *Acta Neuropathol.* 101, 249–255.
- Miyamoto, A., Wake, H., Moorhouse, A.J., Nabekura, J., 2013. Microglia and synapse interactions: fine tuning neural circuits and candidate molecules. *Front. Cell. Neurosci.* 7, 70.
- Miyawaki, T., Goodchild, A.K., Pilowsky, P.M., 2002. Evidence for a tonic GABA-ergic inhibition of excitatory respiratory-related afferents to presympathetic neurons in the rostral ventrolateral medulla. *Brain Res.* 924, 56–62.
- Morrison, H.W., Filosa, J.A., 2013. A quantitative spatiotemporal analysis of microglia morphology during ischemic stroke and reperfusion. *J. Neuroinflamm.* 10, 4.
- Nedoboy, P.E., Mohammed, S., Kapoor, K., Bhandare, A.M., Farnham, M.M., Pilowsky, P.M., 2016. pSer40 tyrosine hydroxylase immunohistochemistry identifies the anatomical location of C1 neurons in rat RVLM that are activated by hypotension. *Neuroscience* 317, 162–172.
- Nikodemova, M., Small, A.L., Smith, S.M.C., Mitchell, G.S., Watters, J.J., 2014. Spinal but not cortical microglia acquire an atypical phenotype with high VEGF, galectin-3 and osteopontin, and blunted inflammatory responses in ALS rats. *Neurobiol. Dis.* 69, 43–53.

- Nimmerjahn, A., Kirchhoff, F., Helmchen, F., 2005. Neuroscience: resting microglial cells are highly dynamic surveillants of brain parenchyma in vivo. *Science* 308, 1314–1318.
- Okamoto, K., Aoki, K., 1963. Development of a strain of spontaneously hypertensive rats. *Jpn. Circ. J.* 27, 282–293.
- Paxinos, G., Watson, C., 2007. *The Rat Brain in Stereotaxic Coordinates*. sixth ed. Elsevier Academic Press.
- Pilowsky, P.M., Lung, M.S., Spirovski, D., McMullan, S., 2009. Differential regulation of the central neural cardiorespiratory system by metabotropic neurotransmitters. *Philos. Trans. R. Soc. Lond. Ser. B Biol. Sci.* 364, 2537–2552.
- Pocock, J.M., Kettenmann, H., 2007. Neurotransmitter receptors on microglia. *Trends Neurosci.* 30, 527–535.
- Pyo, H., Yang, M.S., Jou, I., Joe, E.H., 2003. Wortmannin enhances lipopolysaccharide-induced inducible nitric oxide synthase expression in microglia in the presence of astrocytes in rats. *Neurosci. Lett.* 346, 141–144.
- Rinaman, L., 2011. Hindbrain noradrenergic A2 neurons: diverse roles in autonomic, endocrine, cognitive, and behavioral functions. *Am. J. Phys.* 300, R222–R235.
- Ritter, S., Llewellyn-Smith, I., Dinh, T.T., 1998. Subgroups of hindbrain catecholamine neurons are selectively activated by 2-deoxy-D-glucose induced metabolic challenge. *Brain Res.* 805, 41–54.
- Shi, P., Diez-Freire, C., Jun, J.Y., Qi, Y., Katovich, M.J., Li, Q., Sriramula, S., Francis, J., Summers, C., Raizada, M.K., 2010. Brain microglial cytokines in neurogenic hypertension. *Hypertension* 56, 297–303.
- Sokal, R.R., Rohlf, F.J., 2012. *Biometry*. fourth ed. W.H. Freeman and Company, New York.
- Springell, D.A., Costin, N.S., Pilowsky, P.M., Goodchild, A.K., 2005. Hypotension and short-term anaesthesia induce ERK1/2 phosphorylation in autonomic nuclei of the brainstem. *Eur. J. Neurosci.* 22, 2257–2270.
- Ueno, M., Fujita, Y., Tanaka, T., Nakamura, Y., Kikuta, J., Ishii, M., Yamashita, T., 2013. Layer V cortical neurons require microglial support for survival during postnatal development. *Nat. Neurosci.* 16, 543–551.
- Wake, H., Moorhouse, A.J., Jinno, S., Kohsaka, S., Nabekura, J., 2009. Resting microglia directly monitor the functional state of synapses in vivo and determine the fate of ischemic terminals. *J. Neurosci.* 29, 3974–3980.
- Waki, H., Gouraud, S.S., Maeda, M., Paton, J.F., 2008. Specific inflammatory condition in nucleus tractus solitarius of the SHR: novel insight for neurogenic hypertension? *Auton. Neurosci.* 142, 25–31.
- Waki, H., Gouraud, S.S., Maeda, M., Raizada, M.K., Paton, J.F., 2011. Contributions of vascular inflammation in the brainstem for neurogenic hypertension. *Respir. Physiol. Neurobiol.* 178, 422–428.
- Wei, S.G., Zhang, Z.H., Beltz, T.G., Yu, Y., Johnson, A.K., Felder, R.B., 2013. Subfornical organ mediates sympathetic and hemodynamic responses to blood-borne proinflammatory cytokines. *Hypertension* 62, 118–125.
- Wei, S.G., Yu, Y., Zhang, Z.H., Felder, R.B., 2015. Proinflammatory cytokines upregulate sympathoexcitatory mechanisms in the subfornical organ of the rat. *Hypertension* 65, 1126–1133.
- Windelborn, J.A., Mitchell, G.S., 2012. Glial activation in the spinal ventral horn caudal to cervical injury. *Respir. Physiol. Neurobiol.* 180, 61–68.
- Xavier, A.L., Menezes, J.R., Goldman, S.A., Nedergaard, M., 2014. Fine-tuning the central nervous system: microglial modelling of cells and synapses. *Philos. Trans. R. Soc. Lond. Ser. B Biol. Sci.* 369, 20130593.



DYNAMIC CHANGES IN THE RELATIONSHIP OF MICROGLIA TO CARDIOVASCULAR NEURONS IN RESPONSE TO INCREASES AND DECREASES IN BLOOD PRESSURE

KOMAL KAPOOR,^{a,b} AMOL M. BHANDARE,^{a,b}
POLINA E. NEDOBOY,^b SUJA MOHAMMED,^{b,c}
MELISSA M. J. FARNHAM^{b,c} AND PAUL M. PILOWSKY^{b,c,*}

^a Faculty of Medicine and Health Sciences, Macquarie University, Sydney, New South Wales 2109, Australia

^b The Heart Research Institute, Sydney, New South Wales 2042, Australia

^c Department of Physiology, University of Sydney, Sydney, New South Wales 2006, Australia

Key words: CVLM, RVLM, microglia, blood pressure, sympathetic.

INTRODUCTION

Until recently, microglia were considered to be cells whose sole function was to detect and respond to inflammation, following any internal or external stimulus that threatens the integrity of the brain (Perry et al., 1993; Kreutzberg, 1996; Kettenmann et al., 2011). When subjected to strongly activating stimuli, microglia transform their phenotype from a highly ramified morphology with a small cell body to an amoeboid shape, allowing them to move easily, and phagocytose debris (Stence et al., 2001).

The idea that microglia are only important as inflammatory cells, now seems less certain. A growing body of evidence suggests that microglia are not only constantly alert and active; surveilling their immediate environment (Nimmerjahn et al., 2005; Tremblay et al., 2011), but may also play a physiological role in maintaining normal neuronal function. The idea that microglia constantly maintain neurons within their dynamic physiological working range, by regulating the number of excitatory synapses present on their post-synaptic membrane (Wake et al., 2009; Tremblay et al., 2010), is still poorly understood. Microglia are thought to perform this function by extending or retracting their processes, sensing the presence of any unexpected increase in extracellular chemical ("on-signaling") or absence of any consistently expressed biological molecule ("off-signaling") (van Rossum and Hanisch, 2004; Biber et al., 2007; Hanisch and Kettenmann, 2007). Microglia achieve this role by expressing receptors for all known neurotransmitters, and many other molecules (Pocock and Kettenmann, 2007), and by being in close proximity to neurons at all times (Shapiro et al., 2009). The close apposition of microglial processes to neuronal synapses in higher brain regions, such as the visual cortex, further strengthens the hypothesis of continuous neuron-microglia communication (Wake et al., 2009; Tremblay et al., 2010; Schafer et al., 2013). The possibility that this type of neuron-microglia relationship operates in a physiological state in the autonomic nervous system is unknown.

The caudal- and rostral- ventrolateral medullary (CVLM and RVLM, respectively) neurons of the brainstem are critical for the regulation of the

Abstract—Microglia are present throughout the central nervous system (CNS) and express receptors for every known neurotransmitter. During inflammation, microglia change into a state that either promotes removal of debris (M1), or into a state that promotes soothing (M2). Caudal- and rostral- ventrolateral medullary regions (CVLM and RVLM, respectively) of the brainstem are key nuclei involved in all aspects of the cardiovascular system. In this study, we investigate a novel role for microglia in cardiovascular control in the brainstem of adult male Sprague–Dawley (SD) rat. Here we show, that increases and decreases in blood pressure (BP) triggers alertness in the physiology of microglia in the brainstem region; inducing changes in microglial spatial distribution and the number of synapses in contact with microglial end processes. Following 6 h of acute hypertension, the number of synapses in contact with microglia increased by ~30% in both regions of the brainstem, CVLM and RVLM. Induction of acute hypotension for 6 h causes microglia to reduce the number of synaptic contacts by >20% in both, CVLM and RVLM, nuclei of the brainstem. Our analysis of the morphological characteristics of microglia, and expression levels of M1 and M2, reveals that the changes induced in microglial behavior do not require any obvious dramatic changes in their morphology. Taken together, our findings suggest that microglia play a novel, unexpected, physiological role in the uninjured autonomic nuclei of CNS; we therefore speculate that microglia act cooperatively with brainstem cardiovascular neurons to maintain them in a physiologically receptive state. © 2016 IBRO. Published by Elsevier Ltd. All rights reserved.

*Correspondence to: P. M. Pilowsky, University of Sydney & Heart Research Institute, 7 Eliza Street, Newtown 2042, Australia. Tel: +61-0-2-8208-8938.

E-mail address: paul.pilowsky@hri.org.au (P. M. Pilowsky).

Abbreviations: AUC, area under curve; BP, blood pressure; CNS, central nervous system; CVLM, caudal ventrolateral medulla; Fos-ir, Fos immunoreactivity; MAP, mean arterial pressure; NAsc, nucleus ambiguus (sub compact); NTS, nucleus of the solitary tract; PBS, phosphate-buffered saline; RVLM, rostral ventrolateral medulla; SD, Sprague–Dawley; SNS, sympathetic nervous system; TH, tyrosine hydroxylase.

<http://dx.doi.org/10.1016/j.neuroscience.2016.04.044>

0306-4522/© 2016 IBRO. Published by Elsevier Ltd. All rights reserved.

sympathetic nervous system (SNS) and various reflex control mechanisms such as the chemoreflexes, baroreflex and somatosympathetic reflex (Pilowsky et al., 2009). Propriobulbar CVLM neurons provide an inhibitory GABAergic (γ -Aminobutyric acid) input to the excitatory bulbospinal glutamatergic presympathetic neurons located in the RVLM in response to elevated levels of blood pressure (BP); these inhibited RVLM neurons, in turn, reduces the activity of the sympathetic preganglionic neurons (SPN) located in the spinal cord, thereby lowering BP and sympathetic activity (Guyenet, 2006; Pilowsky et al., 2009). Recently, we reported that inhibition of microglia led to an over-activation of sympathetic output, supporting the concept that microglia play an important physiological role in the SNS (Bhandare et al., 2015). However, the exact morphological relationship between microglia and cardiovascular neurons during the imposition of changes in BP remains unclear.

Here, we aimed to identify, first, the morphological relationship between surveilling microglia and cardiovascular neurons in the CVLM and the RVLM that control sympathetic output pathways, under homeostatic conditions. Secondly, we aimed to establish the extent to which the microglial-neuronal relationship, in the CVLM and RVLM regions of the brainstem, is affected by manipulations introduced in the basal levels of BP. Data concerning microglia were acquired following the induction of acute hyper- (phenylephrine) or hypo- (hydralazine) tension in adult male Sprague–Dawley (SD) rats at four different time points; 0.5, 2, 6 and 10 h (hrs). Our findings indicate that brainstem microglia behave as an essential element of the autonomic arm of the central nervous system (CNS), and that microglial responses to changes in levels of BP are carefully tailored according to the magnitude and duration of disturbances introduced in the homeostatic state. In particular, increased BP causes microglia to change their pattern of distribution, and make more contacts with synapses. On the contrary, decreased levels of BP, causes microglia to decrease the number of contacts with synapses and change their spatial distribution. This microglial behavior has all the characteristics of a physiological, as opposed to an inflammatory, destructive, response.

EXPERIMENTAL PROCEDURES

Animals

Experiments were conducted in 36 adult male SD rats (300–420 g; Animal resource center, Perth, Australia) in accordance with the Australian code of practice for the care and use of animals for scientific purposes. All procedures and protocols performed were approved by the Sydney Local Health District Animal Welfare Committee and the Macquarie University Animal care and Ethics Committee, Sydney, Australia.

Experimental protocol

The external jugular vein, carotid artery and femoral vein were cannulated, in anesthetized rats, for the administration of additional anesthetics, measurement of

arterial BP and administration of BP altering drugs (phenylephrine, saline or hydralazine), respectively. Temperature for all animals was maintained between 36.5 °C and 37.5 °C, for the protocol period, using a rectal probe connected to a homeothermic heating blanket. Experiments were conducted at four time points: 0.5, 2, 6 and 10 h, with three treatment groups at each time point ($n = 3$ each treatment group at each time point): phenylephrine induced hypertension, saline served as control and hydralazine induced hypotension.

0.5, 2 and 6 h: rats were anesthetized with sodium pentobarbital i.p. (50 mg/kg; Cenvet Australia) mixed with atropine sulfate (to reduce bronchial secretions; 0.2 ml/kg; Pfizer). Room air was supplemented with 100% oxygen (rate 0.5–1.0 l/min) through a nose cone. The depth of anesthesia was monitored by observing reflex responses to nociceptive and tactile stimuli (withdrawal reflex to periodic tail/paw pinches), pupillary responses to light stimuli and the corneal touch reflex (involuntary blink). Additional anesthetic – sodium pentobarbital (1.5–2.0 mg) – was injected intravenously, when required, to eliminate nociceptive or corneal touch reflex responses.

10 h: rats were anesthetized with urethane i.p. (1.0–1.5 g/kg) mixed with atropine sulfate (to reduce bronchial secretions prior to vagotomy; 0.2 ml/kg), vagotomized (both, left and right cervical vagus nerves were cut), paralyzed with pancuronium bromide (neuromuscular blockade, 0.2-ml bolus i.v. injection containing 0.4 mg followed by 10% pancuronium in 0.9% saline at a rate of 2 ml/h; AstraZeneca) and artificially ventilated. Animals were vagotomized and paralyzed to prevent entrainment of breathing to the ventilator. The depth of anesthesia, prior to induction of neuromuscular blockade, was monitored by observing reflex responses to nociceptive and tactile stimuli, pupillary responses to light stimuli and the corneal touch reflex (as explained above). Following neuromuscular blockade, the depth of anesthesia was determined by continuously monitoring the resting levels of BP for excessive fluctuations, and any changes in BP in response to nociceptive stimuli. Additional anesthetic – urethane (30–40 mg, 10% urethane i.v.) – was injected intravenously, when nociceptive stimuli evoked changes in BP exceeding 10%.

Prior to the start of the protocol, arterial pressure was allowed to stabilize for at least 10 min. Baseline mean arterial pressure (MAP) was increased or decreased by at least 40 mmHg with the aid of phenylephrine or hydralazine, respectively. A continuous infusion of phenylephrine, at the dose of 10 μ g/kg/min (Graham et al., 1995), was maintained to induce acute hypertension. Rate of phenylephrine infusion was adjusted to maintain elevated levels of MAP. To induce acute hypotension, a bolus injection of hydralazine was given, at the dose of 10 mg/kg (Springell et al., 2005). To match the volume infused in the phenylephrine treatment group, hydralazine and saline treatment groups received a continuous infusion of saline at the rate of 10 μ g/kg/min. Drug concentrations and infusion volumes were carefully determined in preliminary experiments and then adjusted to

limit the maximum volume of infusion to 10 ml for the duration of protocol, to avoid hypervolemia.

Perfusion and tissue processing

All chemical reagents were purchased from Sigma–Aldrich, unless otherwise stated. At the end of the protocol, rats were deeply anesthetized with sodium pentobarbital (> 72 mg/kg i.v.; Cenvet Australia) and were transcardially perfused with 400 ml of ice cold 0.1 M phosphate buffered saline (PBS) followed by fixation with ≈400 ml of ice cold 4% paraformaldehyde in 0.1 M PBS (pH 7.4). Brainstem was carefully extracted and post fixed overnight in the same fixative at 4 °C. Brainstems were sectioned transversely at 40 µm and were sequentially collected in five pots using vibrating microtome (VT1200S, Leica) and stored in cryoprotectant solution (30% sucrose, 30% ethylene glycol, 2% polyvinylpyrrolidone in 0.1 M PBS) at –20 °C, until processed for immunohistochemistry.

Immunohistochemistry

Methods were conducted as previously described (Shahid et al., 2012; Bhandare et al., 2016; Nedoboy et al., 2016). In brief, free floating 40-µm brainstem sections, previously stored in cryoprotectant solution, were washed 3 times, for 30 min each, in 0.1 M PBS containing 0.3% Triton X-100 at room temperature. Post washes, sections were incubated for >48 h in TTPBSm (10 mM Tris–HCl, 0.1 M PBS, 0.9% NaCl, 0.3% Triton X-100 and 0.1% merthiolate at pH 7.4), 10% normal donkey serum and primary antibodies (refer to Table 1) at 4 °C while shaking. Sections were then subsequently washed 3 times, 30 min each, in TPBS (10 mM Tris–HCl, 0.1 M PBS and

0.9% NaCl at pH 7.4). Depending on the primary antibodies, sections were incubated overnight with secondary antibodies (refer to Table 1) in TPBSm (10 mM Tris–HCl, 0.1 M PBS, 0.9% NaCl and 0.1% merthiolate at pH 7.4) with 2% normal donkey serum at room temperature while shaking. Sections were then washed in TPBS 3 times, 30 min each, at room temperature followed by mounting sequentially on glass slides (Thermo Fisher Scientific, Victoria, Australia), cover-slipped with Vectashield (H-1000, Vector Laboratories, CA, USA) and sealed with clear nail polish.

Image acquisition and analysis

Brainstem sections, processed for immunohistochemistry, were imaged using an Axio Imager Z2 (ZEISS, Germany) at 20×, 40× or 63× magnification for subsequent analysis, depending on the target molecule. Images were adjusted for brightness and contrast to best represent the morphological characteristics of microglia. LSM 510 Meta spectral confocal microscope (ZEISS, Germany) was used for obtaining images to demonstrate the microglial-neuronal relationship.

A rat brain atlas was used to define the anatomical location of the neuronal population analyzed in this study (Paxinos and Watson, 2007). The RVLM was defined as a triangular area, containing tyrosine hydroxylase positive (TH⁺) neurons, ventral to the nucleus ambiguus (NAsc), medial to the spinal trigeminal tract and lateral to the pyramidal tracts. Bilateral RVLM images were obtained from 4 serial sections, separated by 200 µm between 12.00 and 12.8 mm caudal to the bregma (Graham et al., 1995; Guyenet et al., 2004). CVLM neurons were defined as the neurons located in close apposition with TH⁺ neurons of the A1 region of

Table 1. Primary and corresponding secondary antibodies used for immunohistochemistry experiments

Name	Immunogen	Host, company/Catalog No.	Concentration used [*]	Secondary antibody ^{**}
CD16	Whole white blood cells (clone ASH 1975)	Mouse monoclonal (IgG2a), US Biological Life Sciences/C2267-32	1:400	AlexaFluor488 Goat anti Mouse – 115-545-206
CD206	Synthetic peptide: within residues 1400 to C-terminus of Human Mannose receptor	Rabbit polyclonal, Abcam/ab693	1:2000	AlexaFluor 488 Donkey anti Rabbit – 711-546-152
c-Fos	Synthetic peptide: amino acid 2–17 in rat	Guinea-Pig polyclonal, Synaptic systems/226,004	1:2000	AlexaFluor 488 Donkey anti Guinea Pig – 706-546-148
Iba1	Synthetic peptide corresponding to C-terminus of Iba1	Rabbit polyclonal, Wako Pure Chemical Industries Ltd./019-19741	1:2000	Cy3 Donkey anti Rabbit – 711-166-152
Iba1	Synthetic peptide: TGPPAKKAISELP	Goat polyclonal, Novus Biological/NB100-1028	1:1000	Cy3 Donkey anti Goat – 705-546-147
Synapsin	Synthetic peptide corresponding to N terminus of rat synapsin protein	Guinea-Pig Polyclonal, Synaptic Systems/106,004	1:1000	AMCA Donkey anti Guinea Pig 706–156-148
TH	Rat PC-12 pheochromocytoma cell tyrosine hydroxylase (clone TH-2)	Mouse monoclonal (IgG1), Sigma–Aldrich/T1299	1:500	Cy5 Donkey anti Mouse – 715-175-151
TH	Synthetic peptide: CPRFIGRRQSLIEDARK	Mouse monoclonal (IgG1κ), Avanti antibodies/#AV1 (Bhandare et al., 2016; Nedoboy et al., 2016)	1:100	Cy5 Donkey anti Mouse – 715-175-151 Cy5 Goat anti-mouse – 115-175-205

^{*} Optimum concentration for all primary antibodies was determined by titration on the basis of manufacturer's recommendations using fixed brainstem tissue collected from SD rats perfused with 0.1 M PBS followed by fixation with 4% paraformaldehyde.

^{**} All the secondary antibodies were purchased from Jacksons Immunoresearch and used at 1:500 concentration unless, otherwise stated.

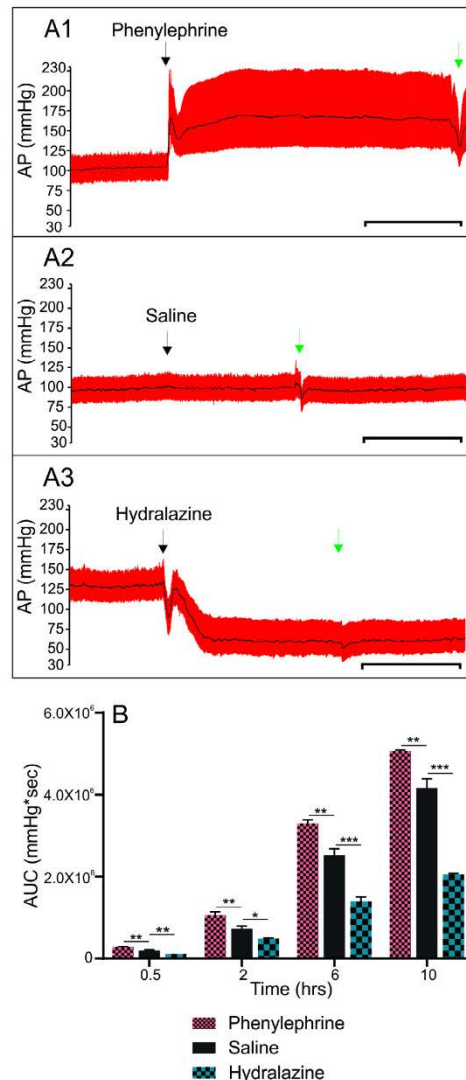


Fig. 1. Effect of intravenous infusion of phenylephrine, saline and hydralazine on blood pressure. (A1) Effect of continuous intravenous infusion of phenylephrine at 10 μ g/kg/min, (A2). Saline infusion and (A3). Effect of bolus injection of hydralazine at 10 mg/kg on arterial blood pressure (AP). Pinch reflex response and administration of additional anesthetic, when required (green arrow; please refer to methods for details). Scale bar = 5 min. (B) Effect of phenylephrine, saline and hydralazine on the area under curve (AUC) for mean arterial pressure (MAP) for the whole protocol period, where the stimulus was maintained continuously for 0.5, 2, 6 and 10 h in 4 separate group of rats ($n = 3$ each). Statistical comparisons were made with saline treatment group, at the particular time point, using one-way ANOVA with Dunnett's multiple comparison tests; $p \leq 0.05$, $^{**}p \leq 0.01$ and $^{***}p \leq 0.001$. Data are expressed as mean \pm SEM, $n = 3$.

brainstem (Graham et al., 1995; Paxinos and Watson, 2007). Bilateral CVLM images were taken between 12.8 and 13.6 mm caudal to the bregma, from four different sections bilaterally, 200 μ m apart (Graham et al., 1995; Guyenet et al., 2004).

Microglial number and morphological analysis at 40 \times . "Z-stack" images at 40 \times magnification were obtained covering an area of 400 μ m \times 400 μ m, 30 μ m in depth, at an interval of 0.62 μ m generating a stack of \approx 46 Z slices. Maximum intensity projection images produced for CVLM and RVLM neurons at 40 \times magnification were used to quantify the overall number of microglia, pattern of distribution and morphological characteristics of microglia. Number of Fos immunoreactive (Fos-ir) neurons and number of microglia were manually counted in the eight images obtained for each region from each repeat. Fos-ir neurons and microglia present at the boundary of images were excluded from the final counts. For spatial distribution analysis, each image was divided into six equal parts using the grid feature in CorelDRAW Graphics Suite X7 and one microglia from each of these six parts was chosen. A series of six concentric circles were drawn around each microglia with the first one centered at the soma of microglia starting at radius of 8 μ m and subsequent circles were drawn with the increasing radii of 5 μ m (Sholl, 1953; Morrison and Filosa, 2013). Microglial cell bodies intersecting with each of these concentric circles were counted to provide an estimate of inter-microglial distance variations with treatment (Fig. 5A). This analysis is an adaptation of Sholl analysis, which is commonly used to quantify neuronal parameters (Sholl, 1953).

The method used to quantify the morphology acquired by microglia in response to different treatment paradigms was as described by Morrison and Filosa (2013) (Morrison and Filosa, 2013). In brief, brightness and contrast for each image was adjusted to highlight all the microglial end point processes. These images were then imported to Image J (NIH) as 8-bit images and 'skeletonized'. The 'skeletonized' image obtained was analyzed using the "AnalyzeSkeleton" Image J plugin to acquire the number of end points and branch length (μ m), which when normalized to the number of microglia in that specific frame, provides an indication of the extent of ramified microglial morphology (Fig. 7A). The percentage (%) of area occupied by microglia was also quantified with the help of in-built "measure" feature in Image J software.

M1 phenotype quantification. "Z-stack" images of the CVLM and the RVLM (Fig. 9F) did not show any significant M1 expression and therefore, M1 expression levels were not quantified.

M2 phenotype quantification. "Z-stack" images at 20 \times magnification were obtained covering an area of 900 μ m \times 600 μ m, 40 μ m in depth, at an interval of 1.39 μ m generating a stack of \approx 29 Z slices. Maximum intensity projection images acquired for the CVLM and the RVLM region at 20 \times magnification were used to

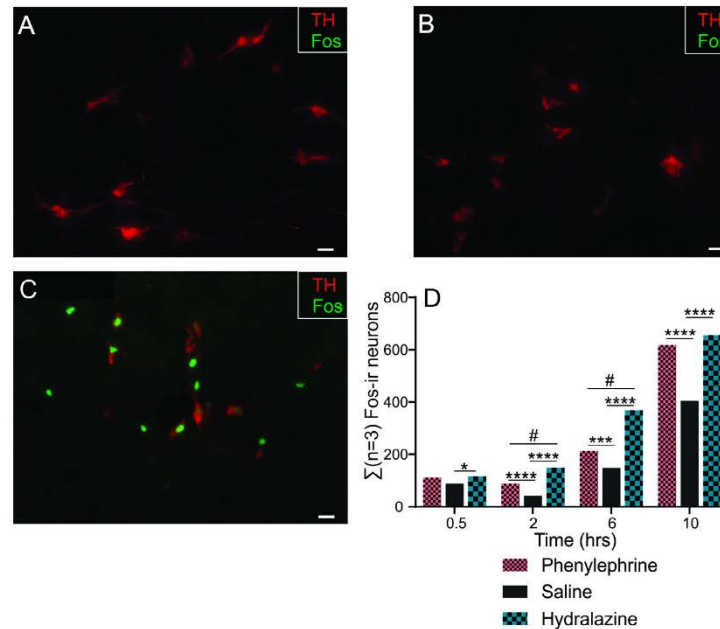


Fig. 2. Effect of three different treatments (intravenous infusion of phenylephrine, saline or hydralazine) on the number of Fos-ir neurons in the RVLM region. (A) Fos-ir decreases in response to intravenous continuous infusion of phenylephrine. (B) Fos-ir stays minimal in response to intravenous continuous infusion of saline. (C) Fos-ir increases in response to intravenous administration of hydralazine. Scale bar = 20 μ m. (D) Number of Fos-ir neurons in the RVLM region when stimuli were provided for 0.5, 2, 6 and 10 h in four separate group of rats ($n = 3$ each). *Statistical comparisons were made with the saline treatment group, at the particular time point, using the Chi-square test for goodness of fit; $p \leq 0.05$, $^{***}p \leq 0.001$ and $^{****}p \leq 0.0001$. #Statistical comparisons were made between phenylephrine and hydralazine treatment groups, at the particular time point, using the Chi-square test for goodness of fit; $p \leq 0.0001$. Data are summed for $n = 3$.

quantify the overall number of microglia (Fig. 9A), with Image J, in the region of interest. The CD206 immunoreactive (CD206⁺) microglia (Fig. 9B), co-localizing with the Iba1 positive (Iba1⁺) microglia (Fig. 9C), were counted in the eight images obtained for each region at each time point in 3 treatment groups ($n = 3$ each). Iba1⁺ and CD206⁺ microglia present at the boundary of images were excluded from the final counts. Expression levels of M2 microglia were expressed as a percentage of CD206⁺ microglia to the total number of microglia (Iba1⁺).

Quantification of number of contacts made by microglial (Iba1) end point processes with synapses (Synapsin) and microglial morphology at 63 \times . “Z-stack” images at 63 \times magnification were obtained covering an area of 400 μ m \times 300 μ m, 30 μ m in depth, at an interval of 0.5 μ m generating a stack of \approx 60 Z slices. For data concerning microglia and synapsin, the RVLM was defined as a triangular area, containing TH⁺ neurons, ventral to the NAsc, medial to the spinal trigeminal tract and lateral to the pyramidal tracts, 12.24 mm caudal to the bregma (Guyenet et al., 2004). CVLM neurons were defined as the neurons located in close apposition with TH⁺ neurons of the A1 region of brainstem, at 13.08 mm caudal to the bregma (Graham et al., 1995; Paxinos and

Watson, 2007). Bilateral images for the CVLM and the RVLM for each animal repeat were obtained. Ten microglia from each image were chosen at random and the numbers of synaptic structures (Synapsin) co-localizing with microglial end point processes (Iba1) were manually counted. Thus, 60 microglia from each animal, from each treatment group (three treatments) at each time point (four time points), were analyzed.

Control experiments in the NAsc (sub compact). The nucleus ambiguus (sub compact; NAsc) was defined as the area, 12.24 mm caudal to bregma, dorsal to the TH⁺ neurons of the RVLM, medial to the spinal trigeminal tract and lateral to the raphe obscurus (Bieger and Hopkins, 1987; Paxinos and Watson, 2007). Images from the NAsc at the 6- and 10-h time point from all three treatment groups (phenylephrine, saline and hydralazine; $n = 3$ each group) served as a control for the images obtained from the CVLM and the RVLM, at each time point. Bilateral ‘Z-stack’ images at 40 \times magnification were obtained covering an area of 400 μ m \times 400 μ m, 30 μ m in depth, at an interval of 0.62 μ m generating a stack of \approx 46 Z slices. Maximum intensity projection images produced for the NAsc at 40 \times magnification were used to quantify the overall number of microglia, pattern of distribution and morphological characteristics of

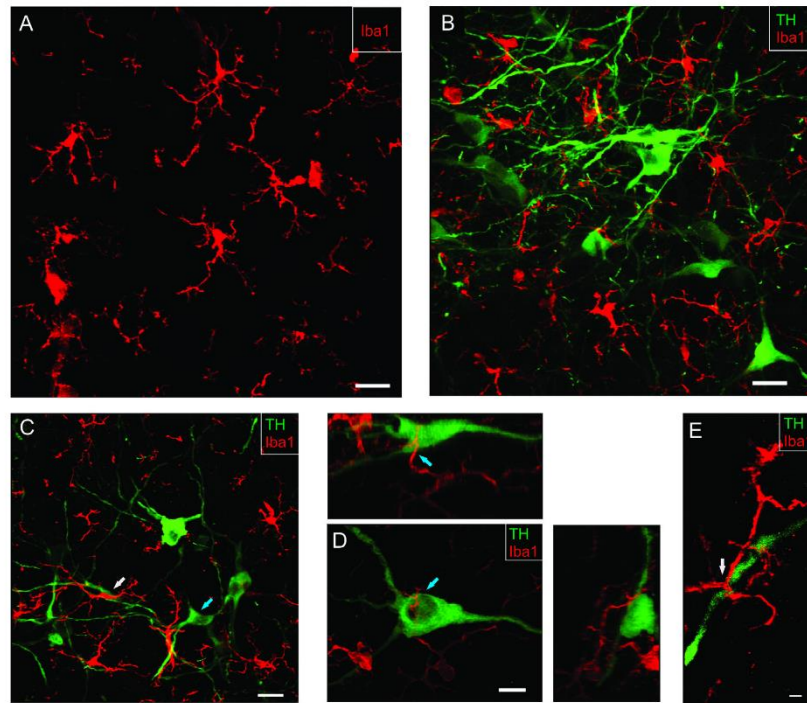


Fig. 3. Evidence of a close yet dynamic relationship between neurons (TH⁺ neurons) and microglia. (A) Microglia are present in the CVLM region. Scale bar = 20 μ m. (B) Surveilling microglia cover the parenchyma of the RVLM region with their dynamic processes. Tyrosine hydroxylase (TH, green) is a marker for adrenergic RVLM neurons. Scale bar = 20 μ m. (C) Microglia are closely apposed to dendrites of TH⁺ RVLM neurons (white arrow) rather than the neuronal cell body (blue arrow). Scale bar = 20 μ m. (See (Kapoor et al., 2015); image used with permission)(D) Microglial processes appear to penetrate a neuronal cell body (blue arrow). Scale bar = 10 μ m. Also see movie 1. (E) Microglial processes are wrapped around the dendrite of a TH⁺ neuron in the RVLM region (white arrow). Scale bar = 2 μ m. Also see movie 2. (For interpretation of the references to color in this figure legend, the reader is referred to the web version of this article.)

microglia: % area covered, number of end point processes/microglia and branch length (μ m)/microglia (similar to the CVLM and RVLM). Bilateral “Z-stack” images at 63 \times magnification were obtained covering an area of 400 μ m \times 300 μ m, 30 μ m in depth, at an interval of 0.5 μ m generating a stack of \approx 60 Z slices. Ten microglia from each image were chosen at random and the number of synaptic structures (Synapsin) co-localizing with microglial end point processes (Iba1) were manually counted (similar to the CVLM and RVLM). Thus, 60 microglia from each animal, from each treatment group (three treatments) at the 6- and 10-h time points, were analyzed.

Data analysis and statistics

Area under curve (AUC) was calculated, using Spike two acquisition and analysis software (version 8.03; Cambridge Electronic Design, Cambridge, UK), for all treatment groups (phenylephrine, saline and hydralazine) at each time point (0.5, 2, 6 and 10 h), and was statistically analyzed using one-way ANOVA with Dunnett’s multiple comparison tests. Non-parametric

non-continuous data, such as the number of Fos-ir neurons, microglia and the number of microglial contacts made with synapses, from each repeat ($n = 3$), was summed and statistically analyzed using the Chi-square test for goodness of fit (Sokal and Rohlf, 2012; Nedoboy et al., 2016). Parameters obtained highlighting the microglial morphology variations between treatments (% of area occupied, number of end point processes per microglia and branch length (μ m) per microglia) and percentage of CD206⁺ microglia to total microglia, were treated as non-parametric continuous data. Non-parametric continuous data were averaged across repeats ($n = 3$) and analyzed using Kruskal–Wallis one-way analysis of variance. All the statistical comparisons were made between treatment group (phenylephrine/hydralazine) and the saline group at the particular time point; no comparisons were made across time points in any of the groups. GraphPad Prism version 6.05 was used to perform all of the above mentioned statistical comparisons; one-way ANOVA, Chi-square test for goodness of fit and Kruskal–Wallis one-way analysis of variance.

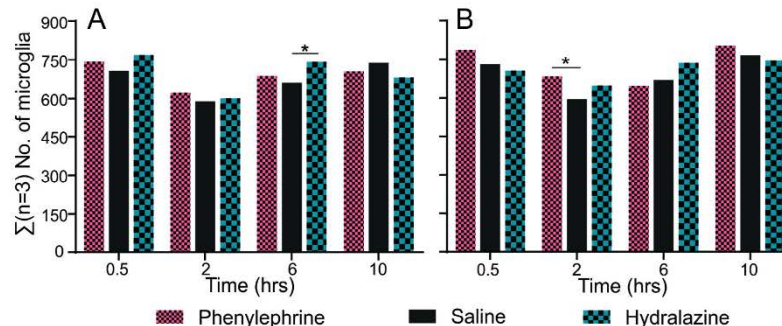


Fig. 4. Effect of intravenous infusion of phenylephrine, saline or hydralazine on the number of microglia in the ventrolateral medullary region of SD rat. Number of microglia in the (A) CVLM and (B) RVLM, when stimuli were provided for 0.5, 2, 6 and 10 h. Statistical comparisons were made with the saline treatment group, at the particular time point, using the Chi-square test for goodness of fit; * $p \leq 0.05$. Data is summed from three animals.

RESULTS

Effects of BP modulations on the CVLM and the RVLM neuronal activity

Variations induced in MAP. Intravenous infusion of phenylephrine (an α_1 -adrenoreceptor agonist, which acts on blood vessels, and does not cross the blood–brain barrier) raised the baseline levels of MAP by 40 ± 10 mmHg, within 1 min following the start of infusion (Fig. 1A1). However, the increase in MAP only lasted for 30 min, without changing the rate of infusion. The gradual reduction in arterial pressure following prolonged phenylephrine infusion is well known, and can be attributed to the desensitization of α_1 -adrenoreceptors (Minami et al., 1997). Therefore, the rate of infusion was adjusted for subsequent time points to maintain the elevated levels of BP, where possible. Intravenous infusion of phenylephrine was maintained for 0.5, 2, 6 and 10 h, in four separate groups of rats ($n = 3$ each). Each group of rats was sacrificed at each time point for analysis. Slight variations in baseline levels of MAP were observed during intravenous infusion of saline in four separate groups of rats: 0.5, 2, 6 and 10 h ($n = 3$ each) (Fig. 1A2) but overall BP levels were not affected.

Intravenous administration of hydralazine caused an instant, and sustained, hypotensive response of 40 ± 10 mmHg (Fig. 1A3). The hypotensive stimulus was maintained for 0.5, 2, 6 and 10 h, respectively, in four separate groups of rats ($n = 3$ each). Maintenance of the acute hyper-, and hypo-, tensile stimuli for the duration of the protocol, evoked significant differences in MAP, shown by AUC analysis (Fig. 1B), indicating that alterations introduced in the MAP were maintained for the duration of the experimental period.

Fos-ir. It is well known that Fos-ir changes in response to altered MAP in the CVLM and the RVLM (Chan and Sawchenko, 1994; Li and Dampney, 1994; Suzuki et al.,

1994; Graham et al., 1995; Minson et al., 1997). Therefore, we did not perform a comprehensive quantification of Fos-ir in the CVLM, in response to provided stimuli; instead, Fos-ir was quantified in the RVLM region to indicate that the stimulus induced the expected changes in neuronal activity.

Neuronal activity in the RVLM increases in response to acute hypotension. In agreement with previous studies, intravenous administration of hydralazine increased the number of Fos-ir neurons in the RVLM (Fig. 2C), when compared to saline infusion (Fig. 2B), at all of the four time points included in the study; 0.5, 2, 6 and 10 h (Graham et al., 1995). At 0.5 h, the number of Fos-ir neurons increased by 32% (88–116; $p \leq 0.05$) when compared with saline (Fig. 2D). Consistent with the previous time point, 2 h of hydralazine administration increased the number of Fos-ir neurons by 255% (42–149; $p \leq 0.0001$, Fig. 2D). The number of Fos-ir neurons in the RVLM continued to increase further by 149% at 6 h (from 148 to 368; $p \leq 0.0001$) and by 62% at 10 h (404–655; $p \leq 0.0001$) (Fig. 2D).

Following 0.5 h of phenylephrine infusion, the number of Fos-ir neurons, observed in the RVLM, were not significantly different from that seen in saline treated rats (Fig. 2D). However, increased levels of Fos-ir neurons were observed in the RVLM samples collected from rats subjected to acute hypertension, when compared with saline, for 2 h (increased by 110%; from 42 to 88; $p \leq 0.0001$), 6 h (increased by 44%; from 148 to 213; $p \leq 0.001$) and 10 h (increased by 53%; from 404 to 618; $p \leq 0.0001$) (Fig. 2D). The increased levels of Fos-ir in the RVLM, in response to phenylephrine infusion when compared with saline infusion, may be attributed to the tendency of BP to return to baseline levels, following the initial 60 min of phenylephrine infusion. However, the Fos-ir observed in the RVLM in response to intravenous phenylephrine (Fig. 2A) was lower than the Fos-ir levels quantified in the same

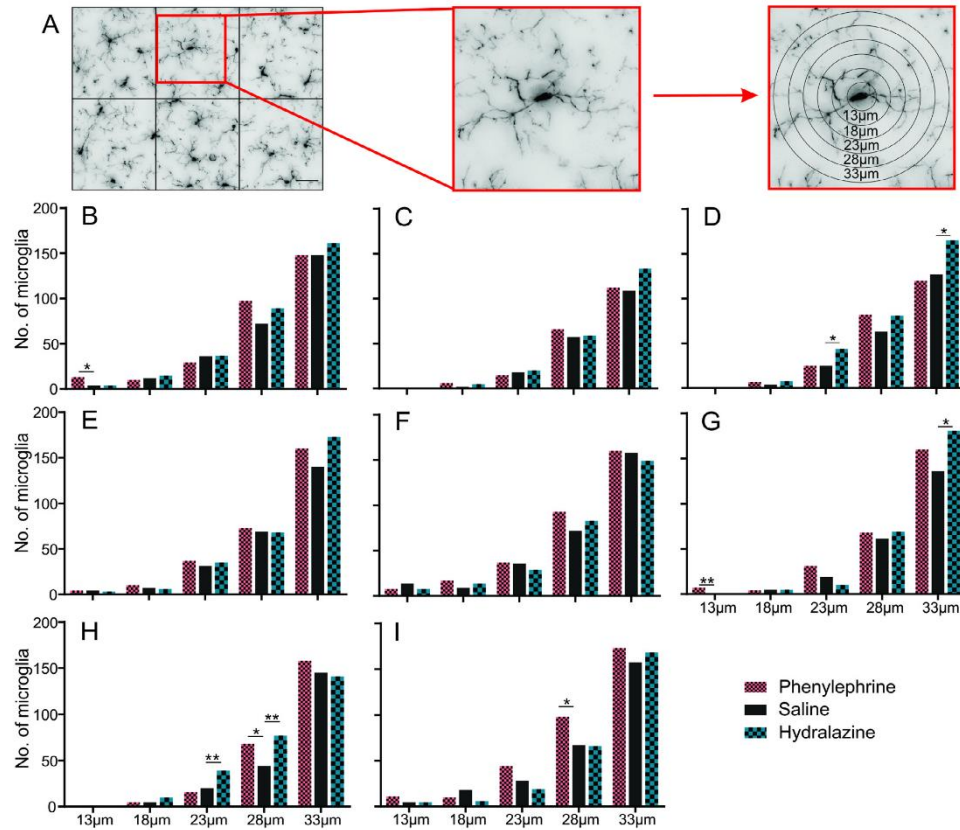


Fig. 5. Effect of intravenous infusion of phenylephrine, saline or hydralazine on the spatial distribution pattern of microglia in the ventrolateral medullary region of SD rat. (A) Spatial distribution analysis: each image was divided into six equal parts using the grid feature in CorelDRAW X7. One microglia was chosen from each of these six regions and a series of six concentric circles were drawn centered around the soma of each of these microglia (modified Sholl analysis; see methods for details). Scale bar = 20 μm . Number of microglia plotted against the inter-microglial distance in the CVLM region when stimuli were provided for (B) 0.5 h, (C) 2 h, (D) 6 h and (E) 10 h and the RVLM region when stimuli were provided for (F) 0.5 h, (G) 2 h, (H) 6 h and (I) 10 h. Statistical comparisons were made with the saline treatment group, at the particular time point, using the Chi-square for goodness of fit; $p \leq 0.05$ and $^{**}p \leq 0.01$. Data is summed from three animals.

region in response to hydralazine administration (Fig. 2C), at the 2 h (lower by 61; $p \leq 0.0001$) and 6 h time points (lower by 155; $p \leq 0.0001$) (Fig. 2D).

Microglial-neuronal relationship under homeostasis

Microglia (Iba1) are homogeneously distributed in the cardiovascular nuclei of the brainstem, the CVLM (Fig. 3A) and the RVLM (Fig. 3B), and create a network with their processes covering the entire neuronal parenchyma. Microglial packing density varies depending on the neuronal packing density (Fig. 3B). Microglial processes were observed to be in closer contact with the dendrites of TH⁺ RVLM neurons than the neuronal cell body (Fig. 3B, C and E). Microglial processes were observed to

wrap themselves around the TH⁺ neuronal cell body (Fig. 3D and movie 1) and dendrites (Fig. 3E and movie 2).

Induction of acute hyper- or hypo-tension causes microglia to change their pattern of distribution in the ventrolateral medullary nuclei

• Overall number of microglia

CVLM: Following intravenous administration of hydralazine, a change in the total number of microglia was only seen 6 h after the stimulus (Fig. 4A), with a slight yet significant increment in the number of microglia (increased by $\approx 12\%$ from 661 to 742; $p \leq 0.05$). This increase returned to normal 10 h after hypotension

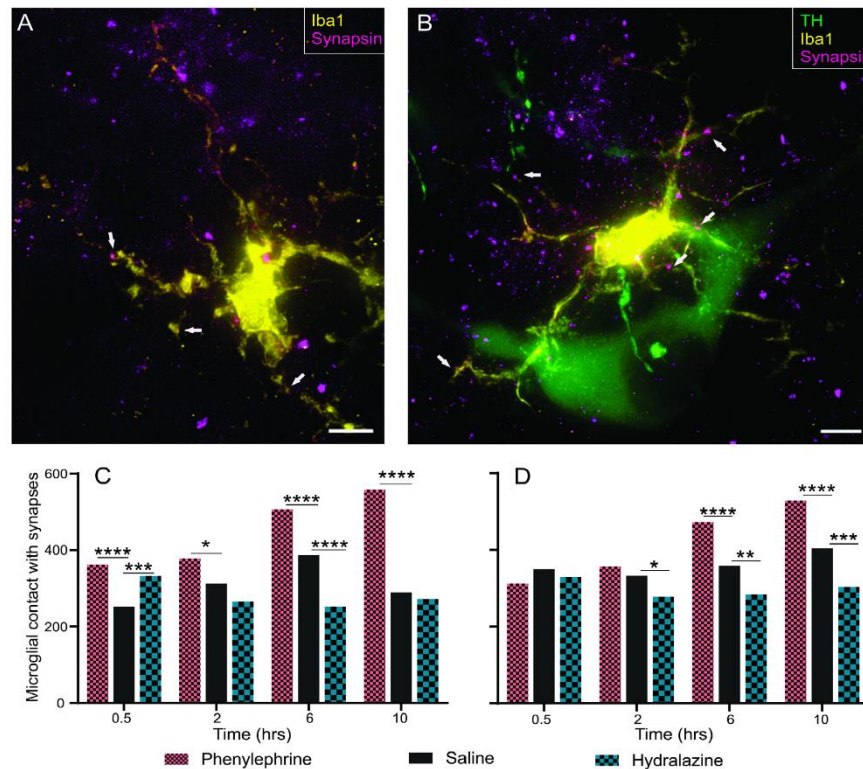


Fig. 6. Effect of intravenous infusion of phenylephrine, saline or hydralazine on the number of synapses in contact with the microglial end point processes in the ventrolateral medullary region of SD rat. (A) Microglial end point processes in close contact with synapses (Synapsin) in the CVLM region (white arrows). Scale bar = 20 μ m. (B) Microglial end point processes in close contact with synapses (Synapsin) in the RVLM region (white arrows). Scale bar = 20 μ m. Yellow – Iba1, Green – TH and Violet – Synapsin. Number of microglia in contact with synapses in the (C) CVLM and the (D) RVLM when stimuli were provided for 0.5, 2, 6 and 10 h. Statistical comparisons were made with the saline treatment group, at the particular time point, using the Chi-square test for goodness of fit; * $p \leq 0.05$, ** $p \leq 0.01$, *** $p \leq 0.001$ and **** $p \leq 0.0001$. Data are summed from three animals. (For interpretation of the references to color in this figure legend, the reader is referred to the web version of this article.)

(Fig. 4A). Intravenous infusion of phenylephrine did not induce any changes in the overall number of microglia in the CVLM (Fig. 4A).

RVLM: Continuous intravenous infusion of phenylephrine for 0.5 h did not change the overall number of microglia (Fig. 4B). However, following 2 h of phenylephrine infusion the number of microglia significantly increased by $\approx 14\%$ (from 596 to 683; $p \leq 0.05$) in the RVLM region when compared with saline (Fig. 4B). These increased numbers of microglia returned to normal baseline levels at 6 h (Fig. 4B) and remained unchanged 10 h following induction of hypertension (Fig. 4B). No significant change in the number of microglia was observed in the hydralazine treatment group at any of the 4 time points analyzed, when compared with saline treated group.

• Inter-microglial distance

CVLM: (Fig. 5B–E). Induction of acute hypertension causes a rapid, but short term, change in the homogenous distribution of microglia. The number of microglia with an inter-microglial distance of $\approx 13 \mu$ m increased from 4 to 13 ($p \leq 0.05$) when compared with the saline group, following 0.5 h of phenylephrine infusion (Fig. 5B). This subtle change in the distribution of microglia returned to normal within 2 h of hypertension induction and stayed that way at subsequent time points (Fig. 5C–E).

No rearrangement in the distribution of microglia was seen following hydralazine administration at 0.5 or 2 h (Fig. 5B and C). However, at the 6-h time point, significant differences were seen in microglial distribution during acute hypotension. Increased numbers of microglia

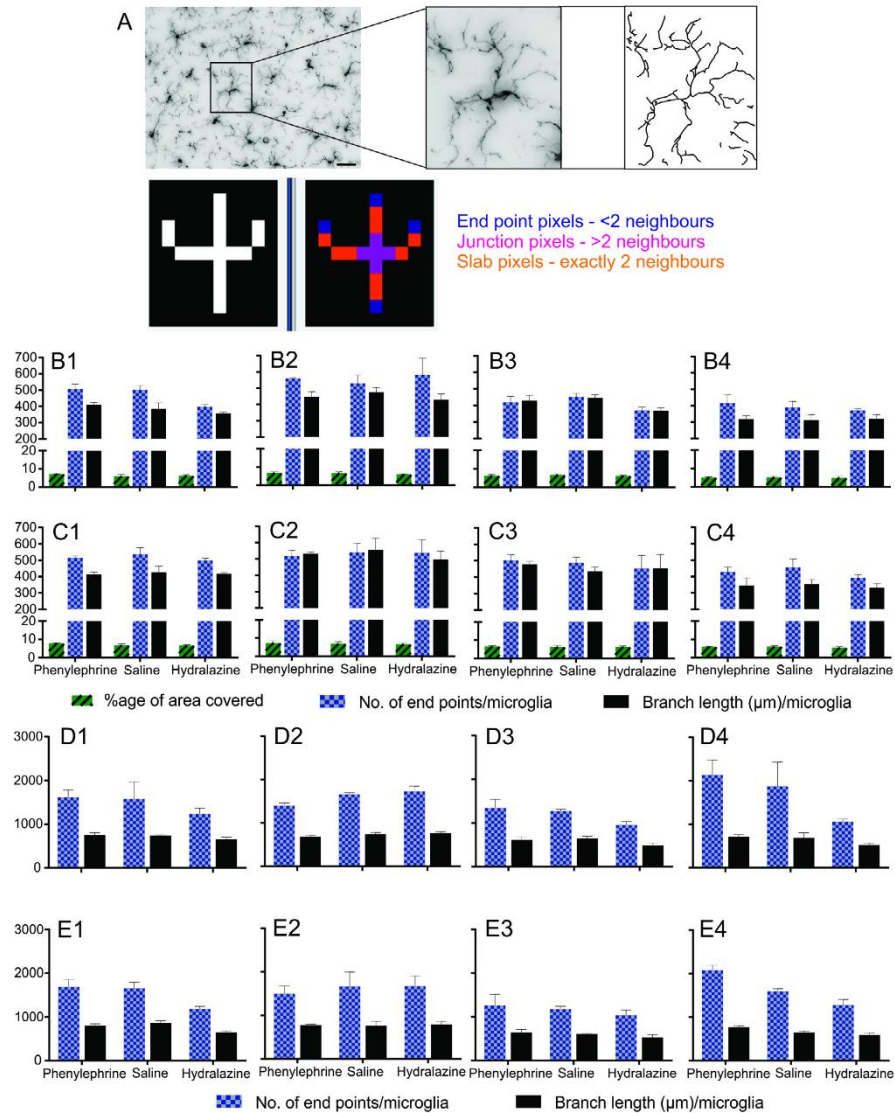


Fig. 7. Effect of intravenous infusion of phenylephrine, saline or hydralazine on the morphological characteristics of microglia in the ventrolateral medullary region of SD rat. (A) Quantification of morphological characteristics: binary images were 'skeletonized' with ImageJ and analyzed with the "AnalyzeSkeleton" plugin. Number of end point pixels (blue) and branch length (orange), obtained using AnalyzeSkeleton plugin of ImageJ, were normalized with the total number of microglia. Scale bar = 20 μm . The morphological characteristics examined at 40 \times magnification were: % of area covered by microglia calculated using ImageJ, No. of end point processes/microglia and branch length (μm)/microglia. Effect of intravenous infusion of blood pressure modulating drugs on the morphological characteristics of microglia (40 \times) in the (B) CVLM region and the (C) RVLM region where the stimulus was maintained for 0.5 h (B1 and C1), 2 h (B2 and C2), 6 h (B3 and C3) and 10 h (B4 and C4). The morphological characteristics examined at 63 \times magnification were: No. of end point processes/microglia and branch length (μm)/microglia. Effect of intravenous infusion of blood pressure modulating drugs on the morphological characteristics of microglia (63 \times) in the (D) CVLM and the (E) RVLM region, where the stimulus was maintained for 0.5 h (D1 and E1), 2 h (D2 and E2), 6 h (D3 and E3) and 10 h (D4 and E4). Kruskal–Wallis one-way analysis of variance didn't show any significant difference between treatments. Data are expressed as mean \pm SEM, $n = 3$. (For interpretation of the references to colour in this figure legend, the reader is referred to the web version of this article.)

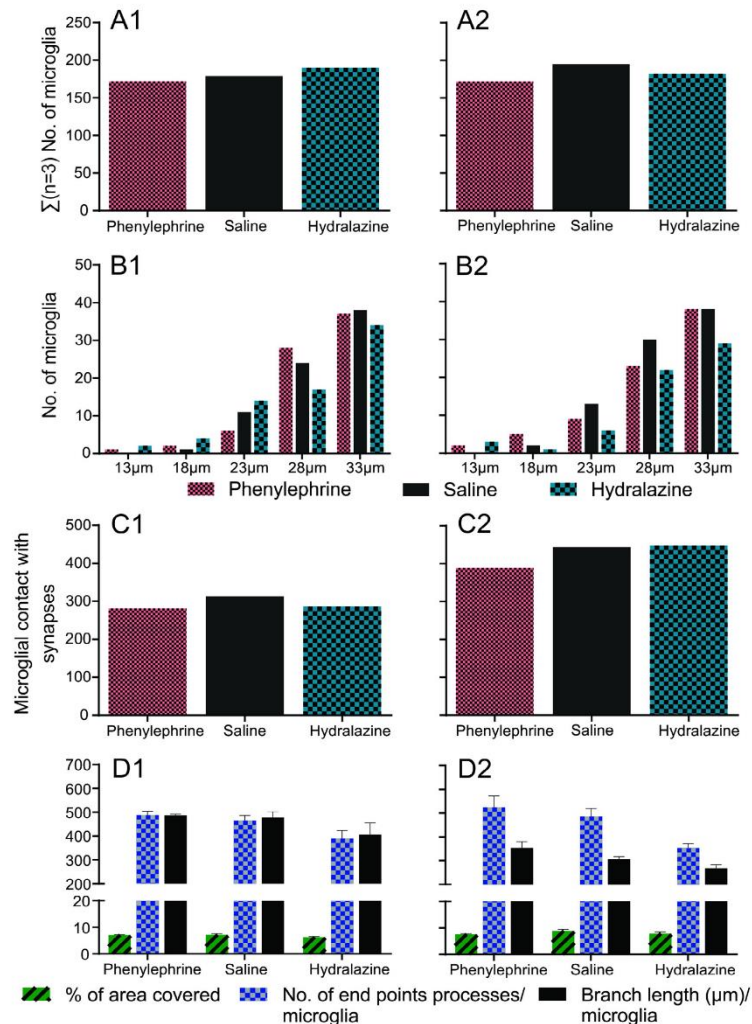


Fig. 8. Microglial response to the intravenous infusion of phenylephrine, saline or hydralazine in the nucleus ambiguus (sub compact; NAsc) at 6 and 10 h time point. (A) Overall number of microglia at (A1) 6 h and (A2) 10 h. (B) Microglial spatial distribution at (B1) 6 h and (B2) 10 h. (C) No. of synapses in contact with microglial end point processes at (C1) 6 h and (C2) 10 h. (D) Microglial morphology: % of area covered, number of end point processes/microglia and branch length (μm)/microglia at (D1) 6 h and (D2) 10 h. The Chi-square test for goodness of fit didn't show any significant differences in the overall No. of microglia, microglial spatial distribution and number of synapses contacted by microglia. Statistical comparisons were made with the saline treatment group, at the particular time point; data is summed from three animals. Kruskal–Wallis one-way analysis of variance didn't show any significant difference between treatment groups. Data are expressed as mean \pm SEM, $n = 3$.

were observed with an inter-microglial distance of $\approx 23 \mu\text{m}$ (increased by 19; $p \leq 0.05$) and $33 \mu\text{m}$ (increased by 38; $p \leq 0.05$), when compared with saline (Fig. 5D). These changes were not observed following 10 h of acute hypotension (Fig. 5E).

RVLM: (Fig. 5F–I). A spatial distribution analysis revealed that the number of microglia with an inter-

microglial distance of $\approx 13 \mu\text{m}$ increased from 0 to 7 ($p \leq 0.01$), when compared with saline, following 2 h of phenylephrine infusion (Fig. 5G). Following 6 h of phenylephrine infusion, significant differences were observed in the number of microglia with an inter-microglial distance of $\approx 28 \mu\text{m}$, indicating the resumption of microglial homeostatic distribution. The number of microglia with an inter-microglial distance of $\approx 28 \mu\text{m}$

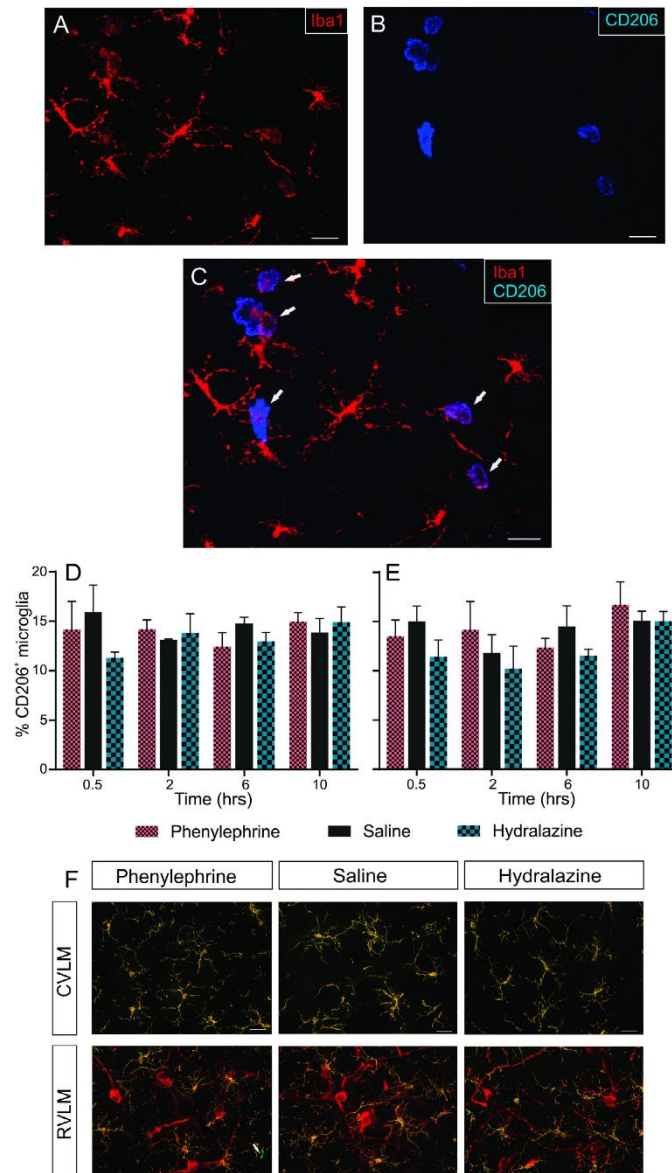


Fig. 9. Effect of intravenous infusion of phenylephrine, saline or hydralazine on the expression levels of M1 and M2 phenotype in the brainstem region of SD rat. (A) Microglia (Iba1, red) in the RVLM region. (B) M2 microglia (CD206, blue) in the RVLM region. (C) Merged image of (A and B) showing the co-localization (white arrows) of M2 microglia and the Iba1 labeled microglia (pan marker for M0, M1 and M2). Scale bar = 20 μ m. % CD206⁺ microglia in response to blood pressure altering drugs in the (D) CVLM and the (E) RVLM when stimuli were provided for 0.5, 2, 6 and 10 h. Statistical comparisons were made using Kruskal–Wallis one-way analysis of variance. Data are expressed as mean \pm SEM, $n = 3$. (F) Representative images showing the expression levels of M1 phenotype (CD16, green, white arrow) and microglia (Iba1, yellow) in the CVLM and RVLM (TH, red) when stimuli were provided for 0.5, 2, 6 and 10 h. Scale bar = 20 μ m. (For interpretation of the references to color in this figure legend, the reader is referred to the web version of this article.)

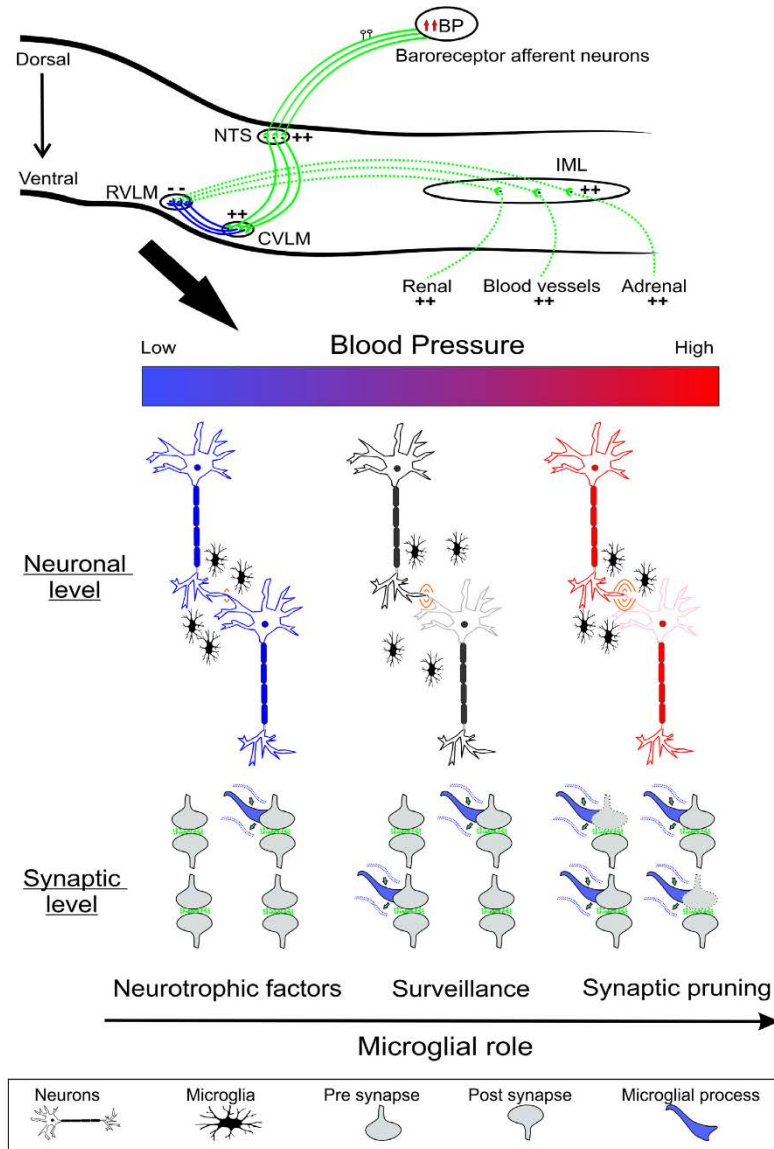


Fig. 10. Microglial alertness induced in response to changes in levels of blood pressure. Baroreceptor afferent neurons located in the carotid sinus and aortic arch provide excitatory input (green) to the nucleus of the solitary tract (NTS) neurons in response to increased levels of blood pressure. Excited NTS neurons then activate (green) the caudal ventrolateral medullary (CVLM) neurons which in turn provide inhibitory input (blue) to rostral ventrolateral medullary (RVLM) neurons. This inhibition of RVLM neurons results in reduced sympatho-excitatory (dotted green) outflow to peripheral organs via neurons located in the intermediolateral (IML) cell column of the spinal cord. Modulations in arterial blood pressure levels further alter the levels of synaptic activity which in turn triggers "on" or "off" signaling alertness in microglial behavior. Low blood pressure levels (blue neurons) may cause "off" signaling microglial alertness resulting in microglia to move closer and reduce the number of synaptic contacts. Whereas, increased levels of blood pressure (red neurons) may trigger "on" signaling in microglial activity causing microglia to move closer to each other and increase the number of contacts made with synapses. (For interpretation of the references to color in this figure legend, the reader is referred to the web version of this article.)

increased from 44 to 68 at 6 h ($p \leq 0.05$) (Fig. 5H) and from 67 to 98 ($p \leq 0.05$) at 10 h (Fig. 5I).

Data from induced hypotension showed a decrease in the inter-microglial distance starting at 2 h, continuing at 6 h and returning to normal at 10 h. The number of microglia at 2 h with an inter-microglial distance of $\approx 33 \mu\text{m}$ increased from 136 to 181 ($p \leq 0.05$) (Fig. 5G). This distance between microglia continues to decrease to $\approx 23 \mu\text{m}$ (microglial number increased from 20 to 39; $p \leq 0.05$) and $28 \mu\text{m}$ (microglial number increased from 44 to 77; $p \leq 0.01$) at 6 h time point (Fig. 5H). These changes in the spatial distribution of microglia returned to normal at 10 h (Fig. 5I).

Microglial contact with synapses increases with the induction of acute hypertension in the ventrolateral medullary nuclei

Microglial end point processes (Iba1) were seen to be in close contact with neuronal synapses (Synapsin), in the CVLM (Fig. 6A) and the RVLM (Fig. 6B) region of the brainstem.

CVLM: Microglial contacts with neuronal synapses increased following 0.5 h of phenylephrine infusion and remained elevated until 10 h (Fig. 6C). At 0.5 h, the number of synapses in close contact with microglial end point processes increased by 44% (from 252 to 362; $p \leq 0.0001$, Fig. 6C). Following 2 h of phenylephrine infusion, the number of synapses in contact with microglia increased by 21% (from 312 to 378; $p \leq 0.05$, Fig. 6C). Similar microglial responses were observed at 6 and 10 h (Fig. 6C). Number of microglial processes in contact with synapses increased by 31% (from 387 to 507; $p \leq 0.0001$) at 6 h and by 93% (from 289 to 558; $p \leq 0.0001$) at 10 h (Fig. 6C).

RVLM: In the RVLM, significant changes in the number of microglial processes contacting neuronal synapses started to appear following 6 h of phenylephrine infusion (Fig. 6D). The number of synapses in contact with microglial end point processes increased by 32% (from 359 to 473; $p \leq 0.0001$) at 6 h and by 31% (from 404 to 529; $p \leq 0.0001$) at 10 h (Fig. 6D).

Microglial contact with synapses decreases with the induction of acute hypotension in the ventrolateral medullary nuclei

CVLM: Following 0.5 h of acute hypotension microglial contacts with neuronal synapses increased by 32% (from 252 to 332; $p \leq 0.001$; Fig. 6C). Microglial contact with CVLM neuronal synapses decreases at 6 h (decreased by 35% from 387 to 252; $p \leq 0.0001$) and returned to normal at 10 h (Figs 6C).

RVLM: Microglial contact with the RVLM neuronal synapses, in response to induction of acute hypotension, decreases with the increase in the duration of the stimulus (Fig. 6D). At 2 h, the number of

synapses contacted by microglia decreased by 17% (from 333 to 278; $p \leq 0.05$) and remained decreased at the following time points (Fig. 6D). Number of synapses contacted by microglial end point processes decreased by 21% (from 359 to 284; $p \leq 0.001$) at 6 h and by 25% (from 404 to 303; $p \leq 0.001$) at 10 h.

Microglia do not change their morphology in response to induction of acute hyper- or hypotension (Fig. 7B–E) in the ventrolateral medullary nuclei

Analysis of the % of area covered by microglia, number of end point processes per microglia and branch length (μm) per microglia at $40\times$ magnification did not show any significant differences between treatment groups. This observation was consistent during induction of acute hyper- or hypotension in either CVLM (Fig. 7B) or RVLM (Fig. 7C). Analysis of microglial morphology (number of end point processes/microglia and branch length (μm)) at higher magnification ($63\times$) also did not show any significant changes in microglial morphological characteristics in either CVLM (Fig. 7D) or RVLM (Fig. 7E).

Induction of acute hyper- or hypotension does not induce any microglial response in the nucleus ambiguus (sub compact; NAsc)

The microglial response to induction of hyper- or hypotension in the NAsc served as a control to the microglial response in the CVLM and the RVLM. No significant differences were observed in the overall number of microglia (Fig. 8A1 and A2), microglial spatial distribution (Fig. 8B1 and B2), number of synapses co-localizing with microglial end point processes (Fig. 8C1 and C2) and microglial morphology (Fig. 8D1 and D2), at either 6 or 10 h time points, regardless of the provided treatment.

Expression levels of M1 or M2 phenotype do not change with the disturbances introduced in BP in the ventrolateral medullary nuclei

Iba1 (a pan marker for microglia) is known to label all microglia in the CNS regardless of their phenotype; M0, M1 or M2 (Fig. 9A). The CD206/mannose receptor was used as a marker to identify activated microglia exhibiting a behavior similar to M2 type macrophages in the periphery (Fig. 9B). The number of CD206⁺ microglia, co-localizing with Iba1 expression (Fig. 9C), was calculated and expressed as the percentage of CD206⁺ microglia to total microglia (% CD206⁺). The % CD206⁺ microglia, signifying the expression levels of M2 microglial phenotype, did not vary significantly between the three treatment groups at any of the four time points; 0.5, 2, 6 and 10 h, in either of the regions analyzed i.e. the CVLM (Fig. 9D) or the RVLM (Fig. 9E).

In addition to this, experiments were performed to quantify the expression levels of the M1 phenotype (labeled with CD16) in the CVLM and the RVLM region when animals were subjected to acute hyper- or hypo-

tension at all of the four time points; 0.5, 2, 6 and 10 h. The results (Fig. 9F) showed very slight, or no, expression of the M1 phenotype at any of the time points analyzed, in any of the treatment groups, in either the CVLM or the RVLM region.

These results were in accordance with other studies, which showed basal M2 expression levels, and lack of M1 expression in the absence of physical CNS injury (Perego et al., 2011).

DISCUSSION

The main finding of our study is that microglia do not play a passive role in the cardiovascular system but actively detect and respond to changes in the levels of BP; microglia dynamically change their distribution pattern and contacts made with synapses in response to changes in BP. Our first finding supports the hypothesis that microglia are well-placed to play a critical role within the CNS (Hanisch and Kettenmann, 2007; Wake et al., 2009; Kettenmann et al., 2013; Dworak et al., 2014) so as to ensure that cardiovascular autonomic neurons remain responsive to excitatory or inhibitory inputs. Secondly, our results reveal that microglia in the ventral medulla oblongata appear to monitor the local environment and respond to the magnitude and persistence of signals. Thirdly, increased or decreased levels of BP, ultimately affecting synaptic activity, changes microglial behavior. Interestingly, this microglial behavior is not manifested as polarization to activated microglial phenotypes, and does not require surveilling microglia to change their ramified morphology significantly. Instead, this modest change in microglial behavior may indicate an enhanced state of microglial alertness whereby they become more attentive to their local environment (Hanisch and Kettenmann, 2007; Karperien et al., 2013; Kapoor et al., 2015). In response to increased BP, the spatial distribution of microglia is affected; as is the number of synapses contacted by surrounding microglia. On the other hand, decreased BP levels cause microglia to change their pattern of distribution, and reduce the number of synaptic structures contacted by microglial processes. This study is the first to describe the spatial distribution of microglia in the resting (saline) or 'stressed' states (hyper- or hypo-tension) within the ventral medulla of the brainstem that are critical for cardiorespiratory regulation.

Our first finding provides evidence for the existence of a mesh created by the fimbria of surveilling microglia covering the entire neuronal population in the CVLM and the RVLM region of brainstem. This microglial state is also defined as the M0 phenotype, which precedes the M1 (inflammatory activated microglia) and M2 (anti-inflammatory activated microglia) phenotypes (Hu et al., 2012; Butovsky et al., 2014).

Induction of acute hypertension increases the glutamatergic input to CVLM neurons of brainstem (Minson et al., 1997; Oshima et al., 2012). This glutamate mediated activation at synapses in the CVLM region induces a rapid microglial response (within 0.5 h), causing microglia to move closer to and contact synapses more

frequently. The rearrangement in the pattern of distribution of microglia was a short term response to increased BP levels and was not seen at any subsequent time points. However, the increased microglial contact with neuronal synapses was a rapid and long term effect and did not return to normal levels even following 10 h of phenylephrine infusion. Augmented inhibitory output (GABAergic transmission) from CVLM neurons, in response to increased BP levels, shuts down neurons in the RVLM region (Pilowsky et al., 1985, 2009). In the RVLM, microglial numbers increased and changed their distribution pattern following 2 h of continuous hypertension. This change observed in the spatial distribution of microglia did not change the level of synapses sampled by microglia. The number of synapses contacted by microglia, in the RVLM region, starts to increase at 6 h and remained elevated at 10 h. A lack of microglial response, in the RVLM region, following 0.5 h of hypertensive stimulus, may be attributed to microglia sensing the decreased synaptic activity in the RVLM region as a temporary disturbance. However, the persistence of stimuli in the RVLM alerts microglia to under-excited neurons.

We performed the same study in another animal group where acute hypotension was induced, by intravenous administration of hydralazine. Lowering of BP reduces the excitatory (glutamatergic) inputs to the CVLM (Miyawaki et al., 1997; Guyenet, 2006; Pilowsky et al., 2009). This reduced synaptic activity of CVLM neurons, in response to reduced glutamatergic input from nucleus of the solitary tract (NTS), caused microglia to increase the number of contacts made with synapses at 0.5 h. Following 6 h of hypotension, microglia changed their pattern of distribution and reduced the number of synaptic contacts. The initial increase (0.5 h) in microglial contacts with synapses, in the CVLM, may be a means by which microglia analyze the nature of any homeostatic disturbance. The lack of a microglial response at 2 h may be attributed to the possibility that microglia assess the homeostatic imbalance as a harmless change. The subsequent persistence of the stimulus may then lead to a microglial reaction. A reduction of inhibitory inputs from CVLM neurons reduces the levels of GABA in the synapses of RVLM neurons and leads to their over-excitation (Miyawaki et al., 1997, 2002). This reduced synaptic activity of RVLM neurons induces a fairly rapid (following 2 h of treatment) change in microglial behavior causing inter-microglial distance to decrease until 6 h of hypotension. This change in the spatial distribution of microglia is accompanied by a reduction in the number of synapses contacted by microglia.

Our data strongly supports the hypothesis that microglia and neurons are constantly communicating with each other (van Rossum and Hanisch, 2004; Pocock and Kettenmann, 2007). Any changes in neuronal activity are, more often than not, accompanied with changes in their neurochemistry that possess the power to disrupt the constitutive release of neurotransmitters, released by neurons in homeostatic circumstances, such as GABA and glutamate (Pilowsky, 2014). Augmented, or reduced, synaptic levels of constitutively expressed neurotransmitters, depending on the stimulus, are sensed

by microglia that may cause them to shift to an 'alerted' state. In this 'alerted/intermediate' state, microglia monitor the local environment with extra vigilance by changing the level of synaptic sampling and conducting the required action (Hanisch and Kettenmann, 2007; Karperien et al., 2013; Kapoor et al., 2015). This shift can be attributed to "on" (due to an increased synaptic activity) or "off" (due to a decreased synaptic activity) signaling mechanisms (Biber et al., 2007). In this study, the microglial behavior induced in response to increased BP levels/synaptic activity, possibly via "on" signaling, causes rearrangement of their pattern of distribution and increases the number of synapses contacted by microglia. This microglial behavior might be necessary to conduct activities such as synaptic pruning (Wake et al., 2009; Miyamoto et al., 2013), to reduce the activity levels of affected synapses. Changes in microglial behavior observed in response to decreased BP levels/synaptic activity, possibly via "off" signaling, can be attributed to their ability to release neurotrophic factors. Such factors may include: insulin growth factor-1 (Ueno et al., 2013) and macrophage-colony stimulating factor (Murase and Hayashi, 1998) that may support, or increase, the activity of silent synapses. In the case of "off signaling", we speculate that fewer microglia may spend longer with affected synapses. The rearrangement induced in the pattern of microglial distribution may or may not be accompanied by changes in the overall number of microglia. In our hands, the first signs of a microglial response, to the changes induced in the basal levels of BP, were observed in the CVLM region, in both hyper-, and hypo-, tension.

It is now believed that microglial responses to any stimuli can no longer be viewed as an "all or none" activity; rather, they elaborate a graded response (Kettenmann et al., 2011). At one extreme, microglia respond to damage caused by inflammation or other severe injury. At the other extreme, the findings presented here support the notion that microglia continuously interact with neuronal synapses in a homeostatic manner to maintain a physiologically balanced state (Wake et al., 2009; Miyamoto et al., 2013). CNS injuries can result in irreversible damage that requires dramatic morphological rearrangement of surveilling microglia, resulting in microglial polarization to either of the activated phenotypes; M1 or M2 (David and Kroner, 2011; Perego et al., 2011). In our case, our morphological analysis revealed that brainstem microglia in cardiovascular nuclei do not significantly change their morphology when subjected to either hyper-, or hypo-, tension. This is further supported by the lack of significant changes observed in the expression levels of M1 or M2 phenotype. Our data also reveal that the brainstem microglial response to increased or decreased levels of BP does not require an obvious change to an "activated phenotype". Therefore, we speculate, in accordance with other studies, that the microglial behavior observed here is may be exhibited as an intermediate state by "alerted microglia" that succeeds the surveilling phenotype (M0), but precedes the activated phenotypes (M1/M2), that are observed during even mild disturbances in the local environment, and act to restore homeostasis (Hanisch and Kettenmann, 2007; Karperien et al., 2013;

Kapoor et al., 2015). Recent literature suggests that microglia, in their ramified state, are capable of a number of neuro-supportive functions, including synaptic pruning (Tremblay et al., 2011), and release of neurotrophic substances (Karperien et al., 2013); this earlier work further supports the hypothesis for the existence of an 'alerted' microglial phenotype in addition to the quiescent M0, and activated M1/M2 states (Hanisch and Kettenmann, 2007; Kettenmann et al., 2011; Karperien et al., 2013). Our findings therefore illustrate a novel dimension to sympathetic neurophysiology, and illustrate the way that 'alerted' microglia may play a critical role in interacting with neurons to maintain a healthy CNS in normal homeostasis.

Microglial migration to the site of injury enables them to execute their immune functions, and requires a highly dynamic morphology (Stence et al., 2001) that comes with the ability to cope with extreme cellular rearrangements in a short period of time (Janssen et al., 2014). There is a possibility that there may be subtle changes introduced in the morphology of surveilling microglia enabling them to change their pattern of distribution while they are in a normal but 'alerted' state. Other studies also suggest that microglia may be capable of migrating short distances to conduct their housekeeping activities without acquiring an ameboid morphology (Amadio et al., 2013; Karperien et al., 2013).

Changes in the levels of BP, by loading or unloading of baroreceptors, affects the synaptic activity levels in the CVLM or the RVLM, fairly rapidly, within minutes of the provided stimulus (Miyawaki et al., 1997; Schreihöfer and Guyenet, 2003). These rapidly induced changes in the levels of synaptic activity may be sensed by microglia in the vicinity of the affected synapses, and microglia may contribute to mechanisms such as baroreflex resetting. Baroreflex resetting is a mechanism by which the operating point of baroreceptor sensitivity changes, over a wide range of BP, and allows elevation of BP during appropriate behaviors such as exercise (DiCarlo and Bishop, 2001; Guyenet, 2006). The earliest time point employed in our study was 0.5 h and the latest time point was 10 h; at 0.5 h no significant changes in the microglial spatial distribution, except in the CVLM following phenylephrine infusion, were observed. Microglia increased the number of CVLM neuronal synapses contacted at 0.5 h, following phenylephrine and hydralazine administration, but no changes were observed in the RVLM. We speculate that the persistence of the stimulus, rather than the appearance, evokes a more settled microglial response. However, the possibility that the microglial response to altered levels of BP, in the ventrolateral medullary nuclei, may begin and peak earlier than 0.5 h cannot be ignored; further work at earlier time points would be needed to clarify such a possibility.

Technical consideration: vertebrates under anesthesia cannot breathe adequately for longer durations without the aid of artificial ventilation: in this study, 6 h was the maximum. Thus, in the 10 h experiments animals were vagotomized (both left and right cervical vagus nerves were cut, to prevent inputs from pulmonary afferent nerves) and paralyzed with

pancuronium bromide (to prevent entrainment of breathing to the ventilator (Pilowsky et al., 1990; Sun et al., 2011)), and were artificially ventilated. In preliminary experiments combining the use of sodium pentobarbital, pancuronium bromide and phenylephrine, there was a severe deterioration in the condition of the animal. Thus, the anesthetic was changed to urethane, so that all three drugs (anesthetic, paralyzing agent and phenylephrine) could be administered in the same animal. The control experiments (saline), at the 10-h time-point were conducted, where the animals were treated in the same way as the test treatments (phenylephrine/hydralazine), to rule out the effect of change in anesthetic and surgical procedures, and isolate the effect of altered BP, on the microglial response. The microglial response observed at the 10-h time point reached a 'plateau phase' where microglial response either returned to baseline or no new additional changes were observed at 10 h compared to 6 h. This is reflected in the data from the control experiments (10 h in the NASc) where no changes were seen in the microglial number, spatial distribution, morphology or level of synaptic sampling, following 10 h of either hyper-, or hypo-, tension.

In summary, we speculate that while changes in BP do not require polarization of microglia to an activation state, but that a transition to an 'alerted' state is essential to maintain a normal homeostatic environment. Microglia constantly sense changes in synaptic activity and change their pattern of distribution or packing density along with the level of synaptic surveillance, but without requiring an obvious transformation in their phenotype. The alertness induced in microglial behavior in response to synaptic activity variations may be attributed to the ability of microglia to conduct neuro-protective/neuro-supportive activities such as synaptic pruning or release of neurotrophic factors, to resume homeostasis without causing inflammation or long-term neuronal damage (Fig. 10).

Our study, therefore, provides the first evidence concerning the relationship of microglia to cardiovascular neurons in the ventral brainstem. Importantly, the microglial response that follows imposed variations in BP does not induce a conventional inflammatory activation of microglia; revealing yet another function of surveilling microglia in the uninjured CNS. With increasing literature suggesting that microglial activation contributes to the exaggerated activity of the SNS (Shi et al., 2010), we propose a plausible neuro-supportive role of microglia in the SNS.

Acknowledgements—Work in the Authors laboratory is supported by funding from the Australian Research Council (DE120100992), the National Health and Medical Research Council of Australia (1082215, 1065485 and 1024489), The Heart Research Institute and Macquarie University (2012112 and 2012219). The Authors acknowledge the support received from the Bosch Institute Advanced Microscopy Facility at the University of Sydney, and the expert help of Facility staff, especially Dr. Louise Cole and Dr. Cathy Payne.

The authors declare no competing financial interests.

REFERENCES

- Amadio S, De Nino A, Montilli C, Businaro L, Gerardino A, Volonte C (2013) Plasticity of primary microglia on micropatterned geometries and spontaneous long-distance migration in microfluidic channels. *BMC Neurosci* 14:121.
- Bhandare A, Mohammed S, Pilowsky PM, Farnham MM (2015) Antagonism of PACAP or microglia function worsens the cardiovascular consequences of kainic acid induced seizures in rats. *J Neurosci* 35:2283–2292.
- Bhandare AM, Kapoor K, Pilowsky PM, Farnham MMJ (2016) Seizure-induced sympathoexcitation is caused by activation of glutamatergic receptors in RVLM that also causes proarrhythmic changes mediated by PACAP and microglia in rats. *J Neurosci* 36:506–517.
- Biber K, Neumann H, Inoue K, Boddeke HW (2007) Neuronal 'On' and 'Off' signals control microglia. *Trends Neurosci* 30:596–602.
- Bieger D, Hopkins DA (1987) Visceromotoric representation of the upper alimentary tract in the medulla oblongata in the rat: the nucleus ambiguus. *J Comp Neurol* 262:546–562.
- Butovsky O, Jedrychowski MP, Moore CS, Cialic R, Lanser AJ, Gabriely G, Koeglsperger T, Dake B, Wu PM, Doykan CE, Fanek Z, Liu L, Chen Z, Rothstein JD, Ransohoff RM, Gygi SP, Antel JP, Weiner HL (2014) Identification of a unique TGF- β -dependent molecular and functional signature in microglia. *Nat Neurosci* 17:131–143.
- Chan RK, Sawchenko PE (1994) Spatially and temporally differentiated patterns of c-fos expression in brainstem catecholaminergic cell groups induced by cardiovascular challenges in the rat. *J Comp Neurol* 348:433–460.
- David S, Kroner A (2011) Repertoire of microglial and macrophage responses after spinal cord injury. *Nat Rev Neurosci* 12:388–399.
- DiCarlo SE, Bishop VS (2001) Central baroreflex resetting as a means of increasing and decreasing sympathetic outflow and arterial pressure. *Ann N Y Acad Sci* 940:324–337.
- Dworak M, Stebbing M, Kompa AR, Rana I, Krum H, Badoer E (2014) Attenuation of microglial and neuronal activation in the brain by ICV minocycline following myocardial infarction. *Auton Neurosci* 185:43–50.
- Graham JC, Hoffman GE, Sved AF (1995) C-Fos expression in brain in response to hypotension and hypertension in conscious rats. *J Auton Nerv Syst* 55:92–104.
- Guyenet PG (2006) The sympathetic control of blood pressure. *Nat Rev Neurosci* 7:335–346.
- Guyenet PG, Stormetta RL, Weston MC, McQuiston T, Simmons JR (2004) Detection of amino acid and peptide transmitters in physiologically identified brainstem cardiorespiratory neurons. *Auton Neurosci* 114:1–10.
- Hanisch UK, Kettenmann H (2007) Microglia: active sensor and versatile effector cells in the normal and pathologic brain. *Nat Neurosci* 10:1387–1394.
- Hu X, Li P, Guo Y, Wang H, Leak RK, Chen S, Gao Y, Chen J (2012) Microglia/macrophage polarization dynamics reveal novel mechanism of injury expansion after focal cerebral ischemia. *Stroke* 43:3063–3070.
- Janssen S, Gudi V, Prajeeth CK, Singh V, Stahl K, Heckers S, Skripuletz T, Pul R, Trebst C, Tsiavaliaris G, Stangel M (2014) A pivotal role of nonmuscle myosin II during microglial activation. *Exp Neurol* 261:666–676.
- Kapoor K, Bhandare AM, Farnham MM, Pilowsky PM (2015) Alerted microglia and the sympathetic nervous system: A novel form of microglia in the development of hypertension. *Respir Physiol Neurobiol*.
- Karperien A, Ahammer H, Jelinek HF (2013) Quantitating the subtleties of microglial morphology with fractal analysis. *Front Cell Neurosci* 1–34.
- Kettenmann H, Hanisch UK, Noda M, Verkhratsky A (2011) Physiology of microglia. *Physiol Rev* 91:461–553.
- Kettenmann H, Kirchhoff F, Verkhratsky A (2013) Microglia: new roles for the synaptic stripper. *Neuron* 77:10–18.

- Kreutzberg GW (1996) Microglia: a sensor for pathological events in the CNS. *Trends Neurosci* 19:312–318.
- Li YW, Dampney RA (1994) Expression of Fos-like protein in brain following sustained hypertension and hypotension in conscious rabbits. *Neuroscience* 61:613–634.
- Minami N, Imai Y, Nishiyama H, Abe K (1997) Role of nitric oxide in the development of vascular alpha 1-adrenoreceptor desensitization and pressure diuresis in conscious rats. *Hypertension* 29:969–975.
- Minson JB, Llewellyn-Smith IJ, Chalmers JP, Pilowsky PM, Arnold LF (1997) C-fos identifies GABA-synthesizing barosensitive neurons in caudal ventrolateral medulla. *NeuroReport* 8:3015–3021.
- Miyamoto A, Wake H, Moorhouse AJ, Nabekura J (2013) Microglia and synapse interactions: fine tuning neural circuits and candidate molecules. *Front Cell Neurosci* 7:70.
- Miyawaki T, Goodchild AK, Pilowsky PM (2002) Evidence for a tonic GABA-ergic inhibition of excitatory respiratory-related afferents to presympathetic neurons in the rostral ventrolateral medulla. *Brain Res* 924:56–62.
- Miyawaki T, Suzuki S, Minson J, Arnold L, Chalmers J, Llewellyn-Smith I, Pilowsky P (1997) Role of AMPA/kainate receptors in transmission of the sympathetic baroreflex in rat CVLM. *Am J Physiol* 272:R800–R812.
- Morrison HW, Filosa JA (2013) A quantitative spatiotemporal analysis of microglia morphology during ischemic stroke and reperfusion. *J Neuroinflammation* 10:4.
- Murase SI, Hayashi Y (1998) Expression pattern and neurotrophic role of the c-fms proto-oncogene M-CSF receptor in rodent Purkinje cells. *J Neurosci* 18:10481–10492.
- Nedobov PE, Mohammed S, Kapoor K, Bhandare AM, Farnham MM, Pilowsky PM (2016) PSer40 tyrosine hydroxylase immunohistochemistry identifies the anatomical location of C1 neurons in rat RVLM that are activated by hypotension. *Neuroscience* 317:162–172.
- Nimmerjahn A, Kirchhoff F, Helmchen F (2005) Neuroscience: resting microglial cells are highly dynamic surveillants of brain parenchyma in vivo. *Science* 308:1314–1318.
- Oshima N, Kumagai H, Iigaya K, Onimaru H, Kawai A, Nishida Y, Saruta T, Itoh H (2012) Baro-excited neurons in the caudal ventrolateral medulla (CVLM) recorded using the whole-cell patch-clamp technique. *Hypertens Res* 35:500–506.
- Paxinos G, Watson C (2007) *The rat brain in stereotaxic coordinates*. Elsevier Academic Press.
- Perego C, Fumagalli S, De Simoni MG (2011) Temporal pattern of expression and colocalization of microglia/macrophage phenotype markers following brain ischemic injury in mice. *J Neuroinflammation* 8:174.
- Perry VH, Andersson P-B, Gordon S (1993) Macrophages and inflammation in the central nervous system. *Trends Neurosci* 16:268–273.
- Pilowsky P, West M, Chalmers J (1985) Renal sympathetic nerve responses to stimulation, inhibition and destruction of the ventrolateral medulla in the rabbit. *Neurosci Lett* 60:51–55.
- Pilowsky PM (2014) Peptides, serotonin, and breathing: the role of the raphe in the control of respiration. *Prog Brain Res* 209:169–189.
- Pilowsky PM, Jiang C, Lipski J (1990) An intracellular study of respiratory neurons in the rostral ventrolateral medulla of the rat and their relationship to catecholamine-containing neurons. *J Comp Neurol* 301:604–617.
- Pilowsky PM, Lung MS, Spirovski D, McMullan S (2009) Differential regulation of the central neural cardiorespiratory system by metabotropic neurotransmitters. *Philos Trans R Soc Lond B Biol Sci* 364:2537–2552.
- Pocock JM, Kettenmann H (2007) Neurotransmitter receptors on microglia. *Trends Neurosci* 30:527–535.
- Schafer DP, Lehrman EK, Stevens B (2013) The “quad-partite” synapse: microglia-synapse interactions in the developing and mature CNS. *Glia* 61:24–36.
- Schreihöfer AM, Guyenet PG (2003) Baro-activated neurons with pulse-modulated activity in the rat caudal ventrolateral medulla express GAD67 mRNA. *J Neurophysiol* 89:1265–1277.
- Shahid IZ, Rahman AA, Pilowsky PM (2012) Orexin A in rat rostral ventrolateral medulla is pressor, sympatho-excitatory, increases barosensitivity and attenuates the somato-sympathetic reflex. *Br J Pharmacol* 165:2292–2303.
- Shapiro LA, Perez ZD, Foresti ML, Arisi GM, Ribak CE (2009) Morphological and ultrastructural features of Iba1-immunolabeled microglial cells in the hippocampal dentate gyrus. *Brain Res* 1266:29–36.
- Shi P, Diez-Freire C, Jun JY, Qi Y, Katovich MJ, Li Q, Sriramula S, Francis J, Sumners C, Raizada MK (2010) Brain microglial cytokines in neurogenic hypertension. *Hypertension* 56:297–303.
- Sholl DA (1953) Dendritic organization in the neurons of the visual and motor cortices of the cat. *J Anat* 87:387–406.
- Sokal RR, Rohlf FJ (2012) *Biometry*: W.H. Freeman and Company, New York.
- Springell DA, Costin NS, Pilowsky PM, Goodchild AK (2005) Hypotension and short-term anaesthesia induce ERK1/2 phosphorylation in autonomic nuclei of the brainstem. *Eur J Neurosci* 22:2257–2270.
- Stence N, Waite M, Dailey ME (2001) Dynamics of microglial activation: a confocal time-lapse analysis in hippocampal slices. *Glia* 33:256–266.
- Sun QJ, Bautista TG, Berkowitz RG, Zhao WJ, Pilowsky PM (2011) The temporal relationship between non-respiratory burst activity of expiratory laryngeal motoneurons and phrenic apnoea during stimulation of the superior laryngeal nerve in rat. *J Physiol* 589:1819–1830.
- Suzuki S, Pilowsky P, Minson J, Arnold L, Llewellyn-Smith IJ, Chalmers J (1994) C-fos antisense in rostral ventral medulla reduces arterial blood pressure. *Am J Physiol Regul Integr Comp Physiol* 266:R1418–R1422.
- Tremblay ME, Lowery RL, Majewska AK (2010) Microglial interactions with synapses are modulated by visual experience. *PLoS Biol* 8.
- Tremblay ME, Stevens B, Sierra A, Wake H, Bessis A, Nimmerjahn A (2011) The role of microglia in the healthy brain. *J Neurosci* 31:16064–16069.
- Ueno M, Fujita Y, Tanaka T, Nakamura Y, Kikuta J, Ishii M, Yamashita T (2013) Layer v cortical neurons require microglial support for survival during postnatal development. *Nat Neurosci* 16:543–551.
- van Rossum D, Hanisch UK (2004) Microglia. *Metab Brain Dis* 19:393–411.
- Wake H, Moorhouse AJ, Jinno S, Kohsaka S, Nabekura J (2009) Resting microglia directly monitor the functional state of synapses in vivo and determine the fate of ischemic terminals. *J Neurosci* 29:3974–3980.

APPENDIX A. SUPPLEMENTARY DATA

Supplementary data associated with this article can be found, in the online version, at <http://dx.doi.org/10.1016/j.neuroscience.2016.04.044>.

(Accepted 28 April 2016)
(Available online 4 May 2016)

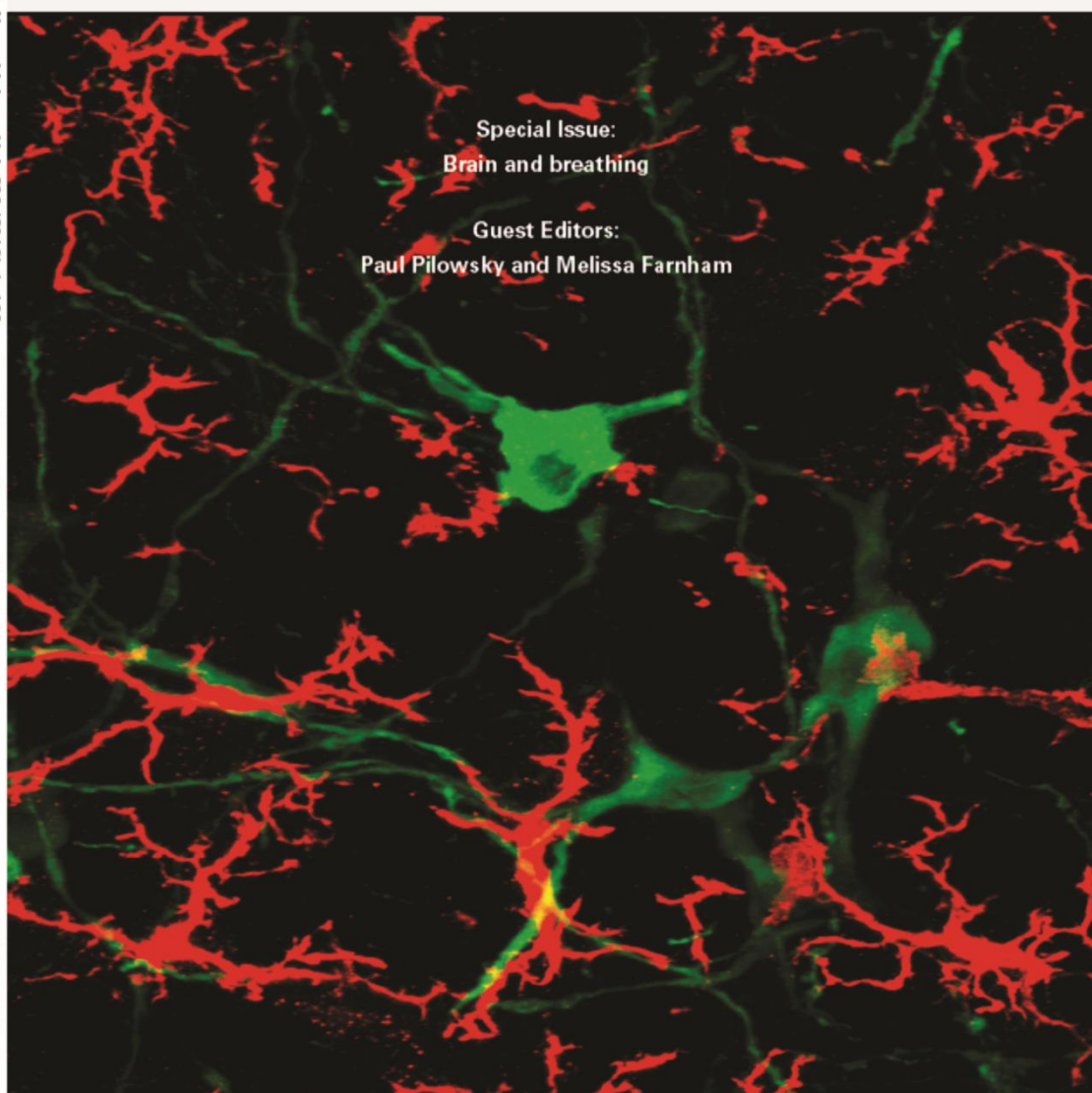


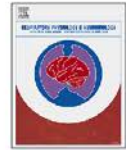
Volume 226, June 2016

ISSN 1569-9048
226 1–160 (2016)

RESPIRATORY PHYSIOLOGY & NEUROBIOLOGY

EDITOR MATHIAS DUTSCHMANN, MELBOURNE ASSOCIATE EDITOR YU RU KOU, TAIPEI





Alerted microglia and the sympathetic nervous system: A novel form of microglia in the development of hypertension



Komal Kapoor^{a,b}, Amol M. Bhandare^{a,b}, Melissa M.J. Farnham^{b,c}, Paul M. Pilowsky^{b,c,*}

^a Faculty of Medicine and Health Sciences, Macquarie University, Sydney, New South Wales 2109, Australia

^b The Heart Research Institute, Sydney, New South Wales 2042, Australia

^c Department of Physiology, University of Sydney, Sydney, New South Wales 2006, Australia

ARTICLE INFO

Article history:

Received 16 September 2015

Received in revised form

24 November 2015

Accepted 25 November 2015

Available online 28 November 2015

Keywords:

Sympathetic nervous system

Microglia

RVLM

CVLM

Blood pressure

ABSTRACT

Microglia, commonly known as the tissue resident macrophages of the central nervous system (CNS), are ubiquitously expressed in the CNS. Microglia, in their resting, or surveilling, stage, play a critical role in the maintenance of normal neuronal physiology and homeostasis. On activation, microglia can acquire either a neurotoxic (M1) or a neuroprotective (M2) phenotype. Prior to development of the M1 or M2 phenotype, little was known about changes in microglial activity, when subjected to stimuli. It is postulated, that an inability of microglia to maintain neuronal physiology within a normal working range can contribute to the development of cardiovascular disorders (CVDs) such as hypertension, but clear evidence supporting this hypothesis is missing. Even though our understanding of microglial function in a state of CNS injury/inflammation is extensive, the literature concerning role of microglia in the healthy CNS, is limited. Involvement of microglia in the pathophysiology of CVDs, in a neuroprotective/neurotoxic manner, is a key area that requires further investigation.

© 2015 Published by Elsevier B.V. All rights reserved.

1. Microglia

Until recently, microglia were considered to play a role solely as immune cells of the CNS, where they were responsible for a wide range of functions during CNS damage (Kettenmann et al., 2011). Recent developments in the field, since 2005 (Nimmerjahn et al., 2005), suggest that microglia are more than just immune cells of the CNS. In fact, it seems that microglia are guardians of the CNS at all times; constantly working to maintain the dynamic neuronal physiology, within its homeostatic levels (Hughes, 2012).

1.1. Origin of microglia

Microglia are cells of mesodermal origin that populate the CNS tissue during early stages of development. Erythroid/myeloid progenitor cells in the yolk sac, during early development, differentiate into tissue resident macrophage progenitor cells. These tissue resident macrophage progenitor cells, with amoeboid morphology, migrate into the brain and invade the brain tissue as microglial cells (Cronk and Kipnis, 2013). These microglial cells are self-renewing (Ajami et al., 2007), in case of depletion, during inflammatory

conditions. However, under special defined circumstances, when microglial cells in the CNS are depleted and are unable to replenish their pool, monocytes from bone marrow are capable of replenishing tissue resident macrophages of the CNS (Cronk and Kipnis, 2013).

1.2. History of microglia

Microglia were also previously known as “Hortega cells”, after Pio del Rio-Hortega first described these cells in the CNS, around 1932 (Kettenmann et al., 2011). According to studies performed by del Rio-Hortega, using a modified silver staining technique, microglia are of mesodermal origin and are homogeneously distributed cells of CNS (Fig. 1), known for their inflammatory response, towards any pathological event disturbing the homeostasis of CNS (Kettenmann et al., 2011). Subsequently, many studies were performed, that aimed to describe these microglial/“Hortega cells” and characterise their functions, but the advances made by Pio del Rio-Hortega still set the benchmark (Kettenmann et al., 2011).

1.3. Conventional activation paradigm

1.3.1. Diverse microglial phenotypes

Taking advantage of modern immunohistochemical methods, it is possible to identify all microglia in the brain using antibody-

* Corresponding author at: University of Sydney & Heart Research Institute, 7 Eliza St, Newtown 2042, Australia.

E-mail address: paul.pilowsky@hri.org.au (P.M. Pilowsky).

<http://dx.doi.org/10.1016/j.resp.2015.11.015>

1569-9048/Crown Copyright © 2015 Published by Elsevier B.V. All rights reserved.

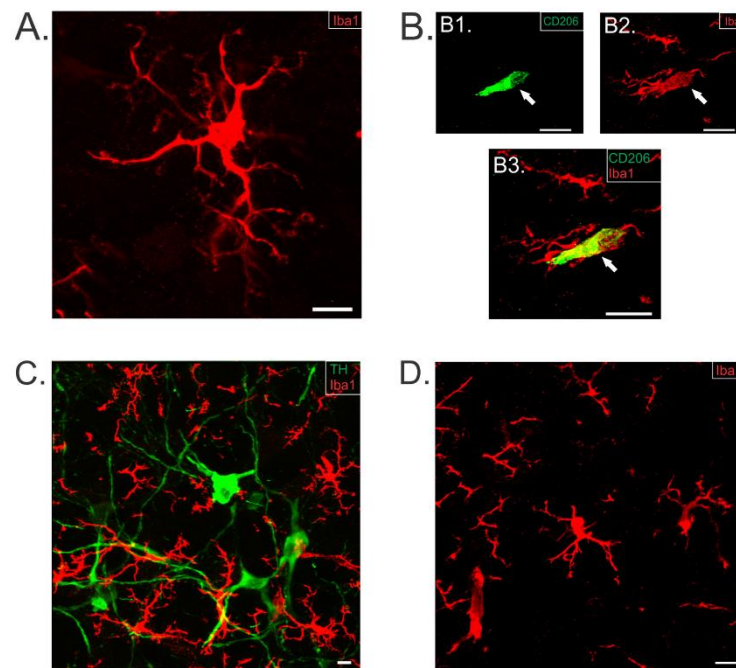


Fig. 1. Microglia in the SNS A. Microglia in the surveilling state in the brainstem of Sprague-Dawley (SD) rat. B. M2 microglia in the brainstem of a SD rat. B1. M2 (CD206 positive, green) microglia. B2. Iba1 (red) positive microglia acquiring an amoeboid morphology. B3. Merged image of B1 and B2 showing co-localization of CD206 expression with Iba1 in M2 microglia. C. Microglia (Iba1, red) are intermingled with the TH-ir (tyrosine hydroxylase-immunoreactive, green) neurons throughout the RVLM. D. Microglia (Iba1, red) in the CVLM region. Scale bar = 10 μ m. (For interpretation of the references to colour in this figure legend, the reader is referred to the web version of this article.)

ies to different markers in addition to the morphology of the cell. Microglial morphology is a useful indicator of its activation state and its potential role. Broadly speaking, microglial morphologies have been classed into 3 categories; M0, M1 or M2 (Butovsky et al., 2014; Hu et al., 2012). The M0 microglial phenotype (Figs. 1 and 2), represents microglia in their resting/surveilling stage, characterised by a small cell body ($\approx 10 \mu$ m diameter) (Kozłowski and Weimer, 2012) and long thin processes/ramifications. On the other hand, M1/M2 phenotypes (Figs. 1 and 2) share similar morphological characteristics; these are amoeboid in shape with shorter or no processes, but differ in their activities. Iba1 (ionized calcium binding adaptor molecule 1) is a calcium binding protein that is also a pan microglial marker. M0, M1 and M2 microglia all express Iba1. Expression of CD16 and CD32 is specific to M1 microglia, whereas expression of CD206 is specific for M2 microglia (David and Kroner, 2011; Hu et al., 2012).

The M0, surveilling microglial phenotype, monitors the local environment for the presence of pathogens, or for changes in the extracellular concentration of constitutively expressed neurochemicals (including neurotransmitters such as neuropeptides, glutamate or GABA) (Nimmerjahn et al., 2005; Tremblay et al., 2011) (Fig. 2). Polarization of the M0 phenotype to an M1/M2 phenotype, signifies a marked activation of microglia. The M1 phenotype, also known as the neurotoxic microglial phenotype, is associated with release of molecules such as IL-6, TNF- α and IL-1 β (Crain et al., 2013) (Fig. 2) that are all associated with apoptosis of cells that express receptors for these molecules. The M2 phenotype, which is a neuroprotective phenotype, releases molecules

such as IL-10. The M2 phenotype is anti-apoptotic, and promotes tissue repair (Crain et al., 2013) (Fig. 2).

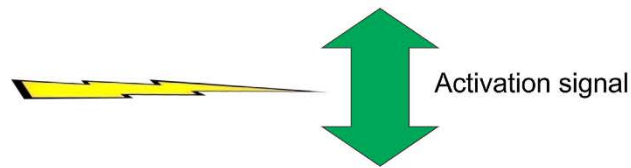
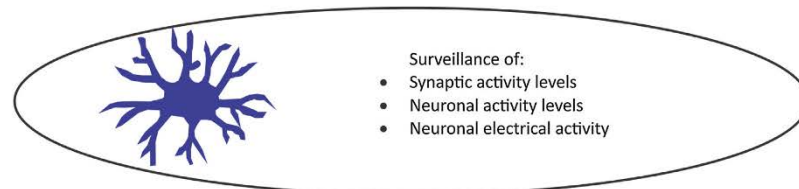
1.3.2. Activation pathway

Most of our understanding related to the activation of microglia, is based on findings from experiments performed *in vitro*, in either cultured microglia, or in freshly prepared brain tissue slices; this situation may differ *in vivo*.

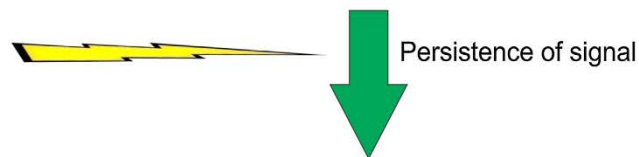
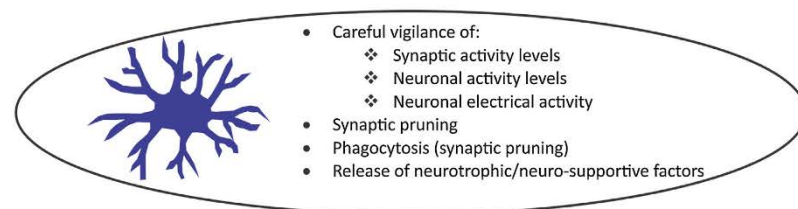
The conventional microglial activation paradigm is divided into 3 distinct stages: a **withdrawal**, a **motility** and a **locomotory** stage (Stence et al., 2001). The ramified resting/surveilling microglia (M0), on sensing the presence of an activation signal, enters a **withdrawal** stage, where these cells start to retract their existing processes. Whilst still withdrawing their existing branches, microglia initiate the process of developing new, short ramifications that are highly dynamic in nature, enabling microglia to become highly motile. Replacement of long microglial fimbria, with short highly dynamic protrusions, permits microglia to enter a **motile** state. In their motile stage, microglia develop a large cell body and very short processes, enabling them to migrate towards the site of injury and participate in inflammatory (M1) or non-inflammatory (M2) related activities (Fig. 2). This last state is known as the **locomotory** stage (Stence et al., 2001).

In addition to the M0 morphological polarization to either M1 or M2, microglia also undergo intracellular re-arrangements, enabling them to translocate their cell body through the tissue. Recent studies indicate that the non-muscle myosin II B (NMIIIB) is one of many intra-microglial molecules involved in microglial movement

Surveilling/resting microglia (M0) - small cell body with long thin processes



Alerted microglia - morphology similar to M0 microglia



Activated microglia (M1/M2) - amoeboid morphology

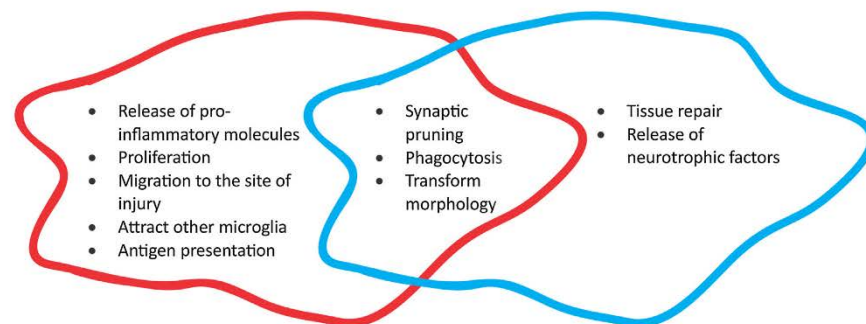


Fig. 2. Various activation stages of microglia in healthy CNS, when subjected to signal disturbing the homeostasis of CNS. Surveilling/resting microglia, in their highly ramified shape (M0), are distributed throughout the CNS. Sudden appearance or disappearance of any unexpected or expected molecule, respectively, triggers alertness in microglia. These “alerted microglia” survey the local environment, with extra vigilance or conduct housekeeping activities, to resume the CNS homeostatic levels. Persistence of the activation signal or when the CNS damage is permanent, M0 microglia polarize into M1 (inflammatory) or M2 (anti-inflammatory), depending on the situation. Although, M1 and M2 perform different set of roles in the CNS, they do share few functions and acquire similar morphology.

(Janssen et al., 2014). Microglial activation triggers the rearrangement of the cellular distribution of NMIIB, enabling amoeboid microglia to become motile (Janssen et al., 2014). Increased expression levels of cell adhesion molecules, such as integrins (Hailer et al., 1996), may also permit amoeboid microglia to be locomotory. While changes observed in the morphology of activated microglia are obvious, subtle changes introduced in extracellular matrix proteins such as laminin (Milner and Campbell, 2002), is another equally crucial process, facilitating microglial movement through tissue.

1.4. Activation signals—“on” or “off”

Neurons are not simply passive recipients of microglial signaling. In fact, microglia and neurons are in constant, dynamic communication, thereby affecting each other's physiological state. The ability of microglia and neurons to communicate, in response to changes in the extracellular environment, suggests a more subtle level of responsiveness by microglia, rather than being solely due to physical damage in the environment. Types of signals that alert microglia to changes in neuronal homeostasis are divided into 2 categories: “on” and “off” signals (Biber et al., 2007). “On” signals are defined as the appearance of unexpected molecules such as a pathogen or increases in the extracellular levels of intracellular constituents (released on cell death). Recently, the list of molecules leading to “on” signaling, has been extended to include enhanced levels of neurotransmitters in the CNS. “Off” signaling, on the other hand, is triggered by the disappearance or disruption of constitutively expressed molecules such as neurotransmitters or fractalkines (CX3CL1). (Biber et al., 2007; Hanisch and Kettenmann, 2007; van Rossum and Hanisch, 2004)

1.5. Microglial reaction to activation signal

Microglial perception of an activating signal and their response to the activating signal are 2 different processes. For example, addition of LPS (lipopolysaccharide) to cultured microglia can lead to the polarization of M0 to M1 (Butovsky et al., 2005); addition of IL-4 to cultured microglia results in the polarization of M0 to M2 (Butovsky et al., 2005). Appearance of both, LPS and IL-4, are examples of “on” signaling however, microglial reaction to these molecules are 2 different extremes of the spectrum. Our difficulty in understanding the role of microglia in the normal physiological state, clearly identifies, a severe gap in our understanding concerning microglial function in the CNS.

2. Microglia and communication

2.1. Inter-microglial communication

Each microglia has its own surveilling territory (Fig. 1), ranging from approx. 15 to 30 μm , and under normal conditions, microglia do not breach each other's territory (Fig. 1C and D). However, the molecular factors that determine inter-microglial distance, and the microglial pattern of distribution, are unknown. Microglia exhibit a heterogeneous distribution pattern, expression profile and morphology which is highly region-specific (de Haas et al., 2008; Lawson et al., 1990; Mittelbronn et al., 2001). The proteins expressed by microglia, which become evident during microglial responses to physiological and pathophysiological situations, are assumed to depend on the neuronal profile of their immediate environment (de Haas et al., 2008). A higher neuronal packing density may require more number of microglia, to maintain neurons in a healthy state. Also, neuronal activity, and their release of signaling molecules, will further affect the microglial expression profile. One can assume that the tessellated pattern of microglial distribution

(Fig. 1C and D) and precise inter-microglial distance is determined by a combination of neuronal packing density and neuronal activity levels, but this remains a matter of speculation.

Microglia release various factors such as cytokines, reactive oxygen species and neurotrophic factors, that not only affect neurons, but may also act on nearby microglia, and other cell types such as astroglia, oligodendrocytes and blood vessels, in a paracrine signaling fashion (Kettenmann et al., 2011). Microglia also act as the antigen presenting cells in the CNS (Kettenmann et al., 2011) thereby, providing positive feedback to other microglia, and to infiltrating macrophages. Inter-microglial communication, over long distances, largely depends on the ability of microglia to translocate through the tissue, when in their amoeboid morphology.

2.2. Microglia and astrocytes

Even though the strands of communication between microglia and neurons are quite obvious, the importance of cross talk between microglia and astrocytes, cannot be ignored. Astrocytes are an essential part of the CNS, mainly known for their supportive role towards neurons. Astrocytes play an important role in dampening the neurotoxic effects, such as release of iNOS (Pyo et al., 2003) and IL-12 (Aloisi et al., 1997), by microglia. Microglia are also able to affect astrocytes. It was recently demonstrated that IL-1, released by activated microglia, promotes the activation of astrocytes (Griffin, 2006). In addition, cultured astrocytes, treated with activated-microglial conditioned media, promote astrocytic gene expression of brain-derived neurotrophic factor (BDNF) (Savli et al., 2004) and astrocyte proliferation (Giulian and Baker, 1985).

2.3. Microglia and neurons

Since 2005, microglia are no longer considered to be passive or dormant cells in the CNS (Nimmerjahn et al., 2005). Rather, microglia are thought of as “busy bees” (Cronk and Kipnis, 2013) or the “constant gardeners” (Hughes, 2012) of the CNS. Microglia continuously monitor their local environment, for the presence of any unexpected changes in the expression level of neurochemicals and other molecules. Microglia can also sense the activity level of synapses (Tremblay et al., 2010; Wake et al., 2009). In response to these changes, microglia constantly extend or retract their processes and survey the whole CNS over periods ranging from minutes to hours (Nimmerjahn et al., 2005). As the tip of the microglial process extends and contacts synapses, it enlarges, enabling the removal of excessive synaptic input, if necessary (Wake et al., 2009).

Microglia and neurons are in constant communication; this communication is possible due to the presence of receptors for nearly every neurotransmitter on the surface of microglia including: PACAP (pituitary adenylate cyclase-activating polypeptide), dopamine, substance P, glutamate and GABA (Pocock and Kettenmann, 2007) (Table 1). Microglia also express receptors for neurohormones/neuromodulators, such as neurotrophin (Kettenmann et al., 2011; Pocock and Kettenmann, 2007) (Table 1). The diverse range of receptors, expressed by microglia, allow them to perceive neuronal signals as an indicator of neuronal health and physiological levels. However, it is not yet clear, whether or not neurons emit microglia-specific signals or the extent to which microglia detect neuron–neuron signalling.

Disruption to healthy neuron–neuron communication, leading to deviations in neuronal homeostasis, can lead to the development of neurological disorders such as Alzheimer's disease or hypertension, depending on the CNS area affected. Disturbances in an otherwise highly dynamic neuronal physiology are, more often than not, accompanied with changes in their neurochemistry, membrane potentials and the concentration of molecules that dif-

Table 1
Neurotransmitter receptors and their corresponding functions in the sympathetic nervous system (SNS) and microglia.

Neurotransmitter	SNS		Microglia	
	Effect	Reference	Effect	Reference
Angiotensin - II	Activates the AT ₁ receptor in circumventricular organs and exerts pressor effects via PVN and RVLM	Cato and Toney (2005) ; Li et al. (2003)	<ul style="list-style-type: none"> • AT₁ receptor expression is upregulated in response to LPS • Angiotensin-II activates microglia in PVN and causes an increased levels of pro-inflammatory cytokines 	Miyoshi et al. (2008) Shi et al. (2010)
Bradykinin	Microinjection of bradykinin in the RVLM elicits hypertensive effect	Privitera et al. (1994)	Induces chemotaxis and enhances motility features	Noda et al. (2003) ; Noda et al. (2006)
Dopamine	Microinjection of dopamine in the PVN results in decreased levels of renal sympathetic nerve activity and blood pressure in SD rats	Zheng et al. (2014)	Stimulation of dopamine receptors enhances microglial migration abilities and suppresses nitric oxide production	Farber et al. (2005)
GABA	Sympatho-inhibitory	Guyenet (2006)	Anti-inflammatory response in microglia	Kuhn et al. (2004) ; Pocock and Kettenmann (2007)
Galanin	<ul style="list-style-type: none"> • Microinjection of galanin in the RVLM elicits a sympatho-inhibitory response by decreasing blood pressure and sympathetic nerve activity • Microinjection of galanin in the respiratory sites of brainstem (BötC or PreBötC) causes a depression in the respiratory output 	Abbott and Pilowsky (2009) Abbott et al. (2009)	Increases microglial motility	Ifuku et al. (2011)
Glutamate	Sympatho-excitatory	Guyenet (2006)	Broadly, activation of glutamate receptors triggers pro-inflammatory responses (except mGluR group III)	Pocock and Kettenmann (2007)
Orexin	Microinjection of orexin A in RVLM causes a pressor and sympatho-excitatory response	Shahid et al. (2012)	<ul style="list-style-type: none"> • Microglial immunoreactivity for orexin 1 receptor increases with activation in response to traumatic brain injury • Orexin inhibits the ATP induced microglial motility 	Mihara et al. (2011) Noda et al. (2011)
PACAP	Sympatho-excitatory	Farnham et al. (2008) ; Farnham et al. (2012) ; Ingloff et al. (2011)	Neuro-protective	Dejda et al. (2005)
Serotonin (5-HT)	Antagonism of 5-HT _{1A} receptor in RVLM blocks the hemorrhage induced sympatho-inhibition of SNS	Dean and Bago (2002)	Serotonin triggers the release of exosomes from microglia via 5-HT receptors	Glebov et al. (2015)
Somatostatin (SST)	Microinjection of SST in RVLM causes a sympatho-inhibitory response and hypotension	Burke et al. (2008)	Neuro-protective (inhibits microglial proliferation)	Feindt et al. (1998)
Substance P	Microinjection of substance P analogue in the RVLM causes an increase in blood pressure, heart rate and sympathetic nerve activity	Makeham et al. (2005)	Neurotoxic/pro-inflammatory	Block et al. (2006) ; Rasley et al. (2002)

fuse across synapses in the extracellular matrix; these changes can be detected by microglia, as abnormal neuronal or synaptic activity ([Biber et al., 2007](#); [Hanisch and Kettenmann, 2007](#)).

Recently, [Glebov et al. \(2015\)](#) showed that serotonergic neurons (derived from stem cells) stimulate the release of exosomes from microglia ([Glebov et al., 2015](#)). These exosomes may be

one way by which microglia are provoked to release proteins, inflammatory molecules and cytokines, into the extracellular environment. Although this study (Glebov et al., 2015) was performed in a co-culture, *in vitro*, system, it does provide an example of direct microglia–neuron communication, driven by neurotransmitter release.

Some examples of microglial receptors corresponding to some commonly expressed neurotransmitters in the CNS include glutamate, GABA, purines, and peptides (see Table 1 for further examples)

2.3.1. Glutamate receptors

Glutamate is an excitatory neurotransmitter in the CNS. Glutamate receptors, broadly, can be divided into 2 subtypes: fast ionotropic (iGluRs) and slower metabotropic (mGluRs). With regards to iGluRs, evidence from transcription analysis has confirmed the presence of GluR1, GluR2, GluR3 and GluR4, on microglia (Kettenmann et al., 2011). Activation of glutamate receptors on microglia, via glutamate or kainate, can lead to the release of the pro-apoptotic peptide TNF- α (Hagino et al., 2004). iGluRs may also be involved in microglial chemotaxis, however, *in vivo* evidence in support of this idea is not yet available.

On the other hand, the evidence regarding the exact role of microglial mGluRs is controversial. Activation of group II mGluRs can enhance the neurotoxicity of microglia (Taylor et al., 2005). Whereas, activation of group III mGluRs, tends to promote the neuroprotective effects of microglia (Taylor et al., 2003).

2.3.2. GABA receptors

Unlike glutamate receptors, the role of GABA receptors in microglial physiology is well established. GABA, acting on GABA receptors is an inhibitory neurotransmitter and acts as a neuroprotective agent by acting on microglial GABA_A and GABA_B receptors (Pocock and Kettenmann, 2007; Lee, 2013). Both subunits of GABA_B receptors are expressed by microglia, with majority of them concentrated in the microglial lamellipodia (Kettenmann et al., 2011). Activation of GABA_B receptors in microglia subjected to LPS, can exert neuroprotective effects by reducing the release of inflammatory cytokines such as IL-6 and IL-12 (Lee, 2013).

2.3.3. Purinergic receptors

Purinergic receptors, and their associated signaling systems, are found in almost all types of cells and tissues. The most abundant purinergic signaling molecule is adenosine triphosphate (ATP). ATP is a critical source of phosphate in kinase reactions that result in phosphorylation of intracellular proteins, and subsequent cellular activation. Purinergic receptors such as P2Y6, P2Y7, P2Y8, P2Y12 and P2X are abundantly expressed on the surface of microglia (Pocock and Kettenmann, 2007). Broadly speaking, activation of purinergic signaling systems results in energy consuming processes such as chemotaxis, movement of microglial fine ramifications, migration and cytokine release (Pocock and Kettenmann, 2007). Most ATP mediated functions are activated in response to physical injury. Activation of P2X4 receptors on microglia may be a cause of chronic neuropathic pain (Inoue, 2006), and drugs that target these receptors are currently being actively investigated for clinical use.

2.3.4. Other neurotransmitter receptors

Microglia also express receptors for peptide neurotransmitters such as substance P and PACAP. Substance P activates neurokinin-1 (NK-1) receptors expressed by microglia, leading to activation of pro-inflammatory pathways such as chemotaxis, and production of intracellular reactive oxygen species (Block et al., 2006; Rasley et al., 2002). Similarly, activation of bradykinin receptors expressed in microglia, can lead to enhancement of microglial motility features (Noda et al., 2003; Noda et al., 2006). Conversely, activation of

PACAP receptors reduces chemokine production, thereby inhibiting the neurotoxic effects of microglia (Dejda et al., 2005).

3. Microglia in CNS

Microglia are ubiquitously distributed throughout the CNS, comprising for approximately 10–20% of the whole CNS cellular population (Kettenmann et al., 2011). Microglial cell bodies, labelled with Iba1 and visualised ultra-structurally, are closely apposed to neuronal cell bodies, implying the existence of close lines of communication between neurons and microglia (Shapiro et al., 2009).

Interestingly, microglial expression profiles throughout the CNS are not the same. For example, expression levels of CD11b, a pan-marker for microglia, are higher in spinal cord as compared to cerebral cortex (de Haas et al., 2008). These data highlight the fact that the microglial profiles are significantly influenced by properties of their local microenvironment. The ability of microglia to be influenced by the neuronal diversity in their immediate environment, to be affected by the neuronal physiology, and to play a critical role in healthy neuron–neuron communication, further adds complexity to the already diverse microglial physiology.

3.1. Microglia in healthy CNS

As previously discussed, neurons are continuously being monitored by microglia (Nimmerjahn et al., 2005). Highly ramified processes on microglia that are closely apposed to sites of neuronal synaptic interaction enables the microglia to monitor their local environment without having to translocate through the tissue. However, it is still possible that microglia are capable of migrating short distances, while still in their surveilling stage (Karperien et al., 2013).

Microglia are also capable of performing activities, such as phagocytosis/synaptic pruning, without changing their morphology (Tremblay et al., 2011). During synaptic surveillance, microglia can sense whether or not synaptic spines are weak or over-worked. If spines are found to be in need of removal, microglia can strip them from the dendrite. Synaptic pruning by microglia is normally a 3 step process: (1) microglia make, rather prolonged, contact with the pre-synaptic structure, (2) microglia attach firmly to, and strip the pre-synaptic structure and (3) phagocytose the stripped pre-synaptic structure (Kettenmann et al., 2013; Wake et al., 2009). It is not yet clear, if microglia also phagocytose the post-synaptic structure.

Microglia are also capable of releasing neurotrophic factors, such as BDNF (Kettenmann et al., 2011), macrophage colony stimulating factor (M-CSF) (Murase and Hayashi, 1998) and insulin growth factor-1 (IGF-1) (Ueno et al., 2013), in order to support neuronal physiology. This is another important, yet poorly understood, function of microglia that does not require polarization to either M1 or M2.

3.2. Microglia during CNS injury

Most of the animal models, used to investigate microglial activation pathways, require either LPS-induced inflammation (Wu et al., 2012), or physical damage to the CNS (leading to neuronal stress and death) (Morrison and Filosa, 2013; Perego et al., 2011).

Previous work, focusing on the characterization of the correlation between neuronal activity and microglial activity, used stimuli such as binocular eye enucleation (Tremblay et al., 2010), tetrodotoxin injection into the retina (Wake et al., 2009), or middle cerebral artery occlusion leading to ischemia (Dworak et al., 2014). These insults to the CNS affect the frequency with which

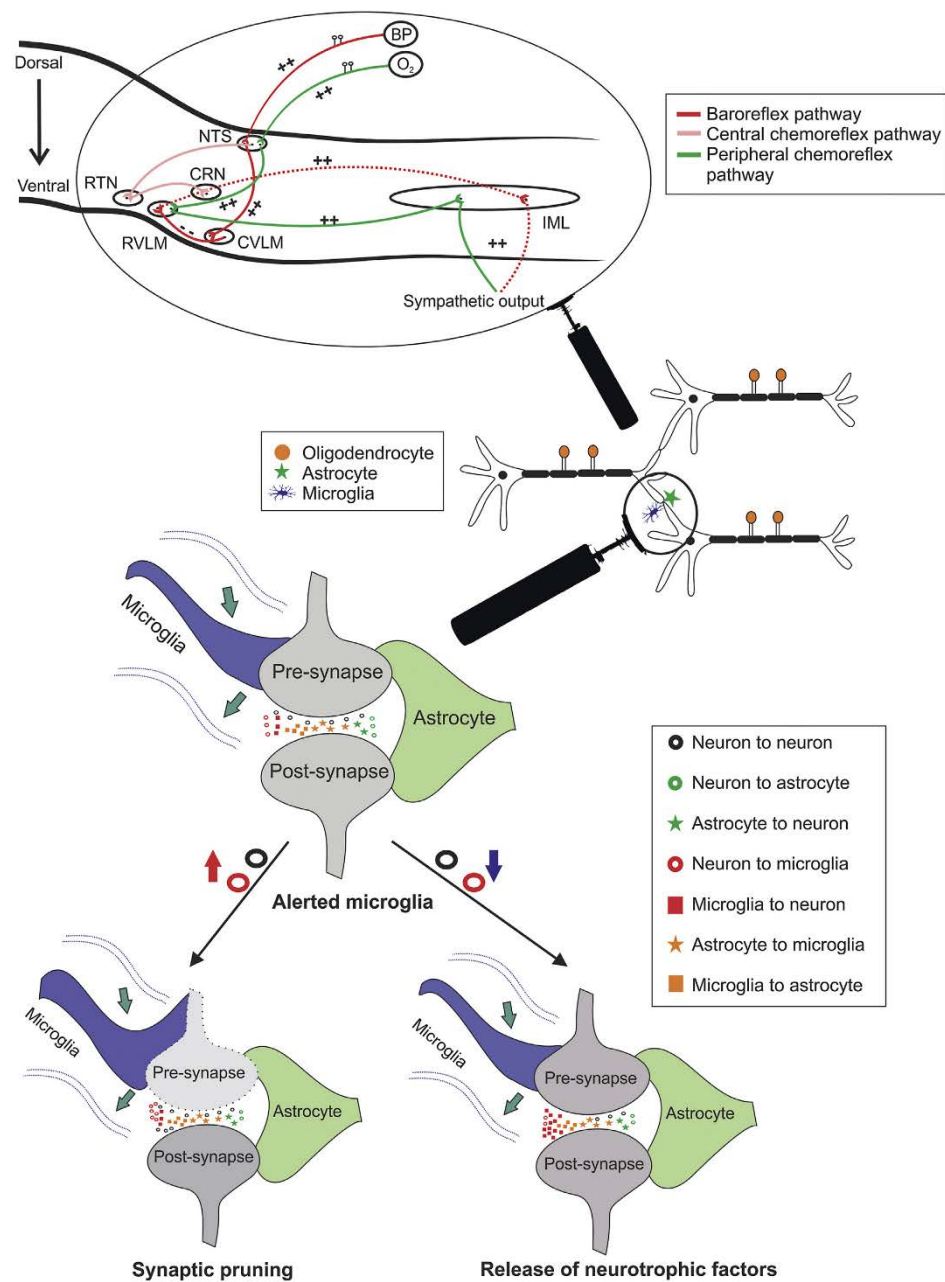


Fig. 3. Microglia play an important role in the normal neuron–neuron communication and form an integral part of the tri-partite synaptic structure (pre-synapse, post synapse and astroglial process) in the SNS. The figure is divided into 3 stages. 1st stage refers to 3 important reflex pathways in the SNS: baroreflex (red), central chemoreflex (pink) and peripheral chemoreflex (green). Please refer to the text for details on these reflex pathways. 2nd stage of the figure shows the presence of different CNS elements, at the autonomic neuronal level. Oligodendrocytes are the supportive cells for neurons, providing the myelin sheath. Astrocytes and microglia are found in close apposition to the neuronal synaptic structure. Stage 3 of the figure shows the dynamics at the synaptic level. Unlike astrocytic process, microglial processes are not permanently associated with the synaptic structure. Rather, microglial processes are constantly moving, surveying the neuronal activity levels. In case of, enhanced levels of neuron–neuron/neuron–microglia communication, microglia perform functions such as synaptic pruning. During synaptic pruning, microglial process envelops the

microglia contact neuronal synapses. For example, reduced neuronal activity, in response to the injection of tetrodotoxin in the retina or hypothermia, can reduce the frequency of microglial contact with synaptic structures by 40–50% (Wake et al., 2009). Furthermore, induction of transient cerebral ischemia, results in prolongation of contacts between surveilling microglial processes and synaptic boutons, in the region of somatosensory cortex, which lasts from about 5 min in the control state to around 80 min in the ischemic state (Wake et al., 2009). This extreme prolongation observed in microglial contact with synapses, can be attributed to microglia carefully sensing synaptic health to, either prune the dead/weak synapses, or trying to restore their normal activity levels. No changes in microglial morphology, affected by transient cerebral ischemia, were reported. Another study showed that the microglial response to an activating signal runs parallel to developing cerebral brain injury, in response to ischemic stroke and reperfusion. The main finding, from this study, was the hyper- and de-ramification of microglia in relation to the necrotic core, caused by the CNS injury (Morrison and Filosa, 2013).

The recent studies discussed above identify a novel “alerted microglial” phenotype, that is more active than “surveilling”, but not yet fully activated. This novel alerted state is characterized by a hyper-ramified or de-ramified morphology, or a morphology that is quite similar to surveilling microglia. Alerted microglia (Hanisch and Kettenmann, 2007; Kettenmann et al., 2011; Karperien et al., 2013) may be the form adopted, prior to acquisition of an extreme activation phenotype, if this is necessary (Fig. 2).

Under extreme circumstances, when ischemic conditions are left to develop for over 7 days, microglia exhibit carefully tailored biphasic behavior that is neuroprotective, before developing into a phagocytic phenotype (Perego et al., 2011). This biphasic response highlights another important trait of microglia: in the first instance, microglia tend to exhibit a neuroprotective/neurosupportive behavior in the CNS. However, when the CNS damage is very severe or irreversible, microglia initiate the process of eradicating dead/affected neurons in order to stop the spread of CNS injury and clear away debris. (Perego et al., 2011)

Although the microglial response to injury, in higher brain regions is well established, studies have also identified these cells as an important mediator of spinal cord injury (Kigerl et al., 2009; Kroner et al., 2014).

4. Microglia and sympathetic nervous system (SNS)

4.1. SNS

The nucleus of solitary tract (NTS), the caudal ventrolateral medulla (CVLM) and the rostral ventrolateral medulla (RVLM), are regions of the brainstem, that are crucial in the regulation of tonic activity of the SNS, and integration of various reflex mechanisms including the somatosympathetic, baro-, and chemo-, reflexes. The activity of sympathoexcitatory neurons in the RVLM is modulated by inputs from other key brain regions such as the NTS (Koshiya and Guyenet, 1996), the CVLM (Burke et al., 2008) and the hypothalamus (Chen et al., 2013; Dworak et al., 2014). Following the integration of these inputs, RVLM neurons cause appropriate changes in physiology via bulbospinal sympathoexcitatory efferent pathways. Sympathetic preganglionic neurons (SPN), found in the intermediolateral (IML) cell column of the spinal cord, receive monosynaptic inputs from RVLM neurons and may be other suprab-

ulbar sites (Guyenet, 2006; Pilowsky et al., 2009, 1994; McAllen et al., 1994; Oshima et al., 2008, 2006).

4.1.1. Baroreflex (Fig. 3)

The baroreflexes are a series of negative feedback loops that are involved in the regulation of blood pressure. One of these reflexes, the sympathetic baroreflex, is critical in the short-term control of blood pressure; the role of the sympathetic baroreflex pathway in the long term regulation of blood pressure remains a topic of considerable debate (Thrasher, 2005). Baroreceptor sensory nerves, that terminate around the carotid sinus and aortic arch, provide an excitatory input (via IX and X cranial nerves) to neurons in the NTS. These baroreceptor afferent nerves respond to increases in arterial blood pressure. NTS neurons process this excitatory input, and further excite neurons located in the CVLM, via glutamatergic projections (Weston et al., 2003). CVLM neurons provide GABAergic inhibitory inputs to presympathetic neurons located in the RVLM, which in turn inhibits the activity of the SPN, thereby lowering blood pressure and sympathetic activity. (Guyenet, 2006; Pilowsky and Goodchild, 2002; Schreihofer and Guyenet, 2002; Sved et al., 2003)

4.1.2. Chemoreflex (Fig. 3)

4.1.2.1. Peripheral chemoreceptors: Carotid bodies, located near the bifurcation of carotid arteries, are chemosensitive cells that are activated in response to falls in the PaO_2 below 100 mmHg and to increases in blood pH. Chemo-stimulation of cells located in the carotid body provides glutamatergic input to NTS neurons (de Paula et al., 2007), ultimately leading to excitation of neurons in the RVLM. RVLM neurons then excite cardiovascular SPNs thereby increasing sympathetic activity, plasma catecholamine levels and total peripheral resistance, leading to an increase in arterial blood pressure (Prabhakar et al., 2012).

4.1.2.2. Central chemoreceptors: There is a dose-dependency in the way that central neurons respond to chemoreceptor inputs. In fact, almost every neuron in the brain will respond to changes in O_2 , CO_2 or acidity depending on the depth and duration. Central chemoreceptors are considered to be those neurons that respond vigorously within a physiological range. Central chemoreceptors, unlike peripheral chemoreceptors, are thought to be distributed over a wide region of the brain including, rostral sites such as the hypothalamus (orexinergic neurons), to caudal sites such as retrotrapezoid nucleus (RTN) and serotonin positive rostral medullary raphe neurons (Nattie and Li, 2012). Kuwaki and colleagues showed that the induction of hypercapnia caused a marked increase in the Fos expression (signifying neuronal activity), in orexin-containing cells of the hypothalamus (Sunanaga et al., 2009). Central chemoreceptors, located in the RTN in the brainstem region, are glutamatergic in nature and are activated in response to changes in CO_2 levels or pH of arterial blood (Guyenet et al., 2012; Mulkey et al., 2004). Efferent neurons from the RTN innervate the central respiratory network (CRN) driving inspiration (Rosin et al., 2006) and the activity of RTN neurons is regulated by NTS neurons (Takakura et al., 2007). In addition to RTN neurons, serotonergic neurons (in particular 5-HT_{2A} receptor), located in the rostral brainstem, are also chemosensitive and are capable of detecting changes in CO_2 levels (Buchanan et al., 2015).

pre-synaptic structure, strip it and phagocytose the residue. On the contrary, decreased neuron–neuron/microglial communication causes microglia to release neurotrophic factors (red squares), to support the weak synapse or increase the neuron–neuron communication. BP: blood pressure, O_2 : oxygen, NTS: nucleus of solitary tract, RVLM: rostral ventrolateral medulla, CVLM: caudal ventrolateral medulla, IML: intermediolateral cell column of spinal cord, RTN: retrotrapezoid nucleus and CRN: central respiratory network. (For interpretation of the references to colour in this figure legend, the reader is referred to the web version of this article.)

4.2. Microglia in SNS

Microglia are present in all parts of the CNS. In the SNS, microglia (Fig. 1C and D) play a crucial role in the surveillance of synaptic and neuronal activity levels. It is therefore somewhat surprising, considering the importance of SNS in the regulation of the cardiorespiratory system, that the role of microglia in the SNS remains relatively unexplored. As discussed in previous sections, microglia express receptors for the vast majority of neurotransmitters, as well as many other chemicals. Table 1 provides a brief overview of some of the neurotransmitters critical for cardiorespiratory function, and the relevant receptors and their function that are present on local microglia.

Intracerebroventricular administration of IL-1 β (a pro-inflammatory cytokine) increases arterial blood pressure, heart rate and renal sympathetic nerve activity, within 20–25 min of administration (Kannan et al., 1996). A recent study from our laboratory found that, inhibition of microglial activation, by minocycline, at the level of spinal cord, exaggerates the increase in sympathetic nerve activity response seen in rats that develop seizures following an intraperitoneal dose of kainic acid (Bhandare et al., 2015). Our findings highlight the neuroprotective effect of microglia during seizure, on sympathetic preganglionic neurons, in the spinal cord. The protective effect of microglia towards seizure induced sympathetic nerve activity, might be mediated through their polarisation towards M2 phenotype and an endogenous production of neurotrophic and anti-apoptotic molecules such as TGF- β and IL-10. Moreover, findings from this study also suggest that, as part of microglia-neuron communication, PACAP might be acting on microglial PAC1 and VPAC-1 receptors causing an increased expression of glutamate transporters on the surface of microglia and increasing glutamate uptake (Bhandare et al., 2015). This data highlights the possible neuroprotective behaviour of microglia when subjected to seizure.

Following myocardial infarction (a model for inflammation), in Sprague-Dawley (SD) rats, there is an increased percentage of activated microglia in the RVLM and NTS (Dworak et al., 2014). Unfortunately, the lack of detailed analysis needed to determine the phenotype (M1 or M2) of the activated microglia (in the RVLM and NTS in response to myocardial infarction), makes it difficult to ascertain, whether or not these activated microglia are playing a neuro-protective, a neuro-supportive, or a neurotoxic role.

The number of possible disorders that can occur, or be worsened by, increases in sympathetic activity is very large and include: hypertension, diabetes, metabolic syndrome and heart failure. Given that microglia can regulate sympathetic activity (Bhandare et al., 2015), there is now a strong possibility that therapies affecting microglial function could play an important role in the treatment of sympathetic nerve related disorders, including cardiovascular disease. We hypothesise that, in addition to the important role that microglia play in the responses to physical injury by adopting an M1 or M2 state, microglia can also detect changes in the level of neuronal/synaptic activity. Microglia may respond to normal adaptive reflexes by triggering a mild level of alertness in their normal behaviour (Fig. 3). This alertness does not require polarisation to their extreme activation phenotypes: M1 or M2 instead, there is a more subtle change in microglial physiology. We propose that 'alerted' microglia have a morphology similar to that of surveilling microglia, but are more attentive of synaptic activity levels (Fig. 2) (Hanisch and Kettenmann, 2007; Kettenmann et al., 2011). Alerted microglia can perform activities such as synaptic pruning, in response to exaggerated levels of synaptic activity. In contrast to this, decreased synaptic activity levels can cause alerted microglia to release neuro-supportive substances, such as BDNF or IGF-1, in order to restore normal homeostasis.

5. Possible involvement of microglia in hypertension

Hypertension is a pathological condition defined as a continuous elevation of arterial blood pressure beyond 130/85 mmHg, and is a risk factor for other cardiovascular and cerebrovascular disorders. Hypertension may be either primary (essential) or secondary. Essential hypertension is responsible for approximately 95% of all cases of hypertension and is generally neurogenic in origin (Guyenet, 2006; Pilowsky et al., 2009). Almost all forms of neurogenic hypertension are associated with an over-excitation of RVLM neurons and the SNS (Schlaich et al., 2004). Development of essential hypertension is also a risk factor for other CVDs, such as heart attack and stroke.

Induction of systemic inflammation (by peripheral LPS injection), can lead to the development of neurogenic hypertension, via activation of microglia and an increase in the levels of oxidative stress in the RVLM (Wu et al., 2012). Genetically hypertensive rats develop larger cerebral infarctions following stroke (De Geyter et al., 2012; Hom et al., 2007); further highlighting a possible relationship between microglia and hypertension.

In the NTS, a critical cardiorespiratory medullary nucleus, SHR (spontaneously hypertensive rats; animal model for essential hypertension) are reported to have a pre-existing inflammatory state in their microvasculature (Waki et al., 2008). In the vascular endothelial cells of NTS of SHR there is over-expression of the pro-inflammatory molecule: junctional adhesion molecule-1 (JAM-1). This over-expression of JAM-1 suggests that inflammation may play an important role in the genesis of neurogenic hypertension. The possibility that JAM-1 plays a mechanistic role in the development of hypertension was addressed by demonstrating that over-expression of JAM-1 in the NTS of the normotensive WKY (wistar-kyoto rats; control for SHR) rat causes hypertension (Waki et al., 2008). This study highlights an alternative explanation to the hypothesis: "microglia/neuro-inflammation may contribute to the pathophysiology of hypertension". According to this study, enhanced inflammation within the microvasculature of cardiovascular nuclei (such as the NTS), may be critical in the development of neurogenic hypertension.

A direct correlation between angiotensin-II induced hypertension and neuroinflammation, in particular in the paraventricular nucleus (PVN), was investigated by Shi et al. (2010). The PVN receives inputs from higher brain regions, and projects to both the RVLM and the IML, and therefore plays an important role in the co-ordination of efferent sympathetic nerve activity (Guyenet, 2006). Angiotensin-II induced hypertension causes an activation of microglia in the PVN of SD rats (Shi et al., 2010). This angiotensin-II mediated hypertension was abrogated almost completely, by intracerebroventricular administration of minocycline (broad spectrum tetracycline known to inhibit microglial activation). On the other hand, over-expression of IL-10 (anti-inflammatory cytokine), decreases the effect of angiotensin-II mediated hypertension. Taken together, these results suggest an important role for microglia in the development of neurogenic hypertension (Shi et al., 2010).

In clinical studies, reports suggest that there is an approximately 35% increase in C-reactive protein levels (marker of systemic inflammation) in patients that are more vulnerable to develop peripheral arterial diseases and hypertension (Ridker et al., 1998). Even though, the detailed mechanism behind these results is not clear, these findings do suggest novel directions in the investigation of microglia as critical players in neuro-inflammation, and hypertension.

6. Technical considerations

The task of gaining a better understanding of the role of microglia in healthy CNS, requires the use of state-of-the-art, microscopy and non-invasive, technologies. Employment of, easily available, extensively invasive techniques, currently utilized in neuroscience, such as direct brain access, opening of the skull or decapitation, may contribute to the activation of microglia on its own (Stence et al., 2001; Xu et al., 2007). Further work is required to not only understand the role of microglia in hypertension but to also identify techniques, with minimal physiological manipulations, enabling us to evaluate the nature and mechanism of morphological changes introduced in the microglial phenotype or the extracellular matrix of the local environment, when subjected to homeostatic disturbances.

7. Conclusion

Clearly, microglia play an important and highly dynamic role in the SNS and carefully tailor their responses to changes in homeostasis (Fig. 3). Emerging evidence suggests that the activation of microglia, can no longer be viewed as an “all or none” process. Rather it is a gradual, morphological and physiological, transformation of microglia, which is reversible up to the point where an extreme activation phenotype (M1 or M2) is acquired. So far, attempting to predict the fate or role (neuro-protective or neuro-toxic) of microglia in the SNS, following a conventional flow chart, is proving to be a formidable task.

Conflict of interest

The authors declare no competing financial interests.

Acknowledgements

This work was supported by the Australian Research Council (Discovery Early Career Researcher Award, DE120100992), the National Health and Medical Research Council of Australia (Grant 1065485 and Fellowship 1024489), and the Heart Research Institute. K.K. and A.M.B. are supported by International Macquarie University Research Excellence Scholarship (No. 2012112 and 2012219, respectively). The authors acknowledge the support received from the Bosch Institute Advanced Microscopy Facility at the University of Sydney, and the expert help of Facility staff, especially Dr. Louise Cole and Dr. Cathy Payne.

References

- Burke, P.G.R., Pilowsky, P.M., 2009. Galanin microinjection into the PreBötzinger or the Böttinger complex terminates central inspiratory activity and reduces responses to hypoxia and hypercapnia in rat. *Respir. Physiol. Neurobiol.* 167, 299–306.
- Abbott, S.B.G., Pilowsky, P.M., 2009. Galanin microinjection into rostral ventrolateral medulla of the rat is hypotensive and attenuates sympathetic chemoreflex. *Am. J. Physiol. Regul. Integr. Comp. Physiol.* 296, R1019–R1026.
- Ajami, B., Bennett, J.L., Krieger, C., Tetzlaff, W., Rossi, F.M.V., 2007. Local self-renewal can sustain CNS microglia maintenance and function throughout adult life. *Nat. Neurosci.* 10, 1538–1543.
- Aloisi, F., Penna, G., Cerase, J., Menendez Iglesias, B., Adorini, L., 1997. IL-12 production by central nervous system microglia is inhibited by astrocytes. *J. Immunol.* 159, 1604–1612.
- Bhandare, A., Mohammed, S., Pilowsky, P.M., Farnham, M.M., 2015. Antagonism of PACAP or microglia function worsens the cardiovascular consequences of kainic acid induced seizures in rats. *J. Neurosci.* 35, 2283–2292.
- Biber, K., Neumann, H., Inoue, K., Boddeke, H.W., 2007. Neuronal ‘On’ and ‘Off’ signals control microglia. *Trends Neurosci.* 30, 596–602.
- Block, M.L., Li, G., Qin, L., Wu, X., Pei, Z., Wang, T., Wilson, B., Yang, J., Hong, J.S., 2006. Potent regulation of microglia-derived oxidative stress and dopaminergic neuron survival: substance P vs. dynorphin. *FASEB J.* 20, 251–258.
- Buchanan, G.F., Smith, H.R., MacAskill, A., Richerson, G.B., 2015. 5-HT2A receptor activation is necessary for CO2-induced arousal. *J. Neurophysiol.* 114, 233–243.
- Burke, P.G.R., Li, Q., Costin, M.L., McMullan, S., Pilowsky, P.M., Goodchild, A.K., 2008. Somatostatin 2A receptor-expressing presympathetic neurons in the rostral ventrolateral medulla maintain blood pressure. *Hypertension* 52, 1127–1133.
- Butovsky, O., Jedrychowski, M.P., Moore, C.S., Cialic, R., Lanser, A.J., Gabriely, G., Koeglsperger, T., Dake, B., Wu, P.M., Doykan, C.E., Fanek, Z., Liu, L., Chen, Z., Rothstein, J.D., Ransohoff, R.M., Gygi, S.P., Antel, J.P., Weiner, H.L., 2014. Identification of a unique TGF- β -dependent molecular and functional signature in microglia. *Nat. Neurosci.* 17, 131–143.
- Butovsky, O., Talpalar, A.E., Ben-Yaakov, K., Schwartz, M., 2005. Activation of microglia by aggregated beta-amyloid or lipopolysaccharide impairs MHC-II expression and renders them cytotoxic whereas IFN-gamma and IL-4 render them protective. *Mol. Cell. Neurosci.* 29, 381–393.
- Cato, M.J., Toney, G.M., 2005. Angiotensin II excites paraventricular nucleus neurons that innervate the rostral ventrolateral medulla: an in vitro patch-clamp study in brain slices. *J. Neurophysiol.* 93, 403–413.
- Chen, J., Xia, C., Wang, J., Jiang, M., Zhang, H., Zhang, C., Zhu, M., Shen, L., Zhu, D., 2013. The effect of orexin-A on cardiac dysfunction mediated by NADPH oxidase-derived superoxide anion in ventrolateral medulla. *PLoS One* 8.
- Crain, J.M., Nikodemova, M., Watters, J.J., 2013. Microglia express distinct M1 and M2 phenotypic markers in the postnatal and adult central nervous system in male and female mice. *J. Neurosci. Res.* 91, 1143–1151.
- Cronk, J.C., Kipnis, J., 2013. Microglia—the brain’s busy bees. *Fl000Prime Rep.* 5, 53.
- David, S., Kroner, A., 2011. Repertoire of microglial and macrophage responses after spinal cord injury. *Nat. Rev. Neurosci.* 12, 388–399.
- De Geyter, D., Stoop, W., Zgavc, T., Sane, S., Michotte, Y., De Keyser, J., Kooijman, R., 2012. Spontaneously hypertensive rats display reduced microglial activation in response to ischemic stroke and lipopolysaccharide. *J. Neuroinflammation* 9, 114.
- de Haas, A.H., Boddeke, H.W., Biber, K., 2008. Region-specific expression of immunoregulatory proteins on microglia in the healthy CNS. *Glia* 56, 888–894.
- de Paula, P.M., Tolstykh, G., Mifflin, S., 2007. Chronic intermittent hypoxia alters NMDA and AMPA-evoked currents in NTS neurons receiving carotid body chemoreceptor inputs. *Am. J. Physiol. Regul. Integr. Comp. Physiol.* 292, R2259–R2265.
- Dean, C., Bago, M., 2002. Renal sympathoinhibition mediated by 5-HT1A receptors in the RVLM during severe hemorrhage in rats. *Am. J. Physiol. Regul. Integr. Comp. Physiol.* 282, R122–R130.
- Dejda, A., Sokolowska, P., Nowak, J.Z., 2005. Neuroprotective potential of three neuropeptides PACAP VIP and PHI. *Pharmacol. Rep.* 57, 307–320.
- Dworak, M., Stebbing, M., Kompa, A.R., Rana, L., Krum, H., Badoer, E., 2014. Attenuation of microglial and neuronal activation in the brain by ICV minocycline following myocardial infarction. *Auton. Neurosci.* 185, 43–50.
- Farber, K., Pannasch, U., Kettenmann, H., 2005. Dopamine and noradrenaline control distinct functions in rodent microglial cells. *Mol. Cell. Neurosci.* 29, 128–138.
- Farnham, M.M.J., Li, Q., Goodchild, A.K., Pilowsky, P.M., 2008. PACAP is expressed in sympathoexcitatory bulbospinal C1 neurons of the brain stem and increases sympathetic nerve activity in vivo. *Am. J. Physiol. Regul. Integr. Comp. Physiol.* 294, R1304–R1311.
- Farnham, M.M.J., Lung, M.S.Y., Tallapragada, V.J., Pilowsky, P.M., 2012. PACAP causes PAC 1/VPAC 2 receptor mediated hypertension and sympathoexcitation in normal and hypertensive rats. *Am. J. Physiol. Heart Circ. Physiol.* 303, H910–H917.
- Feindt, J., Schmidt, A., Mentlein, R., 1998. Receptors and effects of the inhibitory neuropeptide somatostatin in microglial cells. *Mol. Brain Res.* 60, 228–233.
- Giulian, D., Baker, T.J., 1985. Peptides released by ameboid microglia regulate astroglial proliferation. *J. Cell Biol.* 101, 2411–2415.
- Glebov, K., Löchner, M., Jabs, R., Lau, T., Merkel, O., Schloss, P., Steinhäuser, C., Walter, J., 2015. Serotonin stimulates secretion of exosomes from microglia cells. *Glia* 63, 626–634.
- Griffin, W.S., 2006. Inflammation and neurodegenerative diseases. *Am. J. Clin. Nutr.* 83, 470S–474S.
- Guyenet, P.G., 2006. The sympathetic control of blood pressure. *Nat. Rev. Neurosci.* 7, 335–346.
- Guyenet, P.G., Stometta, R.L., Abbott, S.B., Depuy, S.D., Kanbar, R., 2012. The retrotrapezoid nucleus and breathing. *Adv. Exp. Med. Biol.* 758, 115–122.
- Hagino, Y., Kariura, Y., Manago, Y., Amano, T., Wang, B., Sekiguchi, M., Nishikawa, K., Aoki, S., Wada, K., Noda, M., 2004. Heterogeneity and potentiation of AMPA type of glutamate receptors in rat cultured microglia. *Glia* 47, 68–77.
- Hailer, N.P., Jährhult, J.D., Nitsch, R., 1996. Resting microglial cells in vitro: analysis of morphology and adhesion molecule expression in organotypic hippocampal slice cultures. *Glia* 18, 319–331.
- Hanisch, U.K., Kettenmann, H., 2007. Microglia: active sensor and versatile effector cells in the normal and pathologic brain. *Nat. Neurosci.* 10, 1387–1394.
- Hom, S., Fleegal, M.A., Egleton, R.D., Campos, C.R., Hawkins, B.T., Davis, T.P., 2007. Comparative changes in the blood-brain barrier and cerebral infarction of SHR and WKY rats. *Am. J. Physiol. Regul. Integr. Comp. Physiol.* 292, R1881–R1892.
- Hu, X., Li, P., Guo, Y., Wang, H., Leak, R.K., Chen, S., Gao, Y., Chen, J., 2012. Microglia/macrophage polarization dynamics reveal novel mechanism of injury expansion after focal cerebral ischemia. *Stroke* 43, 3063–3070.
- Hughes, V., 2012. Microglia: the constant gardeners. *Nature* 485, 570–572.
- Ifuku, M., Okuno, Y., Yamakawa, Y., Izumi, K., Seifert, S., Kettenmann, H., Noda, M., 2011. Functional importance of inositol-1,4,5-trisphosphate-induced

- intracellular Ca^{2+} mobilization in galanin-induced microglial migration. *J. Neurochem.* 117, 61–70.
- Inglott, M.A., Farnham, M.M.J., Pilowsky, P.M., 2011. Intrathecal PACAP-38 causes prolonged widespread sympathoexcitation via a spinally mediated mechanism and increases in basal metabolic rate in anesthetized rat. *Am. J. Physiol. Heart Circ. Physiol.* 300, H2300–H2307.
- Inoue, K., 2006. The function of microglia through purinergic receptors: neuropathic pain and cytokine release. *Pharmacol. Ther.* 109, 210–226.
- Janssen, S., Gudi, V., Prajeeth, C.K., Singh, V., Stahl, K., Heckers, S., Skripuletz, T., Pul, R., Trebst, C., Tsiavaliaris, G., Stangel, M., 2014. A pivotal role of nonmuscle myosin II during microglial activation. *Exp. Neurol.* 261, 666–676.
- Kannan, H., Tanaka, Y., Kunitake, T., Ueta, Y., Hayashida, Y., Yamashita, H., 1996. Activation of sympathetic outflow by recombinant human interleukin-1 β in conscious rats. *Am. J. Physiol. Regul. Integr. Comp. Physiol.* 270, R479–R485.
- Karperien, A., Ahammer, H., Jelinek, H.F., 2013. Quantitating the subtleties of microglial morphology with fractal analysis. *Front. Cell. Neurosci.* 1–34.
- Kettenmann, H., Hanisch, U.K., Noda, M., Verkhratsky, A., 2011. Physiology of microglia. *Physiol. Rev.* 91, 461–553.
- Kettenmann, H., Kirchhoff, F., Verkhratsky, A., 2013. Microglia: new roles for the synaptic stripper. *Neuron* 77, 10–18.
- Kigerl, K.A., Gensel, J.C., Ankeny, D.P., Alexander, J.K., Donnelly, D.J., Popovich, P.G., 2009. Identification of two distinct macrophage subsets with divergent effects causing either neurotoxicity or regeneration in the injured mouse spinal cord. *J. Neurosci.* 29, 13435–13444.
- Koshiya, N., Guyenet, P.G., 1996. NTS neurons with carotid chemoreceptor inputs arborize in the rostral ventrolateral medulla. *Am. J. Physiol. Regul. Integr. Comp. Physiol.* 270, R1273–1278.
- Kozłowski, C., Weimer, R.M., 2012. An automated method to quantify microglia morphology and application to monitor activation state longitudinally in vivo. *PLoS One* 7, e31814.
- Kroner, A., Greenhalgh, A.D., Zaruk, J.G., PassosdosSantos, R., Gaestel, M., David, S., 2014. TNF and increased intracellular iron alter macrophage polarization to a detrimental M1 phenotype in the injured spinal cord. *Neuron* 83, 1098–1116.
- Kuhn, S.A., van Landeghem, F.K., Zacharias, R., Farber, K., Rappert, A., Pavlovic, S., Hoffmann, A., Nolte, C., Kettenmann, H., 2004. Microglia express GABA(B) receptors to modulate interleukin release. *Mol. Cell. Neurosci.* 25, 312–322.
- Lawson, L.J., Perry, V.H., Dri, P., Gordon, S., 1990. Heterogeneity in the distribution and morphology of microglia in the normal adult mouse brain. *Neuroscience* 39, 151–170.
- Lee, M., 2013. Neurotransmitters and microglial-mediated neuroinflammation. *Curr. Protein Pept. Sci.* 14, 21–32.
- Li, D.P., Chen, S.R., Pan, H.L., 2003. Angiotensin II stimulates spinally projecting paraventricular neurons through presynaptic disinhibition. *J. Neurosci.* 23, 5041–5049.
- Makeham, J.M., Goodchild, A.K., Pilowsky, P.M., 2005. NK1 receptor activation in rat rostral ventrolateral medulla selectively attenuates somato-sympathetic reflex while antagonism attenuates sympathetic chemoreflex. *Am. J. Physiol. Regul. Integr. Comp. Physiol.* 288, R1707–R1715.
- McAllen, R.M., Habler, H.J., Michaelis, M., Peters, O., Janig, W., 1994. Monosynaptic excitation of preganglionic vasomotor neurons by subretrofacial neurons of the rostral ventrolateral medulla. *Brain Res.* 634, 227–234.
- Mihara, Y., Dohi, K., Yofu, S., Nakamachi, T., Ohtaki, H., Shioda, S., Aruga, T., 2011. Expression and localization of the orexin-1 receptor (OX1R) after traumatic brain injury in mice. *J. Mol. Neurosci.* 43, 162–168.
- Milner, R., Campbell, I.L., 2002. Cytokines regulate microglial adhesion to laminin and astrocyte extracellular matrix via protein kinase C-dependent activation of the $\alpha 6 \beta 1$ integrin. *J. Neurosci.* 22, 1562–1572.
- Mittelbronn, M., Dietz, K., Schluesener, H.J., Meyermann, R., 2001. Local distribution of microglia in the normal adult human central nervous system differs by up to one order of magnitude. *Acta Neuropathol.* 101, 249–255.
- Miyoshi, M., Miyano, K., Moriyama, N., Taniguchi, M., Watanabe, T., 2008. Angiotensin type 1 receptor antagonist inhibits lipopolysaccharide-induced stimulation of rat microglial cells by suppressing nuclear factor κ B and activator protein-1 activation. *Eur. J. Neurosci.* 27, 343–351.
- Morrison, H.W., Filosa, J.A., 2013. A quantitative spatiotemporal analysis of microglia morphology during ischemic stroke and reperfusion. *J. Neuroinflammation* 10, 4.
- Mulkey, D.K., Stormetta, R.L., Weston, M.C., Simmons, J.R., Parker, A., Bayliss, D.A., Guyenet, P.G., 2004. Respiratory control by ventral surface chemoreceptor neurons in rats. *Nat. Neurosci.* 7, 1360–1369.
- Murase, S.I., Hayashi, Y., 1998. Expression pattern and neurotrophic role of the c-fms proto-oncogene M-CSF receptor in rodent Purkinje cells. *J. Neurosci.* 18, 10481–10492.
- Nattie, E., Li, A., 2012. Central chemoreceptors: locations and functions. *Comp. Physiol.* 2, 221–254.
- Nimmerjahn, A., Kirchhoff, F., Helmchen, F., 2005. Resting microglial cells are highly dynamic surveillants of brain parenchyma in vivo. *Science* 308, 1314–1318.
- Noda, M., Kariura, Y., Amano, T., Manago, Y., Nishikawa, K., Aoki, S., Wada, K., 2003. Expression and function of bradykinin receptors in microglia. *Life Sci.* 72, 1573–1581.
- Noda, M., Kettenmann, H., Wada, K., 2006. Anti-inflammatory effects of kinins via microglia in the central nervous system. *Biol. Chem.* 387, 167–171.
- Noda, M., Okuno, Y., Ifuku, M., 2011. Neurotransmitter regulation of microglial motility and phagocytosis. *Acta Physiol.*, 203.
- Oshima, N., Kumagai, H., Onimaru, H., Kawai, A., Pilowsky, P.M., Iigaya, K., Takimoto, C., Hayashi, K., Saruta, T., Itoh, H., 2008. Monosynaptic excitatory connection from the rostral ventrolateral medulla to sympathetic preganglionic neurons revealed by simultaneous recordings. *Hypertens. Res.* 31, 1445–1454.
- Oshima, N., McMullan, S., Goodchild, A.K., Pilowsky, P.M., 2006. A monosynaptic connection between baroreceptor neurons in the RVLM and IML in Sprague-Dawley rats. *Brain Res.* 1089, 153–161.
- Perego, C., Fumagalli, S., De Simoni, M.G., 2011. Temporal pattern of expression and colocalization of microglia/macrophage phenotype markers following brain ischemic injury in mice. *J. Neuroinflammation* 8, 174.
- Pilowsky, P., Llewellyn-Smith, I.J., Arnold, L., Minson, J., Chalmers, J., 1994. Intracellular recording from sympathetic preganglionic neurons in cat lumbar spinal cord. *Brain Res.* 656, 319–328.
- Pilowsky, P.M., Goodchild, A.K., 2002. Baroreceptor reflex pathways and neurotransmitters: 10 years on. *J. Hypertens.* 20, 1675–1688.
- Pilowsky, P.M., Lung, M.S., Spirovski, D., McMullan, S., 2009. Differential regulation of the central neural cardiorespiratory system by metabotropic neurotransmitters. *Philos. Trans. R. Soc. Lond. B. Biol. Sci.* 364, 2537–2552.
- Pocock, J.M., Kettenmann, H., 2007. Neurotransmitter receptors on microglia. *Trends Neurosci.* 30, 527–535.
- Prabhakar, N.R., Kumar, G.K., Peng, Y.J., 2012. Sympatho-adrenal activation by chronic intermittent hypoxia. *J. Appl. Physiol.* 113, 1304–1310.
- Privitera, P.J., Thibodeaux, H., Yates, P., 1994. Rostral ventrolateral medulla as a site for the central hypotensive action of kinins. *Hypertension* 23, 52–58.
- Pyo, H., Yang, M.S., Jou, I., Joe, E.H., 2003. Wortmannin enhances lipopolysaccharide-induced inducible nitric oxide synthase expression in microglia in the presence of astrocytes in rats. *Neurosci. Lett.* 346, 141–144.
- Rasley, A., Bost, K.L., Olson, J.K., Miller, S.D., Marriott, L., 2002. Expression of functional NK-1 receptors in murine microglia. *Glia* 37, 258–267.
- Ridker, P.M., Cushman, M., Stampfer, M.J., Tracy, R.P., Hennekens, C.H., 1998. Plasma concentration of C-reactive protein and risk of developing peripheral vascular disease. *Circulation* 97, 425–428.
- Rosin, D.L., Chang, D.A., Guyenet, P.G., 2006. Afferent and efferent connections of the rat retrotrapezoid nucleus. *J. Comp. Neurol.* 499, 64–89.
- Savli, H., Gulkar, M.D., Esen, N., 2004. The effect of stimulated microglia conditioned media on BDNF gene expression of striatal astrocytes: quantification by real-time PCR. *Int. J. Neurosci.* 114, 1601–1612.
- Schlaich, M.P., Lambert, E., Kaye, D.M., Krozowski, Z., Campbell, D.J., Lambert, G., Hastings, J., Aggarwal, A., Esler, M.D., 2004. Sympathetic augmentation in hypertension: role of nerve firing, norepinephrine reuptake, and angiotensin neuromodulation. *Hypertension* 43, 169–175.
- Schreihöfer, A.M., Guyenet, P.G., 2002. The baroreflex and beyond: control of sympathetic vasomotor tone by GABAergic neurons in the ventrolateral medulla. *Clin. Exp. Pharmacol. Physiol.* 29, 514–521.
- Shahid, I.Z., Rahman, A.A., Pilowsky, P.M., 2012. Orexin A in rat rostral ventrolateral medulla is pressor, sympatho-excitatory, increases barosensitivity and attenuates the somato-sympathetic reflex. *Br. J. Pharmacol.* 165, 2292–2303.
- Shapiro, L.A., Perez, Z.D., Foresti, M.L., Anis, G.M., Ribak, C.E., 2009. Morphological and ultrastructural features of Iba1-immunolabeled microglial cells in the hippocampal dentate gyrus. *Brain Res.* 1266, 29–36.
- Shi, P., Diez-Freire, C., Jun, J.Y., Qi, Y., Katovich, M.J., Li, Q., Sriramula, S., Francis, J., Summers, C., Raizada, M.K., 2010. Brain microglial cytokines in neurogenic hypertension. *Hypertension* 56, 297–303.
- Stence, N., Waite, M., Dailey, M.E., 2001. Dynamics of microglial activation: a confocal time-lapse analysis in hippocampal slices. *Glia* 33, 256–266.
- Sunanaga, J., Deng, B.S., Zhang, W., Kanmura, Y., Kuwaki, T., 2009. CO₂ activates orexin-containing neurons in mice. *Respir. Physiol. Neurobiol.* 166, 184–186.
- Sved, A.F., Ito, S., Sved, J.C., 2003. Brainstem mechanisms of hypertension: role of the rostral ventrolateral medulla. *Curr. Hypertens. Rep.* 5, 262–268.
- Takakura, A.C., Moreira, T.S., West, G.H., Gwilt, J.M., Colombari, E., Stormetta, R.L., Guyenet, P.G., 2007. GABAergic pump cells of solitary tract nucleus innervate retrotrapezoid nucleus chemoreceptors. *J. Neurophysiol.* 98, 374–381.
- Taylor, D.L., Diemel, L.T., Pocock, J.M., 2003. Activation of microglial group III metabotropic glutamate receptors protects neurons against microglial neurotoxicity. *J. Neurosci.* 23, 2150–2160.
- Taylor, D.L., Jones, F., Kubota, E.S., Pocock, J.M., 2005. Stimulation of microglial metabotropic glutamate receptor mGlu2 triggers tumor necrosis factor α -induced neurotoxicity in concert with microglial-derived Fas ligand. *J. Neurosci.* 25, 2952–2964.
- Thrasher, T.N., 2005. Baroreceptors, baroreceptor unloading, and the long-term control of blood pressure. *Am. J. Physiol.* 288, R819–R827.
- Tremblay, M.E., Lowery, R.L., Majewska, A.K., 2010. Microglial interactions with synapses are modulated by visual experience. *PLoS Biol.* 8, e1000527.
- Tremblay, M.E., Stevens, B., Sierra, A., Wake, H., Bessis, A., Nimmerjahn, A., 2011. The role of microglia in the healthy brain. *J. Neurosci.* 31, 16064–16069.
- Ueno, M., Fujita, Y., Tanaka, T., Nakamura, Y., Kikuta, J., Ishii, M., Yamashita, T., 2013. Layer V cortical neurons require microglial support for survival during postnatal development. *Nat. Neurosci.* 16, 543–551.
- van Rossum, D., Hanisch, U.K., 2004. Microglia. *Metab. Brain Dis.* 19, 393–411.
- Wake, H., Moorhouse, A.J., Jinno, S., Kohsaka, S., Nabekura, J., 2009. Resting microglia directly monitor the functional state of synapses in vivo and determine the fate of ischemic terminals. *J. Neurosci.* 29, 3974–3980.
- Waki, H., Gouraud, S.S., Maeda, M., Paton, J.F., 2008. Specific inflammatory condition in nucleus tractus solitarius of the SHR: novel insight for neurogenic hypertension? *Auton. Neurosci.* 142, 25–31.

- Weston, M., Wang, H., Stornetta, R.L., Sevigny, C.P., Guyenet, P.G., 2003. Fos expression by glutamatergic neurons of the solitary tract nucleus after phenylephrine-induced hypertension in rats. *J. Comp. Neurol.* 460, 525–541.
- Wu, K.L.H., Chan, S.H.H., Chan, J.Y.H., 2012. Neuroinflammation and oxidative stress in rostral ventrolateral medulla contribute to neurogenic hypertension induced by systemic inflammation. *J. Neuroinflammation* 9, 212.
- Xu, H.T., Pan, F., Yang, G., Gan, W.B., 2007. Choice of cranial window type for in vivo imaging affects dendritic spine turnover in the cortex. *Nat. Neurosci.* 10, 549–551.
- Zheng, H., Liu, X., Li, Y., Mishra, P.K., Patel, K.P., 2014. Attenuated dopaminergic tone in the paraventricular nucleus contributing to sympathoexcitation in rats with type 2 diabetes. *Am. J. Physiol. Regul. Integr. Comp. Physiol.* 306, 138–148.

Neuroscience 317 (2016) 162–172

pSer40 TYROSINE HYDROXYLASE IMMUNOHISTOCHEMISTRY IDENTIFIES THE ANATOMICAL LOCATION OF C1 NEURONS IN RAT RVLM THAT ARE ACTIVATED BY HYPOTENSION

P. E. NEDOBOY,^a S. MOHAMMED,^a K. KAPOOR,^{a,b}
A. M. BHANDARE,^{a,b} M. M. J. FARNHAM^a AND
P. M. PILOWSKY^{a,c,*}

^a The Heart Research Institute, 2042 New South Wales, Australia

^b Australian School of Advanced Medicine, Macquarie University, Sydney, 2109 New South Wales, Australia

^c Department of Physiology, University of Sydney, Sydney, 2006 New South Wales, Australia

Abstract—Identification of neurons, and their phenotype, that are activated in response to specific stimuli is a critical step in understanding how neural networks integrate inputs to produce specific outputs. Here, we developed novel mouse monoclonal antibodies of different IgG isotypes that are specific to tyrosine hydroxylase (TH), and to tyrosine hydroxylase activated at its serine 40 position (pSer40TH), in order to assess changes in the activity of phenotypically identified cardiovascular neurons using fluorescence immunohistochemistry. We find that the proportion of C1 pSer40TH-positive neurons in the central and medial region of the rat rostral ventrolateral medulla (RVLM) increases dramatically following hydralazine treatment, whereas phenylephrine treatment does not significantly change the pSer40TH/TH ratio in these regions compared to control. This finding suggests that there is a mediolateral topology associated with the activation of C1 neurons following baroreceptor loading or unloading. Overall, we conclude first, that our newly characterized monoclonal antibodies are specific, and selective, against TH and pSer40TH. Secondly, that they can be used to label TH and pSer40TH immunoreactive neurons simultaneously, and thirdly that that they can be used to identify the activation state of catecholamine synthesizing neurons after physiological stimuli. Finally, we find that there is basal level of activation of TH neurons in the lateral, central and medial regions (~70%,

30% and 45%, respectively) of the C1 area, but that following unloading of the baroreceptors there is a marked increase in activation of central (~80%) and medial (~90%) C1 neurons in the RVLM. Crown Copyright © 2016 Published by Elsevier Ltd. on behalf of IBRO. All rights reserved.

Key words: tyrosine hydroxylase, phosphorylated tyrosine hydroxylase, RVLM, C1 neurons, IgG subtype-specific monoclonal antibodies, baroreflex.

INTRODUCTION

The rostral ventrolateral medulla (RVLM) is a critical area in the central control of blood pressure (BP) (Pilowsky et al., 2009). With the development of modern immunohistochemical and tract-tracing techniques, it was recognized that bulbospinal neurons that are inhibited by baroreceptor activation (Miyawaki et al., 1995) and hence termed 'sympathoexcitatory' (BS-SE) in the RVLM are extremely heterogeneous in terms of their neurotransmitter content, receptor expression, axon myelination (Schreihofer and Guyenet, 1997; Verberne and Sartor, 2004; Burke et al., 2011), and many other features. In 1974 (Hökfelt et al., 1974), it was demonstrated that in RVLM, all tyrosine hydroxylase (TH) neurons also contained phenylethanolamine-N-methyltransferase (PNMT; adrenaline synthesizing). Subsequently, it was discovered that these same PNMT cells (also termed C1 neurons) projected to the spinal cord where they synapsed exclusively – albeit in very small numbers – with sympathetic preganglionic neurons (Guyenet et al., 1989). Ablation or inhibition of the RVLM causes a catastrophic fall in arterial BP and sympathetic nerve activity (SNA) (Pilowsky et al., 1985; Sun and Reis, 1996; Honiuchi and Dampney, 1998). Depletion of C1 cells in RVLM does not significantly alter arterial pressure or generation of sympathetic vasomotor tone (Schreihofer and Guyenet, 2000); interestingly, depletion of catecholamine neurons does attenuate the pressor and sympathoexcitatory responses to stimulation of the RVLM. Functional identification of baroreceptor inhibited bulbospinal RVLM neurons using morphological criteria has until now been limited to the use of protein product of the feline osteosarcoma oncogene 'c-fos' (Fos) histochemistry combined with other markers (Minson et al., 1996b; Spirovski et al., 2012). A disadvantage of these approaches is that

*Correspondence to: P.M. Pilowsky, The Heart Research Institute, University of Sydney, 7 Eliza Street, Sydney, 2042 New South Wales, Australia. Tel: +61-2-82088938.

E-mail address: paul.pilowsky@hri.org.au (P. M. Pilowsky).

Abbreviations: BP, blood pressure; DMEM, Dulbecco's modified Eagle's medium; ELISA, enzyme-linked immunosorbent assay; FBS, fetal bovine serum; Fos, protein product of the feline osteosarcoma oncogene 'c-fos'; IgG, immunoglobulin G; IHC, immunohistochemistry; mAbs, monoclonal antibodies; MAP, mean arterial pressure; MATF, Monash Antibody Technology Facility; PBS, phosphate-buffered saline; PFA, paraformaldehyde in 0.1 M phosphate buffer; PNMT, phenylethanolamine-N-methyltransferase; pSer40TH, tyrosine hydroxylase phosphorylated at Ser40; pSer40THIgG_{2Bκ}, pSer40TH antibody – IgG_{2Bκ} isotype; RVLM, rostral ventrolateral medulla; SNA, sympathetic nerve activity; TCS, tissue culture supernatants; TH, tyrosine hydroxylase; THIgG_{7A}, TH antibody – IgG_{7A} isotype.

<http://dx.doi.org/10.1016/j.neuroscience.2016.01.012>

0306-4522/Crown Copyright © 2016 Published by Elsevier Ltd. on behalf of IBRO. All rights reserved.

there is heterogeneity of cell types in the RVLM, and the use of Fos on its own is not sufficient to parse out the different groups of cells.

Here, we investigate the possibility of using monoclonal antibodies (mAbs) directed toward TH, and mAbs directed toward TH that has been phosphorylated at the serine 40 residue (pSer40TH), a site that is known to increase TH activity at least 20-fold in most cases (Dunkley et al., 2004). Our objective was to determine if the ratio of phosphorylated to non-phosphorylated neurons would be useful in identifying activity changes in central cardiovascular catecholaminergic neurons in the RVLM.

Our aims in this study were first, to develop and characterize mouse mAbs of different immunoglobulin G (IgG) subclasses to TH, and to pSer40TH. Secondly, to determine that both antibodies exclusively stain catecholaminergic neurons, and thirdly, to establish the extent to which the antibodies could be used to determine increases or decreases in phosphorylation states in catecholaminergic neurons in different regions of the RVLM following baroreceptor loading (phenylephrine) or unloading (hydralazine). If this was the case, we believe that such an approach would enable the identification of TH neurons that were activated in different functional states.

EXPERIMENTAL PROCEDURES

Reagents

Chemicals were from Sigma–Aldrich (NSW, Australia) unless otherwise stated.

Peptide synthesis

Peptide sequences, corresponding to TH and pSer40TH were identified and validated using NCBI BLAST protein database. TH sequence: C-PRFIGRRQSLIEDARK; pSer40TH sequence: C-PRFIGRRQpSLIEDARK. Peptides were produced at >70% purity using standard peptide chemistry by C S Bio Co (CA, USA).

mAb production

mAbs were generated at the Monash Antibody Technology Facility (MATF, Melbourne, <https://platforms.monash.edu/matf/>). Briefly, mice were immunized intraperitoneally with a synthetic peptide, corresponding to the antigen of interest (TH or pSer40TH). Following immunization, the mouse producing the largest amount of the relevant antibody was selected for fusion. Hybridoma cells were produced by fusing SP2/0-Ag14 myeloma cells with mouse spleen cells in the presence of polyethylene glycol and then grown in azaserine hypoxanthine containing medium. Hybridoma cells were screened for reactivity with the antigen by microarray (Antigen MicroArray (AMA), MATF) followed by enzyme-linked immunosorbent assay (ELISA) of any IgG microarray-positive clones. The most responsive ELISA clones were expanded and subcloned by two rounds of serial dilution. Two stable clonal lines that secreted antibodies specific for each antigen were established. The isotype of the

monoclonal antibody being produced was determined by a commercially available assay kit (IsoStrip, Roche, USA). The TH antibody was found to be IgG_{1κ} (THIgG_{1κ}). The pSer40TH antibody was found to be an IgG_{2aκ} (pSer40THIgG_{2aκ}).

Hybridoma cell culture

Newly established hybridoma cell lines were first cultured in Dulbecco's modified Eagle's medium (DMEM, JRH Biosciences) supplemented with 200 mM GlutaMAX (Invitrogen, VIC, Australia), 50 µg/mL gentamicin (Gibco, Invitrogen, VIC, Australia) and 20% fetal bovine serum (FBS). Cells were split every 3–4 days and seeded at 1×10^5 cells/mL in 75 cm³ culture flasks for two weeks. Serum content of the medium was gradually decreased to 10%. Antibody-containing tissue culture supernatants (TCS) were collected after two weeks of culturing cells in 10% FBS-supplemented DMEM. Small aliquots of TCS were frozen and stored at –20 °C for future use.

ELISA

The TCS were tested against each target antigen by ELISA. Briefly, 96-well plates were coated with the peptide of interest (TH or pSer40TH) at a concentration of 4 µg/mL and blocked with 3% bovine serum albumin in phosphate-buffered saline (100 mM phosphate buffer, 0.9% NaCl, pH 7.4; PBS). Undiluted hybridoma TCS was added to the wells followed by the addition of a secondary antibody (donkey anti-mouse IgG (H + L), alkaline phosphatase labeled). A chromogenic reaction was initiated by addition of p-nitrophenylphosphate substrate, and stopped by addition of a stop solution (5 M sodium hydroxide). Absorbance was measured at 405 nm; clones were considered positive if the absorbance readings were more than triple than the negative control (hybridoma cell media).

Double-labeled immunofluorescence labeling of rat brainstem sections

Mouse mAbs produced by hybridoma cells were used for immunohistochemical analysis of free floating rat brain sections. Different IgG isotypes of the primary mAbs in conjunction with IgG-isotype specific secondary antibodies conjugated to two different fluorophores allowed for simultaneous detection of TH and pSer40TH in the tissue. Prior to incubation with the primary mAbs, brainstem sections were washed 3 × 30 min in PBS containing 0.3% Triton X-100 on an orbital shaker (Heidolph Instruments, Germany) at room temperature. Sections were then transferred to the solution containing 1:100 dilution of mouse mAbs against TH (THIgG_{1κ}) and pSer40TH (pSer40THIgG_{2aκ}) described above in Tris–PBS with 0.1% thimerosal, 0.3% Triton X-100 and 10% normal donkey serum, and incubated on an orbital shaker at 4 °C for 72 h. Following incubation with the primary mAbs, brainstem sections were washed with PBS containing 0.3% Triton X-100 (3 × 30 min) and incubated with Cy5-conjugated IgG_{1κ}-specific

(for the detection of TH) and AlexaFluor 488-conjugated IgG_{2ak}-specific (for the detection of pSer40TH) secondary goat anti-mouse antibodies (1:500 dilution, Cat#: 115-175-205 and Cat#: 115-545-206, respectively, Jackson ImmunoResearch Laboratories, PA, USA) in Tris-PBS with 0.1% thimerosal and 2% normal donkey serum on an orbital shaker at room temperature for 24 h, protected from light. The sections were then washed with Tris-PBS (3 × 30 min) and mounted on Superfrost (VWR, PA, USA) glass slides. Mounted sections were air-dried, coverslipped with Vectashield mounting medium (Vector Laboratories, CA, USA) and sealed with nail polish. A Zeiss Axio Imager Z2 microscope was used to assess immunofluorescent staining.

For urethane anesthetized rat the immunolabeling protocol was followed as described above with an addition of a primary polyclonal guinea-pig antibody against c-Fos (1:2000 dilution, Cat#: 226 004, Synaptic Systems, Germany) and secondary donkey anti-guinea-pig AMCA-conjugated antibody (1:500 dilution, Cat#: 706-156-148, Jackson ImmunoResearch Laboratories, PA, USA).

Controls

The pattern of staining of the THIgG_{1k} mAb was compared with a previously characterized commercial polyclonal sheep anti-TH antibody (Cat#: 120-00113, Abcam, UK). Immunofluorescence staining protocol and microscopy was carried out as described above. Brainstem sections were incubated with 1:100 diluted mouse THIgG_{1k} mAb together with 1:3000 diluted sheep anti-TH antibody and then with donkey anti-mouse Cy5-conjugated and donkey anti-sheep FITC-conjugated secondary antibodies (1:500 dilution, Cat#: 715-175-151 and Cat#: 713-096-147, respectively, Jackson ImmunoResearch Laboratories, PA, USA).

The specificity of THIgG_{1k} and pSer40THIgG_{2ak} antibodies was validated by eliminating staining following incubation with the same peptides used to generate the original antibodies. Briefly, 100 µg/mL of immunogen peptide was incubated with 1:100 diluted mouse monoclonal THIgG_{1k} or pSer40THIgG_{2ak} antibody for 30 min at room temperature. Following antigen preabsorption, brainstem sections were incubated with the preabsorbed antibody as per standard immunofluorescence staining protocol (above). Immunostaining with non-preabsorbed antibodies was run in parallel.

In order to assess the specificity of isotype-specific secondary antibodies, one of the primary mAbs (THIgG_{1k} or pSer40THIgG_{2ak}) was omitted from the immunostaining protocol described in Double-labeled immunofluorescence labeling of rat brainstem sections while both secondary antibodies (IgG_{1k}-specific Cy5-conjugated and IgG_{2ak}-specific-AlexaFluor 488-conjugated) were present. In a separate experiment, both primary mAbs were omitted with both secondary antibodies present. Staining was assessed by fluorescence microscopy.

Animal experiments

All procedures and protocols were approved by the Animal Care and Ethics Committee of Macquarie University and the Sydney Local Health District. Adult male Sprague–Dawley (SD, 250–350 g, *N* = 9) rats were anesthetized with an intraperitoneal injection of sodium pentobarbitone (Lethabarb, Virbac; 50–60 mg/kg; ~1 mL/rat) or 10% urethane (*N* = 1, 1.3 g/kg) combined with atropine sulfate (Pfizer, 0.2 mL/kg) using a 26G needle. A cannula was inserted in the external jugular vein for the administration of fluids, additional anesthetic and other intravenous drugs. The right carotid artery was cannulated for measurement of BP. A femoral vein was cannulated for continuous infusion of phenylephrine, hydralazine or saline. Following cannulation, intravenous administration of drugs to alter the baseline mean arterial pressure (MAP) to a fixed amount was initiated. Lowering of MAP by 40 mmHg was triggered in rats via a single intravenous injection of hydralazine hydrochloride at a dose of 10 mg/kg and a continuous infusion of saline for 2 h. Phenylephrine hydrochloride was continuously infused intravenously (10 µg/kg/min) over a period of 2 h to increase MAP by 25–40 mmHg. Control experiments were conducted by the intravenous administration of saline to three sodium pentobarbitone anesthetized animals, and one urethane-anesthetized animal. The depth of anesthesia was monitored by observing reflex responses to nociceptive and tactile stimuli (regular tail/paw pinches), pupillary response to light and corneal response to touch. Additional anesthetic (1.5–2 mg of sodium pentobarbitone or 0.3–0.4 mg of 10% urethane) was infused intravenously if positive responses were observed. Following the 2-h protocol, rats were deeply anesthetized with 80 mg/kg of sodium pentobarbitone or urethane (1.4 g/kg) and perfused transcardially with 400 mL 0.9% PBS followed by 4% (w/v) paraformaldehyde in 0.1 M phosphate buffer (PFA). The brain was extracted and postfixed in 4% PFA overnight. Brain tissue was cut coronally using a vibrating microtome (Leica VT1200) into 40 µm sections. Sections were stored in cryoprotectant solution at –20 °C.

Analysis

Sections were examined by imaging the individual fluorochromes separately with appropriate filter cubes (THIgG_{1k}-Cy5 with 650/673 nm (ex/em) and pSer40THIgG_{2ak}-AlexaFluor 488 with 493/517 nm (ex/em)). Images were adjusted for brightness and contrast only to maximize our ability to count cells and discriminate them from background. No other changes were made to the images. Slides were coded and examined 'blind' to treatment condition to avoid bias. THIgG_{1k}- and pSer40THIgG_{2ak}-immunoreactive (ir) cell bodies that included a nucleus were counted for each experimental condition (control, phenylephrine and hydralazine) bilaterally in the RVLM area that was defined dorsally by the nucleus ambiguus, laterally by the spinal trigeminal tract, and medially by the inferior olive (Hokfelt et al., 1973; Ross et al., 1984; Schreihofer

and Guyenet, 1997; Phillips et al., 2001) at Bregma level -12.36 mm (Map 136, (Paxinos, 2007)). For analysis, a rectangular field ($600 \mu\text{m} \times 1110 \mu\text{m}$) was superimposed on the captured image so as to include all THlgG_{1k}-ir (C1) cells within the RVLM area. The rectangular field was divided vertically into three equal parts to designate lateral, central and medial regions of RVLM. The number of THlgG_{1k}- (Cy5, red fluorescence) and pSer40THlgG_{2ak} (AlexaFluor 488, green fluorescence)-ir neurons in each region from each repeat ($n = 3$, bilaterally, one $40\text{-}\mu\text{m}$ section per animal) was summed, and analyzed (exact test for goodness-of-fit, commonly used to analyze categorical, non-parametric data, such as cell counts, with sample size < 1000 (McDonald, 2014)). GraphPad Prism version 6.05 was used to plot the percentage of double-labeled neurons (pSer40THlgG_{2ak}-ir and THlgG_{1k}-ir) versus single-labeled neurons (THlgG_{1k}-ir) in lateral, medial and central regions of RVLM for each treatment (control, phenylephrine and hydralazine). The numbers reported are the sum of cell counts of three animals in each treatment group.

RESULTS

Both THlgG_{1k} and pSer40THlgG_{2ak} antibodies were tested by ELISA and preabsorption with the immunizing antigen. THlgG_{1k} antibody was also validated by double labeling with a previously characterized commercial antibody.

ELISA

Hybridoma cells that tested positive for the peptide of interest by microarray were subjected to an ELISA test. Each ELISA-positive clone underwent two rounds of subcloning to ensure monoclonality. Supernatant ELISA of each round of subcloning determined the clones producing antibodies of appropriate specificity and thereby deemed suitable for expansion.

Immunolabeling

Specificity of THlgG_{1k} and pSer40THlgG_{2ak} antibodies was demonstrated by immunostaining of catecholaminergic neurons in rat brain and adrenal medulla. The typical pattern of distribution of TH-ir neurons was observed with THlgG_{1k} antibody. Specifically, THlgG_{1k}-positive neurons were found in many regions of the brain, including C2/C3 (Fig. 1A), C1 (Fig. 1B, magenta), A5 (Fig. 1C, magenta), A1 (Fig. 1D, magenta) and hypothalamus (Fig. 1F, magenta). Chromaffin cells of the adrenal medulla also stained positive for THlgG_{1k} (Fig. 1E, magenta). In addition, pSer40THlgG_{2ak} immunoreactivity was also observed in all the areas that were positive for THlgG_{1k} (Fig. 1B–F, green).

THlgG_{1k} antibody incubation with the peptide that was originally used to generate the antibody resulted in the absence of staining following the standard immunohistochemistry (IHC) protocol (Fig. 2A, B). Similar results were obtained when pSer40THlgG_{2ak}

antibody was preabsorbed with its immunizing antigen (Fig. 2C, D).

When THlgG_{1k} (Fig. 2G, H) or pSer40THlgG_{2ak} (Fig. 2E, F) antibody was omitted from the primary antibody cocktail in the presence of both secondary antibodies, there was no staining present in the image channels corresponding to the omitted primary antibody (Fig. 2F, G). This confirms the specificity and lack of cross-reactivity of the secondary antibodies. The presence of low-level, granular background green fluorescence in Fig. 2F is indicative of intrinsic lipofuscin auto-fluorescence, that is particularly evident when tissue is obtained from older animals, and when fixed with formalin; it is most frequently observed when AlexaFluor488-, FITC- or Cy3-fluorophores are used.

Omission of both primary mAbs resulted in the complete absence of specific staining.

No significant differences in staining were observed when THlgG_{1k} mAb was compared with a previously validated TH antibody (see Experimental procedures section). Co-incubation of mouse THlgG_{1k} mAb with sheep TH antibody showed 100% co-localization of staining following an IHC protocol described above (Fig. 2I–K).

pSer40THlgG_{2ak} IHC after baroreceptor loading or unloading

All three treatments revealed the presence of neurons dually labeled with pSer40THlgG_{2ak} and THlgG_{1k} and also cells labeled only with THlgG_{1k}. Rarely, ($\sim 3\%$) cells positive for pSer40THlgG_{2ak} were apparently negative for THlgG_{1k}. The absence of staining might be explained by the fact that phosphorylation of Ser40 at the antigenic site precludes its recognition by antibody that was raised against non-phosphorylated peptide. When phosphorylation is extensive, it is possible that staining with THlgG_{1k} antibody might not be observed. Owing to the fact that cells, in order to be positive for the phosphorylated form of TH, must contain TH, pSer40THlgG_{2ak}-positive/THlgG_{1k}-negative cells were included in the dually labeled pSer40THlgG_{2ak}/THlgG_{1k} category. In order to confirm that the pSer40THlgG_{2ak}-positive cells all contained TH, we also dually labeled using the pSer40THlgG_{2ak} antibody and an antibody to TH raised in sheep (Abcam – see Controls section). In this experiment, all pSer40THlgG_{2ak}-positive cells were found to contain TH, but it was not the case that all TH cells were positive for pSer40THlgG_{2ak} (Fig. 3A–C).

In the hydralazine-treated animals there was the highest number of dual/single (112/41)-labeled cells compared to the control (73/67) and phenylephrine (58/74) treatments. Saline, phenylephrine and hydralazine infusions produced distinctly different mediolateral patterns of pSer40THlgG_{2ak} immunoreactivity (Fig. 4B vs E vs H).

Baroreceptor loading, achieved by a 2-h infusion of phenylephrine, significantly decreased the number of pSer40THlgG_{2ak}-ir neurons in the lateral RVLM compared to the saline control (23/19 vs 46/21, respectively, $P = 0.04$, Fig. 4K, lateral gray bar vs white

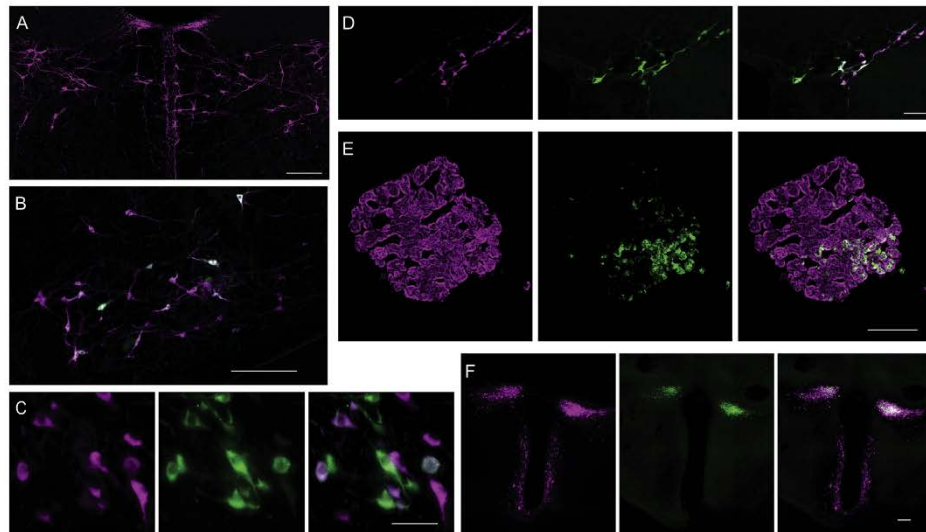


Fig. 1. Representative images of TH and pSer40TH immunolabeling in rat tissues. (A) THlgG_{1k}-ir cells in the C2/C3 region of the rat brainstem; (B) C1 THlgG_{1k} and pSer40THlgG_{2ak}-ir cells in the RVLM; (C) A5 cells in the rat brainstem; (D) A1 region of the brainstem; (E) chromaffin cells in the rat adrenal medulla; and (F) hypothalamus. THlgG_{1k}-Cy5 fluorescence is pseudo-colored magenta, pSer40THlgG_{2ak}-AlexaFluor 488 – green. Scale bars: (A, B, E, F) = 200 μ m; (C) 50 μ m; (D) 100 μ m. (For interpretation of the references to color in this figure legend, the reader is referred to the web version of this article.)

bar). This proportion, however, was not significantly different between phenylephrine treatment and control in the central (21/40 vs 17/34) and medial regions (14/15 vs 10/12) of RVLM ($P > 0.5$ and $P > 1$, respectively, Fig. 4K, central and medial gray bars vs white bars). Conversely, hydralazine treatment significantly increased the number of pSer40THlgG_{2ak}-positive neurons in the central (63/18 vs 17/34) and medial (16/2 vs 10/12) regions of the RVLM ($P < 0.0001$, and $P < 0.01$, respectively, Fig. 4K central and medial black bars vs white bars), while the proportion of pSer40THlgG_{2ak}-ir was not statistically different to control in the lateral RVLM (33/21 vs 46/21, respectively, $P > 0.1$, Fig. 4K, lateral black bar vs white bar).

Immunolabeling for c-Fos in urethane anesthetized rat revealed the absence of co-localization of c-Fos staining with pSer40THlgG_{2ak} in many instances (Fig. 5E, I, white arrowheads).

DISCUSSION

Here, we report for the first time that there is a clear topographical variation in the distribution of activated TH neurons during different physiological states. Under control conditions active C1 neurons appear mostly in the lateral part of the RVLM. However, during baroreceptor unloading, C1 neurons in the medial and central parts of the RVLM become engaged as well. This observation was possible because of the use of novel mAbs of two different IgG isotypes that are specific for TH and pSer40TH. Thus, it was possible to use different labeled secondary antibodies to distinguish

the populations of TH neurons according to their functional state histochemically. Furthermore, we could demonstrate that it is possible to use these two antibodies to detect activation states of catecholaminergic neurons in the C1 cell group, and demonstrate changes in cell numbers following relevant stimuli.

A key novelty of this study is that it is the first to our knowledge that is able to discriminate active catecholamine neurons from inactive catecholamine neurons. Earlier studies have reported the use of antibodies of this type, but these are generally polyclonal and often in the same species (e.g. rabbit; (Xu et al., 1998)) making this type of study impossible. In this study we were able to use the antibodies as functional markers for changes in the activity state of a specific population of neurons. Although it is well understood that in resting conditions, normal MAP is maintained by a rather low resting SNA, it has not been possible to demonstrate any functional phenotypic anatomical correlate within presympathetic neurons in the brainstem that could support this physiological state. Fig. 6 presents a mechanistic interpretation of our data that synthesizes previous physiological work along with our current anatomical findings. Previous studies have demonstrated that changes in arterial BP, that are either imposed or are genetic (Minson et al., 1996a), can lead to increases or decreases in Fos labeling within different populations of neurons in the brainstem. The novel feature of our work is the demonstration of a topography associated with a specific phenotype.

In the control state, only a modest number of dually labeled pSer40THlgG_{2ak}/THlgG_{1k} neurons, concentrated

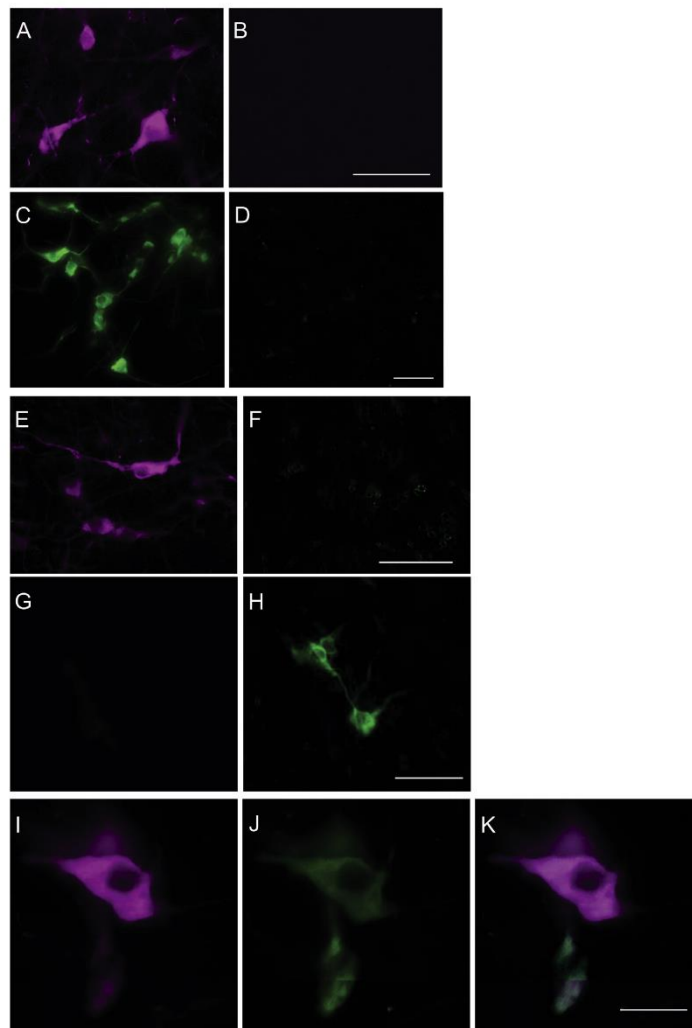


Fig. 2. Immunohistochemical staining for (A) THlgG_{1κ} and (B) preabsorbed THlgG_{1κ}; (C) pSer40THlgG_{2ακ} and (D) preabsorbed pSer40THlgG_{2ακ}; (E–H) Immunostaining pattern when brainstem sections were incubated with (E, F) THlgG_{1κ} or (G, H) pSer40THlgG_{2ακ} mAb followed by a mixture of both secondary antibodies; THlgG_{1κ}-labeled cells bound only anti-IgG_{1κ}-Cy5 secondary antibody (E) and not the anti-IgG_{2ακ}-AlexaFluor 488 (F); pSer40THlgG_{2ακ}-labeled cells bound only anti-IgG_{2ακ}-AlexaFluor 488 secondary antibody (H) and not the anti-IgG_{1κ}-Cy5 (G). A small amount of non-specific lipofuscin granule fluorescence is seen under the green filter (F); (I) mouse monoclonal THlgG_{1κ}; (J) sheep polyclonal TH antibody immunofluorescence; (K) merged image shows extent of co-localization in (I) and (J), which was always 100%; (A–H) THlgG_{1κ}-Cy5 fluorescence is pseudo-colored magenta, pSer40THlgG_{2ακ}-AlexaFluor 488 – green; (I, J) mouse mAb TH-Cy5 fluorescence is pseudo-colored magenta, sheep TH-FITC is pseudo-colored green. Scale bars: (A–H) = 50 μm; (I–K) = 20 μm. (For interpretation of the references to color in this figure legend, the reader is referred to the web version of this article.)

in the lateral segment of the RVLM, are found. Following activation of baroreceptors by intravenous injection of phenylephrine – which would be expected to silence TH neurons in RVLM, there was a small, but significant change in the number of pSer40THlgG_{2ακ} neurons in

RVLM. However, not all TH-positive cells were silenced. This may have been due to C1 neurons with other functions and projections, such as those involved in regulation of adrenaline neurons in the adrenal medulla (Morrison and Cao, 2000) or those that project rostrally.

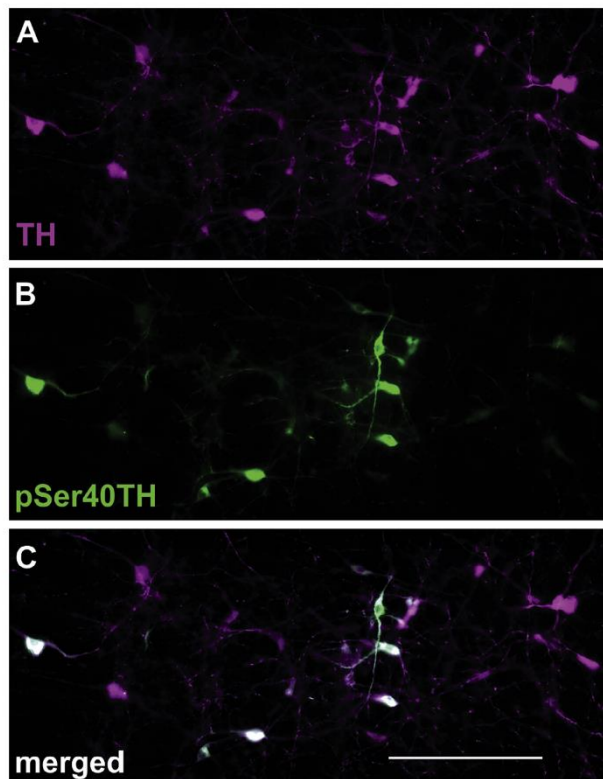


Fig. 3. Tyrosine hydroxylase (TH)-positive neurons are present in the RVLM (A). At the same site, pSer40THIrG_{2aκ}-ir neurons are also present, but in small numbers (B). The merged image shows that not all TH neurons contain pSer40THIrG_{2aκ}, but all pSer40THIrG_{2aκ}-ir neurons are TH immunoreactive (C). Scale bar in (C) is 200 μ m, applicable to (A–C).

Additionally, phenylephrine-induced generalized stress may have caused activation of certain TH-ir in the RVLM (Chan and Sawchenko, 1998; Weston et al., 2003). Following baroreceptor unloading with marked hypotension using hydralazine, there was a dramatic increase in the proportion of pSer40THIrG_{2aκ}-ir neurons in the central and medial regions of the RVLM. Under the control conditions, the proportion of pSer40THIrG_{2aκ}-ir neurons did not exceed 33% in the central RVLM and 45% in the medial RVLM, whereas with hydralazine treatment this ratio increased to 78% and 89%, respectively. This suggests that there is a specific subpopulation of RVLM catecholaminergic neurons that is activated in response to hydralazine-induced hypotension.

Technical considerations

Previous studies have reported changes in TH phosphorylation levels (Raghuraman et al., 2009; Damanhuri et al., 2012; Parker et al., 2015) in the RVLM, but none of these studies have been able to identify the proportion, or region location of TH neurons that become

phosphorylated (activated) following a specific stimulus. Chan and Sawchenko (1994) reported changes in Fos expression in catecholamine cells in the brainstem following hemorrhage, which is a rather complicated stimulus in terms of the evoked autonomic responses. Chan and Sawchenko (1994) did not report a mediolateral change in cell activation of the type seen here.

In functional studies, it was suggested that certain parts of the RVLM have different functions. McAllen and Dampney (1990) reported a differential activation of skeletal versus renal beds, depending on the part of the RVLM that was activated. Our data supports the idea that there are different parts of the RVLM that may be involved in management of sympathetic outflow to different autonomic beds. In previous studies, it was elegantly demonstrated that at rest renal nerve activity is not extremely elevated, however, after treatment with sodium nitroprusside and a collapse in BP there is a massive increase in sympathetic activity (Kunitake and Kannan, 2000). We suggest that the engagement of the centromedial compartment of the RVLM may be important in this response. Clearly, further work now needs to be undertaken to

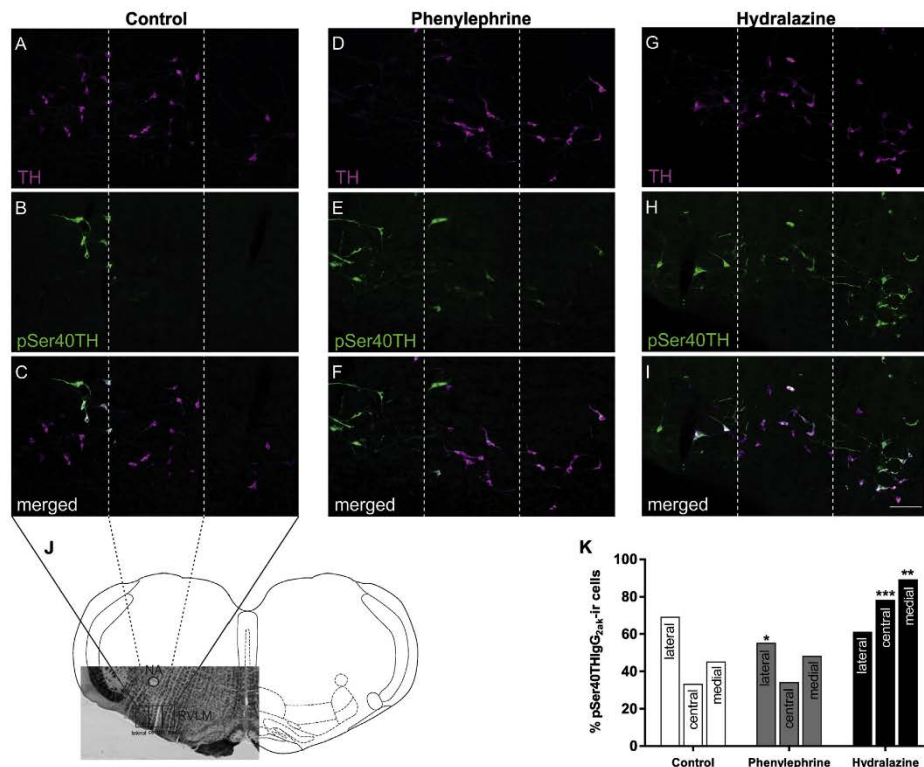


Fig. 4. Representative images of immunohistochemical labeling of RVLM neurons using mouse monoclonal antibodies raised against THlgG_{1k} (magenta) and pSer40THlgG_{2ak} (green) following (A–C) saline, (D–F) phenylephrine and (G–I) hydralazine infusion; (J) Diagram is adapted from Fig. 136 (Paxinos, 2007); boxed area represents lateral, central and medial RVLM, applicable to (A–I) images; (K) lateromedial distribution of pSer40THlgG_{2ak}-ir neurons in the RVLM represented as a percentage of double-labeled (pSer40THlgG_{2ak}-ir/THlgG_{1k}-ir) vs single-labeled (THlgG_{1k}-ir) neurons in the lateral, central and medial RVLM regions following 2-h i.v. infusion of saline (white bars), 10 µg/kg/min of phenylephrine (gray bars) or 10 mg/kg of hydralazine (black bars). Statistical comparisons were made using exact test for goodness-of-fit for the pooled data from 3 animals; * $P < 0.05$, ** $P < 0.01$, *** $P < 0.001$; NA – nucleus ambiguus, RVLM – rostral ventrolateral medulla. Scale bar in (I) = 100 µm, applicable to (A–I). (For interpretation of the references to color in this figure legend, the reader is referred to the web version of this article.)

determine the specificity of such an arrangement, and the use of our two novel mAbs may provide a powerful adjunctive tool to approach such questions in the RVLM and in other nuclei and tissues where TH is used as an enzyme to produce DOPA and dopamine.

What constitutes neuronal activation? Previous studies have attempted to address this question by examining changes in the expression of a number of markers. One of the most popular and stable of these has been Fos protein (Minson et al., 1995; Kovács, 2008). Following neuronal depolarization Fos and Jun form a stable dimer that enters the nucleus and attaches to the cyclic AMP response element binding site to cause a large increase in proteins that include angiotensin related proteins, catecholamine related proteins and many kinases. This process occurs over many hours (Reja et al., 2002, 2006). Although Fos IHC is an extremely useful tool for determining the activation state of

neurons, there are neurons that do not express Fos (Weston et al., 2003). On the other hand, the use of phosphorylated proteins may provide a better 'snapshot' of the activation state of a cell (Xu et al., 1998; Springell et al., 2005a,b). Unfortunately, in some cases protein phosphorylation can be a delicate and ephemeral state that is difficult to capture with IHC as we have reported in the case of MAP kinase (Xu et al., 1998; Springell et al., 2005a,b).

Here we reveal that phosphorylation of TH is indicative of a subset of activated C1 neurons, providing a new and effective tool to study catecholaminergic neurons during or after short physiological challenges.

A critical advantage of pSer40THlgG_{2ak} IHC is that this technique can be used even under urethane anesthesia (see Fig. 5). Fos is quite sensitive to the use of anesthesia, and while it will cope with light pentobarbitone sodium anesthesia, urethane anesthesia can significantly increase the level of baseline

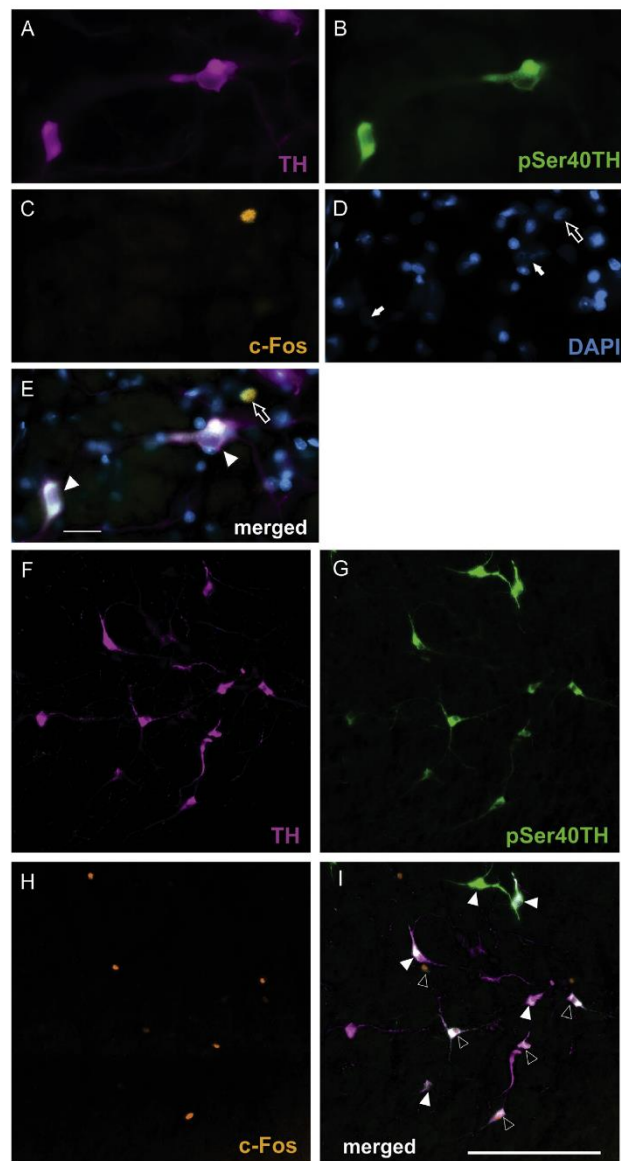


Fig. 5. c-Fos-, pSer40THIgG_{2aκ}- and THIgG_{1κ}-ir in the RVLN following >2 h urethane anesthesia and i.v. saline infusion. (A, F) THIgG_{1κ}-ir neurons; (B, G) pSer40THIgG_{2aκ}-ir neurons; (C, H) c-Fos-ir cells; (D) DAPI nuclear stain; (E, I) co-localized. White arrows represent nuclei of pSer40THIgG_{2aκ}/THIgG_{1κ}-ir neurons; open arrow represents nucleus of c-Fos-ir neuron; open arrowheads indicate co-localization of c-Fos/pSer40THIgG_{2aκ}/THIgG_{1κ}, white arrowheads designate pSer40THIgG_{2aκ}/THIgG_{1κ} co-localization without any c-Fos staining. Scale bars are 50 μm (in E), applicable to (A–E)); 100 μm (in I), applicable to (F–I)).

expression of Fos protein (Rocha and Herbert, 1997). MAP kinase, which we used previously, would not tolerate any long term anesthetic at all (Xu et al., 1998; Springell

et al., 2005a,b). A disadvantage of using phosphorylated TH is that it is only useful in the context of neurons that contain this enzyme. Nevertheless, our findings do

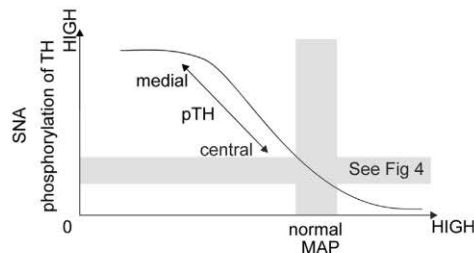


Fig. 6. A simplified mechanistic explanation of the findings in this paper. As is well-known, only a small amount of sympathetic nerve activity (SNA) is required to maintain normal mean arterial pressure (MAP; gray box). Here, we report for the first time that this is reflected not only in the extent of phosphorylation of tyrosine hydroxylase (TH), but also in the location of the phosphorylated tyrosine hydroxylase (pTH) neurons. Normally, pTH is prominent in the lateral rostral ventrolateral medulla (RVLM). As MAP falls, under the influence of hydralazine (see Fig. 4), SNA rises, and as we show here, there is a marked increase in pTH, that is especially notable in the central and medial parts of the RVLM.

suggest that other phenotypic specific opportunities may arise in the future.

The most important advantages of the new antibodies are that they are effective at a high titer, they are completely selective for their antigen (absorption test), and secondary antibodies are commercially available (Jackson ImmunoResearch, Cat. # 115-545-206 and 115-175-205). Samples of the primary mAbs are available on request from the corresponding author.

In summary, we have developed two new mAbs that enabled us to examine activation states in the RVLM. We discovered that in the resting state, during suppression of activity following phenylephrine administration, C1 neurons tended to be activated mostly in the lateral parts of the RVLM, whereas baroreceptor unloading, following hydralazine infusion, resulted in the activation of a significant number of centromedially located TH-ir neurons. The findings reported here demonstrate for the first time that there is a topographical activation state of C1 neurons in response to a physiological stimulus. It remains to be determined if other neurotransmitters, apart from adrenergic transmitters are also differentially organized within cardiovascular neurons in this region. The use of phosphorylated TH and TH antibodies provides a useful first step in probing these possibilities.

GRANTS

This work was supported by the Australian Research Council (Discovery Early Career Researcher Award DE120100992), the National Health and Medical Research Council of Australia (Grants 1065485 and 1082215 and Fellowship 1024489), Macquarie University and the Heart Research Institute.

DISCLOSURES

The authors declare no competing financial interests.

AUTHOR CONTRIBUTIONS

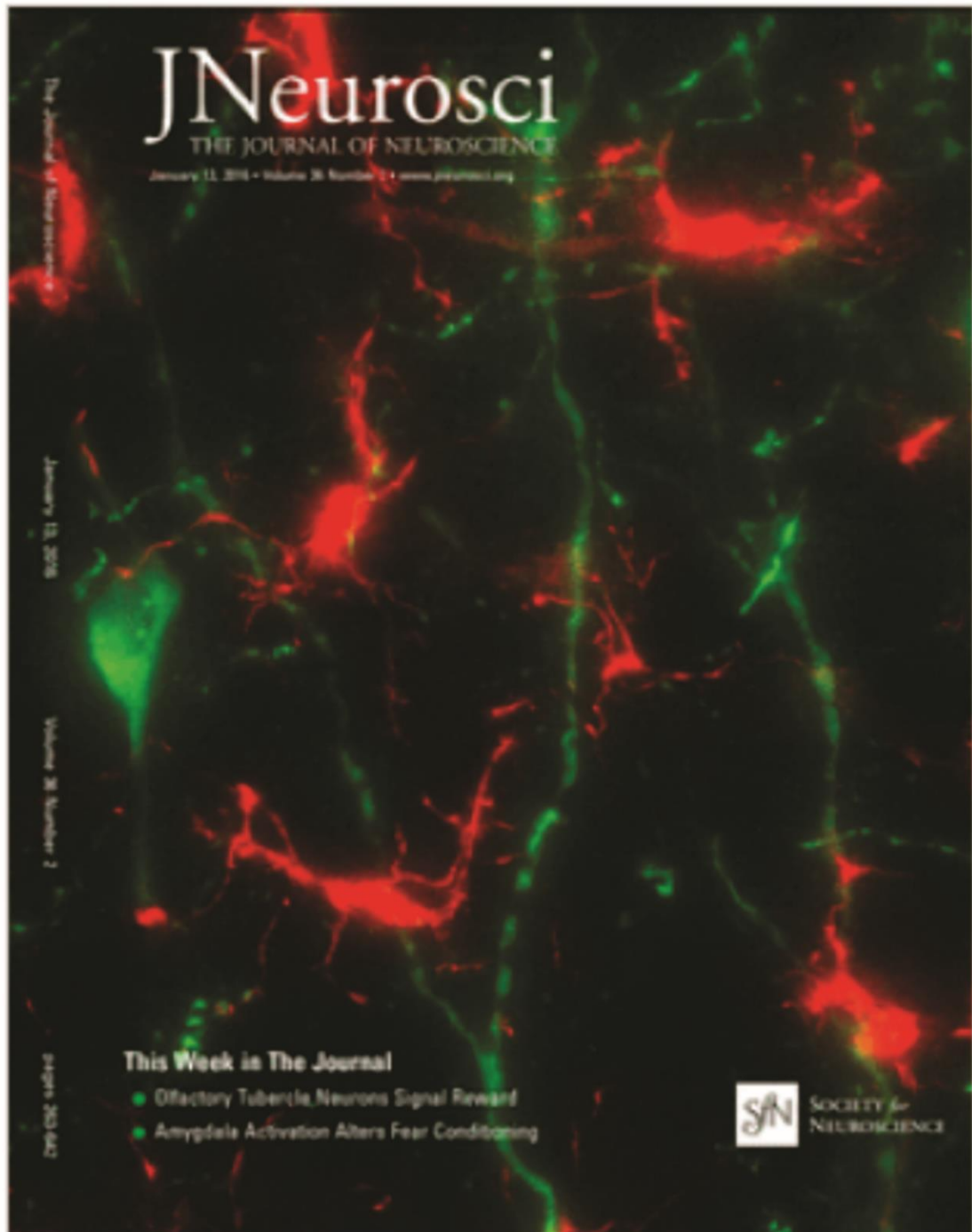
P.E.N., P.M.P. and M.M.J.F. designed research; P.E.N., S.M., K.K., and A.M.B. performed research; P.E.N. and P.M.P. analyzed data; P.E.N., P.M.P. and M.M.J.F. wrote the paper. The authors thank Casey Rieck, Joey Montgomery and Michael Goings for assistance in antibody characterization and buffer preparation.

REFERENCES

- Burke PG, Neale J, Korim WS, McMullan S, Goodchild AK (2011) Patterning of somatosympathetic reflexes reveals nonuniform organization of presympathetic drive from C1 and non-C1 RVLM neurons. *Am J Physiol* 301:R1112–R1122.
- Chan RK, Sawchenko PE (1994) Spatially and temporally differentiated patterns of c-fos expression in brainstem catecholaminergic cell groups induced by cardiovascular challenges in the rat. *J Comp Neurol* 348:433–460.
- Chan RK, Sawchenko PE (1998) Organization and transmitter specificity of medullary neurons activated by sustained hypertension: implications for understanding baroreceptor reflex circuitry. *J Neurosci* 18:371–387.
- Damanhuri HA, Burke PG, Ong LK, Bobrovskaya L, Dickson PW, Dunkley PR, Goodchild AK (2012) Tyrosine hydroxylase phosphorylation in catecholaminergic brain regions: a marker of activation following acute hypotension and glucoprivation. *PLoS One* 7:e50535.
- Dunkley PR, Bobrovskaya L, Graham ME, von Nagy-Felsobuki EI, Dickson PW (2004) Tyrosine hydroxylase phosphorylation: regulation and consequences. *J Neurochem* 91:1025–1043.
- Guyenet PG, Haselton JR, Sun MK (1989) Sympathoexcitatory neurons of the rostral ventrolateral medulla and the origin of the sympathetic vasomotor tone. *Prog Brain Res* 81:105–116.
- Hökfelt T, Fuxe K, Goldstein M, Johansson O (1973) Evidence for adrenaline neurons in the rat brain. *Acta Physiol Scand* 89:286–288.
- Hökfelt T, Fuxe K, Goldstein M, Johansson O (1974) Immunohistochemical evidence for the existence of adrenaline neurons in the rat brain. *Brain Res* 66:235–251.
- Horiuchi J, Dampney RAL (1998) Dependence of sympathetic vasomotor tone on bilateral inputs from the rostral ventrolateral medulla in the rabbit: role of baroreceptor reflexes. *Neurosci Lett* 248:113–116.
- Kovács KJ (2008) Measurement of immediate-early gene activation: c-fos and beyond. *J Neuroendocrinol* 20:665–672.
- Kunitake T, Kannan H (2000) Discharge pattern of renal sympathetic nerve activity in the conscious rat: spectral analysis of integrated activity. *J Neurophysiol* 84:2859–2867.
- McAllen RM, Dampney RA (1990) Vasomotor neurons in the rostral ventrolateral medulla are organized topographically with respect to type of vascular bed but not body region. *Neurosci Lett* 110:91–96.
- McDonald JH (2014) Handbook of biological statistics. 3rd ed. Baltimore, Maryland: Sparky House Publishing.
- Minson JB, Suzuki S, Llewellyn-Smith IJ, Pilowsky PM, Arnold LF, Chalmers JP (1995) C-FOS expression in central cardiovascular pathways. *Clin Exp Hypertens* 17:67–79.
- Minson J, Arnold L, Llewellyn-Smith I, Pilowsky P, Chalmers J (1996a) Altered c-fos in rostral medulla and spinal cord of spontaneously hypertensive rats. *Hypertension* 27:433–441.
- Minson JB, Arnold LF, Llewellyn-Smith IJ, Pilowsky PM, Suzuki S, Chalmers JP (1996b) Immediate early genes in blood pressure regulation. *Clin Exp Hypertens* 18:279–290.
- Miyawaki T, Pilowsky P, Sun QJ, Minson J, Suzuki S, Arnold L, Llewellyn-Smith I, Chalmers J (1995) Central inspiration increases barosensitivity of neurons in rat rostral ventrolateral medulla. *Am J Physiol* 268:R909–R918.

- Morrison SF, Cao WH (2000) Different adrenal sympathetic preganglionic neurons regulate epinephrine and norepinephrine secretion. *Am J Physiol* 279:R1763–R1775.
- Parker LM, Kumar NN, Lonergan T, McMullan S, Goodchild AK (2015) Distribution and neurochemical characterization of neurons in the rat ventrolateral medulla activated by glucoprivation. *Brain Struct Funct* 220:117–134.
- Paxinos G (2007) *The rat brain in stereotaxic coordinates*/George Paxinos, Charles Watson. Amsterdam: Elsevier.
- Phillips JK, Goodchild AK, Dubey R, Sesiasvili E, Takeda M, Chalmers J, Pilowsky PM, Lipski J (2001) Differential expression of catecholamine biosynthetic enzymes in the rat ventrolateral medulla. *J Comp Neurol* 432:20–34.
- Pilowsky P, West M, Chalmers J (1985) Renal sympathetic nerve responses to stimulation, inhibition and destruction of the ventrolateral medulla in the rabbit. *Neurosci Lett* 60:51–55.
- Pilowsky PM, Lung MS, Spirovski D, McMullan S (2009) Differential regulation of the central neural cardiorespiratory system by metabotropic neurotransmitters. *Philos Trans R Soc Lond B Biol Sci* 364:2537–2552.
- Raghuraman G, Rai V, Peng YJ, Prabhakar NR, Kumar GK (2009) Pattern-specific sustained activation of tyrosine hydroxylase by intermittent hypoxia: role of reactive oxygen species-dependent downregulation of protein phosphatase 2A and upregulation of protein kinases. *Antioxid Redox Signal* 11:1777–1789.
- Reja V, Goodchild AK, Pilowsky PM (2002) Catecholamine-related gene expression correlates with blood pressures in SHR. *Hypertension* 40:342–347.
- Reja V, Goodchild AK, Phillips JK, Pilowsky PM (2006) Upregulation of angiotensin AT1 receptor and intracellular kinase gene expression in hypertensive rats. *Clin Exp Pharmacol Physiol* 33:690–695.
- Rocha MJ, Herbert H (1997) Effects of anesthetics on Fos protein expression in autonomic brain nuclei related to cardiovascular regulation. *Neuropharmacology* 36:1779–1781.
- Ross CA, Ruggiero DA, Joh TH, Park DH, Reis DJ (1984) Rostral ventrolateral medulla: selective projections to the thoracic autonomic cell column from the region containing C1 adrenaline neurons. *J Comp Neurol* 228:168–185.
- Schreihofer AM, Guyenet PG (1997) Identification of C1 presympathetic neurons in rat rostral ventrolateral medulla by juxtacellular labeling in vivo. *J Comp Neurol* 387:524–536.
- Schreihofer AM, Guyenet PG (2000) Role of presympathetic C1 neurons in the sympatholytic and hypotensive effects of donidine in rats. *Am J Physiol* 279:R1753–R1762.
- Spirovski D, Li Q, Pilowsky PM (2012) Brainstem galanin-synthesizing neurons are differentially activated by chemoreceptor stimuli and represent a subpopulation of respiratory neurons. *J Comp Neurol* 520:154–173.
- Springell DA, Costin NS, Pilowsky PM, Goodchild AK (2005a) Hypotension and short-term anaesthesia induce ERK1/2 phosphorylation in autonomic nuclei of the brainstem. *Eur J Neurosci* 22:2257–2270.
- Springell DA, Powers-Martin K, Phillips JK, Pilowsky PM, Goodchild AK (2005b) Phosphorylated extracellular signal-regulated kinase 1/2 immunoreactivity identifies a novel subpopulation of sympathetic preganglionic neurons. *Neuroscience* 133:583–590.
- Sun MK, Reis DJ (1996) Medullary vasomotor activity and hypoxic sympathoexcitation in pentobarbital-anesthetized rats. *Am J Physiol* 270:R348–R355.
- Verberne AJ, Sartor DM (2004) CCK-induced inhibition of presympathetic vasomotor neurons: dependence on subdiaphragmatic vagal afferents and central NMDA receptors in the rat. *Am J Physiol* 287:R809–R816.
- Weston M, Wang H, Stornetta RL, Sevigny CP, Guyenet PG (2003) Fos expression by glutamatergic neurons of the solitary tract nucleus after phenylephrine-induced hypertension in rats. *J Comp Neurol* 460:525–541.
- Xu ZQ, Lew JY, Harada K, Aman K, Goldstein M, Deutch A, Haycock JW, Hokfelt T (1998) Immunohistochemical studies on phosphorylation of tyrosine hydroxylase in central catecholamine neurons using site- and phosphorylation state-specific antibodies. *Neuroscience* 82:727–738.

(Accepted 5 January 2016)
(Available 12 January 2016)



Seizure-Induced Sympathoexcitation Is Caused by Activation of Glutamatergic Receptors in RVLM That Also Causes Proarrhythmogenic Changes Mediated by PACAP and Microglia in Rats

Amol M. Bhandare,^{1,2} Komal Kapoor,^{1,2} Paul M. Pilowsky,^{1,3} and Melissa M.J. Farnham^{1,3}

¹The Heart Research Institute, Sydney 2042, New South Wales, Australia, ²Faculty of Medicine and Health Sciences, Macquarie University, Sydney 2109, New South Wales, Australia, and ³Department of Physiology, University of Sydney, Sydney 2006, New South Wales, Australia

Cardiovascular autonomic dysfunction in seizure is a major cause of sudden unexpected death in epilepsy. The catecholaminergic neurons in the rostral ventrolateral medulla (RVLM) maintain sympathetic vasomotor tone and blood pressure through their direct excitatory projections to the intermediolateral (IML) cell column. Glutamate, the principal excitatory neurotransmitter in brain, is increased in seizures. Pituitary adenylate cyclase activating polypeptide (PACAP) is an excitatory neuropeptide with neuroprotective properties, whereas microglia are key players in inflammatory responses in CNS. We investigated the roles of glutamate, PACAP, and microglia on RVLM catecholaminergic neurons during the cardiovascular responses to 2 mg/kg kainic acid (KA)-induced seizures in urethane anesthetized, male Sprague Dawley rats. Microinjection of the glutamate antagonist, kynurenic acid (50 nM; 100 mM) into RVLM, blocked the seizure-induced $43.2 \pm 12.6\%$ sympathoexcitation ($p \leq 0.05$), and abolished the pressor responses, tachycardia, and QT interval prolongation. PACAP or microglia antagonists (50 nM) (PACAP(6–38), 15 pmol; minocycline 10 mg/ml) microinjected bilaterally into RVLM had no effect on seizure-induced sympathoexcitation, pressor responses, or tachycardia but abolished the prolongation of QT interval. The actions of PACAP or microglia on RVLM neurons do not cause sympathoexcitation, but they do elicit proarrhythmogenic changes. An immunohistochemical analysis in 2 and 10 mg/kg KA-induced seizure rats revealed that microglia surrounding catecholaminergic neurons are in a “surveillance” state with no change in the number of M2 microglia (anti-inflammatory). In conclusion, seizure-induced sympathoexcitation is caused by activation of glutamatergic receptors in RVLM that also cause proarrhythmogenic changes mediated by PACAP and microglia.

Key words: glutamate; microglia; PACAP; rat; seizure; sympathetic

Significance Statement

Sudden unexpected death in epilepsy is a major cause of death in epilepsy. Generally, seizures are accompanied by changes in brain function leading to uncontrolled nerve activity causing high blood pressure, rapid heart rate, and abnormal heart rhythm. Nevertheless, the brain chemicals causing these cardiovascular changes are unknown. Chemicals, such as glutamate and pituitary adenylate cyclase activating polypeptide, whose expression is increased after seizures, act on specific cardiovascular nuclei in the brain and influence the activity of the heart, and blood vessels. Microglia, which manage excitation in the brain, are commonly activated after seizure and produce pro- and/or anti-inflammatory factors. Hence, we aimed to determine the effects of blocking glutamate, pituitary adenylate cyclase activating polypeptide, and microglia in the RVLM and their contribution to cardiovascular autonomic dysfunction in seizure.

Introduction

Seizure-induced cardiovascular autonomic dysfunction is a common cause of sudden unexpected death in epilepsy (SUDEP),

which accounts for 5%–17% deaths in people with epilepsy (Sakamoto et al., 2008; Surges et al., 2009; Bardai et al., 2012; Massey et al., 2014). The rostral ventrolateral medulla (RVLM)

Received July 8, 2015; revised Oct. 6, 2015; accepted Nov. 25, 2015.

Author contributions: A.M.B., P.M.P., and M.M.J.F. designed research; A.M.B., K.K., and M.M.J.F. performed research; A.M.B., K.K., P.M.P., and M.M.J.F. contributed unpublished reagents/analytic tools; A.M.B., K.K., P.M.P., and M.M.J.F. analyzed data; A.M.B., K.K., P.M.P., and M.M.J.F. wrote the paper.

This work was supported by Australian Research Council Discovery Early Career Researcher Award DE120100992, and National Health and Medical Research Council of Australia Grants 1024489, 1065485, and 1082215. A.M.B. and K.K. were supported by International Macquarie University Research Excellence Scholarships 2012/219 and 2012/112, the Heart Research Institute, and the University of Sydney.

contains sympathetic premotor neurons (C1), which are a subset of catecholaminergic neurons that express all of the enzymes necessary for the synthesis of adrenaline (Schreihofer and Guyenet, 1997; Phillips et al., 2001). Sympathetic vasomotor tone and blood pressure are regulated by C1 neurons, and another smaller population of neurons that is also located in the RVLM, through their direct projections to the intermediolateral (IML) cell column (Ross et al., 1984; Guyenet, 2006; Pilowsky et al., 2009). Seizure-induced increased activity of C1 catecholaminergic neurons (*c-fos*) is well documented (Kanter et al., 1995; Silveira et al., 2000). Seizure causes an increase in sympathetic nerve activity (SNA) and has significant effect on cardiac electrophysiology and heart rate (HR) (Nei et al., 2004; Metcalf et al., 2009; Damasceno et al., 2013). There is no information about the neurotransmitters mediating activation of brainstem catecholaminergic neurons contributing to the autonomic manifestations that frequently accompany epileptic seizures.

As we have documented previously, low-dose kainic acid (KA)-induced seizures in rat cause sympathoexcitation, increases in mean arterial pressure (MAP) and HR, and proarrhythmic changes, including prolongation of the QT interval (Bhandare et al., 2015). The evidence suggests that pituitary adenylate cyclase activating polypeptide (PACAP) and microglia have a protective effect on sympathetic preganglionic neurons in the IML cell column where they ameliorate the sympathoexcitatory effect of seizures. PACAP is well established to be neuroprotective (Shioda et al., 1998; Ohtaki et al., 2006), through its effect on microglia (Wada et al., 2013). Recently, we investigated the excitatory effect of PACAP in cardiovascular autonomic nuclei (Farnham et al., 2008, 2012). KA-induced seizures dramatically increase PACAP expression in central autonomic nuclei (paraventricular nucleus) (Nomura et al., 2000). Additionally, microglia can be pro- or anti-inflammatory in some models of diseases, such as temporal lobe epilepsy (Shapiro et al., 2008; Mirrione et al., 2010; Vinet et al., 2012). In seizure, there is extensive activation of microglia in patients and in animal models (Beach et al., 1995; Shapiro et al., 2008; Eyo et al., 2014). Moreover, there are reports suggesting that PACAP modulates the activated microglial state (Wada et al., 2013; Brifault et al., 2015). This important relationship between PACAP, microglia, and seizure-induced increase in its expression or activation in cardiovascular autonomic nuclei makes them a very promising target in the development of therapy for seizure-induced sympathoexcitation and cardiovascular dysfunction. In addition, brain glutamate levels are increased in patients and animal models of temporal lobe epilepsy (Meldrum et al., 1999; Blümcke et al., 2000) and play a major pathogenic role for neuronal hyperexcitability. However, glutamatergic drive within RVLM neurons is not important for maintenance of basal tonic activity of catecholaminergic neurons or blood pressure (Guyenet et al., 1987; Araujo et al., 1999; Sved et al., 2002). Collectively, the sympathoexcitation during seizure may be due to an increased glutamate turnover that could be reversed by glutamate antagonist microinjection into RVLM without affecting basal sympathetic output and blood pressure.

Overall, the aims of this study were to identify the role of PACAP, microglia, and glutamatergic receptors in the RVLM to regulate catecholaminergic neuronal hyperexcitability and other

cardiovascular changes following low-dose KA-induced seizures in rats. To achieve these aims, we used a combination of electrophysiological and neuroanatomical approaches with KA-induced seizures in rats. Seizures were induced with 2 mg/kg intraperitoneal KA injection in urethane anesthetized, vagotomized, paralyzed, and artificially ventilated rats and 50 nl of each PACAP antagonist, PACAP(6–38); microglia antagonist, minocycline; or glutamate antagonist, kynurenic acid (KYNA) were microinjected into the RVLM of different group of rats. The changes in microglial morphology and the expression of the anti-inflammatory M2 microglial phenotype in the vicinity of RVLM catecholaminergic neurons in response to 2 and 10 mg/kg KA-induced seizures in rats were analyzed with immunohistochemistry.

Materials and Methods

Animals. The animal usage and protocols were in accordance with the Australian code of practice for the care and use of animals for scientific purposes. The protocols were approved by the Animal Care and Ethics Committee of Macquarie University and the Sydney Local Health District. All electrophysiology and histology experiments were conducted on adult male Sprague-Dawley rats (250–350 g; Animal Resources Centre).

Surgical preparations. For electrophysiology experiments ($n = 31$), rats were anesthetized with 10% urethane (ethyl carbamate; 1.3–1.5 g/kg i.p.; Sigma-Aldrich) and for histology experiments ($n = 15$) with 3% sodium pentobarbital (50 mg/kg i.p.; Virbac). The depth of anesthesia was monitored by observing reflex responses (withdrawal or pressor >10 mmHg) to nociceptive stimuli (periodic tail/paw pinches). Additional anesthetic was injected (30–40 mg, 10% urethane i.v. or 1.5–2.0 mg, sodium pentobarbital i.v.), if reflex responses were observed. Atropine sulfate (100 μ g/kg, i.p.; Pfizer) was administered with the first dose of anesthetics to prevent bronchial secretions. After the completion of the general surgical procedures described below, rats were secured in a stereotaxic frame and body temperature was recorded and maintained between 36.5°C and 37.5°C throughout the experiment using a homeothermic blanket (TC-1000; CWE).

General surgical procedures and electroencephalogram (EEG) electrode placement. Procedures were performed as described previously (Bhandare et al., 2015). Briefly, the right carotid artery and jugular vein were cannulated for recording of blood pressure, and for administration of drugs and fluids, respectively, with a tracheostomy to enable mechanical ventilation. A three lead electrocardiogram (ECG; front paws, hindpaw) was recorded, and HR was derived from it. Rats were vagotomized, artificially ventilated with oxygen-enriched room air, and paralyzed with pancuronium bromide. Arterial blood gases were analyzed with an electrolyte and blood gas analyzer (IDEXX, Vetstat). PaCO_2 was maintained at 40 ± 2 and pH between 7.35 and 7.45.

For the placement of EEG electrodes, burr holes were drilled bilaterally for recording over the dorsal hippocampus (5.2 mm anterior to lambda, 3 mm lateral to midline, and 2–3 mm below the skull surface), and electrode positions were confirmed with cresyl violet staining. A single 75 μ m Teflon-insulated stainless steel wire (A-M Systems) was inserted into each hole using stereotaxic manipulator. The signals were amplified (CWE, BMA-931 Bioamplifier), bandpass filtered from 1 Hz to 10 kHz, and digitized at 20 kHz with a $100\times$ gain.

Seizure induction. For electrophysiology experiments, seizures were induced by intraperitoneal injection of 2 mg/kg KA in Sprague Dawley rats (Bhandare et al., 2015). In the histology study, two doses of KA (2 and 10 mg/kg; i.p.) were used to elicit mild and severe seizures in rats to analyze their effects on the morphology of microglia in the vicinity of catecholaminergic neurons in RVLM; 2 mg/kg is the lowest dose of KA required to induce seizure and sympathoexcitation (Bhandare et al., 2015), whereas 10 mg/kg KA induces status epilepticus with generalized tonic-clonic seizures in rats (Nadler, 1981; Sperk et al., 1983). However, in our study, rats were paralyzed and had no behavioral seizures. KA responses were recorded for 2 h after KA injection, during which continuous monitoring of EEG was used to identify the development of sei-

The authors declare no competing financial interests.

Correspondence should be addressed to Dr. Paul M. Pilowsky, Heart Research Institute, 7 Eliza Street, Sydney 2042, NSW, Australia. E-mail: paul.pilowsky@hri.org.au.

DOI:10.1523/JNEUROSCI.2584-15.2016

Copyright © 2016 the authors 0270-6474/16/360507-12\$15.00/0

zures. To investigate the duration of seizure-induced cardiovascular responses, 2 mg/kg KA-induced seizures were recorded until cardiovascular parameters returned to baseline ($n = 4$).

In vivo electrophysiology: isolation and preparation of nerves. The left greater splanchnic sympathetic nerve at a site proximal to the celiac ganglion, and the left phrenic nerve were isolated, dissected, and tied with 5/0 silk thread. Nerve activity was recorded using bipolar stainless steel electrodes. Signals were amplified (CWE, BMA-931 Bioamplifiers) (sampling rate: 6 kHz, gain: 2000, filtering: 30–3000 Hz) and filtered with a 50/60 Hz line frequency filter (Humboldt Quest Scientific).

RVLM site detection, confirmation and microinjection. The dorsal surface of the medulla oblongata was exposed by occipital craniotomy and the dura was removed. The bilateral RVLM stereotaxic coordinates were measured with respect to calamus scriptorius and confirmed if a 50 nl microinjection of 100 mmol/L glutamate increased blood pressure > 30 mmHg. After glutamate confirmation, stable baseline parameters were recorded for at least for 30 min.

In vehicle and KA control groups of rats ($n = 5$), 50 nl of 10 mmol/L PBS was microinjected bilaterally in the RVLM; 50 nl of 15 pmol of PACAP(6–38) (150 μ mol/L in 100 nl) (Auspep, Selleck) was microinjected bilaterally in the RVLM ($n = 6$) (Farnham et al., 2012). Minocycline (10 mg/ml) ($n = 6$) (LeBlanc et al., 2011) and KYNA (100 mM) ($n = 5$) (Miyawaki et al., 2002) were bilaterally microinjected in the RVLM in doses of 50 nl in different groups of rats. In all rats, microinjections were made 15 min before intraperitoneal KA or PBS injection. Microinjections were not made in $n = 4$ rats that were used to investigate the duration of KA-induced cardiovascular effects. At the conclusion of the experiment, 50 nl of Chicago Sky Blue (2%) was microinjected at the site of the RVLM, and rats were either killed with 0.5 ml of 3 M potassium chloride (KCl; i.v.) or deeply anesthetized and perfused with 400 ml of ice-cold 0.9% saline followed by 400 ml of 4% PFA solution. The brains were removed from the perfused rats and postfixed in the same fixative overnight. Cerebrum and brainstem were sectioned coronally (100 μ m) and stained with cresyl violet for histological verification of the EEG electrode positions in hippocampus and microinjection site in RVLM, respectively.

Histology: perfusions. At the conclusion of the experiment, rats used for histology study (in all groups; $n = 5$) were deeply anesthetized with an overdose of sodium pentobarbital and given 1 ml of heparin via the venous line. Rats were transcardially perfused with 400 ml of ice-cold 0.9% saline followed by 400 ml of 4% PFA solution. The brains were then removed and postfixed in the same fixative for 18–24 h.

Sectioning and immunohistochemistry. Immunohistochemical analysis was done in $n = 3$ of 5 rats in each group. Brainstems were sectioned coronally (40 μ m thick) with a vibrating microtome (Leica, VT1200S) and collected sequentially into five different pots containing a cryoprotectant solution and stored at -20°C until further processing. Free floating sections were used for all histological procedures. Sections were rinsed, blocked, and incubated in primary antibodies: mouse anti-tyrosine hydroxylase (TH) (1:500; Sigma-Aldrich), rabbit anti-CD206 (1:2000; Abcam), and goat anti-Iba1 (1:1000; Novus Biologicals). After 48 h, sections were rinsed and TH, CD-206, and Iba1 immunoreactivity was subsequently revealed by overnight incubation with the following secondary antibodies at 1:500 dilutions (Jackson ImmunoResearch Laboratories): Cy5-conjugated donkey anti-mouse, AlexaFluor-488-conjugated donkey anti-rabbit, and Cy3-conjugated donkey anti-goat. Sections were rinsed, mounted sequentially on glass slides, and coverslipped with Vectashield (Vector Laboratories).

Data acquisition and analysis: electrophysiology data. Data were acquired using a CED 1401 ADC system (Cambridge Electronic Design) and Spike 2 acquisition and analysis software (version 8.03; Cambridge Electronic Design). The EEG activity raw data were DC removed. The power in the “gamma” frequency range (25–45 Hz) was analyzed, as previously shown (Olsson et al., 2006; Gurbanova et al., 2008). A power spectrum analysis was done from 5 min blocks taken 1 min before microinjection or intraperitoneal injection and 60 and 120 min after intraperitoneal injection. The percentage change in power spectrum area was calculated for each rat at 60 and 120 min after intraperitoneal injection compared with pretreatment area (taken as 100%) and grouped together.

Phrenic nerve activity (PNA) was rectified and smoothed ($\tau 0.5$ s). PNA was analyzed from 1 min blocks taken 1 min before microinjection and 60 and 120 min after intraperitoneal injection. The percentage change in PNA area under curve (AUC) was analyzed at 60 and 120 min and compared with the pretreatment area (taken as 100%). SNA was rectified, smoothed ($\tau 2$ s), and normalized to zero by subtracting the residual activity 5–10 min after death. The integrated SNA trace was calibrated (baseline as 100%) and analyzed for AUC between 60 and 120 min after intraperitoneal KA or PBS injection. MAP and HR were analyzed from 1 min blocks taken 1 min before microinjection or intraperitoneal injection and 30, 60, 90, and 120 min after intraperitoneal injection (only 120 min results are shown in graphs). End-tidal CO_2 and core temperature were analyzed from 1 min blocks taken 1 min before microinjection or intraperitoneal injection and 30, 60, 90, and 120 min after intraperitoneal injection of either KA or PBS. Arterial blood gas levels (PaCO_2 and pH) were measured 10 min before microinjection or intraperitoneal injection and 120 min after KA or PBS injections in all animals. In the rats used to investigate the duration of KA-induced seizures, the duration of effect was analyzed from the time of intraperitoneal KA injection up to the point where SNA, MAP, and HR returned to baseline. Changes in EEG activity were analyzed at the point where SNA returned to baseline and compared against the pre-KA (control) and 60 min post-KA injection (seizure control) period. A log transformation was applied to EEG raw values because variances were not normally distributed, and/or heterogeneous. Statistical analysis was performed in GraphPad Prism software (version 6.05). Statistical significance was determined using one-way ANOVA followed by t tests with the Holm–Sidak correction. Multiple comparisons were done between groups. $p \leq 0.05$ was considered significant.

Histology imaging and analysis. All images were acquired using a Zeiss Axio Imager Z2 (Zeiss). Images were captured at $20\times$ and $40\times$ magnifications. The RVLM is defined as a triangular area ventral to the nucleus ambiguus, medial to the spinal trigeminal tract, and lateral to the inferior olive or the pyramidal tracts. A 0.16 mm^2 box was then placed within the imaged RVLM, and this area was used for analysis. The morphological analysis (branch length and number of endpoint processes) of Iba1-labeled microglial cells in the vicinity of TH-labeled RVLM neurons was performed using ImageJ plugin software, and GraphPad Prism (version 6.05) was used for χ^2 test for goodness of fit. The proportions of CD206-labeled anti-inflammatory M2 microglia in the RVLM of 2 and 10 mg/kg KA treated rats were compared with the vehicle-treated group. The proportion of M2 microglia is equal to the number of M2 microglia divided by the total number of microglia multiplied by 100. Statistical significance was determined using nonparametric Kruskal–Wallis test (Sokal and Rohlf, 2012).

Calculation of corrected QT (QTc) interval. QT, PR, and RR intervals were calculated from the ECG recordings. ECG raw data were processed (DC remove), wherever baseline fluctuations were prominent. QTc interval was calculated by dividing the QT interval in seconds by the square root of the R–R interval in seconds (Bazett, 1920). The QTc was obtained before and 120 min after vehicle or KA injection. The PR and QTc interval statistical analysis was performed in GraphPad Prism software (version 6.05). Statistical significance was determined using one-way ANOVA between treatment groups followed by t tests with the Holm–Sidak correction. Multiple comparisons were done between groups. $p \leq 0.05$ was considered significant.

Results

Sympathoexcitation, tachycardia, and pressor responses due to KA-induced seizures in rats

Intraperitoneal injection of 2 mg/kg KA induces seizures, and subsequently, increases HR, MAP, and SNA in KA control group of rats (Fig. 1A). KA (2 mg/kg i.p.) leads to development of hippocampal seizure activity within ~ 15 –20 min. At this time, there are no changes in sympathetic activity (Fig. 2), blood pressure, or heart rate (Fig. 1A). Ten to 15 min after the start of the hippocampal seizure activity, SNA, MAP, and HR began to increase (Figs. 1A, 2). Autonomic changes are entirely downstream effects of hippocampal seizures as there was no seizure activity (increase in

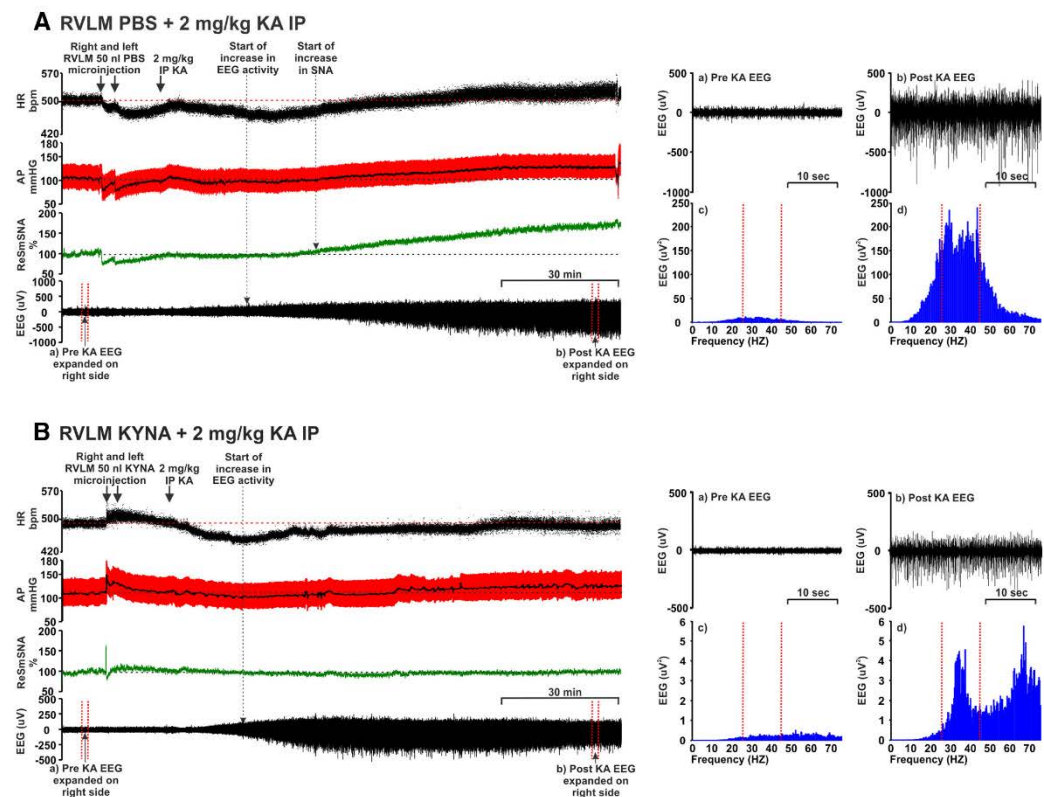


Figure 1. Effect of bilateral RVLM microinjection of (A) PBS (50 nl) and (B) KYNA (50 nl; 100 mM) followed by 2 mg/kg intraperitoneal KA in an anesthetized rat (see Materials and Methods) showing the effect on the following: from the top, (i) HR (bpm), (ii) AP (arterial pressure; mmHg), (iii) SNA (%), and (iv) EEG (μV). Arrow indicates time of RVLM microinjections and intraperitoneal KA. Dotted arrows indicate the starting points for increase in EEG and/or SNA activity. Right side panels, Pre (a) and post (b) KA EEG represents the expanded waveform from respective period. Baseline (a), which is a pre-KA period with desynchronous waves, and (b) post-KA period with increased γ range frequencies and followed by the data from the same EEG, drawn as a power spectrum (c, d, respectively) (during post-KA period γ range frequencies, which is shown between two dotted lines) are increased. Increase in gamma range frequency (25–45 Hz) is characteristic property of KA-induced seizures (Olsson et al., 2006; Gurbanova et al., 2008).

gamma frequency, which is typical sign of KA-induced seizures) in the sympathetic nerve recording until at least 70 min after KA injection, whereas SNA started to increase 25–30 min after KA injection (Fig. 2). Together, these findings indicate that central autonomic nuclei are not the source of KA-induced seizures. Between 60 and 120 min after KA injection, SNA AUC was increased by $43.2 \pm 12.6\%$ ($p = 0.04$) compared with the vehicle control group (Fig. 3A). In the KA-induced seizure group, MAP and HR were increased by 21 ± 4 mmHg ($p = 0.008$) and 32 ± 7 bpm ($p = 0.0001$), respectively, compared with the vehicle-treated group (Fig. 3B, C): the findings support the notion that seizure is the cause of the dramatic increase in sympathetic nerve activity, tachycardia, and pressor effects (Sakamoto et al., 2008; Bealer et al., 2010). Bilateral microinjection of PBS (50 nl) had a transient and nonsignificant effect on MAP, HR, and SNA, that lasted for only a few minutes (Fig. 1A).

The induction of seizures was confirmed with hippocampal EEG recordings; the power spectra were obtained from the same expanded EEG waveforms as indicated (Fig. 1A). The spectral

changes in EEG at 60 and 120 min after KA injection were obtained using Fourier analysis of 5 min EEG intervals and the AUC between gamma frequency range (25–45 Hz). The steep increase in γ wave amplitude was observed at both 60 ($\Delta 1038 \pm 402\%$, $p = 0.0001$) and 120 min ($\Delta 1329 \pm 390\%$, $p = 0.0005$) after KA injection (Figs. 1A, 3D, E). This finding also shows that KA-induced seizures in rats continued for at least 120 min following KA injection, which is consistent with results of the experiments performed to analyze the duration of seizure-induced cardiovascular effects.

KA (2 mg/kg)-induced seizures and its effects on SNA, MAP, and HR lasted for ~ 3 h. After this time, SNA, MAP, and HR returned to baseline values at 170, 196, and 160 min, respectively. At these time points, EEG activity was significantly reduced compared with the seizure period (at 60 min after KA) but did not return to baseline.

We did not observe any changes in PNA, expired CO_2 , or body temperature in any of the groups (results not shown). Blood gas analysis confirmed that PaCO_2 and pH were within normal phys-

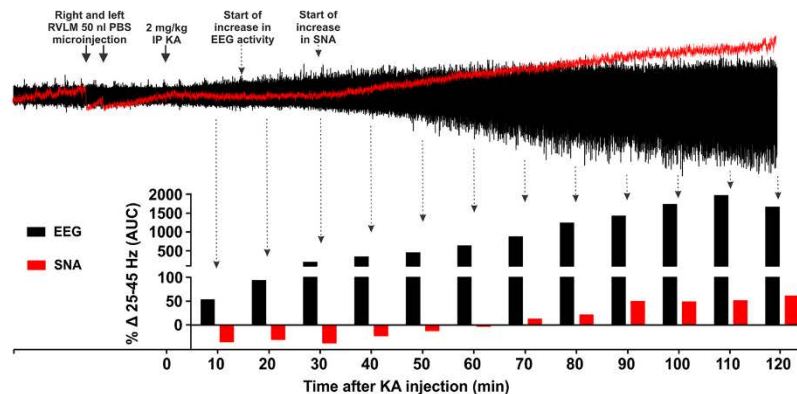


Figure 2. Effects of KA treatment on induction of seizures in hippocampus and central autonomic nuclei. Change in gamma range frequency (25–45 Hz) in hippocampal EEG and sympathetic nerve recordings every 10 min after 2 mg/kg KA injection. Arrow indicates time of RVLM microinjections and intraperitoneal KA. Dotted arrows indicate the starting points for increase in EEG and/or SNA activity. Induction of seizure activity in sympathetic nerve activity does not start at least until 70 min after KA injection, whereas hippocampal seizure activity starts ~15–20 min after KA injection followed by an increase in SNA at 25–30 min. Time-dependent increases in hippocampal seizure activity occur up to 110 min after KA injection followed by a fall.

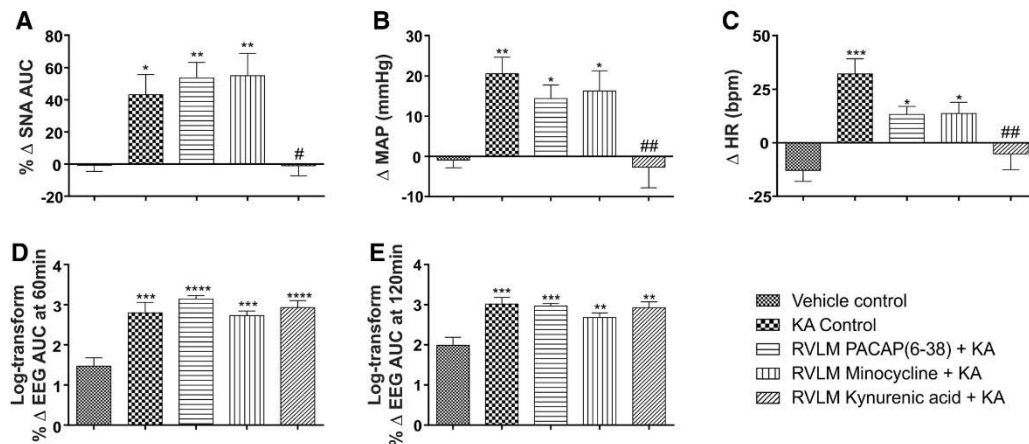


Figure 3. *In vivo* effects of RVLM microinjection of PBS, PACAP(6–38), minocycline, and KYNA in 2 mg/kg KA-induced seizure rats. Change in SNA (AUC) between 60 and 120 min after intraperitoneal treatment (A), change in MAP 120 min after intraperitoneal PBS or KA injection (B), change in HR at 120 min after intraperitoneal PBS or KA injection (C), and log transform of percentage change in EEG activity (gamma wave frequency AUC), at 60 min (D) and 120 min (E) after intraperitoneal PBS or KA injection in different groups of rats after development of seizure. Statistical significance was determined using one-way ANOVA followed by *t* tests with a Holm–Sidak correction. Data are mean \pm SEM. **** $p \leq 0.0001$ compared with vehicle control group. *** $p \leq 0.001$ compared with vehicle control group. ** $p \leq 0.01$ compared with vehicle control group. * $p \leq 0.05$ compared with vehicle control group. # $p \leq 0.05$ compared with KA control group. ## $p \leq 0.01$.

iological range (PaCO₂ was 40 ± 2 and pH between 7.35 and 7.45) throughout the experiment.

Sympathoexcitation, tachycardia, and pressor effects during seizure are caused by glutamatergic receptors in the RVLM and not by PACAP or microglial activation

Our findings demonstrate that sympathoexcitation during seizure is caused by glutamatergic receptor activation in the RVLM because bilateral microinjection of glutamate antagonist KYNA completely abolished the seizure-induced sympathoexcitation in rats (Figs. 1B, 3A). After microinjection of KYNA in five rats, KA-induced seizures were present (Figs. 1B, 3D,E), but pressor and heart rate responses were blocked ($p = 0.005$ and $p = 0.001$,

respectively) compared with KA control group (Figs. 1B, 3B,C). The KA-induced seizures caused no change ($\Delta -1.0 \pm 6.2\%$) in SNA after bilateral microinjection of KYNA and was significantly reduced compared with KA control group ($p = 0.04$). In these groups of rats, MAP and HR were not significantly changed compared with the vehicle-treated group ($\Delta -3 \pm 5$ mmHg and $\Delta -5 \pm 7$ bpm, respectively; Fig. 3B,C). The findings reveal that KA-induced sympathoexcitation, tachycardia, pressor responses along with changes in QT interval are downstream effects of seizure and do not have a direct effect on cardiomyocytes.

Bilateral microinjection of PACAP(6–38) into the RVLM of KA-induced seizure rats did not ameliorate the significant in-

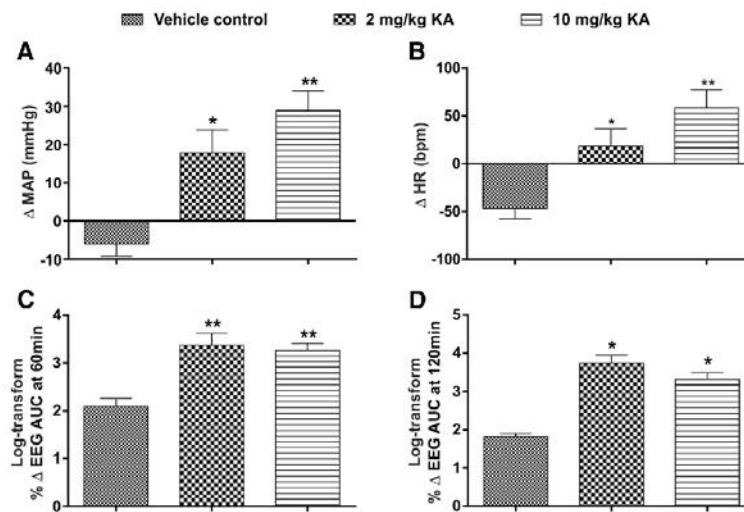


Figure 4. *In vivo* effects of PBS and KA-induced (2 and 10 mg/kg) seizures in rats studied for histology. Change in MAP (A) and HR (B), at 120 min after intraperitoneal PBS or KA (2 and 10 mg/kg) injection and percentage change in EEG activity (gamma wave frequency AUC), at 60 min (C) and 120 min (D) after intraperitoneal PBS or KA (2 and 10 mg/kg) injection in different groups of rats. In all groups, $n = 5$. Statistical significance was determined using one-way ANOVA followed by t tests with a Holm–Šidák correction. Data are mean \pm SEM. ** $p \leq 0.01$ compared with vehicle control group. * $p \leq 0.05$ compared with vehicle control group.

crease in SNA ($\Delta 53.7 \pm 9.6\%$; $p = 0.007$) compared with the vehicle-treated group (Fig. 3A). The HR and MAP responses in PACAP(6–38) group were still significantly increased compared with the vehicle control group of rats (Fig. 3B,C). The lack of response to the PACAP antagonist (PACAP(6–38)) was replicated following bilateral RVLM microinjection of minocycline in seizure-induced rats. Following minocycline, there was a significant increase in SNA ($\Delta 55.1 \pm 13.8\%$; $p = 0.006$; Fig. 3A), as well as MAP and HR ($\Delta 16 \pm 5$ mmHg and $\Delta 14 \pm 5$ bpm; $p = 0.04$ and $p = 0.02$, respectively; Fig. 3B,C) compared with vehicle control group of rats.

After KA induced seizures, microglia are in surveillance state in the vicinity of the RVLM neurons with no change in the proportion of M2 phenotype

Immunohistochemical analysis was done in rats with vehicle treatment and 2 and 10 mg/kg intraperitoneal KA ($n = 3$) to analyze the morphology of Iba1-labeled microglia and proportion of anti-inflammatory M2 phenotype in the vicinity of TH-labeled RVLM neurons. The effect of different doses of KA on MAP, HR, and EEG are shown in Figure 4 ($n = 5$). At 120 min after 2 and 10 mg/kg KA treatment, the MAP ($\Delta 18 \pm 6$ and $\Delta 29 \pm 5$; $p = 0.02$ and 0.001 , respectively; Fig. 4A), HR ($\Delta 18 \pm 18$ and $\Delta 58 \pm 19$; $p = 0.05$ and 0.002 , respectively; Fig. 4B), EEG activity at 60 min ($\Delta 1791 \pm 622$ and $\Delta 1651 \pm 400$; $p = 0.007$ and 0.007 ; respectively; Fig. 4C), and EEG activity at 120 min ($\Delta 4164 \pm 2504$ and $\Delta 1995 \pm 563$; $p = 0.04$ and 0.04 ; respectively; Fig. 4D) were significantly increased compared with vehicle-treated rats. The findings are consistent with *in vivo* electrophysiology data and our previous studies. Immunohistochemical analysis revealed that TH-immunoreactive (ir) neurons were surrounded with typical resting microglial cells in all three groups (Fig. 5A–C). In all three groups, microglia appeared with a round cell body and processes that appeared normal with few ramifications (Fig. 5A–C). The total number of microglia in each group

are shown in Figure 5D. A branch length, and number of endpoint analysis, was performed to identify the activated microglia. There were no differences in mean branch length, and number of endpoint processes of Iba1-labeled microglia between vehicle control and seizure-induced rats (Fig. 5E,F). The proportion of anti-inflammatory M2 phenotype of microglia was $14.2 \pm 1.4\%$ in saline-treated rats, which was similar in 2 and 10 mg/kg KA-treated rats ($10.1 \pm 2.5\%$ and $9.6 \pm 2.4\%$, respectively; Fig. 5G). The findings revealed that microglia are in a surveillance state with no differences in their morphology and proportion of M2 phenotype, at least in the RVLM, between vehicle and seizure-induced groups. These results are consistent with our electrophysiology findings where microinjection of a microglia antagonist had no effect on increase in SNA, MAP, and HR in KA-induced seizure rats.

Proarrhythmic ECG changes during seizures are driven by activation of glutamatergic receptors, PACAP, and microglia

The 2 mg/kg KA-induced seizures caused prolongation of QT interval. The Δ QTc was significantly increased in KA control group ($\Delta 8.2 \pm 2.5$ ms; $p = 0.02$) compared with vehicle treatment (Fig. 6A). These changes in QT interval are most clearly seen in Poincaré plots before and after treatment; representative QT Poincaré plots from each group are shown in Fig. 7A. KA control group showed almost complete dispersion of the QT interval along with arrhythmic behavior in heart rate (multiple ellipses) (Fig. 7AII). Despite this, there was no evidence of atrial fibrillation, although there was evidence of dramatic decrease in PR interval after KA treatment (Figs. 6B, 7BII). The prolongation of QT interval (Δ QTc) was completely blocked by administration of glutamate receptors antagonist KYNA in the RVLM ($p = 0.02$; Figs. 6A, 7AV); nevertheless, bilateral microinjection of KYNA has no effect on seizure-induced shortened PR interval (Figs. 6B, 7BV). PACAP(6–38) and minocycline microinjections also

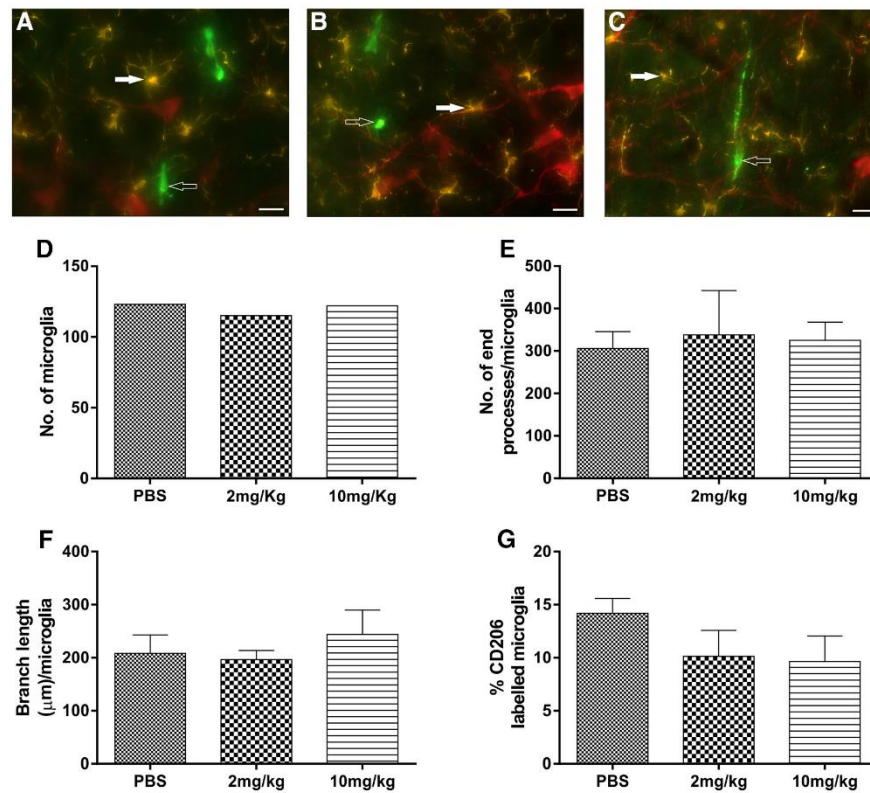


Figure 5. Fluorescence images of RVLM area containing TH⁺-ir (red), Iba1-labeled microglia (yellow), and CD206-labeled M2 microglial cells (green) and their morphological analysis in different treatment groups of rats. Scale bar, 20 μ m. TH, Iba1 and CD206 immunoreactivity in RVLM in PBS (A), 2 mg/kg KA (B), and 10 mg/kg KA (C) treated rats. In all of these three groups, TH⁺-ir neurons (red) were surrounded with microglia with its round cell body and normal appearing processes with few ramifications (closed arrow) and no change in number of anti-inflammatory M2 microglia (open arrow). Quantitative analysis of number of microglial cells in mean square area (D), number of end processes/microglia (E), branch length (μ m)/microglia of Iba1-labeled microglial cells (F), and percentage of CD206-labeled M2 microglial cells (G) in the RVLM of vehicle-treated and KA-induced seizure (2 and 10 mg/kg i.p.) rats.

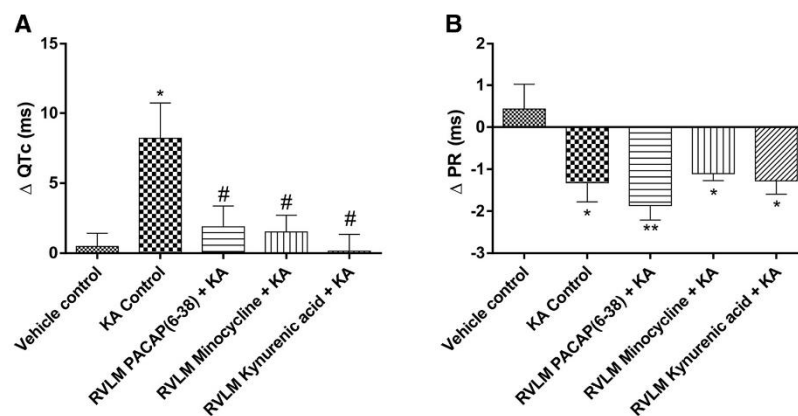


Figure 6. Proarrhythmic effects of seizures. Group data showing changes in QTc interval (A) and PR interval (B) 120 min after intraperitoneal injection of PBS or KA in different groups of rats. Statistical significance was determined using one-way ANOVA followed by *t* tests with a Holm-Sidak correction. Data are mean \pm SEM. ** p \leq 0.01 compared with vehicle control group. * p \leq 0.05 compared with vehicle control group. # p \leq 0.05 compared with KA control group.

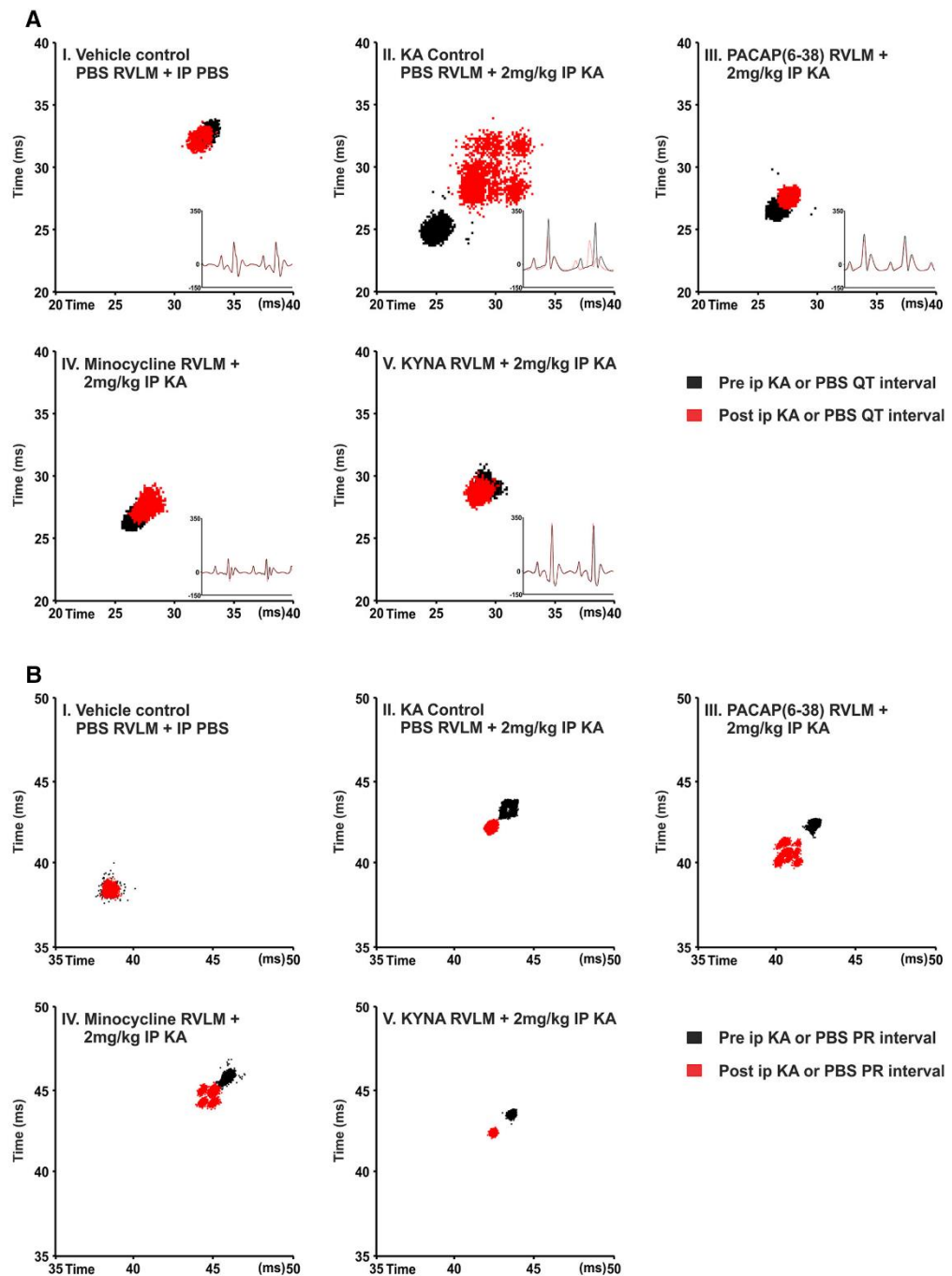


Figure 7. Representative Poincaré plots illustrate the changes in QT interval (**A**) and PR interval (**B**) following KA-induced seizures in rats. **A**, Treatment with KA causes a dramatic dispersion in the QT interval (prolongation) and arrhythmic behavior in the heart rate (multiple ellipses) (**II**). In rats treated with the PACAP antagonist (PACAP(6–38)) or (Figure legend continues.)

significantly reduced ΔQTC interval compared with KA control group of rats ($\Delta 1.9 \pm 1.5$; $p = 0.03$ and $\Delta 1.5 \pm 1.2$; $p = 0.03$; Fig. 6A). In PACAP(6–38) and minocycline-treated groups, prolongation of QT interval and dysrhythmia is abolished. As shown in Figure 7A, PACAP(6–38) and minocycline treatment in KA-induced seizure rats has almost similar patterns of pre- and post-QT interval as the vehicle-treated group (Fig. 7A,III,IV). The seizure-induced prolongation of QT interval is very obvious in KA control, which was significantly blocked in PACAP(6–38) and minocycline-microinjected rats. The PR interval was significantly reduced in the 2 mg/kg KA-induced seizure group compared with the vehicle control group of rats (Fig. 6B). This is clearly represented in Poincaré plots (Fig. 7B). In contrast to the improvements seen in the QT interval, RVLM microinjection of PACAP(6–38), minocycline, or KYNA did not prevent changes in seizure-induced shortening of PR interval (Fig. 6B). However, PACAP(6–38) (Fig. 7B,III) and minocycline (Fig. 7B,IV) showed quantally dispersed PR intervals as evidenced by multiple ellipses, rather than complete R-R dispersion, and an absence of P-waves, which is clearly not suggestive of atrial fibrillation.

Discussion

This study provides the first direct evidence that the sympathoexcitation, tachycardia, pressor responses, and proarrhythmic changes during seizures are driven by activation of glutamatergic receptors, which leads to increased activity of the sympathetic premotor neurons in the RVLM. The sympathoexcitatory effect does not appear due to increases or decreases in PACAP secretion, or microglial activation. However, PACAP and microglial activity in the vicinity of RVLM neurons mediate the proarrhythmic changes during seizures. Central autonomic nuclei are not the source of KA-induced seizures (2 mg/kg). We confirm that the induction of seizures does not cause changes in the state of microglia within the RVLM, and microglia remain in a surveillance state with no change in the number of M2 phenotypes, supporting our *in vivo* electrophysiology findings.

Our results strengthen the findings that seizures have a devastating effects on the cardiovascular system (Sakamoto et al., 2008; Brotherton et al., 2010; Bhandare et al., 2015), with immediate cardiovascular effects that last for ~3 h (Lothman et al., 1981). Importantly, these cardiovascular changes are downstream effects of seizure-induced autonomic overactivity and mediated by the action of the excitatory amino acid, L-glutamate, on sympathetic premotor neurons in the RVLM as the bilateral microinjection of ionotropic glutamate receptor antagonist KYNA completely abolished these changes. Glutamatergic synapses are important in the development of seizures, as seizure elevates the glutamate levels in the extracellular fluid of the rat hippocampus (Chapman, 1998; Faingold and Casebeer, 1999; Ueda et al., 2001; Kanamori and Ross, 2011). The RVLM contains sympathetic premotor neurons responsible for maintaining tonic excitation of sympathetic preganglionic neurons involved in cardiovascular

regulation (Guyenet, 2006; Pilowsky et al., 2009). Increased activity of sympathetic premotor RVLM neurons has significant effect on cardiac electrophysiology and is arrhythmogenic during seizures (Metcalf et al., 2009; Damasceno et al., 2013). Microinjection of L-glutamate into the RVLM causes pressor responses and sympathoexcitation that is completely blocked with KYNA (Ito and Sved, 1997; Araujo et al., 1999; Dampney et al., 2003). KYNA microinjection into RVLM on its own does not affect basal blood pressure and sympathetic activity (Guyenet et al., 1987; Kiely and Gordon, 1994; Araujo et al., 1999). Subsequently, Ito and Sved (1997) observed that, if the caudal ventrolateral medulla (inhibitory drive to the RVLM) is inhibited first, subsequent blockade of glutamate receptor in the RVLM markedly reduces blood pressure. In this paradigm, glutamatergic input to the RVLM directly excites presympathetic neurons and indirectly inhibit gamma-GABAergic inhibition of the RVLM, and the lack of change in arterial pressure with KYNA in the RVLM reflects the balance of these two actions. Miyawaki et al. (2002) also observed that, after blockade of GABAergic input within the RVLM, injection of KYNA produced inhibition of splanchnic and lumbar sympathetic nerve activity. Together, these findings illustrate that there is a tonic glutamatergic input with the existence of additional sources of neurotransmitter drive to RVLM neurons. We hypothesized that the increased concentration of glutamate in the RVLM during seizure leads to sympathoexcitation, tachycardia, and pressor responses. In turn, the responses can be antagonized by microinjection of KYNA into RVLM; indeed, our findings support this hypothesis. The findings suggest that not only sympathoexcitation but also proarrhythmic changes during seizures are mediated through glutamatergic receptor activation in RVLM catecholaminergic neurons. RVLM microinjection of KYNA (as well as PACAP(6–38) and minocycline) was unable to block the reduction in PR interval. In this paradigm, it is possible that the KA treatment had peripheral effects on dromotropy at the level of the AV node.

Generalized seizures in rats cause the expression of Fos, a protein marker of recently activated neurons (Minson et al., 1994), in brainstem catecholaminergic neurons in RVLM (Silveira et al., 2000). Earlier studies also suggests that C1 neurons are activated following seizure (Kanter et al., 1995), findings that were supported in our previous, and current work (Bhandare et al., 2015), where KA-induced seizures in rats elicited sympathoexcitation, tachycardia, and pressor responses. Together, the findings confirm that during seizure most of the excitatory effects of glutamate in RVLM are mediated by ionotropic receptors because the broad-spectrum ionotropic glutamate receptor (NMDA, AMPA, and kainate) antagonist (KYNA) completely abolished these effects.

PACAP is a 38 amino acid pleiotropic neuropeptide. The effects of PACAP are mediated via three different G-protein receptors (PAC1R, VPAC1R, and VPAC2R); all are positively coupled to adenylate cyclase. PACAP gene expression is increased in the paraventricular nucleus of the hypothalamus after KA-induced temporal lobe epilepsy in rats (Nomura et al., 2000), whereas PACAP is sympathoexcitatory (Lai et al., 1997; Farnham et al., 2008, 2012; Gaede et al., 2012), anti-inflammatory, and neuroprotective (Shioda et al., 1998) on sympathetic preganglionic neurons during seizure (Bhandare et al., 2015). Therefore, we aimed to determine whether or not PACAP also has a sympathoexcitatory or neuroprotective effect on RVLM sympathetic premotor neurons during seizures. The findings show that blockade of PACAP receptors (PAC1 and VPAC2) in the RVLM does not affect seizure-induced sympathoexcitation, tachycardia, and hypertension but does abolish prolongation of the QT

(Figure legend continued.) with the microglial antagonist minocycline, prolongation of QT interval and the dysrhythmia is abolished (III, IV). Following treatment with KYNA, the HR and QT are restored to normal (V). HR-triggered ECG was drawn before and after treatment and shown in the right side corner of each box. Continuous black and dotted red lines indicate pretreatment and post-treatment ECG, respectively. B, Induction of seizures with intraperitoneal KA injection shortened the PR interval (II) compared with vehicle control. RVLM microinjection of PACAP(6–38) (III), minocycline (IV), or KYNA (V) did not show changes in seizure-induced short PR interval; however, PACAP(6–38) (III) and minocycline (IV) showed more dispersed PR interval with multiple ellipses. Scale bars are in milliseconds.

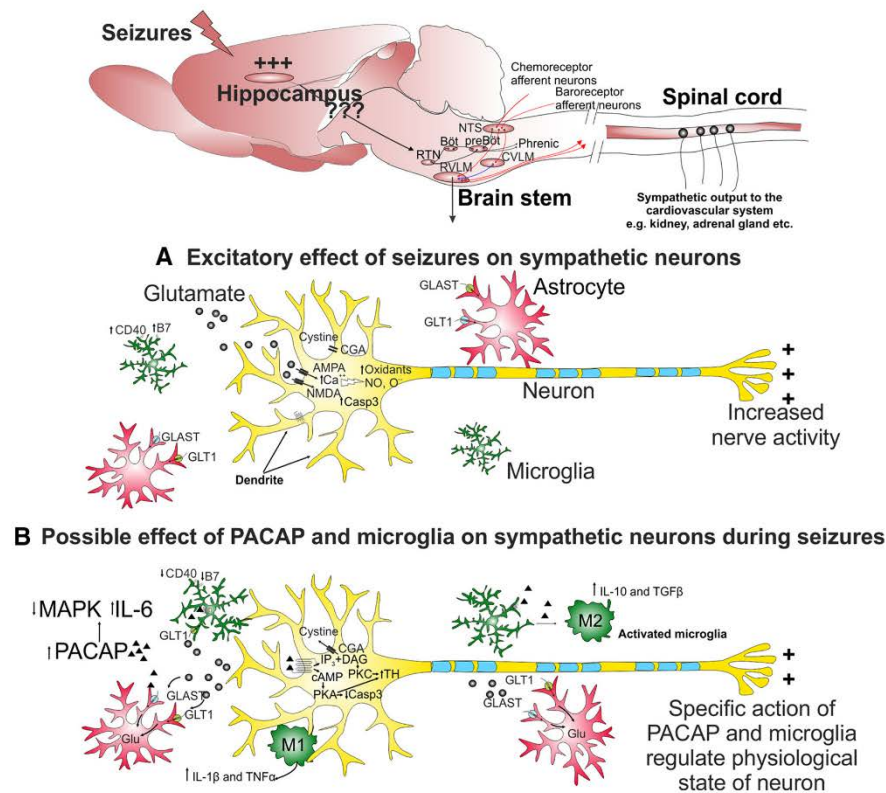


Figure 8. A proposed mechanism by which hippocampal seizures induce increased activity of sympathetic premotor neurons in the RVLM and role of glutamate, PACAP, and microglia. **A**, Seizure elevates synaptic glutamate release that can act on postsynaptic AMPA or NMDA receptors. Activation of AMPA or NMDA receptors leads to inhibition of cysteine uptake and influx of extracellular calcium, which stimulates production of oxidants, NO and O_2^- . Under repetitive and extreme neuronal activation, neurotoxic effects are mediated through increased production of apoptotic factor-like caspase-3. Glutamate transporters are expressed by astrocytes and play an important role in rapid clearance of the synaptically released glutamate, whose expression is downregulated in seizure. Together, increased oxidative stress and cellular excitability cause increased activity of sympathetic premotor neurons. **B**, Increased PACAP expression can act via cAMP-mediated PKA and/or PKC pathways and produce either excitatory effect through phosphorylation of TH at serine 40 or neuroprotective effect regulated through decreased caspase 3, increased glial-glutamate transporters, and redirecting microglia toward anti-inflammatory M2 phenotype. In neurons, PACAP inhibits MAPK and increases IL-6 production. Microglia are activated by PACAP binding to PAC1 and VPAC1 receptors. Subsequently, microglia increase production and release of IL-10 and TGF-β and decrease production and release of TNF-α, as well as downregulating CD40 and B7 surface protein expression, with a neuroprotective effect. Conversely, the pro-inflammatory phenotype of activated microglia can produce IL-1β and TNF-α that may increase the sensitivity of neurons to activation.

interval. This response to PACAP (6–38) suggests that the excitatory action of PACAP (Fig. 8) on RVLM sympathetic premotor neurons mediates proarrhythmic changes, but not seizure-induced sympathoexcitation. Possible explanations could be that PACAP expression in the RVLM at 2 h after 2 mg/kg KA injection may be insufficient to produce sympathoexcitation, but enough to induce proarrhythmic effects. This idea is supported by the findings that PACAP gene expression reaches a maximum at 12 h after 12 mg/kg KA-induced seizures in the paraventricular nucleus of the hypothalamus (Nomura et al., 2000).

Microglia are the principal resident immune cells of the CNS, contributing ~10% of the total brain cell population. Activated microglia respond to environmental perturbations by adopting either a “pro-inflammatory M1” or “anti-inflammatory M2” phenotype (Li et al., 2007; Lai and Todd, 2008; Pisanu et al., 2014). Seizure causes extensive microglial activation in patients (Beach et al., 1995), and in animal models (Drage et al., 2002). There is considerable controversy surrounding the pro- (Shapiro

et al., 2008) or anti-inflammatory (Mirrione et al., 2010; Eyo et al., 2014) role played by microglia during seizure. Our recent findings demonstrate that microglia are protective during seizure on sympathetic preganglionic neurons within spinal cord (Bhandare et al., 2015). The findings of the current study show that blockade of microglial activation with minocycline microinjection in RVLM abolishes the prolongation of QT interval caused by KA-induced seizures but causes no change in sympathoexcitation, tachycardia, or hypertension. Our immunohistochemical analysis revealed that there are no changes in microglial morphology or phenotype in the vicinity of RVLM neurons (branch length or number of endpoint processes) or proportion of the M2 phenotype following induction of seizures. The increased RVLM neuronal activity may have activated microglia (which might be insufficient to differentiate with immunohistochemistry) producing an excitatory effect and contributed to the seizure-induced prolongation of QT interval (Fig. 8).

A possible mechanism to explain the increased glutamate release from presynaptic cells during seizure, and sympathoexcitation, is

proposed in Figure 8. The oxidative stress and inflammation in RVLM during seizure (Tsai et al., 2012) could be mediated through increased glutamate levels or functional failure of glutamate transporters. Increased synthesis and release of PACAP during seizure acts via cAMP-mediated PKA and/or PKC pathways that may have either excitatory effects through phosphorylation of TH at serine 40 (Bobrovskaya et al., 2007) or neuroprotective effects regulated through decreased caspase 3 (Dejda et al., 2011), increased glial-glutamate transporters, and redirecting microglia toward anti-inflammatory M2 phenotype (Brifault et al., 2015). PACAP inhibits MAPK and increases IL-6 (Shioda et al., 1998), whereas its action on the PAC1 and VPAC1 receptors of activated microglia increase production of IL-10, TGF- β and decrease TNF- α (Wada et al., 2013). Whereas polarization of activated microglia toward pro-inflammatory M1 phenotype increase IL-1 β and TNF- α . Overall, depending on the type, severity, and intensity of stimulus, selective actions of PACAP and microglia regulate the physiological state of neurons. In the current study, both PACAP and microglia may regulate excitatory effects as their antagonism results in restoration of QT prolongation.

This is the first evidence to indicate that an increase in sympathetic nerve discharge and cardiovascular dysfunction in seizure is due to activation of glutamatergic receptors within the RVLM. Second, antagonism of PACAP and microglial activity in RVLM did not abolish the seizure-induced sympathoexcitation, hypertension, and tachycardia. Interestingly, minocycline, a drug that has central bioavailability following oral administration, and PACAP antagonist, restores the proarrhythmogenic effects of seizures to normal. This is the evidence for the physiological interaction between neurons and microglia. Third, the finding that microglia are not activated, and there is no change in the proportion of M2 phenotype during seizures, is consistent with our physiological findings.

In conclusion, the implications of the current findings are that, in patients with seizure, targeting glutamatergic receptors in RVLM catecholaminergic neurons and tailoring activity of PACAP and microglia in the vicinity of sympathetic premotor neurons may have protective effects and lead to novel therapies for seizure-induced cardiovascular dysfunction and SUDEP.

References

- Araújo GC, Lopes OU, Campos RR (1999) Importance of glycinergic and glutamatergic synapses within the rostral ventrolateral medulla for blood pressure regulation in conscious rats. *Hypertension* 34:752–755. [CrossRef Medline](#)
- Bardai A, Lamberts RJ, Blom MT, Spanjaart AM, Berdowski J, van der Staal SR, Brouwer HJ, Koster RW, Sander JW, Thijs RD, Tan HL (2012) Epilepsy is a risk factor for sudden cardiac arrest in the general population. *PLoS One* 7:e42749. [CrossRef Medline](#)
- Bazett HC (1920) An analysis of the time-relations of electrocardiograms. *Heart* 7:353–370.
- Beach TG, Woodhurst WB, MacDonald DB, Jones MW (1995) Reactive microglia in hippocampal sclerosis associated with human temporal lobe epilepsy. *Neurosci Lett* 191:27–30. [CrossRef Medline](#)
- Bealer SL, Little JG, Metcalf CS, Brewster AL, Anderson AE (2010) Autonomic and cellular mechanisms mediating detrimental cardiac effects of status epilepticus. *Epilepsy Res* 91:66–73. [CrossRef Medline](#)
- Bhandare AM, Mohammed S, Pilowsky PM, Farnham MM (2015) Antagonism of PACAP or microglia function worsens the cardiovascular consequences of kainic acid-induced seizures in rats. *J Neurosci* 35:2191–2199. [CrossRef Medline](#)
- Blümcke I, Becker AJ, Klein C, Scheiwe C, Lie AA, Beck H, Waha A, Friedl MG, Kuhn R, Emson P, Elger C, Wiestler OD (2000) Temporal lobe epilepsy associated upregulation of metabotropic glutamate receptors: correlated changes in mGluR1 mRNA and protein expression in experimental animals and human patients. *J Neuropathol Exp Neurol* 59:1–10. [Medline](#)
- Bobrovskaya L, Gelain DP, Gilligan C, Dickson PW, Dunkley PR (2007) PACAP stimulates the sustained phosphorylation of tyrosine hydroxylase at serine 40. *Cell Signal* 19:1141–1149. [CrossRef Medline](#)
- Brifault C, Gras M, Liot D, May V, Vaudry D, Wurtz O (2015) Delayed pituitary adenylate cyclase-activating polypeptide delivery after brain stroke improves functional recovery by inducing M2 microglia/macrophage polarization. *Stroke* 46:520–528. [CrossRef Medline](#)
- Brotherstone R, Blackhall B, McLellan A (2010) Lengthening of corrected QT during epileptic seizures. *Epilepsia* 51:221–232. [CrossRef Medline](#)
- Chapman AG (1998) Glutamate receptors in epilepsy. *Prog Brain Res* 116:371–383. [CrossRef Medline](#)
- Damasceno DD, Saverghini SQ, Gomes ER, Guatimosim S, Ferreira AJ, Doretto MC, Almeida AP (2013) Cardiac dysfunction in rats prone to audiogenic epileptic seizures. *Seizure* 22:259–266. [CrossRef Medline](#)
- Dampney RA, Horiuchi J, Tagawa T, Fontes MA, Potts PD, Polson JW (2003) Medullary and supramedullary mechanisms regulating sympathetic vasomotor tone. *Acta Physiol Scand* 177:209–218. [CrossRef Medline](#)
- Dejda A, Seaborn T, Bourgault S, Touzani O, Fournier A, Vaudry H, Vaudry D (2011) PACAP and a novel stable analog protect rat brain from ischemia: insight into the mechanisms of action. *Peptides* 32:1207–1216. [CrossRef Medline](#)
- Drage MG, Holmes GL, Seyfried TN (2002) Hippocampal neurons and glia in epileptic EL mice. *J Neurocytol* 31:681–692. [CrossRef Medline](#)
- Eyo UB, Peng J, Swiatkowski P, Mukherjee A, Bispo A, Wu LJ (2014) Neuronal hyperactivity recruits microglial processes via neuronal NMDA receptors and microglial P2Y12 receptors after status epilepticus. *J Neurosci* 34:10528–10540. [CrossRef Medline](#)
- Faingold C, Casebeer D (1999) Modulation of the audiogenic seizure network by noradrenergic and glutamatergic receptors of the deep layers of superior colliculus. *Brain Res* 821:392–399. [CrossRef Medline](#)
- Farnham MM, Li Q, Goodchild AK, Pilowsky PM (2008) PACAP is expressed in sympathoexcitatory bulbospinal C1 neurons of the brain stem and increases sympathetic nerve activity in vivo. *Am J Physiol Regul Integr Comp Physiol* 294:1304–1311. [CrossRef Medline](#)
- Farnham MM, Lung MS, Tallapragada VJ, Pilowsky PM (2012) PACAP causes PAC1/VPAC2 receptor mediated hypertension and sympathoexcitation in normal and hypertensive rats. *Am J Physiol Heart Circ Physiol* 303:910–917. [CrossRef Medline](#)
- Gaede AH, Ingloff MA, Farnham MM, Pilowsky PM (2012) Catestatin has an unexpected effect on the intrathecal actions of PACAP dramatically reducing blood pressure. *Am J Physiol Regul Integr Comp Physiol* 303:R719–R726. [CrossRef Medline](#)
- Gurbanova AA, Aker RG, Sirvanci S, Demiralp T, Onat FY (2008) Intramygdaloid injection of kainic acid in rats with genetic absence epilepsy: the relationship of typical absence epilepsy and temporal lobe epilepsy. *J Neurosci* 28:7828–7836. [CrossRef Medline](#)
- Guyenet PG (2006) The sympathetic control of blood pressure. *Nat Rev Neurosci* 7:335–346. [CrossRef Medline](#)
- Guyenet PG, Filtz TM, Donaldson SR (1987) Role of excitatory amino acids in rat vagal and sympathetic baroreflexes. *Brain Res* 407:272–284. [CrossRef Medline](#)
- Ito S, Sved AF (1997) Tonic glutamate-mediated control of rostral ventrolateral medulla and sympathetic vasomotor tone. *Am J Physiol Regul Integr Comp Physiol* 273:487–494. [Medline](#)
- Kanamori K, Ross BD (2011) Chronic electrographic seizure reduces glutamine and elevates glutamate in the extracellular fluid of rat brain. *Brain Res* 1371:180–191. [CrossRef Medline](#)
- Kanter RK, Strauss JA, Sauro MD (1995) Seizure-induced c-fos expression in rat medulla oblongata is not dependent on associated elevation of blood pressure. *Neurosci Lett* 194:201–204. [CrossRef Medline](#)
- Kiely JM, Gordon FJ (1994) Role of rostral ventrolateral medulla in centrally mediated pressor responses. *Am J Physiol Heart Circ Physiol* 267:H1549–H1556. [Medline](#)
- Lai AY, Todd KG (2008) Differential regulation of trophic and proinflammatory microglial effectors is dependent on severity of neuronal injury. *Glia* 56:259–270. [CrossRef Medline](#)
- Lai CC, Wu SY, Lin HH, Dun NJ (1997) Excitatory action of pituitary adenylate cyclase activating polypeptide on rat sympathetic preganglionic neurons in vivo and in vitro. *Brain Res* 748:189–194. [CrossRef Medline](#)
- LeBlanc BW, Zerah ML, Kadasi LM, Chai N, Saab CY (2011) Minocycline injection in the ventral posterolateral thalamus reverses microglial reac-

- tivity and thermal hyperalgesia secondary to sciatic neuropathy. *Neurosci Lett* 498:138–142. [CrossRef Medline](#)
- Li L, Lu J, Tay SS, Mochhala SM, He BP (2007) The function of microglia, either neuroprotection or neurotoxicity, is determined by the equilibrium among factors released from activated microglia in vitro. *Brain Res* 1159:8–17. [CrossRef Medline](#)
- Lothman EW, Collins RC, Ferrendelli JA (1981) Kainic acid-induced limbic seizures: electrophysiologic studies. *Neurology* 31:806–812. [CrossRef Medline](#)
- Massey CA, Sowers LP, Dlouhy BJ, Richerson GB (2014) Mechanisms of sudden unexpected death in epilepsy: the pathway to prevention. *Nat Rev Neurol* 10:271–282. [CrossRef Medline](#)
- Meldrum BS, Akbar MT, Chapman AG (1999) Glutamate receptors and transporters in genetic and acquired models of epilepsy. *Epilepsy Res* 36:189–204. [CrossRef Medline](#)
- Metcalfe CS, Poelzing S, Little JG, Bealer SL (2009) Status epilepticus induces cardiac myofilament damage and increased susceptibility to arrhythmias in rats. *Am J Physiol Heart Circ Physiol* 297:H2120–H2127. [CrossRef Medline](#)
- Minson JB, Llewellyn-Smith IJ, Arnolda LF, Pilowsky PM, Oliver JR, Chalmers JP (1994) Disinhibition of the rostral ventral medulla increases blood pressure and Fos expression in bulbospinal neurons. *Brain Res* 646:44–52. [CrossRef Medline](#)
- Mirriione MM, Konomos DK, Gravanis I, Dewey SL, Aguzzi A, Heppner FL, Tsirka SE (2010) Microglial ablation and lipopolysaccharide preconditioning affects pilocarpine-induced seizures in mice. *Neurobiol Dis* 39:85–97. [CrossRef Medline](#)
- Miyawaki T, Goodchild AK, Pilowsky PM (2002) Evidence for a tonic GABA-ergic inhibition of excitatory respiratory-related afferents to pre-sympathetic neurons in the rostral ventrolateral medulla. *Brain Res* 924:56–62. [CrossRef Medline](#)
- Nadler JV (1981) Kainic acid as a tool for the study of temporal lobe epilepsy. *Life Sci* 29:2031–2042. [CrossRef Medline](#)
- Nei M, Ho RT, Abou-Khalil BW, Drislane FW, Liporace J, Romeo A, Sperling MR (2004) EEG and ECG in sudden unexplained death in epilepsy. *Epilepsia* 45:338–345. [CrossRef Medline](#)
- Nomura M, Ueta Y, Hannibal J, Serino R, Yamamoto Y, Shibuya I, Matsumoto T, Yamashita H (2000) Induction of pituitary adenylate cyclase-activating polypeptide mRNA in the medial parvocellular part of the paraventricular nucleus of rats following kainic-acid-induced seizure. *Neuroendocrinology* 71:318–326. [CrossRef Medline](#)
- Ohtaki H, Nakamachi T, Dohi K, Aizawa Y, Takaki A, Hodoyama K, Yofu S, Hashimoto H, Shintani N, Baba A, Kopf M, Iwakura Y, Matsuda K, Arimura A, Shioda S (2006) Pituitary adenylate cyclase-activating polypeptide (PACAP) decreases ischemic neuronal cell death in association with IL-6. *Proc Natl Acad Sci U S A* 103:7488–7493. [CrossRef Medline](#)
- Olsson T, Broberg M, Pope KJ, Wallace A, Mackenzie L, Blomstrand F, Nilsson M, Willoughby JO (2006) Cell swelling, seizures and spreading depression: an impedance study. *Neuroscience* 140:505–515. [CrossRef Medline](#)
- Phillips JK, Goodchild AK, Dubey R, Sesiashvili E, Takeda M, Chalmers J, Pilowsky PM, Lipski J (2001) Differential expression of catecholamine biosynthetic enzymes in the rat ventrolateral medulla. *J Comp Neurol* 432:20–34. [CrossRef Medline](#)
- Pilowsky PM, Lung MS, Spirovski D, McMullan S (2009) Differential regulation of the central neural cardiorespiratory system by metabotropic neurotransmitters. *Philos Trans R Soc Lond B Biol Sci* 364:2537–2552. [CrossRef Medline](#)
- Pisanu A, Lecca D, Mulas G, Wardas J, Simbula G, Spiga S, Carta AR (2014) Dynamic changes in pro- and anti-inflammatory cytokines in microglia after PPAR- γ agonist neuroprotective treatment in the MPTP mouse model of progressive Parkinson's disease. *Neurobiol Dis* 71:280–291. [CrossRef Medline](#)
- Ross CA, Ruggiero DA, Joh TH, Park DH, Reis DJ (1984) Rostral ventrolateral medulla: selective projections to the thoracic autonomic cell column from the region containing C1 adrenaline neurons. *J Comp Neurol* 228:168–185. [CrossRef Medline](#)
- Sakamoto K, Saito T, Orman R, Koizumi K, Lazar J, Saliciccioli L, Stewart M (2008) Autonomic consequences of kainic acid-induced limbic cortical seizures in rats: peripheral autonomic nerve activity, acute cardiovascular changes, and death. *Epilepsia* 49:982–996. [CrossRef Medline](#)
- Schreihöfer AM, Guyenet PG (1997) Identification of C1 presympathetic neurons in rat rostral ventrolateral medulla by juxtacellular labeling in vivo. *J Comp Neurol* 387:524–536. [CrossRef Medline](#)
- Shapiro LA, Wang L, Ribak CE (2008) Rapid astrocyte and microglial activation following pilocarpine-induced seizures in rats. *Epilepsia* 49:33–41. [CrossRef Medline](#)
- Shioda S, Ozawa H, Dohi K, Mizushima H, Matsumoto K, Nakajo S, Takaki A, Zhou CJ, Nakai Y, Arimura A (1998) PACAP protects hippocampal neurons against apoptosis: involvement of JNK/SAPK signaling pathway. *Ann N Y Acad Sci* 865:111–117. [CrossRef Medline](#)
- Silveira DC, Schachter SC, Schomer DL, Holmes GL (2000) Flurothyl-induced seizures in rats activate Fos in brainstem catecholaminergic neurons. *Epilepsy Res* 39:1–12. [CrossRef Medline](#)
- Sokal RR, Rohlf FJ (2012) *Biometry*, Ed 4. New York: Freeman.
- Sperk G, Lassmann H, Baran H, Kish SJ, Seitelberger F, Hornykiewicz O (1983) Kainic acid induced seizures: neurochemical and histopathological changes. *Neuroscience* 10:1301–1315. [CrossRef Medline](#)
- Surges R, Thijs RD, Tan HL, Sander JW (2009) Sudden unexpected death in epilepsy: risk factors and potential pathomechanisms. *Nat Rev Neurol* 5:492–504. [CrossRef Medline](#)
- Sved AF, Ito S, Yajima Y (2002) Role of excitatory amino acid inputs to the rostral ventrolateral medulla in cardiovascular regulation. *Clin Exp Pharmacol Physiol* 29:503–506. [CrossRef Medline](#)
- Tsai CY, Chan JY, Hsu KS, Chang AY, Chan SH (2012) Brain-derived neurotrophic factor ameliorates brain stem cardiovascular dysregulation during experimental temporal lobe status epilepticus. *PLoS One* 7:e33527. [CrossRef Medline](#)
- Ueda Y, Doi T, Tokumaru J, Yokoyama H, Nakajima A, Mitsuyama Y, Ohya-Nishiguchi H, Kamada H, Willmore LJ (2001) Collapse of extracellular glutamate regulation during epileptogenesis: down-regulation and functional failure of glutamate transporter function in rats with chronic seizures induced by kainic acid. *J Neurochem* 76:892–900. [CrossRef Medline](#)
- Vinet J, van Weering HRJ, Heinrich A, Kalin RE, Wegner A, Brouwer N, Heppner FL, van Rooijen N, Boddeke HWGM, Biber K (2012) Neuroprotective function for ramified microglia in hippocampal excitotoxicity. *J Neuroinflamm* 9:27. [CrossRef Medline](#)
- Wada Y, Nakamachi T, Endo K, Seki T, Ohtaki H, Tsuchikawa D, Hori M, Tsuchida M, Yoshikawa A, Matkovits A, Kagami N, Imai N, Fujisaka S, Usui I, Tobe K, Koide R, Takahashi H, Shioda S (2013) PACAP attenuates NMDA-induced retinal damage in association with modulation of the microglia/macrophage status into an acquired deactivation subtype. *J Mol Neurosci* 51:493–502. [CrossRef Medline](#)



Microglia PACAP and glutamate: Friends or foes in seizure-induced autonomic dysfunction and SUDEP?



Amol M. Bhandare^{a,b}, Komal Kapoor^{a,b}, Melissa M.J. Farnham^{b,c}, Paul M. Pilowsky^{b,c,*}

^a Department of Biomedical Sciences, Faculty of Medicine and Health Sciences, Macquarie University, Sydney 2109 New South Wales, Australia

^b The Heart Research Institute, 7 Eliza Street, Sydney 2042 New South Wales, Australia

^c Department of Physiology, University of Sydney, Sydney 2006 New South Wales, Australia

ARTICLE INFO

Article history:

Received 26 November 2015

Received in revised form 18 January 2016

Accepted 21 January 2016

Available online 26 January 2016

Keywords:

Seizure

SUDEP

Cardiorespiratory system

Microglia

PACAP

Glutamate

Inflammation

Ventrolateral medulla

ABSTRACT

Seizure-induced cardiorespiratory autonomic dysfunction is a major cause of sudden unexpected death in epilepsy (SUDEP), and the underlying mechanism is unclear. Seizures lead to increased synthesis, and release of glutamate, pituitary adenylate cyclase activating polypeptide (PACAP), and other neurotransmitters, and cause extensive activation of microglia at multiple regions in the brain including central autonomic cardiorespiratory brainstem nuclei. Glutamate contributes to neurodegeneration, and inflammation in epilepsy. PACAP has neuroprotective, and anti-inflammatory properties, whereas microglia are key players in inflammatory responses in CNS. Seizure-induced increase in PACAP is neuroprotective. PACAP produces neuroprotective effects acting on microglial PAC1 and VPAC1 receptors. Microglia also express glutamate transporters, and their expression can be increased by PACAP in response to harmful or stressful situations such as seizures. Here we discuss the mechanism of autonomic cardiorespiratory dysfunction in seizure, and the role of PACAP, glutamate and microglia in regulating cardiorespiratory brainstem neurons in their physiological state that could provide future therapeutic options for SUDEP.

© 2016 Elsevier B.V. All rights reserved.

1. Introduction

Epilepsy affects about 50 million people worldwide (WHO, 2005). Sudden unexpected death in epilepsy (SUDEP) is an important but poorly-appreciated disorder (Massey et al., 2014) that accounts for 5–17% of deaths in people with epilepsy, and 50% in refractory epilepsy (Ficker et al., 1998; Holst et al., 2013). The first evidence of SUDEP was published nearly 50 years ago (Hirsch and Martin, 1971), but the underlying mechanism remains obscure. The classical mechanism of SUDEP is extensively studied, and accounts for seizure-induced central autonomic and cardiorespiratory dysfunction (Figs. 1–2). Maximal electroshock applied by two ear electrodes, in freely moving rats, leads to seizure causing cardiac arrhythmia that is precisely correlated with the ictal period (Darbin et al., 2002). In human, seizure is commonly associated with profound apnoea and oxygen desaturation (Bateman et al., 2008; Dlouhy et al., 2015). Here we survey new data and propose a role for microglia (innate immune cells of the CNS), and the neurotransmitters, pituitary adenylate cyclase activating polypeptide

(PACAP), and glutamate in the context of seizure induced cardiorespiratory dysfunction (Fig. 3). These novel findings suggest probable mechanisms of cardiorespiratory dysfunction in seizure, and point to future therapeutic strategies that may help in the management, and prevention of SUDEP.

Cardiorespiratory disturbances such as arrhythmia and apnoea that occur during, and after seizures are the leading cause of SUDEP in both humans, and animals (Fig. 1) (Dlouhy et al., 2015; Johnston et al., 1997; Metcalf et al., 2009; Naggat et al., 2014). Cardiac sympathovagal imbalances with sympathetic dominance, baroreflex dysfunction, tachycardia or bradycardia with severe ictal ECG abnormalities are common in patients and animals (Bhandare et al., 2015; Nei et al., 2000; Opherk et al., 2002; Ponnusamy et al., 2012; Sakamoto et al., 2008). Seizure-related respiratory dysfunction, with associated hypoxaemia, is common, as seen in video-electroencephalogram (EEG) telemetry (Fig. 4), from patients in epilepsy monitoring units (Bateman et al., 2008; Dlouhy et al., 2015; Seyal et al., 2010).

Recent studies have uncovered a novel mechanism of seizure-induced cardiorespiratory dysfunction in animal models of seizure and epilepsy that involves three important mediators: microglia, which are immune cells in the CNS, PACAP, a pleiotropic neuropeptide, and glutamate, a major excitatory neurotransmitter in the brain (Fig. 3).

* Corresponding author at: The Heart Research Institute, 7 Eliza Street, Sydney 2042 New South Wales, Australia.

E-mail address: paul.pilowsky@hri.org.au (P.M. Pilowsky).

<http://dx.doi.org/10.1016/j.resp.2016.01.003>

1569-9048/© 2016 Elsevier B.V. All rights reserved.

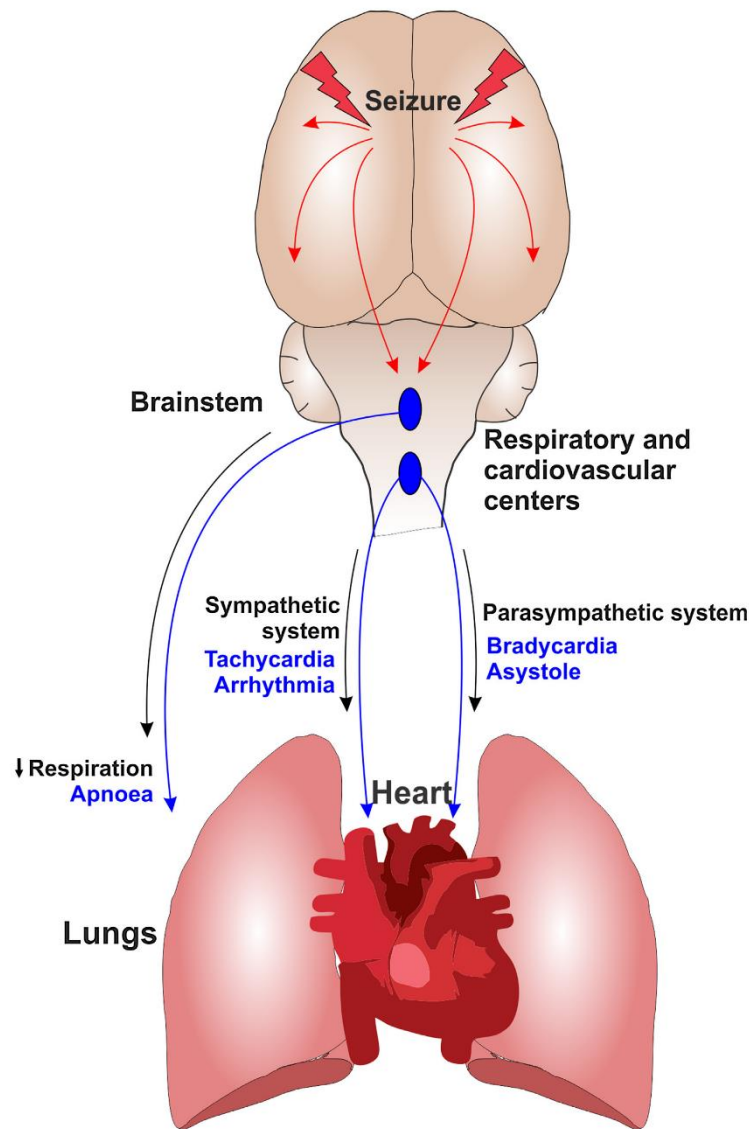


Fig. 1. A schematic diagram of mechanism of seizure-induced central autonomic cardiorespiratory dysfunction. Seizures propagate from higher brain region into the cardiorespiratory brainstem autonomic nuclei, and disturb the normal cardiorespiratory activity and reflexes. Seizure-induced excitation of sympathetic neurons leads to tachycardia and arrhythmia, whereas activation of parasympathetic system causes bradycardia and asystole. Moreover, spread of seizures could result in postictal coma, and loss of protective airway reflexes eventually causing decreased respiratory drive, apnoea and hypoventilation.

Microglia are ubiquitously distributed throughout the CNS, including in the vicinity of sympathetic premotor rostral ventrolateral medullary (RVLM) neurons (Fig. 5) (Kapoor et al., 2016). Microglia can be either neuroprotective or neurodegenerative, depending on circumstances (Li et al., 2007; Vinet et al., 2012). Extensive microglial activation is evident in animal models of seizure (Beach et al., 1995; Drage et al., 2002; Shapiro et al., 2008).

During the acute phase of seizure, preconditioning of hippocampal microglia reduces the seizure score in mice (Mirrione et al., 2010). Moreover, antagonism of microglia activation, with intrathecal administration of minocycline, during acute phase seizures in rats produces more sympathoexcitation (Bhandare et al., 2015).

PACAP expression increases in the paraventricular nucleus (PVN) of the hypothalamus, after kainic acid-induced seizure in

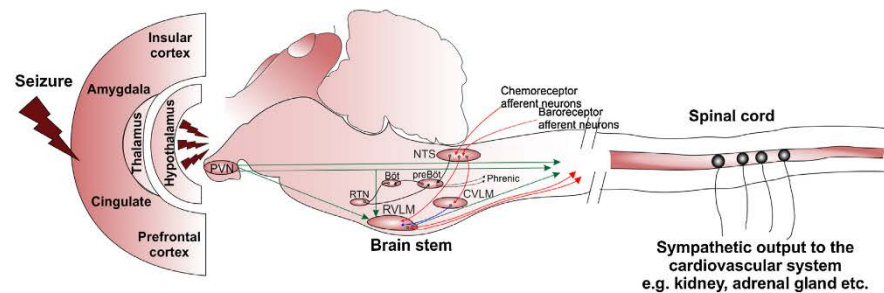


Fig. 2. The classical mechanism of seizure-induced central autonomic and cardiorespiratory dysfunction. Cardiorespiratory homeostasis is maintained by autonomic output, which is determined by balance of medullary reflexes, and influence of cerebral cortex. The sympathetic output to the heart is mediated by neurons from the RVLM through their direct projections to the IML cell column (red). The PVN affects sympathetic output through three different pathways; first, a direct descending projections to the IML, secondly, a projection to the vasomotor neurons of the RVLM, and thirdly, collateral projections to both IML and RVLM (Fig. 2) (Pyner and Coote, 2000; Shafston et al., 1998). Arterial baroreceptors are situated in the aortic arch and carotid sinus, and peripheral chemoreceptors are located in carotid and aortic bodies, providing afferent signals to NTS (red). The NTS integrates afferent information and relays it to activate (red) inhibitory neurons in the CVLM that in turn inhibit (blue) neurons in the RVLM. Astrocytes, and RTN neurons, act as central respiratory chemoreceptors that are exquisitely sensitive to changes in CO_2 . Peripheral chemosensory afferent in NTS provide information to the pre-Bötzinger complex influencing the rate and shape of respiratory rhythm, which in turn regulates respiratory motoneurons including the phrenic, intercostal and hypoglossal neurons. Bulbar respiratory interneurons also modulate the activity of cardiovascular neurons. During seizures, electrical disturbances occur, and excitation propagates throughout the central autonomic network, disturbing the normal autonomic control of vital cardiorespiratory functions.

rats (Nomura et al., 2000). PACAP is sympathoexcitatory and pressor when injected into the subarachnoid space or into the RVLM (Farnham et al., 2012, 2011). During seizures, infusion of PACAP antagonist into the intrathecal space produces more sympathoexcitation (Bhandare et al., 2015), where PACAP may be reducing neurotoxicity, a possibility that requires further investigation. The multifaceted findings of PACAP make it a promising player in the central autonomic cardiorespiratory dysfunction in seizure.

Finally, glutamate, the principal excitatory neurotransmitter in brain, is increased in rat hippocampus following seizures (Kanamori and Ross, 2011), suggesting that glutamatergic synapses play an important role in the development of seizures (Ueda et al., 2001). Activation of glutamatergic receptors in RVLM mediate sympathoexcitatory as well as proarrhythmic changes during seizure in rats (Bhandare et al., 2016), making them an attractive target for SUDEP therapy. Very recently, a role for microglia, PACAP, and glutamate, in seizure-induced cardiorespiratory responses is becoming a topic of considerable interest (Fig. 3).

2. Autonomic control of cardiorespiratory function

Normally, short-term cardiorespiratory homeostasis is tightly regulated by a balance between the sympathetic and parasympathetic activity (Young, 2010). The overall autonomic output to the cardiorespiratory system is determined by medullary reflexes, and the influence of the cerebral cortex (Fig. 2) (Guo et al., 2002; Westerhaus and Loewy, 2001). Findings in rats after pseudorabies virus injection in cardiac sympathetic target organs, such as adrenal gland and stellate ganglion, showed that higher brain centres exert a descending control on autonomic outflow to the heart (Fig. 2) (Westerhaus and Loewy, 2001). Stimulation of cardiac sympathetic afferents in cats, which evokes excitatory cardiovascular reflexes, confirmed that the neurons in the medulla, especially ventrolateral medulla, regulate the cardiovascular sympathetic reflexes (Guo et al., 2002). Medullary neurons regulate automatism of the sinus node, atrioventricular conduction, ventricular excitability and contractility. Sympathetic reflexes (baro, chemo and somatosympathetic) and blood pressure is regulated by C1, and non-C1, neurons in the RVLM, via direct projections to the IML cell column (intermediolateral cell column) (Madden and Sved, 2003; Nedoboy et al., 2016; Ross et al., 1984a,b). The PVN integrates the specific afferent inputs to generate a differential sympathetic out-

put. The PVN affects the sympathetic output (Allen, 2002) through three different pathways; projections to RVLM (Pyner and Coote, 1999), direct descending projections to IML, and collateral projections to both IML and RVLM (Fig. 2) (Pyner and Coote, 2000; Shafston et al., 1998). Arterial baroreceptors, situated in the aortic arch and carotid sinus, respond to changes in BP (Guo et al., 1982). Parasympathetic output to the heart is mediated by the vagus nerve, which originates from the dorsal motor nucleus, and more ventrally located nucleus ambiguus in the medulla (ter Horst et al., 1984). Respiratory centres in the brainstem provide an input to vagal efferents, which increases their activity decreasing heart rate, atrio-ventricular conduction, and ventricular excitability (Jones et al., 1998).

Brainstem neurons are also responsible for generating respiratory rhythm (Chitravanshi and Sapru, 1999; Mutolo et al., 2005). The findings in rabbits show that the respiratory rhythm is generated by glutamatergic interneurons, where the broad spectrum glutamate receptor antagonist, kynurenic acid, microinjection in pre-Bötzinger or Böttinger complex induces a pattern of breathing characterised by low-amplitude, high-frequency irregular oscillations, superimposed on tonic phrenic nerve activity (Mutolo et al., 2005). The respiratory interneurons project to bulbar, phrenic, and other spinal motoneurons (Chitravanshi and Sapru, 1999). Peripheral chemoreceptors are located in the carotid and aortic bodies, and monitor blood chemicals (e.g. CO_2 , O_2 , H^+ , glucose) to maintain their homeostasis through initiation of respiratory, and cardiovascular reflexes (Heeringa et al., 1979; Moraes et al., 2014). Astrocytes, and neurons in the retrotrapezoid nucleus (RTN) act as central respiratory chemoreceptors (Wenker et al., 2010). Serotonin (5-hydroxytryptamine (5-HT)) (Massey et al., 2015) and many neuropeptides (Pilowsky et al., 2009; Rahman et al., 2011) can modify the excitability of central chemoreceptors. 5-HT neurons have projections to all parts of the CNS, and are important in arousal. The arousal response to hypercapnia is significantly diminished in genetically modified mice lacking 5-HT neurons (Hodges et al., 2008; Hodges et al., 2009).

The nucleus of the solitary tract (NTS) acts as a relay centre for both peripheral chemoreceptors, and baroreceptors (Callera et al., 1997). Suzuki and colleagues conducted experiments in rats, and showed that the glutamatergic NTS neurons excite both the RVLM and CVLM neurons, and the GABAergic (γ -aminobutyric acid) NTS and CVLM neurons inhibit the sympathetic activity of RVLM neu-

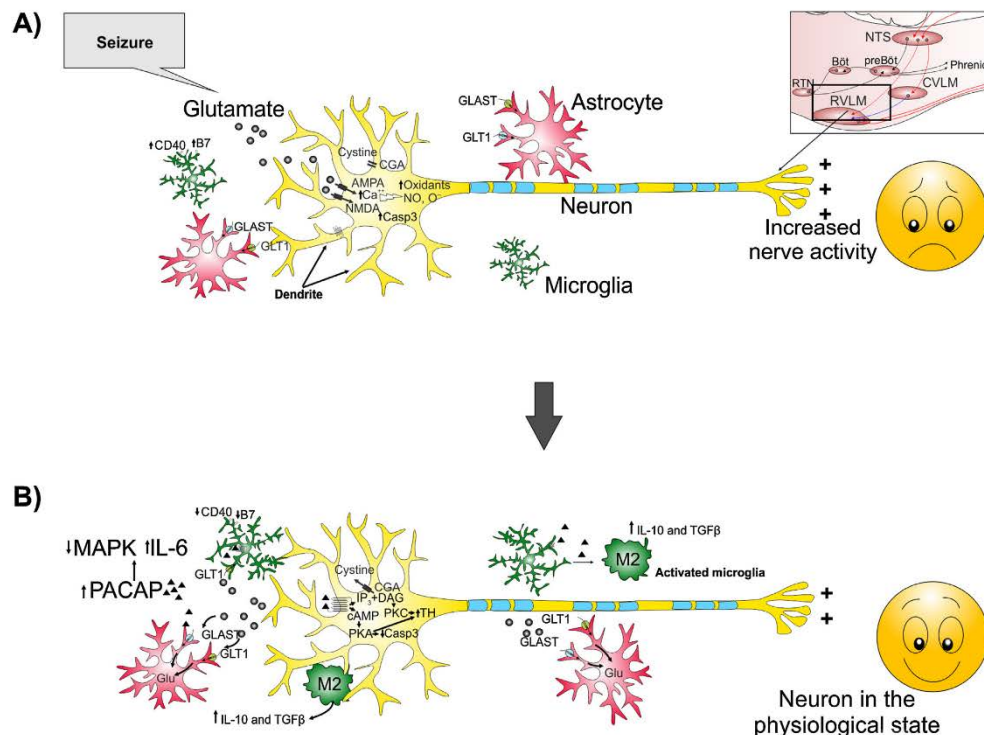


Fig. 3. A proposed model of the possible effect of PACAP, microglia, and glutamate on cardiorespiratory brainstem neurons during seizure. **A)** During seizures induced intense neuronal hyperactivity, neurons release glutamate from presynaptic terminals that can act on postsynaptic AMPA or NMDA receptors. Activation of AMPA or NMDA receptors inhibits cysteine uptake, and influx of calcium stimulating production of oxidants, NO , and $\text{O}^{\cdot -}$. Under repetitive and extreme neuronal activation, neurotoxic effects are mediated through increased production of apoptotic factors such as caspase-3. Glutamate transporters expressed by astrocytes, play an important role in the rapid clearance of synaptically released glutamate. Expression of astrocytic glutamate transporters is downregulated in seizure. Altogether, increased oxidative stress, and cellular excitability, causes increased activity of cardiorespiratory neurons, and in extreme situations neuronal death. **B)** Increased PACAP expression during seizure may produce a neuroprotective effect on microglia in several ways. PACAP acts on neuronal PAC1 or VPAC2 receptors, to increase intracellular cAMP. PACAP can inhibit increases in caspase 3, via PKA and PKC pathways. Increased cAMP mimics the effect of glial glutamate transporter expression to further enhance glutamate clearance from the synaptic cleft. Microglia also express glutamate transporters in response to harmful or stressful situations such as seizures. PACAP can redirect the microglia towards the neuroprotective M2 phenotype. PACAP achieves its effects via actions on the MAP kinase family (and by inhibiting activation of JNK/SAPK, while it activates ERK), and increasing IL-6. Activation of PAC1 and VPAC1 receptors on activated microglia increases the production of IL-10, TGF- β , and decreases TNF- α as well as downregulating CD40, and B7 surface protein expression. Taken together, the action of PACAP and microglia may lead to protective effects on cardiorespiratory brainstem neuron to keep them in a physiological state.

rons (Suzuki et al., 1997). NTS plays a critical integrative role in regulation of cardiovascular, and respiratory system since it is the initial step in processing barosensory, and chemosensory information that culminates in homeostatic reflex responses (Callera et al., 1997). It is important to note that seizure upregulates the c-fos expression in brainstem cardiorespiratory nuclei including RVLM, and NTS (Sakamoto et al., 2008; Silveira et al., 2000). These findings confirm that seizure activates the neurons in the major cardiorespiratory nuclei in brainstem, and causes cardiorespiratory and autonomic dysfunction.

3. Cardiorespiratory dysfunction in seizure and SUDEP

There are many different types of epilepsy depending on signs, symptoms and origin of seizures (WHO, 2005). SUDEP is operationally defined as “sudden, unexpected, witnessed or unwitnessed, non-traumatic and non-drowning death in patients with epilepsy, with or without evidence of a seizure, and excluding documented status epilepticus, where post-mortem examination does

not reveal a toxicological or anatomical cause of death” (Nashef, 1997). The mechanism of SUDEP is still unknown, and is the major hurdle in finding the best therapeutic solution for its prevention. Plausible mechanisms of SUDEP (Fig. 1) include ictal arrhythmias (Auerbach et al., 2013; Darbin et al., 2002), ictal and postictal central apnoea (Bateman et al., 2008; Seyal et al., 2010), acute neurogenic pulmonary edema (Kennedy et al., 2015), and autonomic dysfunction (Naggar et al., 2014) for each of which a case report has been documented and described further in detail. It therefore seems unlikely that SUDEP is a failure of a single system; rather it is more likely to be due to the collapse of multiple systems leading to fatal cardiac and respiratory dysfunction (Fig. 1).

Findings in SUDEP and temporal lobe epilepsy patients compared to controls shows that there is a significant volume loss in specific cardiorespiratory brainstem autonomic nuclei such as the periaqueductal gray, colliculi, raphe and reticular formation extending into the diencephalon particularly the medial posterior thalamus (Mueller et al., 2014). More importantly, in contrast to temporal lobe epilepsy patients, this volume loss was not only

more severe in SUDEP but also more widespread and extended into the dorsal section of the pons and even upper medulla. These findings specifically suggest that the neurodegeneration in central cardiorespiratory autonomic nuclei could be the mechanism for SUDEP (Mueller et al., 2014).

3.1. Cardiovascular dysfunction

3.1.1. Acute cardiac changes in epilepsy

Studies into the mechanisms of SUDEP, in human and animal, show that seizure causes major cardiovascular changes with significant sympathovagal imbalance, tachy- or brady- cardia, and abnormal changes in the electrocardiogram (ECG) (Fig. 1) (Bhandare et al., 2016, 2015; Naggar et al., 2014; Ponnusamy et al., 2012). Acute seizure causes a ~100% increase in sympathetic activity, pressor effects, tachycardia, and prolongation of QT interval in rat (Bhandare et al., 2016, 2015; Naggar et al., 2014; Sakamoto et al., 2008). Increase in both sympathetic and parasympathetic activity, baro-reflex dysfunction, and hypoperfusion of brain and heart is evidenced as the major cause of death in seizure-induced rats (Sakamoto et al., 2008). Pilocarpine-induced status epilepticus causes severe shifts in sympathovagal balance towards a sympathetic predominance in rats (Metcalfe et al., 2009). Kainic acid-induced chronic seizures in rats showed decreased vagal tone, increased QT dispersion, and eccentric cardiac hypertrophy without significant cardiac fibrosis (Naggar et al., 2014). Peri-ictal and ictal ECG changes are potential that can be used to detect seizure risk. In patients with refractory or well controlled temporal lobe epilepsy, heart rate variation during normal breathing, and tilting was lower, compared to control subjects (Ansakorpi et al., 2000). In temporal lobe epilepsy patients, heart rate variability changes (RR interval, low and high frequency domain analysed from ictal ECG recording) were significantly lower, and cardiosympathetic index was higher, compared to patients with psychogenic nonepileptic seizures (Ponnusamy et al., 2012). SUDEP is closely linked to ictal cardiovascular changes. ECG abnormalities, including ST segment elevation or depression, and T-wave inversion, occur in around 49% of patients during or after epileptic discharges, and are common in generalised seizure (Nei et al., 2000; Opherk et al., 2002). Tachycardia is present in 76–99% patients in epilepsy monitoring unit, suggestive of most probable clinical sign of convulsive and non-convulsive seizures (Moseley et al., 2011; Opherk et al., 2002). Activation of the central autonomic cardiovascular network, including the RVLM, causes cardiac changes observed in epilepsy (Silveira et al., 2000; Tsai et al., 2012). Overall, epileptic discharges are thought to propagate to the central autonomic nuclei in the brainstem, and disturb the normal autonomic control through sympathetic and parasympathetic pathways (Figs. 1–2). Our findings reveal that cardiovascular changes are always preceded by induction of seizures in rats (Bhandare et al., 2016, 2015). Temporal lobe epileptic discharges are also associated with ictal bradycardia, and asystole in 2–4% of seizure cases (Nei et al., 2000), and may occur due to the collapse of multiple systems.

3.1.2. Chronic cardiac changes in epilepsy

Neurocardiac channelopathies are the most significant chronic cardiovascular changes in patients with epilepsy. These changes lead to altered membrane excitability both in the brain and the heart (Ludwig et al., 2003), and pose an increased risk of autonomic dysfunction, and cardiac arrhythmia (Biet et al., 2015). Patch-clamp recordings reveal that, as in brain, epilepsy is associated with an increased expression of the neuronal isoform Nav1.1 in cardiomyocytes (Biet et al., 2015). In mice, the HCN channel plays a physiological role in regulating the resting membrane potential, required for regular cardiac and neuronal rhythmicity (Ludwig et al., 2003). In Genetic Absence Epilepsy Rats from Strasbourg

(GAERS) and acquired temporal lobe epilepsy rats, the significant reduction in HCN2 mRNA and protein expression is the mechanism for abnormal cardiac electrophysiology (Powell et al., 2014).

Genetic mutations in the KCNQ1 gene cause familial long QT syndrome due to prolonged cardiac action potential (Goldman et al., 2009). Mutations in the KCNQ1 gene in forebrain neuronal networks, and in brainstem autonomic nuclei can produce seizures, and dysregulate the autonomic control of heart (Goldman et al., 2009).

Dravet syndrome is associated with a loss of function mutation in gene SCN1A encoding for voltage-gated sodium channel Nav1.5 that leads to ECG abnormalities. Increased excitability, prolongation of action potential duration, and triggered activity was recorded in isolated Dravet syndrome ventricular myocytes (Auerbach et al., 2013). Patients with Dravet syndrome have reduced heart rate variability (HRV) that shows imbalance in autonomic cardiac function (Delogu et al., 2011). The findings in SCN1A heterozygous knockout mice show that increase in parasympathetic activity following tonic-clonic seizures causes bradycardia and subsequently SUDEP (Kalume et al., 2013). SCN1A mutant mice have lower threshold for spreading depression that causes bradycardia, apnoea and SUDEP (Aiba and Noebels, 2015).

Loss of function mutations of the SCN5A gene causes Brugada syndrome, and is characterised with ECG abnormalities including ST segment elevation, syncope as well as seizures, and sleep abnormalities (Wang et al., 2015).

HRV is used as a functional tool to investigate the state of the autonomic nervous system. Reduced HRV is seen in epilepsy patients compared to their controls (Ponnusamy et al., 2012), and is associated with increased mortality in patients with heart failure. Abnormal blood pressure variability with higher vasomotor tone is observed in patients with chronic epilepsy (Devinsky et al., 1994).

3.2. Respiratory dysfunction

In epilepsy patients with severe respiratory dysfunction, as demonstrated using video-EEG telemetry, the ictal period is associated with a severe poikilopapnic hypoxia (Fig. 4) (Bateman et al., 2008; Seyal et al., 2010). Ictal and post-ictal ETCO₂ increased above 50 mmHg in 11 out of the 33 epilepsy patients with the post-ictal increase in respiratory rate, and amplitude (Seyal et al., 2010). In human, peri-ictal respiratory disturbances are likely to play a critical role in the pathophysiology of SUDEP (Dlouhy et al., 2015). Central apnoea is common in a sheep model of epileptic sudden death (Johnston et al., 1997). In audiogenic seizure-prone DBA/2 mice death due to respiratory arrest can be prevented by mechanical ventilation (Venit et al., 2004). Interestingly SUDEP in DBA/2 mice can also be prevented by treatment with a selective serotonin reuptake inhibitor (Tupal and Faingold, 2006). Serotonergic and/or glutamatergic neuronal abnormalities are associated with central respiratory dysfunction (Hodges et al., 2008, 2009). Impaired ventilatory responses to hypercapnia may lead to SUDEP by adversely affecting patients' ability to reposition their head when prone after convulsion.

Clinical evidence suggests that post-ictal pulmonary edema, which may be mediated by vasoconstriction induced by a massive seizure-related sympathetic outburst with increased pulmonary vascular resistance, could be associated with the pathophysiology of SUDEP (Kennedy et al., 2015). Forensic autopsies of 52 cases of SUDEP showed marked pulmonary congestion, and edema with an average combined lung weight of 1182 g, compared with the normal average combined lung weight of 840 g in men (Zhuo et al., 2012). In epileptic baboons that died suddenly without apparent cause, 96% had pulmonary congestion or edema, whereas only 12%

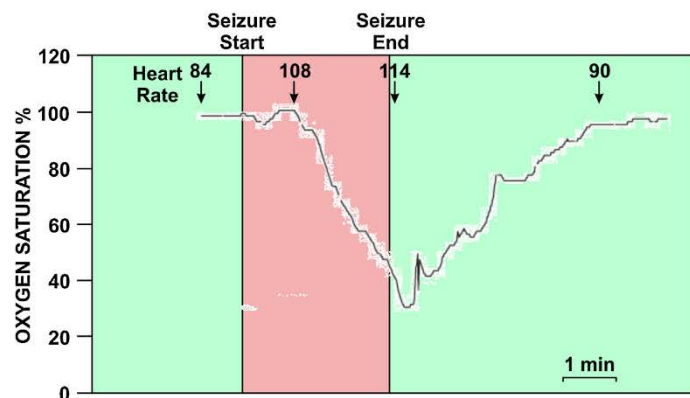


Fig. 4. Oxygen saturation falling below 40% in a 19 year old male patient with a complex partial seizure without generalisation. Seizure duration is shown in red with heart rate in the top panel. (With permission from Guarantors of Brain/Oxford University Press from – Bateman, L.M., Li, C.S., Seyal, M., 2008. Ictal hypoxemia in localization-related epilepsy: Analysis of incidence, severity and risk factors, Brain 131, 3239–3245).

of the control animals had pulmonary edema (Ákos Szabó et al., 2009).

4. Neurotransmitters in cardiorespiratory control

Glutamate, GABA and glycine are the three major ionotropic neurotransmitters within the central nervous system that are responsible for regulating cardiorespiratory activity and reflexes (Ross et al., 1984a; Suzuki et al., 1997). Antagonism of any of these three neurotransmitter systems causes major, or even complete, disruption of central cardiorespiratory control (Ross et al., 1984a). Microinjection of the broad spectrum ionotropic glutamate receptor antagonist, kynurenic acid, into either NTS or ventrolateral medulla reduces the vagal and sympathetic baroreflex (Guyenet et al., 1987). Selective inhibition of NMDA and AMPA/kainate receptors in the CVLM has a similar effect (Miyawaki et al., 1996a,b, 1997). On the other hand, other neurotransmitters and peptides, such as serotonin, catecholamines, PACAP, opioids, substance P, neuropeptide Y, somatostatin, galanin, orexin and angiotensin II also play significant roles in modulating cardiorespiratory function, and reflexes (Callera et al., 1997; Farnham et al., 2011; Kashiwara et al., 2008; Miyawaki et al., 2002a; Pilowsky et al., 2009; Rahman et al., 2011; Shahid et al., 2011). Here we discuss the potential role of PACAP, and glutamate on brainstem cardiorespiratory neurons, in relation to seizure, and SUDEP.

4.1. Pituitary Adenylate Cyclase Activating Polypeptide (PACAP)

PACAP is a 38 amino acid pleiotropic neuropeptide that acts through three different G-protein coupled receptors (PAC1, VPAC1 and VPAC2) (Joo et al., 2004) to stimulate adenylate cyclase activity (Vaudry et al., 1998). It belongs to the glucagon-secretin-vasoactive intestinal polypeptide (VIP) super family of peptides. Since the discovery of PACAP, many studies have emphasised its neuroprotective, and anti-inflammatory role *in vivo*, and *in vitro*, models of neurodegenerative diseases (Bhandare et al., 2015; Brifault et al., 2015; Delgado et al., 1999; Shioda et al., 1998). PACAP is positively coupled to act on its membrane bound receptors and activate adenylate cyclase and generate increased intracellular levels of cAMP. Subsequently, the increased level of cAMP leads to enhanced phosphorylation and changes intracellular proteins expressions such as the MAP kinase proteins (inhibit activation of Jun N-

terminal kinase (JNK)/stress activated protein kinase (SAPK), while it activate extracellular signal-regulated kinase (ERK)), and stimulates IL-6 secretion (Shioda et al., 1998; Shoge et al., 1999). PACAP administration after permanent cerebral ischemia by electrocauterization of middle cerebral artery improves function and recovery in mice by redirecting the microglial response toward a neuroprotective M2 phenotype (Brifault et al., 2015). In cardiovascular regulation, PACAP acts as an excitatory neurotransmitter at central autonomic nuclei in brainstem, and spinal cord (Farnham et al., 2012, 2011, 2008). PACAP is present in the brainstem, and spinal cord autonomic nuclei that are important in central cardiorespiratory regulation (Farnham et al., 2008). The PAC1 receptor is specific for PACAP with a 1000 times lower affinity for VIP, whereas VPAC1 and VPAC2 receptors have equal affinity for PACAP and VIP (Buscail et al., 1990; Miyata et al., 1989). PAC and VPAC receptors are present at specific locations throughout the CNS, on both neurons and microglia (Joo et al., 2004). PAC1 and VPAC1 (but not VPAC2) receptors are present on microglia (Delgado, 2002a,b; Kim et al., 2000; Nunan et al., 2014; Pocock and Kettenmann, 2007). PACAP immunoreactivity is found in regions of the brainstem and spinal cord, including the PVN (Hannibal et al., 1995). PACAP immunoreactive fibers innervate the PVN (Das et al., 2007), the RVLM (Farnham et al., 2008), the ventromedial hypothalamus (Mackawa et al., 2006), the arcuate nucleus (Dürr et al., 2007), and in the IML cell column (Chiba et al., 1996), which are major autonomic nuclei.

Kainic acid-induced seizure increases PACAP expression in PVN of the hypothalamus in rats (Nomura et al., 2000). Previously we found that low dose kainic acid-induced seizures in rats causes sympathoexcitation, increased mean arterial pressure and heart rate, and pro-arrhythmogenic changes including prolongation of the QT interval. The evidence suggests that PACAP has a protective effect on sympathetic preganglionic neurons in the IML cell column during seizures (Bhandare et al., 2015). In patients with epilepsy and SUDEP, PACAP might have “neuroprotective” or “excitatory” effect on sympathetic neurons, which depends on multiple factors, and leads to non-fatal or fatal seizure consequences. The outcome of seizure depends on the type and severity of seizure, the path of spread of seizure to autonomic nuclei, duration of seizure history, the presence of other cardiorespiratory complications etc. (Dlouhy et al., 2015; Hitiris et al., 2007). During seizures, the location of PACAP secretion and its concentration play an important role in modifying sympathetic activity and overall seizure outcome, e.g.

PACAP has different effects on sympathetic neurons at the RVLM and the IML cell column during seizures in rats (Bhandare et al., 2016, 2015).

There are a number of possibilities that could explain the way in which PACAP is exerting its effects, and contributing to either decrease or increase the seizure-induced sympathoexcitation. First, PACAP maintains the sympathetic neuronal firing threshold under control through inhibition of MAP kinase (Shioda et al., 1998), and synaptic glutamate levels (Figiel and Engele, 2000; Shoge et al., 1999) to keep them in healthy condition. Secondly, activation of PACAP on microglial PAC1, and VPAC1 receptors may polarise microglia toward an M2 (anti-inflammatory) phenotype, and increase the endogenous production of the anti-inflammatory cytokines, TGF- β , and IL-10 (Brifault et al., 2015; Suk et al., 2004). Thirdly, as reported earlier, PACAP may produce excitatory effect on the catecholaminergic neurons, and mediate sympathoexcitatory responses along with major effects on the ECG (Farnham et al., 2008; Lai et al., 1997). There is strong evidence that PACAP may play a neuroprotective role.

First, PACAP is anti-inflammatory, and protects neurons against various *in vitro* toxic insults (Delgado et al., 1999; Kim et al., 2000). Following ischemia, PACAP treatment inhibits the activation of JNK/SAPK, and increases secretion of IL-6, which further inhibits activation of JNK/SAPK (Shioda et al., 1998). The protective effect of PACAP is also seen in *in vivo* models of cerebral ischemia where its expression was increased after ischemic injury in rats and mice (Chen et al., 2006; Skoglösa et al., 1999a). PACAP is upregulated following sciatic nerve injury, suggesting a role for PACAP in post-injury recovery of nervous system (Zhang et al., 1996). PACAP also influences the development of the nervous system; specifically it has neurotrophic action on mesencephalic dopaminergic primary culture of neurons (Skoglösa et al., 1999b; Takei et al., 1998). The survival of the immature sympathetic neurons depends on NGF, and in its absence neurons undergo a decrease in intracellular cAMP levels, and programmed cell death (Chang and Korolev, 1997; Przywara et al., 1998). However, treatment with PACAP can increase the cAMP levels, and delay neuronal death caused by NGF deprivation. PACAP can rescue chick embryonic sympathetic neurons from apoptosis when the supply of NGF is compromised (Przywara et al., 1998). These findings indicate that under normal conditions, PACAP might not play a major role as a neurotrophic molecule for sympathetic neuroblasts because NGF is sufficient, and is a dominant neurotrophic factor. However, if neurons become vulnerable as a result of unavailable NGF, PACAP released from presynaptic sites could prevent neurons from apoptosis. Also the caspases 3, 6 and 7 cleave protein substrates within cell to trigger the final phase of apoptosis. PACAP inhibits the caspase 3 in NGF-deprived chicken sympathetic embryonic neuroblasts, which could be mediated through PKA and PKC, but not by ERK-type MAPK transduction pathways (Dejda et al., 2011; Vaudry et al., 1998).

PACAP has a protective effect against glutamate induced toxicity *in vitro* (Shoge et al., 1999). In cultured retinal neurons, a 10 min exposure to 1 mM glutamate followed by a further 24-h incubation significantly decreases cell viability. Application of PACAP simultaneously with glutamate attenuates the glutamate induced neurotoxicity, and prevents the decrease in viability, via cAMP/PKA/MAPK pathways (Shoge et al., 1999). Glutamate transporters play an important role in the rapid clearance of synaptically released excess glutamate. RT-PCR analysis of PACAP mRNA shows that PACAP is synthesised exclusively by neurons, and not by glia, and exposure of cortical astroglia to PACAP increases the maximal velocity of glutamate uptake by promoting the expression of GLT-1 and GLAST transporters (Figiel and Engele, 2000). PACAP also induces expression of glutamine synthetase, which metabolises glutamate into glu-

tamine. PACAP induced increased expression of glial glutamate transporter by astrocytes is likely mediated through activation of cAMP-dependant pathways (Figiel and Engele, 2000; Swanson et al., 1997). The results suggest that PACAP regulates glutamate transport, and metabolism that may contribute to its neuroprotective effect on cardiorespiratory neurons during seizure. Overall PACAP reduces the excessive firing of sympathetic neurons during seizures through the cAMP mediated mechanism, and needs further investigation, which inhibits JNK/SAPK, activates ERK, increases IL-6, inhibits caspase-3, and increases glutamate uptake via astrocytes (Fig. 3).

Secondly, PACAP can produce neuroprotective effects through its action on microglial PAC1 and VPAC1 receptors (Kim et al., 2000); causing release of substances such as IL-10, and TGF- β ; compounds that protect neurons from overexcitation. PACAP suppresses NMDA-induced cell loss in the ganglion cell layer of the retina, and significantly elevates the mRNA levels of anti-inflammatory cytokines IL-10, and TGF- β by increasing the number of microglia and macrophages (Wada et al., 2013). PACAP inhibits activated microglia induced production of TNF- α by a cAMP dependent pathway in *in vivo*, and *in vitro* (Kim et al., 2000). The action of PACAP on microglial cell surface receptors increases IL-10 protein expression, causing downregulation of CD40, and B7 mRNA in activated microglia, thereby acting as a potent anti-inflammatory agent (Delgado et al., 1999; Kim et al., 2002). PACAP inhibits the activation of the MAPK family such as JNK (Delgado, 2002b; Shioda et al., 1998), and stimulates the secretion of IL-6 in CSF (Gottschall et al., 1994; Shioda et al., 1998). Under hypoxic condition, PACAP attenuates activation of inflammatory microglia, and protects co-cultured PC12 cells from microglial neurotoxicity via reduction of hypoxia induced activation of p38 MAPK (Suk et al., 2004). As explained later in detail, activated microglia can polarise into two different phenotypes depending on the type of stimulus, and participate in either neuroprotection or neurotoxicity. However, PACAP treatment can redirect the microglial response toward a neuroprotective M2 phenotype in the late phase of brain ischemia, suggesting that PACAP has a neuroprotective effect on activated microglia (Brifault et al., 2015). Altogether, the actions of PACAP may produce neuroprotective effect on cardiorespiratory neurons in the brainstem during neurotoxic insults such as epilepsy.

A third possibility that is also very promising occurs when increased PACAP expression during seizures may excite catecholaminergic neurons, and mediate sympathoexcitatory responses along with ECG abnormalities. PACAP infusion into the intrathecal space (Farnham et al., 2011; Lai et al., 1997), or microinjection into RVLM (Farnham et al., 2012) has long lasting sympathoexcitatory effects along with variable pressor responses in rats. Systemic administration of low doses of PACAP in rats decreases the threshold for the development of febrile convulsions. Conversely, administration of higher doses of PACAP increased the threshold (Chepurnova et al., 2002). The observed effect is most likely to be an indirect effect of PACAP-induced arginine vasopressin expression, where arginine vasopressin is known to mediate the hypothermia-induced seizures (Kasting et al., 1981). In these circumstances PACAP seems to mediate the induction of seizures, and acts as an excitatory neurotransmitter, which may cause further sympathoexcitatory effects.

4.2. Glutamate

Glutamate is the principal excitatory neurotransmitter of the CNS. Glutamate induced activation of the ionotropic NMDA and AMPA receptors leads to influx of Ca²⁺ and Na⁺. During prolonged excitation, glutamate causes neurotoxic insults through disruption of ionic homeostasis, and increases in oxidative stress (Fig. 3) (Hoyt et al., 1998). Glutamate transporters play an important role in

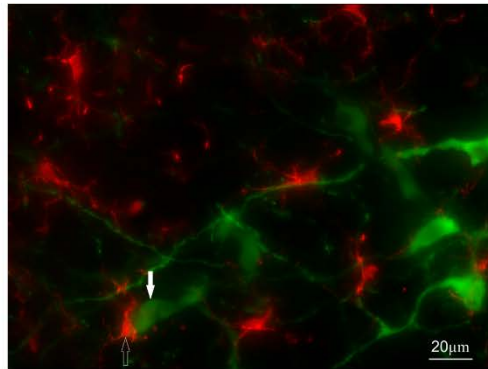


Fig. 5. Microglia (Iba1 immunoreactive; red) with a round cell body and normal processes with few ramifications are distributed in the vicinity of premotor tyrosine hydroxylase immunoreactive RVLM neurons (green). Sympathetic premotor RVLM neurons (green) are shown with a closed arrow and microglia (red) with open arrow.

rapid clearance of the synaptically released glutamate. High affinity sodium-dependant glutamate transporters include GLAST/EAAT1, GLT-1/EAAT2, EAAC1/EAAT3, EAAT4, and EAAT5. The GLAST1 and GLT-1 are expressed predominantly by glia (Swanson et al., 1997). Astrocytes are known to perform the majority of glutamate uptake in the brain, and unlike neurons, are capable of metabolising incorporated glutamate into glutamine by glutamine synthetase (Figiel et al., 2003).

Glutamate is the primary fast neurotransmitter of sympathetic premotor RVLM neurons, as all of these neurons express vesicular glutamate transporter 2 mRNA (Stornetta et al., 2002a,b), and phosphate activated glutaminase is present in both respiratory (Pilowsky et al., 1997) and cardiovascular neurons (Minson et al., 1991). Physiological findings confirmed that bulbospinal RVLM neurons use glutamate as their major neurotransmitter. Microinjection of L-glutamate into the RVLM produces pressor responses along with sympathoexcitation that are completely blocked by kynurenic acid (Araujo et al., 1999; Ito and Sved, 1997). Kynurenic acid microinjection into RVLM on its own has no effect on basal blood pressure, suggesting that glutamatergic synapses have little input to the RVLM in maintaining basal blood pressure, and sympathetic activity. On the other hand, the increase in blood pressure and sympathetic activity that follows blockade of inputs from CVLM to RVLM is dramatically attenuated by blocking glutamatergic excitation into the RVLM (Ito and Sved, 1997; Miyawaki et al., 2002b). Collectively, findings suggest that there is a glutamatergic input to the RVLM neurons and that this glutamatergic input is in balance with inhibitory pathways from CVLM.

Glutamatergic pathways are involved in acute and chronic neurodegenerative diseases including epilepsy, where it is more specific only in some types such as temporal lobe epilepsy (Mueller et al., 2014; Thom, 2004). Activation of both ionotropic and metabotropic glutamate receptors is pro-convulsant (Chapman, 1998). Seizure elevates glutamate levels in the extracellular fluid of the rat hippocampus (Kanamori and Ross, 2011), and produces down-regulation, and functional failure of glutamate transporters (Ueda et al., 2001). The RVLM contains sympathetic premotor neurons responsible for maintaining tonic excitation of sympathetic preganglionic neurons involved in cardiovascular regulation (Madden and Sved, 2003). The activity of pre-sympathetic RVLM neurons is directly correlated with sympathetic nerve activity, and stimulation of neuronal cell bodies in the RVLM with glutamate produces dose-dependent increases in arterial pres-

sure, that is sympathetically mediated (Madden and Sved, 2003). Seizure-induced sympathoexcitation is caused by activation of glutamatergic receptors in RVLM that also causes proarrhythmic changes in rats (Bhandare et al., 2016). Seizure-related increased glutamate expression causes autonomic cardiovascular changes, since the microinjection of kynurenic acid, completely abolished these effects.

It is most likely that increased glutamate levels during seizure induces excitotoxicity of pre-synaptic RVLM neurons, and may contribute to neurodegeneration, and inflammation in epilepsy that might contribute to SUDEP (Mueller et al., 2014). Increased oxidative stress, and inflammation in RVLM during seizure (Tsai et al., 2012) could be mediated through increased glutamate levels or functional failure of glutamate transporters on astrocytes (Ueda et al., 2001). Extracellular glutamate activates either AMPA, NMDA or group I metabotropic receptors, resulting in oxidative stress and cellular excitability (Coyle and Puttfarcken, 1993), and causes sympathoexcitation. Group I metabotropic receptors (mGlu1 and mGlu5) are predominantly located postsynaptically, and activate phospholipase C, which catalyse the production of inositol trisphosphate, and thereby trigger the release of Ca^{2+} from intracellular stores. Mitochondrial activation is a plausible event in glutamate induced oxidative stress, and cellular excitability causing sympathoexcitation (Fig. 3) (Coyle and Puttfarcken, 1993).

5. Microglia and their effect on the physiological state of cardiorespiratory neurons during seizure

Microglia are the principal resident immune cells of the CNS, contributing ~10% of total brain population (Benarroch, 2013; Helmut et al., 2011). Since the first morphological characterisation of microglia, enormous research is conducted, and still their precise role in the healthy and diseased CNS remains unclear. Initially, microglia were classified into two types, “resting” microglia, which are “inactive”, and present in uninjured CNS; and “activated” microglia that are present in response to injury. However, recent work suggests that this classical active/inactive classification is misleading. Using *in vivo* two photon imaging of fluorescently labelled neurons and microglia in mice, it is shown that resting microglia continuously survey their microenvironment for the homeostatic conditions by making brief, and direct contact with synapses. The frequency of microglial contact is directly proportional to neuronal activity, and also reflects the functional status of the synapses (Wake et al., 2009). On the other hand, resting microglia undergo drastic changes, and transform into an activated state. Activated microglia are ramified, with an amoeboid morphology, and acquire their phenotype depending on the type of stimulus; participating in either neuroprotection or neurotoxicity (Ayoub and Salm, 2003). Thus the important role of highly dynamic microglial cells is to maintain synaptic and neuronal homeostasis during both normal and diseased CNS conditions (Helmut et al., 2011; Wake et al., 2009).

Extensive microglial activation is well described in animal models of seizure (Drage et al., 2002; Shapiro et al., 2008), as well as in humans (Beach et al., 1995). Patients with intractable seizures display an 11-fold increase in microglial reactivity in the hippocampus suggesting that microglia change their state in response to altered neuronal activity (Beach et al., 1995). As explained earlier, brainstem and spinal cord autonomic nuclei are important in central cardiorespiratory regulation whose function is disturbed in seizure cases (Bhandare et al., 2015; Naggar et al., 2014; Sakamoto et al., 2008). Microglia are closely associated with sympathetic premotor RVLM neurons (Fig. 5) (Kapoor et al., 2016), and help to maintain a normal homeostatic state. During seizure, microglial responses are

not necessarily neurotoxic. Ablation of preconditioned hippocampal microglia in mice causes significant increases in acute seizure scores compared to non-ablated and preconditioned microglia in control mice, suggestive of a protective effect of microglia (Mitrione et al., 2010). Other studies reported a neuroprotective role of microglia in different animal models of neurodegenerative diseases. In TNF- α and IL-1 β -deficient mice, sodium nitroprusside-induced acute neurotoxicity was increased, which supports a neuroprotective role for pro-inflammatory cytokines released by microglia (Turrin and Rivest, 2006). Marked increases in infarct size and neuronal apoptosis was evident when proliferation of resident microglia was selectively ablated in a mouse model of cerebral ischemia (Lalancette-Hébert et al., 2007). Similar findings were observed in *in vitro* studies, where ablation of ramified microglia severely enhanced NMDA induced neuronal cell death (Vinet et al., 2012). However, neurotoxic effects of microglia occur in cases of overshooting, and uncontrolled stimulation, and are widely attributed to release of cytokines such as caspases, TNF- α and IL-1 β (Burguillos, 2011; Li et al., 2007). Activated microglia are major contributors to neuroinflammation, via secretion of pro-inflammatory cytokines, and chemokines, in addition to non-specific inflammatory mediators such as ROS, and NO. Fresh frozen tissue samples from autism patients showed marked activation of microglia with significant increase in proinflammatory cytokines profile in CSF (Vargas et al., 2005). However, there is little information available about the effect of seizure on microglial activation in brainstem, and spinal cord cardiorespiratory autonomic nuclei, and their possible neuroprotective or neurotoxic effect.

Recent findings provide increasing evidence for microglial communication with neurons (Wake et al., 2009). During early development, microglia clear apoptotic neurons, promote survival of cortical neurons, and prune synapses (Awasaki and Ito, 2004) whereas in the mature CNS they perform highly dynamic functions. Exquisitely motile process and stationary somata of microglial cells make contacts with neurons, and synapses to constantly survey the microenvironment (Fig. 5) (Wake et al., 2009). As explained earlier, glutamate plays a crucial role in development of seizure, and is a major neurotransmitter in cardiorespiratory reflexes. Increased glutamate levels in seizure activates neuronal NMDA receptors followed by calcium influx, and ATP release, which attracts microglial processes through activation of P2Y₁₂ receptors (Eyo et al., 2014). Normally, astroglial glutamate transporters, GLT-1 and GLAST, perform the majority of glutamate uptake in the brain to mediate a high signal to noise ratio in synaptic signaling. However, in pathological conditions such as epilepsy, astroglial glutamate transporter proteins are downregulated, causing excitotoxicity (Ueda et al., 2001). It is possible that microglia may be neuroprotective during seizure by increasing glutamate transporter (GLT-1) expression, and reducing synaptic glutamate concentrations, as demonstrated during facial nerve axotomy (López-Redondo et al., 2000), infectious diseases (Persson et al., 2007), and neurodegenerative diseases (Chrétien et al., 2004). Collectively, the findings support the notion that during seizures, microglia may exert a neuroprotective effect on cardiorespiratory neurons in brainstem that is in part mediated by PACAP (Fig. 3).

6. Conclusion

In epilepsy, the increased expression of glutamate contributes to neurodegeneration, and inflammation. PACAP, and its action on microglia may mediate the neuroprotective effect on central cardiorespiratory neurons in the brainstem. PACAP is neuroprotective by causing production of anti-inflammatory factors such as TGF- β , and IL-6. Additionally, PACAP not only increases the expression of glutamate transporters on microglia, which accelerate glutamate

clearance from the synaptic cleft, but also polarise microglia toward an anti-inflammatory M2 phenotype. Hence, tailoring the effect of PACAP and microglia in the vicinity of cardiorespiratory brainstem neurons may be neuroprotective, and lead to possible novel therapeutic approaches for SUDEP.

Acknowledgements

Authors are recipients of grants from the Australian Research Council (Discovery Early Career Researcher Award; DE120100992), National Health and Medical Research Council of Australia (1024489, 1065485 and 1082215). A.M.B. and K.K. are supported by international Macquarie University Research Excellence Scholarship (2012219 and 2012112), The Heart Research Institute (HRI) and The University of Sydney.

References

- Aiba, I., Noebels, J.L., 2015. Spreading depolarization in the brainstem mediates sudden cardiorespiratory arrest in mouse SUDEP models. *Sci. Transl. Med.* 7, 282ra46.
- Akos Szabó, C., Knappe Michelle Leland, K.D.M., Feldman, J., McCoy, K.J.M., Hubbard, G.B., Williams, J.T., 2009. Mortality in captive baboons with seizures: a new model for SUDEP? *Epilepsia* 50, 1995–1998.
- Allen, A.M., 2002. Inhibition of the hypothalamic paraventricular nucleus in spontaneously hypertensive rats dramatically reduces sympathetic vasomotor tone. *Hypertension* 39, 275–280.
- Ansakorpi, H., Korpeläinen, J.T., Suominen, K., Tolonen, K., Myllylä, V.V., Isojärvi, J.T., 2000. Interictal cardiovascular autonomic responses in patients with temporal lobe epilepsy. *Epilepsia* 41, 42–47.
- Araujo, G.C., Lopes, O.U., Campos, R.R., 1999. Importance of glycinergic and glutamatergic synapses within the rostral ventrolateral medulla for blood pressure regulation in conscious rats. *Hypertension* 34, 752–755.
- Auerbach, D.S., Jones, J., Clawson, B.C., Offord, J., Lenk, G.M., Ogiwara, I., Yamakawa, K., Meisler, M.H., Parent, J.M., Isom, L.L., 2013. Altered cardiac electrophysiology and SUDEP in a model of Dravet syndrome. *PLoS One* 8, e77843.
- Awasaki, T., Ito, K., 2004. Engulfing action of glial cells is required for programmed axon pruning during *Drosophila* metamorphosis. *Curr. Biol.* 14, 668–677.
- Ayoub, A.E., Salm, A.K., 2003. Increased morphological diversity of microglia in the activated hypothalamic supraoptic nucleus. *J. Neurosci.* 23, 7759–7766.
- Bateman, L.M., Li, C.S., Seyal, M., 2008. Ictal hypoxemia in localization-related epilepsy: analysis of incidence, severity and risk factors. *Brain* 131, 3239–3245.
- Beach, T.G., Woodhurst, W.B., MacDonald, D.B., Jones, M.W., 1995. Reactive microglia in hippocampal sclerosis associated with human temporal lobe epilepsy. *Neurosci. Lett.* 191, 27–30.
- Benarroch, E.E., 2013. Microglia: Multiple roles in surveillance, circuit shaping, and response to injury. *Neurology* 81, 1079–1088.
- Bhandare, A.M., Kapoor, K., Pilowsky, P.M., Farnham, M.M.J., 2016. Seizure-Induced Sympathoexcitation Is Caused by Activation of Glutamatergic Receptors in RVLM That Also Causes Proarrhythmic Changes Mediated by PACAP and Microglia in Rats. *J. Neurosci.* 36, 506–517.
- Bhandare, A.M., Mohammed, S., Pilowsky, P.M., Farnham, M.M.J., 2015. Antagonism of PACAP or microglia function worsens the cardiovascular consequences of kainic acid-induced seizures in rats. *J. Neurosci.* 35, 2191–2199.
- Biet, M., Morin, N., Lessard-Beaudoin, M., Graham, R.K., Duss, S., Gagné, J., Sanon, N.T., Carmant, L., Dumaine, R., 2015. Prolongation of action potential duration and QT interval during epilepsy linked to increased contribution of neuronal sodium channels to cardiac late Na⁺ current. *Circ. Arrhythmia Electrophysiol.* 8, 912–920.
- Brifault, C., Gras, M., Liot, D., May, V., Vaudry, D., Wurtz, O., 2015. Delayed pituitary adenylate cyclase-activating polypeptide delivery after brain stroke improves functional recovery by inducing M2 microglia/macrophage polarization. *Stroke* 46, 520–528.
- Burguillos, M.A.D.T.E.A.N.-Q.A.J.P.E.J.L.J.B., 2011. Caspase signalling controls microglia activation and neurotoxicity. *Nature* 472, 319–324.
- Buscail, L., Gourlet, P., Cauvin, A., De Neef, P., Gossen, D., Arimura, A., Miyata, A., Coy, D.H., Robberecht, P., Christophe, J., 1990. Presence of highly selective receptors for PACAP (pituitary adenylate cyclase activating peptide) in membranes from the rat pancreatic acinar cell line AR 4-2J. *FEBS Lett.* 262, 77–81.
- Callera, J.C., Sévoz, C., Laguzzi, R., Machado, B.H., 1997. Microinjection of a serotonin₃ receptor agonist into the NTS of unanesthetized rats inhibits the bradycardia evoked by activation of the baro- and chemoreflexes. *J. Auton. Nerv. Syst.* 63, 127–136.
- Chang, J.Y., Korolev, V.V., 1997. Cyclic AMP and sympathetic neuronal programmed cell death. *Neurochem. Int.* 31, 161–167.
- Chapman, A.G., 1998. Glutamate receptors in epilepsy. *Prog. Brain Res.* 116, 371–383.

- Chen, Y., Samal, B., Hamelink, C.R., Xiang, C.C., Chen, Y., Chen, M., Vaudry, D., Brownstein, M.J., Hallenbeck, J.M., Eiden, L.E., 2006. Neuroprotection by endogenous and exogenous PACAP following stroke. *Regul. Peptides* 137, 4–19.
- Chepurnova, N.E., Ponomarenko, A.A., Chepurinov, S.A., 2002. Peptidergic mechanisms of hyperthermia-evoked convulsions in rats in early postnatal ontogenesis. *Neurosci. Behav. Physiol.* 32, 505–511.
- Chiba, T., Tanaka, K., Tatsuoaka, H., Dun, S.L., Dun, N.J., 1996. The synaptic structure of PACAP immunoreactive axons in the intermedialateral nucleus of the rat. *Neurosci. Lett.* 214, 65–68.
- Chitravanshi, V.C., Sapru, H.N., 1999. Phrenic nerve responses to chemical stimulation of the subregions of ventral medullary respiratory neuronal group in the rat. *Brain Res.* 821, 443–460.
- Chrétien, F., Le Pavec, G., Vallat-Decouvelaere, A.V., Delisle, M.B., Uro-Coste, E., Ironside, J.W., Gambetti, P., Parchi, P., Crémillon, C., Dormont, D., Mikol, J., Gray, F., Gras, G., 2004. Expression of excitatory amino acid transporter-1 (EAAT-1) in brain macrophages and microglia of patients with prion diseases. *J. Neuropath. Exp. Neur.* 63, 1058–1071.
- Coyle, J.T., Puttfarcken, P., 1993. Oxidative stress, glutamate, and neurodegenerative disorders. *Science* 262, 689–695.
- Darbin, O., Casebeer, D.J., Naritoku, D.K., 2002. Cardiac dysrhythmia associated with the immediate postictal state after maximal electroshock in freely moving rat. *Epilepsia* 43, 326–341.
- Das, M., Vihlen, C.S., Legradi, G., 2007. Hypothalamic and brainstem sources of pituitary adenylate cyclase-activating polypeptide nerve fibers innervating the hypothalamic paraventricular nucleus in the rat. *J. Comp. Neurol.* 500, 761–776.
- Dejda, A., Seaborn, T., Bourgault, S., Touzani, O., Fournier, A., Vaudry, H., Vaudry, D., 2011. PACAP and a novel stable analog protect rat brain from ischemia: Insight into the mechanisms of action. *Peptides* 32, 1207–1216.
- Delgado, M., 2002a. Vasoactive intestinal peptide and pituitary adenylate cyclase-activating polypeptide inhibit CBP–NF- κ B interaction in activated microglia. *Biochem. Biophys. Res. Commun.* 297, 1181–1185.
- Delgado, M., 2002b. Vasoactive intestinal peptide and pituitary adenylate cyclase-activating polypeptide inhibit the MEKK1/MEK4/JNK signaling pathway in endotoxin-activated microglia. *Biochem. Biophys. Res. Commun.* 293, 771–776.
- Delgado, M., Munoz-Elias, E.J., Gomariz, R.P., Ganea, D., 1999. Vasoactive intestinal peptide and pituitary adenylate cyclase-activating polypeptide enhance IL-10 production by murine macrophages: in vitro and in vivo studies. *J. Immunol.* 162, 1707–1716.
- Delogu, A.B., Spinelli, A., Battaglia, D., Dravet, C., De Nisco, A., Saracino, A., Romagnoli, C., Lanza, G.A., Crea, F., 2011. Electrical and autonomic cardiac function in patients with Dravet syndrome. *Epilepsia* 52, 55–58.
- Devinsky, O., Perrine, K., Theodore, W.H., 1994. Interictal autonomic nervous system function in patients with epilepsy. *Epilepsia* 35, 199–204.
- Dlouhy, B.J., Gehlbach, B.K., Kreple, C.J., Kawasaki, H., Oya, H., Buzza, C., Granner, M.A., Welsh, M.J., Howard, M.A., Wemmie, J.A., Richerson, G.B., 2015. Breathing inhibited when seizures spread to the amygdala and upon amygdala stimulation. *J. Neurosci.* 35, 10281–10289.
- Drage, M.G., Holmes, G.L., Seyfried, T.N., 2002. Hippocampal neurons and glia in epileptic EL mice. *J. Neurocytol.* 31, 681–692.
- Dürr, K., Norsted, E., Gömüç, B., Suarez, E., Hannibal, J., Meister, B., 2007. Presence of pituitary adenylate cyclase-activating polypeptide (PACAP) defines a subpopulation of hypothalamic POMC neurons. *Brain Res.* 1186, 203–211.
- Eyo, U.B., Peng, J., Swiatkowski, P., Mukherjee, A., Bispo, A., Wu, L.J., 2014. Neuronal hyperactivity recruits microglial processes via neuronal NMDA receptors and microglial P2Y12 receptors after status epilepticus. *J. Neurosci.* 34, 10528–10540.
- Farnham, M.M., Lung, M.S., Tallapragada, V.J., Pilowsky, P.M., 2012. PACAP causes PAC1/VPAC2 receptor mediated hypertension and sympathoexcitation in normal and hypertensive rats. *Am. J. Physiol.-Heart C* 303, 910–917.
- Farnham, M.M.J., Ingloff, M.A., Pilowsky, P.M., 2011. Intrathecal PACAP-38 causes increases in sympathetic nerve activity and heart rate but not blood pressure in the spontaneously hypertensive rat. *Am. J. Physiol.-Heart C* 300, 214–222.
- Farnham, M.M.J., Li, Q., Goodchild, A.K., Pilowsky, P.M., 2008. PACAP is expressed in sympathoexcitatory bulbospinal C1 neurons of the brain stem and increases sympathetic nerve activity in vivo. *Am. J. Physiol.-Regul.* 294, 1304–1311.
- Ficker, D.M., So, E.L., Shen, W.K., Annegers, J.F., O'Brien, P.C., Cascino, G.D., Belau, P.O., 1998. Population-based study of the incidence of sudden unexplained death in epilepsy. *Neurology* 51, 1270–1274.
- Figiel, M., Engele, J., 2000. Pituitary adenylate cyclase-activating polypeptide (PACAP), a neuron- derived peptide regulating glial glutamate transport and metabolism. *J. Neurosci.* 20, 3596–3605.
- Figiel, M., Maucher, T., Rozyczka, J., Bayatti, N., Engele, J., 2003. Regulation of glial glutamate transporter expression by growth factors. *Exp. Neurol.* 183, 124–135.
- Goldman, A.M., Glasscock, E., Yoo, J., Chen, T.T., Klassen, T.L., Noebels, J.L., 2009. Arrhythmia in heart and brain: KCNQ1 mutations link epilepsy and sudden unexplained death. *Sci. Transl. Med.* 1, 2ra6.
- Gottschall, P.E., Tatsuno, I., Arimura, A., 1994. Regulation of interleukin-6 (IL-6) secretion in primary cultured rat astrocytes: Synergism of interleukin-1 (IL-1) and pituitary adenylate cyclase activating polypeptide (PACAP). *Brain Res.* 637, 197–203.
- Guo, G.B., Thames, M.D., Abboud, F.M., 1982. Differential baroreflex control of heart rate and vascular resistance in rabbits. Relative role of carotid aortic, and cardiopulmonary baroreceptors. *Circ. Res.* 50, 554–565.
- Guo, Z.-L., Lai, H.-C., Longhurst, J.C., 2002. Medullary pathways involved in cardiac sympathoexcitatory reflexes in the cat. *Brain Res.* 925, 55–66.
- Guyenet, P.G., Filtz, T.M., Donaldson, S.R., 1987. Role of excitatory amino acids in rat vagal and sympathetic baroreflexes. *Brain Res.* 407, 272–284.
- Hannibal, J., Mikkelsen, J.D., Clausen, H., Holst, J.J., Wulff, B.S., Fahrenkrug, J., 1995. Gene expression of pituitary adenylate cyclase activating polypeptide (PACAP) in the rat hypothalamus. *Regul. Peptides* 55, 133–148.
- Heeringa, J., Berkenbosch, A., De Goede, J., Olivier, C.N., 1979. Relative contribution of central and peripheral chemoreceptors to the ventilatory response to CO₂ during hyperoxia. *Resp. Physiol.* 37, 365–379.
- Helmut, K., Hanisch, U.K., Noda, M., Verkhatsky, A., 2011. Physiology of microglia. *Physiol. Rev.* 91, 461–553.
- Hirsch, C.S., Martin, D.L., 1971. Unexpected death in young epileptics. *Neurology* 21, 682–690.
- Hitiris, N., Suratman, S., Kelly, K., Stephen, L.J., Sills, G.J., Brodie, M.J., 2007. Sudden unexpected death in epilepsy: a search for risk factors. *Epilepsy Behav.* 10, 138–141.
- Hodges, M.R., Tattersall, G.J., Harris, M.B., McEvoy, S.D., Richerson, D.N., Deneris, E.S., Johnson, R.L., Chen, Z.F., Richerson, G.B., 2008. Defects in breathing and thermoregulation in mice with near-complete absence of central serotonin neurons. *J. Neurosci.* 28, 2495–2505.
- Hodges, M.R., Wehner, M., Augst, J., Smith, J.C., Richerson, G.B., 2009. Transgenic mice lacking serotonin neurons have severe apnea and high mortality during development. *J. Neurosci.* 29, 10341–10349.
- Holst, A.G., Winkel, B.G., Risgaard, B., Nielsen, J.B., Rasmussen, P.V., Haunsø, S., Sabers, A., Uldall, P., Tfelt-Hansen, J., 2013. Epilepsy and risk of death and sudden unexpected death in the young: a nationwide study. *Epilepsia* 54, 1613–1620.
- Hoyt, K.R., Arden, S.R., Aizenman, E., Reynolds, I.J., 1998. Reverse Na⁺/Ca²⁺ exchange contributes to glutamate-induced intracellular Ca²⁺ concentration increases in cultured rat forebrain neurons. *Mol. Pharmacol.* 53, 742–749.
- Ito, S., Sved, A.F., 1997. Tonic glutamate-mediated control of rostral ventrolateral medulla and sympathetic vasomotor tone. *Am. J. Physiol.-Regul.* 273, 487–494.
- Johnston, S.C., Siedenberg, R., Min, J.K., Jerome, E.H., Laxer, K.D., 1997. Central apnea and acute cardiac ischemia in a sheep model of epileptic sudden death. *Ann. Neurol.* 42, 588–594.
- Jones, J.F.X., Wang, Y., Jordan, D., 1998. Activity of C fibre cardiac vagal efferents in anaesthetized cats and rats. *J. Physiol.* 507, 869–880.
- Joo, K.M., Chung, Y.H., Kim, M.K., Nam, R.H., Lee, B.L., Lee, K.H., Cha, C.I., 2004. Distribution of vasoactive intestinal peptide and pituitary adenylate cyclase-activating polypeptide receptors (VPAC1, VPAC2, and PAC1 receptor) in the rat brain. *J. Comp. Neurol.* 476, 388–413.
- Kalume, F., Westenbroek, R.E., Cheah, C.S., Yu, F.H., Oakley, J.C., Scheuer, T., Catterall, W.A., 2013. Sudden unexpected death in a mouse model of Dravet syndrome. *J. Clin. Invest.* 123, 1798–1808.
- Kanamori, K., Ross, B.D., 2011. Chronic electrographic seizure reduces glutamine and elevates glutamate in the extracellular fluid of rat brain. *Brain Res.* 1371, 180–191.
- Kapoor, K., Bhandare, A.M., Farnham, M.M.J., Pilowsky, P.M., 2016. Alerted microglia and the sympathetic nervous system: A novel form of microglia in the development of hypertension. *Respir. Physiol. Neurobiol.* 226, 51–62.
- Kashihara, K., McMullan, S., Lonergan, T., Goodchild, A.K., Pilowsky, P.M., 2008. Neuropeptide Y in the rostral ventrolateral medulla blocks somatosympathetic reflexes in anesthetized rats. *Auton. Neurosci.-Basic* 142, 64–70.
- Kasting, N.W., Veale, W.L., Cooper, K.E., Lederis, K., 1981. Vasopressin may mediate febrile convulsions. *Brain Res.* 213, 327–333.
- Kennedy, J.D., Hardin, K.A., Parikh, P., Li, C.S., Seyal, M., 2015. Pulmonary edema following generalized tonic clonic seizures is directly associated with seizure duration. *Seizure* 27, 19–24.
- Kim, W.-K., Kan, Y., Ganea, D., Hart, R.P., Gozes, I., Jonakait, G.M., 2000. Vasoactive intestinal peptide and pituitary adenylate cyclase-activating polypeptide inhibit tumor necrosis factor- α production in injured spinal cord and in activated microglia via a cAMP-dependent pathway. *J. Neurosci.* 20, 3622–3630.
- Kim, W.K., Ganea, D., Jonakait, G.M., 2002. Inhibition of microglial CD40 expression by pituitary adenylate cyclase-activating polypeptide is mediated by interleukin-10. *J. Neuroimmunol.* 126, 16–24.
- Lai, C.C., Wu, S.Y., Lin, H.H., Dun, N.J., 1997. Excitatory action of pituitary adenylate cyclase activating polypeptide on rat sympathetic preganglionic neurons in vivo and in vitro. *Brain Res.* 748, 189–194.
- Lalancette-Hébert, M., Gowing, G., Simard, A., Yuan, C.W., Kriz, J., 2007. Selective ablation of proliferating microglial cells exacerbates ischemic injury in the brain. *J. Neurosci.* 27, 2596–2605.
- Li, L., Lu, J., Tay, S.S.W., Mochhala, S.M., He, B.P., 2007. The function of microglia, either neuroprotection or neurotoxicity, is determined by the equilibrium among factors released from activated microglia in vitro. *Brain Res.* 1159, 8–17.
- López-Redondo, F., Nakajima, K., Honda, S., Kohsaka, S., 2000. Glutamate transporter GLT-1 is highly expressed in activated microglia following facial nerve axotomy. *Mol. Brain Res.* 76, 429–435.
- Ludwig, A., Budde, T., Stieber, J., Moosmang, S., Wahl, C., Holthoff, K., Langebartels, A., Wotjak, C., Munsch, T., Zong, X., Feil, R., Lancel, M., Chien, K.R., Konnerth, A., Pape, H.C., Biel, M., Hofmann, F., 2003. Absence epilepsy and sinus dysrhythmia in mice lacking the pacemaker channel HCN2. *EMBO J.* 22, 216–224.
- Madden, C.J., Sved, A.F., 2003. Cardiovascular regulation after destruction of the C1 cell group of the rostral ventrolateral medulla in rats. *Am. J. Physiol. Heart C* 285, 2734–2748.

- Maekawa, F., Fujiwara, K., Tsukahara, S., Yada, T., 2006. Pituitary adenylate cyclase-activating polypeptide neurons of the ventromedial hypothalamus project to the midbrain central gray. *Neuroreport* 17, 221–224.
- Massey, C.A., Iceman, K.E., Johansen, S.L., Wu, Y., Harris, M.B., Richerson, G.B., 2015. Isoflurane abolishes spontaneous firing of serotonin neurons and masks their pH/CO₂ chemosensitivity. *J. Neurophysiol.* 113, 2879–2888.
- Massey, C.A., Sowers, L.P., Dlouhy, B.J., Richerson, G.B., 2014. Mechanisms of sudden unexpected death in epilepsy: The pathway to prevention. *Nat. Rev. Neurol.* 10, 271–282.
- Metcalf, C.S., Radwanski, P.B., Bealer, S.L., 2009. Status epilepticus produces chronic alterations in cardiac sympathovagal balance. *Epilepsia* 50, 747–754.
- Minson, J., Pilowsky, P., Llewellyn-Smith, I., Kaneko, T., Kapoor, V., Chalmers, J., 1991. Glutamate in spinally projecting neurons of the rostral ventral medulla. *Brain Res.* 555, 326–331.
- Mirriione, M.M., Kononos, D.K., Gravanis, I., Dewey, S.L., Aguzzi, A., Heppner, F.L., Tsirka, S.E., 2010. Microglial ablation and lipopolysaccharide preconditioning affects pilocarpine-induced seizures in mice. *Neurobiol. Dis.* 39, 85–97.
- Miyata, A., Arimura, A., Dahl, R.R., Minamino, N., Uehara, A., Jiang, L., Culler, M.D., Coy, D.H., 1989. Isolation of a novel 38 residue-hypothalamic polypeptide which stimulates adenylate cyclase in pituitary cells. *Biochem. Biophys. Res. Commun.* 164, 567–574.
- Miyawaki, T., Goodchild, A.K., Pilowsky, P.M., 2002a. Activation of mu-opioid receptors in rat ventrolateral medulla selectively blocks baroreceptor reflexes while activation of delta opioid receptors blocks somato-sympathetic reflexes. *Neuroscience* 109, 133–144.
- Miyawaki, T., Goodchild, A.K., Pilowsky, P.M., 2002b. Evidence for a tonic GABA-ergic inhibition of excitatory respiratory-related afferents to presympathetic neurons in the rostral ventrolateral medulla. *Brain Res.* 924, 56–62.
- Miyawaki, T., Minson, J., Arnold, L., Chalmers, J., Llewellyn-Smith, I., Pilowsky, P., 1996a. Role of excitatory amino acid receptors in cardiorespiratory coupling in ventrolateral medulla. *Am. J. Physiol.-Regul.* 1271, 1221–1230.
- Miyawaki, T., Minson, J., Arnold, L., Llewellyn-Smith, I., Chalmers, J., Pilowsky, P., 1996b. AMPA/kainate receptors mediate sympathetic chemoreceptor reflex in the rostral ventrolateral medulla. *Brain Res.* 726, 64–68.
- Miyawaki, T., Suzuki, S., Minson, J., Arnold, L., Chalmers, J., Llewellyn-Smith, I., Pilowsky, P., 1997. Role of AMPA/kainate receptors in transmission of the sympathetic baroreflex in rat CVLM. *Am. J. Physiol.-Regul.* 1272, 800–812.
- Morales, D.J.A., Bonagamba, L.G.H., Costa, K.M., Costa-Silva, J.H., Zoccal, D.B., Machado, B.H., 2014. Short-term sustained hypoxia induces changes in the coupling of sympathetic and respiratory activities in rats. *J. Physiol.* 592, 2013–2033.
- Moseley, B.D., Wirrell, E.C., Nickels, K., Johnson, J.N., Ackerman, M.J., Britton, J., 2011. Electrocardiographic and oximetric changes during partial complex and generalized seizures. *Epilepsy Res.* 95, 237–245.
- Mueller, S.G., Bateman, L.M., Laxer, K.D., 2014. Evidence for brainstem network disruption in temporal lobe epilepsy and sudden unexplained death in epilepsy. *Neuroimage Clin.* 5, 208–216.
- Mutolo, D., Bongianini, F., Nardone, F., Pantaleo, T., 2005. Respiratory responses evoked by blockades of ionotropic glutamate receptors within the Bötzing complex and the pre-Bötzing complex of the rabbit. *Eur. J. Neurosci.* 21, 122–134.
- Naggar, I., Lazar, J., Kamran, H., Orman, R., Stewart, M., 2014. Relation of autonomic and cardiac abnormalities to ventricular fibrillation in a rat model of epilepsy. *Epilepsy Res.* 108, 44–56.
- Nashef, L., 1997. Sudden unexpected death in epilepsy: terminology and definitions. *Epilepsia* 38, S6–S8.
- Nedobov, P.E., Mohammed, S., Kapoor, K., Bhandare, A.M., Farnham, M.M.J., Pilowsky, P.M., 2016. pSer40 tyrosine hydroxylase immunohistochemistry identifies the anatomical location of C1 neurons in rat RVLM that are activated by hypotension. *Neuroscience* 317, 162–172. <http://dx.doi.org/10.1016/j.neuroscience.2016.01.012>.
- Nei, M., Ho, R.T., Sperling, M.R., 2000. EKG abnormalities during partial seizures in refractory epilepsy. *Epilepsia* 41, 542–548.
- Nomura, M., Ueta, Y., Hannibal, J., Serino, R., Yamamoto, Y., Shibuya, I., Matsumoto, T., Yamashita, H., 2000. Induction of pituitary adenylate cyclase-activating polypeptide mRNA in the medial parvocellular part of the paraventricular nucleus of rats following kainic-acid-induced seizure. *Neuroendocrinology* 71, 318–326.
- Nunan, R., Sivasathiaselam, H., Khan, D., Zaben, M., Gray, W., 2014. Microglial VPAC1R mediates a novel mechanism of neuroimmune-modulation of hippocampal precursor cells via IL-4 release. *Glia* 62, 1313–1327.
- Opherk, C., Coromilas, J., Hirsch, L.J., 2002. Heart rate and EKG changes in 102 seizures: Analysis of influencing factors. *Epilepsy Res.* 52, 117–127.
- Persson, M., Brantefjord, M., Liljeqvist, J.A., Bergström, T., Hansson, E., Rönnbäck, L., 2007. Microglial GLT-1 is upregulated in response to herpes simplex virus infection to provide an antiviral defence via glutathione. *Glia* 55, 1449–1458.
- Pilowsky, P., Sun, Q.J., Llewellyn-Smith, I., Arnold, L., Chalmers, J., Minson, J., 1997. Phosphate-activated glutaminase immunoreactivity in brainstem respiratory neurons. *J. Auton. Nerv. Syst.* 63, 85–90.
- Pilowsky, P.M., Lung, M.S.Y., Spirovski, D., McMullan, S., 2009. Differential regulation of the central neural cardiorespiratory system by metabotropic neurotransmitters. *Philos. T Roy Soc. B* 364, 2537–2552.
- Pocock, J.M., Kettenmann, H., 2007. Neurotransmitter receptors on microglia. *Trends Neurosci.* 30, 527–535.
- Ponnusamy, A., Marques, J.L.B., Reuber, M., 2012. Comparison of heart rate variability parameters during complex partial seizures and psychogenic nonepileptic seizures. *Epilepsia* 53, 1314–1321.
- Powell, K.L., Jones, N.C., Kennard, J.T., Ng, C., Urmaliya, V., Lau, S., Tran, A., Zheng, T., Ozturk, E., Dezzi, G., Megatia, I., Delbridge, L.M., Pinaut, D., Reid, C.A., White, P.J., O'Brien, T.J., 2014. HCN channelopathy and cardiac electrophysiologic dysfunction in genetic and acquired rat epilepsy models. *Epilepsia* 55, 609–620.
- Przywara, D.A., Kulkarni, J.S., Wakade, T.D., Leontiev, D.V., Wakade, A.R., 1998. Pituitary adenylate cyclase-activating polypeptide and nerve growth factor use the proteasome to rescue nerve growth factor-deprived sympathetic neurons cultured from chick embryos. *J. Neurochem.* 71, 1889–1897.
- Pyner, S., Coote, J.H., 1999. Identification of an efferent projection from the paraventricular nucleus of the hypothalamus terminating close to spinally projecting rostral ventrolateral medullary neurons. *Neuroscience* 88, 949–957.
- Pyner, S., Coote, J.H., 2000. Identification of branching paraventricular neurons of the hypothalamus that project to the rostral ventrolateral medulla and spinal cord. *Neuroscience* 100, 549–556.
- Rahman, A.A., Shahid, I.Z., Pilowsky, P.M., 2011. Intrathecal neuromedin U induces biphasic effects on sympathetic vasomotor tone, increases respiratory drive and attenuates sympathetic reflexes in rat. *Brit. J. Pharmacol.* 164, 617–631.
- Ross, C., Ruggiero, D., Park, D., Joh, T., Sved, A., Fernandez-Pardal, J., Saavedra, J., Reis, D., 1984a. Tonic vasomotor control by the rostral ventrolateral medulla: effect of electrical or chemical stimulation of the area containing C1 adrenergic neurons on arterial pressure, heart rate, and plasma catecholamines and vasopressin. *J. Neurosci.* 4, 474–484.
- Ross, C.A., Ruggiero, D.A., Joh, T.H., Park, D.H., Reis, D.J., 1984b. Rostral ventrolateral medulla: selective projections to the thoracic autonomic cell column from the region containing C1 adrenergic neurons. *J. Comp. Neurol.* 228, 168–185.
- Sakamoto, K., Saito, T., Orman, R., Koizumi, K., Lazar, J., Saliciccioli, L., Stewart, M., 2008. Autonomic consequences of kainic acid-induced limbic cortical seizures in rats: peripheral autonomic nerve activity, acute cardiovascular changes, and death. *Epilepsia* 49, 982–996.
- Seyal, M., Bateman, L.M., Albertson, T.E., Lin, T.C., Li, C.S., 2010. Respiratory changes with seizures in localization-related epilepsy: analysis of pericardial hypercapnia and airflow patterns. *Epilepsia* 51, 1359–1364.
- Shafon, A.D., Ryan, A., Badoer, E., 1998. Neurons in the hypothalamic paraventricular nucleus send collaterals to the spinal cord and to the rostral ventrolateral medulla in the rat. *Brain Res.* 801, 239–243.
- Shahid, I.Z., Rahman, A.A., Pilowsky, P.M., 2011. Intrathecal orexin A increases sympathetic outflow and respiratory drive, enhances baroreflex sensitivity and blocks the somato-sympathetic reflex. *Brit. J. Pharmacol.* 162, 961–973.
- Shapiro, L.A., Wang, L., Ribak, C.E., 2008. Rapid astrocyte and microglial activation following pilocarpine-induced seizures in rats. *Epilepsia* 49, 33–41.
- Shioda, S., Ozawa, H., Dohi, K., Mizushima, H., Matsumoto, K., Nakajo, S., Takaki, A., Zhou, C.J., Nakai, Y., Arimura, A., 1998. PACAP protects hippocampal neurons against apoptosis: Involvement of JNK/SAPK signaling pathway. *Ann. NY Acad. Sci.* 865, 111–117.
- Shoge, K., Mishima, H.K., Saitoh, T., Ishihara, K., Tamura, Y., Shiomi, H., Sasa, M., 1999. Attenuation by PACAP of glutamate-induced neurotoxicity in cultured retinal neurons. *Brain Res.* 839, 66–73.
- Silveira, D.C., Schachter, S.C., Schomer, D.L., Holmes, G.L., 2000. Flurothyl-induced seizures in rats activate Fos in brainstem catecholaminergic neurons. *Epilepsy Res.* 39, 1–12.
- Skoglösa, Y., Lewén, A., Takei, N., Hillered, L., Lindholm, D., 1999a. Regulation of pituitary adenylate cyclase activating polypeptide and its receptor type 1 after traumatic brain injury: Comparison with brain-derived neurotrophic factor and the induction of neuronal cell death. *Neuroscience* 90, 235–247.
- Skoglösa, Y., Takei, N., Lindholm, D., 1999b. Distribution of pituitary adenylate cyclase activating polypeptide mRNA in the developing rat brain. *Mol. Brain Res.* 65, 1–13.
- Stornetta, R.L., Sevigny, C.P., Guyenet, P.G., 2002a. Vesicular glutamate transporter DNPI/VGLUT2 mRNA is present in C1 and several other groups of brainstem catecholaminergic neurons. *J. Comp. Neurol.* 444, 191–206.
- Stornetta, R.L., Sevigny, C.P., Schreihöfer, A.M., Rosin, D.L., Guyenet, P.G., 2002b. Vesicular glutamate transporter DNPI/VGLUT2 is expressed by both C1 adrenergic and nonadrenergic presympathetic vasomotor neurons of the rat medulla. *J. Comp. Neurol.* 444, 207–220.
- Suk, K., Park, J.-H., Lee, W.-H., 2004. Neurotrophic PACAP inhibits hypoxic activation of brain microglia: a protective mechanism against microglial neurotoxicity in ischemia. *Brain Res.* 1026, 151–156.
- Suzuki, T., Takayama, K., Miura, M., 1997. Distribution and projection of the medullary cardiovascular control neurons containing glutamate, glutamic acid decarboxylase, tyrosine hydroxylase and phenylethanolamine N-methyltransferase in rats. *Neurosci Res.* 27, 9–19.
- Swanson, R.A., Liu, J., Miller, J.W., Rothstein, J.D., Farrell, K., Stein, B.A., Longuemare, M.C., 1997. Neuronal regulation of glutamate transporter subtype expression in astrocytes. *J. Neurosci.* 17, 932–940.
- Takei, N., Skoglösa, Y., Lindholm, D., 1998. Neurotrophic and neuroprotective effects of pituitary adenylate cyclase-activating polypeptide (PACAP) on mesencephalic dopaminergic neurons. *J. Neurosci. Res.* 54, 698–706.
- ter Horst, G.J., Luiten, P.G.M., Kuipers, F., 1984. Descending pathways from hypothalamus to dorsal motor vagus and ambiguous nuclei in the rat. *J. Auton. Nerv. Syst.* 11, 59–75.
- Thom, M., 2004. Neuropathological findings in epilepsy. *Curr. Diagn. Pathol.* 10, 93–105.

- Tsai, C.-Y., Chan, J.Y.H., Hsu K.-s., Chang, A.Y.W., Chan, S.H.H., 2012. Brain-derived neurotrophic factor ameliorates brain stem cardiovascular dysregulation during experimental temporal lobe status epilepticus. *PLoS One* 7, e33527.
- Tupal, S., Faingold, C.L., 2006. Evidence supporting a role of serotonin in modulation of sudden death induced by seizures in DBA/2 mice. *Epilepsia* 47, 21–26.
- Turrin, N.P., Rivest, S., 2006. Tumor necrosis factor α but not interleukin 1β mediates neuroprotection in response to acute nitric oxide excitotoxicity. *J. Neurosci.* 26, 143–151.
- Ueda, Y., Doi, T., Tokumaru, J., Yokoyama, H., Nakajima, A., Mitsuyama, Y., Ohya-Nishiguchi, H., Kamada, H., James Willmore, L., 2001. Collapse of extracellular glutamate regulation during epileptogenesis: Down-regulation and functional failure of glutamate transporter function in rats with chronic seizures induced by kainic acid. *J. Neurochem.* 76, 892–900.
- Vargas, D.L., Nascimbene, C., Krishnan, C., Zimmerman, A.W., Pardo, C.A., 2005. Neuroglial activation and neuroinflammation in the brain of patients with autism. *Ann. Neurol.* 57, 67–81.
- Vaudry, D., Gonzalez, B.J., Basille, M., Anouar, Y., Fournier, A., Vaudry, H., 1998. Pituitary adenylate cyclase-activating polypeptide stimulates both *c-fos* gene expression and cell survival in rat cerebellar granule neurons through activation of the protein kinase A pathway. *Neuroscience* 84, 801–812.
- Venit, E.L., Shepard, B.D., Seyfried, T.N., 2004. Oxygenation prevents sudden death in seizure-prone mice. *Epilepsia* 45, 993–996.
- Vinet, J., van Weering, H.R.J., Heinrich, A., Kälin, R.E., Wegner, A., Brouwer, N., Heppner, F.L., van Rooijen, N., Boddeke, H.W.G.M., Biber, K., 2012. Neuroprotective function for ramified microglia in hippocampal excitotoxicity. *J. Neuroinflamm.* 9, 27.
- Wada, Y., Nakamachi, T., Endo, K., Seki, T., Ohtaki, H., Tsuchikawa, D., Hori, M., Tsuchida, M., Yoshikawa, A., Matkovits, A., Kagami, N., Imai, N., Fujisaka, S., Usui, I., Tobe, K., Koide, R., Takahashi, H., Shioda, S., 2013. PACAP attenuates NMDA-induced retinal damage in association with modulation of the microglia/macrophage status into an acquired deactivation subtype. *J. Mol. Neurosci.* 51, 493–502.
- Wake, H., Moorhouse, A.J., Jinno, S., Kohsaka, S., Nabekura, J., 2009. Resting microglia directly monitor the functional state of synapses in vivo and determine the fate of ischemic terminals. *J. Neurosci.* 29, 3974–3980.
- Wang, L., Meng, X., Yuchi, Z., Zhao, Z., Xu, D., Fedida, D., Wang, Z., Huang, C., 2015. De novo mutation in the SCN5A gene associated with brugada syndrome. *Cell Physiol. Biochem.* 36, 2250–2262.
- Wenker, I.C., Kréneisz, O., Nishiyama, A., Mulkey, D.K., 2010. Astrocytes in the retrotrapezoid nucleus sense H^+ by inhibition of a Kir4.1-Kir5.1-like current and may contribute to chemoreception by a purinergic mechanism. *J. Neurophysiol.* 104, 3042–3052.
- Westerhaus, M.J., Loewy, A.D., 2001. Central representation of the sympathetic nervous system in the cerebral cortex. *Brain Res.* 903, 117–127.
- WHO, 2005 Atlas: Epilepsy Care in the World Department of Mental Health and Substance Abuse. W.H.O. (Ed.), Geneva.
- Young, D., 2010. Control of Cardiac Output. San Rafael: Morgan & Claypool Life Sciences. San Rafael.
- Zhang, Y.Z., Hannibal, J., Zhao, Q., Moller, K., Danielsen, N., Fahrenkrug, J., Sundler, F., 1996. Pituitary adenylate cyclase activating peptide expression in the rat dorsal root ganglia: Up-regulation after peripheral nerve injury. *Neuroscience* 74, 1099–1110.
- Zhuo, L., Zhang, Y., Zielke, H.R., Levine, B., Zhang, X., Chang, L., Fowler, D., Li, L., 2012. Sudden unexpected death in epilepsy: Evaluation of forensic autopsy cases. *Forensic Sci. Int.* 223, 171–175.

Appendix 3

Ethics

Appendix 3 (pp. 381-388) has been removed as it contains confidential material